

Dissecting iron and heme regulatory networks and adaptation to heme stress in *Corynebacterium glutamicum*

Aileen Krüger

Schlüsseltechnologien / Key Technologies

Band / Volume 266

ISBN 978-3-95806-686-1

Forschungszentrum Jülich GmbH
Institut für Bio-und Geowissenschaften
Biotechnologie (IBG-1)

Dissecting iron and heme regulatory networks and adaptation to heme stress in *Corynebacterium glutamicum*

Aileen Krüger

Schriften des Forschungszentrums Jülich
Reihe Schlüsseltechnologien / Key Technologies

Band / Volume 266

ISSN 1866-1807

ISBN 978-3-95806-686-1

Bibliografische Information der Deutschen Nationalbibliothek.
Die Deutsche Nationalbibliothek verzeichnet diese Publikation in der
Deutschen Nationalbibliografie; detaillierte Bibliografische Daten
sind im Internet über <http://dnb.d-nb.de> abrufbar.

Herausgeber und Vertrieb: Forschungszentrum Jülich GmbH
Zentralbibliothek, Verlag
52425 Jülich
Tel.: +49 2461 61-5368
Fax: +49 2461 61-6103
zb-publikation@fz-juelich.de
www.fz-juelich.de/zb

Umschlaggestaltung: Grafische Medien, Forschungszentrum Jülich GmbH

Druck: Grafische Medien, Forschungszentrum Jülich GmbH

Copyright: Forschungszentrum Jülich 2023

Schriften des Forschungszentrums Jülich
Reihe Schlüsseltechnologien / Key Technologies, Band / Volume 266

D 61 (Diss. Düsseldorf, Univ., 2022)

ISSN 1866-1807
ISBN 978-3-95806-686-1

Vollständig frei verfügbar über das Publikationsportal des Forschungszentrums Jülich (JuSER)
unter www.fz-juelich.de/zb/openaccess.



This is an Open Access publication distributed under the terms of the [Creative Commons Attribution License 4.0](https://creativecommons.org/licenses/by/4.0/), which permits unrestricted use, distribution, and reproduction in any medium, provided the original work is properly cited.

The thesis has been conducted at the Institute of Bio- and Geosciences, IBG-1: Biotechnology, Forschungszentrum Jülich, from March 2019 until October 2022 under the supervision of Prof. Dr. Julia Frunzke.

Published by permission of the Faculty of Mathematics and Natural Sciences at Heinrich-Heine-University Düsseldorf.

Supervisor: Prof. Dr. Julia Frunzke
Institute of Bio- and Geosciences
IBG-1: Biotechnology
Forschungszentrum Jülich, Jülich

Mentor: Prof. Dr. Lutz Schmitt
Institute of Biochemistry I
Heinrich-Heine-University Düsseldorf, Düsseldorf

Date of oral examination: 16.01.2023

“This is a strange land, an environment dangerous for those unprepared for it.”

– Iron Man (1974, Vol 1 68, Marvel Comics Group)

The studies presented in this doctoral thesis have been published or summarized for publication in the following articles and manuscripts:

Keppel M.*, Hünnefeld M.*, Filipchuk A.*, Viets U., Davoudi C. F., **Krüger A.**, Mack C., Pfeifer E., Polen T., Baumgart M., Bott M., and Frunzke J. (2020): HrrSA orchestrates a systemic response to heme and determines prioritization of terminal cytochrome oxidase expression. *Nucleic Acids Research*, 48:6547–62. DOI: 10.1093/nar/gkaa415.

Krüger A., Keppel M., Sharma V., and Frunzke J. (2022): The diversity of heme sensor systems - heme-responsive transcriptional regulation mediated by transient heme protein interactions. *FEMS Microbiology Reviews*, 46(3). DOI: 10.1093/femsre/fuac002.

Krüger A., Frunzke J. (2022): A pseudokinase version of the histidine kinase ChrS promotes high heme tolerance of *Corynebacterium glutamicum*. *Frontiers in Microbiology*, 13:997448. DOI: 10.3389/fmicb.2022.997448.

Krüger A., Viets U., Filipchuk A., Frunzke J. (2022): A genome-wide analysis of the interconnection of iron- and heme-dependent regulatory networks governed by DtxR and HrrA in *Corynebacterium glutamicum*. *To be submitted*.

Results of further projects not discussed in this thesis have been published in:

Krüger A.*, Wiechert J.*, Gätgens C., Polen T., Mahr R., Frunzke J. (2019): Impact of CO₂/HCO₃⁻ Availability on Anaplerotic Flux in Pyruvate Dehydrogenase Complex-Deficient *Corynebacterium glutamicum* Strains. *Journal of Bacteriology*, 201(20). DOI: 10.1128/JB.00387-19.

* *These authors contributed equally to this work.*

Abbreviations

a.u.	Arbitrary units	<i>eyfp</i>	Enhanced yellow fluorescent protein
aa	Amino acids		
ALA	δ -aminolevulinic acid	HK	Histidine kinase
ALE	Adaptive laboratory evolution	HPLC	High performance liquid chromatography
ATCC	American type culture collection	HRM	Heme-regulatory motif
ATP	Adenosine triphosphate	IPTG	Isopropyl-thio- β -D-galactopyranosid
BACTH	Bacterial two-hybrid	OD ₆₀₀	Optical density at 600 nm
BHI(S)	Brain-heart infusion(+ sorbitol)	OP	Output domain
bp	Base pairs	REC	Receiver domain
CA domain	Catalytical domain	RNA	Ribonucleic acid
ChAP	Chromatin affinity purification	ROS	Reactive oxygen species
ChIP	Chromatin immunoprecipitation	RR	Response regulator
DHp domain	Dimerization and histidine phosphotransfer domain	Seq	Sequencing
DNA	Deoxyribonucleic acid	TCA	Tricarboxylic acid
e.g.	<i>exempli gratia</i>	TCS	Two-component system
ECF	Extracytoplasmic function	TM domain	Transmembrane domain
EMSA	Electrophoretic mobility shift assay	TMPD	N,N,N',N'-tetramethyl- <i>p</i> -phenylenediamine
et al.	<i>et alii</i>	v/v	Volume per volume
etc.	<i>et cetera</i>	w/v	Weight per volume
		WT	Wild type

Further abbreviations not included in this section are used according to international standards, as e.g. listed in the author guidelines of the Journal of Cell Biology (<http://jcb.rupress.org/content/standard-abbreviations>).

Table of Contents

1. Summary.....	1
2. Scientific context and key results of this thesis.....	3
2.1 Iron – a crucial micronutrient for cellular life	3
2.2 A versatile alternative resource of iron: Heme	3
2.3 Coping with the environment: Control of iron and heme homeostasis	5
2.3.1 Iron-responsive gene regulation	5
2.3.2 Heme-responsive control of gene expression.....	7
2.4 Genome-wide binding profiles of iron and heme regulatory networks in <i>C. glutamicum</i>	15
2.4.1 In vivo profiling of DtxR promoter occupancies.....	16
2.4.2 In vivo profiling of HrrA promoter occupancies.....	20
2.4.3 Relevance of weak binding sites in ChAP-Seq analyses	23
2.4.4 From static regulons to dynamic networks.....	25
2.5 Evolution towards high heme tolerance	28
2.5.1 Heme export by HrtBA plays a pivotal role for adaptation to elevated heme levels	29
2.5.2 The role of pseudokinases in signaling cascades.....	33
2.5.3 Mode of action of pseudokinase ChrS_CA-fs	35
2.5.4 Heme sequestration or alternative transport systems counteracting heme toxicity.....	40
2.6 A glimpse into heme as valuable resource in community.....	42
2.7 Evolution towards the production of heme	44
2.8 Conclusion and Outlook	48
2.9 References.....	50
3. Publications and manuscripts.....	69
3.1 The diversity of heme sensor systems - heme-responsive transcriptional regulation mediated by transient heme protein interactions	70
3.2 A genome-wide analysis of the interconnection of iron- and heme-dependent regulatory networks governed by DtxR and HrrA in <i>Corynebacterium glutamicum</i>	90
3.3 HrrSA orchestrates a systemic response to heme and determines prioritization of terminal cytochrome oxidase expression	115
3.4 A pseudokinase version of the histidine kinase ChrS promotes high heme tolerance of <i>Corynebacterium glutamicum</i>	132

4. Appendix.....	149
4.1 Supplemental material to “A genome-wide analysis of the interconnection of iron- and heme-dependent regulatory networks governed by DtxR and HrrA in <i>Corynebacterium glutamicum</i> ”..	149
4.2 Supplemental material to “HrrSA orchestrates a systemic response to heme and determines prioritization of terminal cytochrome oxidase expression” ..	174
4.3 Supplemental material to “A pseudokinase version of the histidine kinase ChrS promotes high heme tolerance of <i>Corynebacterium glutamicum</i> ”.....	199
4.4 Supplemental material to section “2.7 Evolution towards the production of heme” ..	218
4.5 Impact of CO ₂ /HCO ₃ ⁻ Availability on Anaplerotic Flux in Pyruvate Dehydrogenase Complex-Deficient <i>Corynebacterium glutamicum</i> Strains.....	221
4.6 Supplemental material to “Impact of CO ₂ /HCO ₃ ⁻ Availability on Anaplerotic Flux in Pyruvate Dehydrogenase Complex-Deficient <i>Corynebacterium glutamicum</i> Strains” ..	244
Acknowledgements	273

1. Summary

Transcription factors enable organisms to modulate the expression of numerous genes in response to different environmental stimuli. They are embedded in complex and sophisticated regulatory networks to ensure balanced responses and survival in fluctuating environments. The aim of this doctoral thesis was to enlarge the knowledge on corynebacterial iron and heme regulatory networks, their interactions and their plasticity in response to stress.

The trace element iron is vital for almost every cellular organism acting in various essential biological processes, like electron transport, tricarboxylic acid cycle or peroxide reduction. An important form of bound iron is the porphyrin structure heme. Besides its role as alternative iron resource in iron-scarce environments, heme serves as the prosthetic group of several critical proteins like cytochromes, hydroxylases or catalases. Despite being essential for survival, a certain toxicity is associated with iron and heme at elevated levels *inter alia* caused by the generation of oxidative stress via Fenton reaction. With the intention to maintain robust iron and heme homeostasis, the Gram-positive soil bacterium *Corynebacterium glutamicum* relies on a transcriptional network comprised of the master regulator of iron DtxR and the paralogous heme-responsive two-component systems HrrSA and ChrSA. While HrrSA represents a global regulatory system of heme homeostasis, ChrSA is specific for heme detoxification by regulating the expression of the heme exporter HrtBA.

In the framework of this doctoral thesis, *in vivo* genome-wide profiling of DtxR binding sites confirmed many targets known from *in vitro* data, but further expanded the repertoire of DtxR targets by genes involved in DNA recombination, methionine synthesis and oxidative stress as well as several prophage genes. Remarkably, binding was illustrated to be dependent from the iron source present and a similar observation was made when deciphering conditional and time-resolved binding patterns of HrrA. Here, identification of more than 200 target genes of *inter alia* heme biosynthesis, respiratory chain, oxidative stress or cell envelope remodeling unraveled HrrA as global regulator of heme homeostasis. Strikingly, a significant anti-proportional correlation of binding peak intensity and the differential gene expression was determined for both DtxR and HrrA data sets, i.e. weaker binding correlated with a higher differential gene expression in strains lacking the respective regulator. Furthermore, this comparative, genome-wide approach led to the identification of several shared targets of DtxR and HrrA underlining the interconnection of these two global regulatory networks.

Focusing on heme, this study further aimed at the examination of strategies applied by *C. glutamicum* to cope with heme toxicity. An adaptive laboratory evolution experiment towards heme tolerance resulted in an evolved strain carrying a beneficial frameshift mutation in the catalytic domain of the histidine kinase ChrS, yielding a pseudokinase variant. This strain had an exceptionally elevated heme tolerance provided by highly increased expression of *hrtBA* encoding a conserved heme exporter, which was shown to be crucial for heme detoxification. Expression of *hrtBA* is mediated by the response regulator ChrA, but different from the native context, the phosphorylation of ChrA in the evolved strain is completely dependent on the paralogous non-cognate histidine kinase HrrS. This activation is presumably enforced by the pseudokinase variant of ChrS. Thus, adaptation to elevated heme levels occurred via altered communication between the paralogous two-component systems HrrSA and ChrSA. Apart from that, another regulatory layer on the histidine kinase level by heterodimerization of native ChrS and HrrS could be revealed within this study. Moreover, additional minor heme detoxification strategies were postulated, like sequestration via heme binding proteins or alternate transport to counteract toxicity.

In conclusion, this thesis provides comprehensive insights into the control of iron and heme homeostasis by the global transcriptional regulators DtxR and HrrA. The presented results emphasize the importance of *in vivo* genome-wide binding analyses to decipher interactions and interference between global regulatory networks. Furthermore, adaptive laboratory evolution experiments revealed the high evolutionary plasticity of TCSs cascades composed of paralogous systems, as exemplified by HrrSA and ChrSA, facilitating the rapid adaptation to environmental stresses.

2. Scientific context and key results of this thesis

2.1 Iron – a crucial micronutrient for cellular life

Every organism depends on metals required for growth and survival. It can be estimated that half of all enzymes, which have been characterized, rely on one or more metal ions for their function (Chandrangsu et al., 2017; Waldron et al., 2009). The most important metals for bacterial metabolism are inter alia zinc, copper and iron (Hughes and Poole, 1989). Throughout this thesis, the focus will be on iron and especially on the iron-bound compound heme as well as on the homeostatic regulation thereof, vital for cellular life.

Iron is one of the four most abundant elements on earth (Weber et al., 2006) and it is even claimed to be involved in the origin of life (Camprubi et al., 2017; Thiel et al., 2019). This trace element has been determined as a physiological requirement of almost every living organism as it plays important roles in numerous biological processes, like electron transport, tricarboxylic acid cycle (TCA), peroxide reduction or DNA biosynthesis and repair (Andrews et al., 2003; Cornelis et al., 2011). Within prosthetic groups, iron is the most common redox active metal found in proteins (Andreini et al., 2008). While being vital, iron is a scarce and growth-limiting resource, as it is not readily available at aerobic conditions. There it remains primarily in the insoluble ferric form (Fe^{3+}) (solubility: 10^{-18} M at pH 7) as a result of the corrosive reaction of the soluble form Fe^{2+} with O_2 (Andrews et al., 2003). Although the soluble ferrous state of iron (Fe^{2+}) is essential for life, it can induce serious damage to cells. The main cause is the pro-oxidant characteristic of Fe^{2+} reacting with H_2O_2 to yield reactive oxygen species (ROS), as depicted by Fenton/Haber-Weiss reaction (Fenton, 1894):



The resulting hydroxyl radicals can induce severe damage on DNA, proteins and lipids (Pierre and Fontecave, 1999; Sousa et al., 2020). To protect from this damage, iron must be tightly controlled to maintain the free intracellular iron at low levels. Nevertheless, iron levels must still be sufficient to meet the required needs. Therefore, besides the avoidance of toxic levels, strategies to counteract iron limitation are required in iron-scarce environments. In this context, many bacteria rely on the use of siderophores, which are metal-chelating agents that capture iron from the habitat, as summarized in several reviews (Ahmed and Holmström, 2014; Saha et al., 2016).

2.2 A versatile alternative resource of iron: Heme

In certain iron-depleted environments, the versatile molecule heme can act as an alternative iron resource. This is especially the case for pathogens sequestering heme from their hosts, like bacteria infecting vertebrates where the major fraction of iron comes in the form of heme bound to hemoglobin

(~70%) (Contreras et al., 2014; Nobles and Maresso, 2011; Wallace, 2016). Nevertheless, also non-pathogenic bacteria rely on heme-bound iron (Andrews et al., 2003; Frunzke et al., 2011; Noya et al., 1997), e.g. in soil from decaying organic material.

Heme is a complex with an iron coordinated via four nitrogen atoms as part of a protoporphyrin ring (protoporphyrin IX) (Ponka, 1999) (Figure 1). Similar to iron, this versatile molecule is essential for both prokaryotes and eukaryotes, because - apart from serving as alternative iron resource - it is also inevitably required as prosthetic group of manifold enzymes of critical cellular processes including cytochromes, hydroxylases, catalases and peroxidases (Layer et al., 2010). Thereby, heme serves a vital role in processes like electron transfer, respiration and oxygen metabolism (Ajioka et al., 2006).

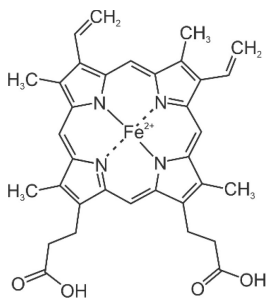


Figure 1: Structure of heme *b*. Ferrous iron (Fe^{2+}) is bound by four nitrogen atoms in a porphyrin ring structure. Heme *b* (protoheme IX) is the most abundant form of heme.

Apart from acquiring from the environment, heme can also be synthesized by many cells (Barupala et al., 2016; Choby and Skaar, 2016; Layer, 2021). The early precursor δ -aminolevulinic acid (ALA) is essential and universal for heme biosynthesis in eukaryotes and prokaryotes alike, although it is synthesized from different pathways. Many eukaryotes and alphaproteobacteria utilize the C4-pathway to generate ALA from glycine and succinyl-CoA (Shemin and Kumin, 1952; Shemin and Rittenberg, 1945), while most prokaryotes and plants employ the C5-pathway, which uses glutamyl-tRNA^{Glu} as precursor molecule (Beale et al., 1975). Over a long period, it was assumed that the heme biosynthesis pathway following ALA is highly conserved in all organisms. This remained true for the protoporphyrin-dependent pathway found among eukaryotic organisms. However, for bacteria and archaea different routes for heme biosynthesis were established (Dailey et al., 2017). While for many Gram-negative bacteria the same route as for eukaryotic systems is employed, many Gram-positives rely on the coproporphyrin-dependent pathway and sulfate-reducing bacteria as well as archaea make use of the most ancient siroheme-dependent pathway. These pathways differ in their enzymatic setup yielding different intermediates, as summarized in detail throughout several recent literature (Dailey et al., 2017; Layer, 2021; Layer et al., 2010).

Analogously to iron, there is also a certain toxicity of heme at elevated levels ascribed to the generation of ROS, which is attributed to the redox-active iron (Kumar and Bandyopadhyay, 2005). Due to its

highly hydrophobic character, free heme accumulates at biological membranes where it promotes oxidation and consequent cell lysis (Aft and Mueller, 1984). Previous studies suggested that there might be a non-iron related toxicity of the porphyrin structure itself (Stojiljkovic et al., 1999), which is not yet unraveled.

2.3 Coping with the environment: Control of iron and heme homeostasis

In principle, any substance is potentially able to turn to a lethal threat and harm living organisms if present at elevated concentrations, even if it is an essential nutrient. This was already claimed by the famous Renaissance physician Paracelsus (1493-1541):

“What is there that is not poison? All things are poison and nothing is without poison. Solely the dose determines that a thing is not a poison.”

As a consequence, organisms have evolved a vast amount of strategies to cope with valuable, but toxic resources allowing to survive under diverse and rapidly changing conditions and finally inhabit almost every environment on earth (Boor, 2006). As metals cannot be synthesized or degraded, organisms have evolved sophisticated strategies maintaining homeostasis. In this context, DNA-binding transcription factors sensing environmental changes and subsequently modulating the expression of relevant target genes represent a key solution.

2.3.1 Iron-responsive gene regulation

The mechanisms of any organism employed to deal with proper iron homeostasis are dependent on the ecological niche and the environmental conditions it is exposed to. However, in general, there are common strategies employed by bacteria to maintain iron homeostasis: (i) iron transport for scavenging iron from the surroundings by e.g. siderophores, (ii) iron storage for later resort, (iii) counteraction of resulting redox stress, and (iv) controlled iron consumption by downregulation of genes coding for iron-requiring proteins (Andrews et al., 2003). Consequently, these manifold genes involved in the different strategies of iron homeostasis require iron-responsive regulatory systems to orchestrate proper functionality. Iron-dependent control of gene expression is of superior importance to meet the necessity for iron without intoxication. For eukaryotic systems, this is primarily regulated by posttranscriptional mechanisms, as summarized earlier (Dlouhy and Outten, 2013; Rouault and Klausner, 1997). In bacteria, there are two widely distributed transcriptional regulators that play a major role in the control of iron homeostasis: Fur and DtxR.

The ferric-uptake regulator (Fur) is a global DNA-binding transcriptional regulator found in several Gram-negative bacteria (e.g. *Escherichia coli* (Bagg and Neilands, 1987), *Neisseria meningitidis* (Delany et al., 2004), *Helicobacter pylori* (Bereswill et al., 2000)) and additionally some low GC-content Gram-

positives (e.g. *Bacillus subtilis* (Bsat et al., 1998)) (Saito and Williams, 1991). In the presence of iron, the Fur protein exists as homodimer with a Zn^{2+} structural binding site, as well as a regulatory active Fe^{2+} site coupling its activity to the presence of intracellular iron (Pecqueur et al., 2006). Fur utilizes Fe^{2+} as co-repressor to regulate transcription of directly and indirectly iron-related genes (Bagg and Neilands, 1987). Thoroughly studied in *Escherichia coli*, more than 80 target genes were shown to be directly controlled by this regulator via binding to a Fur box in the presence of iron, especially including the repression of genes important for iron-acquisition or the biosynthesis of siderophores (McHugh et al., 2003; Seo et al., 2014). More than 10 targets were demonstrated to be directly activated by Fur; including *ftnB* encoding a ferritin-like protein or the TCA cycle related aconitases encoded by *acnA* or *acnB* (Gruer and Guest, 1994; Seo et al., 2014). Concerning the latter ones, it is worth to note that aconitases, upon conformational changes, additionally play an important dual role as iron regulatory proteins (IRPs) in eukaryotes (Narahari et al., 2000; Volz, 2008), while there are also hints for prokaryotes (Tang and Guest, 1999; Tang et al., 2005). Apart from that, the Fur regulator was shown to interact with the expression of small RNAs to further indirectly influence the gene expression of several other targets. In the case of *E. coli*, Fur acts as repressor for the expression of the small RNA RhyB. In iron-limited milieu, *rhyB* is derepressed from Fur in order to degrade several mRNAs which were positively regulated by Fur, e.g. aconitase (*acnA*), succinate dehydrogenase (*sdhCDAB*) or ferritin (*ftn*) (Massé and Arguin, 2005; Massé and Gottesman, 2002; Massé et al., 2007). A dual regulation of the same targets by Fur and RhyB, like in the case for *acnA*, enables rapid adaptation to fluctuating environments (O'Brien et al., 2013; Seo et al., 2014). Further homologs of RhyB were found in other bacteria like *Pseudomonas aeruginosa* (Wilderman et al., 2004). Recently, it was claimed that the reversible binding of Fur to [2Fe-2S]-cluster is conserved among bacteria to sense intracellular iron concentrations as shown for *E. coli* and *Hemophilus influenza* (Fontenot et al., 2020).

Beyond Fur, Gram-positive bacteria with medium to high GC-content rather rely on the global iron regulator DtxR. Firstly discovered in *Corynebacterium diphtheriae*, the diphtheria toxin regulator DtxR was initially revealed to repress the *tox* gene (Boyd et al., 1990; Pappenheimer and Johnson, 1936). The diphtheria toxin is encoded in the genome of several corynephages and is derepressed by the genome-encoded DtxR under iron-limiting conditions (Pappenheimer, 1977; Schmitt and Holmes, 1991; Welkos and Holmes, 1981). On a pathogenic view, this yields toxin production as soon as infecting the host, as the bloody milieu in vertebrates is iron-scarce. In fact, several pathogenic bacteria sense their host environment via iron availability to induce their toxin production (Litwin and Calderwood, 1993). DtxR-like homologs were found in numerous Gram-positive bacteria like IdeR of *Mycobacterium tuberculosis* (Manabe et al., 1999) or MntR of *Staphylococcus aureus* (Ando et al., 2003) and are often described as master regulator of iron homeostasis. However, DtxR is not only relevant in pathogenic, but also in non-pathogenic species, like the soil bacterium *Corynebacterium*

glutamicum (Brune et al., 2006; Wennerhold and Bott, 2006). Although Fur and DtxR do not share significant similarity on the protein level (Fur of *E. coli* with DtxR of *C. diphtheriae*: 28% (global alignment, Needleman-Wunsch)), they are functional homologs. Comparable to Fur, DtxR-like regulators form dimers in complex with Fe²⁺ in order to orchestrate an iron-dependent gene expression by binding to the respective target DNA (White et al., 1998). Different from Fur, DtxR requires two Fe²⁺ ions per monomer. Thorough research in corynebacteria demonstrated that this regulator controls more than 50 targets and most of them are also involved in the repression of iron acquisition genes encompassing iron uptake and siderophore biosynthesis as well as iron utilization (Brune et al., 2006; Kunkle and Schmitt, 2005; Wennerhold and Bott, 2006; Yellaboina et al., 2004). Further, DtxR directly activates genes encoding iron storage proteins like ferritin (*ftn*) or the starvation-induced DNA protection protein (*dps*) as well as the assembly of [Fe-S] cluster by controlling the *suf* operon (Wennerhold and Bott, 2006). Strikingly, DtxR was shown to regulate the expression of further transcriptional regulators. One example is the iron-starvation regulator RipA (repressor of iron proteins A). RipA represses non-essential iron-dependent gene expression, e.g. of genes coding for an aconitase or succinate dehydrogenase, to save resources at iron-limited conditions (Wennerhold et al., 2005). Nevertheless, DtxR does not only repress iron-related, but also heme-related genes like the heme importer *hmuTUV* or the heme oxygenase *hmuO* (Bibb et al., 2007; Brune et al., 2006; Kunkle and Schmitt, 2003; Wennerhold and Bott, 2006). This further matches the observation that DtxR of *C. glutamicum* regulates the expression of the heme-responsive transcriptional response regulator HrrA belonging to the corynebacterial two-component system HrrSA (Wennerhold and Bott, 2006), which will be further described throughout section 2.3.2.1. Interestingly, this regulation of *hrrA* was not identified for DtxR in *C. diphtheriae* (Bibb et al., 2007).

2.3.2 Heme-responsive control of gene expression

Throughout the domains of life, the multifaceted molecule heme has led to the evolution of diverse regulatory systems. There are two types of heme sensor systems: Heme can either be sensed directly, or it can act as sensor of gases such as O₂, CO or NO (Girvan and Munro, 2013). However, within this study, we will focus on the former type. These heme sensor systems act as transcriptional regulators and are involved in diverse issues, like the circadian rhythm (e.g. mammalian NPAS2 (Dioum et al., 2002)), demethylases (e.g. yeast Gis1 (Lal et al., 2018)) or also glucose metabolism (e.g. mammalian Rev-erb α (Yin et al., 2007)). In addition, several systems are engaged in the control of heme homeostasis via various mechanisms (Krüger et al., 2022), some of which will be described in further detail in the following sections.

The evolution of complex and sophisticated regulatory systems sensing heme is not only influenced by the environment, but further by the overall chemical versatility of this molecule, especially due to the

highly hydrophobic and poorly soluble character in the physiological cellular context. Apart from heme bound irreversibly as prosthetic group to proteins, there is potentially free heme, which was newly synthesized or released from hemoproteins. Strikingly, excess free heme only exists transiently as it rather tends to bind fast and non-specifically to lipids, proteins or further macromolecules within the cell imposing a respective cytotoxicity (Chiabrando et al., 2014). Heme, which is accessible and transiently binds to proteins, is referred to as exchangeable heme. The term 'regulatory heme' was adopted in many research fields for the pool of respective free and exchangeable heme portions, which is accessible for heme sensor systems regulating e.g. heme homeostasis (Gallio et al., 2021; Granick et al., 1975; Shimizu et al., 2019). Regulatory heme binds transiently to heme-sensing regulatory proteins for situation-dependent responses with micromolar affinities, allowing a rapid reaction to environmental fluctuations. Although the transient binding mode of heme by regulatory proteins largely remains to be further elucidated, some heme-regulatory motifs (HRMs) have been identified. The most prominent HRMs among those known are CP(cysteine-proline)-motifs, with a cysteine residue acting as direct ligand of the heme-iron, and the proline supporting the coordination by incorporating bends in mainly alpha helices and avoid formation of hydrogen bonds (Kühl et al., 2011; Lathrop and Timko, 1993; Li et al., 2011). However, there are further non-CP-motifs for heme binding, which are quite diverse. Early studies already demonstrated that especially histidine residues are frequently involved in heme binding (Dawson et al., 1982). Nevertheless, structural information and biochemical data are still missing for both CP- and non-CP-motifs, illustrating a yet remaining blind spot for our understanding of transient heme-protein interactions (Krüger et al., 2022). Although specific sequence features were identified that positively influence heme binding like a hydrophobic binding pocket or a positive net charge (Wißbrock et al., 2019), experimental data is inevitably necessary for further verification. This is due to the fact that actual heme binding affinities are strongly influenced by the individual configuration of further surrounding amino acids, providing a strong individual diversity among HRMs and corresponding binding affinities (Krüger et al., 2022; Kühl et al., 2013; Schubert et al., 2015; Wißbrock et al., 2019).

Upon heme sensing in diverse modalities, heme-responsive sensor systems provide the regulation of adequate heme homeostasis at different levels shaped by the respective environmental niche. Across the domains of life, there is a high variability of strategies for heme homeostasis, while the most prominent ones are (i) the control of heme biosynthesis genes, (ii) heme sequestration by heme binding proteins or by conversion into a nontoxic form, (iii) regulation of heme import, (iv) heme degradation, or (v) direct export of heme or its toxic degradation products (Anzaldi and Skaar, 2010; Choby and Skaar, 2016). Within the review 'The diversity of heme sensor systems – heme-responsive transcriptional regulation mediated by transient heme protein interactions', a comparative overview covering eukaryotic and prokaryotic heme sensor systems regulating heme homeostasis-related genes

is provided (Krüger et al., 2022). Comparison across the domains of life underlined the different strategies, mechanisms and functions of heme sensing systems, but also revealed a common logic of the underlying networks, e.g. comparing Gram-negative and -positives. While in Gram-negative bacteria extracytoplasmic function (ECF) σ -factors based systems are the predominant form of heme sensing, Gram-positives mostly employ two-component systems. In general, these two signal-transduction mechanisms are widely distributed in bacteria and often even merge (Marcos-Torres et al., 2022; Staroń et al., 2009). However, this distinct separation of heme-responsive mechanisms according to the Gram-status might have evolved based on the respective habitat facing different challenges and/or cell wall composition.

As example, the heme assimilation (Has) system is responsible for heme acquisition and utilization in *Pseudomonas* (Dent and Wilks, 2020) and *Serratia* (Biville et al., 2004) (Figure 2A). In general, σ -factors are subunits of the RNA-polymerase important for the initiation of transcription, while ECF σ -factors are specialized σ -factors that are associated with signal sensing pathways. At the cell surface, they are sequestered by their anti- σ -factors and released upon stimulus reception (Helmann, 2002; Staroń et al., 2009). Within the Has system of *Pseudomonas aeruginosa*, HasI represents the ECF σ -factor and HasS the anti- σ -factor. For activation of this system, the hemophore HasA, which is a high-affinity heme-binding protein that scavenges heme from the environment, binds to the membrane receptor HasR, which imports heme to the periplasm in a TonB-dependent manner. Consequently, the N-terminal plug domain of HasR interacts with HasS leading to its inactivation and release of HasI. HasI recruits the core RNA polymerase to regulate the transcriptional activation of the *hasRA* operon for further heme acquisition (Dent et al., 2019; Dent and Wilks, 2020; Ochsner et al., 2000). A similar mechanism is also found for the ECF σ -factor Rhul and the untypical activating anti- σ -factor RhuR controlling heme acquisition in Burkholderiales (Murphy et al., 2002). Conservation of ECF σ -factor-based heme homeostasis regulation in Gram-negative bacteria is further confirmed by the data platform 'ECF Hub', where all known heme-responsive ECF σ -factors belong to Gram-negatives (Casas-Pastor et al., 2021).

Regarding Gram-positive bacteria, heme-responsive two-component signaling is thoroughly described for *Bacillales* (Figure 2B) and *Corynebacteriaceae* (Frunzke et al., 2011; Schmitt, 1999; Stauff and Skaar, 2009b). In *Bacillales* like *Staphylococcus aureus* or *Bacillus anthracis*, the two-component system (TCS) HssRS is required for the regulation of detoxification from heme by heme export. This encompasses HssS as sensor histidine kinase and HssR as response regulator activating the expression of *hrtBA* encoding a heme exporter (Stauff and Skaar, 2009a, b). As heme-responsive two-component systems (TCSs) will be a focus of this work, but with emphasizes to the biotechnologically relevant *Corynebacterium glutamicum*, the basics of TCSs will be introduced throughout the following section.

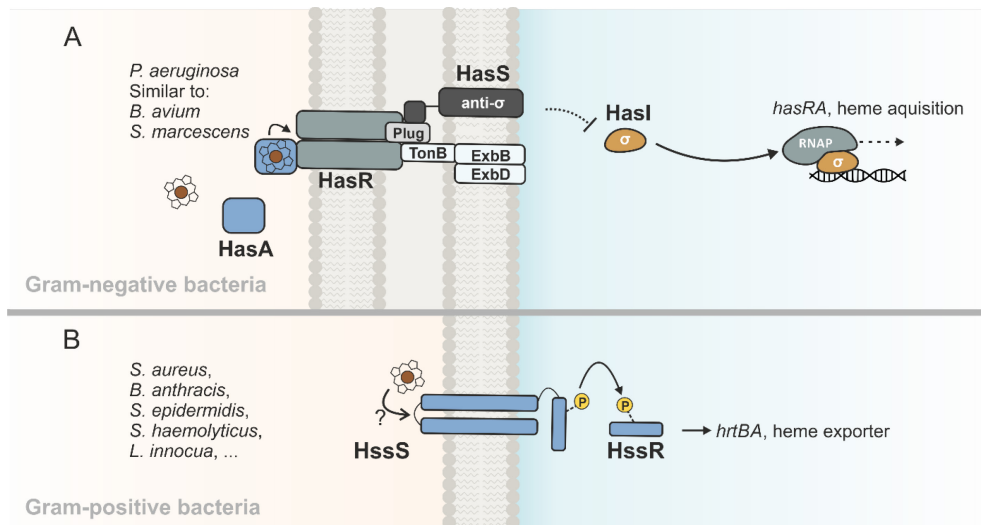


Figure 2: Prokaryotic heme sensor systems controlled by transient heme binding. Schematic overview of prokaryotic heme sensor systems using the examples of Gram-negative *Pseudomonadales* and Gram-positive *Bacillales*. (A) In *Pseudomonas aeruginosa*, the Has system responds to the presence of heme for the regulation of its acquisition. The system consists of the outer membrane receptor HasR (grey) with a N-terminal plug domain (light grey), the membrane bound anti- σ -factor HasS (dark grey) shown with TonB-ExbBD (white) and the extracytoplasmic function (ECF) σ -factor HasI (yellow). HasR senses heme with the help of the hemophore HasA, transduces a signal to HasS, which releases HasI initiating transcription. Imported heme further activates PhuTUV for uptake into the cytoplasm, where heme is transported by the heme binding protein PhuS to the heme oxygenase HemO (not shown). (B) In *Bacillales*, the two-component system HssSR (blue) activates the expression its target in a heme-dependent manner. Upon sensing of heme, autophosphorylation (yellow circles) of the histidine kinase HssS allows phosphotransfer to the response regulator HssR for its activation. HssR then functions as a transcriptional regulator for the activation of the expression of *hrtBA* encoding a heme exporter. Adapted from Krüger et al. (2022).

2.3.2.1 Two-component systems: The pre-dominant form of heme-sensing in Gram-positive bacteria

Identified for manifold functions among various microorganisms, TCSs in general perceive and transduce environmental stimuli in order to generate an appropriate cellular response. This allows the regulation of diverse functions like e.g. cell metabolism, development, pathogenicity or chemotaxis in response to a diverse set of chemical or physical stimuli (Mascher et al., 2006; Stock et al., 2000). TCSs are widely distributed among bacteria and archaea, while seldomly found in eukaryotic systems and absent in the animal kingdom (Ortet et al., 2014). Canonical TCSs consist of a membrane bound histidine kinase (HK) and a cytoplasmic response regulator (RR), exemplary and schematically represented in Figure 3.

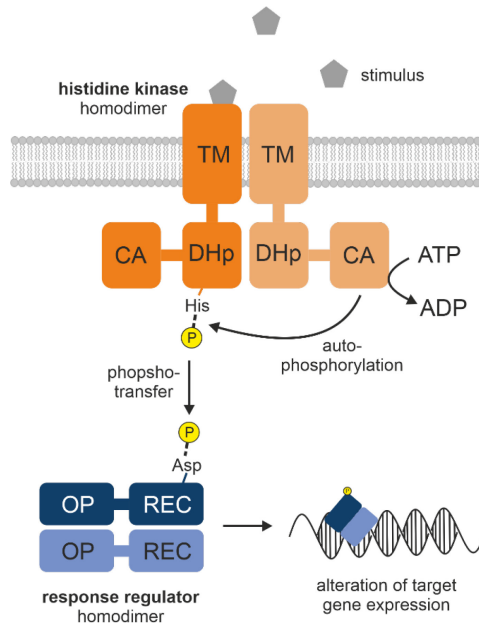


Figure 3: Canonical two-component signaling. This simplified schematic overview demonstrates a classical setup for a two-component system with a histidine kinase (shades of orange) and its cognate response regulator (shades of blue). The histidine kinase is depicted as a typical transmembrane homodimer version. Upon stimulus (grey) reception via the sensor domain of the transmembrane domain (TM), the conserved histidine residue located in the dimerization and histidine-phosphotransfer (DHp) domain is autophosphorylated mediated by the catalytic and ATPase (CA) domain. Thereafter, the phosphoryl group (yellow) is transferred to the conserved aspartate (Asp) present in the receiver (REC) domain of the response regulator. Phosphorylation typically triggers homodimerization and subsequent activation of the output (OP) domain, which initiates a physiological output, e.g. acting as transcriptional regulator by altering gene expression. Further outputs can be protein interactions, enzymatic activities or RNA binding (Galperin, 2006).

A prototypical HK acts as transmitter and may be composed of multiple domains comprising an N-terminal transmembrane domain and a C-terminal transmitter domain. The sensing domains in the N-terminal transmembrane (TM) domain are highly variable in sequence, which reflects the variability of the wide range of environmental cues that can be detected among TCSs (Krell et al., 2010). Examples of stimuli detected range from temperature changes (Albanesi et al., 2009), over gases (Kamps et al., 2004) to small molecules like heme (Keppel et al., 2018) (section 2.3.2.2). Sensing domains in HKs can be soluble, intramembrane or extracytoplasmic, with the latter being most abundant (Mascher et al., 2006). Many HKs feature additional C-terminal extensions between the TM domain and transmitter domain that act as support for signal transmission or aid at the integration of further signals (Galperin et al., 2001; Möglich et al., 2009; Parkinson, 2010). These elements are referred to as HAMP, PAS and GAF domains (Zschiedrich et al., 2016). The subsequent C-terminal transmitter domain becomes active caused by intramolecular changes in response to the stimulus reception of the sensor domain (Mascher et al., 2006; Wolanin et al., 2002). This transmitter domain is further divided in two sub-domains: (i) the dimerization and histidine phosphotransfer (DHp) domain followed by (ii) the

catalytical and ATPase (CA) domain (Dutta et al., 1999) (Figure 3). In general, the CA-domain executes binding of ATP in a pocket and transfers the γ -phosphoryl group to the conserved histidine residue in the DHp domain. For that, four common sequence motifs can be identified inside the CA-domain, i.e. N, G1, F, and G2 boxes (Parkinson and Kofoid, 1992; Wolanin et al., 2002). In detail, the F-box is required for binding to ATP, while the G-boxes build an ATP lid and the N-box builds a pocket, where the phosphate is finally shuttled to the histidine. The histidine residue, which is thereby autophosphorylated upon stimulus reception, is present in the H box motif within the DHp-domain (Dutta et al., 1999). Additionally, the DHp-domain harbors an X box motif, which is required for dimerization. Strikingly, many HKs are bifunctional acting not only as kinase, but also as phosphatase for the RR (Laub and Goulian, 2007; Perego and Hoch, 1996). This is typically accomplished by conserved glutamine, asparagine or threonine residues in a conserved phosphatase motif, which are required for the formation of hydrogen bonds with a nucleophilic water molecule and the orientation for hydrolysis of the phosphoryl group (Huynh and Stewart, 2011). Such a switch of activities allows a rapid reaction to fluctuating environments.

To date, the majority (>60%) of identified HKs are membrane-associated and act as homodimers (Jacob-Dubuisson et al., 2018). However, along with research, further complex regulations by HKs are revealed. This includes for example heterodimeric HKs, like the HK RetS of *Pseudomonas aeruginosa* directly controlling the HK GacS by heterooligomerization (Francis et al., 2018; Goodman et al., 2009).

The input detected by HKs can subsequently be transmitted to the RR via phosphotransfer. A flexible linker sequence in between the DHp- and CA-domain of HKs presumably supports keeping the RR in place during the phosphotransfer reaction (Casino et al., 2009). Canonical RRs consists of two domains with (i) an N-terminal receiver domain (REC) connected to (ii) a C-terminal output domain (OP) (Figure 3). The REC domain contains a conserved aspartate residue that receives the phosphoryl group from the conserved histidine residue of the HK. In vitro studies demonstrated that RRs not only passively receive the phosphoryl group but actively take part in the catalysis (Lukat et al., 1992). Two acidic residues are present for Mg^{2+} ion binding, which is important for a coordinated phosphorylation, and a conserved lysine residue was described to be required for structural rearrangements upon phosphorylation, which activates the RR (Gao et al., 2007; Lukat et al., 1991; West and Stock, 2001).

For many RR, phosphorylation leads to homodimer or –multimer formation rendering the RR active (Boudes et al., 2014; Kou et al., 2018; Menon and Wang, 2011). However, some RR also undergo heterodimerization, like CheY in *E. coli* that complexes with the flagellar motor switch protein FliM (Lee et al., 2001). Dimerization results in the activation of the output domain. Similar to the sensory domain of HKs, there is a significant diversity of OP domains across different RRs adapted to different ways of regulations for respective signals. Based on the kind of response, RRs can be divided in five classes:

(i) DNA binding, (ii) RNA binding, (iii) enzymatically active, (iv) protein-binding or (v) single-domain (Zschiedrich et al., 2016). However, the majority of RRs act as DNA-binding transcription factors, binding to respective DNA-binding motifs and regulating target gene expression (Gao et al., 2007; Zschiedrich et al., 2016).

Throughout the numerous TCSs in microorganisms, several variations from the herein schematically depicted version of signal transduction can be found. This includes for example hybrid kinase variants, where transmitter and receiver modules are combined, i.e. the phosphoryl group is firstly transferred to an internal receiver domain. Such hybrid kinases are dominant in fungi (Defosse et al., 2015), but were also identified for some prokaryotic systems, like ShkA of *Caulobacter crescentus* for timing G1/S cell cycle transition (Dubey et al., 2020). Further, there are also examples of multiple HKs phosphorylating a single RR, or a single HK phosphorylating several RRs (Francis and Porter, 2019). For example, the five HKs KinA-E are involved in the phosphorylation of the RR Spo0A mediating the sporulation of *B. subtilis* (Jiang et al., 2000), thereby integrating different signals into one signaling cascade. By contrast, the HK CheA of *E. coli* phosphorylates both RRs CheY and CheB involved in chemotaxis (Li et al., 1995), yielding a multiple signal output. Another recently emerging field are pseudokinases, which are catalytically inactive variants of HKs acting as important signaling modulators by various mechanisms (Kung and Jura, 2019; Kwon et al., 2019; Mace and Murphy, 2021; Raju and Shaw, 2015), like e.g. the pseudokinase DivL in *Caulobacter crescentus* (Tsokos et al., 2011). Some of these pseudokinases inherit important roles involved in cellular signaling, like allosteric activation of other kinases, aiding in the assembly of complexes or as competitive inhibitors (Mace and Murphy, 2021), and will be discussed in detail within section 2.5.2.

2.3.2.2 Paralogous two-component systems ChrSA and HrrSA in *Corynebacterium glutamicum*

A special set-up of paralogous TCSs can be found across the family of *Corynebacteriaceae*, where actually two TCSs are responding to the same stimulus - heme. The interactions and regulons of the two TCSs ChrSA and HrrSA have been studied particularly in the pathogen *C. diphtheriae* (Bibb and Schmitt, 2010; Burgos and Schmitt, 2016; Schmitt, 1999) and in the closely related, biotechnologically-relevant soil bacterium *C. glutamicum* (Frunzke et al., 2011; Heyer et al., 2012), which is the focus of this study. Still, there are few exceptions of *Corynebacteriaceae*, which only possess one of those TCSs, with *C. efficiens* only harboring HrrSA and *C. jeikeium* only ChrSA (Bott and Brocker, 2012).

Heme availability is sensed by the HKs ChrS and HrrS via direct intramembrane interactions (Ito et al., 2009; Keppel et al., 2018) and the signal is transmitted to the respective RRs ChrA and HrrA. These two paralogous TCSs are responsible for maintenance of heme homeostasis by integrating various aspects. In *C. glutamicum*, ChrSA is mainly responsible for the detoxification from heme, while HrrSA globally

regulates heme homeostasis (Figure 4). Upon stimulus reception, ChrSA activates the *hrtBA* operon encoding the heme export system (Heyer et al., 2012). While only suggested and indirectly shown for a long period, recent studies were able to demonstrate that heme is actively exported by the HrtBA exporter in *C. diphtheriae* (Nakamura et al., 2022), therefore abandoning toxic levels by direct outward transfer. This transfer is described to be accomplished by two HrtA ATPase- and two HrtB permease-subunits, where dimerization of HrtA squeezes the heme-binding site to foster the release of the heme molecule.

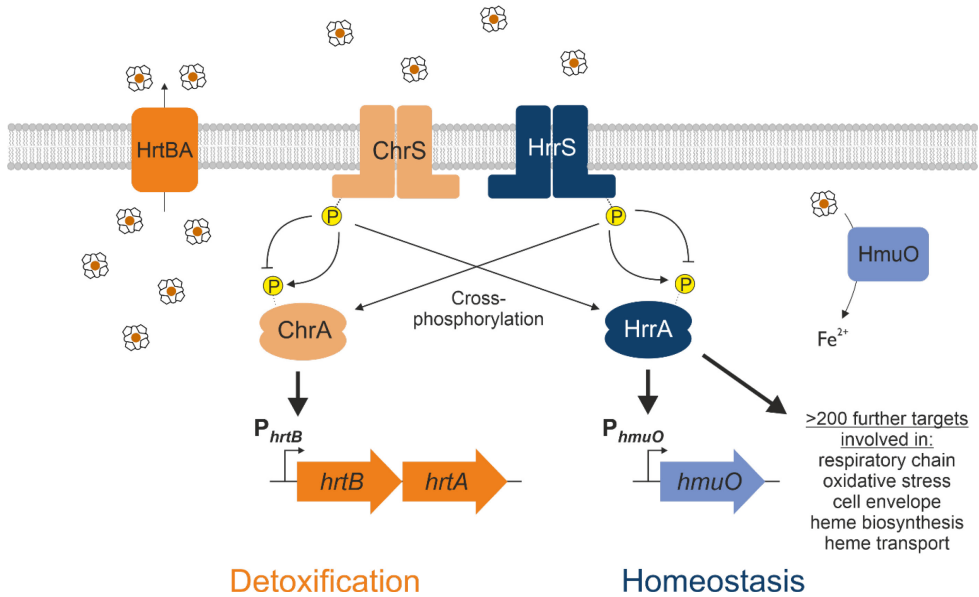


Figure 4: Heme-responsive two-component systems ChrSA and HrrSA in *Corynebacterium glutamicum*. The simplified representation shows the interaction of the two paralogous TCSs ChrSA (orange) and HrrSA (blue) and each a representative genetic target. ChrSA regulates detoxification from heme by activation of *hrtBA* expression (Heyer et al., 2012). HrrSA was shown, in context of this thesis, to act as regulator for heme homeostasis, controlling heme oxygenase *hmuO* as well as more than 200 further genes involved in heme biosynthesis, respiratory chain, oxidative stress or cell envelope remodeling (Keppel et al., 2020). The HKs undergo autophosphorylation in response to heme, activating the respective RR. Cross-phosphorylation of the non-cognate response regulator has been demonstrated, while the phosphatase activity remains specific for the respective cognate response regulator (Hentschel et al., 2014). Figure adapted from Krüger and Frunzke (2022).

The export of heme is a conserved strategy among several pathogenic and non-pathogenic bacteria counteracting cytotoxic free heme levels (Bibb and Schmitt, 2010; Fernandez et al., 2010; Heyer et al., 2012; Krüger et al., 2022; Stauff and Skaar, 2009a) and was even described in human cells (Quigley et al., 2004). Particularly, *in silico* analysis demonstrated that the heme regulated ABC transporter HrtBA is a highly conserved TCS-regulated target among Firmicutes and Actinobacteria. Orthologues of the exporter were found in 3,232 of 39,096 analyzed bacterial genomes with 99% belonging to one of these phyla (Krüger et al., 2022). As depicted in literature, HrtBA of Firmicutes is mainly under the control of the TCS HssRS or homologs, as shown for *Staphylococcus aureus* or *Bacillus anthracis* (Stauff

and Skaar, 2009a; Torres et al., 2007) (Figure 2B). By contrast, actinobacterial TCSs rely on ChrSA or homologs for the control of *hrtBA*, like shown for corynebacterial species (Bibb and Schmitt, 2010; Heyer et al., 2012). This distribution became even more evident when inspecting 5 kb up- and downstream of the identified *hrtBA* orthologues, where the respective TCSs are encoded in close proximity. Here, heme-responsive HssRS-like TCSs were present in more than 40% of the loci in Firmicutes, and even more than 50% with ChrSA-like TCSs in actinobacterial genomes (Krüger et al., 2022).

Apart from autoregulation, *hrtBA* is suggested to be the only target of ChrA regulation (Heyer et al., 2012). While the activity of ChrSA activating *hrtBA* expression is quite specific, HrrSA is controlling several aspects of heme homeostasis. This global regulator was shown to regulate the expression of more than 200 genomic targets including genes involved in heme biosynthesis, cell respiration, and oxidative stress, among others (section 2.4.2) (Keppel et al., 2020).

A high level of cross-phosphorylation between the two paralogous system has been observed (Hentschel et al., 2014). Consequently, within the corynebacterial heme-responsive TCSs, loss of one HK can be compensated by the other via cross-phosphorylation of the non-cognate RR (Keppel et al., 2019). Importantly, unwanted activation of the RRs was shown to be prevented by the specific phosphatase activity. Both RRs, ChrA and HrrA, are only dephosphorylated by their cognate HK (Hentschel et al., 2014).

2.4 Genome-wide binding profiles of iron and heme regulatory networks in *C. glutamicum*

As depicted, diverse transcription factors play an essential role in the complex iron and heme metabolism of bacteria. In *Corynebacterium glutamicum*, the key players for iron and heme homeostasis include the above-portrayed master regulator of iron DtxR and the global heme regulator HrrA of the TCS HrrSA. Although previous biochemical and genetic studies already gave valuable insights about binding of DtxR and HrrA to several targets (Brune et al., 2006; Frunzke et al., 2011; Wennerhold and Bott, 2006), these data rely on in vitro experiments under defined conditions. However, combining in vitro data with further in vivo studies provides the unprecedented opportunity for more detailed and complex insights into promoter occupancies in the cellular context. Additionally, merging regulatory patterns of these two pathways with strongly interconnected stimuli can emerge into a big regulatory picture of positive and negative interferences. Therefore, within this study we performed chromatin affinity purification coupled to sequencing (ChAP-Seq) experiments to reveal the global genome-wide binding profile of both DtxR and HrrA in *C. glutamicum* (Keppel et al., 2020; Krüger et al., to be submitted).

ChAP-Seq is an alternative method to the frequently used chromatin immunoprecipitation (ChIP)-Seq procedure (Myers et al., 2015). Within this method, protein and DNA is cross-linked, followed by employing an antibody specific for the DNA-binding protein for purification and consequent identification of enriched genomic loci of binding. Firstly developed by Gilmour and Lis, the ChIP technique was already used in the 1980s for studying RNA polymerase II binding in the genome of *E. coli* and *Drosophila melanogaster* (Gilmour and Lis, 1984, 1985, 1986). Further improvement of fixation methods using formaldehyde for protein-DNA cross-linking led to this sophisticated method as it is used and adapted today (Solomon et al., 1988). Many studies utilize this rapidly and steadily evolving technique across all fields and kingdoms. Among numerous further examples, in mammalian cells ChIP-seq was employed to study the circadian control of transcription (Takahashi et al., 2015), cancer-related factors like NF- κ B (Lu et al., 2013) or even circular RNAs (Liang et al., 2022). A prominent pathogenic bacterial example is the study on the combination of the binding profiles of 50 different transcription factors in *Mycobacterium tuberculosis* (Galagan et al., 2013b; Minch et al., 2015). Within this vast study, a direct relation between hypoxic response, lipid catabolism and anabolism, as well as cell wall lipid production could be drawn. This knowledge provided important insights into the mechanisms underlying different aspects of pathogenesis and yet poorly understood persistence of *M. tuberculosis* inside the host. Moreover, recent studies established automated ChIP-Seq protocols for supporting such high-throughput analyses (Dainese et al., 2020; Gasper et al., 2014; Wu et al., 2012).

Within this thesis, ChAP-Seq instead of ChIP-Seq was employed. Former ChIP-Seq approaches for DtxR were not successful as it permitted only low yields paired with excessive background signals after purification. Instead of using an antibody for immunoprecipitation, the herein applied ChAP-Seq experiment utilizes a tagged variant of the regulatory protein of interest for purification. In the context of this study, we performed a genome-wide condition-dependent binding analysis of both DtxR and HrrA (Krüger et al., to be submitted) as well as a time-resolved binding analysis for HrrA (Keppel et al., 2020). Identification of novel yet unknown genetic targets expanded the current knowledge of these two transcriptional regulators, while an ultimate aim of these studies was a direct comparison of their binding profiles to add dynamic network information based on their interaction and interferences with each other, as summarized in the following.

2.4.1 In vivo profiling of DtxR promoter occupancies

About 60 DtxR-regulated targets were identified for *C. glutamicum* via comparative transcriptome analyses in iron excess and limitation conditions as well as electrophoretic mobility shift assays (EMSAs) (Brune et al., 2006; Wennerhold and Bott, 2006). Our study aimed to enlarge this knowledge on an in vivo scale assessing DtxR binding patterns once in iron excess (100 μ M FeSO₄) and once iron-

scarcely in the presence of heme (4 μM hemin, further referred to as heme). Interestingly, an overall similar binding pattern was obtained from ChAP-seq analysis for growth on both conditions (Figure 5A). This reflects the efficient and well-balanced iron and heme homeostatic processes in *C. glutamicum* that stabilize the intracellular pool of chelatable Fe^{2+} and heme. In iron-starved, but heme rich conditions, heme is efficiently used as alternative iron source via heme oxygenase HmuO (Wilks and Schmitt, 1998). Analogously, at conditions of sufficient iron supply, the high amounts of iron present lead to proper heme synthesis (Frunzke et al., 2011; Layer, 2021). Nevertheless, calculated Pearson correlations clearly showed slight but substantial differences between the binding patterns at the two growth conditions that allowed determination of several yet unidentified targets and relations.

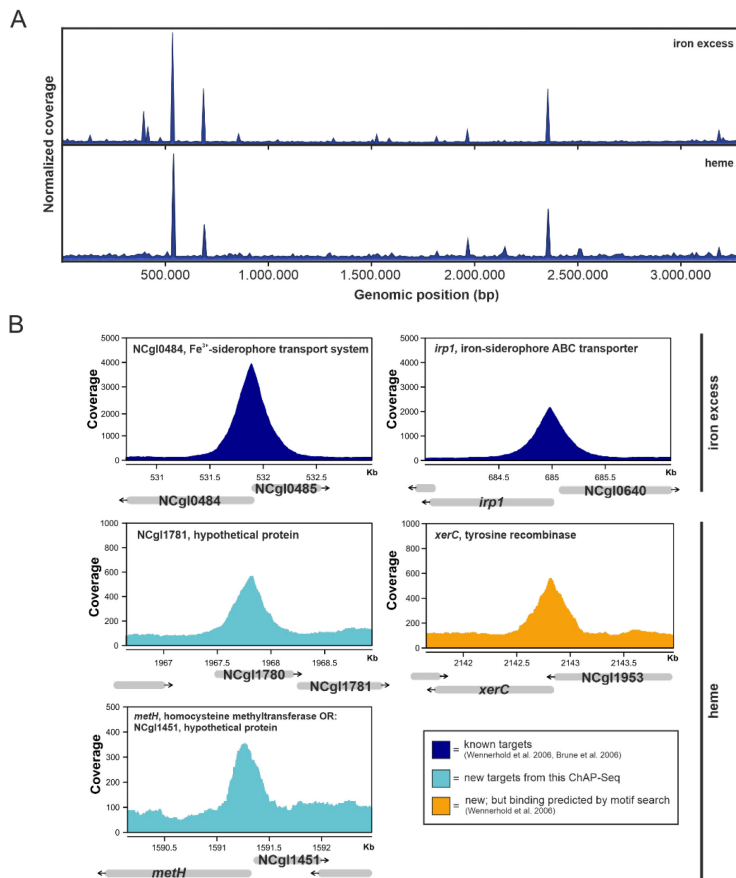


Figure 5: Genome-wide profiling of DtxR DNA-binding in *C. glutamicum*. (A) Representative mapping of ChAP-seq reads to the whole *C. glutamicum* ATCC 13032 genome. DNA was obtained by affinity purification of DtxR from cultures grown under iron excess (100 μM FeSO_4) (top) or in the presence of heme (4 μM) (bottom). (B) Coverage of binding peaks plotted against the respective genomic region as indicated by grey arrows below. Among the peaks are known targets (dark blue; (Brune et al., 2006; Wennerhold and Bott, 2006)), novel targets identified within this study (light blue) and targets predicted by previous studies (orange). Shown is one representative peak of three biological replicates. Upper graphs were taken as identified from iron excess condition, while all of them were also found in the heme condition. Peak graphs below are peaks identified in the heme condition. Except for NCgl1781, these peaks were only found in heme condition. Adapted from Krüger et al. (to be submitted).

Of overall 45 identified peaks across the conditions, 21 genomic target locations were already previously known, while further 24 novel targets of diverse functions could be determined within this study. Regarding these new targets, approximately two-third were found in the heme condition, which has not yet been investigated before, indicating the importance of environmental influences for revealing regulatory systems (section 2.4.4.2). Selected identified binding peaks of DtxR can be found in Figure 5B and are briefly discussed in the following.

In particular, the siderophore transporters NCgl0484 and *irp1* were recognized as most prominent targets in both iron and heme conditions. Siderophores are iron-chelating molecules, that organisms produce in response to iron-scarce environments (Ahmed and Holmström, 2014; Sheldon and Heinrichs, 2015). After sequestration of iron, siderophores are transported into the cell and iron is released either by reduction of iron or by hydrolysis of the siderophore. *C. diphtheriae* produces the endogenous siderophore called corynebactin for iron scavenging from the host (Russell et al., 1984; Zajdowicz et al., 2012). First, this corynebactin was also identified in *C. glutamicum* (Budzikiewicz et al., 1997), but a decade later it was proven to be mistakenly interchanged with the siderophore bacillibactin from *Bacillus subtilis* (Dertz et al., 2006), i.e. *C. glutamicum* does not produce siderophores on its own. The lack of the own siderophore production clusters might be an environmental adaptation of this soil bacterium in comparison to its pathogenic relative. Suggested by the presence of several siderophore transporter genes (Ikeda and Nakagawa, 2003; Kalinowski et al., 2003), it potentially has been an evolutionary advantage in the environmental niche of *C. glutamicum* to rather rely on the uptake of xenosiderophores, thereby saving production costs. The expression of several of these operons was previously shown to be tightly regulated by the iron availability (Brune et al., 2006; Wennerhold and Bott, 2006), allowing energy-efficient usage when required.

Focusing on novel targets, Figure 5B also represents the binding peaks in the promoter region of three selected newly identified targets: NCgl1781, *xerC* and *methH*. A quite intense peak for binding of DtxR is given for NCgl1781 in both iron excess and heme condition. Although being a hypothetical protein, it is known that NCgl1781 is located in the prophage region of CGP4. *C. glutamicum* ATCC 13032 contains in total four prophage elements (CGP1-4). Among those, CGP3 is by far the largest one, while it contains CGP4. CGP3 is the only inducible prophage, i.e. it can excise from the genome and autonomously replicate inside the cell (Frunzke et al., 2008; Nanda et al., 2014; Pfeifer et al., 2016). An RNA-seq workflow determined an increased cellular SOS response induction upon increased iron levels (Freiherr von Boeselager et al., 2018), which is associated with CGP3 induction (Helfrich et al., 2015; Nanda et al., 2014). This might be triggered by iron itself or by the resulting oxidative stress. Although a *ΔdtxR* mutant demonstrated an overall higher rate of CGP3 induction (Frunzke et al., 2008), the possibility of a direct influence of DtxR on prophages genes remains to be elucidated. Additionally, the function of many prophage genes remains unknown, like for the hypothetical protein NCgl1781.

Another novel DtxR-regulated target is represented by the tyrosine recombinase encoding gene *xerC*. This target was previously suggested by motif prediction, but in vitro binding could not yet be verified (Wennerhold and Bott, 2006). However, in these ChAP-seq experiments, a clear peak was observed, but only for the heme condition. Tyrosine recombinases in general are responsible for site-specific DNA recombination to result in a variety of genetic rearrangements like integration, excision or inversion. (Grindley et al., 2006). In *E. coli*, XerC as well as XerD recombinase aid at proper plasmid and chromosome segregation during cell division by converting dimers of its bacterial chromosome to monomers, working together with the DNA-translocase FtsK protein (Aussel et al., 2002; Blakely et al., 1991). Remarkably, these Xer proteins are highly conserved in many bacteria, including *C. glutamicum*. Although XerC from *E. coli* and *C. glutamicum* share only ~30% sequence identity and ~50% similarity on the protein level (global alignment (Needleman-Wunsch)), it might have a similar function during cell division. However, the functional DtxR-homolog Fur was not described to regulate *xerC* in *E. coli* (Seo et al., 2014). Experimental data on *xerC* of *C. glutamicum* in its general function as well as on its regulation by DtxR should be further addressed, especially in terms of expression data in the presence of heme. This would allow to evaluate a potential connection between iron homeostasis and recombination control in *C. glutamicum*, e.g. for rapid repair of redox stress damage or, by contrast, to halt recombination events at specific lower iron levels.

The present ChAP-seq study additionally established a binding site of DtxR in the promoter region of *metH* encoding a homocysteine methyltransferase. In *C. glutamicum*, methionine is generated from homoserine, while MetH and MetE catalyze the last step by methylation of homocysteine (Rückert et al., 2003). Unlike earlier steps of the methionine synthesis, the last step utilizing both MetH and MetE is conserved among several further bacterial species, like *E. coli* (Thanbichler et al., 1999) or *Pseudomonas putida* (Alaminos and Ramos, 2001). Although the methionine and cysteine biosynthesis repressor (McbR) was shown to control *metY*, *metK* and *hom* of methionine biosynthesis in *C. glutamicum*, the expression of other numerous genes thereof are not influenced by this regulator, including *metH* (Rey et al., 2003). In *C. diphtheriae*, DtxR was already predicted to contribute to methionine synthesis regulating the genes *metA* and *mapA* (Yellaboina et al., 2004). Further, comparable to our ChAP-seq results, the iron regulator Fur of *E. coli* binds to *metH* (Stojiljkovic et al., 1994). In general, methionine has the ability to act as antioxidant, as it has a high susceptibility to be oxidized to methionine sulfoxide (Levine et al., 1996; Slyshenkov et al., 2002), which is reduced back to methionine by methionine sulfoxide reductases (Brot and Weissbach, 1983). Such a process is likewise applied in Corynebacteria like *C. glutamicum* as well as *C. diphtheriae* utilizing the methionine sulfoxide reductase MsrA, which is regulated by the ECF σ -factor SigH (Si et al., 2015; Tossounian et al., 2015). Consequently, a regulatory connection between iron inducing ROS and methionine synthesis could be valuable for oxidative stress counteraction. Overall, in this context, DtxR can be suggested to

activate the expression of *metH* to promote methionine synthesis. Nevertheless, it is striking that the binding peak for *metH* can only be found in the heme-rich condition. When contrary assuming that DtxR represses *metH*, it can be hypothesized that repression is only accomplished when iron is scarce. At these conditions, methionine might not be required for counteracting low levels iron-related oxidative stress, saving energy. Growing under iron excess conditions, derepression of *metH* by DtxR might be required for additionally counteracting redox stress. This would include a concentration-dependent response as outlined in section 2.4.4.2, which might also be assumed for *xerC*. Broadening the view on methionine synthesis in eukaryotes, studies in endothelial cells examined that methionine additionally promotes the catalytical activity of heme oxygenase as well as ferritin. This supports suppression of free radical formation by acceleration of the heme degradation and subsequent sequestration process (Erdmann et al., 2005). Although further investigation is required to reveal the influence of DtxR on *metH* in *C. glutamicum*, its general regulation adds up on the knowledge about a strong interconnection between iron homeostasis and oxidative stress, as is already underlined by the fact that DtxR is only activated by Fe^{2+} and not Fe^{3+} (Spiering et al., 2003). Note that this binding peak could also reveal regulation of the gene expression for the hypothetical protein NCgl1451.

Finally, these vague theories on several newly identified targets of DtxR demonstrate the need for future expression and binding studies, which should be related to the herein presented ChAP-Seq results. These studies potentially expand the DtxR regulon for further functions regarding prophages, DNA recombination and methionine synthesis connected to oxidative stress.

2.4.2 In vivo profiling of HrrA promoter occupancies

Conditional ChAP-Seq for DtxR binding demonstrated inter alia the efficiency of iron and heme homeostatic processes in *C. glutamicum*. This can only be achieved in collaboration with further heme regulation factors. As depicted in earlier sections, heme homeostasis in *C. glutamicum* is achieved by the TCSs ChrSA and HrrSA (section 2.3.2.2). While ChrSA is suggested to play a rather defined regulatory role focused on heme detoxification (Heyer et al., 2012), HrrSA was shown to act as a global regulator (Frunzke et al., 2011; Keppel et al., 2020).

Thus far, several genomic targets regulated by HrrA in *C. glutamicum* were confirmed, mostly coordinating genes involved in processes like heme utilization and synthesis (Frunzke et al., 2011). However, it is unlikely that this rather small number of targets reflects the whole complexity of heme, which influences various vital cellular processes. Within this study, a first in vivo analysis of the dynamic response of HrrA in the presence of heme extended our current awareness from approximately 30 to more than 200 different genomic targets (Keppel et al., 2020). Combining this time-resolved ChAP-Seq analysis with further comparative transcriptome analysis via RNA-Seq ($\Delta hrrA$ /wild type), HrrSA could be verified as a global player of a systemic response to the external addition of heme. This TCS

regulates genes encoding proteins of various functions, including e.g. heme biosynthesis, glucose uptake, cell envelope remodeling, oxidative stress response and respiratory chain regulation. The latter two are briefly summarized in the following.

Apart from ChrA cross-phosphorylation, the presented ChAP-Seq analysis confirmed also a direct role of HrrSA in coping with the toxic character of heme by activating genes of antioxidant enzymes, like *katA* encoding a catalase (Teramoto et al., 2013), *trxB* coding for a thioredoxin reductase or *mpx* for a mycothiol peroxidase (Si et al., 2015). Additionally, HrrA regulates *sigH* expression, which encodes an ECF σ -factor regulating several stress responses (Kim et al., 2005), including the above-mentioned methionine sulfoxide reductase MsrA (section 2.4.1) (Si et al., 2015). This provides a sophisticated and variable redox stress response regulated by HrrSA. Analogously, we could demonstrate that a $\Delta hrrA$ strain was more sensitive to hydrogen peroxide manifested in a growth defect. However, a further role of HrrA in context of coping with heme and resulting oxidative stress via counteraction of consequences was detected. For example, HrrA could be shown to regulate *gapA* and *gapB* encoding glyceraldehyde-3-phosphate dehydrogenases of glycolysis and gluconeogenesis. These enzymes were shown to be inhibited by oxidative stress in *C. diphtheriae* (Hillion et al., 2017). Activation of *gapA* by HrrA might counteract the impaired glycolysis in the presence of heme-induced oxidative stress thereby stabilizing metabolic flux under these conditions.

In particular, HrrA was identified to prominently bind in the promoter regions of genes involved in the respiratory chain, changing their expression significantly. In *C. glutamicum*, the electron transport chain is branched consisting of cytochrome *bc*₁-*aa*₃ supercomplex (*ctaD*, *ctaCF*, *ctaE-qcrCAB*) harboring six heme molecules and the cytochrome *bd* oxidase (*cydABCD*) with three heme molecules for their function (Bott and Niebisch, 2003). All of these genes were bound by HrrA, while the promoter regions around *ctaD* and *ctaE* even possessed inter alia the highest identified peak intensities. Besides, our comparative N,N,N',N'-tetramethyl-*p*-phenylenediamine (TMPD) oxidase assays confirmed the positive regulation of HrrA on cytochrome *aa*₃ oxidase activity. These findings enlarged the identified repertoire of respiratory chain genes controlled by HrrA upon heme availability. Interestingly, the ECF σ -factor encoded by *sigC*, which regulates the activation of the *cydABCD* operon (Toyoda and Inui, 2016), was found to be repressed by HrrA. This slight repression of *sigC* expression by HrrA in the presence of heme yields a delay in *cydAB* expression and consequently hints for HrrA aiding at prioritization of the more efficient cytochrome *bc*₁-*aa*₃ supercomplex.

After identification of numerous targets of HrrA from a time-resolved analysis, our following study aimed at promoter occupation analysis under heme and iron conditions (Krüger et al., to be submitted). Cultivation under the same conditions as in the ChAP-Seq for DtxR (section 2.4.1), these analyses laid the foundation to unravel interaction and interference between iron and heme regulatory

networks, as discussed in section 2.4.4.1. Regarding HrrA, conditional binding studies allowed identification of additional ~180 potential targets. These target genes vary in their function, while most encode hypothetical proteins. Overall 80 of these ~180 additional targets identified within this following study were only identified in the iron excess condition, i.e. cultivated without exogenous heme addition as performed in the former study (Keppel et al., 2020). Strikingly, this includes several bound regions of genes encoding ribosomal proteins (*rplJ*, *rplK*, *rplU*, *rpmB*, *rpmH*, *rpsF*, *rpsH*, *rpsL*). Genes coding for ribosomal proteins drive ribosome biogenesis and are regulated in response to fluctuating environments in order to adapt for rapid cell growth. Recently, ribosomal protein genes of yeast were also described to be regulated by transcription factors in response to nutrients and stress factors (Petibon et al., 2021; Zencir et al., 2020). Although analyzed in the presence of heme, comparative RNA-Seq data ($\Delta hrrA$ /wild type) suggested that these targets are rather repressed by HrrA. As this repression is more apparent in the iron excess condition, this hints towards a contribution to ribosome synthesis based on the concentration of the stimulus (section 2.4.4.2).

Moreover, among those new targets found at iron excess conditions, there are further genes of the central carbon metabolism, including e.g. *aceE* encoding the E1 subunit of pyruvate dehydrogenase, *pfkA* encoding the 6-phosphofructokinase or *pck* encoding the phosphoenolpyruvate carboxykinase. Studies in *S. aureus* claimed a yet unsolved interconnection between heme biosynthesis and central carbon metabolism as repression of steps of the upper glycolysis impaired heme production (Mike et al., 2013), probably due to redirection of flux.

Further novel binding targets of HrrA under iron excess condition include *rpoB* encoding the β subunit of a DNA-directed RNA polymerase, *ohr* encoding a putative organic hydroperoxide resistance and detoxification protein or the universal stress protein encoded by *uspA3*, further underlining the participation of HrrSA in oxidative stress response. These additionally identified targets show at least minor effects on the expression level upon deletion of *hrrA*, as depicted from comparative RNA-Seq results ($\Delta hrrA$ /wild type) performed at the heme condition. Nevertheless, further transcriptome analyses including the respective iron excess condition could give more detailed insights into the extent of the influence of HrrA on these newly identified targets concerning inter alia ribosome synthesis, central carbon metabolism and oxidative stress responses at the differing conditions.

Unravelling HrrA as a global regulator of heme homeostasis also revealed similarities to the regulon of the eukaryotic BTB and CNC homology 1 (BACH1) transcription factor. BACH1 is the mammalian key player for balancing heme content, by regulating the expression of heme oxygenase *HMOX1* as well as 50 further targets involved in iron storage, oxidative stress, apoptosis or subcellular transport (Warnatz et al., 2011). In general, BACH1 forms heterodimers with Maf proteins thereby acting as repressor for the respective downstream targets. Upon heme binding, BACH1 degrades and Maf proteins are able

to bind the transcription factor Nrf2 for the activation of several target genes (Ogawa et al., 2001) (further summarized by Krüger et al. (2022)). Although HrrA and BACH1 encompass completely different regulatory mechanisms, the similar regulatory logic is noteworthy. Both global heme sensing systems not only regulate the expression of their respective heme oxygenase, but also genes encoding antioxidant enzymes, i.e. catalases, thioredoxin reductases or mycothiol peroxidases, coupling heme utilization with oxidative stress response. Furthermore, both regulate several genes of the central carbon metabolism.

Finally, these analyses demonstrated HrrA to be a global regulator in *C. glutamicum* for manifold functions influenced by heme availability. By contrast, in *C. diphtheriae* a considerable overlap of HrrSA and ChrSA regulons was suggested instead of having HrrA as global and ChrA as narrow, specific regulator (Bibb et al., 2005; Bibb and Schmitt, 2010). Although in vivo data is not yet available in *C. diphtheriae*, it might hint for plasticity of TCSs signaling adapting to the respective ecological niche.

2.4.3 Relevance of weak binding sites in ChAP-Seq analyses

The profiling of genome-wide binding patterns of each DtxR and HrrA in *C. glutamicum* encompassed several peaks at both known and unknown target sites, which feature only weak peak intensities. Such weak binding sites are frequently found throughout ChIP/ChAP-Seq experiments (Cao et al., 2010; Rhee and Pugh, 2011). In order to address their physiological relevance, we correlated previously obtained comparative transcriptomic data, including microarrays (Wennerhold and Bott, 2006) and qPCR (Brune et al., 2006), with the underlying peak intensities obtained from this ChAP-Seq at iron excess conditions (Figure 6A). Clearly, an anti-proportional correlation of peak intensities with the differential gene expression ($\Delta dtxR$ /wild type) was observed. While the binding peaks with the highest coverage among selected targets are represented by *irp1* and *hmuO*, the differential expression levels comparing expression of wild type with a $\Delta dtxR$ strain were rather low. Analogously, the highest differential gene expression levels were found for NCgl0123 coding for a hypothetical protein and NCgl1646 encoding a putative secreted hydrolase in the prophage CGP3 region. Both targets showed only a low binding coverage. Remarkably, this observation concerning an anti-correlation between differential gene expression and peak binding intensity was also made for HrrA comparing ChAP-Seq binding peaks and RNA-Seq expression data ($\Delta hrrA$ /wild type) (Figure 6B). Here, this is clearly demonstrated by *subB* encoding a myo-inositol-1 or 4-monophosphatase in contrast to *hmuO* encoding a heme oxygenase.

Although many studies define weak binding sites as false-positives, the reproducibility or the presence of a respective binding motif argues against the exclusion of those as random artefacts (Galagan et al., 2013a; Rhee and Pugh, 2011). Consideration will, however, always require the inclusion of further, complementary analyses such as transcriptome data. Overall, the observed anti-correlation suggests

that targets bound with weaker binding peak intensity react more sensitive to environmental changes. Potentially, this is a result of varying binding strengths at these genomic locations or accessibility (Johnson et al., 2007; Myers et al., 2013) yielding a fine-tuned network, which is able to quickly integrate information about rapidly changing environments (Rhee and Pugh, 2011). For example, the weak binding to *ripA* encoding a regulator of iron-dependent proteins could enable a fast derepression by DtxR upon decreasing iron levels to ensure a subsequent rapid response by this regulator. Our study emphasized the physiological relevance of several weak binding sites in ChAP-Seq experiments, which should not be ignored.

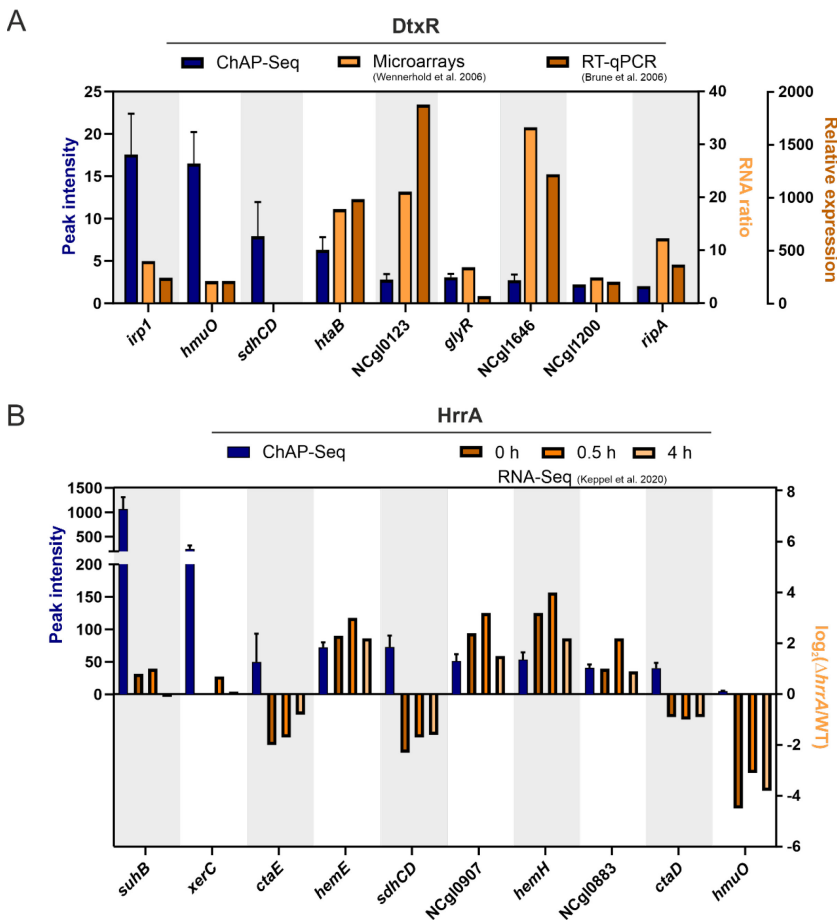


Figure 6: Correlation of DtxR and HrrA peak intensities with comparative expression data. (A) Correlation of peak intensities of the ChAP-Seq for DtxR (dark blue) with the RNA ratio ($\Delta dtxR$ /wild type) from a microarray analysis (dark orange; (Wennerhold and Bott, 2006)) as well as to the relative expression in the deletion strain $\Delta dtxR$ compared to wild type analyzed via RT-qPCR (light orange; (Brune et al., 2006)). All cultivations were conducted at iron excess conditions (100 μ M FeSO_4). (B) Correlation of selected peak intensities of the ChAP-Seq of HrrA (dark blue) was compared to the $\log_2(\Delta hrrA/\text{wild type})$ obtained from the time-resolved RNA-seq (Keppel et al., 2020) (shades of orange). Each cultivation was performed in the presence of heme (4 μ M). Adapted from Krüger et al. (to be submitted).

2.4.4 From static regulons to dynamic networks

Identification of regulatory targets of a specific transcriptional regulator at defined conditions brings undeniably valuable input. Nevertheless, cellular organisms are vibrant systems facing fluctuating environmental challenges, employing not only complex, but interdependent regulatory systems. Therefore, unveiling the complexity of regulatory networks requires the merging of static regulons to dynamic networks.

2.4.4.1 A glimpse into the connection of iron and heme regulatory pathways

Conducting ChAP-Seq analyses for both DtxR and HrrA at the same conditions allowed direct comparison of binding patterns for shared targets of these regulators for the first time *in vivo*. Regarding overlaps of these networks, in total 16 shared targets of DtxR and HrrA could be identified, while some targets hint for competitive and others for cooperative binding. A clear interconnection can be observed for DtxR and HrrA binding with a significant overlap upstream of *hmuO* encoding the heme oxygenase for degrading heme to iron, carbon monoxide and bilirubin (Figure 7A). While DtxR repressing *hmuO* demonstrated a slightly higher binding peak coverage at iron excess compared with heme, binding of HrrA for activation is higher at heme conditions. This could demonstrate a fine-tuning dependent on environmental conditions by these two regulators counteracting each other at different conditions. Not counteracting, but rather direct competition at the same conditions might be expected from DtxR and HrrA (auto)regulating *hrrA*, with no overlapping, but close binding peak sites (Figure 7B). For both regulators, the peak intensity is significantly higher in the presence of heme, while for DtxR there was even no identified peak at all in iron excess. This fine-tuning regulation rather illustrates a direct interference between the regulators.

By contrast, DtxR and HrrA are binding upstream to *sdhCD* encoding a succinate:menaquinone oxidoreductase, but binding sites are separated by ~100 bp (Figure 7C). In this case, there is again a higher peak intensity coverage on the specific stimulus, i.e. for DtxR on iron and for HrrA on heme. As this oxidoreductase is important for cell respiration and uses both iron and heme for functioning, this target is probably coordinatively activated by both DtxR and HrrA. Due to the location of binding, there is a potential, that e.g. HrrA also regulates nearby *ramB*, as several studies demonstrated that binding of transcription factors at large distances from promoters is also possible (Belitsky and Sonenshein, 1999; Czaplewski et al., 1992).

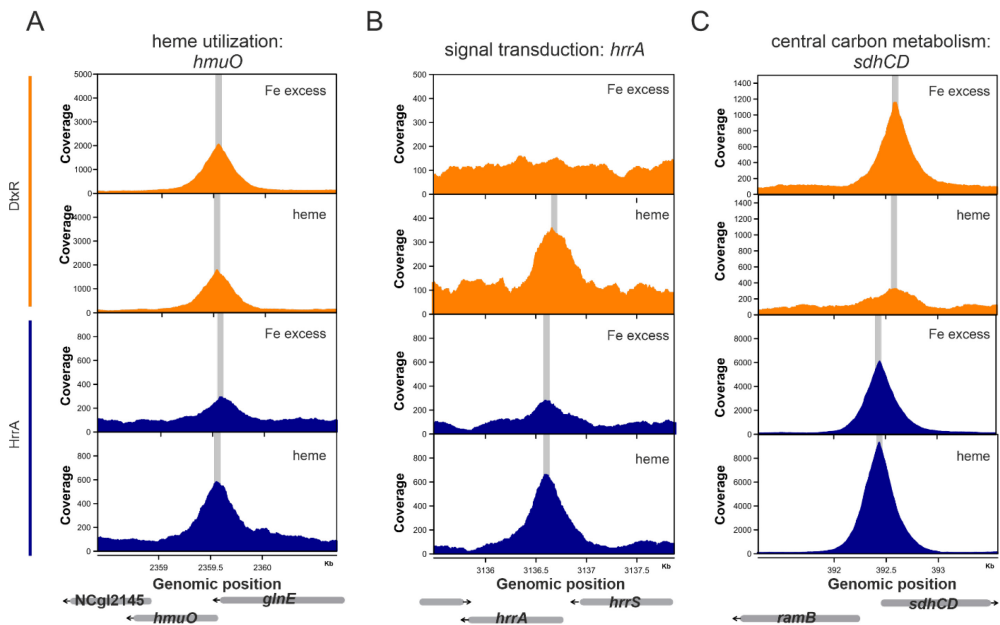


Figure 7: Shared targets of the transcriptional regulators DtxR and HrrA show interconnection between iron and heme regulatory networks. Peak detection in the region of (A) *hmuO*, (B) *hrrA* and (C) *sdhCD*, as represented by grey arrows below. Orange peaks show binding of DtxR, blue ones of HrrA. The grey vertical line illustrates the peak maxima. One representative peak of three biological replicates. For more detailed information, compare supplemental material 4.1, Figure S3. Adapted from Krüger et al. (to be submitted).

In the end, no conclusive trend that summarizes the regulatory connection of DtxR and HrrA at several promoter regions of shared targets can be extracted, demonstrating the complexity beyond potential interference of two global regulators. By analyzing the ratios of peak intensities of targets that were bound in both iron and heme conditions, we could derive hints for a trend towards higher peak intensities of DtxR binding in iron conditions than in the presence of heme and analogously for HrrA at heme conditions (compare supplemental section 4.1, Figure S4). Although this trend needs further examination, this might emphasize the stimulus-dependent interferences of these two regulators on each other. In order to profoundly evaluate the regulatory influences of DtxR and HrrA on each other, further ChAP-seq analyses with each a deletion strain of one of these regulators should be addressed coupled with expression analyses. In- or decreased binding of the remaining regulator and target expression changes would allow further detailed assessment. Recently, algorithms estimating coordinative regulator binding on ChIP-Seq peak intensities were published (Datta et al., 2018) that could add information.

Recent bioinformatic analyses established that the regulatory network in *C. glutamicum* is dependent on nine global regulators (*sigA*, *hrrA*, *ramA*, *glxR*, *sigH*, *ramB*, *atIR*, *mcbR* and *dtxR*). In the *all evidence* network (as identified by Abasy (Ibarra-Arellano et al., 2016)), HrrA is involved in the transcription of

21% of the regulatory nodes and DtxR for 3% (Escorcia-Rodríguez et al., 2021). In relation, this is in line with the count of overall targets identified in this study (relation percentage: $3/21 = 0.143$; relation targets: $45/334 = 0.135$ (Krüger et al., to be submitted)). ChAP-Seq analyses coupled to expression data of further global regulators demonstrate a possibility for revelation of basic regulatory network interactions in *C. glutamicum*, while for iron and heme regulatory networks an additional combined genome-wide binding analysis of RipA, ChrA or SigC would be of special interest.

2.4.4.2 Influence of surplus iron or heme on complex binding behavior

The presented ChAP-Seq experiments at different conditional and temporal conditions yielding slightly different binding patterns illustrated the importance of multiple growth conditions when evaluating the functionality of a transcription factor. This issue was already addressed in other studies, leading to identifications of novel mechanisms and especially connections to other regulatory pathways (Knijnenburg et al., 2007). Several (novel) genetic targets of the herein analyzed transcriptional regulators were found in the respective stimulus-scarce condition, e.g. DtxR only binds *metH* or *xerC* in the presence of heme, but not at iron excess. Subsequently, two hypotheses can be established.

The first would include a graded response of the transcriptional regulators dependent on the concentration of the stimulus. A prominent example is a recent ChIP-Seq analysis of the functional DtxR-homolog Fur in *Bacillus subtilis*, which could reveal a graded response based on varying protein-DNA-binding affinities, i.e. Fur derepresses its targets stepwise depending on iron concentrations. When iron concentrations change from replete to deficient, genes of iron uptake systems are derepressed at first, followed by derepression of genes for siderophore import systems as well as siderophore synthesis and finally, when iron is nearly depleted, the genes coding for the small RNA FsrA and respective cooperating proteins are derepressed to block the expression of non-essential iron-dependent proteins to save iron resources (Pi and Helmann, 2017, 2018). In order to assess the general possibility of such graded response of DtxR or HrrA, future studies should aim at ChAP-Seq experiments with further cultivation conditions, e.g. stepwise iron limitation or even starvation. Another option would be to perform reporter assays for several selected targets at different cultivation conditions. Nevertheless, evaluable prerequisites for a graded response are present for DtxR: Early studies claimed that a monomer of DtxR in *C. diphtheriae* has two-metal binding sites with varying affinities for iron. Binding of iron at the first site induces conformational changes that subsequently allow binding of another iron atom at the second binding site resulting in further conformation altering (Love et al., 2003; Spiering et al., 2003; Tao et al., 1994). Furthermore, it was suggested that for efficient repression by DtxR two dimers are required (Spiering et al., 2003; White et al., 1998). These variations in conformation depending on the amount of ions bound might lead to different binding affinities of the regulator, which potentially hints for a graded response. This strategy was also observed for other regulatory systems, like the zinc deprivation response by Zur in *B. subtilis* (Shin and

Helmann, 2016), providing a malleable tool for prioritization of cellular metal response. Several other variable modes for transcription factor DNA-binding had been summarized earlier (Siggers and Gordân, 2013).

Apart from that, a second explanation for the variation in genetic target binding at the different cultivation conditions can be found beyond a single transcription factor, but within interdependent regulatory networks including further factors. For example, a direct antagonizing activity of the DtxR homolog IdeR with the histone-like protein Lsr2 was demonstrated in *M. tuberculosis* for *bfrB* encoding an iron storage protein (Kurthkoti et al., 2015). Beyond that, whole interfering dynamic networks were also recognized from ChIP-Seq experiments in *E. coli* analyzing the global regulator of anaerobiosis FNR (Myers et al., 2013). Examination in both aerobic and anaerobic conditions led to varying binding patterns, while additionally, these different conditions influenced the FNR regulon concerning other transcription factors with condition-specific regulons. The authors claimed different categories of these interconnections, including e.g. co-activation of FNR by NarL and NarP in the presence of NO_3^- or NO_2^- or repression of FNR regulation by Fur in the presence of iron. Such combinatorial regulation by other transcription factors could also be of importance for unveiling the complexity of regulatory networks of DtxR and HrrA, besides interference on each other (section 2.4.4.1). Basically, not only other transcription factors but also e.g. nucleoid-associated proteins could mask DtxR or HrrA binding in vivo, resulting in variation of observed genetic targets at different conditions (Myers et al., 2013; Pfeifer et al., 2016).

In the end, shifting analyses from static regulons with a single defined condition, for a single regulator, at a single time point to a rather dynamic network analysis could give unprecedented insights into the complex and sophisticated regulatory setup of bacteria coping with their environment (Keppel et al., 2020; Krüger et al., to be submitted).

2.5 Evolution towards high heme tolerance

Coping with the environment is of particular importance for bacteria, which rely on the acquisition of iron from their surroundings. In general, the availability of free iron is rather low. For example, the iron reservoir for pathogenic bacteria acquirable from the vertebrate host is limited due to nutritional immunity, i.e. the host keeps iron sequestered making this nutrient inaccessible for the pathogen and thereby limiting bacterial replication (Bilitewski et al., 2017; Weinberg, 1974). On this purpose, heme represents the most abundant form of iron in adult humans (~ 70%) (Ponka, 1997), with an average of $21 \pm 2 \mu\text{M}$ free heme in human blood (Aich et al., 2015). Consequently, the usage of heme as alternative resource needs to be rapidly adapted, but further there is a special interest for adaptation to the elevated and toxic heme levels inside the host (Choby and Skaar, 2016). This issue is not only

encountered by pathogenic, but also by non-pathogenic species acquiring heme e.g. from soil, where decaying organic material results in local elevated heme levels. In framework of this thesis, it was aimed to investigate on the adaptation to elevated heme levels as encountered by many bacteria in fluctuating environments. For that, we made use of the soil bacterium *C. glutamicum* as model organism (Krüger and Frunzke, 2022), a close relative to the pathogenic species *C. diphtheriae*.

To evaluate and understand mechanisms of bacterial heme tolerance, we performed an adaptive laboratory evolution (ALE) experiment of *C. glutamicum* on increasing concentrations of heme. ALE is a frequently used strategy where the employment of a specific selection pressure leads to the generation of microbial strains with desired characteristics (Dragosits and Mattanovich, 2013; Mavrommati et al., 2022; Portnoy et al., 2011; Stella et al., 2019), based on the theory of biological evolution (Darwin, 1872). Depending on the experimental setup, ALE can improve process performance in terms of increased growth rates, higher product titers, or even stress and product tolerance (Stella et al., 2019). ALE strategies were efficiently applied to mutate strains towards the production of numerous products, e.g. amino acids (Har et al., 2021; Prell et al., 2021), ethanol (Catrileo et al., 2020) or lipids (Wang et al., 2021b); or to tolerate products like esters (Matson et al., 2022), antioxidants (Lu et al., 2022) or methanol (Wang et al., 2020) - to name only a few recent examples. In addition, ALE approaches bear the potential to provide novel insights into bacterial metabolism and biological pathway regulation. In the presented study, ALE on increasing heme levels evolved a highly heme tolerant strain, which had a mutation in the CA-domain of the HK ChrS (section 2.3.2.2). This mutation yielded a pseudokinase variant of ChrS that provokes a highly upregulated expression of the *hrtBA* operon encoding the heme export system HrtBA. This activation is mediated by the response regulator ChrA, but completely dependent from the paralogous HK HrrS (Krüger and Frunzke, 2022), as further described throughout the following sections.

2.5.1 Heme export by HrtBA plays a pivotal role for adaptation to elevated heme levels

Concentrations below 5 μM heme are not sufficient to meet the iron need of *C. glutamicum* cells as demonstrated by reduced growth rates. However, concentrations above 5 μM heme are toxic, which manifests especially in elongated lag phases (Frunzke et al., 2011). The previously described heme exporter HrtBA was established to be of special importance for heme detoxification, as a deletion of the *hrtBA* operon resulted in even significantly increased lag phase times during growth on high heme concentrations compared to the wild type (Heyer et al., 2012). Confirmation that HrtBA is a key player of heme tolerance was further accomplished with a comparative ALE experiment of the wild type and a $\Delta hrtBA$ strain on increasing concentrations of heme as described in this thesis. While for the wild type a stepwise increase from 10 μM to 60 μM heme over several inoculations could be achieved, a

strain lacking *hrtBA* was not able to evolve towards higher heme tolerance. This underlines the general importance of heme export in *C. glutamicum* for the adaptation to fluctuating heme concentrations.

Genome sequencing of the successfully evolved wild type strains revealed mutations affecting the CA-domain of the HK ChrS in every clone that allowed growth at heme concentrations of up to 100 μM . Analysis of the evolved populations after different time points indicated that the mutational adaptation to heme was accomplished already at inoculation in concentrations between 20 and 25 μM heme. Remarkably, the most advantageous mutation in the context of providing heme tolerance was a single nucleotide polymorphism inducing a frameshift directly after the DHp-domain (ChrS-Ala245fs). Interestingly, exactly this mutation was found in two independently evolved clones. This emphasizes this frameshift mutation as highly efficient in providing elevated heme tolerance to cells exposed to a strong selection pressure. Figure 8A exemplarily depicts the improved growth of the evolved clone carrying the frameshift mutation, further referred to as 1.fs. The respective strain was shown to outcompete the wild type under all tested conditions, except iron starvation conditions. As a result of the frameshift, the CA-domain is replaced by newly generated 60 amino acids (Figure 8B).

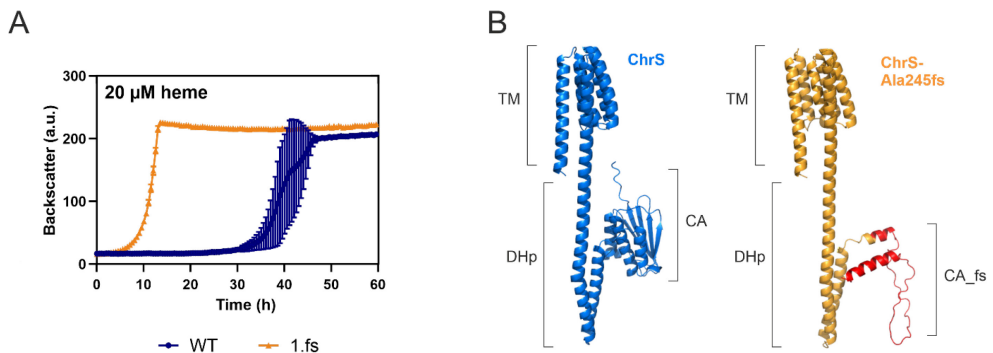


Figure 8: Adaptive laboratory evolution of *C. glutamicum* to high heme concentrations resulted in mutation of the CA-domain of ChrS. (A) Growth of the wild type (blue) in comparison to the evolved clone 1.fs (orange). Growth analyses were performed in the Biolector® microtiter cultivation system (Kensy et al., 2009) using CGXII media supplemented with 2% glucose, no iron and 20 μM heme. Data represents average of three biological replicates including standard deviations depicted as error bars. (B) Predicted protein structures of ChrS (blue) and the truncated ChrS-Ala245fs variant (orange, with 60 additional amino acids caused by the frameshift shown in red) as present in 1.fs. Structure prediction was performed using AlphaFold2 (Jumper et al., 2021; Varadi et al., 2021). Domain arrangements are shown next to the protein structures. TM = transmembrane domain, DHp = dimerization- and histidine-phosphotransfer-domain, CA = catalytic- and ATPase-domain. Adapted from Krüger and Frunzke (2022).

Subsequent mutational studies as well as reporter-assays on *hrtB* expression – the main target of ChrSA – provided insights into the mechanisms behind the elevated heme tolerance (Figure 9). Comparing the growth of 1.fs with the wild type and further mutant strains on increasing concentrations of heme demonstrated the enormous heme tolerance of this strain, while reintegration of the ChrS-Ala245fs

mutation confirmed the causality of the single frameshift mutation (Figure 9A). Consistent with the fact that the $\Delta hrtBA$ strain could not evolve any advantageous mutations in ALE experiments, the expression of *hrtBA* was highly elevated in the evolved wild type mutant strain, accounting for its heme tolerance (Figure 9B). Transcriptome analysis of the evolved variant revealed a ~ 150 -fold increase in *hrtBA* expression compared to a wild type strain and reporter assays (using pJC1- P_{hrtB} -*eyfp* from Heyer et al. (2012)) demonstrated a continuously high *hrtBA* expression in 1.fs, which is not shut down as usual after stimulus decline (Keppel et al., 2019). Interestingly, *hrtB* expression was also observed in 1.fs under standard conditions, i.e. without any exogenously added heme stimulus.

Deletion of the complete *chrS* gene also led to an improved growth on heme compared to the wild type (Figure 9A). This was enabled by the constant activation of *hrtBA* gene expression for heme export in this mutant, accomplished by cross-talk with HrrS as underlined by the denied growth of a $\Delta chrS \Delta hrrS$ strain (Figure 9B). The *hrtB* expression did not decline in $\Delta chrS$ due to the missing dephosphorylation of ChrA, which is only specifically achieved by ChrS. The significant delay in the *hrtB* signal in $\Delta chrS$ was caused by the lower heme sensitivity of HrrS. ChrS was demonstrated to be the fast-acting HK in order to prioritize detoxification for survival before regulating homeostasis by slower reacting HrrS (Keppel et al., 2019). Nevertheless, it is evident that the evolved clone 1.fs possesses a higher level of heme tolerance than $\Delta chrS$, encompassed by a significantly higher and faster *hrtB* expression. Regarding the continuous expression of *hrtB*, we further compared 1.fs to a phosphatase mutant *chrS*-Q191A, with a mutation of a glutamine residue at position 191 in the phosphatase motif DxxxQ located in the DHp-domain (Hentschel et al., 2014). This motif is conserved in several HKs of different bacteria (Huynh et al., 2010). However, the heme tolerance of 1.fs was significantly higher than that of the phosphatase strain, demonstrated in growth (Figure 9A). Although the extreme high levels of *hrtB* expression were comparable, the difference lies in the end signal: In both strains, *hrtB* expression was never shut off, but for 1.fs it remained at a higher final continuous level (Figure 9B). Therefore, the ChrS-Ala245fs variant, further referred to as ChrS_CA-fs, must play an important active role in elevated activation kinetics beyond only an abolished phosphatase activity.

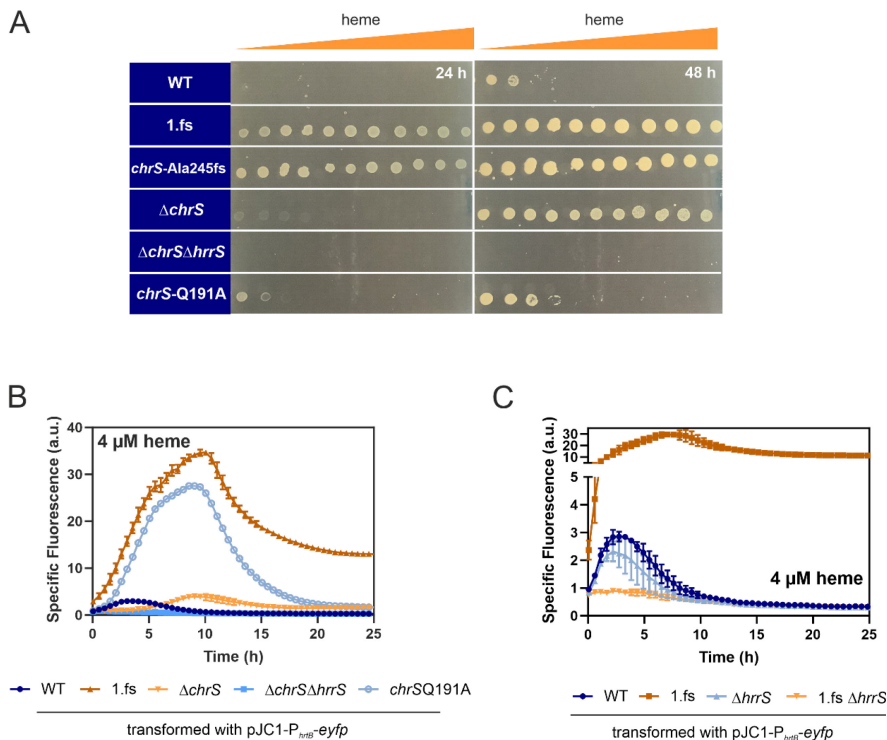


Figure 9: Mutational analyses to provide insights into improved heme tolerance of 1.fs. (A) Different mutant strains were spotted on heme gradient plates with elevating concentrations to the right (CGXII media, 2% glucose, no iron). Photos of plates were taken after 24 and 48 h. (B) Reporter assays visualizing *hrtBA*-expression using the plasmid pJC1-P_{*hrtB*}-*eyfp* for transformation of the wild type (WT) (dark blue), the evolved clone 1.fs (dark orange), Δ *chrS* (light orange), Δ *chrS* Δ *hrrS* (mid-blue), and *chrS*-Q191A (light blue). (C) Reporter assays for *hrtB*-expression using pJC1-P_{*hrtB*}-*eyfp* upon deletion of *hrrS* in 1.fs (shades of orange) and the wild type (shades of blue). Specific fluorescent analyses were performed in the Biolector® microtiter cultivation system (Kensy et al., 2009) using CGXII media supplemented with 2% glucose, no iron, 4 μ M heme and 25 μ g/ml kanamycin. Specific fluorescence was calculated as measured fluorescence per backscatter. Data represent average of three biological replicates including standard deviations depicted as error bars. Adapted from Krüger and Frunzke (2022).

As there is significant cross-talk between the paralogous HKs and their non-cognate RRs (Hentschel et al., 2014), *hrtBA* activation kinetics was further evaluated by examining the effect of an additional deletion of *hrrS* in the 1.fs background. Here, it became apparent that the extreme high *hrtB* expression is completely dependent from HrrS. When this paralogous HK is missing, the growth advantage on heme of 1.fs is abolished, which is also reflected by the shutdown of its *hrtB* expression (Figure 9C). Transcriptomic analyses examined that the expression of *hrrS* is not elevated in 1.fs, hinting for an increased ChrA activation performance by HrrS. Moreover, deletion of *chrA* had a drastic influence on heme tolerance of 1.fs, while deletion of *hrrA* did not. Analogously, an overexpression of ChrA did improve heme tolerance, but not comparable to the immensely improved growth of 1.fs, where ChrA must be rather phosphorylated more efficiently. Interestingly, a plasmid-based direct overexpression of *hrtBA*, which led to a ~400-fold increase in expression level, did not improve growth on heme, but

even worsens it compared to the wild type (compare supplemental section 4.3, Figures S5 and S6). Finally, all of these aspects underline a well-balanced expression kinetics achieved by mutated ChrS_CA-fs and native HrrS in the evolved heme tolerant 1.fs strain.

However, the observation that an exchange of the autophosphorylation residue at position 186 in ChrS_CA-fs did not affect the high heme tolerance of this strain suggests that this kinase does no more participate in the typical phosphotransfer reaction. Although autophosphorylation should be further addressed by phosphorylation assays in vitro, it can be proposed that ChrS_CA-fs does not serve a canonical role in catalysis in 1.fs. Kinases that are not catalytically active, but still perform important tasks in signal transduction, were classified as pseudokinases. Pseudokinases vary enormously in their mode of actions, as outlined in the following section.

2.5.2 The role of pseudokinases in signaling cascades

Referred to as dead or even zombie proteins, pseudokinases are detectable across all kingdoms of life. However, these special kinases are not simply dead evolutionary relicts, but rather play roles in signal transduction pathways beyond catalytical functions, e.g. serving as protein-interaction partners. While the first pseudokinase was already found in the late 80's in the sea urchin *Arabica punctulata* (Singh et al., 1988), there is emerging appreciation in recent research (Kwon et al., 2019; Mace and Murphy, 2021). In the human proteome approximately 10% of all protein kinases are pseudokinases (Manning et al., 2002). Canonical kinases require ATP binding, coordination of Mg^{2+} and catalysis of phosphoryl transfer for their kinase activity. Some or all of these functions might be lost in pseudokinases (Kwon et al., 2019; Murphy et al., 2014). However, the exact mechanism for the function of pseudokinases remains obscure in many cases. One factor is that e.g. some pseudokinases with highly degraded catalytic components are catalytically inactive, but act as protein-interaction partners, while others even retain a small phosphorylation activity (Beraki et al., 2019; Zhu et al., 2016) (referred to as low activity or active pseudokinases (Zeqiraj and van Aalten, 2010)). Such factors make it nearly impossible to predict functions from bioinformatics analysis only and consequently experimental validation on the molecular level is required to unravel their role in the respective signal transduction cascade (Mace and Murphy, 2021; Zeqiraj and van Aalten, 2010). However, increasing research revealed in general four different types of functional mechanisms of pseudokinases mediating specialized non-catalytical functions, yet still with a main focus on eukaryotic systems (Mace and Murphy, 2021; Murphy et al., 2017).

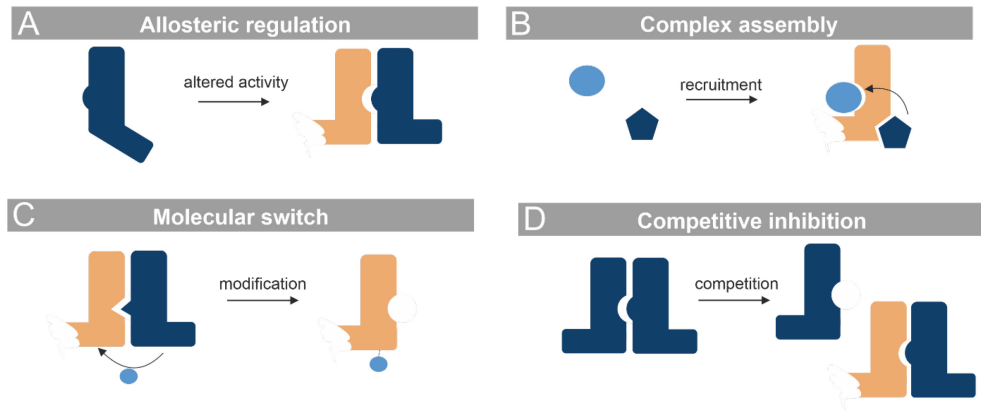


Figure 10: Overview of pseudokinase functions. (A) Allosteric regulation for the activation or inhibition of a cognate protein kinase (blue). (B) Assembly of complexes for recruitment of multiple relevant interaction partners, like kinases, phosphatases, regulatory proteins, etc (blue). (C) Molecular switch by receiving post-translation modification, e.g. phosphorylation (light blue), from another upstream regulator like a kinase (dark blue) that promote conformational switching and effector functions. (D) Competitive inhibition by blocking catalytic activity or substrate access of other kinases or proteins (blue). The pseudokinase variant is depicted always in orange. Adapted from Mace and Murphy (2021) and Murphy et al. (2017).

Allosteric regulation of cognate kinases is a well-characterized function of pseudokinases, encompassing intermolecular interactions as heterooligomers supporting active or inactive conformation of a respective kinase (Figure 10A). This mode of action is found in the yet best-characterized bacterial pseudokinase throughout literature: In *Caulobacter crescentus*, the pseudokinase DivL directly interacts with the kinase CckA to regulate cell division (Iniesta et al., 2010). Although the mechanism is not yet revealed, the direct interaction with the pseudokinase is required for maximal kinase activity of CckA. In this context, neither the ATPase domain nor an autophosphorylation residue of DivL is required (Reisinger et al., 2007). This kinase:pseudokinase interaction is further mediated by the phosphorylation status of the RR DivK, further implementing the kinases PleC and DivJ (Iniesta et al., 2010; Tsokos et al., 2011). This example represents the introduction of an activating pseudokinase into a multikinase network to balance several signals regulating cell division (Francis et al., 2018).

Another function described for pseudokinases is to act as signaling scaffold for the formation of larger signaling complexes (Figure 10B). Some pseudokinases were reported to interact with substrates, regulators or several other binding partners to allow recruitment of components and thereby facilitate the connection of signaling cascades. The vertebrate titin kinase proves such a scaffold function by coupling the ubiquitin ligases MuRF1 and MuRF2. This pseudokinase thereby connects divergent stimuli of muscle response to metabolic stress (Bogomolovas et al., 2014). Further, vertebrate KSR1 pseudokinases dimerize with Raf and MEK kinases to activate them, while additionally serving as

docking site for various other involved players of this cascade, like phosphatases, RAF proteins or regulatory 14-3-3 proteins (Lavoie et al., 2018; McKay et al., 2009).

An interesting function of pseudokinases is to act as molecular switches, where they receive information from a regulator to control a subsequent downstream output (Figure 10C). Pseudokinases thereby act as molecular switch upon post-translational modifications, like phosphorylation in a common example of the vertebrate mixed lineage kinase domain-like (MLKL) pseudokinase. The upstream protein kinase RIPK3 phosphorylates the pseudokinase domain thereby inducing a conformational change in MLKL and releasing it from an N-terminal four-helix bundle domain. MLKL is consequently able to oligomerize and translocate to the plasma membrane, where it accumulates and thereby permeabilizes the lipid bilayer causing lytic cell death (Hildebrand et al., 2014; Murphy et al., 2013; Samson et al., 2020).

So far rather less described, but still abundant, pseudokinases can also act as competitors within signal transduction (Figure 10D), where they are able to attenuate the catalysis or block substrate access of another protein kinase in order to inhibit the signaling cascade. Recently, within the human IRAK (interleukin-1 receptor associated kinase) family, the pseudokinase IRAK3 dimer was proposed to inhibit the kinase IRAK4 dimer, blocking its active sites (Lange et al., 2021). Consequently, the inflammatory signaling in the complex of IRAK proteins (myddosome) in the immune response to pathogens is attenuated (Moncrieffe et al., 2020).

Recent analysis of >30,000 pseudokinase sequences underlined that pseudokinases have fundamental roles across all kingdoms of life (Kwon et al., 2019). Most likely, these evolved from gene-duplication events from canonical kinases (Eyers and Murphy, 2016). However, it is not excluded that some canonical kinases have evolved from pseudokinases, just like for other pseudoenzymes (Clifton et al., 2018; Kaltenbach et al., 2018; Kwon et al., 2019).

2.5.3 Mode of action of pseudokinase ChrS_CA-fs

In our study, a pseudokinase variant of ChrS was shown to promote high heme tolerance in *C. glutamicum* (Krüger and Frunzke, 2022). With ChrS_CA-fs being no more involved in canonical phosphotransfer, three main hypotheses explaining an increase of the activation kinetics of ChrA by HrrS were suggested (Figure 11). It is important to note that this adaptation is made possible by the specialty of *C. glutamicum* possessing the paralogous systems ChrSA and HrrSA reacting to the same stimulus heme. Paralogs have already been demonstrated to be valuable for efficient adaptations (Bratlie et al., 2010; Gevers et al., 2004). Our study further emphasizes gene duplication as powerful tool for adaptation shaped by the respective environmental niche.

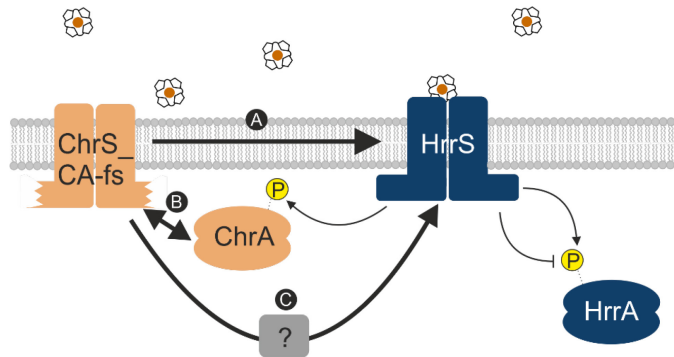


Figure 11: Three hypotheses concerning the influence of the pseudokinase ChrS_CA-fs on elevated heme tolerance. The pseudokinase ChrS-CA-fs (orange) and the HK HrrS (blue) are shown in their homodimeric forms. There are three different assumptions for the suggested communication on HK level in the evolved strain 1.fs possessing the pseudokinase that allow elevated expression of *hrtBA*. (A) Direct communication on HK level by e.g. transient interactions. (B) Recruitment of the response regulator ChrA for more efficient activation by HrrS. (C) Indirect communication on HK level using a third, yet unknown component. ChrS-CA-fs = ChrS with a frameshift mutation at alanine on position 245, P = phosphate.

2.5.3.1 Direct communication on the histidine kinase level for elevated activation

A first hypothesis would include allosteric activation (Figure 10A, Figure 11A) of HrrS by heterodimerization with ChrS_CA-fs. This could lead e.g. to beneficial switching from 'off' to 'on' state of HrrS by interaction with ChrS_CA-fs. Further, if there is alternate, minor phosphorylation activity remaining for ChrS_CA-fs it could also support fast activation of ChrA by phosphorylation on the HK-level. For analysis, dimerization characteristics were investigated using bacterial two-hybrid (BACTH) assays on plates as well as coupled to liquid β -galactosidase assays (Figure 12, left part). While homodimerization could be confirmed for all of the three HKs tested, heterodimerization of the ChrS_CA-fs variant with HrrS could not be revealed.

However, heterodimerization for the native kinases ChrS and HrrS was reported for the first time. As the respective Dhp domains of these HKs share 58% sequence identity and even 72% similarity on the protein level in *C. glutamicum* (global alignment (Needleman-Wunsch)), this observation was reasonable. However, the question remains if and how this influences native TCSs signaling in these paralogous systems and how this might affect the altered ChrS_CA-fs signaling. Up to date, HK communication on the level of heterodimerization is rather less reported, but also because it is only rarely examined. Nevertheless, a prominent example is the heterooligomerization of the HKs RetS and GacS in *P. aeruginosa*. During infection of a host, the hybrid HK RetS downregulates the activity of the unorthodox HK GacS in three different mechanisms: Either (i) by inhibition of the autophosphorylation reaction of GacS, (ii) by deprivation of the phosphoryl group from the histidine residue of GacS or (iii) by cross-phosphatase activity of RetS on the REC domain of GacS. This cross-communication between the HKs allows switching between motile and biofilm lifestyles of this bacterium (Francis et al., 2018;

Ryan Kaler et al., 2021). Overall, heterodimerization of HKs might be an underestimated mechanism to expand signaling pathways to a multikinase network. In the case of ChrS and HrrS in *C. glutamicum*, it remains to be elucidated if heterodimers could play a significant role in vivo or if the observed interaction is an in vitro artefact. Previous studies investigating on dissociation constants for different modes of dimerization of the HKs EnvZ and RstB in *E. coli* demonstrated that homodimers of these HKs are significantly more stable than heterodimers, summarizing heterodimerization of these HKs are rather unstable in vivo (Ashenberg et al., 2011). However, these *E. coli* systems only share ~30% identity, which is significantly less than the paralogous HKs of *C. glutamicum* responding to the same stimulus heme. Previous studies demonstrated that HrrS acts as ‘kickstarter’ of the ChrS-mediated response, as HrrS presence is required for instantaneous promoter activation of *hrtBA* (Keppel et al., 2019), which could be explained by transient activating interactions between these HKs upon heterodimerization. Inhibiting events on the other HK would rather be excluded, as activities of HK targets are not elevated upon deletion of the other HK (Hentschel et al., 2014).

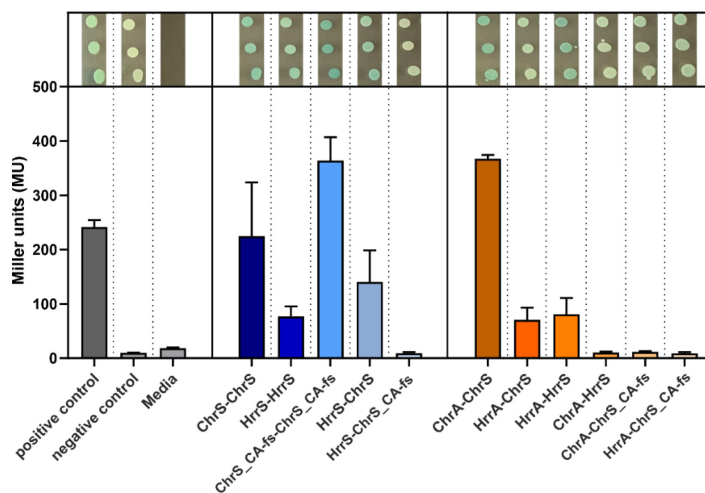


Figure 12: Bacterial two-hybrid assays (BACTH) reveal heterodimerization of native ChrS and HrrS. BACTH interactions between the histidine kinases ChrS, HrrS and the evolved ChrS variant (ChrS_CA-fs) as well as their interaction with the RRs ChrA and HrrA were analyzed as C-terminal tag fusions. Drop assay was performed in triplicates, where blueish color of the colonies indicate interaction, while white colonies indicate no interaction (Euromedex, Souffelweyersheim, France). The bar graph represents a quantitative analysis of these respective triplicates using β -galactosidase assay according to Griffith and Wolf (2002). Colorimetric β -galactosidase activity is given in Miller units. Grey bars represent controls, while blue ones show the interaction between HKs and orange ones for HKs with RRs. Positive control = pKTN25-zip with pUT18-zip, negative control = pKTN25 with pUT18, media = CGXII basis with 2% glucose. Adapted from Krüger and Frunzke (2022).

The performed BACTH assays might disprove the potential allosteric activation of HrrS by interaction with the evolved ChrS_CA-fs. Nevertheless, the native situation points out that there is already interaction between the HKs that may be shifted towards HrrS-mediated ChrA activation in the evolution mutant. It should be taken into account that these *E. coli* based in vitro BACTH assays do not

perfectly reflect the in vivo situation of *C. glutamicum*. For example, as HKs are transmembrane proteins, there might be an issue about the intracellular folding of these proteins (Mehla et al., 2017). Using fluorescence resonance energy transfer (FRET) analyses might be an option to shift to an examination in *C. glutamicum*. Furthermore, dimerization modes of kinases can be quite diverse ranging in its 'on' and 'off' state conformation by rotation and bending events of the DHp- and CA-domains (Cai et al., 2017; Casino et al., 2009; Stewart, 2010) as well as varying from head-to-head and back-to-back, over head-to-tail to parallel or transverse side-to-side (Lavoie et al., 2014; Mace and Murphy, 2021). As the pseudokinase might retain different structural properties, this could potentially impede tag interactions in BACTH. Also highly efficient homodimerization by ChrS_CA-fs could obscure any minor heterodimerization with HrrS in this assay, which could, however, be relevant in vivo.

2.5.3.2 Recruitment of the response regulator for facilitated phosphorylation

Apart from activation by ChrS_CA-fs, another explanation for the ChrA activity increase could be recruitment of ChrA by ChrS_CA-fs to facilitate its phosphorylation by HrrS (Figure 10B, Figure 11B). In this context, BACTH assays were also performed examining on HKs and RRs interactions (Figure 12, right part). Known interactions of native HKs with their cognate RRs could be validated by this assay. However, the already demonstrated cross-talk with non-cognate partners (Hentschel et al., 2014) could only be confirmed for ChrS and HrrA, not for HrrS and ChrA. This highlights again the limits of BACTH assays for protein-interactions in this case and therefore, it cannot be completely excluded that the RRs also interact with the pseudokinase ChrS_CA-fs. Please note that β -galactosidase assays in liquid assays did not show any signal for RRs and pseudokinase interactions, but a blueish coloration was observed on plates.

Consequently, the hypotheses about allosteric activation and recruitment of RR cannot yet completely be excluded based on BACTH assays. A further comprehensive explanation, apart from in vitro conditions, might be found in the experimental limitation that BACTH can only assess binary interactions. It might be possible that heterodimerization of HrrS with ChrS_CA-fs in response to heme availability and recruiting of ChrA by ChrS_CA-fs is required simultaneously for proper interactions. These issues should be addressed in further studies. Although bacterial three-hybrid assays might be used to prove the latter hypothesis, it might be a more promising option to assess protein-interactions via co-immunoprecipitation allowing evaluation in the natural *C. glutamicum* context. On top, to unravel molecular characteristics of this pseudokinase variant of ChrS, its ability for nucleotide binding could be investigated using thermal shift assays (Murphy et al., 2014), while it would be of further interest to assess if there is an alternative ATP-binding site, which could facilitate such conformational changes.

2.5.3.3 Indirect communication between histidine kinases employing a third component

Apart from the communication of HKs on a direct level as presented above, a third hypothesis about indirect communication can be proposed (Figure 11C). This would include another, third component that interacts with the HKs, which could be e.g. a small protein (Buelow and Raivio, 2010; Salvado et al., 2012). Small proteins have been described as underestimated participant in signal transduction with regulatory functions. Due to their small size (< 100 amino acids (aa) (Yadavalli and Yuan, 2022)), they typically lack enzymatic activities, but have been described to act as inhibitors or activators influencing interactions between proteins or induce conformational changes (Storz et al., 2014). Therefore, small proteins have not only been established as 'TCS modulators', but also as 'TCSs connector' proteins. In *E. coli* a small 65 amino acid protein SafA (formerly known as B1500) acts as such a connector protein linking the TCSs EvgSA and PhoQP for mediation of acid resistance. Expression of the gene encoding the membrane protein SafA is increased by EvgSA activity, while SafA further directly interacts and activates the PhoQP system by either promoting kinase activity or decreasing phosphatase activity (Eguchi et al., 2011; Eguchi et al., 2007). Similarly, another 123 aa protein MzrA connects the two TCSs CpxAR and EnvZ/OmpR upon cell envelope stress in *E. coli* (Gerken et al., 2009). Most interactions with a connector protein were suggested on transmembrane domain level (Szurmant et al., 2008), as for many small proteins in general (Storz et al., 2014). If such a (small) protein would aid at communication between the native HKs ChrS and HrrS in *C. glutamicum*, an altered activity might endure in the evolved 1.fs context, where the remaining transmembrane domain or even DHP-domain of ChrS_CA-fs could still interact with potential TCS connector proteins, constantly elevating the activity of HrrS. As such open-reading frames are often co-localized, a preliminary look on the genomic region around these TCSs drew attention to cg3249 that codes for a larger 183 aa putative protein in close proximity to *hrrSA*. The expression of this gene was also shown to be downregulated in a $\Delta hrrA$ mutant (Frunzke et al., 2011). Fitting into the scheme of small proteins, subsequent cg3250 encodes a putative membrane protein of 50 aa nearby the region of *hrrSA*. Nevertheless, profound analysis of potential (small) proteins involved in indirect HK communication between these two paralogous systems should be further performed by pull-down assays or reconstitution of the complexes in proteoliposomes to establish defined systems for in vitro characterization.

Not only small, but also RNA-binding proteins gained recent interest throughout research (Beckmann et al., 2016; Holmqvist and Vogel, 2018). This type of proteins was also described in the context of TCSs regulation. Recently, a significant cross-talk at transcriptional as well as phosphorylation level between the heme-responsive TCSs HssRS and the cell envelope stress-related TCSs HitRS (HrrRS interfacing TCS) was demonstrated in *Bacillus anthracis* (Mike et al., 2014; Pi et al., 2020). Subsequent research further established that the RNA-binding protein KrrA activates the TCSs HitRS by binding its transcript

and modulating mRNA stability (Pi et al., 2022). Although KrrA does not influence the activity of the other TCSs HssRS, it was established to bind further ~70 RNA targets. Therefore, it might not be excluded that regulation of further downstream components also connects these signals.

Connecting signal transduction pathways via multiple kinases, RRs, and further small or RNA-binding proteins demonstrates a high level of complexity, which is required to enable fast adaptation to fluctuating environmental conditions. It is therefore not unlikely that further players are involved in ChrSA and HrrSA signaling, which have not been unraveled so far.

2.5.3.4 Altered phosphatase kinetics for constant activation

Independent from the exact mechanism of the evolved pseudokinase ChrS_CA-fs elevating *hrtB* activation kinetics, it is suggested that it is overall further supported by a missing dephosphorylation activity of ChrS_CA-fs. Although the ChrS_CA-fs variant does still possess the DxxxQ phosphatase motif in its DHP-domain (Figure 8B), we concluded that there is no more or at least attenuated phosphatase activity based on the continuous *hrtB* activation. The CA-domain is missing due to the frameshift mutation, while several studies described an essential role for this domain in phosphatase activity interacting with DHP-domain (Carmany et al., 2003; Zhu et al., 2000). Throughout clinical pathogenic strains, there are various studies describing single nucleotide polymorphisms in HKs evolved around the CA-domain that lead to an increased output of the RR and consequently highly elevated target gene expression due to an abolished phosphatase activity. Exemplarily, this was demonstrated for clinical and virulent *M. tuberculosis* strains isolated after infection of the host (Baena et al., 2019; Waturuocha et al., 2021a; Waturuocha et al., 2021b). Here, in vitro phosphorylation assays might confirm the lack of ChrS_CA-fs phosphatase activity.

In the end, this ALE-based approach provided important mechanistic insights into the interaction of the HrrSA and ChrSA systems. It also demonstrates the high evolutionary flexibility based on two paralogous TCSs, which enables rapid adaptation to changing environmental conditions.

2.5.4 Heme sequestration or alternative transport systems counteracting heme toxicity

Although the ChrS_CA-fs mediated export of heme was demonstrated as key strategy of the evolved 1.fs strain in terms of heme tolerance, further players beyond heme exporters might be involved in counteracting heme toxicity in *C. glutamicum*.

Comparative transcriptome analysis via microarrays revealed a high upregulation of all genes encoding (potential) heme-binding proteins, i.e. *htaA*, *htaB*, *htaC*, *htaD* and *hmuT*, in the evolved heme tolerant 1.fs strain compared to the wild type in the presence of heme (supplemental section 4.3, Table S4). Deletion of all these genes resulted in a strain possessing reduced tolerance to moderate levels of heme (~10 μ M). As there were no more differences on lower or higher heme concentrations, it was

suggested that membrane-bound heme-binding proteins rather play a minor – but significant – role in heme detoxification by sequestering heme at the cell periphery thereby shielding it from cytosolic components. Heme sequestration and/or storage as detoxification strategy by heme-binding proteins was already described for several bacterial organisms. Members of the HemS-family, like HemS of *Yersinia enterocolitica* (Stojiljkovic and Hantke, 1994), ShuS of *Shigella dysenteriae* (Wilks, 2001) or PhuS of *P. aeruginosa* play a role for heme tolerance by binding heme and safely trafficking it within the cell (Lansky et al., 2006). Recently, the heme-binding protein HupZ of Group A *Streptococcus* was demonstrated to be involved in heme tolerance and was proposed to act as heme chaperone (Lyles et al., 2022). All of these heme-binding proteins possess at least one other function, acting, for example, in heme import or as heme oxygenase. This is also true for the corynebacterial heme-binding proteins HtaA and HmuT, which are involved in heme import (Allen and Schmitt, 2009; Drazek et al., 2000). Moreover, in *C. diphtheriae*, HtaA was shown to transfer heme to HtaB, suggesting that HtaB is also involved in heme import as intermediate sequestration protein (Allen and Schmitt, 2011). As *htaC* is located in the same operon, HtaC might assist in the import process. Further confirmation of these functions as well as investigation on HtaD, which is encoded in a different location than the other heme-binding protein genes, is required to unravel their potential role in heme scavenging and detoxification. In future studies, overexpression of respective heme-binding protein genes or even addition of the purified proteins to cultivations at high heme levels could provide valuable insights. Such an overexpression of the heme binding protein C (HbpC) in the Gram-negative *Bartonella henselae* was shown to increase its heme tolerance and consequently its ability to infect its host (Liu et al., 2012; Roden et al., 2012). Interestingly, HbpC was found in outer membrane vesicles shedding from the bacterial surface, which allow to sequester local toxic concentrations of heme (Roden et al., 2012). The excretion of outer membrane vesicles as strategy for the sequestration of several toxic compounds have been described for other bacteria (McBroom and Kuehn, 2007; Schooling and Beveridge, 2006). *Dietzia sp.* of the order *Corynebacteriales* were recently shown to release membrane vesicles containing heme binding proteins (Wang et al., 2021a). In general, membrane vesicles were shown to be formed by *C. glutamicum* (Nagakubo et al., 2021), but whether this vesicle formation could also play a role in this bacterium remains to be elucidated, e.g. by membrane vesicle isolation and protein content analysis via mass spectrometry (Prados-Rosales et al., 2014).

Apart from heme sequestration by binding proteins and heme export, also other transport systems might matter for detoxification. Strikingly, the transcriptome analysis further depicted differential expression of genes coding for various transport systems in the evolved 1.fs strain (supplemental section 4.3, Table S4). The upregulation of the operon comprising *cg2675* to *cg2678* (NCgl2350 to NCgl2353) coding for an ABC-type transport system is of special interest, as our genome-wide binding studies already demonstrated that this system is also positively regulated by heme-responsive HrrA

(Keppel et al., 2020). Co-transcribed with the gene *ahpD* encoding an alkyl hydroperoxidase, this operon was recently connected to oxidative stress regulation (Hong et al., 2019). As the substrate translocated by this transport system is yet unknown, only vague hypotheses about the involvement in heme detoxification can be made. Apart from direct export of heme or toxic heme-related products, it might be an additional option to import neutralizing compounds aiding heme detoxification. Such a potential role was found for the import of manganese to counteract oxidative stress, with Mn(II) acting as scavenger of superoxide or hydrogen peroxide (Horsburgh et al., 2002). In *E. coli*, manganese was shown to replace the iron in the ribulose-5-phosphate 3-epimerase to avoid ROS generation in vitro (Sobota and Imlay, 2011) and in *Neisseria gonorrhoeae* the Mn(II) uptake system directly imports manganese to counteract elevated oxidative stress (Seib et al., 2004; Tseng et al., 2001). However, also excessive manganese concentrations have the potential to result again in redox stress (Sachla et al., 2021). Finally, the influence of such transport systems and further compounds affecting heme homeostasis should be addressed in future studies, as these might outline important issues to overcome heme-induced oxidative stress.

2.6 A glimpse into heme as valuable resource in community

As heme represents an essential cofactor for many enzymes and an important alternative iron source for many microbes, the above-portrayed conserved key strategy of exporting heme for detoxification is inevitably accompanied by losing this valuable resource. Therefore, the question raises whether it might be possible for *C. glutamicum* to keep heme in close proximity, e.g. for an own later resort or even to share it within microbial communities. This issue was already addressed when visually comparing pelleted cells, which were cultivated in the presence and absence of heme (Figure 13A). Here, heme-subjected cells showed a dark brownish color. Due to the hydrophobic nature of the molecule, there is the possibility that heme passively sticks to the cell membrane when not yet imported or after export. However, also active scavenging, e.g. by heme-binding proteins, in the cell envelope of *C. glutamicum* could be hypothesized. Overall five heme-binding proteins HmuT, HtaA, HtaB, HtaC and HtaD are encoded in the genome of this bacterium, giving not only the opportunity to sequester heme for detoxification (section 2.5.4), but possibly also for external heme storage. Such a reservoir could be helpful in rapidly heme-depleted environments. Future experiments with modified heme-binding proteins or mutants defective in the production of the hydrophobic mycolic acid layer should give insights into the mechanisms involved in heme scavenging.

Upon holding heme in close proximity of cells – no matter if passively or actively – it can be further questioned whether heme can be shared in a community or is rather privatized for own use. First investigations to evaluate heme as such a public good were made via co-cultivations using a donor and

a recipient strain. The donor strain was pulsed with heme by inoculation with 20 μM heme or none as control, before mixing it with an iron depleted recipient strain transformed with a *hrtB* reporter plasmid (pJC1-*P_{hrtB}-eyfp* from Heyer et al. (2012)) to monitor if this strain encounters heme (Figure 13B). There is a slight but significant higher fluorescent output for the co-cultivation encompassing a heme pulse, meaning that the recipient strain indeed came into contact with (more) heme. Another co-cultivation in the same manner was tested on plates using constitutively fluorescing donor and recipient cells yielding similar results based on growth (Figure 13C). These investigations gave hints for a potential heme sharing, probably enabled by heme export of the donor strain to the cell surface. Nevertheless, further aspects must inevitably be tested.

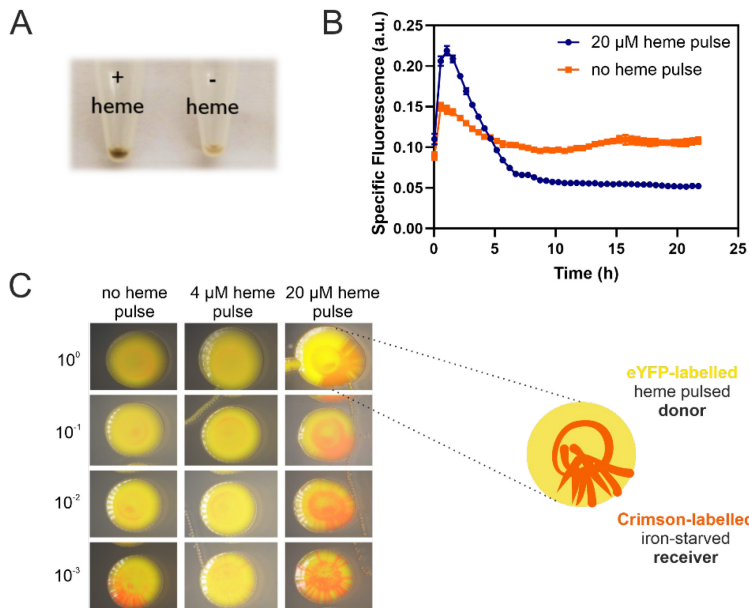


Figure 13: Potential heme sharing in *C. glutamicum*. (A) *C. glutamicum* wild-type cells were incubated either with 20 μM heme (+) or without (-) for 15 minutes and pelleted by centrifugation. (B) A donor strain was pulsed in the same way with 20 μM heme or none as control and co-cultivated with an iron-starved recipient strain, which was transformed with a pJC1-*P_{hrtB}-eyfp* reporter plasmid. Specific fluorescence analyses were performed in the Biolector[®] microtiter cultivation system (Kensy et al., 2009) using CGXII media with 2% glucose, no iron and kanamycin. Specific fluorescence was calculated as measured fluorescence per backscatter. Data represent average of three biological replicates including standard deviations depicted as error bars. (C) Pulsed donor strain (no, 4 μM or 20 μM heme) was labelled with eYFP fluorescent protein and the iron-starved receiver strain with Crimson, whose gene expressions were controlled by a constitutive P_{tac} promoter. Cells were mixed and dropped on iron-depleted CGXII agar plates with 2% glucose in 1:10 dilutions. Images were taken using a stereomicroscope Nikon SMZ18 (merged picture, λ_{Ex} : 500/20 nm, λ_{Em} : 535/30 nm; λ_{Ex} : 562/20 nm, λ_{Em} : 604-1100 nm).

There is a variety of bacterial interactions secreting and exchanging metabolites shaping a global ecological network (Faust and Raes, 2012; Phelan et al., 2011), while there are also examples for partial privatization of public goods to avoid cheater at respective conditions (Jin et al., 2018; Scholz and Greenberg, 2015). To assess the sharing dynamics, conditional co-cultivations should also be achieved

with deletion strains of e.g. heme export ($\Delta hrtBA$), but also heme import ($\Delta hmuTUV$) and heme binding proteins ($\Delta hmuT \Delta htaA \Delta htaBC \Delta htaD$). On top, it should be excluded that the high heme pulse not only kills a high fraction of donor strains allowing the recipients to grow on the released nutrients. The evolved strain 1.fs with the pseudokinase ChrS_CA-fs could also be employed for further tests, since this strain features an extraordinary level of *hrtBA* expression - superiorly balanced compared to the level achieved by simple overexpression (section 2.5).

Regarding the potential sharing process, it should further be noted that several Gram-positive bacteria, including *C. glutamicum*, have a thick mycolic acid layer (Eggeling and Sahm, 2001; Minnikin and Goodfellow, 1980). Recent studies claimed that the Gram-positive strain *Dietzia sp.* DQ12-45-1b shares heme using mycomembrane vesicles packed with heme binding proteins and, interestingly, this recycling process was even shown to occur interspecifically, as depicted for *Dietzia* with *C. glutamicum* (Wang et al., 2021a). As both these strains occur in soil, this interaction could be of relevance for community interactions. However, whether *C. glutamicum* is also able to form these membrane vesicles, or if it only relies on heme-packed vesicles delivered by other microbes, remains to be elucidated. As the membrane of *Corynebacteria* is comparable to that of *Dietzia* in terms of thickness (Zuber et al., 2008) and *C. glutamicum* was shown to form membrane vesicles in general (Nagakubo et al., 2021), there might be a potential for vesicle mediated heme sharing. The proteins present in these vesicles could further be examined using e.g. LC-MS/MS. Moreover, the strain $\Delta hmuTUV$, harboring deletion of the heme import genes (Frunzke et al., 2011), could be analyzed in regard if it is still able to take up heme from a bacterial community, e.g. by heme-packed vesicles, beyond the conventional import system.

Finally, bacterial cells should be considered in a multivalent and spatial environment, where they could demonstrate several strategies for competition or cooperation on heme usage on both species and interspecies level.

2.7 Evolution towards the production of heme

Throughout the former sections, the relevance of heme tolerance and usage in the context of bacterial survival was discussed. Within recent years, also the production of heme from microorganisms gained increasing attention, because microbial produced heme entails the avoidance of heme extraction from animal blood. Since heme is an important flavor carrier in conventional meat, this molecule plays an important role in the production of animal-free meat alternatives. Besides plants and yeasts (Espinass et al., 2012; Fraser et al., 2017; Ishchuk et al., 2021), also bacteria were recently engineered for an alternative high-yielding heme production (Choi et al., 2022; Kwon et al., 2003; Zhao et al., 2018). In

particular, high heme yields were recently shown for engineered *C. glutamicum* strains (0.61 mmol_{heme} per mol_{glucose}, with a maximum titer of 309.18 ± 16.43 mg l⁻¹) (Ko et al., 2021).

Within section 2.5, ALE experiments were performed to unravel strategies to counteract heme intoxication using increasing concentrations of heme as selection pressure. In a similar manner, ALE could be used to reveal further pathways and mechanisms that possibly improve bacterial heme production and transport. The most important prerequisite for an evolution towards heme production is to couple it to cellular growth providing a selection pressure. The traditional approach would be a heme auxotrophic strain, but as heme synthesis is an essential pathway it was not possible in the context of this study to obtain such a strain of *C. glutamicum*. However, several strategies for synthetic growth-coupled product formation have been described throughout literature (Buerger et al., 2019). Recently, the application of a transcription factor-based biosensor was successful in coupling growth to enhanced levels of amino acid production in *C. glutamicum* (Stella et al., 2021), where the principle of the previously generated Lrp biosensor (Mustafi et al., 2012) was key for the generation of a selection pressure towards production. The genomic region encompassing the gene encoding the transcription factor Lrp, the intergenic region between *Lrp* and *brnFE* as well as the first 30 bp of the Lrp-target *brnF* were introduced upstream of a growth-regulating gene. In the presence of its effector molecules - i.e. the amino-acids L-valine, L-methionine, L-leucine or L-isoleucine - Lrp binds P_{brnF} and induces the expression of the selected growth-regulating gene *pfkA* encoding the phosphofructokinase of central carbon metabolism or *hisD* coding for the histidinol-dehydrogenase involved in L-histidine biosynthesis (Stella et al., 2021). Thereby, a selection pressure towards amino acid production was implemented and cells with improved production performances could be isolated after ALE experiments.

In a comparable approach, in context of the master thesis of Janik Göddecke (2022), which was supervised as part of this doctoral project, biosensor constructs were designed, coupling heme production to the expression of the growth-regulating genes *aceE*, *pgi* or *pfkA*. The *aceE* gene encodes the E1 subunit of the pyruvate dehydrogenase complex linking glycolysis and TCA, making it essential for growth on glucose (Schreiner et al., 2005). Pgi represents the glucose-6-phosphate isomerase catalyzing the reversible reaction from glucose-6-phosphate to fructose-6-phosphate, while the phosphofructokinase PfkA is responsible for the reaction of fructose-6-phosphate to fructose-1,6-bisphosphate. Upon deletion of *pgi* or *pfkA*, the glucose catabolism is inevitably forced to progress via pentose phosphate pathway, resulting in a severe growth defect (Lindner et al., 2013; Siedler et al., 2013). In the following, the focus will be on the biosensor construct that is based on *pfkA*.

For coupling *pfkA* expression and, thereby, growth to heme production, we made use of the heme-responsive TCS ChrSA controlling the expression of the *hrtBA* operon (Figure 14A). As P_{hrtB} is efficiently

activated by ChrA upon the presence of heme, this promoter region was placed in front of *pfkA* rendering its expression heme-dependent. Monitoring growth of the WT::P_{*hrtB*}-*pfkA* strain, further referred to as biosensor strain, revealed a significant growth defect in the absence of heme, which can be counteracted already by the addition of 1 μ M heme (Figure 14B), making this construct applicable for growth-coupled evolution. Note that it was not necessary to add another copy of ChrSA into the biosensor construct. Stella et al. (2021) comprehensively determined that selection on plates is more advantageous for these biosensor constructs than using e.g. liquid culture, as cheaters that show simple promoter mutations in the biosensor circuit can be circumvented more easily. Therefore, this ALE was performed by streaking on iron-rich but heme-depleted agar plates (Figure 14C). In direct comparison to the wild type, the biosensor strain showed impaired growth revealed by growth delay and yielded colonies of different size. Moreover, the transformation of these strains with a reporter plasmid for *hrtB* expression (pJC1-P_{*hrtBA*}-*eyfp* (Heyer et al., 2012)) revealed that the majority of big colonies showed a fluorescent signal indicating the elevated expression of *hrtB* and potentially the presence of increased heme levels. Interestingly, several smaller colonies accumulated around these big potential producer colonies, which presumably gain either glycolysis intermediates or even heme (section 2.6) from the producing strain in order to support their growth.

Subsequently, several potentially producing clones were selected and analyzed using high performance liquid chromatography (HPLC) with a linear gradient of ammonium acetate and methanol (Figure 14D) (compare supplemental section 4.4). In order to gain an evaluable output, the total heme content of the cells was screened. After a fast screening, two potential candidates exhibiting higher heme contents (\sim 4.43 and 2.68 μ M) than the wild type (\sim 2.48 μ M) were selected for genome sequencing, represented as clones 1 and 21 in Figure 14D. The highest heme production was observed for clone 1, where two amino acid exchange mutations in *cydD* were identified. CydD is annotated as a component of a heterodimeric ABC transporter, essential for cytochrome *bd* oxidase assembly. Regarding the respiratory chain, a connection between CydDC and heme was suggested in earlier studies, while heme was established to bind and modulate CydDC activity in *E. coli* (Shepherd, 2015; Yamashita et al., 2014). Although a connection is clear, exact influences remain controversial. A recent pre-print claimed that CydDC bears a function in heme export in *E. coli* (Wu et al., 2022).

Furthermore, in clone 21 we identified a mutation in the CA-domain of ChrS – comparable to the evolved mutant described in section 2.5. Consequently, this mutation presumably leads to an extreme upregulation of *hrtB*, and concomitant growth-required *pfkA* expression. On the one hand, this uncouples *pfkA* expression from heme production due to continuous *hrtB* expression, but on the other hand, the constant heme export potentially stimulates the inherent heme biosynthesis to some extent.

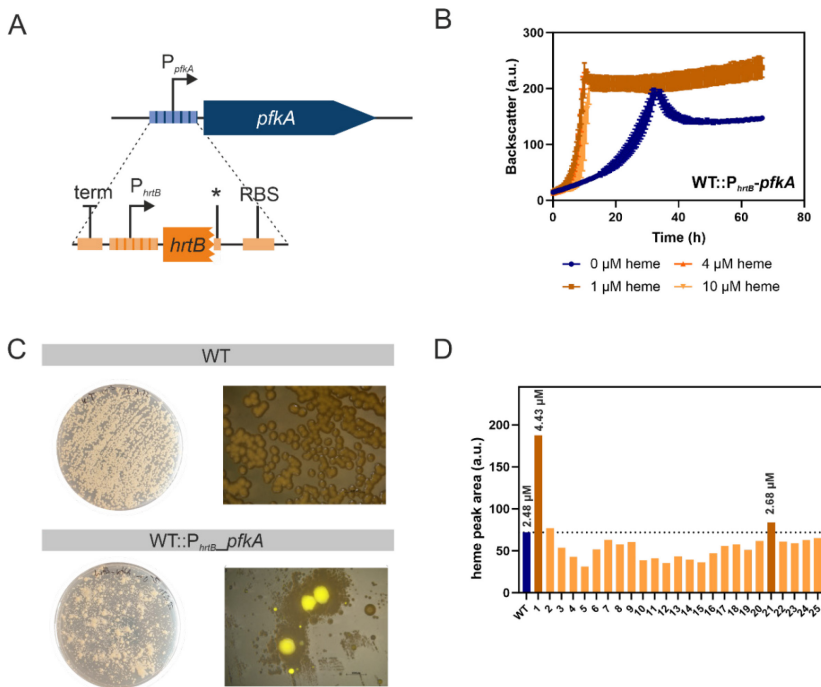


Figure 14: Coupling heme production to cellular growth of *C. glutamicum*. (A) Schematic overview of *hrtB*-based biosensor coupling heme production to the expression of *pfkA*. term = terminator, * = stop, RBS = ribosomal binding site. (B) Growth analysis of the WT::*P_{hrtB}-pfkA* biosensor strain in CGXII media with 2% glucose, no iron and increasing concentrations of heme from none (blue) to 1, 4 and 10 μM (shades of orange). Data represent average values measured in the Biolector[®] microtiter cultivation system (Kensy et al., 2009) as three biological replicates including standard deviations depicted as error bars. (C) ALE on iron-rich CGXII agar plates (100 μM FeSO_4 , 2% glucose). Strains as depicted were transformed with a *pJC1-P_{hrtB}-eyfp* reporter plasmid, to indicate the presence of heme in the respective colony. Zoomed in images were taken using a stereomicroscope Nikon SMZ18 (λ_{Ex} : 500/20, λ_{Em} : 535/30). (D) HPLC analysis of total heme content after 24 h cultivation in iron-rich CGXII media supplemented with 2% glucose to screen for heme producing evolved mutants. Measured in unicates. Blue represents wild type as control, with the horizontal dotted line demonstrating wild type level. Orange bars represent picked evolved clones, while dark orange ones showed increased heme content. Values depicted above bar graphs represent calculated heme content in μM . Presented data was generated in the context of the herein supervised master thesis of Janik Göddecke (2022).

Finally, sequence analyses demonstrate the necessity for larger screens of more evolved strains, as cheater strains remain inevitable. Automated evolutionary selection could support such high-throughput approaches (Radek et al., 2017), as well as faster pre-screenings for heme content making use of oxalic acid assays (Sassa, 1976) or apo-horseradish-peroxidase-assays (Atamna et al., 2015). Nevertheless, it could be elucidated that the concept of biosensor-based evolution towards heme can be successful and potentially provides further beneficial mutations that improve heme production. Future studies will focus not only on larger screenings, but also on heme-responsive biosensor circuits in front of further growth-regulating genes, like *aceE* or *pgi*.

2.8 Conclusion and Outlook

Iron is an essential mineral of cellular life involved in many crucial processes, as is the iron-bound protoporphyrin heme. Simultaneously, both this ion and molecule entail the risk of cell-damaging oxidative stress, i.e. they are “toxic, but tasty” (Keppel et al., 2019), and consequently posture the requirement for sophisticated regulatory networks maintaining homeostatic conditions within cells.

This doctoral thesis contributed to the understanding of iron and heme regulatory networks of *C. glutamicum* dealing with these stimuli and provides genome-wide insights into the binding pattern of the global regulators governing iron and heme homeostasis: DtxR and HrrA (Keppel et al., 2020; Krüger et al., to be submitted). Hitherto unknown genetic targets of each of these transcriptional regulators could be identified, which expand their known range of regulatory tasks from iron and heme homeostasis to numerous further global functions like e.g. counteraction of oxidative stress or important roles for cell respiration and central carbon metabolism. In this context, it became clear that cultivation at different conditions is inevitably necessary to comprehensively unravel a complete regulon, taking into account graded responses and interactions with other condition-dependent factors. By determining an anti-proportional trend of transcription factor binding peak intensity and comparative target gene expression, an importance was assigned to weak binding peaks of ChAP-Seq experiments, which must not be ignored. Such analyses further examine interference effects that validate a sophisticated co-evolution of DtxR and HrrA regulation balancing strongly interdependent iron and heme contents.

Apart from genome-wide binding profiling, this thesis specifically provides mechanistic insights into the interaction of the heme-responsive corynebacterial two-component systems ChrSA and HrrSA in the context of heme detoxification. The advantage of paralogous systems in the adaptation to fluctuating environments could be demonstrated eliciting heme tolerance by elevated activation kinetics for heme export (Krüger and Frunzke, 2022). The obtained frameshift version of ChrS resulted in a pseudokinase variant, which efficiently drives the activation of the heme exporter HrtBA in *C. glutamicum*. This activation was completely dependent on the phosphotransfer from HrrS to ChrA. Finally, this ALE approach resulted in a *C. glutamicum* strain with the highest heme tolerance reported so far, thereby providing a powerful basis for future engineering of heme production strains with high end-product tolerance. Further paralogous systems reacting to the same stimulus should be analysed in similar fashion to evaluate if pseudokinases are a universal adaptation mechanism of paralogous systems.

So far, interconnection of transcriptional regulation of the paralogous two-component systems HrrSA and ChrSA was demonstrated on the histidine kinase-response regulator level based on cross-phosphorylation (Hentschel et al., 2014). In this thesis, we proved another regulatory layer on the

histidine kinase level based on the heterodimerization of the native histidine kinases. This interaction might represent an underestimated phenomenon of paralogous TCSs integrating multikinase networks to allow fast adaptations to changing environmental conditions.

While the function of HrtBA in heme detoxification is well accepted (Heyer et al., 2012; Krüger and Frunzke, 2022), the role of heme export in microbial community interactions has not been comprehensively studied thus far. In a microbial community context, exported heme might further be accessible to neighbouring cells, if not sequestered and privatized for own later resort, to avoid the loss of a valuable resource. The establishment of defined co-cultures would be prerequisite to decipher the potential role of HrtBA in heme-dependent networking and to monitor heme sharing at the community level.

2.9 References

- Aft, R.L., and Mueller, G.C. (1984). Hemin-mediated oxidative degradation of proteins. *J Biol Chem*, 259(1): 301-305. doi: 10.1016/S0021-9258(17)43657-X.
- Ahmed, E., and Holmström, S.J. (2014). Siderophores in environmental research: roles and applications. *Microb Biotechnol*, 7(3): 196-208. doi: 10.1111/1751-7915.12117.
- Aich, A., Freundlich, M., and Vekilov, P.G. (2015). The free heme concentration in healthy human erythrocytes. *Blood Cells Mol Dis*, 55(4): 402-409. doi: 10.1016/j.bcmd.2015.09.003.
- Ajioka, R.S., Phillips, J.D., and Kushner, J.P. (2006). Biosynthesis of heme in mammals. *Biochim Biophys Acta Mol Cell Res*, 1763(7): 723-736. doi: 10.1016/j.bbamcr.2006.05.005.
- Alaminos, M., and Ramos, J.L. (2001). The methionine biosynthetic pathway from homoserine in *Pseudomonas putida* involves the *metW*, *metX*, *metZ*, *metH* and *metE* gene products. *Arch Microbiol*, 176(1-2): 151-154. doi: 10.1007/s002030100293.
- Albanesi, D., Martín, M., Trajtenberg, F., Mansilla, M.C., Haouz, A., Alzari, P.M., de Mendoza, D., and Buschiazzi, A. (2009). Structural plasticity and catalysis regulation of a thermosensor histidine kinase. *Proc Natl Acad Sci USA*, 106(38): 16185-16190. doi: 10.1073/pnas.0906699106.
- Allen, C., and Schmitt, M. (2009). HtaA Is an Iron-Regulated Hemin Binding Protein Involved in the Utilization of Heme Iron in *Corynebacterium diphtheriae*. *J Bacteriol*, 191: 2638-2648. doi: 10.1128/JB.01784-08.
- Allen, C.E., and Schmitt, M.P. (2011). Novel hemin binding domains in the *Corynebacterium diphtheriae* HtaA protein interact with hemoglobin and are critical for heme iron utilization by HtaA. *J Bacteriol*, 193(19): 5374-5385. doi: 10.1128/jb.05508-11.
- Ando, M., Manabe, Y.C., Converse, P.J., Miyazaki, E., Harrison, R., Murphy, J.R., and Bishai, W.R. (2003). Characterization of the role of the divalent metal ion-dependent transcriptional repressor MntR in the virulence of *Staphylococcus aureus*. *Infect Immun*, 71(5): 2584-2590. doi: 10.1128/iai.71.5.2584-2590.2003.
- Andreini, C., Bertini, I., Cavallaro, G., Holliday, G.L., and Thornton, J.M. (2008). Metal ions in biological catalysis: from enzyme databases to general principles. *J Biol Inorg Chem*, 13(8): 1205-1218. doi: 10.1007/s00775-008-0404-5.
- Andrews, S.C., Robinson, A.K., and Rodríguez-Quiñones, F. (2003). Bacterial iron homeostasis. *FEMS Microbiol Rev*, 27(2-3): 215-237. doi: 10.1016/s0168-6445(03)00055-x.
- Anzaldí, L.L., and Skaar, E.P. (2010). Overcoming the heme paradox: heme toxicity and tolerance in bacterial pathogens. *Infect Immun*, 78(12): 4977-4989. doi: 10.1128/iai.00613-10.
- Ashenberg, O., Rozen-Gagnon, K., Laub, M.T., and Keating, A.E. (2011). Determinants of homodimerization specificity in histidine kinases. *J Mol Biol*, 413(1): 222-235. doi: 10.1016/j.jmb.2011.08.011.
- Atamna, H., Brahmabhatt, M., Atamna, W., Shanower, G.A., and Dhahbi, J.M. (2015). ApoHRP-based assay to measure intracellular regulatory heme. *Metallomics*, 7(2): 309-321. doi: 10.1039/c4mt00246f.
- Aussel, L., Barre, F.-X., Aroyo, M., Stasiak, A., Stasiak, A.Z., and Sherratt, D. (2002). FtsK Is a DNA Motor Protein that Activates Chromosome Dimer Resolution by Switching the Catalytic State of the XerC and XerD Recombinases. *Cell*, 108(2): 195-205. doi: 10.1016/S0092-8674(02)00624-4.
- Baena, A., Cabarcas, F., Alvarez-Eraso, K.L.F., Isaza, J.P., Alzate, J.F., and Barrera, L.F. (2019). Differential determinants of virulence in two *Mycobacterium tuberculosis* Colombian clinical isolates of the LAM09 family. *Virulence*, 10(1): 695-710. doi: 10.1080/21505594.2019.1642045.
- Bagg, A., and Neilands, J.B. (1987). Ferric uptake regulation protein acts as a repressor, employing iron (II) as a cofactor to bind the operator of an iron transport operon in *Escherichia coli*. *Biochemistry*, 26(17): 5471-5477. doi: 10.1021/bi00391a039.
- Barupala, D.P., Dzul, S.P., Riggs-Gelasco, P.J., and Stemmler, T.L. (2016). Synthesis, delivery and regulation of eukaryotic heme and Fe-S cluster cofactors. *Arch Biochem Biophys*, 592: 60-75. doi: 10.1016/j.abb.2016.01.010.
- Beale, S.I., Gough, S.P., and Granick, S. (1975). Biosynthesis of delta-aminolevulinic acid from the intact carbon skeleton of glutamic acid in greening barley. *Proc Natl Acad Sci USA*, 72(7): 2719-2723.

- Beckmann, B.M., Castello, A., and Medenbach, J. (2016). The expanding universe of ribonucleoproteins: of novel RNA-binding proteins and unconventional interactions. *Pflügers Arch*, 468(6): 1029-1040.
- Belitsky, B.R., and Sonenshein, A.L. (1999). An enhancer element located downstream of the major glutamate dehydrogenase gene of *Bacillus subtilis*. *Proc Natl Acad Sci USA*, 96(18): 10290-10295. doi: 10.1073/pnas.96.18.10290.
- Beraki, T., Hu, X., Broncel, M., Young, J.C., O'Shaughnessy, W.J., Borek, D., Treeck, M., and Reese, M.L. (2019). Divergent kinase regulates membrane ultrastructure of the *Toxoplasma parasitophorous* vacuole. *Proc Natl Acad Sci USA*, 116(13): 6361-6370. doi: 10.1073/pnas.1816161116.
- Bereswill, S., Greiner, S., van Vliet, A.H., Waidner, B., Fassbinder, F., Schiltz, E., Kusters, J.G., and Kist, M. (2000). Regulation of ferritin-mediated cytoplasmic iron storage by the ferric uptake regulator homolog (Fur) of *Helicobacter pylori*. *J Bacteriol*, 182(21): 5948-5953. doi: 10.1128/jb.182.21.5948-5953.2000.
- Bibb, L.A., King, N.D., Kunkle, C.A., and Schmitt, M.P. (2005). Analysis of a heme-dependent signal transduction system in *Corynebacterium diphtheriae*: deletion of the *chrAS* genes results in heme sensitivity and diminished heme-dependent activation of the *hmuO* promoter. *Infect Immun*, 73(11): 7406-7412. doi: 10.1128/iai.73.11.7406-7412.2005.
- Bibb, L.A., Kunkle, C.A., and Schmitt, M.P. (2007). The ChrA-ChrS and HrrA-HrrS signal transduction systems are required for activation of the *hmuO* promoter and repression of the *hemA* promoter in *Corynebacterium diphtheriae*. *Infect Immun*, 75(5): 2421-2431. doi: 10.1128/iai.01821-06.
- Bibb, L.A., and Schmitt, M.P. (2010). The ABC transporter HrtAB confers resistance to hemin toxicity and is regulated in a hemin-dependent manner by the ChrAS two-component system in *Corynebacterium diphtheriae*. *J Bacteriol*, 192(18): 4606-4617. doi: 10.1128/jb.00525-10.
- Bilitewski, U., Blodgett, J.A.V., Duhme-Klair, A.K., Dallavalle, S., Laschat, S., Routledge, A., and Schobert, R. (2017). Chemical and Biological Aspects of Nutritional Immunity-Perspectives for New Anti-Infectives that Target Iron Uptake Systems. *Angew Chem Int Ed Engl*, 56(46): 14360-14382. doi: 10.1002/anie.201701586.
- Biville, F., Cwerman, H., Létoffé, S., Rossi, M.-S., Drouet, V., Ghigo, J.M., and Wandersman, C. (2004). Haemophore-mediated signalling in *Serratia marcescens*: a new mode of regulation for an extra cytoplasmic function (ECF) sigma factor involved in haem acquisition. *Mol Microbiol*, 53(4): 1267-1277. doi: 10.1111/j.1365-2958.2004.04207.x.
- Blakely, G., Colloms, S., May, G., Burke, M., and Sherratt, D. (1991). *Escherichia coli* XerC recombinase is required for chromosomal segregation at cell division. *New Biol*, 3(8): 789-798.
- Bogomolovas, J., Gasch, A., Simkovic, F., Rigden, D.J., Labeit, S., and Mayans, O. (2014). Titin kinase is an inactive pseudokinase scaffold that supports MuRF1 recruitment to the sarcomeric M-line. *Open Biol*, 4(5): 140041. doi: 10.1098/rsob.140041.
- Boor, K.J. (2006). Bacterial stress responses: what doesn't kill them can make them stronger. *PLoS Biol*, 4(1): e23. doi: 10.1371/journal.pbio.0040023.
- Bott, M., and Brocker, H. (2012). Two-component signal transduction in *Corynebacterium glutamicum* and other corynebacteria: on the way towards stimuli and targets. *Appl Microbiol Biotechnol*, 94(5): 1131-1150. doi: 10.1007/s00253-012-4060-x.
- Bott, M., and Niebisch, A. (2003). The respiratory chain of *Corynebacterium glutamicum*. *J Biotechnol*, 104(1-3): 129-153. doi: 10.1016/s0168-1656(03)00144-5.
- Boudes, M., Sanchez, D., Graille, M., van Tilbeurgh, H., Durand, D., and Quevillon-Cheruel, S. (2014). Structural insights into the dimerization of the response regulator ComE from *Streptococcus pneumoniae*. *Nucleic Acids Res*, 42(8): 5302-5313. doi: 10.1093/nar/gku110.
- Boyd, J., Oza, M.N., and Murphy, J.R. (1990). Molecular cloning and DNA sequence analysis of a diphtheria toxin iron-dependent regulatory element (*dtxR*) from *Corynebacterium diphtheriae*. *Proc Natl Acad Sci USA*, 87(15): 5968-5972. doi: 10.1073/pnas.87.15.5968.
- Brot, N., and Weissbach, H. (1983). Biochemistry and physiological role of methionine sulfoxide residues in proteins. *Arch Biochem Biophys*, 223(1): 271-281. doi: 10.1016/0003-9861(83)90592-1.

- Brune, I., Werner, H., Hüser, A.T., Kalinowski, J., Pühler, A., and Tauch, A. (2006). The DtxR protein acting as dual transcriptional regulator directs a global regulatory network involved in iron metabolism of *Corynebacterium glutamicum*. *BMC Genomics*, 7: 21. doi: 10.1186/1471-2164-7-21.
- Bsat, N., Herbig, A., Casillas-Martinez, L., Setlow, P., and Helmann, J.D. (1998). *Bacillus subtilis* contains multiple Fur homologues: identification of the iron uptake (Fur) and peroxide regulon (PerR) repressors. *Mol Microbiol*, 29(1): 189-198. doi: 10.1046/j.1365-2958.1998.00921.x.
- Budzikiewicz, H., Bössenkamp, A., Taraz, K., Pandey, A., and Meyer, J.-M. (1997). Corynebactin, a Cyclic Catecholate Siderophore from *Corynebacterium glutamicum* ATCC 14067 (*Brevibacterium sp.* DSM 20411). *Z Naturforsch* 52(7-8): 551-554. doi: 10.1515/znc-1997-7-820.
- Buelow, D.R., and Raivio, T.L. (2010). Three (and more) component regulatory systems – auxiliary regulators of bacterial histidine kinases. *Mol Microbiol*, 75(3): 547-566. doi: 10.1111/j.1365-2958.2009.06982.x.
- Buerger, J., Gronenberg, L.S., Genee, H.J., and Sommer, M.O.A. (2019). Wiring cell growth to product formation. *Curr Opin Biotechnol*, 59: 85-92. doi: 10.1016/j.copbio.2019.02.014.
- Burgos, J.M., and Schmitt, M.P. (2016). The ChrSA and HrrSA Two-Component Systems Are Required for Transcriptional Regulation of the hemA Promoter in *Corynebacterium diphtheriae*. *J Bacteriol*, 198(18): 2419-2430. doi: 10.1128/jb.00339-16.
- Cai, Y., Su, M., Ahmad, A., Hu, X., Sang, J., Kong, L., Chen, X., Wang, C., Shuai, J., and Han, A. (2017). Conformational dynamics of the essential sensor histidine kinase Walk. *Acta Crystallogr D Struct Biol*, 73(Pt 10): 793-803. doi: 10.1107/s2059798317013043.
- Camprubi, E., Jordan, S.F., Vasiliadou, R., and Lane, N. (2017). Iron catalysis at the origin of life. *IUBMB Life*, 69(6): 373-381. doi: 10.1002/iub.1632.
- Cao, Y., Yao, Z., Sarkar, D., Lawrence, M., Sanchez, G.J., Parker, M.H., MacQuarrie, K.L., Davison, J., Morgan, M.T., Ruzzo, W.L., *et al.* (2010). Genome-wide MyoD binding in skeletal muscle cells: a potential for broad cellular reprogramming. *Dev Cell*, 18(4): 662-674. doi: 10.1016/j.devcel.2010.02.014.
- Carmany, D.O., Hollingsworth, K., and McCleary, W.R. (2003). Genetic and biochemical studies of phosphatase activity of PhoR. *J Bacteriol*, 185(3): 1112-1115. doi: 10.1128/jb.185.3.1112-1115.2003.
- Casas-Pastor, D., Müller, R.R., Jaenicke, S., Brinkrolf, K., Becker, A., Buttner, M.J., Gross, C.A., Mascher, T., Goesmann, A., and Fritz, G. (2021). Expansion and re-classification of the extracytoplasmic function (ECF) σ factor family. *Nucleic Acids Res*, 49(2): 986-1005. doi: 10.1093/nar/gkaa1229.
- Casino, P., Rubio, V., and Marina, A. (2009). Structural insight into partner specificity and phosphoryl transfer in two-component signal transduction. *Cell*, 139(2): 325-336. doi: 10.1016/j.cell.2009.08.032.
- Catrileo, D., Acuña-Fontecilla, A., and Godoy, L. (2020). Adaptive Laboratory Evolution of Native *Torulaspota delbrueckii* YCPUC10 With Enhanced Ethanol Resistance and Evaluation in Co-inoculated Fermentation. *Front Microbiol*, 11: 595023. doi: 10.3389/fmicb.2020.595023.
- Chandrangsu, P., Rensing, C., and Helmann, J.D. (2017). Metal homeostasis and resistance in bacteria. *Nat Rev Microbiol*, 15(6): 338-350. doi: 10.1038/nrmicro.2017.15.
- Chiabrando, D., Vinchi, F., Fiorito, V., Mercurio, S., and Tolosano, E. (2014). Heme in pathophysiology: a matter of scavenging, metabolism and trafficking across cell membranes. *Front Pharmacol*, 5. doi: 10.3389/fphar.2014.00061.
- Choby, J.E., and Skaar, E.P. (2016). Heme Synthesis and Acquisition in Bacterial Pathogens. *J Mol Biol*, 428(17): 3408-3428. doi: 10.1016/j.jmb.2016.03.018.
- Choi, K.R., Yu, H.E., Lee, H., and Lee, S.Y. (2022). Improved production of heme using metabolically engineered *Escherichia coli*. *Biotechnol Bioeng*, 119(11): 3178-3193. doi: 10.1002/bit.28194.
- Clifton, B.E., Kaczmarek, J.A., Carr, P.D., Gerth, M.L., Tokuriki, N., and Jackson, C.J. (2018). Evolution of cyclohexadienyl dehydratase from an ancestral solute-binding protein. *Nat Chem Biol*, 14(6): 542-547. doi: 10.1038/s41589-018-0043-2.
- Contreras, H., Chim, N., Credali, A., and Goulding, C.W. (2014). Heme uptake in bacterial pathogens. *Curr Opin Chem Biol*, 19: 34-41. doi: 10.1016/j.cbpa.2013.12.014.

- Cornelis, P., Wei, Q., Andrews, S.C., and Vinckx, T. (2011). Iron homeostasis and management of oxidative stress response in bacteria. *Metallomics*, 3(6): 540-549. doi: 10.1039/c1mt00022e.
- Czaplewski, L.G., North, A.K., Smith, M.C.M., Baumberg, S., and Stockley, P.G. (1992). Purification and initial characterization of AhrC: the regulator of arginine metabolism genes in *Bacillus subtilis*. *Mol Microbiol*, 6(2): 267-275. doi: 10.1111/j.1365-2958.1992.tb02008.x.
- Dailey, H.A., Dailey, T.A., Gerdes, S., Jahn, D., Jahn, M., O'Brian, M.R., and Warren, M.J. (2017). Prokaryotic Heme Biosynthesis: Multiple Pathways to a Common Essential Product. *Microbiol Mol Biol Rev*, 81(1): e00048-00016. doi: 10.1128/MMBR.00048-16.
- Dainese, R., Gardeux, V., Llimos, G., Alpern, D., Jiang, J.Y., Meireles-Filho, A.C.A., and Deplancke, B. (2020). A parallelized, automated platform enabling individual or sequential ChIP of histone marks and transcription factors. *Proc Natl Acad Sci USA*, 117(24): 13828-13838. doi: 10.1073/pnas.1913261117.
- Darwin, C. (1872). Darwinism. *Ind Med Gaz*, 7(2): 47.
- Datta, V., Siddharthan, R., and Krishna, S. (2018). Detection of cooperatively bound transcription factor pairs using ChIP-seq peak intensities and expectation maximization. *PLoS One*, 13(7): e0199771. doi: 10.1371/journal.pone.0199771.
- Dawson, J.H., Andersson, L.A., and Sono, M. (1982). Spectroscopic investigations of ferric cytochrome P-450-CAM ligand complexes. Identification of the ligand trans to cysteinate in the native enzyme. *J Biol Chem*, 257(7): 3606-3617.
- Defosse, T.A., Sharma, A., Mondal, A.K., Dugé de Bernonville, T., Latgé, J.-P., Calderone, R., Giglioli-Guivarc'h, N., Courdavault, V., Clastre, M., and Papon, N. (2015). Hybrid histidine kinases in pathogenic fungi. *Mol Microbiol*, 95(6): 914-924. doi: 10.1111/mmi.12911.
- Delany, I., Rappuoli, R., and Scarlato, V. (2004). Fur functions as an activator and as a repressor of putative virulence genes in *Neisseria meningitidis*. *Mol Microbiol*, 52(4): 1081-1090. doi: 10.1111/j.1365-2958.2004.04030.x.
- Dent, A.T., Mouriño, S., Huang, W., and Wilks, A. (2019). Post-transcriptional regulation of the *Pseudomonas aeruginosa* heme assimilation system (Has) fine-tunes extracellular heme sensing. *J Biol Chem*, 294(8): 2771-2785. doi: 10.1074/jbc.RA118.006185.
- Dent, A.T., and Wilks, A. (2020). Contributions of the heme coordinating ligands of the *Pseudomonas aeruginosa* outer membrane receptor HasR to extracellular heme sensing and transport. *J Biol Chem*, 295(30): 10456-10467. doi: 10.1074/jbc.RA120.014081.
- Dertz, E.A., Stintzi, A., and Raymond, K.N. (2006). Siderophore-mediated iron transport in *Bacillus subtilis* and *Corynebacterium glutamicum*. *J Biol Inorg Chem*, 11(8): 1087-1097. doi: 10.1007/s00775-006-0151-4.
- Dioum, E.M., Rutter, J., Tuckerman, J.R., Gonzalez, G., Gilles-Gonzalez, M.A., and McKnight, S.L. (2002). NPAS2: a gas-responsive transcription factor. *Science*, 298(5602): 2385-2387. doi: 10.1126/science.1078456.
- Dlouhy, A.C., and Outten, C.E. (2013). The iron metallome in eukaryotic organisms. *Met Ions Life Sci*, 12: 241-278. doi: 10.1007/978-94-007-5561-1_8.
- Dragosits, M., and Mattanovich, D. (2013). Adaptive laboratory evolution – principles and applications for biotechnology. *Microb Cell Fact*, 12(1): 64. doi: 10.1186/1475-2859-12-64.
- Drazek, E.S., Hammack, C.A., and Schmitt, M.P. (2000). *Corynebacterium diphtheriae* genes required for acquisition of iron from haemin and haemoglobin are homologous to ABC haemin transporters. *Mol Microbiol*, 36(1): 68-84. doi: 10.1046/j.1365-2958.2000.01818.x.
- Dubey, B.N., Agustoni, E., Böhm, R., Kaczmarczyk, A., Mangia, F., von Arx, C., Jenal, U., Hiller, S., Plaza-Menacho, I., and Schirmer, T. (2020). Hybrid histidine kinase activation by cyclic di-GMP-mediated domain liberation. *Proc Natl Acad Sci USA*, 117(2): 1000-1008. doi: 10.1073/pnas.1911427117.
- Dutta, R., Qin, L., and Inouye, M. (1999). Histidine kinases: diversity of domain organization. *Mol Microbiol*, 34(4): 633-640. doi: 10.1046/j.1365-2958.1999.01646.x.
- Eggeling, L., and Sahm, H. (2001). The cell wall barrier of *Corynebacterium glutamicum* and amino acid efflux. *J Biosci Bioeng*, 92(3): 201-213. doi: 10.1016/S1389-1723(01)80251-6.

- Eguchi, Y., Ishii, E., Hata, K., and Utsumi, R. (2011). Regulation of Acid Resistance by Connectors of Two-Component Signal Transduction Systems in *Escherichia coli*. *J Bacteriol*, 193(5): 1222-1228. doi: 10.1128/JB.01124-10.
- Eguchi, Y., Itou, J., Yamane, M., Demizu, R., Yamato, F., Okada, A., Mori, H., Kato, A., and Utsumi, R. (2007). B1500, a small membrane protein, connects the two-component systems EvgS/EvgA and PhoQ/PhoP in *Escherichia coli*. *Proc Natl Acad Sci USA*, 104(47): 18712-18717. doi: 10.1073/pnas.0705768104.
- Erdmann, K., Grosser, N., and Schroder, H. (2005). L-methionine reduces oxidant stress in endothelial cells: role of heme oxygenase-1, ferritin, and nitric oxide. *Aaps j*, 7(1): E195-200. doi: 10.1208/aapsj070118.
- Escorcia-Rodríguez, J.M., Tauch, A., and Freyre-González, J.A. (2021). *Corynebacterium glutamicum* Regulation beyond Transcription: Organizing Principles and Reconstruction of an Extended Regulatory Network Incorporating Regulations Mediated by Small RNA and Protein-Protein Interactions. *Microorganisms*, 9(7): 1395. doi: 10.3390/microorganisms9071395.
- Espinas, N.A., Kobayashi, K., Takahashi, S., Mochizuki, N., and Masuda, T. (2012). Evaluation of unbound free heme in plant cells by differential acetone extraction. *Plant Cell Physiol*, 53(7): 1344-1354. doi: 10.1093/pcp/pcs067.
- Eyers, P.A., and Murphy, J.M. (2016). The evolving world of pseudoenzymes: proteins, prejudice and zombies. *BMC Biol*, 14(1): 98. doi: 10.1186/s12915-016-0322-x.
- Faust, K., and Raes, J. (2012). Microbial interactions: from networks to models. *Nat Rev Microbiol*, 10(8): 538-550. doi: 10.1038/nrmicro2832.
- Fenton, H.J.H. (1894). Oxidation of tartaric acid in presence of iron. *J Chem Soc, Trans*, 65: 899-910.
- Fernandez, A., Lechardeur, D., Derré-Bobillot, A., Couvé, E., Gaudu, P., and Gruss, A. (2010). Two coregulated efflux transporters modulate intracellular heme and protoporphyrin IX availability in *Streptococcus agalactiae*. *PLoS Pathog*, 6(4): e1000860. doi: 10.1371/journal.ppat.1000860.
- Fontenot, C.R., Tasnim, H., Valdes, K.A., Popescu, C.V., and Ding, H. (2020). Ferric uptake regulator (Fur) reversibly binds a [2Fe-2S] cluster to sense intracellular iron homeostasis in *Escherichia coli*. *J Biol Chem*, 295(46): 15454-15463. doi: 10.1074/jbc.RA120.014814.
- Francis, V.I., and Porter, S.L. (2019). Multikinase Networks: Two-Component Signaling Networks Integrating Multiple Stimuli. *Annu Rev Microbiol*, 73: 199-223. doi: 10.1146/annurev-micro-020518-115846.
- Francis, V.I., Waters, E.M., Finton-James, S.E., Gori, A., Kadioglu, A., Brown, A.R., and Porter, S.L. (2018). Multiple communication mechanisms between sensor kinases are crucial for virulence in *Pseudomonas aeruginosa*. *Nat Commun*, 9(1): 2219. doi: 10.1038/s41467-018-04640-8.
- Fraser, R., Davis, S.C., and O'Reilly Brown, P. (2017). Secretion of heme-containing polypeptides. US20170342131A1. (Redwood City, CA (US): Impossible Foods Inc).
- Freiherr von Boeselager, R., Pfeifer, E., and Frunzke, J. (2018). Cytometry meets next-generation sequencing - RNA-Seq of sorted subpopulations reveals regional replication and iron-triggered prophage induction in *Corynebacterium glutamicum*. *Sci Rep*, 8(1): 14856. doi: 10.1038/s41598-018-32997-9.
- Frunzke, J., Bramkamp, M., Schweitzer, J.E., and Bott, M. (2008). Population Heterogeneity in *Corynebacterium glutamicum* ATCC 13032 caused by prophage CGP3. *J Bacteriol*, 190(14): 5111-5119. doi: 10.1128/jb.00310-08.
- Frunzke, J., Gätgens, C., Bocker, M., and Bott, M. (2011). Control of heme homeostasis in *Corynebacterium glutamicum* by the two-component system HrrSA. *J Bacteriol*, 193(5): 1212-1221. doi: 10.1128/jb.01130-10.
- Galagan, J., Lyubetskaya, A., and Gomes, A. (2013a). ChIP-Seq and the complexity of bacterial transcriptional regulation. *Curr Top Microbiol Immunol*, 363: 43-68. doi: 10.1007/82_2012_257.
- Galagan, J.E., Minch, K., Peterson, M., Lyubetskaya, A., Azizi, E., Sweet, L., Gomes, A., Rustad, T., Dolganov, G., Glotova, I., et al. (2013b). The *Mycobacterium tuberculosis* regulatory network and hypoxia. *Nature*, 499(7457): 178-183. doi: 10.1038/nature12337.

- Gallio, A.E., Fung, S.S., Cammack-Najera, A., Hudson, A.J., and Raven, E.L. (2021). Understanding the Logistics for the Distribution of Heme in Cells. *JACS Au*, 1(10): 1541-1555. doi: 10.1021/jacsau.1c00288.
- Galperin, M.Y. (2006). Structural classification of bacterial response regulators: diversity of output domains and domain combinations. *J Bacteriol*, 188(12): 4169-4182. doi: 10.1128/jb.01887-05.
- Galperin, M.Y., Nikolskaya, A.N., and Koonin, E.V. (2001). Novel domains of the prokaryotic two-component signal transduction systems. *FEMS Microbiol Lett*, 203(1): 11-21. doi: 10.1111/j.1574-6968.2001.tb10814.x.
- Gao, R., Mack, T.R., and Stock, A.M. (2007). Bacterial response regulators: versatile regulatory strategies from common domains. *Trends Biochem Sci*, 32(5): 225-234. doi: 10.1016/j.tibs.2007.03.002.
- Gaspar, W.C., Marinov, G.K., Pauli-Behn, F., Scott, M.T., Newberry, K., DeSalvo, G., Ou, S., Myers, R.M., Vielmetter, J., and Wold, B.J. (2014). Fully automated high-throughput chromatin immunoprecipitation for ChIP-seq: Identifying ChIP-quality p300 monoclonal antibodies. *Sci Rep*, 4(1): 5152. doi: 10.1038/srep05152.
- Gerken, H., Charlson, E.S., Cicirelli, E.M., Kenney, L.J., and Misra, R. (2009). MzrA: a novel modulator of the EnvZ/OmpR two-component regulon. *Mol Microbiol*, 72(6): 1408-1422. doi: 10.1111/j.1365-2958.2009.06728.x.
- Gilmour, D.S., and Lis, J.T. (1984). Detecting protein-DNA interactions in vivo: distribution of RNA polymerase on specific bacterial genes. *Proc Natl Acad Sci USA*, 81(14): 4275-4279. doi: 10.1073/pnas.81.14.4275.
- Gilmour, D.S., and Lis, J.T. (1985). In vivo interactions of RNA polymerase II with genes of *Drosophila melanogaster*. *Mol Cell Biol*, 5(8): 2009-2018. doi: 10.1128/mcb.5.8.2009-2018.1985.
- Gilmour, D.S., and Lis, J.T. (1986). RNA polymerase II interacts with the promoter region of the noninduced hsp70 gene in *Drosophila melanogaster* cells. *Mol Cell Biol*, 6(11): 3984-3989. doi: 10.1128/mcb.6.11.3984-3989.1986.
- Girvan, H.M., and Munro, A.W. (2013). Heme sensor proteins. *J Biol Chem*, 288(19): 13194-13203. doi: 10.1074/jbc.R112.422642.
- Goodman, A.L., Merighi, M., Hyodo, M., Ventre, I., Filloux, A., and Lory, S. (2009). Direct interaction between sensor kinase proteins mediates acute and chronic disease phenotypes in a bacterial pathogen. *Genes Dev*, 23(2): 249-259. doi: 10.1101/gad.1739009.
- Granick, S., Sinclair, P., Sassa, S., and Grieninger, G. (1975). Effects by heme, insulin, and serum albumin on heme and protein synthesis in chick embryo liver cells cultured in a chemically defined medium, and a spectrophotometric assay for porphyrin composition. *J Biol Chem*, 250(24): 9215-9225. doi: 10.1016/S0021-9258(19)40633-9.
- Griffith, K.L., and Wolf, R.E., Jr. (2002). Measuring beta-galactosidase activity in bacteria: cell growth, permeabilization, and enzyme assays in 96-well arrays. *Biochem Biophys Res Commun*, 290(1): 397-402. doi: 10.1006/bbrc.2001.6152.
- Grindley, N.D.F., Whiteson, K.L., and Rice, P.A. (2006). Mechanisms of Site-Specific Recombination. *Annu Rev Biochem*, 75(1): 567-605. doi: 10.1146/annurev.biochem.73.011303.073908.
- Gruer, M.J., and Guest, J.R. (1994). Two genetically-distinct and differentially-regulated aconitases (AcnA and AcnB) in *Escherichia coli*. *Microbiology (Reading)*, 140(10): 2531-2541. doi: 10.1099/00221287-140-10-2531.
- Har, J.R.G., Agee, A., Bennett, R.K., Papoutsakis, E.T., and Antoniewicz, M.R. (2021). Adaptive laboratory evolution of methylotrophic *Escherichia coli* enables synthesis of all amino acids from methanol-derived carbon. *Appl Microbiol Biotechnol*, 105(2): 869-876. doi: 10.1007/s00253-020-11058-0.
- Helfrich, S., Pfeifer, E., Krämer, C., Sachs, C.C., Wiechert, W., Kohlheyer, D., Nöh, K., and Frunzke, J. (2015). Live cell imaging of SOS and prophage dynamics in isogenic bacterial populations. *Mol Microbiol*, 98(4): 636-650. doi: 10.1111/mmi.13147.
- Helmann, J.D. (2002). The extracytoplasmic function (ECF) sigma factors. *Adv Microb Physiol*, 46: 47-110. doi: 10.1016/s0065-2911(02)46002-x.

- Hentschel, E., Mack, C., Gätgens, C., Bott, M., Brocker, M., and Frunzke, J. (2014). Phosphatase activity of the histidine kinases ensures pathway specificity of the ChrSA and HrrSA two-component systems in *Corynebacterium glutamicum*. *Mol Microbiol*, 92(6): 1326-1342. doi: 10.1111/mmi.12633.
- Heyer, A., Gätgens, C., Hentschel, E., Kalinowski, J., Bott, M., and Frunzke, J. (2012). The two-component system ChrSA is crucial for haem tolerance and interferes with HrrSA in haem-dependent gene regulation in *Corynebacterium glutamicum*. *Microbiology (Reading)*, 158(12): 3020-3031. doi: 10.1099/mic.0.062638-0.
- Hildebrand, J.M., Tanzer, M.C., Lucet, I.S., Young, S.N., Spall, S.K., Sharma, P., Pierotti, C., Garnier, J.M., Dobson, R.C., Webb, A.I., *et al.* (2014). Activation of the pseudokinase MLKL unleashes the four-helix bundle domain to induce membrane localization and necroptotic cell death. *Proc Natl Acad Sci USA*, 111(42): 15072-15077. doi: 10.1073/pnas.1408987111.
- Hillion, M., Imber, M., Pedre, B., Bernhardt, J., Saleh, M., Loi, V.V., Maaß, S., Becher, D., Astolfi Rosado, L., Adrian, L., *et al.* (2017). The glyceraldehyde-3-phosphate dehydrogenase GapDH of *Corynebacterium diphtheriae* is redox-controlled by protein S-mycothiolation under oxidative stress. *Sci Rep*, 7(1): 5020. doi: 10.1038/s41598-017-05206-2.
- Holmqvist, E., and Vogel, J. (2018). RNA-binding proteins in bacteria. *Nat Rev Microbiol*, 16(10): 601-615. doi: 10.1038/s41579-018-0049-5.
- Hong, E.J., Jeong, H., Lee, D.S., Kim, Y., and Lee, H.S. (2019). The *ahpD* gene of *Corynebacterium glutamicum* plays an important role in hydrogen peroxide-induced oxidative stress response. *J Biochem*, 165(2): 197-204. doi: 10.1093/jb/mvy097.
- Horsburgh, M.J., Wharton, S.J., Karavolos, M., and Foster, S.J. (2002). Manganese: elemental defence for a life with oxygen. *Trends Microbiol*, 10(11): 496-501. doi: 10.1016/S0966-842X(02)02462-9.
- Hughes, M.N., and Poole, R.K. (1989). Metals and micro-organisms. *Lancet*, 175(4519): 1014-1015. doi: 10.1016/S0140-6736(01)14139-5.
- Huynh, T.N., Noriega, C.E., and Stewart, V. (2010). Conserved mechanism for sensor phosphatase control of two-component signaling revealed in the nitrate sensor NarX. *Proc Natl Acad Sci USA*, 107(49): 21140-21145. doi: 10.1073/pnas.1013081107.
- Huynh, T.N., and Stewart, V. (2011). Negative control in two-component signal transduction by transmitter phosphatase activity. *Mol Microbiol*, 82(2): 275-286. doi: 10.1111/j.1365-2958.2011.07829.x.
- Ibarra-Arellano, M.A., Campos-González, A.I., Treviño-Quintanilla, L.G., Tauch, A., and Freyre-González, J.A. (2016). Abasy Atlas: a comprehensive inventory of systems, global network properties and systems-level elements across bacteria. *Database*, 2016. doi: 10.1093/database/baw089.
- Ikeda, M., and Nakagawa, S. (2003). The *Corynebacterium glutamicum* genome: features and impacts on biotechnological processes. *Appl Microbiol Biotechnol*, 62(2-3): 99-109. doi: 10.1007/s00253-003-1328-1.
- Iniesta, A.A., Hillson, N.J., and Shapiro, L. (2010). Cell pole-specific activation of a critical bacterial cell cycle kinase. *Proc Natl Acad Sci USA*, 107(15): 7012-7017. doi: 10.1073/pnas.1001767107.
- Ishchuk, O.P., Frost, A.T., Muñiz-Paredes, F., Matsumoto, S., Laforge, N., Eriksson, N.L., Martínez, J.L., and Petranovic, D. (2021). Improved production of human hemoglobin in yeast by engineering hemoglobin degradation. *Metab Eng*, 66: 259-267. doi: 10.1016/j.ymben.2021.05.002.
- Ito, Y., Nakagawa, S., Komagata, A., Ikeda-Saito, M., Shiro, Y., and Nakamura, H. (2009). Heme-dependent autophosphorylation of a heme sensor kinase, ChrS, from *Corynebacterium diphtheriae* reconstituted in proteoliposomes. *FEBS Lett*, 583(13): 2244-2248. doi: 10.1016/j.febslet.2009.06.001.
- Jacob-Dubuisson, F., Mechaly, A., Betton, J.-M., and Antoine, R. (2018). Structural insights into the signalling mechanisms of two-component systems. *Nat Rev Microbiol*, 16(10): 585-593. doi: 10.1038/s41579-018-0055-7.
- Jiang, M., Shao, W., Perego, M., and Hoch, J.A. (2000). Multiple histidine kinases regulate entry into stationary phase and sporulation in *Bacillus subtilis*. *Mol Microbiol*, 38(3): 535-542. doi: 10.1046/j.1365-2958.2000.02148.x.

- Jin, Z., Li, J., Ni, L., Zhang, R., Xia, A., and Jin, F. (2018). Conditional privatization of a public siderophore enables *Pseudomonas aeruginosa* to resist cheater invasion. *Nat Commun*, 9(1): 1383. doi: 10.1038/s41467-018-03791-y.
- Johnson, D.S., Mortazavi, A., Myers, R.M., and Wold, B. (2007). Genome-wide mapping of in vivo protein-DNA interactions. *Science*, 316(5830): 1497-1502. doi: 10.1126/science.1141319.
- Jumper, J., Evans, R., Pritzel, A., Green, T., Figurnov, M., Ronneberger, O., Tunyasuvunakool, K., Bates, R., Žídek, A., Potapenko, A., et al. (2021). Highly accurate protein structure prediction with AlphaFold. *Nature*, 596(7873): 583-589. doi: 10.1038/s41586-021-03819-2.
- Kalinowski, J., Bathe, B., Bartels, D., Bischoff, N., Bott, M., Burkovski, A., Dusch, N., Eggeling, L., Eikmanns, B.J., Gaigalat, L., et al. (2003). The complete *Corynebacterium glutamicum* ATCC 13032 genome sequence and its impact on the production of L-aspartate-derived amino acids and vitamins. *J Biotechnol*, 104(1-3): 5-25. doi: 10.1016/s0168-1656(03)00154-8.
- Kaltenbach, M., Burke, J.R., Dindo, M., Pabis, A., Munsberg, F.S., Rabin, A., Kamerlin, S.C.L., Noel, J.P., and Tawfik, D.S. (2018). Evolution of chalcone isomerase from a noncatalytic ancestor. *Nat Chem Biol*, 14(6): 548-555. doi: 10.1038/s41589-018-0042-3.
- Kamps, A., Achebach, S., Fedtke, I., Unden, G., and Götz, F. (2004). Staphylococcal NreB: an O₂-sensing histidine protein kinase with an O₂-labile iron-sulphur cluster of the FNR type. *Mol Microbiol*, 52(3): 713-723. doi: 10.1111/j.1365-2958.2004.04024.x.
- Kensy, F., Zang, E., Faulhammer, C., Tan, R.-K., and Büchs, J. (2009). Validation of a high-throughput fermentation system based on online monitoring of biomass and fluorescence in continuously shaken microtiter plates. *Microb Cell Fact*, 8(1): 31. doi: 10.1186/1475-2859-8-31.
- Keppel, M., Davoudi, E., Gätgens, C., and Frunzke, J. (2018). Membrane Topology and Heme Binding of the Histidine Kinases HrrS and ChrS in *Corynebacterium glutamicum*. *Front Microbiol*, 9: 183. doi: 10.3389/fmicb.2018.00183.
- Keppel, M., Hünnefeld, M., Filipchuk, A., Viets, U., Davoudi, C.-F., Krüger, A., Mack, C., Pfeifer, E., Polen, T., Baumgart, M., et al. (2020). HrrSA orchestrates a systemic response to heme and determines prioritization of terminal cytochrome oxidase expression. *Nucleic Acids Res*, 48(12): 6547-6562. doi: 10.1093/nar/gkaa415.
- Keppel, M., Piepenbreier, H., Gätgens, C., Fritz, G., and Frunzke, J. (2019). Toxic but tasty - temporal dynamics and network architecture of heme-responsive two-component signaling in *Corynebacterium glutamicum*. *Mol Microbiol*, 111(5): 1367-1381. doi: 10.1111/mmi.14226.
- Kim, T.H., Kim, H.J., Park, J.S., Kim, Y., Kim, P., and Lee, H.S. (2005). Functional analysis of *sigH* expression in *Corynebacterium glutamicum*. *Biochem Biophys Res Commun*, 331(4): 1542-1547. doi: 10.1016/j.bbrc.2005.04.073.
- Knijnenburg, T.A., de Winde, J.H., Daran, J.M., Daran-Lapujade, P., Pronk, J.T., Reinders, M.J., and Wessels, L.F. (2007). Exploiting combinatorial cultivation conditions to infer transcriptional regulation. *BMC Genomics*, 8: 25. doi: 10.1186/1471-2164-8-25.
- Ko, Y.J., Kim, M., You, S.K., Shin, S.K., Chang, J., Choi, H.J., Jeong, W.Y., Lee, M.E., Hwang, D.H., and Han, S.O. (2021). Animal-free heme production for artificial meat in *Corynebacterium glutamicum* via systems metabolic and membrane engineering. *Metab Eng*, 66: 217-228. doi: 10.1016/j.ymben.2021.04.013.
- Kou, X., Liu, Y., Li, C., Liu, M., and Jiang, L. (2018). Dimerization and Conformational Exchanges of the Receiver Domain of Response Regulator PhoB from *Escherichia coli*. *J Phys Chem B*, 122(22): 5749-5757. doi: 10.1021/acs.jpcc.8b01034.
- Krell, T., Lacal, J., Busch, A., Silva-Jiménez, H., Guazzaroni, M.E., and Ramos, J.L. (2010). Bacterial sensor kinases: diversity in the recognition of environmental signals. *Annu Rev Microbiol*, 64: 539-559. doi: 10.1146/annurev.micro.112408.134054.
- Krüger, A., and Frunzke, J. (2022). A pseudokinase version of the histidine kinase ChrS promotes high heme tolerance of *Corynebacterium glutamicum*. *Front Microbiol*, 13: 997448. doi: 10.3389/fmicb.2022.997448
- Krüger, A., Keppel, M., Sharma, V., and Frunzke, J. (2022). The diversity of heme sensor systems - heme-responsive transcriptional regulation mediated by transient heme protein interactions. *FEMS Microbiol Rev*, 46(3): fuac002. doi: 10.1093/femsre/fuac002.

- Krüger, A., Viets, U., Filipchuk, A., and Frunzke, J. (to be submitted). A genome-wide analysis of the interconnection of iron- and heme-dependent regulatory networks governed by DtxR and HrrA in *Corynebacterium glutamicum*.
- Kühl, T., Sahoo, N., Nikolajski, M., Schlott, B., Heinemann, S.H., and Imhof, D. (2011). Determination of Hemin-Binding Characteristics of Proteins by a Combinatorial Peptide Library Approach. *ChemBioChem*, 12(18): 2846-2855. doi: 10.1002/cbic.201100556.
- Kühl, T., Wißbrock, A., Goradia, N., Sahoo, N., Galler, K., Neugebauer, U., Popp, J., Heinemann, S.H., Ohlenschläger, O., and Imhof, D. (2013). Analysis of Fe(III) heme binding to cysteine-containing heme-regulatory motifs in proteins. *ACS Chem Biol*, 8(8): 1785-1793. doi: 10.1021/cb400317x.
- Kumar, S., and Bandyopadhyay, U. (2005). Free heme toxicity and its detoxification systems in human. *Toxicol Lett*, 157(3): 175-188. doi: 10.1016/j.toxlet.2005.03.004.
- Kung, J.E., and Jura, N. (2019). Prospects for pharmacological targeting of pseudokinases. *Nat Rev Drug Discov*, 18(7): 501-526. doi: 10.1038/s41573-019-0018-3.
- Kunkle, C.A., and Schmitt, M.P. (2003). Analysis of the *Corynebacterium diphtheriae* DtxR regulon: identification of a putative siderophore synthesis and transport system that is similar to the *Yersinia* high-pathogenicity island-encoded yersiniabactin synthesis and uptake system. *J Bacteriol*, 185(23): 6826-6840. doi: 10.1128/jb.185.23.6826-6840.2003.
- Kunkle, C.A., and Schmitt, M.P. (2005). Analysis of a DtxR-regulated iron transport and siderophore biosynthesis gene cluster in *Corynebacterium diphtheriae*. *J Bacteriol*, 187(2): 422-433. doi: 10.1128/jb.187.2.422-433.2005.
- Kurthkoti, K., Tare, P., Paitchowdhury, R., Gowthami, V.N., Garcia, M.J., Colangeli, R., Chatterji, D., Nagaraja, V., and Rodriguez, G.M. (2015). The mycobacterial iron-dependent regulator IdeR induces ferritin (*bfrB*) by alleviating Lsr2 repression. *Mol Microbiol*, 98(5): 864-877. doi: 10.1111/mmi.13166.
- Kwon, A., Scott, S., Taujale, R., Yeung, W., Kochut, K.J., Evers, P.A., and Kannan, N. (2019). Tracing the origin and evolution of pseudokinases across the tree of life. *Sci Signal*, 12(578): eaav3810. doi: 10.1126/scisignal.aav3810.
- Kwon, S.J., de Boer, A.L., Petri, R., and Schmidt-Dannert, C. (2003). High-level production of porphyrins in metabolically engineered *Escherichia coli*: systematic extension of a pathway assembled from overexpressed genes involved in heme biosynthesis. *Appl Environ Microbiol*, 69(8): 4875-4883. doi: 10.1128/aem.69.8.4875-4883.2003.
- Lal, S., Comer, J.M., Konduri, P.C., Shah, A., Wang, T., Lewis, A., Shoffner, G., Guo, F., and Zhang, L. (2018). Heme promotes transcriptional and demethylase activities of Gis1, a member of the histone demethylase JMJD2/KDM4 family. *Nucleic Acids Res*, 46(1): 215-228. doi: 10.1093/nar/gkx1051.
- Lange, S.M., Nelen, M.I., Cohen, P., and Kulathu, Y. (2021). Dimeric Structure of the Pseudokinase IRAK3 Suggests an Allosteric Mechanism for Negative Regulation. *Structure*, 29(3): 238-251.e234. doi: 10.1016/j.str.2020.11.004.
- Lansky, I.B., Lukat-Rodgers, G.S., Block, D., Rodgers, K.R., Ratliff, M., and Wilks, A. (2006). The cytoplasmic heme-binding protein (PhuS) from the heme uptake system of *Pseudomonas aeruginosa* is an intracellular heme-trafficking protein to the delta-regioselective heme oxygenase. *J Biol Chem*, 281(19): 13652-13662. doi: 10.1074/jbc.M600824200.
- Lathrop, J.T., and Timko, M.P. (1993). Regulation by Heme of Mitochondrial Protein Transport Through a Conserved Amino Acid Motif. *Science*, 259(5094): 522-525. doi: 10.1126/science.8424176.
- Laub, M.T., and Goulian, M. (2007). Specificity in two-component signal transduction pathways. *Annu Rev Genet*, 41: 121-145. doi: 10.1146/annurev.genet.41.042007.170548.
- Lavoie, H., Li, J.J., Thevakumaran, N., Therrien, M., and Sicheri, F. (2014). Dimerization-induced allostery in protein kinase regulation. *Trends Biochem Sci*, 39(10): 475-486. doi: 10.1016/j.tibs.2014.08.004.
- Lavoie, H., Sahmi, M., Maisonneuve, P., Marullo, S.A., Thevakumaran, N., Jin, T., Kurinov, I., Sicheri, F., and Therrien, M. (2018). MEK drives BRAF activation through allosteric control of KSR proteins. *Nature*, 554(7693): 549-553. doi: 10.1038/nature25478.

- Layer, G. (2021). Heme biosynthesis in prokaryotes. *Biochim Biophys Acta Mol Cell Res*, 1868(1): 118861. doi: 10.1016/j.bbamcr.2020.118861.
- Layer, G., Reichelt, J., Jahn, D., and Heinz, D.W. (2010). Structure and function of enzymes in heme biosynthesis. *Protein Sci*, 19(6): 1137-1161. doi: 10.1002/pro.405.
- Lee, S.-Y., Cho, H.S., Pelton, J.G., Yan, D., Henderson, R.K., King, D.S., Huang, L.-s., Kustu, S., Berry, E.A., and Wemmer, D.E. (2001). Crystal structure of an activated response regulator bound to its target. *Nat Struct Biol*, 8(1): 52-56. doi: 10.1038/83053.
- Levine, R.L., Mosoni, L., Berlett, B.S., and Stadtman, E.R. (1996). Methionine residues as endogenous antioxidants in proteins. *Proc Natl Acad Sci USA*, 93(26): 15036-15040. doi: 10.1073/pnas.93.26.15036.
- Li, J., Swanson, R.V., Simon, M.I., and Weis, R.M. (1995). The response regulators CheB and CheY exhibit competitive binding to the kinase CheA. *Biochemistry*, 34(45): 14626-14636. doi: 10.1021/bi00045a003.
- Li, T., Bonkovsky, H.L., and Guo, J.-t. (2011). Structural analysis of heme proteins: implications for design and prediction. *BMC Struct Biol*, 11(1): 13. doi: 10.1186/1472-6807-11-13.
- Liang, L., Zhu, Y., Li, J., Zeng, J., and Wu, L. (2022). ALKBH5-mediated m6A modification of circCCDC134 facilitates cervical cancer metastasis by enhancing HIF1A transcription. *J Exp Clin Cancer Res*, 41(1): 261. doi: 10.1186/s13046-022-02462-7.
- Lindner, S.N., Petrov, D.P., Hagemann, C.T., Henrich, A., Krämer, R., Eikmanns, B.J., Wendisch, V.F., and Seibold, G.M. (2013). Phosphotransferase system-mediated glucose uptake is repressed in phosphoglucosomerase-deficient *Corynebacterium glutamicum* strains. *Appl Environ Microbiol*, 79(8): 2588-2595. doi: 10.1128/aem.03231-12.
- Litwin, C.M., and Calderwood, S.B. (1993). Role of iron in regulation of virulence genes. *Clin Microbiol Rev*, 6(2): 137-149. doi: 10.1128/cmr.6.2.137.
- Liu, M., Ferrandez, Y., Bouhsira, E., Monteil, M., Franc, M., Boulouis, H.J., and Biville, F. (2012). Heme binding proteins of *Bartonella henselae* are required when undergoing oxidative stress during cell and flea invasion. *PLoS One*, 7(10): e48408. doi: 10.1371/journal.pone.0048408.
- Love, J.F., vanderSpek, J.C., and Murphy, J.R. (2003). The *src* Homology 3-Like Domain of the Diphtheria Toxin Repressor (DtxR) Modulates Repressor Activation through Interaction with the Ancillary Metal Ion-Binding Site. *J Bacteriol*, 185(7): 2251-2258. doi: 10.1128/JB.185.7.2251-2258.2003.
- Lu, Q., Zhou, X.-L., and Liu, J.-Z. (2022). Adaptive laboratory evolution and shuffling of *Escherichia coli* to enhance its tolerance and production of astaxanthin. *Biotechnol Biofuels*, 15(1): 17. doi: 10.1186/s13068-022-02118-w.
- Lu, T., Yang, M., Huang, D.B., Wei, H., Ozer, G.H., Ghosh, G., and Stark, G.R. (2013). Role of lysine methylation of NF- κ B in differential gene regulation. *Proc Natl Acad Sci USA*, 110(33): 13510-13515. doi: 10.1073/pnas.1311770110.
- Lukat, G.S., Lee, B.H., Mottonen, J.M., Stock, A.M., and Stock, J.B. (1991). Roles of the highly conserved aspartate and lysine residues in the response regulator of bacterial chemotaxis. *J Biol Chem*, 266(13): 8348-8354. doi: 10.1016/S0021-9258(18)92982-0.
- Lukat, G.S., McCleary, W.R., Stock, A.M., and Stock, J.B. (1992). Phosphorylation of bacterial response regulator proteins by low molecular weight phospho-donors. *Proc Natl Acad Sci USA*, 89(2): 718-722. doi: 10.1073/pnas.89.2.718.
- Lyles, K.V., Thomas, L.S., Ouellette, C., Cook, L.C.C., and Eichenbaum, Z. (2022). HupZ, a Unique Heme-Binding Protein, Enhances Group A *Streptococcus* Fitness During Mucosal Colonization. *Front Cell Infect Microbiol*, 12: 867963. doi: 10.3389/fcimb.2022.867963.
- Mace, P.D., and Murphy, J.M. (2021). There's more to death than life: Noncatalytic functions in kinase and pseudokinase signaling. *J Biol Chem*, 296: 100705. doi: 10.1016/j.jbc.2021.100705.
- Manabe, Y.C., Saviola, B.J., Sun, L., Murphy, J.R., and Bishai, W.R. (1999). Attenuation of virulence in *Mycobacterium tuberculosis* expressing a constitutively active iron repressor. *Proc Natl Acad Sci USA*, 96(22): 12844-12848. doi: 10.1073/pnas.96.22.12844.
- Manning, G., Whyte, D.B., Martinez, R., Hunter, T., and Sudarsanam, S. (2002). The protein kinase complement of the human genome. *Science*, 298(5600): 1912-1934. doi: 10.1126/science.1075762.

- Marcos-Torres, F.J., Moraleda-Muñoz, A., Contreras-Moreno, F.J., Muñoz-Dorado, J., and Pérez, J. (2022). Mechanisms of Action of Non-Canonical ECF Sigma Factors. *Int J Mol Sci*, 23(7): 3601. doi: 10.3390/ijms23073601.
- Mascher, T., Helmann, J.D., and Uden, G. (2006). Stimulus perception in bacterial signal-transducing histidine kinases. *Microbiol Mol Biol Rev*, 70(4): 910-938. doi: 10.1128/mubr.00020-06.
- Massé, E., and Arguin, M. (2005). Ironing out the problem: new mechanisms of iron homeostasis. *Trends Biochem Sci*, 30(8): 462-468. doi: 10.1016/j.tibs.2005.06.005.
- Massé, E., and Gottesman, S. (2002). A small RNA regulates the expression of genes involved in iron metabolism in *Escherichia coli*. *Proc Natl Acad Sci USA*, 99(7): 4620-4625. doi: 10.1073/pnas.032066599.
- Massé, E., Salvail, H., Desnoyers, G., and Arguin, M. (2007). Small RNAs controlling iron metabolism. *Curr Opin Microbiol*, 10(2): 140-145. doi: 10.1016/j.mib.2007.03.013.
- Matson, M.M., Cepeda, M.M., Zhang, A., Case, A.E., Kavvas, E.S., Wang, X., Carroll, A.L., Tagkopoulos, I., and Atsumi, S. (2022). Adaptive laboratory evolution for improved tolerance of isobutyl acetate in *Escherichia coli*. *Metab Eng*, 69: 50-58. doi: 10.1016/j.ymben.2021.11.002.
- Mavrommati, M., Daskalaki, A., Papanikolaou, S., and Aggelis, G. (2022). Adaptive laboratory evolution principles and applications in industrial biotechnology. *Biotechnol Adv*, 54: 107795. doi: 10.1016/j.biotechadv.2021.107795.
- McBroom, A.J., and Kuehn, M.J. (2007). Release of outer membrane vesicles by Gram-negative bacteria is a novel envelope stress response. *Mol Microbiol*, 63(2): 545-558. doi: 10.1111/j.1365-2958.2006.05522.x.
- McHugh, J.P., Rodríguez-Quinoñes, F., Abdul-Tehrani, H., Svistunenko, D.A., Poole, R.K., Cooper, C.E., and Andrews, S.C. (2003). Global iron-dependent gene regulation in *Escherichia coli*. A new mechanism for iron homeostasis. *J Biol Chem*, 278(32): 29478-29486. doi: 10.1074/jbc.M303381200.
- McKay, M.M., Ritt, D.A., and Morrison, D.K. (2009). Signaling dynamics of the KSR1 scaffold complex. *Proc Natl Acad Sci USA*, 106(27): 11022-11027. doi: 10.1073/pnas.0901590106.
- McNutt, M.K., Bradford, M., Drazen, J.M., Hanson, B., Howard, B., Jamieson, K.H., Kiermer, V., Marcus, E., Pope, B.K., Schekman, R., et al. (2018). Transparency in authors' contributions and responsibilities to promote integrity in scientific publication. *Proc Natl Acad Sci USA*, 115(11): 2557-2560. doi: 10.1073/pnas.1715374115.
- Mehla, J., Caufield, J.H., Sakhawalkar, N., and Uetz, P. (2017). A Comparison of Two-Hybrid Approaches for Detecting Protein-Protein Interactions. *Methods Enzymol*, 586: 333-358. doi: 10.1016/bs.mie.2016.10.020.
- Menon, S., and Wang, S. (2011). Structure of the response regulator PhoP from *Mycobacterium tuberculosis* reveals a dimer through the receiver domain. *Biochemistry*, 50(26): 5948-5957. doi: 10.1021/bi2005575.
- Mike, L.A., Choby, J.E., Brinkman, P.R., Olive, L.Q., Dutter, B.F., Ivan, S.J., Gibbs, C.M., Sulikowski, G.A., Stauff, D.L., and Skaar, E.P. (2014). Two-Component System Cross-Regulation Integrates *Bacillus anthracis* Response to Heme and Cell Envelope Stress. *PLoS Pathog*, 10(3): e1004044. doi: 10.1371/journal.ppat.1004044.
- Mike, L.A., Dutter, B.F., Stauff, D.L., Moore, J.L., Vitko, N.P., Aranmolate, O., Kehl-Fie, T.E., Sullivan, S., Reid, P.R., DuBois, J.L., et al. (2013). Activation of heme biosynthesis by a small molecule that is toxic to fermenting *Staphylococcus aureus*. *Proc Natl Acad Sci USA*, 110(20): 8206-8211. doi: 10.1073/pnas.1303674110.
- Minch, K.J., Rustad, T.R., Peterson, E.J.R., Winkler, J., Reiss, D.J., Ma, S., Hickey, M., Brabant, W., Morrison, B., Turkarslan, S., et al. (2015). The DNA-binding network of *Mycobacterium tuberculosis*. *Nat Commun*, 6(1): 5829. doi: 10.1038/ncomms6829.
- Minnikin, D.E., and Goodfellow, M. (1980). Lipid composition in the classification and identification of acid-fast bacteria. *Soc Appl Bacteriol Symp Ser*, 8: 189-256.
- Möglich, A., Ayers, R.A., and Moffat, K. (2009). Structure and signaling mechanism of Per-ARNT-Sim domains. *Structure*, 17(10): 1282-1294. doi: 10.1016/j.str.2009.08.011.

- Moncrieffe, M.C., Bollschweiler, D., Li, B., Penczek, P.A., Hopkins, L., Bryant, C.E., Klenerman, D., and Gay, N.J. (2020). MyD88 Death-Domain Oligomerization Determines Myddosome Architecture: Implications for Toll-like Receptor Signaling. *Structure*, 28(3): 281-289.e283. doi: 10.1016/j.str.2020.01.003.
- Murphy, E.R., Sacco, R.E., Dickenson, A., Metzger, D.J., Hu, Y., Orndorff, P.E., and Connell, T.D. (2002). BhuR, a virulence-associated outer membrane protein of *Bordetella avium*, is required for the acquisition of iron from heme and hemoproteins. *Infect Immun*, 70(10): 5390-5403. doi: 10.1128/iai.70.10.5390-5403.2002.
- Murphy, J.M., Czabotar, P.E., Hildebrand, J.M., Lucet, I.S., Zhang, J.G., Alvarez-Diaz, S., Lewis, R., Lalaoui, N., Metcalf, D., Webb, A.I., *et al.* (2013). The pseudokinase MLKL mediates necroptosis via a molecular switch mechanism. *Immunity*, 39(3): 443-453. doi: 10.1016/j.immuni.2013.06.018.
- Murphy, J.M., Mace, P.D., and Evers, P.A. (2017). Live and let die: insights into pseudoenzyme mechanisms from structure. *Curr Opin Struct Biol*, 47: 95-104. doi: 10.1016/j.sbi.2017.07.004.
- Murphy, J.M., Zhang, Q., Young, S.N., Reese, M.L., Bailey, F.P., Evers, P.A., Ungureanu, D., Hammaren, H., Silvennoinen, O., Varghese, L.N., *et al.* (2014). A robust methodology to subclassify pseudokinases based on their nucleotide-binding properties. *Biochem J*, 457(2): 323-334. doi: 10.1042/bj20131174.
- Mustafi, N., Grünberger, A., Kohlheyer, D., Bott, M., and Frunzke, J. (2012). The development and application of a single-cell biosensor for the detection of l-methionine and branched-chain amino acids. *Metab Eng*, 14(4): 449-457. doi: 10.1016/j.ymben.2012.02.002.
- Myers, K.S., Park, D.M., Beauchene, N.A., and Kiley, P.J. (2015). Defining bacterial regulons using ChIP-seq. *Methods*, 86: 80-88. doi: 10.1016/j.ymeth.2015.05.022.
- Myers, K.S., Yan, H., Ong, I.M., Chung, D., Liang, K., Tran, F., Keleş, S., Landick, R., and Kiley, P.J. (2013). Genome-scale Analysis of *Escherichia coli* FNR Reveals Complex Features of Transcription Factor Binding. *PLoS Genet*, 9(6): e1003565. doi: 10.1371/journal.pgen.1003565.
- Nagakubo, T., Tahara, Y.O., Miyata, M., Nomura, N., and Toyofuku, M. (2021). Mycolic acid-containing bacteria trigger distinct types of membrane vesicles through different routes. *iScience*, 24(1): 102015. doi: 10.1016/j.isci.2020.102015.
- Nakamura, H., Hisano, T., Rahman, M.M., Tosha, T., Shirouzu, M., and Shiro, Y. (2022). Structural basis for heme detoxification by an ATP-binding cassette-type efflux pump in gram-positive pathogenic bacteria. *Proc Natl Acad Sci USA*, 119(27): e2123385119. doi: 10.1073/pnas.2123385119.
- Nanda, A.M., Heyer, A., Krämer, C., Grünberger, A., Kohlheyer, D., and Frunzke, J. (2014). Analysis of SOS-induced spontaneous prophage induction in *Corynebacterium glutamicum* at the single-cell level. *J Bacteriol*, 196(1): 180-188. doi: 10.1128/jb.01018-13.
- Narahari, J., Ma, R., Wang, M., and Walden, W.E. (2000). The aconitase function of iron regulatory protein 1. Genetic studies in yeast implicate its role in iron-mediated redox regulation. *J Biol Chem*, 275(21): 16227-16234. doi: 10.1074/jbc.M910450199.
- Nobles, C.L., and Maresso, A.W. (2011). The theft of host heme by Gram-positive pathogenic bacteria. *Metallomics*, 3(8): 788-796. doi: 10.1039/c1mt00047k.
- Noya, F., Arias, A., and Fabiano, E. (1997). Heme compounds as iron sources for nonpathogenic Rhizobium bacteria. *J Bacteriol*, 179(9): 3076-3078. doi: 10.1128/jb.179.9.3076-3078.1997.
- O'Brien, E.J., Lerman, J.A., Chang, R.L., Hyduke, D.R., and Palsson, B. (2013). Genome-scale models of metabolism and gene expression extend and refine growth phenotype prediction. *Mol Syst Biol*, 9: 693. doi: 10.1038/msb.2013.52.
- Ochsner, U.A., Johnson, Z., and Vasil, M.L. (2000). Genetics and regulation of two distinct haem-uptake systems, *phu* and *has*, in *Pseudomonas aeruginosa*. *Microbiology (Reading)*, 146(1): 185-198. doi: 10.1099/00221287-146-1-185.
- Ogawa, K., Sun, J., Taketani, S., Nakajima, O., Nishitani, C., Sassa, S., Hayashi, N., Yamamoto, M., Shibahara, S., Fujita, H., *et al.* (2001). Heme mediates derepression of Maf recognition element through direct binding to transcription repressor Bach1. *Embo j*, 20(11): 2835-2843. doi: 10.1093/emboj/20.11.2835.

- Ortet, P., Whitworth, D.E., Santaella, C., Achouak, W., and Barakat, M. (2014). P2CS: updates of the prokaryotic two-component systems database. *Nucleic Acids Res*, 43(D1): D536-D541. doi: 10.1093/nar/gku968.
- Pappenheimer, A.M., Jr. (1977). Diphtheria toxin. *Annu Rev Biochem*, 46: 69-94. doi: 10.1146/annurev.bi.46.070177.000441.
- Pappenheimer, A.M.J., and Johnson, S.J. (1936). Studies in Diphtheria Toxin Production. I: The Effect of Iron and Copper. *Br J Exp Pathol*, 17(5): 335-341.
- Parkinson, J.S. (2010). Signaling mechanisms of HAMP domains in chemoreceptors and sensor kinases. *Annu Rev Microbiol*, 64: 101-122. doi: 10.1146/annurev.micro.112408.134215.
- Parkinson, J.S., and Kofoid, E.C. (1992). Communication modules in bacterial signaling proteins. *Annu Rev Genet*, 26: 71-112. doi: 10.1146/annurev.ge.26.120192.000443.
- Pecqueur, L., D'Autréaux, B., Dupuy, J., Nicolet, Y., Jacquamet, L., Brutscher, B., Michaud-Soret, I., and Bersch, B. (2006). Structural changes of *Escherichia coli* ferric uptake regulator during metal-dependent dimerization and activation explored by NMR and X-ray crystallography. *J Biol Chem*, 281(30): 21286-21295. doi: 10.1074/jbc.M601278200.
- Perego, M., and Hoch, J.A. (1996). Protein aspartate phosphatases control the output of two-component signal transduction systems. *Trends Genet*, 12(3): 97-101. doi: 10.1016/0168-9525(96)81420-x.
- Petibon, C., Malik Ghulam, M., Catala, M., and Abou Elela, S. (2021). Regulation of ribosomal protein genes: An ordered anarchy. *Wiley Interdiscip Rev RNA*, 12(3): e1632. doi: 10.1002/wrna.1632.
- Pfeifer, E., Hünnefeld, M., Popa, O., Polen, T., Kohlheyer, D., Baumgart, M., and Frunzke, J. (2016). Silencing of cryptic prophages in *Corynebacterium glutamicum*. *Nucleic Acids Res*, 44(21): 10117-10131. doi: 10.1093/nar/gkw692.
- Phelan, V.V., Liu, W.T., Pogliano, K., and Dorrestein, P.C. (2011). Microbial metabolic exchange-the chemotype-to-phenotype link. *Nat Chem Biol*, 8(1): 26-35. doi: 10.1038/nchembio.739.
- Pi, H., Chu, M., Ivan, S., Latario, C., Toth, A., Carlin, S., Hillebrand, G., Lin, H., Reppart, J., Stauff, D., et al. (2020). Directed evolution reveals the mechanism of HitRS signaling transduction in *Bacillus anthracis*. *PLoS Pathog*, 16: e1009148. doi: 10.1371/journal.ppat.1009148.
- Pi, H., and Helmann, J.D. (2017). Sequential induction of Fur-regulated genes in response to iron limitation in *Bacillus subtilis*. *Proc Natl Acad Sci USA*, 114(48): 12785-12790. doi: 10.1073/pnas.1713008114.
- Pi, H., and Helmann, J.D. (2018). Genome-Wide Characterization of the Fur Regulatory Network Reveals a Link between Catechol Degradation and Bacillibactin Metabolism in *Bacillus subtilis*. *mBio*, 9(5): e01451-01418. doi: 10.1128/mBio.01451-18.
- Pi, H., Weiss, A., Laut, C.L., Grunenwald, C.M., Lin, H.K., Yi, X.I., Stauff, D.L., and Skaar, E.P. (2022). An RNA-binding protein acts as a major post-transcriptional modulator in *Bacillus anthracis*. *Nat Commun*, 13(1): 1491. doi: 10.1038/s41467-022-29209-4.
- Pierre, J.L., and Fontecave, M. (1999). Iron and activated oxygen species in biology: the basic chemistry. *Biometals*, 12(3): 195-199. doi: 10.1023/a:1009252919854.
- Ponka, P. (1997). Tissue-Specific Regulation of Iron Metabolism and Heme Synthesis: Distinct Control Mechanisms in Erythroid Cells. *Blood*, 89(1): 1-25. doi: 10.1182/blood.V89.1.1.
- Ponka, P. (1999). Cell biology of heme. *Am J Med Sci*, 318(4): 241-256. doi: 10.1097/00000441-199910000-00004.
- Portnoy, V.A., Bezdan, D., and Zengler, K. (2011). Adaptive laboratory evolution-harnessing the power of biology for metabolic engineering. *Curr Opin Biotechnol*, 22(4): 590-594. doi: 10.1016/j.copbio.2011.03.007.
- Prados-Rosales, R., Brown, L., Casadevall, A., Montalvo-Quirós, S., and Luque-Garcia, J.L. (2014). Isolation and identification of membrane vesicle-associated proteins in Gram-positive bacteria and mycobacteria. *MethodsX*, 1: 124-129. doi: 10.1016/j.mex.2014.08.001.
- Prell, C., Busche, T., Rückert, C., Nolte, L., Brandenbusch, C., and Wendisch, V.F. (2021). Adaptive laboratory evolution accelerated glutarate production by *Corynebacterium glutamicum*. *Microb Cell Fact*, 20(1): 97. doi: 10.1186/s12934-021-01586-3.

- Quigley, J.G., Yang, Z., Worthington, M.T., Phillips, J.D., Sabo, K.M., Sabath, D.E., Berg, C.L., Sassa, S., Wood, B.L., and Abkowitz, J.L. (2004). Identification of a human heme exporter that is essential for erythropoiesis. *Cell*, 118(6): 757-766. doi: 10.1016/j.cell.2004.08.014.
- Radek, A., Tenhaef, N., Müller, M.F., Brüsseler, C., Wiechert, W., Marienhagen, J., Polen, T., and Noack, S. (2017). Miniaturized and automated adaptive laboratory evolution: Evolving *Corynebacterium glutamicum* towards an improved d-xylose utilization. *Bioresour Technol*, 245(Pt B): 1377-1385. doi: 10.1016/j.biortech.2017.05.055.
- Raju, S., and Shaw, A.S. (2015). What is the point of pseudokinases? *Elife*, 4: e07771. doi: 10.7554/eLife.07771.
- Reisinger, S.J., Huntwork, S., Viollier, P.H., and Ryan, K.R. (2007). DivL performs critical cell cycle functions in *Caulobacter crescentus* independent of kinase activity. *J Bacteriol*, 189(22): 8308-8320. doi: 10.1128/jb.00868-07.
- Rey, D.A., Pühler, A., and Kalinowski, J. (2003). The putative transcriptional repressor McbR, member of the TetR-family, is involved in the regulation of the metabolic network directing the synthesis of sulfur containing amino acids in *Corynebacterium glutamicum*. *J Biotechnol*, 103(1): 51-65. doi: 10.1016/s0168-1656(03)00073-7.
- Rhee, H.S., and Pugh, B.F. (2011). Comprehensive genome-wide protein-DNA interactions detected at single-nucleotide resolution. *Cell*, 147(6): 1408-1419. doi: 10.1016/j.cell.2011.11.013.
- Roden, J.A., Wells, D.H., Chomel, B.B., Kasten, R.W., and Koehler, J.E. (2012). Hemin Binding Protein C Is Found in Outer Membrane Vesicles and Protects *Bartonella henselae* against Toxic Concentrations of Hemin. *Infect Immun*, 80(3): 929-942. doi: 10.1128/IAI.05769-11.
- Rouault, T., and Klausner, R. (1997). Regulation of iron metabolism in eukaryotes. *Curr Top Cell Regul*, 35: 1-19. doi: 10.1016/s0070-2137(97)80001-5.
- Rückert, C., Pühler, A., and Kalinowski, J. (2003). Genome-wide analysis of the L-methionine biosynthetic pathway in *Corynebacterium glutamicum* by targeted gene deletion and homologous complementation. *J Biotechnol*, 104(1-3): 213-228. doi: 10.1016/s0168-1656(03)00158-5.
- Russell, L.M., Cryz, S.J., Jr., and Holmes, R.K. (1984). Genetic and biochemical evidence for a siderophore-dependent iron transport system in *Corynebacterium diphtheriae*. *Infect Immun*, 45(1): 143-149. doi: 10.1128/iai.45.1.143-149.1984.
- Ryan Kaler, K.M., Nix, J.C., and Schubot, F.D. (2021). RetS inhibits *Pseudomonas aeruginosa* biofilm formation by disrupting the canonical histidine kinase dimerization interface of GacS. *J Biol Chem*, 297(4): 101193. doi: 10.1016/j.jbc.2021.101193.
- Sachla, A.J., Luo, Y., and Helmann, J.D. (2021). Manganese impairs the QoxABCD terminal oxidase leading to respiration-associated toxicity. *Mol Microbiol*, 116(3): 729-742. doi: 10.1111/mmi.14767.
- Saha, M., Sarkar, S., Sarkar, B., Sharma, B.K., Bhattacharjee, S., and Tribedi, P. (2016). Microbial siderophores and their potential applications: a review. *Environ Sci Pollut Res Int*, 23(5): 3984-3999. doi: 10.1007/s11356-015-4294-0.
- Saito, T., and Williams, R.J. (1991). The binding of the ferric uptake regulation protein to a DNA fragment. *Eur J Biochem*, 197(1): 43-47. doi: 10.1111/j.1432-1033.1991.tb15880.x.
- Salvado, B., Vilaprinyo, E., Karathia, H., Sorribas, A., and Alves, R. (2012). Two Component Systems: Physiological Effect of a Third Component. *PLoS One*, 7(2): e31095. doi: 10.1371/journal.pone.0031095.
- Samson, A.L., Zhang, Y., Geoghegan, N.D., Gavin, X.J., Davies, K.A., Mlodzianoski, M.J., Whitehead, L.W., Frank, D., Garnish, S.E., Fitzgibbon, C., et al. (2020). MLKL trafficking and accumulation at the plasma membrane control the kinetics and threshold for necroptosis. *Nat Commun*, 11(1): 3151. doi: 10.1038/s41467-020-16887-1.
- Sassa, S. (1976). Sequential induction of heme pathway enzymes during erythroid differentiation of mouse Friend leukemia virus-infected cells. *J Exp Med*, 143(2): 305-315. doi: 10.1084/jem.143.2.305.
- Schmitt, M.P. (1999). Identification of a Two-Component Signal Transduction System from *Corynebacterium diphtheriae* That Activates Gene Expression in Response to the Presence of

- Heme and Hemoglobin. *J Bacteriol*, 181(17): 5330-5340. doi: 10.1128/JB.181.17.5330-5340.1999.
- Schmitt, M.P., and Holmes, R.K. (1991). Iron-dependent regulation of diphtheria toxin and siderophore expression by the cloned *Corynebacterium diphtheriae* repressor gene *dtxR* in *C. diphtheriae* C7 strains. *Infect Immun*, 59(6): 1899-1904. doi: 10.1128/iai.59.6.1899-1904.1991.
- Scholz, R.L., and Greenberg, E.P. (2015). Sociality in *Escherichia coli*: Enterochelin Is a Private Good at Low Cell Density and Can Be Shared at High Cell Density. *J Bacteriol*, 197(13): 2122-2128. doi: 10.1128/jb.02596-14.
- Schooling, S.R., and Beveridge, T.J. (2006). Membrane vesicles: an overlooked component of the matrices of biofilms. *J Bacteriol*, 188(16): 5945-5957. doi: 10.1128/jb.00257-06.
- Schreiner, M.E., Fiur, D., Holátko, J., Pátek, M., and Eikmanns, B.J. (2005). E1 Enzyme of the Pyruvate Dehydrogenase Complex in *Corynebacterium glutamicum*: Molecular Analysis of the Gene and Phylogenetic Aspects. *J Bacteriol*, 187(17): 6005-6018. doi: 10.1128/JB.187.17.6005-6018.2005.
- Schubert, E., Florin, N., Duthie, F., Brewitz, H.H., Kühl, T., Imhof, D., Hagelueken, G., and Schiemann, O. (2015). Spectroscopic Studies on Peptides and Proteins with Cysteine-Containing Heme Regulatory Motifs (HRM). *J Inorg Biochem*, 148: 49-56. doi: 10.1016/j.jinorgbio.2015.05.008.
- Seib, K.L., Tseng, H.-J., McEwan, A.G., Apicella, M.A., and Jennings, M.P. (2004). Defenses against Oxidative Stress in *Neisseria gonorrhoeae* and *Neisseria meningitidis*: Distinctive Systems for Different Lifestyles. *J Infect Dis*, 190(1): 136-147. doi: 10.1086/421299.
- Seo, S.W., Kim, D., Latif, H., O'Brien, E.J., Szubin, R., and Palsson, B.O. (2014). Deciphering Fur transcriptional regulatory network highlights its complex role beyond iron metabolism in *Escherichia coli*. *Nat Commun*, 5: 4910. doi: 10.1038/ncomms5910.
- Sheldon, J.R., and Heinrichs, D.E. (2015). Recent developments in understanding the iron acquisition strategies of gram positive pathogens. *FEMS Microbiol Rev*, 39(4): 592-630. doi: 10.1093/femsre/fuv009.
- Shemin, D., and Kumin, S. (1952). The mechanism of porphyrin formation. *J Biol Chem*, 198: 827. doi: 10.1016/S0021-9258(18)55541-1.
- Shemin, D., and Rittenberg, D. (1945). The utilization of glycine for the synthesis of a porphyrin. *J Biol Chem*, 159(2): 567-568. doi: 10.1016/S0021-9258(17)35200-6.
- Shepherd, M. (2015). The CydDC ABC transporter of *Escherichia coli*: new roles for a reductant efflux pump. *Biochem Soc Trans*, 43(5): 908-912. doi: 10.1042/bst20150098.
- Shimizu, T., Lengalova, A., Martínek, V., and Martíňková, M. (2019). Heme: emergent roles of heme in signal transduction, functional regulation and as catalytic centres. *Chem Soc Rev*, 48(24): 5624-5657. doi: 10.1039/C9CS00268E.
- Shin, J.-H., and Helmann, J.D. (2016). Molecular logic of the Zur-regulated zinc deprivation response in *Bacillus subtilis*. *Nat Commun*, 7(1): 12612. doi: 10.1038/ncomms12612.
- Si, M., Zhang, L., Chaudhry, M.T., Ding, W., Xu, Y., Chen, C., Akbar, A., Shen, X., and Liu, S.J. (2015). *Corynebacterium glutamicum* methionine sulfoxide reductase A uses both mycoredoxin and thioredoxin for regeneration and oxidative stress resistance. *Appl Environ Microbiol*, 81(8): 2781-2796. doi: 10.1128/aem.04221-14.
- Siedler, S., Lindner, S.N., Bringer, S., Wendisch, V.F., and Bott, M. (2013). Reductive whole-cell biotransformation with *Corynebacterium glutamicum*: improvement of NADPH generation from glucose by a cyclized pentose phosphate pathway using *pfkA* and *gapA* deletion mutants. *Appl Microbiol Biotechnol*, 97(1): 143-152. doi: 10.1007/s00253-012-4314-7.
- Siggers, T., and Gordán, R. (2013). Protein–DNA binding: complexities and multi-protein codes. *Nucleic Acids Res*, 42(4): 2099-2111. doi: 10.1093/nar/gkt1112.
- Singh, S., Lowe, D.G., Thorpe, D.S., Rodriguez, H., Kuang, W.-J., Dangott, L.J., Chinkers, M., Goeddel, D.V., and Garbers, D.L. (1988). Membrane guanylate cyclase is a cell-surface receptor with homology to protein kinases. *Nature*, 334(6184): 708-712. doi: 10.1038/334708a0.
- Slyshenkov, V.S., Shevalye, A.A., Liopo, A.V., and Wojtczak, L. (2002). Protective role of L-methionine against free radical damage of rat brain synaptosomes. *Acta Biochim Pol*, 49(4): 907-916.

- Sobota, J.M., and Imlay, J.A. (2011). Iron enzyme ribulose-5-phosphate 3-epimerase in *Escherichia coli* is rapidly damaged by hydrogen peroxide but can be protected by manganese. *Proc Natl Acad Sci USA*, 108(13): 5402-5407. doi: 10.1073/pnas.1100410108.
- Solomon, M.J., Larsen, P.L., and Varshavsky, A. (1988). Mapping protein-DNA interactions in vivo with formaldehyde: evidence that histone H4 is retained on a highly transcribed gene. *Cell*, 53(6): 937-947. doi: 10.1016/s0092-8674(88)90469-2.
- Sousa, L., Oliveira, M.M., Pessôa, M.T.C., and Barbosa, L.A. (2020). Iron overload: Effects on cellular biochemistry. *Clinica Chimica Acta*, 504: 180-189. doi: 10.1016/j.cca.2019.11.029.
- Spiering, M.M., Ringe, D., Murphy, J.R., and Marletta, M.A. (2003). Metal stoichiometry and functional studies of the diphtheria toxin repressor. *Proc Natl Acad Sci USA*, 100(7): 3808-3813. doi: 10.1073/pnas.0737977100.
- Staroń, A., Sofia, H.J., Dietrich, S., Ulrich, L.E., Liesegang, H., and Mascher, T. (2009). The third pillar of bacterial signal transduction: classification of the extracytoplasmic function (ECF) sigma factor protein family. *Mol Microbiol*, 74(3): 557-581. doi: 10.1111/j.1365-2958.2009.06870.x.
- Stauff, D.L., and Skaar, E.P. (2009a). *Bacillus anthracis* HssRS signalling to HrtAB regulates haem resistance during infection. *Mol Microbiol*, 72(3): 763-778. doi: 10.1111/j.1365-2958.2009.06684.x.
- Stauff, D.L., and Skaar, E.P. (2009b). The heme sensor system of *Staphylococcus aureus*. *Contrib Microbiol*, 16: 120-135. doi: 10.1159/000219376.
- Stella, R.G., Gertzen, C.G.W., Smits, S.H.J., Gätgens, C., Polen, T., Noack, S., and Frunzke, J. (2021). Biosensor-based growth-coupling and spatial separation as an evolution strategy to improve small molecule production of *Corynebacterium glutamicum*. *Metab Eng*, 68: 162-173. doi: 10.1016/j.ymben.2021.10.003.
- Stella, R.G., Wiechert, J., Noack, S., and Frunzke, J. (2019). Evolutionary engineering of *Corynebacterium glutamicum*. *Biotechnol J*, 14(9): e1800444. doi: 10.1002/biot.201800444.
- Stewart, R.C. (2010). Protein histidine kinases: assembly of active sites and their regulation in signaling pathways. *Curr Opin Microbiol*, 13(2): 133-141. doi: 10.1016/j.mib.2009.12.013.
- Stock, A.M., Robinson, V.L., and Goudreau, P.N. (2000). Two-component signal transduction. *Annu Rev Biochem*, 69: 183-215. doi: 10.1146/annurev.biochem.69.1.183.
- Stojiljkovic, I., Bäumlner, A.J., and Hantke, K. (1994). Fur regulon in gram-negative bacteria: Identification and characterization of new iron-regulated *Escherichia coli* genes by a Fur titration assay. *J Mol Biol*, 236(2): 531-545. doi: 10.1006/jmbi.1994.1163.
- Stojiljkovic, I., and Hantke, K. (1994). Transport of haemin across the cytoplasmic membrane through a haemin-specific periplasmic binding-protein-dependent transport system in *Yersinia enterocolitica*. *Mol Microbiol*, 13(4): 719-732. doi: 10.1111/j.1365-2958.1994.tb00465.x.
- Stojiljkovic, I., Kumar, V., and Srinivasan, N. (1999). Non-iron metalloporphyrins: potent antibacterial compounds that exploit haem/Hb uptake systems of pathogenic bacteria. *Mol Microbiol*, 31(2): 429-442. doi: 10.1046/j.1365-2958.1999.01175.x.
- Storz, G., Wolf, Y.I., and Ramamurthi, K.S. (2014). Small proteins can no longer be ignored. *Annu Rev Biochem*, 83: 753-777. doi: 10.1146/annurev-biochem-070611-102400.
- Szurmant, H., Bu, L., Brooks, C.L., and Hoch, J.A. (2008). An essential sensor histidine kinase controlled by transmembrane helix interactions with its auxiliary proteins. *Proc Natl Acad Sci USA*, 105(15): 5891-5896. doi: 10.1073/pnas.0800247105.
- Takahashi, J.S., Kumar, V., Nakashe, P., Koike, N., Huang, H.-C., Green, C.B., and Kim, T.-K. (2015). Chapter Fourteen - ChIP-seq and RNA-seq Methods to Study Circadian Control of Transcription in Mammals. In *Methods Enzymol*, A. Sehgal, ed. (Academic Press), pp. 285-321.
- Tang, Y., and Guest, J.R. (1999). Direct evidence for mRNA binding and post-transcriptional regulation by *Escherichia coli* aconitases. *Microbiology (Reading)*, 145(11): 3069-3079. doi: 10.1099/00221287-145-11-3069.
- Tang, Y., Guest, J.R., Artymiuk, P.J., and Green, J. (2005). Switching aconitase B between catalytic and regulatory modes involves iron-dependent dimer formation. *Mol Microbiol*, 56(5): 1149-1158. doi: 10.1111/j.1365-2958.2005.04610.x.

- Tao, X., Schiering, N., Zeng, H.Y., Ringe, D., and Murphy, J.R. (1994). Iron, DtxR, and the regulation of diphtheria toxin expression. *Mol Microbiol*, 14(2): 191-197. doi: 10.1111/j.1365-2958.1994.tb01280.x.
- Teramoto, H., Inui, M., and Yukawa, H. (2013). OxyR acts as a transcriptional repressor of hydrogen peroxide-inducible antioxidant genes in *Corynebacterium glutamicum* R. *FEBS J*, 280(14): 3298-3312. doi: 10.1111/febs.12312.
- Thanbichler, M., Neuhierl, B., and Böck, A. (1999). S-methylmethionine metabolism in *Escherichia coli*. *J Bacteriol*, 181(2): 662-665. doi: 10.1128/jb.181.2.662-665.1999.
- Thiel, J., Byrne, J.M., Kappler, A., Schink, B., and Pester, M. (2019). Pyrite formation from FeS and H₂S is mediated through microbial redox activity. *Proc Natl Acad Sci USA*, 116(14): 6897-6902. doi: 10.1073/pnas.1814412116.
- Torres, V.J., Stauff, D.L., Pishchany, G., Bezbradica, J.S., Gordy, L.E., Iturregui, J., Anderson, K.L., Dunman, P.M., Joyce, S., and Skaar, E.P. (2007). A *Staphylococcus aureus* regulatory system that responds to host heme and modulates virulence. *Cell Host Microbe*, 1(2): 109-119. doi: 10.1016/j.chom.2007.03.001.
- Tossounian, M.-A., Pedre, B., Wahni, K., Erdogan, H., Vertommen, D., Van Molle, I., and Messens, J. (2015). *Corynebacterium diphtheriae* Methionine Sulfoxide Reductase A Exploits a Unique Mycothiol Redox Relay Mechanism. *J Biol Chem*, 290(18): 11365-11375. doi: 10.1074/jbc.M114.632596.
- Toyoda, K., and Inui, M. (2016). The extracytoplasmic function σ factor σ^c regulates expression of a branched quinol oxidation pathway in *Corynebacterium glutamicum*. *Mol Microbiol*, 100(3): 486-509. doi: 10.1111/mmi.13330.
- Tseng, H.J., Srikhanta, Y., McEwan, A.G., and Jennings, M.P. (2001). Accumulation of manganese in *Neisseria gonorrhoeae* correlates with resistance to oxidative killing by superoxide anion and is independent of superoxide dismutase activity. *Mol Microbiol*, 40(5): 1175-1186. doi: 10.1046/j.1365-2958.2001.02460.x.
- Tsokos, C.G., Perchuk, B.S., and Laub, M.T. (2011). A dynamic complex of signaling proteins uses polar localization to regulate cell-fate asymmetry in *Caulobacter crescentus*. *Dev Cell*, 20(3): 329-341. doi: 10.1016/j.devcel.2011.01.007.
- Varadi, M., Anyango, S., Deshpande, M., Nair, S., Natassia, C., Yordanova, G., Yuan, D., Stroe, O., Wood, G., Laydon, A., et al. (2021). AlphaFold Protein Structure Database: massively expanding the structural coverage of protein-sequence space with high-accuracy models. *Nucleic Acids Res*, 50(D1): D439-D444. doi: 10.1093/nar/gkab1061.
- Volz, K. (2008). The functional duality of iron regulatory protein 1. *Curr Opin Struct Biol*, 18(1): 106-111. doi: 10.1016/j.sbi.2007.12.010.
- Waldron, K.J., Rutherford, J.C., Ford, D., and Robinson, N.J. (2009). Metalloproteins and metal sensing. *Nature*, 460(7257): 823-830. doi: 10.1038/nature08300.
- Wallace, D.F. (2016). The Regulation of Iron Absorption and Homeostasis. *Clin Biochem Rev*, 37(2): 51-62.
- Wang, M., Nie, Y., and Wu, X.L. (2021a). Extracellular heme recycling and sharing across species by novel mycomembrane vesicles of a Gram-positive bacterium. *Isme j*, 15(2): 605-617. doi: 10.1038/s41396-020-00800-1.
- Wang, S., Wan, W., Wang, Z., Zhang, H., Liu, H., Arunakumara, K., Cui, Q., and Song, X. (2021b). A Two-Stage Adaptive Laboratory Evolution Strategy to Enhance Docosahexaenoic Acid Synthesis in *Oleaginous Thraustochytrid*. *Front Nutr*, 8: 795491. doi: 10.3389/fnut.2021.795491.
- Wang, Y., Fan, L., Tuyishime, P., Liu, J., Zhang, K., Gao, N., Zhang, Z., Ni, X., Feng, J., Yuan, Q., et al. (2020). Adaptive laboratory evolution enhances methanol tolerance and conversion in engineered *Corynebacterium glutamicum*. *Commun Biol*, 3(1): 217. doi: 10.1038/s42003-020-0954-9.
- Warnatz, H.J., Schmidt, D., Manke, T., Piccini, I., Sultan, M., Borodina, T., Balzereit, D., Wruck, W., Soldatov, A., Vingron, M., et al. (2011). The BTB and CNC homology 1 (BACH1) target genes are involved in the oxidative stress response and in control of the cell cycle. *J Biol Chem*, 286(26): 23521-23532. doi: 10.1074/jbc.M111.220178.

- Waturuocha, U.W., Krishna, M.S., Malhotra, V., Dixit, N.M., and Saini, D.K. (2021a). A Low-Prevalence Single-Nucleotide Polymorphism in the Sensor Kinase PhoR in *Mycobacterium tuberculosis* Suppresses Its Autophosphatase Activity and Reduces Pathogenic Fitness: Implications in Evolutionary Selection. *Front Microbiol*, 12: 724482. doi: 10.3389/fmicb.2021.724482.
- Waturuocha, U.W., P, J.A., Singh, K.K., Malhotra, V., Krishna, M.S., and Saini, D.K. (2021b). A high-frequency single nucleotide polymorphism in the MtrB sensor kinase in clinical strains of *Mycobacterium tuberculosis* alters its biochemical and physiological properties. *PLoS One*, 16(9): e0256664. doi: 10.1371/journal.pone.0256664.
- Weber, K.A., Achenbach, L.A., and Coates, J.D. (2006). Microorganisms pumping iron: anaerobic microbial iron oxidation and reduction. *Nat Rev Microbiol*, 4(10): 752-764. doi: 10.1038/nrmicro1490.
- Weinberg, E.D. (1974). Iron and susceptibility to infectious disease. *Science*, 184(4140): 952-956. doi: 10.1126/science.184.4140.952.
- Welkos, S.L., and Holmes, R.K. (1981). Regulation of toxinogenesis in *Corynebacterium diphtheriae*. I. Mutations in bacteriophage beta that alter the effects of iron on toxin production. *J Virol*, 37(3): 936-945. doi: 10.1128/jvi.37.3.936-945.1981.
- Wennerhold, J., and Bott, M. (2006). The DtxR regulon of *Corynebacterium glutamicum*. *J Bacteriol*, 188(8): 2907-2918. doi: 10.1128/jb.188.8.2907-2918.2006.
- Wennerhold, J., Krug, A., and Bott, M. (2005). The AraC-type regulator RipA represses aconitase and other iron proteins from *Corynebacterium* under iron limitation and is itself repressed by DtxR. *J Biol Chem*, 280(49): 40500-40508. doi: 10.1074/jbc.M508693200.
- West, A.H., and Stock, A.M. (2001). Histidine kinases and response regulator proteins in two-component signaling systems. *Trends Biochem Sci*, 26(6): 369-376. doi: 10.1016/s0968-0004(01)01852-7.
- White, A., Ding, X., vanderSpek, J.C., Murphy, J.R., and Ringe, D. (1998). Structure of the metal-ion-activated diphtheria toxin repressor/tox operator complex. *Nature*, 394(6692): 502-506. doi: 10.1038/28893.
- Wilderman, P.J., Sowa, N.A., FitzGerald, D.J., FitzGerald, P.C., Gottesman, S., Ochsner, U.A., and Vasil, M.L. (2004). Identification of tandem duplicate regulatory small RNAs in *Pseudomonas aeruginosa* involved in iron homeostasis. *Proc Natl Acad Sci USA*, 101(26): 9792-9797. doi: 10.1073/pnas.0403423101.
- Wilks, A. (2001). The ShuS protein of *Shigella dysenteriae* is a heme-sequestering protein that also binds DNA. *Arch Biochem Biophys*, 387(1): 137-142. doi: 10.1006/abbi.2000.2250.
- Wilks, A., and Schmitt, M.P. (1998). Expression and Characterization of a Heme Oxygenase (HmuO) from *Corynebacterium diphtheriae*: Iron Acquisition Requires Oxidative Cleavage of the Heme Macrocycle. *J Biol Chem*, 273(2): 837-841. doi: 10.1074/jbc.273.2.837.
- Wißbrock, A., Paul George, A.A., Brewitz, H.H., Köhl, T., and Imhof, D. (2019). The molecular basis of transient heme-protein interactions: analysis, concept and implementation. *Biosci Rep*, 39(1): BSR20181940. doi: 10.1042/bsr20181940.
- Wolanin, P.M., Thomason, P.A., and Stock, J.B. (2002). Histidine protein kinases: key signal transducers outside the animal kingdom. *Genome Biol*, 3(10): Reviews3013. doi: 10.1186/gb-2002-3-10-reviews3013.
- Wu, A.R., Kawahara, T.L.A., Rapicavoli, N.A., Riggelen, J.v., Shroff, E.H., Xu, L., Felsher, D.W., Chang, H.Y., and Quake, S.R. (2012). High throughput automated chromatin immunoprecipitation as a platform for drug screening and antibody validation. *Lab Chip*, 12(12): 2190-2198. doi: 10.1039/C2LC21290K.
- Wu, D., Mehdipour, A., Finke, F., Goojani, H., Groh, R., Grund, T., Reichhart, T.M.B., Zimmermann, R., Welsch, S., Bald, D., et al. (2022). Dissecting the conformational complexity and flipping mechanism of a prokaryotic heme transporter. *bioRxiv* (preprint). doi: 10.1101/2022.04.07.487047.
- Yadavalli, S.S., and Yuan, J. (2022). Bacterial Small Membrane Proteins: the Swiss Army Knife of Regulators at the Lipid Bilayer. *J Bacteriol*, 204(1): e0034421. doi: 10.1128/jb.00344-21.

- Yamashita, M., Shepherd, M., Booth, W.I., Xie, H., Postis, V., Nyathi, Y., Tzokov, S.B., Poole, R.K., Baldwin, S.A., and Bullough, P.A. (2014). Structure and function of the bacterial heterodimeric ABC transporter CydDC: stimulation of ATPase activity by thiol and heme compounds. *J Biol Chem*, 289(33): 23177-23188. doi: 10.1074/jbc.M114.590414.
- Yellaboina, S., Ranjan, S., Chakhaiyar, P., Hasnain, S.E., and Ranjan, A. (2004). Prediction of DtxR regulon: identification of binding sites and operons controlled by Diphtheria toxin repressor in *Corynebacterium diphtheriae*. *BMC Microbiol*, 4: 38. doi: 10.1186/1471-2180-4-38.
- Yin, L., Wu, N., Curtin, J., Qatanani, M., Szwegold, N., Reid, R., Waitt, G., Parks, D., Pearce, K., Wisely, G., *et al.* (2007). Rev-erba, a Heme Sensor That Coordinates Metabolic and Circadian Pathways. *Science*, 318: 1786-1789. doi: 10.1126/science.1150179.
- Zajdowicz, S., Haller, J.C., Krafft, A.E., Hunsucker, S.W., Mant, C.T., Duncan, M.W., Hodges, R.S., Jones, D.N., and Holmes, R.K. (2012). Purification and structural characterization of siderophore (corynebactin) from *Corynebacterium diphtheriae*. *PLoS One*, 7(4): e34591. doi: 10.1371/journal.pone.0034591.
- Zencir, S., Dilg, D., Rueda, M.P., Shore, D., and Albert, B. (2020). Mechanisms coordinating ribosomal protein gene transcription in response to stress. *Nucleic Acids Res*, 48(20): 11408-11420. doi: 10.1093/nar/gkaa852.
- Zeqiraj, E., and van Aalten, D.M.F. (2010). Pseudokinases-remnants of evolution or key allosteric regulators? *Curr Opin Struct Biol*, 20(6): 772-781. doi: 10.1016/j.sbi.2010.10.001.
- Zhao, X.R., Choi, K.R., and Lee, S.Y. (2018). Metabolic engineering of *Escherichia coli* for secretory production of free haem. *Nat Catal*, 1(9): 720-728. doi: 10.1038/s41929-018-0126-1.
- Zhu, Q., Venzke, D., Walimbe, A.S., Anderson, M.E., Fu, Q., Kinch, L.N., Wang, W., Chen, X., Grishin, N.V., Huang, N., *et al.* (2016). Structure of protein O-mannose kinase reveals a unique active site architecture. *Elife*, 5: e22238. doi: 10.7554/eLife.22238.
- Zhu, Y., Qin, L., Yoshida, T., and Inouye, M. (2000). Phosphatase activity of histidine kinase EnvZ without kinase catalytic domain. *Proc Natl Acad Sci USA*, 97(14): 7808-7813. doi: 10.1073/pnas.97.14.7808.
- Zschiedrich, C.P., Keidel, V., and Szurmant, H. (2016). Molecular Mechanisms of Two-Component Signal Transduction. *J Mol Biol*, 428(19): 3752-3775. doi: 10.1016/j.jmb.2016.08.003.
- Zuber, B., Chami, M., Houssin, C., Dubochet, J., Griffiths, G., and Daffé, M. (2008). Direct visualization of the outer membrane of mycobacteria and corynebacteria in their native state. *J Bacteriol*, 190(16): 5672-5680. doi: 10.1128/jb.01919-07.

3. Publications and manuscripts

The Contributor Roles Taxonomy (CRediT) describes the respective author contributions to scientific publications (McNutt et al., 2018). The following table is based on the publication of McNutt et al. (2018) and was used to assign author contributions to the manuscripts, which were presented throughout this thesis.

Contributor role	Role definition
Conceptualization	Ideas; formulation or evolution of overarching research goals and aims
Formal analysis	Application of statistical, mathematical, computational, or other formal techniques to analyse or synthesize study data
Investigation/Experiments	Conducting a research and investigation process, specifically performing the experiments, or data/evidence collection
Methodology	Development or design of methodology; creation of models
Project administration	Management and coordination responsibility for the research activity planning and execution
Software	Programming, software development; designing computer programs; implementation of the computer code and supporting algorithms; testing of existing code components
Supervision	Oversight and leadership responsibility for the research activity planning and execution, including mentorship external to the core team
Visualization	Preparation, creation and/or presentation of the published work, specifically visualization/data presentation
Writing – original draft	Preparation, creation and/or presentation of the published work, specifically writing the initial draft (including substantive translation)
Writing – review & editing	Preparation, creation and/or presentation of the published work by those from the original research group, specifically critical review, commentary or revision – including pre- or post-publication stages

3.1 The diversity of heme sensor systems - heme-responsive transcriptional regulation mediated by transient heme protein interactions

Krüger A., Keppel M., Sharma V., and Frunzke J.

Published in *FEMS Microbiology Reviews*, 2022.

Contributor Role	Contributor
Conceptualization	60% AK, 30% JF, 10% MK
Formal Analysis	-
Investigation/Experiments	-
Methodology	-
Project Administration	60% AK, 40% JF
Software	100% VS
Supervision	50% AK, 50% JF
Visualization	90% AK, 10% MK
Writing – Original Draft Preparation	70% AK, 25% JF, 3% MK, 2% VS
Writing – Review & Editing	60% AK, 40% JF

Overall contribution AK: 75%

The writing of the original draft was mainly done by AK, which was reviewed and edited by AK and JF. Figures and Tables were conceptualized and visualized mainly by AK, with some additions of MK. The bioinformatic analysis (Figure 3), which was conducted by VS and further visualized by AK.



The diversity of heme sensor systems – heme-responsive transcriptional regulation mediated by transient heme protein interactions

Aileen Krüger, Marc Keppel, Vikas Sharma and Julia Frunzke

Forschungszentrum Jülich GmbH, Institute for Bio- and Geosciences 1, IBG1, Wilhelm-Johnen-Strasse, 52425 Jülich, Germany

*Corresponding author: Wilhelm-Johnen-Strasse, Institute for Bio- and Geosciences 1, IBG-1: Biotechnology, 52425 Jülich, Germany. E-mail: j.frunzke@fz-juelich.de

One sentence summary: This review covers diverse prokaryotic and eukaryotic heme sensor systems and discusses the mechanisms of signal perception, heme-binding pockets and network architectures focusing on systems with a role in the control of heme homeostasis.

Editor: Jan Roelof van der Meer

Abstract

Heme is a versatile molecule that is vital for nearly all cellular life by serving as prosthetic group for various enzymes or as nutritional iron source for diverse microbial species. However, elevated levels of heme is toxic to cells. The complexity of this stimulus has shaped the evolution of diverse heme sensor systems, which are involved in heme-dependent transcriptional regulation in eukaryotes and prokaryotes. The functions of these systems are manifold—ranging from the specific control of heme detoxification or uptake systems to the global integration of heme and iron homeostasis. This review focuses on heme sensor systems, regulating heme homeostasis by transient heme protein interaction. We provide an overview of known heme-binding motifs in prokaryotic and eukaryotic transcription factors. Besides the central ligands, the surrounding amino acid environment was shown to play a pivotal role in heme binding. The diversity of heme-regulatory systems, therefore, illustrates that prediction based on pure sequence information is hardly possible and requires careful experimental validation. Comprehensive understanding of heme-regulated processes is not only important for our understanding of cellular physiology, but also provides a basis for the development of novel antibacterial drugs and metabolic engineering strategies.

Keywords: heme, heme sensor systems, heme-protein interaction, heme regulatory motifs, heme homeostasis, HrtBA

Introduction

Heme—iron bound protoporphyrin IX—is an essential molecule for nearly all cells and is synthesized and used by prokaryotes and eukaryotes alike (Ponka 1999). It has an important role in critical cellular processes like electron transfer, respiration and oxygen metabolism (Ajioka et al. 2006) where it serves as prosthetic group of cytochromes, hydroxylases, catalases, peroxidases and hemoglobins (Layer et al. 2010). Since hemoglobin is the most abundant reservoir of iron in the human body, host synthesized heme is often the only reliable source of iron for many pathogenic bacteria (Contreras et al. 2014). However, also many non-pathogenic bacteria rely on the salvage of heme-bound iron in iron-depleted environments (Wilks 2002).

Similar to iron, heme causes severe toxicity at elevated levels. In human cells, the toxicity is speculated to partly originate from the redox-active iron, triggering the formation of reactive oxygen species via the Fenton and the Haber–Weiss reaction, thereby damaging lipids, proteins and genomic DNA (Kumar and Bandyopadhyay 2005). Additionally, heme is capable of promoting oxidation after accumulation in biological membranes inducing cell lysis (Aft and Mueller 1984). The mechanism of how this molecule affects bacterial cells is not conclusively unraveled (Anzaldi and Skaar 2010), but previous studies indicated that also non-iron metalloporphyrins can show a significant antibacterial activity (Stojiljkovic et al. 1999). This hints at a general, iron-independent toxicity of certain porphyrin structures. These probably stimulate

the generation of reactive oxygen species, especially upon illumination (Nakahigashi et al. 1991).

Heme is chemically versatile and allows a variety of potential interactions with proteins (Brewitz et al. 2017). A schematic overview of some common heme interacting proteins is given in Fig. 1. One can in general distinguish between two types of heme sensing systems (Fig. 1A): either heme can be sensed directly, or the porphyrin can act as a sensor of gases such as O₂, CO or NO as well as of the redox state of the cell (Girvan and Munro 2013).

In hemoproteins, heme is bound with high-affinity coordination motifs and serves as prosthetic group (Fig. 1B) for enzymes of essential reactions, including electron transfer, cell respiration or oxygen metabolism (Smith et al. 2010; Li et al. 2011). In contrast, transient binding allows for situation-dependent responses and rapid reactions to environmental fluctuations (Granick et al. 1975). Transient heme binding is found for several heme-responsive sensor systems involved in transcriptional regulation. Targets of these systems are highly diverse ranging from genes involved in the circadian rhythm (e.g. NPAS2 (Dioum et al. 2002), Rev-erba and Rev-erbb (Raghuram et al. 2007)), demethylases (e.g. Gls1 (Lal et al. 2018)) or glucose metabolism (Rev-erba (Yin et al. 2007)). Intuitively, another important role of heme sensor systems is the control of heme homeostasis, which is the focus of this review. Heme-protein interactions can also trigger protein degradation (Qi, Hamza and O'Brian 1999; Ogawa et al. 2001; Dent et al. 2019)), the regulation of K⁺-channels (e.g. mammalian Kv1.4 channels

Received: September 28, 2021. Revised: December 21, 2021. Accepted: January 11, 2022

© The Author(s) 2022. Published by Oxford University Press on behalf of FEMS. All rights reserved. For permissions, please e-mail: journals.permissions@oup.com

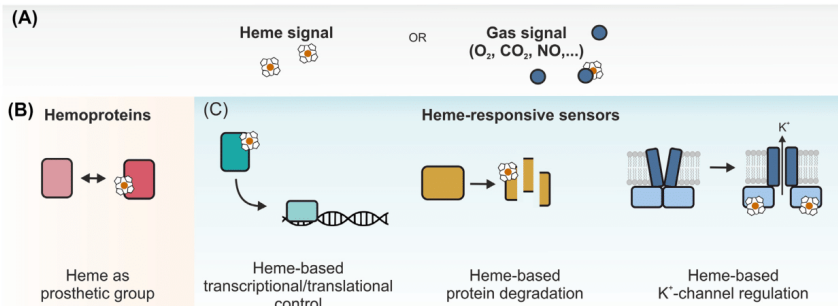


Figure 1. Diversity of heme-binding proteins. Schematic overview of the most common types of heme proteins. **(A)** In general, we can distinguish between two types of heme sensors: proteins, which directly sense heme and proteins, where heme serves as sensor for gases or redox stress. **(B)** Hemoproteins are enzymes that use heme as prosthetic group and have diverse functions, including electron transfer, oxygen transport, oxygen storage, reduction of peroxides, etc. (Chapman, Daff and Munro 1997). **(C)** Transient Heme-protein interaction may have diverse physiological consequences, including regulation of transcription, proteasome-dependent or -independent protein degradation, regulation of K⁺-channels. Further examples are the regulation of tRNA synthetases, mRNA splicing, or other protein-protein interactions, which are further summarized e.g. in Shimizu et al. (2019).

(Tang et al. 2003; Sahoo et al. 2013)) or the heme-based regulation of tRNA synthesis, mRNA splicing, or protein-protein interactions, which are further summarized e.g. in the review article by Shimizu et al. (2019).

In this review, we will focus on heme sensor systems directly involved in heme sensing, but will not discuss the role of heme-binding proteins in gas sensing (here, the interested reader is referred to the following articles: Green et al. (2009); Girvan and Munro (2013); Martínková et al. (2013); Shimizu et al. (2015)). Here, we will compare and discuss transient heme sensor systems across the kingdoms, which contribute to the transcriptional regulation of heme/iron homeostasis, including heme utilization, heme biosynthesis, detoxification, or related responses. In general, we will discuss similarities and differences of prokaryotic and eukaryotic heme sensor systems with respect to signal perception, transduction and regulon structure. The examples also highlight the variability in heme binding motifs in the different systems across domains of life. An overview of the heme sensor systems discussed in this review is presented in Fig. 2 and Table 1.

Heme sensor systems in eukaryotes

In eukaryotes, mainly two different heme sensor systems acting as transient heme sensors have been described: The transcription factor BACH1 balancing the cellular heme content of mammalian cells, and Hap1 of the yeast *Saccharomyces cerevisiae*, which regulates the expression of heme-requiring enzymes like cytochromes in a heme-dependent manner in response to hypoxia.

BTB and CNC homology 1 (BACH1) in mammalian cells

In mammalian cells, the activity of a conserved transcription factor named BTB and CNC homology 1 (BACH1, Fig. 2A) is influenced by heme-binding (Ogawa et al. 2001). This protein acts as a key player in balancing the cellular heme content by regulating HMOX1, encoding a heme oxygenase (Sun et al. 2002), as well as the iron storage protein ferritin, a thioredoxin reductase (Hintze et al. 2007), the NAD(P)H:menadiol oxidoreductase 1 (Dhakshinamoorthy et al. 2005) and more than 50 other target genes (Wernatz et al. 2011).

(Wernatz et al. 2011).

In the absence of heme, BACH1 was shown to heterodimerize with small Maf proteins (e.g. MafF, MafG, MafK), which represent conserved transcription factors among vertebrates (Simile et al. 2018). BACH1-Maf heterodimers bind to the promoter regions of Maf recognition elements (MARE) in order to inhibit the transcription of numerous target genes, like e.g. HMOX1 encoding a heme oxygenase (Igarashi et al. 1994; Oyake et al. 1996; Motohashi et al. 1997; Igarashi et al. 1998). In order to achieve dimerization with Maf proteins, BACH1 contains at least two functional domains: (i) an N-terminal BTB/POZ domain containing the protein interaction motif to form a multivalent DNA-binding complex (Bardwell and Treisman 1994; Zollman et al. 1994; Igarashi et al. 1998), and (ii) a C-terminal bZip domain which binds DNA and consequently mediates the heterodimerization (Oyake et al. 1996).

The presence of intracellular heme negatively regulates the repressor activities of BACH1 (Oyake et al. 1996). This is achieved by a direct interaction of heme with BACH1, binding with high affinity to the cysteine-proline (CP) motifs of the heme-responsive motifs (HRMs). CP-motifs are well known heme binding motifs (Lathrop and Tímko 1993), which will be discussed in the context of HRMs more detailed throughout chapter 5. BACH1 overall contains six CP-motifs: two downstream the BTB/POZ domain (CP1-2) and four surrounding the bZip domain (CP3-6). However, it was shown that only the latter ones are pivotal for function (Ogawa et al. 2001). Interestingly, no single CP-motif is essential, but simultaneous mutation of all four motifs (CP3, CP4, CP5 and CP6) abolished interaction with heme, suggesting cooperativity between CPs (Ogawa et al. 2001). While the exact molecular mechanism of heme-responsive activation remains to be elucidated, a recent study in mice suggests a binding of a CP-motif to heme via a 5-coordination (Segawa et al. 2019). Upon heme binding, structural changes around the bZip domain are likely, which finally lead to the dissociation of BACH1 from the enhancers and a derepression of target genes (Ogawa et al. 2001). For example, derepressed MafK can bind to the transcription factor Nrf2 that activate several protective antioxidant genes (Dhakshinamoorthy et al. 2005). In addition, a nuclear export signal for BACH1 is activated, as well

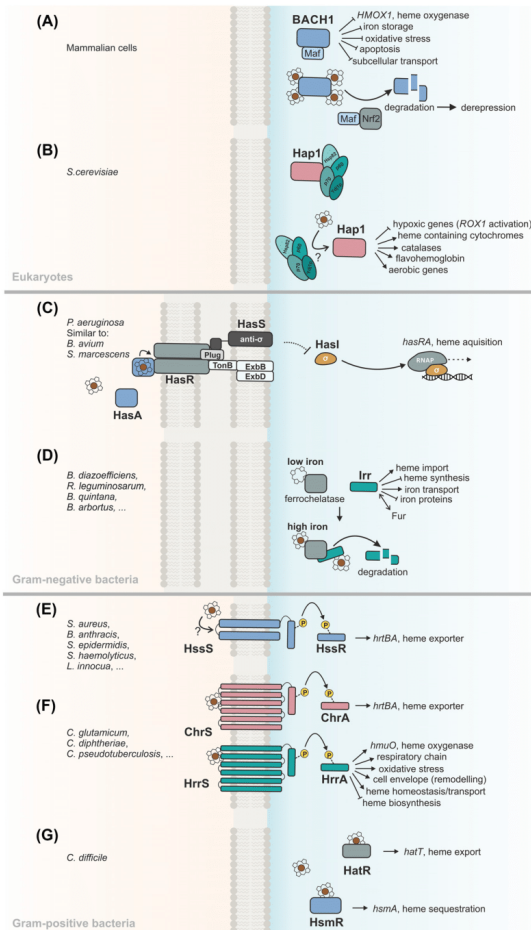


Figure 2. Heme sensor systems controlled by transient heme-protein interaction: **(A)** In *Saccharomyces cerevisiae*, Hap1 (pink) regulates heme containing enzymes like e.g. cytochromes in response to hypoxia sensed indirectly via the availability of heme. Upon heme binding to the protein, Hap1 is released from the high-molecular weight complex (shades of turquoise) allowing it to bind to target promoter regions and control gene expression. **(B)** In mammalian cells, BACH1 (dark blue) regulates more than 50 genes involved in heme homeostasis. BACH1 forms heterodimers with Maf proteins (light blue) to inhibit transcription of its targets. Upon heme binding, BACH1 is dissociated and Maf proteins can bind to the transcription factor Nrf2 (grey), which activates several genes encoding protective antioxidants. **(C)** In *Pseudomonas aeruginosa*, the Has system responds to the presence of heme for the regulation of its acquisition. The system consists of the outer membrane receptor HasR (grey) with a N-terminal plug domain (light grey), the membrane bound anti-sigma factor HasS (dark grey) shown with TonB-ExbB (white) and the extracytoplasmic function (ECF) σ factor HasI (yellow). HasR senses heme with the help of the hemophore HasA, transduces a signal to HasS, which releases HasI initiating transcription. Imported heme further activates PhuTUV for uptake into the cytoplasm, where heme is transported by the heme binding protein PhuS to the heme oxygenase HemO. **(D)** The Irr protein (turquoise) represents the global regulator of iron/heme homeostasis in rhizobia, by sensing iron pools indirectly via heme. When iron is present, the ferrochelatase (grey) inserts iron into protoporphyrin IX yielding heme. The heme-loaded ferrochelatase binds to Irr, thereby inhibiting it. Heme binding to Irr leads to proteins degradation and derepression of its target genes. **(E)** In Gram-positive bacteria, two-component systems represent a common mode of heme sensing. In *Bacillales*, the two-component system HssSR (blue) activates the expression its target in a heme-dependent manner. Upon sensing of heme, autophosphorylation (yellow circles) of the histidine kinase HssS allows phosphotransfer to the response regulator HssR for its activation. HssR then functions as a transcriptional regulator for the activation of the expression of *hrtBA* encoding a heme exporter. **(F)** In *Corynebacteria*, the two paralogous two-component systems ChrSA (pink) and HrrSA (turquoise) show a high level of cross-talk and control heme detoxification and heme homeostasis, respectively. **(G)** In anaerobic Clostridia, the two transcriptional regulators HatR (grey) and HsmR (blue) are necessary for heme detoxification. Upon heme binding, HatR activates the heme efflux pump *hat*, while HsmR activates HsmA important for heme sequestration. For more detailed information on these systems refer to Fig. 4.

Table 1. Overview of heme sensor systems.

Heme sensor	Organisms	Heme effect ¹	Components ²	Heme binding	Mode of action/Function	Target sequence	Selected references
Hap1	<i>S. cerevisiae</i>	+	Transcription factor Hap1 , Hsp82, p70, p60, Ydj1p	Mainly C-terminal HRM7 with CP motif (C1192-P); additionally HRM1-6	Transcriptional regulator in cell respiration (cytochromes), also redox stress and oxygen sensing; $K_D < 20 \mu\text{M}$ (with peptide)	CGGnnnTAnCGG	Zhang and Guarente (1995), Hon et al. (2000), Lee et al. (2003)
BACH1	Mammalian cells	-	BACH1 , Maf	Four pivotal, cooperative CP motifs (CP3-6) out of six; CP6; C ⁶⁹ -P; binding via S-coordinated bond	Repressor for heme oxygenase, iron storage, oxidative stress, etc.; $K_D \approx 13.7 \mu\text{M}$	TCCTGAC(G)TCAGCA (MARE)	Ogawa et al. (2001); Zenke-Kawasaki et al. (2007); Segawa et al. (2019)
HasR/ HaeS/ HasI/ HaeA	<i>P. aeruginosa</i> , <i>S. marcescens</i>	+	Hemophore HaeA , sensor domain HasR , anti- σ -factor HaeS , σ -factor HasI	In <i>P. aeruginosa</i> : HasA, H ⁸² , Y ⁷⁵ , H ⁸³ , HasR; consensus FRAP domain (N ⁶⁵⁹ -R-P-P), NPNL domain (N ⁸³⁴ -P-F-I), histidine residue in between (H ⁶⁵⁴)	Transcriptional activator for heme acquisition and utilization	n.d.	Dent and Wilks (2020)
BhuR/ RhuR/ RhuI	<i>B. avium</i> , <i>B. pertussis</i>	+	sensor domain BhuR , extracytoplasmic sigma factor RhuI , regulator RhuR	In <i>B. avium</i> : consensus FRAP domain (Y ⁶⁹⁴ -R-A-P), NPNL domain (N ⁸²⁷ -P-N-L), tyrosine residue in between (Y ⁶⁸⁹)	Transcriptional activator for heme acquisition (and utilization)	n.d.	Murphy et al. (2002)
Irr	<i>B. diazoefficiens</i> , <i>R. leguminosarum</i> , <i>B. quiniana</i> , <i>B. arborius</i>	-	Irr	In <i>B. diazoefficiens</i> : High-affinity site for oxidized heme: CP motif (C ²⁸ -C-P-W-H-D); Low-affinity site for reduced heme: His-rich motif (H ¹¹²⁻¹¹⁹)	Iron sensing via heme, transcriptional regulator for heme synthesis, import and utilization, oxidative stress; $K_D \approx 0.01 \mu\text{M}$ for oxidized heme	TTTAGAAmmTTCTAAA	(Qi et al. 1999; Yang et al. 2005; Rudolph et al. 2006; Singleton et al. 2010)
HssSR	<i>S. aureus</i> , <i>B. anthracis</i> , <i>S. epidermis</i> , <i>S. haemolyticus</i> , <i>L. imicola</i>	+	Histidine kinase HssS and response regulator, HssR , ABC-transporter HrtBA	? ; suggested to be indirect	Detoxification from heme; signalling/DNA binding	GTTCATATTnnGTTTCATATT	(Stauff et al. 2007; Stauff and Staar 2009b)
ChrSA/ HrsA	<i>C. glutamicum</i> , <i>C. diptheria</i> , <i>C. pseudotuberculosis</i>	+	ChrS/ HrsS and response regulators ChrA / HrA	ChrS potentially extracellular sensing; HrsS rather inside the membrane; HrsS in <i>C. glutamicum</i> : Y ¹¹² , F ¹¹⁵ , F ¹¹⁸	Detoxification from/Utilization of heme	n.d.	Bibb et al. (2007); Keppel et al. (2018)
HatR/ HsmR	<i>C. difficile</i>	+	Transcriptional regulators HatR and HsmR	Involved histidine residues: H ⁶⁹ in HatR , H ⁶⁶ in HsmR	Detoxification from heme	n.d.	Knippel et al. (2020)

¹ + heme leads to higher levels of this protein; — = heme leads to lower levels/degradation of this protein. ² - Proteins, which sense the heme, are bold.

therefore represents a typical anti-sigma factor, which is involved in the activation of HasI (Dent et al. 2019).

In addition to this heme response for heme acquisition, heme is also transported through the HasR receptor in a TonB-dependent manner. TonB is an energy-transducing protein, and the acquisition of heme as an alternative iron source has already been shown to be TonB-dependent in several Gram-negative bacteria (e.g. (Biswas et al. 1997; Elkins et al. 1998; Occhino et al. 1998)). In *P. aeruginosa*, HasR-imported heme is then further translocated to the cytoplasm by the periplasmic heme import system PhuT-PhuUV. In this case, it was described that the Has system is mainly required for heme sensing, while the *Pseudomonas* heme uptake (Phu) system is additionally required as major heme transporter for efficient import into the cytosol (Smith and Wilks 2015; Dent et al. 2019; Dent and Wilks 2020). Comparing it to *S. marcescens*, there is also a non-hemophore heme uptake system (Hem). However, this system appears to have no significant role in heme uptake—in contrast to the *Pseudomonas* system (Benevides-Matos and Biville 2010; Dent et al. 2019), underlining possible diversity in regulations among these systems.

In the cytoplasm of *P. aeruginosa*, heme is bound by the heme binding protein PhuS, which further transfers the porphyrin to the heme oxygenase HemO, which cleaves the tetrapyrrole ring yielding iron, CO and biliverdin IX β and IX δ . The latter two heme metabolites then act as positive feedback regulators of the hemophore HasA (Mouriño et al. 2016). Apart from biliverdin IX β - and IX δ -dependent regulation of protein level, it was also shown in *P. aeruginosa* that post-transcriptional processing of *hasRA* mRNA contributes to the Has systems regulation. This processing is suggested to be performed by small regulatory RNAs (sRNAs) and results in different stabilities for a differentially regulated expression of the co-transcribed genes *hasR* and *hasA* (Dent et al. 2019). Even further, the *hasRA* operon is also regulated by Fur (Ochsner et al. 2000), integrating the utilization of heme in the global iron network of the cell. However, in *S. marcescens*, the Has system is rather regulated at the level of transcription with HasI regulating HasS (Biville et al. 2004). In general, when heme levels decline, HasS is activated and sequesters HasI again, thereby resulting in a down-regulation of the Has systems dependent on availability of heme (Biville et al. 2004; Dent et al. 2019).

RhuR and the sigma factor RhuI in Burkholderiales

The Gram-negative bacterium *Bordetella avium* responds to heme by controlling expression of the *bhuRSTUV* heme acquisition system also via an ECF σ -factor system. This three-component system includes (i) BhuR, the outer membrane receptor for heme (Murphy et al. 2002), (ii) RhuR, a membrane bound activator protein (Kirby et al. 2004) and (iii) the ECF σ -factor RhuI (Kirby et al. 2001). The components of these systems are homolog to the Has systems of *Pseudomonales* described in the section before. For HasR-BhuR, HasS-RhuR and HasI-RhuI, there are identities above 26% and significant similarities above 40% (NCBIResourceCoordinators 2016). However, no homolog to the hemophore HasA of *P. aeruginosa* or *S. marcescens* is present in *B. avium*, implying a significant difference between these systems not only concerning heme acquisition but also regulation. However, a HasA homolog with 35% identity to that of *P. aeruginosa* can be found for *B. petrii*.

Two promoters, P_{bhuR} and $P_{bhuRSTUV}$ control the expression of the *rhuI*-*bhuRSTUV* cluster (King et al. 2005). Overall, this regulatory cascade also responds to both iron stress and the presence of heme and hemoglobin (Kirby et al. 2001; Murphy et al. 2002).

In the presence of iron, transcription of the *bhuRSTUV* operon as well as that of *rhuI* is repressed by Fur, the global iron-dependent transcriptional repressor (Kirby et al. 2001). Upon iron starvation, P_{bhuR} is derepressed, and in addition to RhuI and RhuR, low levels of *bhuR* are expressed supporting recognition of heme at the outer membrane. It is assumed that this is the result of an incomplete termination of *rhuR* transcription. This rare 'read-through transcription' allows a fast response if heme becomes available as an alternative iron source (Kirby et al. 2004; King et al. 2005). In the presence of extracellular heme, the cascade starts by binding of heme to the outer membrane receptor BhuR. This receptor also includes a consensus FRAP- and NPFL motif, with Y⁶⁰⁴-R-A-P and N⁶²⁷-P-N-L in *B. avium*, respectively (Bracken et al. 1999; Ahn et al. 2005; Fusco et al. 2013). However, unlike in other bacterial outer membrane heme receptors, BhuR does not contain the conserved histidine between the FRAP and the NPFL domain, but a similar tyrosine at position 616 (Murphy et al. 2002). Both histidine and tyrosine were described to be involved in transient heme binding (Li et al. 2011) (compare section 5). Further, two TonB boxes are present in BhuR, required for the interaction with TonB for functioning of the heme utilization system (Murphy et al. 2002; Richard et al. 2019).

BhuR subsequently transduces a signal across the periplasm to RhuR, which was proposed to contain a C-terminal periplasmically exposed controller domain for signal interception. The exact mechanism of how the signal is actually transduced is not yet known, but the signal is further propagated through the cytoplasmic membrane to RhuI. Activation of RhuI is achieved by its interaction with the N-terminal 97-amino-acid region of RhuR and some conformational changes. Therefore, RhuR represents an untypical anti-sigma factor, which is involved in the activation of RhuI instead of simple sequestration and inactivation. Consequently, activated RhuI escorts the RNA polymerase to P_{bhuR} directly or indirectly, leading to high transcription levels of *bhuR* as well as *bhuSTUV* encoding for the heme uptake system (Kirby et al. 2001; Vanderpool and Armstrong 2003; Kirby, King and Connell 2004). RhuI is described as an absolute necessary activator of BhuR for a respective response to heme utilization (King et al. 2005). When iron requirements are met again, Fur-dependent regulation allows for a rapid downregulation of heme acquisition.

This three-component signal transduction cascade seems to be highly conserved among *Bordetella* species, as similar loci have been described in the mammalian pathogens *B. pertussis* and *B. bronchiseptica* (*hurI*-*bhuRSTUV*) (Vanderpool and Armstrong 2001; King-Lyons et al. 2007). These systems resemble the control of the ferric dicitrate uptake system *fecI*R-*fecABCDE* of *E. coli* (Pressler et al. 1988).

Indirect sensing via Irr in Rhizobiales

In contrast to other model organisms, rhizobia feature a unique way of controlling iron homeostasis. Their setup is particularly interesting because these bacteria integrate heme and iron homeostasis into one regulon and thereby sense 'functional' iron pools in the form of heme instead of free iron (Johnston et al. 2007; O'Brian 2015).

The iron response regulator protein (Irr) (Fig. 2D) was originally identified in the nitrogen-fixing, symbiotic bacterium *Bradyrhizobium diazoefficiens* (former *B. japonicum*) (Hamza et al. 1998) and was identified as key transcriptional regulator of iron homeostasis controlling heme biosynthesis, import and utilization (Qi et al. 1999). Further Irr orthologues were analyzed in *Rhizobium leguminosarum* (Singleton et al. 2010), *Bartonella quintana* (Parrow et al.

2009), and *Bruceella abortus* (Martinez et al. 2005). Irr proteins were found to have both activator and repressor functions. Upon iron limitation, Irr accumulates and acts as a repressor for, e.g. *hemB*, which encodes the delta-aminolevulinic acid dehydratase of the heme biosynthesis pathway. Thereby, Irr repression avoids the accumulation of toxic porphyrin precursors due to lack of iron (Hamza et al. 1998). Furthermore, Irr serves as an activator of the *hmuVUT* operon, encoding a heme-import system, and further genes responsible for the uptake of ferric iron, to allow fast uptake when these resources become available (Hamza et al. 1998; Rudolph et al. 2006). Binding to the respective target DNA depends on a cis-acting DNA element, called iron control element (ICE) upstream of the promoter (Rudolph et al. 2006).

Although Irr is a Fur-like protein, it does not bind to iron directly, but senses the iron pool indirectly via heme. Under iron-replete conditions, heme directly interacts with Irr at a heme regulatory motif (HRM) near its N-terminus in *B. diazoefficiens* (Qi et al. 1999; Qi and O'Brian 2002). This HRM contains the putative motif G²⁸-C-P-W-H-D, with C²⁹P³⁰ belonging to the known CP-motif, was shown to be essential for binding (Qi et al. 1999). Apart from this high-affinity binding site at the HRM for ferric (oxidized) heme, further studies postulated that there is an additional low-affinity ferrous (reduced) heme-binding site with a histidine-rich motif (H¹¹⁷⁻¹¹⁹) (Qi et al. 1999; Qi and O'Brian 2002; Yang et al. 2005). Based on mutational studies, both binding sites were suggested to be required for rapid turnover (Yang et al. 2005). In order to properly respond to the iron availability in the cell, it is important that Irr does not sense the extracellular free heme, but only newly synthesized heme. How can this be accomplished? Qi and O'Brian showed that there is a direct interaction of Irr and ferrochelatase, the enzyme catalyzing the terminal step of heme biosynthesis by inserting an iron into protoporphyrin IX (Qi and O'Brian 2002). This Irr-ferrochelatase complex is only formed under high iron conditions i.e. when heme is produced. Consequently, complex formation leads to an inhibition of Irr by the ferrochelatase and allows interaction of Irr with the ferrochelatase-generated heme (Qi and O'Brian 2002). Heme binding finally leads to a degradation of Irr and the consequent derepression of its target genes. This degradation might be accomplished either by changes in the conformation of Irr upon heme binding in such a way that it becomes accessible to proteolysis or the binding leads to protein damage due to the formation of local reactive oxygen species and subsequent proteolytic degradation (Qi et al. 1999; Yang et al. 2006; Kitasujii et al. 2016; Kobayashi et al. 2016).

In *Rhodobacter sphaeroides*, Irr was found to be involved in the oxidative stress response, e.g. repressing the expression of the catalase gene *katE* under non-stress conditions (Peuser et al. 2012). It is worth noting that some alphaproteobacteria rely entirely on Irr for their iron-responsive gene regulation, while Fur possesses a rather minor role compared to *E. coli*, where it represents the global regulator of iron homeostasis (Johnston et al. 2007). These findings highlight the special role of this Fur-like protein as heme/iron sensor system in Rhizobia.

Fur orthologue Har in Bacteroidales

A recent study has emphasized the heme-associated regulator (Har) protein as a heme-dependent transcriptional regulator in *Porphyromonas gingivalis*—a Gram-negative oral pathogen associated with the biofilm-mediated periodontal disease. Har is a Fur orthologue and plays a role in hemin-responsive biofilm development. In the presence of heme, Har binds it via a CP-motif (C⁵⁷) triggering structural changes within Har. This consequently af-

fects the expression of several genes, including *hmuY*, which is a hemophore scavenging heme from various hemoproteins, and the replication initiator *dnaA*. Overall, Har was described as a positive regulator of biofilm formation (Butler et al. 2014). However, recent studies claimed that the heme binding cannot be shown for all Har variants of different *P. gingivalis* strains (Śmiga et al. 2019). Thus, further experimental clarification is needed to understand the role of this system in heme-responsive gene expression depending on the strain background.

Heme-responsive two-component systems of Gram-positive bacteria

In Gram-positive bacteria, two-component systems (TCS) appear to be the predominant form of heme sensing. Prototypical TCSs consist of a membrane bound histidine kinase and a cytoplasmic response regulator receiving the signal from the sensor kinase (Hoch 2000; Mascher et al. 2006). Upon stimulus perception, e.g. heme-binding, the histidine kinase undergoes autophosphorylation at a conserved histidine residue. The phosphoryl group is subsequently transferred to a conserved aspartate residue of the response regulator. Typically, the phosphorylated form of the response regulator represents its 'active' state, in which it initiates an appropriate cellular output, commonly by binding to the promoter regions of target genes and thereby acting as a transcriptional regulator (Stock et al. 2000; Mascher et al. 2006; Capra and Laub 2012). Two different examples of heme sensor systems based on TCSs are known in Gram-positive bacteria: the HssRS system and the paralogous systems HrtSA and ChrSA. Similarities and differences in heme-responsive TCS-signaling are discussed in the following.

The heme exporter HrtBA is a prevalent target of heme-responsive TCSs in Gram-positive bacteria

Strikingly, there is one conserved target controlled by all known heme-responsive TCSs in Gram-positive species: The heme-regulated ABC transporter HrtBA. This exporter is required to counteract toxic heme levels and it consists of two components: the ATPase component HrtA and the permease HrtB. Until now, it could not be directly shown that heme is the substrate of export for HrtBA, or if it is rather a toxic intermediate (Stauff et al. 2008). However, increased levels of intracellular heme in mutants lacking HrtBA (e.g. *Staphylococcus aureus* as well as *Lactococcus lactis*) (Joubert et al. 2014; Wakeman et al. 2014), are in favor of the hypothesis that heme is, indeed, the respective substrate of this exporter. Studies confirmed that the activity of HrtAB is essential for e.g. *Staphylococcus aureus* and *Corynebacterium glutamicum* to allow growth at toxic heme levels (Torres et al. 2007; Stauff et al. 2008; Bibb and Schmitt 2010; Heyer et al. 2012). There are many orthologues of the heme exporter HrtBA in Gram-positives (Torres et al. 2006; Stauff and Skaar 2009a; Bibb and Schmitt 2010; Heyer et al. 2012), as well as further efflux systems, e.g. PefAB or PefRCD in *Streptococcus agalactiae* (Fernandez et al. 2010). Therefore, the strategy of efflux to cope with the toxicity of heme seems to be conserved, especially among pathogenic bacteria.

In silico analysis of overall 39 096 bacterial genomes revealed the presence of *hrtBA* orthologues in 3232 of them, from which almost 99% belong to the phyla of Firmicutes or Actinobacteria (Fig. 3A). Among those, overall 4750 genomic hits were found for the *hrtBA* locus. In approximately half of the analyzed Actinobacteria (443 of 905) even two or more copies of *hrtBA* orthologues are present and the same applies for Firmicutes (1000 of 2286).

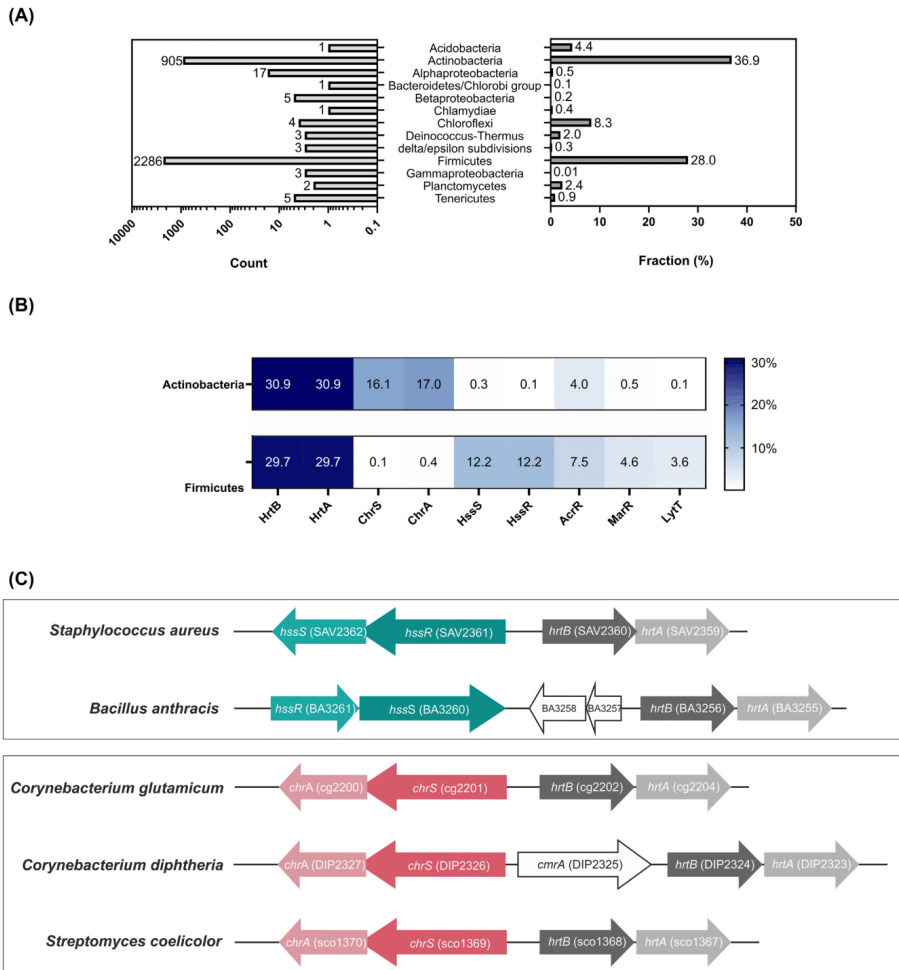


Figure 3. Analysis of *hrtB* synteny. The heme exporter HrtB is a conserved target of two-component systems (TCS) in Gram-positive bacteria. **(A)** In silico analysis revealed 3232 bacterial genomes possessing *hrtBA* orthologues. On the y-axis the phyla are listed. Bars to the left indicate the count of bacterial genomes having a hit in the respective phylum; bars to the right represent the fraction of genomes of the particular phylum harboring *hrtBA* orthologues **(B)** Analysis of co-occurrences of *hrtBA* and genes encoding transcriptional regulators, including TCSs. Overall 4704 *hrtBA* loci were found among 2286 Firmicutes and 905 Actinobacteria genomes. Numbers represent the percentage of the respective transcriptional regulator domain found 5 kb up- and downstream of *hrtBA* in Actinobacteria and Firmicutes. The analysis confirms a conserved synteny of *hssRS* with *hrtBA* in Firmicutes, while *chrSA* is predominantly found in vicinity to *hrtBA* in actinobacterial genomes **(C)** Genomic organization of the *hrtBA* loci in different Gram-positive species. The *hrtBA* operon is shown in shades of grey, the TCS operons in shades of green and pink.

When inspecting 5 kb up- and downstream of the identified *hrtBA* operon using the COG database (clusters of orthologous groups of proteins (Tatusov et al. 2000)), we found a HssRS-like TCS in more than 40% of the loci in Firmicutes and a ChrSA-like TCS in > 50% of the actinobacterial genomes containing a *hrtBA* locus (Fig. 3B). Among the 20 most abundant domains found at the *hrtBA* locus, we identified three further transcriptional regulator

domains—namely AcrR, MarR and LytT (Fig. 3B). Although being in close proximity, no conserved pattern in terms of synteny could be identified, as it is evident for the ChrSA and HssRS TCSs.

A schematic genomic organization of the HrtBA locus and a respective TCS encoded in close proximity for different species is shown in Fig. 3C. These two-component systems will be described in the following sections.

Two-component system HssRS in Bacillales

The pathogenic species *Bacillus anthracis* and *Staphylococcus aureus* have been the model systems to investigate the function of the TCS called the heme sensor system HssRS, which plays a crucial role in the heme-dependent activation of the expression of the genes encoding the heme exporter HrtBA in these species (Fig. 2E) (Stauff and Skaar 2009a,b). The TCS is composed of the cytoplasmic response regulator HssR and the histidine kinase HssS that is anchored to the membrane via two transmembrane helices (Torres et al. 2007). The operons of *hssRS* and *hrtAB* are divergently oriented (Torres et al. 2007) (Fig. 3C).

The periplasmic sensing domain of HssS consisting of 132 amino acids is flanked by two transmembrane helices (Stauff and Skaar 2009a). Nevertheless, the actual heme sensing mechanism is not yet fully understood—a blind spot for all heme-responsive TCS so far. No potential heme-binding domain in HssS could be revealed and its sensing domain does not contain any conserved heme-binding site found in other heme proteins (Torres et al. 2007). Interestingly, it was suggested that the *S. aureus* kinase HssS might not sense heme molecules directly. The application of several non-iron metalloporphyrins showed that, instead, secondary effects of heme toxicity (e.g. heme-induced cell-wall damage or membrane disruption) might influence the activity of this system (Stauff and Skaar 2009b; Wakeman et al. 2014). The presence of heme or its toxic effects triggers autophosphorylation of a histidine residue (H²⁴⁹ in *S. aureus*) in HssS, with consequent phosphotransfer to the aspartic acid residue of the response regulator HssR (D⁵² in *S. aureus*) (Stauff et al. 2007). HssR is thereby activated—probably via conformational changes (Bronner et al. 2004)—and binds to the promoter region of *hrtAB* (Torres et al. 2007). *S. aureus* codes for a set of proteins, which are designated as iron-regulated surface determinants (Isd) as well as the heme transport system (Hts). These proteins are important for the utilization of heme as alternative iron source. However, Stauff et al. claimed that HssRS probably does not regulate the expression of these genes, but is rather specific for *hrtAB* (Stauff et al. 2007).

A recent study demonstrated significant cross-talk between HssRS and a second system called HssRS interfacing TCS (HitRS) in *B. anthracis* (Mike et al. 2014; Pi et al. 2020). HitRS was shown to respond to compounds, which induce cell envelope stress, and consequently influence the expression of the operon *hitPQRS*, which includes a yet unstudied ABC transporter HitPQ (Mike et al. 2014). HitRS cross-regulates P_{Hrt} at the transcriptional level, while HssRS cross-regulates P_{hit} at both transcriptional as well as on the level of phosphorylation. This interaction of HssRS and HitRS nicely demonstrates an additional integration of cell envelope stress into the heme-responsive HssRS regulon.

In general, the activation of the transporter by the TCS HssRS was shown to be highly important for coping with heme stress as deletion of either component resulted in drastically elevated heme sensitivity and an attenuated virulence of *S. aureus* (Stauff et al. 2007; Torres et al. 2007). Homologous TCSs can be found in *Lactococcus lactis*, *Staphylococcus epidermidis* or *Listeria innocua* (Stauff and Skaar 2009a). Notably, *hssRS* homologs seem to be absent in non-pathogenic Bacillales like *B. subtilis* or *B. licheniformis* and this was attributed to the higher demand of heme tolerance for bacterial species infecting mammalian hosts (Stauff and Skaar 2009b). However, the relevance of the HrtBA transporter and its control by a heme-responsive TCS was also described for the non-pathogenic actinobacterium *Corynebacterium glutamicum*, which uses heme as an important alternative iron source. Here, control is mediated by a different TCS setup described in the next section.

Two-component systems HrrSA and ChrSA in Corynebacteriaceae

A special setup of heme sensor systems can be found in most members of the *Corynebacteriaceae* family. Here, two paralogous TCSs, named HrrSA and ChrSA, represent key players in the control of heme homeostasis. The interaction and regulons of these systems have in particular been studied in the human pathogen *C. diphtheriae* as well as the biotechnologically relevant soil bacterium *C. glutamicum* (Schmitt 1999; Bibb and Schmitt 2010; Frunzke et al. 2011; Heyer et al. 2012; Burgos and Schmitt 2016) (Fig. 2F). Remarkably, this is one example of two paralogous systems reacting to the same stimulus, which is in this case heme; other examples are the NarX-NarL and NarQ-NarP systems of *Escherichia coli*, which both respond to nitrate (Noriega et al. 2010). Nevertheless, Bott and Brocker also reported several exceptions of *Corynebacteriaceae* possessing only one of those TCS e.g. *C. efficiens* (only HrrSA) or *C. jeikeium* (only ChrSA) (Bott and Brocker 2012).

Since the two TCSs HrrSA and ChrSA share significant sequence identity (*C. glutamicum* HrrS versus ChrS: 39%; HrrA versus ChrA: 57% (Heyer et al. 2012)), cross-talk at the level of phosphorylation and regulation of target genes was no surprise for both *C. glutamicum* (Hentschel et al. 2014) (Fig. 4) as well as *C. diphtheriae* (Bibb et al. 2007).

Both systems, ChrSA and HrrSA, show marked differences with respect to their regulons in *C. glutamicum*. While HrrSA acts as a global regulator of heme homeostasis, the function of ChrSA appears to be focused on the detoxification of heme (Frunzke et al. 2011; Heyer et al. 2012; Hentschel et al. 2014) (Fig. 4). Recently, genome-wide mapping of HrrA-binding led to the identification of more than 200 different genomic targets of HrrA (Keppel et al. 2020). Among these targets are inter alia *hmuO* encoding the heme oxygenase, as well as genes involved in heme biosynthesis, the respiratory chain, oxidative stress response, and cell envelope remodeling (Keppel et al. 2020). In contrast, the only target promoter of ChrA is the operon encoding the HrtBA heme exporter, which is divergently located to *chrSA* (Fig. 3C) (Ito et al. 2009; Heyer et al. 2012).

However, in contrast to *C. glutamicum*, several studies in *C. diphtheriae* suggest considerable overlap of the HrrSA and ChrSA regulons in this species (Bibb et al. 2005; Bibb and Schmitt 2010). Here, ChrSA was proposed to be the major TCS required for *hmuO* activation (80%), with a rather minor contribution of HrrSA (20%) (Bibb et al. 2007). These examples illustrate the plasticity of heme-responsive TCS signaling which is continuously adapting to the genetic environment and the ecological niche of the particular organism.

Both histidine kinases HrrS and ChrS are embedded into the cytoplasmic membrane via six α -helices and have been proposed to sense the hydrophobic heme molecule via an intramembrane sensing mechanism (Ito et al. 2009; Bibb and Schmitt 2010; Keppel et al. 2018). The heme-binding pocket appears to be different for ChrS and HrrS. For HrrS, the three amino acids Y¹¹², F¹¹⁵ and F¹¹⁸ were identified to be crucial for heme binding. However, mutation of the respective Y⁸⁷-F⁹⁰-F⁹⁴ motif in ChrS did not abolish heme sensing but caused only a red shift of the Soret band (Keppel et al. 2018). This underlines differences of heme signal perception in both histidine kinases (compare section 5). For transient heme binding in *C. diphtheriae*, a conserved tyrosine residue Y⁶¹ located in the second transmembrane helix of ChrS was described to be crucial (Bibb and Schmitt 2010). However, mutation of the analogous region Y⁷⁴ in HrrS of *C. glutamicum* did not lead to significant effects on heme binding (Keppel et al. 2018).

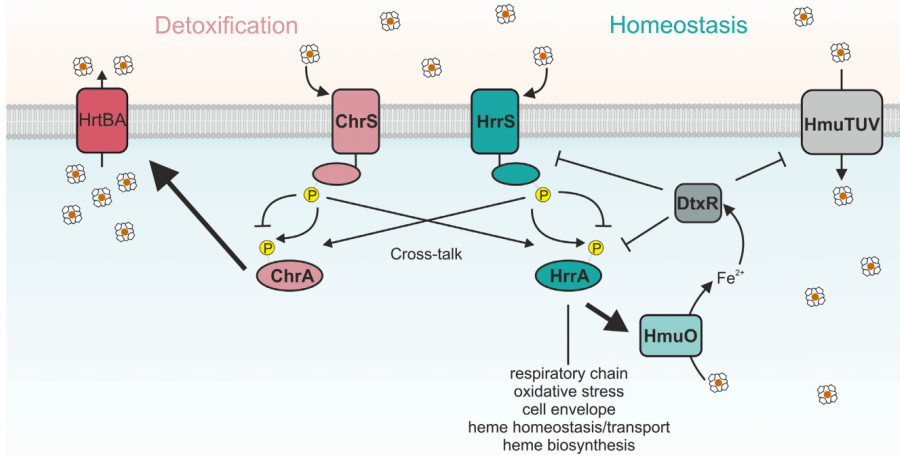


Figure 4. Heme homeostasis and detoxification is mediated by the two paralogous two-component systems HrrSA and ChrSA in *C. glutamicum*. The simplified schematic representation shows the interaction of the two TCS HrrSA (blue) and ChrSA (pink) and their targets *hmuO* and *hrtBA* respectively. HrrSA was recently shown to act as a global regulator of heme homeostasis controlling genes involved in the respiratory chain, heme biosynthesis, oxidative stress or cell envelope remodeling (Keppel et al. 2020). The histidine kinases ChrS as well as HrrS undergo autophosphorylation in response to heme. Both systems display cross-phosphorylation of the respective non-cognate response regulator, but no other TCS of *C. glutamicum* has been shown to activate HrrA or ChrA. In contrast, phosphatase activity of the kinases is specific towards the respective cognate response regulator. The HrrSA-regulated heme oxygenase (HmuO) can degrade heme to release iron for important cellular processes. The released iron can be sensed by DtxR, which consequently represses the expression of *hmuO*, *hrrA* and also *hmuTUV*.

The high similarity between the paralogous TCS provides the basis for cross-talk. In the case of *C. glutamicum* ChrSA and HrrSA, cross-phosphorylation was shown to facilitate a faster onset of the heme detoxification response upon heme stimulus. Here, the HrrS kinase appears to contribute as a 'kickstarter' by activating the non-cognate response regulator ChrA, allowing a faster induction of the *hrtBA* operon (Keppel et al. 2019).

The fast shut-off of P_{HrtBA} is mediated by the phosphatase activity of the ChrS kinase upon stimulus decline, which is very specific to its cognate response regulator ChrA (Hentschel et al. 2014; Keppel et al. 2019). In contrast, both the gene encoding the response regulator HrrA as well as its target gene *hmuO* are under direct control by the global iron regulator DtxR resulting in a delayed activation of *hmuO* upon heme stimulus due to the repression by DtxR (Wennerhold and Bott 2006; Keppel et al. 2019). This hierarchy thereby integrates information on iron availability in the regulation of heme utilization and homeostasis.

For *C. diphtheriae* HrrS a study proposed only minimal kinase activity, but it primarily functions as a phosphatase (Burgos and Schmitt 2016). In summary, several studies have provided insights in the dynamic interplay between ChrSA and HrrSA at the level of phosphorylation, dephosphorylation, and cross-regulation. The interaction with the DtxR regulon provide insights in the homeostatic network coordinated by these systems integrating responses to heme, iron and related stress responses.

Transcriptional regulator HatRT in anaerobic Clostridia

A new concept of sensing heme in the context of detoxification was recently reported for the obligate anaerobic pathogen *Clostrid-*

oides difficile (Knippel et al. 2018; Knippel et al. 2020) (Fig. 2G). *Clostridioides difficile* infection of the host's colon is accompanied by a significant release of heme molecules into the lumen due to erythrocyte lysis and necrotic cell death (Chumberl et al. 2012). In fact, this bacterium is exposed to increased heme levels during infection and is in demand for efficient detoxification strategies. Knippel et al. (2018) identified the heme activated transporter system (HatRT), which is involved in detoxification from heme. This includes the TetR family transcriptional regulator HatR, which binds heme probably transiently ($K_D = 9.2 \pm 1.8 \mu\text{M}$) with H⁵⁹ as critical residue. Formation of the HatR-heme complex derepresses the *hatRT* operon, allowing the expression of the transporter HatT, which functions as a heme efflux pump. Apart from detoxification, this system was also shown to be important for full pathogenicity in a murine model (Knippel et al. 2018).

The same group also identified another heme-sensing membrane protein system HsmRA in *C. difficile* also required for heme tolerance. Heme was shown to bind to the transcriptional regulator HsmR ($K_D = 6.6 \pm 1.1 \mu\text{M}$) at a conserved H⁵⁰ residue, probably placing heme in a cleft between the dimer interfaces and the DNA-binding domain. HsmR then acts as an activator of the *hsmRA* operon. Absorption spectroscopy revealed that the membrane-bound HsmA is able to sequester heme with high-affinity. Heme-bound HsmA then also offers increased resistance to oxidative stress generating compounds, like the clinically relevant antibiotics vancomycin or metronidazole (Knippel et al. 2020) providing another example of the diverse strategies of microbes to deal with elevated heme levels and the resulting oxidative stress.

Diversity of transient heme binding in regulatory proteins

Different heme-responsive sensor systems regulating heme homeostasis across kingdoms were presented in the previous sections (summarized in Fig. 2 and Table 1). Here, we will take a closer look at the necessity of transient binding of regulatory heme, its general features and challenges and compare the binding mechanisms associated with CP- or non-CP-motifs of the different heme sensor systems.

The challenge to sense 'free' heme

Heme is a versatile signaling molecule. Due to its hydrophobic and poorly soluble nature, it can non-specifically bind to lipids, proteins and further macromolecules causing cytotoxicity. Therefore, it is unlikely that there are large amounts of 'free' heme present in the cell. Recent studies claimed that intracellular 'free' heme, which has been newly synthesized or released from hemoproteins due to oxidative stress, can only exist transiently in low amounts and is weakly coordinated with water molecules (Chiabrando et al. 2014; Gallio et al. 2021; Walter et al. 2021). In addition to 'free' heme and heme bound irreversibly to hemoproteins, further studies adopted the term 'exchangeable heme' for another portion of total heme present in the cell. This term describes the part of the heme pool which is transiently bound to proteins or small molecules, so that it can serve as kind of reservoir for heme reflecting its bioavailability (Atamna et al. 2015; de Villiers and Egan 2021; Gallio et al. 2021). These rather low amounts of the free heme and exchangeable heme can collectively be referred to as regulatory heme, which can engage in transient heme-protein interactions and is therefore accessible to the heme sensor systems discussed in this review (Atamna et al. 2015).

Heme responsive motifs (HRMs)

While heme binding in hemoproteins or oxygen-sensor systems is well established in terms of structural aspects or sequence features (Gong et al. 2000; Schneider et al. 2007; Smith et al. 2010; Li et al. 2011), the transient binding of heme by regulatory proteins is less understood, as it becomes evident from the examples covered by this review (summarized in Table 1).

Unlike in hemoproteins, the described heme sensor systems do not covalently bind heme moieties or feature high-affinity heme coordination motifs. They rather display a weak but specific heme binding on the protein surface for temporary events and situation-dependent responses with micromolar affinities (e.g. $K_D \approx 13.7 \mu\text{M}$ for BACH1 (Segawa et al. 2019)), and the ability to rapidly react to environmental fluctuations (Granick et al. 1975; Zhang and Guarente 1995; Qi et al. 1999; Shimizu 2012).

Heme-regulatory motifs (HRMs) are structural characteristics found in several systems. In general, it was described that the central iron ion of heme is coordinated by a heteroatom-containing amino acid side chain at the HRM of the protein. Most often, this amino acid is cysteine (like in Hap1, BACH1 or Irr), but can also be histidine or tyrosine (like in HrrS); nonetheless in few cases it can also be methionine or lysine (Li, Bonkovsky and Guo 2011). However, surrounding amino acids are further contributing to hydrophobic interactions via non-polar amino acids, π - π stacking by the porphyrin ring, electrostatic interactions or hydrogen bonds formed with the propionate side chains (Schneider et al. 2007; Li et al. 2011; Wißbrock et al. 2019). For example, the protein-heme interface was shown to be most often dominated by hydrophobic amino acids, including the aliphatic hydrophobic

amino acids leucine, isoleucine, methionine, valine and alanine. The polar amino acids threonine, serine and aspartate are typically not involved as ligands in observed structures in heme proteins (Reedy and Gibney 2004).

CP-motif heme binding

The most prominent and best-explored HRM encompasses cysteine-proline (CP) motifs (Lathrop and Timko 1993; Kühl et al. 2011). In CP motifs, the cysteine residue acts as direct ligand of the heme-iron ion (Kühl et al. 2011), while the proline supports the coordination of the cysteine in the thiolate form of the Fe(III) heme complex by incorporating a bend for mainly alpha helices and avoiding the formation of hydrogen bonds (Li et al. 2011; Shimizu 2012). For the systems discussed in this review, CP-motifs are present in the eukaryotic Hap1 and BACH1 as well as in the prokaryotic Irr protein.

CP-motifs are typically located in hydrophobic protein environments, but the heme binding affinities of the particular heme sensing system is of course strongly influenced by the particular amino acids configurations (Fig. 5A). The binding affinity of the particular system is the result of adaptation to the prevailing environmental conditions and the physiological function of the heme sensor system. This is, for example, mirrored by the heme binding affinity of human BACH1 ($K_D \approx 13.7 \mu\text{M}$), which is in the range of the heme concentration in human blood ($\sim 21 \mu\text{M}$) (Aich et al. 2015). The binding affinities of the Hap1 protein is in a similar, low-micromolar range ($K_D < 20 \mu\text{M}$) matching the reported intracellular heme concentration of yeast (Hanna et al. 2018).

The prokaryotic example of a CP-motif discussed in this review is the rhizobial Irr protein, which is—like BACH1—degraded upon heme binding. The bulky amino acids tryptophan and histidine right adjacent to the CP-motif of Irr (Fig. 5A) were described to assist steric hindrance for preventing hydrogen bond formation (Ishimori and Watanabe 2014). In contrast to BACH1 and Hap1, Irr features significantly higher heme binding affinity than the eukaryotic systems (oxidized heme in *R. leguminosarum*: $K_D \approx 0.01 \mu\text{M}$) (White et al. 2011). Considering the low iron availability of iron in the soil (Colombo et al. 2014), this high affinity is likely required for efficient iron utilization and the establishment of the symbiotic relationships with legumes (O'Hara 2001). In fact, symbiotic legumes were shown to have a higher iron demand for proper nodule initiation and development (Brear et al. 2013).

Remarkably, all of the three described systems show a heterogeneous heme binding. Analysis of Soret bands displays broad peaks suggested a rather unusual heme binding environment and speaks for multiple configurations of heme binding in BACH1 (Hira et al. 2007), Hap1 (Zhang and Guarente 1995) and Irr (Ishikawa et al. 2011). As already described in the sections before, Hap1 contains seven HRMs (Zhang and Guarente 1995), while mammalian BACH1 has four HRMs (Ogawa et al. 2001). This leads to the remaining question if all HRMs of a protein are of equal relevance for the respective function, which is rather assessed as unlikely (Lee et al. 2003). For the regulator BACH1, it was shown that heme binding to the different HRM varies dependent on the heme concentration. Consequently, this leads to two separate activities: DNA-binding at low heme concentrations or nuclear export of BACH1 at high heme concentrations (Hira et al. 2007). Interestingly for Irr there are multiple configurations of low-spin and high-spin heme binding to the cysteine C²⁹ residue of Irr, which could influence the respective affinities (Ishikawa et al. 2011). This emphasizes that this labile binding is highly sensitive and shaped by the surrounding amino acid environment as well as the local heme con-

(A)	CP-motifs
Hap1 (<i>S. cerevisiae</i> , HRM7)	DQLQKCPVYQDA
BACH1 (<i>Homo sapiens</i> , CP6)	YSAADCP ^u LSFLI
Irr (<i>B. diazoefficiens</i>)	PALTGC ^u P ^u HW ^u DVN
(B)	non-CP-motifs
Irr (<i>B. diazoefficiens</i>)	TNVTT ^u HH ^u HY ^u YLEN
HatR (<i>C. difficile</i>)	FINKV ^u HN ^u IQ ^u YN
HsmR (<i>C. difficile</i>)	IKLVA ^u HN ^u QELT
HrrS (<i>C. glutamicum</i>)	VPVSI ^u Y ^u LL ^u FP ^u LF ^u LY ^u LQ
ChrS (<i>C. glutamicum</i>)*	GPEPAYLV ^u FP ^u M ^u FF ^u LA ^u VL
ChrS (<i>C. diphtheria</i>)	TLGIF ^u Y ^u M ^u IG ^u TA
HasR (<i>P. aeruginosa</i>)	TYGKG ^u WR ^u PP ^u AV ^u TES ^u LIT ^u GR ^u PH ^u GGA ^u EN ^u MY ^u NP ^u N ^u LP ^u LS ^u PERS
BhuR (<i>B. avium</i>)	QYAYG ^u Y ^u RP ^u APS ^u ASE ^u LY ^u TNY ^u GG ^u AG ^u TY ^u RL ^u GN ^u PN ^u L ^u K ^u PETS

Figure 5. Overview of CP- and non-CP heme-binding motifs. Shown are the heme-responsive motifs of the systems summarized in this review, including five amino acids up- and downstream of the respective residues. **(A)** Most important CP-motif of eukaryotic Hap1 and BACH1 and prokaryotic Irr proteins. **(B)** Non-CP-motif like histidine-rich residues in Irr of Rhizobia or HatR and HsmR in Clostridia, tyrosine (and phenylalanine) motifs of Corynebacteria TCS and FRAP/NPNL like motifs of HasR of Pseudomonales or BhuR of Burkholderiales are shown. Vertical lines between the two paralogous systems HrrS and ChrS emphasize same amino acids. * = in contrast to HrrS, mutations of these residues in ChrS does not fully abolish heme binding.

centration in the particular microenvironment. In addition to the 5-coordinated CP-motif, an additional histidine residue (H¹¹⁷⁻¹¹⁹) acts as secondary transient heme binding site of Irr, suggested with a 6-coordinated heme binding fortifying a rapid turnover (Yang et al. 2005; Ishikawa et al. 2011).

Non-CP-motif heme binding

Generally, it was reported, that CP motifs are a favored amino acid arrangement for heme binding, but also other, non-CP motifs were described, further highlighting the diversity of transient heme binding modes (Igarashi et al. 2008). The already above-mentioned second heme binding site of Irr in Rhizobiales, which is described to be histidine-rich, represents such an example (Yang et al. 2005). This histidine-rich region is conserved in Irr homologs, while the CP-motif is not present in all of its representatives (Yang et al. 2005). Histidine residues were already early described to be frequently involved in heme binding (Dawson et al. 1982). The shortly presented *C. difficile* HatR and HsmRA systems also contain histidine residues important for heme binding (Knippel et al. 2018; Knippel et al. 2020). Transient heme binding affinities for these systems are however lower than for Irr (HatR: $K_D \approx 9.2 \mu\text{M}$, HsmR: $K_D \approx 6.6 \mu\text{M}$), which can be explained by the fact that *C. difficile* is usually found in the host's colon, where heme concentrations are higher than in the soil.

The high diversity in heme binding modes is further underlined by the heme-responsive TCS of Gram-positive bacteria. Although the two paralogous histidine kinases HrrS and ChrS of *C.*

glutamicum share 39% identity, the N-terminal heme sensor domains share only 8.5%. Regarding the histidine kinase HrrS, three amino acids encompassing tyrosine and phenylalanines (Y¹¹², F¹¹⁵ and F¹¹⁸) are crucial for heme binding. Here, Y¹¹² was discussed to be important for the interaction with the iron atom of heme, which was also shown for several NEAT proteins (nearly to iron transport) (Andrade et al. 2002; Grigg et al. 2007; Sharp et al. 2007; Villareal et al. 2008; Keppel et al. 2018). NEAT domains are also suggested to play important roles in heme binding and transport probably generating a heme binding-cleft. However, their high diversity in sequence makes them hard to predict (Grigg et al. 2007). The phenylalanine residues F¹¹⁵ and F¹¹⁸ of HrrS have been proposed to be involved in aromatic stacking interactions with the porphyrin ring (Schneider et al. 2007; Smith et al. 2010; Li et al. 2011). By contrast, mutation of the corresponding amino acids in Y⁸⁷, F⁹⁰ and F⁹³ in ChrS did not abolish heme binding (Keppel et al. 2018), although the respective amino acid environment shows a high degree of similarity (Fig. 5B). While the transcriptional response mediated by ChrSA shows a higher sensitivity towards heme, structural data and the heme-binding affinity are missing.

Besides cysteine residues in CP motifs and histidine residues, tyrosine represents a frequently found ligand of proteins involved in transient heme sensing. This is also exemplified by the RhuR/RhuL heme sensor of Burkholderiales where a tyrosine residue (T⁶¹⁶) is flanked by a FRAP motif and a NP^uNL motif (Fig. 5B). In general, histidine residues in between these motifs were described in context of heme binding, like it is also the case for the

herein described HasR of *P. aeruginosa* (Fig. 5B). These conserved motifs represent a common structure in heme receptors of several proteins found in Gram-negative bacteria, like e.g. HemR of *Y. enterocolitica* (Bracken et al. 1999; Murphy et al. 2002; Richard et al. 2019). However, this type of transient heme binding is less described in the context of heme sensor systems, but rather heme utilization proteins or heme transporters, which do not propagate a signal but the heme molecule itself. The general mechanism of transient heme binding and transport around FRAP/NPNL-motifs is not completely established, as they are also highly variable with respect to their surrounding protein environment (Bracken et al. 1999; Murphy et al. 2002; Fusco et al. 2013).

Comparing heme sensor systems, it is striking, that Gram-positive bacteria seem to dedicate at least one TCS to heme-responsive gene regulation, which seems not to be the case for Gram-negative bacteria. Here, ECF σ -factor based systems appear to present a predominant form of heme sensing, as described for the systems found in Burkholderiales (Murphy et al. 2002), *P. aeruginosa* (Dent and Wilks 2020) or *S. marcescens* (Biville et al. 2004).

Comparable to CP-motif based transient heme binding it becomes evident that for all of these systems structural information and detailed biochemical data are still missing. In some cases, the residues involved in heme binding have not yet been identified, illustrating the large number of blind spots in our understanding of transient heme-protein interactions. However, it can be summarized that there are several similarities as well as variations between CP-motif and non-CP-motif HRMs in the context of heme homeostasis shaped by the environmental niche.

Sense and sensitivity—the challenge to predict transient heme-protein interactions and their physiological function

Known heme sensor systems already cover astonishing diversity of heme binding modes and physiological functions. While some systems act as global regulators of heme homeostasis, like e.g. corynebacterial HrrS or the mammalian BACH1, other systems display a specific control of heme uptake or detoxification. Across kingdoms, global systems typically integrate further responses, including responses to oxidative stress, oxygen availability, cell envelope damage or iron availability (Johnston et al. 2007; Warnatz et al. 2011; Keppel et al. 2020). The example of the paralogous TCS HrrSA and ChrSA of *C. glutamicum* nicely illustrate that simple prediction of the physiological function based on pure sequence homology is not possible—but the context provides more insights. While the ChrSA system is genetically linked to its probably only target operon (*hrtBA*), the expression of the response regulator *hrrA* is repressed by the global iron regulator DtxR, thereby creating a link between iron and heme homeostasis (Keppel et al. 2019).

Can we actually predict heme-protein interactions based on the amino acid sequence of a protein? The simple answer is: not with sufficient certainty. For some systems, which do not contain typical heme-binding motifs, the heme-binding ligands have not yet been identified. However, towards this goal, several heme-binding proteins were predicted using combinatorial peptide library screens and database searches or the implemented prediction tool 'SeqD-HBM' for heme-binding motifs described by Wißbrock et al. (2019). This includes e.g. bacterial proteins like FeoB (Schubert et al. 2015), hemolysin C (Peherstorfer et al. 2018) or the human dipeptidylpeptidase 8 (Kühl et al. 2013). Specific sequence features could be revealed which have positive effects on

heme-protein-binding, like a positive net charge or hydrophobic residues (Wißbrock et al. 2019).

However, experimental studies will always be needed for verification of transient heme binding and the physiological function of the respective system. Since binding motifs are highly diverse and the above described examples probably just represent the tip of the iceberg, it is almost impossible to predict transient heme binding based on sequence information only (Kühl et al. 2013; Schubert et al. 2015; Wißbrock et al. 2019). When it comes to heme-binding affinities, it becomes even more difficult.

In addition to that, it is also important to note that currently, we rely on the 'bulk' measurements of heme pools, but do account for the potential spatial differences and gradients within cells and communities. This is particularly relevant when we consider the hydrophobic nature of the molecule heme, which can concentrate in cellular membranes and at hydrophobic protein environments. In this context, advanced imaging technologies and fluorescent sensors might bring light into the spatial biology of heme sensing (Song et al. 2015).

From static regulons to dynamic networks

Heme-regulatory systems discussed in this review are controlled by a transient interaction with the effector molecule heme. This already emphasizes a dynamic nature in their response to heme availability. For most systems, however, we only know a limited number of genomic targets that are controlled by a specific regulator under defined conditions. In a recent study, Keppel et al. analyzed the dynamic response controlled by the HrrSA TCS in response to a heme stimulus in *C. glutamicum* (Keppel et al. 2020). Chromatin affinity purification of the response regulator HrrA followed by sequencing of its bound genomic targets revealed a dynamic binding to more than 200 different genomic targets involved in heme biosynthesis, respiration, stress responses and cell envelope remodeling. This genome-wide and time-resolved analysis provided unprecedented insights in the timing and hierarchy of this systemic response coordinated by HrrSA in response to heme.

Insights gained from these approaches have also the potential to challenge canonical models of transcriptional regulation revealing substantial binding of regulatory proteins to regions outside of promoter regions and the surprisingly high number of weak and so far unknown binding sites (Galagan et al. 2013). While some may be considered as experimental artefacts, the high reproducibility rather suggests that binding of transcription factors exists along a continuum of weak, medium and high affinity sites, raising the question of physiological significance (Rhee and Pugh 2011). Can we define a proper threshold for physiological significance, if we appreciate that cells are analog systems? This is especially relevant for binding sites for which no impact on gene expression has been observed—under the defined experimental conditions. However, genome-wide approaches including different transcription factors revealed a high level of context dependency. Coming back to the example of the corynebacterial HrrSA system, it is the interplay with the global iron regulator DtxR which enables a proper integration of iron and heme regulatory networks fine-tuning the cellular behavior to the actual environmental conditions (including iron/heme availability, cell envelope and oxidative stress responses) (Keppel et al. 2020). Here, heme-triggered HrrA binding to the promoter of *hmuO*, encoding the heme oxygenase, will not further enhance gene expression as long as the iron-bound form of DtxR is repressing it.

Importance of heme sensor systems for medicine and biotechnology

The heme-regulatory systems discussed in this review highlight the diversity of mechanisms organisms have evolved to respond to the multifaceted stimulus heme. The study of these systems not only provides important insights into cellular physiology and bacterial virulence, but also has a high potential for the development of novel antimicrobial drugs. Due to the fact that TCSs are found in nearly all sequenced bacterial genomes, but are absent in animals and humans, several studies have emphasized them as an attractive targets for antimicrobials (Hirakawa *et al.* 2020; Ma and Phillips-Jones 2021). As a specific example, decreased clinical efficacy of metronidazole in patients suffering from a *C. difficile* infection was recently described to be heme-associated (Gonzales-Luna *et al.* 2021; Wu *et al.* 2021). This further underlines the clinical relevance of the herein described heme sensor systems as a potential antimicrobial drug target and the importance of a mechanistic understanding of their role in microbial pathogenicity.

However, heme sensor systems are not only important in fighting bacterial diseases, but also for example in cancer progression. The mammalian heme sensing transcription factor BACH1 was shown to play a role in tumorigenesis as it is involved in the expression of genes e.g. associated with breast-, colon- or prostate cancer metastasis (Liang *et al.* 2012; Shajari *et al.* 2018; Zhu *et al.* 2018; Igarashi *et al.* 2021). Several studies already suggested BACH1 as a potential therapeutic target for adjuvant cancer therapy, e.g. by silencing therapies (Davoudian *et al.* 2016; Shajari *et al.* 2018). Recently, BACH1 was also considered to be of interest as target for developing COVID-19 candidate drugs. SARS-CoV-2 was shown to inhibit NRF2, which could be potentially counteracted by the inhibition of BACH1 leading to a derepression of Maf proteins and consequent activation of NRF2 (Liu *et al.* 2019; Cuadrado *et al.* 2020; Olgner *et al.* 2020). Given the tight link between iron/heme metabolism and microbial growth and virulence, an integrated view on the function of heme sensor systems is highly relevant for medical applications and drug development.

Besides medical applications, another example where knowledge about heme sensor systems bear potential for the industry is the food sector. For instance, the animal-free production of heme has recently attracted attention as ingredient mimicking the meat flavor in artificial meat (Fraser *et al.* 2017; Waltz 2019), which could contribute to a necessary reduction of meat consumption (González *et al.* 2020). Hence, engineering of microbial cell factories is required to achieve high-yield production of animal-free heme. A recent systems metabolic engineering approach resulted in the establishment of animal-free heme production using the biotechnological production strain *C. glutamicum* (Ko *et al.* 2021). Further future metabolic engineering approaches will therefore strongly benefit from a comprehensive understanding of heme-regulation to foster efficient development of microbial cell factories.

Acknowledgments

We thank Michael Bott for critically reading this manuscript.

Funding

This work was supported by the Helmholtz Association (Grant number W2/W3-096) and the European Research Council (ERC Starting Grant, Grant number 757563).

Conflicts of interest. None declared.

References

- Aft RL, Mueller GC. Hemin-mediated oxidative degradation of proteins. *J Biol Chem* 1984;**259**:301–5.
- Ahn SH, Han JH, Lee JH *et al.* Identification of an iron-regulated hemin-binding outer membrane protein, HupO, in *Vibrio fluvialis*: effects on hemolytic activity and the oxidative stress response. *Infect Immun* 2005;**73**:722–9.
- Aich A, Freundlich M, Vekilov PG. The free heme concentration in healthy human erythrocytes. *Blood Cells Mol Dis* 2015;**55**:402–9.
- Ajioka RS, Phillips JD, Kushner JP. Biosynthesis of heme in mammals. *Biochimica et Biophysica Acta (BBA) - Mol Cell Res* 2006;**1763**:723–36.
- Andrade MA, Ciccarelli FD, Perez-Iratxeta C *et al.* NEAT: a domain duplicated in genes near the components of a putative Fe³⁺-siderophore transporter from Gram-positive pathogenic bacteria. *Genome Biol* 2002;**3**:Research0047.
- Anzaldi LL, Skaar EP. Overcoming the heme paradox: heme toxicity and tolerance in bacterial pathogens. *Infect Immun* 2010;**78**:4977–89.
- Atamna H, Brahmabhatt M, Atamna W *et al.* ApoHRP-based assay to measure intracellular regulatory heme. *Metallomics* 2015;**7**:309–21.
- Bardwell VJ, Treisman R. The POZ domain: a conserved protein-protein interaction motif. *Genes Dev* 1994;**8**:1664–77.
- Benevides-Matos N, Biville F. The hem and has haem uptake systems in *Serratia marcescens*. *Microbiology* 2010;**156**:1749–57.
- Bibb LA, King ND, Kunkle CA *et al.* Analysis of a heme-dependent signal transduction system in *Corynebacterium diphtheriae*: deletion of the *chrAS* genes results in heme sensitivity and diminished heme-dependent activation of the *hmuO* promoter. *Infect Immun* 2005;**73**:7406–12.
- Bibb LA, Kunkle CA, Schmitt MP. The ChrA-ChrS and HrrA-HrrS signal transduction systems are required for activation of the *hmuO* promoter and repression of the *hemA* promoter in *Corynebacterium diphtheriae*. *Infect Immun* 2007;**75**:2421–31.
- Bibb LA, Schmitt MP. The ABC transporter HrtAB confers resistance to hemin toxicity and is regulated in a hemin-dependent manner by the ChrAS two-component system in *Corynebacterium diphtheriae*. *J Bacteriol* 2010;**192**:4606–17.
- Biswas GD, Anderson JE, Sparling PF. Cloning and functional characterization of *Neisseria gonorrhoeae* *tonB*, *exbB* and *exbD* genes. *Mol Microbiol* 1997;**24**:169–79.
- Biville F, Cwerman H, Létoffé S *et al.* Haemophore-mediated signalling in *Serratia marcescens*: a new mode of regulation for an extra cytoplasmic function (ECF) sigma factor involved in haem acquisition. *Mol Microbiol* 2004;**53**:1267–77.
- Bott M, Brocker M. Two-component signal transduction in *Corynebacterium glutamicum* and other *Corynebacteria*: on the way towards stimuli and targets. *Appl Microbiol Biotechnol* 2012;**94**:1131–50.
- Bracken CS, Baer MT, Abdur-Rashid A *et al.* Use of heme-protein complexes by the *Yersinia enterocolitica* HemR receptor: histidine residues are essential for receptor function. *J Bacteriol* 1999;**181**:6063–72.
- Breuer E, Day D, Smith P. Iron: an essential micronutrient for the legume-rhizobium symbiosis. *Front Plant Sci* 2013;**4**.
- Brewitz HH, Hagelueken G, Imhof D. Structural and functional diversity of transient heme binding to bacterial proteins. *Biochimica et Biophysica Acta (BBA) - General Subjects* 2017;**1861**:683–97.
- Bronner S, Monteil H, Prévost G. Regulation of virulence determinants in *Staphylococcus aureus*: complexity and applications. *FEMS Microbiol Rev* 2004;**28**:183–200.

- Buisson N, Labbe-Bois R. Flavohemoglobin expression and function in *Saccharomyces cerevisiae*. No relationship with respiration and complex response to oxidative stress. *J Biol Chem* 1998;**273**: 9527–33.
- Burgos JM, Schmitt MP. The ChrSA and HrrSA two-component systems are required for transcriptional regulation of the *hemA* promoter in *Corynebacterium diphtheriae*. *J Bacteriol* 2016;**198**:2419–30.
- Butler CA, Dashper SG, Zhang L et al. The *Porphyromonas gingivalis* ferric uptake regulator orthologue binds hemin and regulates hemin-responsive biofilm development. *PLoS One* 2014;9.
- Capra EJ, Laub MT. Evolution of two-component signal transduction systems. *Annu Rev Microbiol* 2014 2012;**66**:325–47.
- Chapman SK, Daff S, Munro AW. Heme: The most versatile redox centre in biology?. In: HAO Hill, PJ Sadler, AJ Thomson (eds). *Metal Sites in Proteins and Models: Iron Centres*. Berlin, Heidelberg: Springer Berlin Heidelberg, 1997, 39–70. 978-3-540-69035-1.
- Chiabrando D, Vinchi F, Fiorito V et al. Heme in pathophysiology: a matter of scavenging, metabolism and trafficking across cell membranes. *Front Pharmacol* 2014;**5**.
- Chumbler NM, Farrow MA, Lapiere LA et al. Clostridium difficile toxin b causes epithelial cell necrosis through an autoprocessing-independent mechanism. *PLoS Pathog* 2012;**8**.
- Colombo C, Palumbo G, He J-Z et al. Review on iron availability in soil: interaction of Fe minerals, plants, and microbes. *J Soils Sediments* 2014;**14**:538–48.
- Contreras H, Chim N, Credali A et al. Heme uptake in bacterial pathogens. *Curr Opin Chem Biol* 2014;**19**:34–41.
- Creusot F, Verdier J, Gaisne M et al. CYP1 (HAP1) regulator of oxygen-dependent gene expression in yeast. I. Overall organization of the protein sequence displays several novel structural domains. *J Mol Biol* 1988;**204**:263–76.
- Cuadrado A, Pajares M, Benito C et al. Can activation of NRF2 be a strategy against COVID-19? *Trends Pharmacol Sci* 2020;**41**:598–610.
- Davoudian S, Shajari N, Kazemi T et al. BACH1 silencing by siRNA inhibits migration of HT-29 colon cancer cells through reduction of metastasis-related genes. *Biomed Pharmacother* 2016;**84**: 191–8.
- Dawson JH, Andersson LA, Sono M. Spectroscopic investigations of ferric cytochrome P-450-CAM ligand complexes. Identification of the ligand trans to cysteinyl in the native enzyme. *J Biol Chem* 1982;**257**:3606–17.
- de Villiers KA, Egan TJ. Heme detoxification in the malaria parasite: a target for antimalarial drug development. *Acc Chem Res* 2021;**54**:2649–59.
- Dent AT, Brimberry M, Albert T et al. Axial heme coordination by the tyr-his motif in the extracellular hemophore hasap is critical for the release of heme to the HasR receptor of *Pseudomonas aeruginosa*. *Biochemistry* 2021;**60**:2549–59.
- Dent AT, Mourião S, Huang W et al. Post-transcriptional regulation of the *Pseudomonas aeruginosa* heme assimilation system (Has) fine-tunes extracellular heme sensing. *J Biol Chem* 2019;**294**: 2771–85.
- Dent AT, Wilks A. Contributions of the heme coordinating ligands of the *Pseudomonas aeruginosa* outer membrane receptor HasR to extracellular heme sensing and transport. *J Biol Chem* 2020;**295**:10456–67.
- Dhakshinamoorthy S, Jain AK, Bloom DA et al. BACH1 competes with nrf2 leading to negative regulation of the antioxidant response element (ARE)-mediated NAD(P)H:quinone oxidoreductase 1 gene expression and induction in response to antioxidants. *J Biol Chem* 2005;**280**:16891–900.
- Dioum EM, Rutter J, Tuckerman JR et al. NPAS2: a gas-responsive transcription factor. *Science* 2002;**298**:2385–7.
- Elkins C, Totten PA, Olsen B et al. Role of the *Haemophilus ducreyi* ton system in internalization of heme from hemoglobin. *Infect Immun* 1998;**66**:151–60.
- Fernandez A, Lechardeur D, Derré-Bobillot A et al. Two coregulated efflux transporters modulate intracellular heme and protoporphyrin IX availability in *Streptococcus agalactiae*. *PLoS Pathog* 2010;**6**.
- Fraser R, Davis SC, O'Reilly Brown P. Secretion of heme-containing polypeptides. California: R.C. Impossible Foods Inc., 2017.
- Frunzke J, Gätgens C, Brocker M et al. Control of heme homeostasis in *Corynebacterium glutamicum* by the two-component system HrrSA. *J Bacteriol* 2011;**193**:1212–21.
- Fusco WG, Choudhary NR, Council SE et al. Mutational analysis of hemoglobin binding and heme utilization by a bacterial hemoglobin receptor. *J Bacteriol* 2013;**195**:3115–23.
- Galagan J, Lyubetskaya A, Gomes A. ChIP-Seq and the complexity of bacterial transcriptional regulation. *Curr Top Microbiol Immunol* 2013;**363**:43–68.
- Gallio AE, Fung SSP, Cammack-Najera A et al. Understanding the logistics for the distribution of heme in cells. *JACS Au* 2021;**1**, 1541–55.
- Girvan HM, Munro AW. Heme sensor proteins. *J Biol Chem* 2013;**288**:13194–203.
- Gong W, Hao B, Chan MK. New mechanistic insights from structural studies of the oxygen-sensing domain of *Bradyrhizobium japonicum* fixL. *Biochemistry* 2000;**39**:3955–62.
- Gonzales-Luna AJ, Olaitan AO, Shen W-J et al. Reduced susceptibility to metronidazole is associated with initial clinical failure in Clostridioides difficile infection. *Open Forum Infectious Diseases* 2021;**8**:ofab365.
- González N, Marqués M, Nadal M et al. Meat consumption: which are the current global risks? A review of recent (2010-2020) evidences. *Food Res Int* 2020;**137**:109341.
- Granic S, Sinclair P, Sassa S et al. Effects by heme, insulin, and serum albumin on heme and protein synthesis in chick embryo liver cells cultured in a chemically defined medium, and a spectrofluorometric assay for porphyrin composition. *J Biol Chem* 1975;**250**:9215–25.
- Green J, Crack JC, Thomson AJ et al. Bacterial sensors of oxygen. *Curr Opin Microbiol* 2009;**12**:145–51.
- Grigg JC, Vermeiren CL, Heinrichs DE et al. Haem recognition by a *Staphylococcus aureus* NEAT domain. *Mol Microbiol* 2007;**63**:139–49.
- Guarente L, Mason T. Heme regulates transcription of the CYC1 gene of *S. cerevisiae* via an upstream activation site. *Cell* 1983;**32**: 1279–86.
- Hach A, Hon T, Zhang L. A new class of repression modules is critical for heme regulation of the yeast transcriptional activator hap1. *Mol Cell Biol* 1999;**19**:4324–33.
- Hamza I, Chauhan S, Hassett R et al. The bacterial irr protein is required for coordination of heme biosynthesis with iron availability. *J Biol Chem* 1998;**273**:21669–74.
- Hanna DA, Hu R, Kim H et al. Heme bioavailability and signaling in response to stress in yeast cells. *J Biol Chem* 2018;**293**:12378–93.
- Hentschel E, Mack C, Gatgens C et al. Phosphatase activity of the histidine kinases ensures pathway specificity of the ChrSA and HrrSA two-component systems in *Corynebacterium glutamicum*. *Mol Microbiol* 2014;**92**:1326–42.
- Heyer A, Gatgens C, Hentschel E et al. The two-component system ChrSA is crucial for haem tolerance and interferes with HrrSA in haem-dependent gene regulation in *Corynebacterium glutamicum*. *Microbiology* 2012;**158**:3020–31.
- Hintze KJ, Katoh Y, Igarashi K et al. Bach1 repression of ferritin and thioredoxin reductase1 is heme-sensitive in cells and in vitro and coordinates expression with heme oxygenase1, beta-globin,

- and NAD(P)(H) quinone (oxido) reductase1. *J Biol Chem* 2007;**282**:34365–71.
- Hira S, Tomita T, Matsui T et al. Bach1, a heme-dependent transcription factor, reveals presence of multiple heme binding sites with distinct coordination structure. *IUBMB Life* 2007;**59**:542–51.
- Hirakawa H, Kurushima J, Hashimoto Y et al. Progress overview of bacterial two-component regulatory systems as potential targets for antimicrobial chemotherapy. *Antibiotics* 2020;**9**:635.
- Hoch JA. Two-component and phosphorelay signal transduction. *Curr Opin Microbiol* 2000;**3**:165–70.
- Hon T, Dodd A, Dirmeier R et al. A mechanism of oxygen sensing in yeast. Multiple oxygen-responsive steps in the heme biosynthetic pathway affect hap1 activity. *J Biol Chem* 2003;**278**:50771–80.
- Hon T, Hach A, Lee HC et al. Functional analysis of heme regulatory elements of the transcriptional activator hap1. *Biochem Biophys Res Commun* 2000;**273**:584–91.
- Hon T, Lee HC, Hach A et al. The hsp70-ydj1 molecular chaperone represses the activity of the heme activator protein hap1 in the absence of heme. *Mol Cell Biol* 2001;**21**:7923–32.
- Hon T, Lee HC, Hu Z et al. The heme activator protein hap1 represses transcription by a heme-independent mechanism in *Saccharomyces cerevisiae*. *Genetics* 2005;**169**:1343–52.
- Igarashi J, Murase M, Iizuka A et al. Elucidation of the heme binding site of Heme-regulated eukaryotic initiation factor α ; kinase and the role of the regulatory motif in heme sensing by spectroscopic and catalytic studies of mutant proteins. *J Biol Chem* 2008;**283**:18782–91.
- Igarashi K, Hoshino H, Muto A et al. Multivalent DNA binding complex generated by small maf and bach1 as a possible biochemical basis for globin locus control region complex. *J Biol Chem* 1998;**273**:11783–11790.
- Igarashi K, Kataokata K, Itoh K et al. Regulation of transcription by dimerization of erythroid factor NF-E2 p45 with small maf proteins. *Nature* 1994;**367**:568–72.
- Igarashi K, Nishizawa H, Saiki Y et al. The transcription factor BACH1 at the crossroads of cancer biology: from epithelial-mesenchymal transition to ferroptosis. *J Biol Chem* 2021;**297**:101032.
- Ishikawa H, Nakagaki M, Bamba A et al. Unusual heme binding in the bacterial iron response regulator protein: spectral characterization of heme binding to the heme regulatory motif. *Biochemistry* 2011;**50**:1016–22.
- Ishimori K, Watanabe Y. Unique heme environmental structures in Heme-regulated proteins using heme as the signaling molecule. *Chem Lett* 2014;**43**:1680–9.
- Ito Y, Nakagawa S, Komagata A et al. Heme-dependent autophosphorylation of a heme sensor kinase, ChrS, from *Corynebacterium diphtheriae* reconstituted in proteoliposomes. *FEBS Lett* 2009;**583**:2244–8.
- Jepkorir G, Rodríguez JC, Rui H et al. Structural, NMR spectroscopic, and computational investigation of heme loading in the hemophore hasap from *Pseudomonas aeruginosa*. *J Am Chem Soc* 2010;**132**:9857–72.
- Johnston AWB, Todd JD, Curson AR et al. Living without fur: the subtlety and complexity of iron-responsive gene regulation in the symbiotic bacterium rhizobium and other α -proteobacteria. *Biometals* 2007;**20**:501–11.
- Joubert L, Derré-Bobillot A, Gaudu P et al. HrtBA and menaquinones control haem homeostasis in *Lactococcus lactis*. *Mol Microbiol* 2014;**93**:823–33.
- Keppel M, Davoudi E, Gätgens C et al. Membrane topology and heme binding of the histidine kinases HrsS and ChrS in *corynebacterium glutamicum*. *Front Microbiol* 2018;**9**:183.
- Keppel M, Hünnefeld M, Filipchuk A et al. HrrSA orchestrates a systemic response to heme and determines prioritization of terminal cytochrome oxidase expression. *Nucleic Acids Res* 2020;**48**:6547–62.
- Keppel M, Piepenbreier H, Gätgens C et al. Toxic but tasty – temporal dynamics and network architecture of heme-responsive two-component signaling in *Corynebacterium glutamicum*. *Mol Microbiol* 2019;**111**:1367–81.
- King ND, Kirby AE, Connell TD. Transcriptional control of the *rhuR-bhuRSTUV* heme acquisition locus in *Bordetella avium*. *Infect Immun* 2005;**73**:1613–24.
- King-Lyons ND, Smith KF, Connell TD. Expression of *hwrP*, a gene encoding a prospective site 2 protease, is essential for heme-dependent induction of *bhuR* in *Bordetella bronchiseptica*. *J Bacteriol* 2007;**189**:6266–75.
- Kirby AE, King ND, Connell TD. RhuR, an extracytoplasmic function sigma factor activator, is essential for heme-dependent expression of the outer membrane heme and hemoprotein receptor of *Bordetella avium*. *Infect Immun* 2004;**72**:896–907.
- Kirby AE, Metzger DJ, Murphy ER et al. Heme utilization in *Bordetella avium* is regulated by RhuI, a heme-responsive extracytoplasmic function sigma factor. *Infect Immun* 2001;**69**:6951–61.
- Kitatsuji C, Izumi K, Nambu S. Protein oxidation mediated by heme-induced active site conversion specific for heme-regulated transcription factor, iron response regulator. *Sci Rep* 2016;**6**:18703.
- Knippel RJ, Wexler AG, Miller JM et al. *Clostridioides difficile* senses and hijacks host heme for incorporation into an oxidative stress defense system. *Cell Host & Microbe* 2020;**28**:411–21.
- Knippel RJ, Zackular JP, Moore JL et al. Heme sensing and detoxification by HatRT contributes to pathogenesis during *Clostridium difficile* infection. *PLoS Pathog* 2018;**14**:e1007486.
- Ko YJ, Kim M, You SK et al. Animal-free heme production for artificial meat in *Corynebacterium glutamicum* via systems metabolic and membrane engineering. *Metab Eng* 2021;**66**:217–28.
- Kobayashi K, Nakagaki M, Ishikawa H et al. Redox-Dependent dynamics in heme-bound bacterial iron response regulator (Irr) protein. *Biochemistry* 2016;**55**:4047–54.
- Krieg S, Huché F, Diederichs K et al. Heme uptake across the outer membrane as revealed by crystal structures of the receptor-hemophore complex. *Proc Natl Acad Sci* 2009;**106**:1045–50.
- Kühl T, Sahoo N, Nikolajski M et al. Determination of heme-binding characteristics of proteins by a combinatorial peptide library approach. *ChemBioChem* 2011;**12**:2846–55.
- Kühl T, Wissbrock A, Goradia N et al. Analysis of Fe(III) heme binding to cysteine-containing heme-regulatory motifs in proteins. *ACS Chem Biol* 2013;**8**:1785–93.
- Kumar R, Matsumura H, Lovell S et al. Replacing the axial ligand tyrosine 75 or its hydrogen bond partner histidine 83 minimally affects heme acquisition by the hemophore hasap from *Pseudomonas aeruginosa*. *Biochemistry* 2014;**53**:2112–25.
- Kumar S, Bandyopadhyay U. Free heme toxicity and its detoxification systems in human. *Toxicol Lett* 2005;**157**:175–88.
- Lai S, Comer JM, Konduri PC et al. Heme promotes transcriptional and demethylase activities of gis1, a member of the histone demethylase JMJD2/KDM4 family. *Nucleic Acids Res* 2018;**46**:215–28.
- Lathrop J, Timko M. Regulation by heme of mitochondrial protein transport through a conserved amino acid motif. *Science* 1993;**259**:522–5.
- Layer G, Reichelt J, Jahn D et al. Structure and function of enzymes in heme biosynthesis. *Protein Sci* 2010;**19**:1137–61.
- Lee HC, Hon T, Lan C et al. Structural environment dictates the biological significance of heme-responsive motifs and the role of

- hsp90 in the activation of the heme activator protein hap1. *Mol Cell Biol* 2003;**23**:5857–66.
- Létouffé S, Deniau C, Wolff N et al. Haemophore-mediated bacterial haem transport: evidence for a common or overlapping site for haem-free and haem-loaded haemophore on its specific outer membrane receptor. *Mol Microbiol* 2001;**41**:439–50.
- Li T, Bonkovsky HL, Guo J-t. Structural analysis of heme proteins: implications for design and prediction. *BMC Struct Biol* 2011;**11**:13.
- Liang Y, Wu H, Lei R et al. Transcriptional network analysis identifies BACH1 as a master regulator of breast cancer bone metastasis. *J Biol Chem* 2012;**287**:33533–44.
- Liu Q, Gao Y, Ci X. Role of nrf2 and its activators in respiratory diseases. *Oxid Med Cell Longev* 2019;**2019**.
- Lowry CV, Zitomer RS. ROX1 encodes a heme-induced repression factor regulating ANB1 and CYC7 of *Saccharomyces cerevisiae*. *Mol Cell Biol* 1988;**8**:4651–8.
- Ma P, Phillips-Jones MK. Membrane sensor histidine kinases: insights from structural, ligand and inhibitor studies of full-length proteins and signalling domains for antibiotic discovery. *Molecules* 2021;**26**:5110.
- Martinez M, Ugalde R, Almiron M. Dimeric *brucella abortus* irr protein controls its own expression and binds haem. *Microbiology* 2005;**151**:3427–33.
- Martínková M, Kitanishi K, Shimizu T. Heme-based Globin-coupled oxygen sensors: linking oxygen binding to functional regulation of diguanylate cyclase, histidine kinase, and Methyl-accepting chemotaxis. *J Biol Chem* 2013;**288**:27702–11.
- Mascher T, Helmann JD, Unden G. Stimulus perception in bacterial signal-transducing histidine kinases. *Microbiol Mol Biol Rev* 2006;**70**:910–38.
- Mike LA, Choby JE, Brinkman PR et al. Two-component system cross-regulation integrates bacillus anthracis response to heme and cell envelope stress. *PLoS Pathog* 2014;**10**:e1004044.
- Motohashi H, Shavit JA, Igarashi K et al. The world according to maf. *Nucleic Acids Res* 1997;**25**:2953–9.
- Mourinho S, Giardina BJ, Reyes-Caballero H et al. Metabolite-driven regulation of heme uptake by the biliverdin IX β / δ -Selective heme oxygenase (HemO) of *Pseudomonas aeruginosa*. *J Biol Chem* 2016;**291**:20503–15.
- Murphy ER, Sacco RE, Dickenson A et al. BhuR, a virulence-associated outer membrane protein of *Bordetella avium*, is required for the acquisition of iron from heme and hemoproteins. *Infect Immun* 2002;**70**:5390–403.
- Nakahigashi K, Nishimura K, Miyamoto K et al. Photosensitivity of a protoporphyrin-accumulating, light-sensitive mutant (*visA*) of *Escherichia coli* K-12. *Proc Natl Acad Sci* 1991;**88**:10520–4.
- NCBIResourceCoordinators. Database resources of the national center for biotechnology information. *Nucleic Acids Res* 2016;**44**:D7–D19.
- Nienaber A, Hennecke H, Fischer H-M. Discovery of a haem uptake system in the soil bacterium *Bradyrhizobium japonicum*. *Mol Microbiol* 2001;**41**:787–800.
- Noriega CE, Lin HY, Chen LL et al. Asymmetric cross-regulation between the nitrate-responsive NarX-NarL and NarQ-NarP two-component regulatory systems from *Escherichia coli* K-12. *Mol Microbiol* 2010;**75**:394–412.
- O'Brian MR. Perception and homeostatic control of iron in the rhizobia and related bacteria. *Annu Rev Microbiol* 2015;**69**:229–45.
- O'Hara GW. Nutritional constraints on root nodule bacteria affecting symbiotic nitrogen fixation: a review. *Australian Journal of Experimental Agriculture* 2001;**41**:417–33.
- Occhino DA, Wyckoff EE, Henderson DP et al. *Vibrio cholerae* iron transport: haem transport genes are linked to one of two sets of *tonB*, *exbB*, *exbD* genes. *Mol Microbiol* 1998;**29**:1493–507.
- Ochsner UA, Johnson Z, Vasil ML. Genetics and regulation of two distinct haem-uptake systems, *phu* and *has*, in *Pseudomonas aeruginosa*. *Microbiology* 2000;**146**:185–98.
- Ogawa K, Sun J, Taketani S et al. Heme mediates derepression of maf recognition element through direct binding to transcription repressor bach1. *EMBO J* 2001;**20**:2835–43.
- Olagnier D, Farahani E, Thyrtsted J et al. SARS-CoV2-mediated suppression of NRF2-signaling reveals potent antiviral and anti-inflammatory activity of 4-octyl-itaconate and dimethyl fumarate. *Nat Commun* 2020;**11**:4938.
- Oyake T, Itoh K, Motohashi H. Bach proteins belong to a novel family of BTB-basic leucine zipper transcription factors that interact with MafK and regulate transcription through the NF-E2 site. *Mol Cell Biol* 1996;**16**:6083–95.
- Parrow NL, Abbott J, Lockwood AR et al. Function, regulation, and transcriptional organization of the hemin utilization locus of *Bar-tonella quintana*. *Infect Immun* 2009;**77**:307–16.
- Peherstorfer S, Brewitz HH, Paul George AA et al. Insights into mechanism and functional consequences of heme binding to hemolysin-activating lysine acyltransferase HlyC from *Escherichia coli*. *Biochimica et Biophysica Acta (BBA) - General Subjects* 2018;**1862**:1964–72.
- Peuser V, Remes B, Klug G. Role of the irr protein in the regulation of iron metabolism in *Rhodobacter sphaeroides*. *PLoS One* 2012;**7**:e42231.
- Pfeifer K, Kim KS, Kogan S et al. Functional dissection and sequence of yeast HAP1 activator. *Cell* 1989;**56**:291–301.
- Pi H, Chu ML, Ivan SJ et al. Directed evolution reveals the mechanism of HitRS signaling transduction in *Bacillus anthracis*. *PLoS Pathog* 2020;**16**:e1009148.
- Ponka P. Cell biology of heme. *Am J Med Sci* 1999;**318**:241–56.
- Pressler U, Staudenmaier H, Zimmermann L et al. Genetics of the iron dicitrate transport system of *Escherichia coli*. *J Bacteriol* 1988;**170**:2716–24.
- Qi Z, Hamza I, O'Brian MR. Heme is an effector molecule for iron-dependent degradation of the bacterial iron response regulator (Irr) protein. *Proc Natl Acad Sci* 1999;**96**:13056–61.
- Qi Z, O'Brian MR. Interaction between the bacterial iron response regulator and ferroxidase mediates genetic control of heme biosynthesis. *Mol Cell* 2002;**9**:155–62.
- Raghuram S, Stayrook KR, Huang P et al. Identification of heme as the ligand for the orphan nuclear receptors REV-ERBa and REV-ERBb. *Nat Struct Mol Biol* 2007;**14**:1207–13.
- Reedy CJ, Gibney BR. Heme protein assemblies. *Chem Rev* 2004;**104**:617–50.
- Rhee HS, Pugh BF. Comprehensive genome-wide protein-DNA interactions detected at single-nucleotide resolution. *Cell* 2011;**147**:1408–19.
- Richard KL, Kelley BR, Johnson JG. Heme uptake and utilization by Gram-negative bacterial pathogens. *Front Cell Infect Microbiol* 2019;**9**:81.
- Rossi MS, Paquelin A, Ghigo JM et al. Haemophore-mediated signal transduction across the bacterial cell envelope in *Serratia marcescens*: the inducer and the transported substrate are different molecules. *Mol Microbiol* 2003;**48**:1467–80.
- Rudolph G, Semini G, Hauser F et al. The iron control element, acting in positive and negative control of iron-regulated *Bradyrhizobium japonicum* genes, is a target for the irr protein. *J Bacteriol* 2006;**188**:733–44.

- Sahoo N, Goradia N, Ohlenschläger O et al. Heme impairs the ball-and-chain inactivation of potassium channels. *Proc Natl Acad Sci* 2013;**110**:E4036–4044.
- Schmitt MP. Identification of a two-component signal transduction system from *Corynebacterium diphtheriae* that activates gene expression in response to the presence of heme and hemoglobin. *J Bacteriol* 1999;**181**:5330–40.
- Schneider JC, Guarente L. Regulation of the yeast *CYT1* gene encoding cytochrome c1 by HAP1 and HAP2/3/4. *Mol Cell Biol* 1991;**11**:4934–42.
- Schneider S, Marles-Wright J, Sharp KH et al. Diversity and conservation of interactions for binding heme in b-type heme proteins. *Nat Prod Rep* 2007;**24**:621–30.
- Schubert E, Florin N, Duthie F et al. Spectroscopic studies on peptides and proteins with cysteine-containing heme regulatory motifs (HRM). *J Inorg Biochem* 2015;**148**:49–56.
- Segawa K, Watanabe-Matsui M, Matsui T et al. Functional heme binding to the intrinsically disordered C-Terminal region of bch1, a transcriptional repressor. *Tohoku J Exp Med* 2019;**247**:153–9.
- Shajari N, Davudian S, Kazemi T et al. Silencing of BACH1 inhibits invasion and migration of prostate cancer cells by altering metastasis-related gene expression. *Artificial Cells, Nanomedicine, and Biotechnology* 2018;**46**:1495–504.
- Sharp KH, Schneider S, Cockayne A et al. Crystal structure of the Heme-IsdC complex, the central conduit of the *isd* iron/heme uptake system in *Staphylococcus aureus*. *J Biol Chem* 2007;**282**:10625–31.
- Shimizu T, Huang D, Yan F et al. Gaseous O₂, NO, and CO in signal transduction: structure and function relationships of heme-based gas sensors and heme-redox sensors. *Chem Rev* 2015;**115**:6491–533.
- Shimizu T, Lengalova A, Martinek V et al. Heme: emergent roles of heme in signal transduction, functional regulation and as catalytic centres. *Chem Soc Rev* 2019;**48**:5624–57.
- Shimizu T. Binding of cysteine thiolate to the fe(III) heme complex is critical for the function of heme sensor proteins. *J Inorg Biochem* 2012;**108**:171–7.
- Simile MM, Latte G, Pascale RM. MAF proteins: a family of regulating and regulated molecules. *Digest Med Res* 2018;**1**.
- Singleton C, White G, Todd J et al. Heme-responsive DNA binding by the global iron regulator *irr* from *Rhizobium leguminosarum*. *J Biol Chem* 2010;**285**:16023–31.
- Šmíga M, Bielecki M, Olczak M et al. *Porphyromonas gingivalis* pgf_{ur} is a member of a novel fur subfamily with Non-canonical function. *Front Cell Infect Microbiol* 2019;**9**.
- Smith AD, Wilks A. Differential contributions of the outer membrane receptors PhuR and HasR to heme acquisition in *Pseudomonas aeruginosa*. *J Biol Chem* 2015;**290**:7756–66.
- Smith LJ, Kahraman A, Thornton JM. Heme proteins—Diversity in structural characteristics, function, and folding. *Proteins Struct Funct Bioinf* 2010;**78**:2349–68.
- Song Y, Yang M, Wegner SV et al. A genetically encoded FRET sensor for intracellular heme. *ACS Chem Biol* 2015;**10**:1610–5.
- Stauff DL, Bagaley D, Torres VJ et al. *Staphylococcus aureus* HrtA is an ATPase required for protection against heme toxicity and prevention of a transcriptional heme stress response. *J Bacteriol* 2008;**190**:3588–96.
- Stauff DL, Skaar EP. *Bacillus anthracis* HssRS signalling to HrtAB regulates haem resistance during infection. *Mol Microbiol* 2009a;**72**:763–78.
- Stauff DL, Skaar EP. The heme sensor system of *Staphylococcus aureus*. *Contrib Microbiol* 2009b;**16**:120–35.
- Stauff DL, Torres VJ, Skaar EP. Signaling and DNA-binding activities of the *Staphylococcus aureus* HssR-HssS two-component system required for heme sensing. *J Biol Chem* 2007;**282**:26111–21.
- Stock AM, Robinson VL, Goudreau PN. Two-Component signal transduction. *Annu Rev Biochem* 2000;**69**:183–215.
- Stojilkovic I, Hwa V, de Saint Martin L et al. The *Neisseria meningitidis* haemoglobin receptor: its role in iron utilization and virulence. *Mol Microbiol* 1995;**15**:531–41.
- Stojilkovic I, Kumar V, Srinivasan N. Non-iron metalloporphyrins: potent antibacterial compounds that exploit haem/Hb uptake systems of pathogenic bacteria. *Mol Microbiol* 1999;**31**:429–42.
- Sun J, Hoshino H, Takaku K et al. Hemoprotein bch1 regulates enhancer availability of heme oxygenase-1 gene. *EMBO J* 2002;**21**:5216–24.
- Tang XD, Xu R, Reynolds MF et al. Haem can bind to and inhibit mammalian calcium-dependent slo1 BK channels. *Nature* 2003;**425**:531–5.
- Tatusov RL, Galperin MY, Natale DA et al. The COG database: a tool for genome-scale analysis of protein functions and evolution. *Nucleic Acids Res* 2000;**28**:33–36.
- Ter Linde JJ, Steensma HY. A microarray-assisted screen for potential hap1 and rox1 target genes in *Saccharomyces cerevisiae*. *Yeast* 2002;**19**:825–40.
- Torres VJ, Pishchany G, Humayun M et al. *Staphylococcus aureus* IsdB is a hemoglobin receptor required for heme iron utilization. *J Bacteriol* 2006;**188**:8421–9.
- Torres VJ, Stauff DL, Pishchany G et al. A *Staphylococcus aureus* regulatory system that responds to host heme and modulates virulence. *Cell Host & Microbe* 2007;**1**:109–19.
- Vanderpool CK, Armstrong SK. Heme-responsive transcriptional activation of *borderetella bhu* genes. *J Bacteriol* 2003;**185**:909–17.
- Vanderpool CK, Armstrong SK. The *borderetella bhu* locus is required for heme iron utilization. *J Bacteriol* 2001;**183**:4278–87.
- Villareal VA, Pilpa RM, Robson SA et al. The IsdC protein from *Staphylococcus aureus* uses a flexible binding pocket to capture heme. *J Biol Chem* 2008;**283**:31591–600.
- Wakeman CA, Stauff DL, Zhang Y et al. Differential activation of *Staphylococcus aureus* heme detoxification machinery by heme analogues. *J Bacteriol* 2014;**196**:1335–42.
- Walter ERH, Ge Y, Mason JC et al. A coumarin–porphyrin FRET break-apart probe for heme Oxygenase-1. *J Am Chem Soc* 2021;**143**:6460–9.
- Waltz E. Appetite grows for biotech foods with health benefits. *Nat Biotechnol* 2019;**37**:573–80.
- Warnatz HJ, Schmidt D, Manke T et al. The BTB and CNC homology 1 (BACH1) target genes are involved in the oxidative stress response and in control of the cell cycle. *J Biol Chem* 2011;**286**:23521–32.
- Wennerhold J, Bott M. The DtxR regulon of *Corynebacterium glutamicum*. *J Bacteriol* 2006;**188**:2907–18.
- White GF, Singleton C, Todd JD et al. Heme binding to the second, lower-affinity site of the global iron regulator *irr* from *Rhizobium leguminosarum* promotes oligomerization. *FEBS J* 2011;**278**:2011–21.
- Wilks A. Heme oxygenase: evolution, structure, and mechanism. *Antioxid Redox Signal* 2002;**4**:603–14.
- Winkler H, Adam G, Mattes E et al. Co-ordinate control of synthesis of mitochondrial and non-mitochondrial hemoproteins: a binding site for the HAP1 (CYP1) protein in the UAS region of the yeast catalase t gene (CTT1). *EMBO J* 1988;**7**:1799–804.
- Wißbrock A, Paul George AA, Brewitz HH et al. The molecular basis of transient heme-protein interactions: analysis, concept and implementation. *Biosci Rep* 2019;**39**:BSR20181940.

- Wu X, Shen W-J, Deshpande A et al. The integrity of heme is essential for reproducible detection of metronidazole-resistant *Clostridioideis difficile* by agar dilution susceptibility tests. *J Clin Microbiol* 2021;**59**:e00585–00521.
- Yang J, Ishimori K, O'Brian MR. Two heme binding sites are involved in the regulated degradation of the bacterial iron response regulator (Irr) protein. *J Biol Chem* 2005;**280**:7671–6.
- Yang J, Panek HR, O'Brian MR. Oxidative stress promotes degradation of the irr protein to regulate haem biosynthesis in *Bradyrhizobium japonicum*. *Mol Microbiol* 2006;**60**:209–18.
- Yin L, Wu N, Curtin JC et al. Rev-erba, a heme sensor that coordinates metabolic and circadian pathways. *Science* 2007;**318**:1786–9.
- Yukl ET, Jepakorir G, Alontaga AY et al. Kinetic and spectroscopic studies of hemin acquisition in the hemophore hasap from *Pseudomonas aeruginosa*. *Biochemistry* 2010;**49**:6646–54.
- Zenke-Kawasaki Y, Dohi Y, Katoh Y et al. Heme induces ubiquitination and degradation of the transcription factor bach1. *Mol Cell Biol* 2007;**27**:6962–71.
- Zhang L, Bermingham-McDonogh O, Turcotte B et al. Antibody-promoted dimerization bypasses the regulation of DNA binding by the heme domain of the yeast transcriptional activator HAP1. *Proc Natl Acad Sci* 1993;**90**:2851–5.
- Zhang L, Guarente L. Evidence that TUP1/SSN6 has a positive effect on the activity of the yeast activator HAP1. *Genetics* 1994a;**136**:813–7.
- Zhang L, Guarente L. HAP1 is nuclear but is bound to a cellular factor in the absence of heme. *J Biol Chem* 1994b;**269**:14643–7.
- Zhang L, Guarente L. Heme binds to a short sequence that serves a regulatory function in diverse proteins. *EMBO J* 1995;**14**:313–20.
- Zhang L, Guarente L. The yeast activator HAP1-a GAL4 family member-binds DNA in a directly repeated orientation. *Genes Dev* 1994c;**8**:2110–9.
- Zhang L, Hach A, Wang C. Molecular mechanism governing heme signaling in yeast: a higher-order complex mediates heme regulation of the transcriptional activator HAP1. *Mol Cell Biol* 1998;**18**:3819–28.
- Zhang L, Hach A. Molecular mechanism of heme signaling in yeast: the transcriptional activator hap1 serves as the key mediator. *Cell Mol Life Sci (CMLS)* 1999;**56**:415–26.
- Zhu GD, Liu F, OuYang S et al. BACH1 promotes the progression of human colorectal cancer through BACH1/CXCR4 pathway. *Biochem Biophys Res Commun* 2018;**499**:120–7.
- Zitomer RS, Carrico P, Deckert J. Regulation of hypoxic gene expression in yeast. *Kidney Int* 1997;**51**:507–13.
- Zollman S, Godt D, Privé GG et al. The BTB domain, found primarily in zinc finger proteins, defines an evolutionarily conserved family that includes several developmentally regulated genes in drosophila. *Proc Natl Acad Sci* 1994;**91**:10717–21.

3.2 A genome-wide analysis of the interconnection of iron- and heme-dependent regulatory networks governed by DtxR and HrrA in *Corynebacterium glutamicum*

Krüger A., Viets U., Filipchik A., Frunzke J.

Draft, to be submitted.

Contributor Role	Contributor
Conceptualization	60% AK, 40% JF
Formal Analysis	100% AK
Investigation/Experiments	60% AK, 40% UV
Methodology	85% AK, 15% UV
Project Administration	50% AK, 50% JF
Software	100% AF
Supervision	50% AK, 50% JF
Visualization	100% AK
Writing – Original Draft Preparation	70% AK, 30% JF
Writing – Review & Editing	-

Overall contribution AK: 75%

All of the presented experimental work on the ChAP-Seq data was conducted by AK and UV. The bioinformatic analysis was performed by AK using the scripts written by AF. Visualization of all earned data was performed by AK. The manuscript was mainly written by AK.

A genome-wide analysis of the interconnection of iron- and heme-dependent regulatory networks governed by DtxR and HrrA in *Corynebacterium glutamicum*

Aileen Krüger¹, Ulrike Viets¹, Andrei Filipchuk¹, Julia Frunzke^{1*}

¹ Forschungszentrum Jülich GmbH, Institute for Bio- and Geosciences 1, IBG1, 52425 Jülich, Germany

*Corresponding Author: Julia Frunzke, j.frunzke@fz-juelich.de

Iron and heme are valuable resources, which are essential for nearly all living organisms, but paradoxically bear the potential to be toxic at elevated concentrations. Therefore, many organisms make use of sophisticated regulatory networks maintaining homeostasis. In *Corynebacterium glutamicum*, DtxR is the master regulator of more than 60 iron-related genetic targets, while the global regulator HrrA of the two-component system HrrSA is regulating more than 200 targets of heme homeostasis. In vitro studies already gave insights into the respective regulons. Within this study, we provide enlarged and comparative in vivo insights into the genome-wide binding profiles of these two global transcriptional regulators at iron- or heme-rich conditions using chromatin affinity purification sequencing (ChAP-seq). Apart from confirmation of known targets, several yet unknown targets of both DtxR and HrrA could be identified, differing under varying environmental conditions. Strikingly, our data emphasize a significant anti-proportional correlation of the ChAP-Seq peak intensity and the impact of the regulator on the differential gene expression. As an overall trend, weak peak intensities correlated with a higher sensitivity regarding the regulation by the respective transcription factor. Further, our analysis revealed several shared targets highlighting the high level of interconnection between these two global regulatory networks. In the end, this study provides additional important parameters for comprehensive revealing of the two regulatory networks.

Keywords: DtxR, HrrA, iron, heme, transcription factors, chromatin affinity purification and sequencing, iron homeostasis

The essential trace element iron is required for the activity of vital enzymes and regulatory proteins as cofactors or as part of cytochromes involved in the respiratory chain (Andrews et al., 2003; Cornelis et al., 2011). Thereby, iron is inevitably necessary for virtually all living organisms. Recently, iron was even claimed to be involved in the development of life (Thiel et al., 2019). Although iron belongs to the most abundant elements in earth's crust, it is predominantly not readily available due to poor solubility under aerobic conditions (Andrews et al., 2003). In its reduced state, ferrous iron (Fe²⁺) is toxic to the cells at elevated levels, mainly caused by its reaction with H₂O₂ (Fenton

reaction) generating reactive oxygen species (Cornelis et al., 2011). Consequently, there is a need for sophisticated regulatory networks for coping with iron homeostasis. DNA-binding transcription factors that sense intracellular Fe²⁺ levels and subsequently modulate the expression of relevant target genes represent important factors coordinating iron homeostatic strategies.

In Gram-positive *Corynebacteria* the master regulator of iron is DtxR (diphtheria toxin repressor) (Brune et al., 2006; Kunkle and Schmitt, 2005; Wennerhold and Bott, 2006). Homologs to DtxR in other Gram-positive organisms have been characterized,

including IdeR in *Mycobacterium tuberculosis* (Gold et al., 2001) or MntR in *Staphylococcus aureus* (Ando et al., 2003). In the first place, this protein was found to regulate the expression of the diphtheria toxin in the pathogenic strain *Corynebacterium diphtheriae* (Boyd et al., 1990; Pappenheimer and Johnson, 1936). Later, it was also identified in other *Corynebacteria*, like also the herein focused soil bacterium *Corynebacterium glutamicum*, and was further attributed with the regulation of more than 60 genes involved in iron acquisition, storage as well as iron-sulfur cluster assembly (Brune et al., 2006; Wennerhold and Bott, 2006). DtxR is active as a dimer in complex with Fe²⁺ in iron sufficient conditions, while Fe²⁺ dissociates from DtxR when iron becomes limiting, rendering the protein inactive (White et al., 1998). Active DtxR functions as a repressor of genes involved in iron uptake and utilization, while also a low proportion of targets related to iron storage and DNA protection are activated (Drazek et al., 2000; Wennerhold and Bott, 2006). Interestingly, DtxR also represses genes encoding other transcriptional regulators like *ripA* or *hrrA*. By contrast to DtxR, RipA (repressor of iron proteins) acts under iron-limited conditions thereby repressing the expression of non-essential iron-dependent proteins (e.g. aconitase or succinate dehydrogenase) (Wennerhold et al., 2005). HrrA is the response regulator of the two-component system HrrSA controlling heme homeostasis (Frunzke et al., 2011; Keppel et al., 2020). Notably, heme-related genes like the heme oxygenase (*hmuO*) or the heme uptake system (*hmuTUV*) are also regulated by DtxR (Drazek et al., 2000; Wennerhold and Bott, 2006) indicating that there is considerable overlap of the DtxR and HrrA regulons.

Heme is an iron-bound protoporphyrin IX and acts as prosthetic group for critical cellular processes like e.g. electron transfer, oxygen metabolism or cell respiration (Ajioka et al., 2006; Ponka, 1999). Depending on the organism, heme can either be acquired from the environment and/or synthesized by the

cell itself. Notably, heme can serve as alternative iron source when acquired from an iron-scarce environment, relevant for e.g. pathogens in the human body (Contreras et al., 2014), but also for non-pathogenic bacteria (Andrews et al., 2003; Wilks, 2002). Similar to iron, elevated levels of heme are harmful to organisms due to the iron-related redox potential (Aft and Mueller, 1984; Kumar and Bandyopadhyay, 2005), but presumably also due to an iron-independent toxicity of the porphyrin structure (Stojiljkovic et al., 1999). Correspondingly, heme homeostasis requires sophisticated mechanisms to be regulated properly.

Among the kingdoms, there are several diverse strategies involved in the maintenance of heme homeostasis (Krüger et al., 2022). For Gram-positive bacteria, a widespread strategy is the regulation of heme homeostasis by two component-systems (TCSs) (Frunzke et al., 2008; Schmitt, 1999; Stauff and Skaar, 2009). Focusing on *C. glutamicum*, this bacterium possesses two-paralogous TCSs dedicated to the stimulus heme: ChrSA and the aforementioned HrrSA (Frunzke et al., 2011; Heyer et al., 2012). Strikingly, homologs are also found in other corynebacterial species, like *C. diphtheriae* (Bibb et al., 2007; Schmitt, 1999). In general, a typical TCS is composed of a membrane-bound histidine kinase (HK) and a cytoplasmic response regulator (RR). After sensing of the stimulus, the HK is autophosphorylated at a conserved histidine residue. Phosphotransfer to a conserved arginine residue in the RR typically activates the RR, which initiates a proper cellular output - commonly transcriptional regulation (Capra and Laub, 2012; Mascher et al., 2006; Stock et al., 2000). In *C. glutamicum*, ChrSA is responsible for heme detoxification by the heme exporter HrtBA, while HrrSA regulates heme homeostasis. The HKs ChrS and HrrS interact by intermembrane interactions with heme and thereby perceive transient changes in heme levels (Keppel et al., 2018). ChrA was shown to bind to the intergenic region of *chrSA* and *hrtBA* activating both operons (Heyer et al., 2012). In contrast,

HrrSA mediates the control of more than 200 target genes involved in heme biosynthesis, respiration and cell envelope remodeling, thereby acting as a global regulator of heme homeostasis (Keppel et al., 2020). Cross-phosphorylation between these two systems was observed, while dephosphorylation remains to be specific to the cognate HK-RR pair (Hentschel et al., 2014).

Several previous studies focused on the elucidation of the DtxR regulon or on the control of single components. Our current understanding about the regulation of iron homeostasis regulated by DtxR in *C. glutamicum* has become quite broad (Brune et al., 2006; Wennerhold and Bott, 2006). However, this knowledge is mainly based on in vitro expression data and there is still a lack of knowledge about detailed in vivo and genome-wide binding patterns of this global iron-dependent regulator. Genome-wide approaches offer a valuable potential for giving insights into the binding dynamics as well as structural and regulatory influence of transcription factors. A prominent example are several studies aimed at the systematic mapping of the binding sites for every transcription factor in the genome of the human pathogen *Mycobacterium tuberculosis*, in order to gain a deeper understanding about its pathogenesis (Galagan et al., 2013a; Park et al., 2014). Using chromatin immunoprecipitation and sequencing (ChIP-Seq) binding profiles of 50 transcription factors in *M. tuberculosis* could already be assessed (Galagan et al., 2013b). Combining such genome-wide binding data with further expression analyses can even broaden our knowledge on regulation as demonstrated in numerous studies across domains of life (MacPhillamy et al., 2022; Qin et al., 2022; Rustad et al., 2014).

Within this study, we used chromatin affinity purification and sequencing (ChAP-Seq) aiming to compare DtxR and HrrA genome-wide binding patterns in *C. glutamicum* growing in iron- and heme-rich conditions. Comparative analysis of ChAP-Seq peak

intensities with differential gene expressions revealed a significant anti-proportional behavior showing higher changes in RNA levels in a strain lacking the regulator especially for targets with a low peak coverage. Consequently, our genome-wide studies provided important insights into the binding dynamics, interaction and interference of the two global regulators orchestrating iron- and heme homeostasis in *Corynebacterium glutamicum*.

MATERIAL AND METHODS

Bacterial strains and growth conditions

The bacterial strains used within this study are listed in Table 1. *Escherichia coli* strains were cultivated in Lysogeny Broth (Difco LB, Heidelberg, Germany) media shaking at 37°C. If appropriate, 50 µg/ml kanamycin was added to the media for selection. For general cultivation, the *Corynebacterium glutamicum* ATCC 13032 wild type strain or its derivatives were cultivated in liquid BHI (brain heart infusion, Difco BHI, BD, Heidelberg, Germany), inoculated from a fresh agar plate. As complex media, CGXII with 2% (w/v) glucose was used as minimal media. When hemin was added (throughout this paper further referred to as heme), no iron was supplemented to the media. Cells were cultivated shaking at 30°C.

Recombinant DNA work and cloning techniques

Standard molecular methods were performed according to standard protocols (Sambrook and Russell, 2001). DNA fragments were amplified via polymerase chain reactions (PCR), using chromosomal DNA of *C. glutamicum* ATCC 13032 as template and the oligonucleotides listed in Table 2. Preparation was performed as described previously (Eikmanns et al., 1994).

Plasmids were constructed by enzymatically assembling the generated DNA fragments into a cut vector backbone using Gibson assembly (Gibson et al., 2009). Sequencing of

the final plasmids was performed by Eurofins Genomics (Ebersberg, Germany).

For the integration of the His-Tag and a linker (GGGS₂) at the C-terminus of DtxR in the genome of *C. glutamicum*, the suicide vector pK19-*mobsacB* was used (Schäfer et al., 1994). Electrocompetent *C. glutamicum* cells

were transformed with the isolated plasmid by electroporation (van der Rest et al., 1999). Then, the first and second recombination events were performed and verified as described in previous studies (Niebisch and Bott, 2001). The respective deletion was reviewed by amplification and sequencing by Eurofins Genomics (Ebersberg, Germany).

Table 1: Bacterial strains and plasmids used in this study

Strain	Characteristics	Reference
<i>Escherichia coli</i>		
DH5α	F ⁻ Φ80 <i>lacZ</i> ΔM15 Δ(<i>lacZYA-argF</i>) U169 <i>recA1 endA1 hsdR17</i> (r _k ⁻ , m _k ⁺) <i>phoA supE44 thi-1 gyrA96 relA1</i> λ ⁻ ; for general cloning purposes	Invitrogen
<i>Corynebacterium glutamicum</i>		
<i>C. glutamicum</i> ATCC13032	Biotin-auxotrophic wild type strain	Kinoshita et al. (2004)
<i>C. glutamicum</i> ATCC13032:: <i>dtxR</i> -C-linker-His	Derivative of ATCC 13032 encoding a C-terminally His-tagged version of DtxR (NCgl1845) with a flexible linker sequence in between (GGGGSGGGGS).	This work
<i>C. glutamicum</i> ATCC13032:: <i>hrrA</i> -C-twinstrep	Derivative of ATCC 13032 encoding a C-terminally twinstrep-tagged version of HrrA (NCgl2834).	Keppel et al. (2020)
Plasmids		
pK19- <i>mobsacB</i>	Contains negative (<i>sacB</i>) and positive (<i>kan</i> ^r) selection markers for genomic integration and deletion, MCS cut with EcoRI/BamHI	Schäfer et al. (1994)
pK19- <i>mobsacB</i> - <i>dtxR</i> -C-linker-His	Derivative of pK19 <i>mobsacB</i> for C-terminal integration of a His-Tag and a flexible linker in between; Kan ^r	This work

Table 2: Oligonucleotides used in this study provided by Eurofins Genomics (Ebersberg, Germany).

Oligonucleotide	Sequence 5' → 3'	Usage
A280-leftflank-dtxR-C_fw	CAGGTCGACTCTAGAGGATC CGACGGTCTTGTGCA CGTCAGC	Left flank for tag
A290-leftflank-dtxR-His-C- 2-rv	TGATGATGATGTGAGCCGCCGCCCTGAGCCGC CGCCGCCGCCCTCAACCTTTTCTACGC	integration to <i>dtxR</i>
A291-rightflank-dtxR-His-C- 2-fw	GCGGCGGCTCACATCATCATCATCATCA TCATCATTAACACACGATGAAGCTTCT	Right flank for tag
A283-rightflank-dtxR-C-rv	GTAAACGACGGCCAGTGAATTG CGATGTTCCG TATGCGCCAGC	integration to <i>dtxR</i>
A296-dtxR-Tag-C-seq-fw	CAGTCCGGCCCAACTGTCTAG	Sequencing
A297-dtxR-Tag-C-seq-rv	CCGGTTGCTACCTGCAGCAC	primers for tag integration

bold = overlap to backbone, **orange** = flank overlap

Chromatin affinity purification-sequencing (ChAP-Seq) – sample preparation

The protocol for obtaining DNA was adapted to recent studies (Keppel et al., 2020; Pfeifer et al., 2016). The strains *C. glutamicum* ATCC 13032::*dtxR*-C-linker-His and *C. glutamicum* ATCC 13032::*hrrA*-C-twinstrep were cultivated each in triplicates from a fresh agar plate in 20 ml BHI in 100 ml shaking flasks and incubated at 30°C for 8 h in a rotary shaker. Cells were transferred into a second pre-culture with 200 ml CGXII media containing 2% (w/v) glucose for further ~16 h incubation. For the heme condition no iron was added to this pre-culture to starve these cells from iron, while for the iron excess condition the standard amount of iron was used (36 μM FeSO₄). From this overnight culture, the main culture was inoculated at an OD₆₀₀ of 3 in 1 l CGXII with 2% (w/v) glucose and either 100 μM FeSO₄ (Fe excess condition) or 0 μM FeSO₄ but 4 μM heme (heme condition) in 5 l shaking flasks. After 2 h cultivation at 30°C in a rotary shaker, cells were harvested (5,000 x g, 4°C, 10 min). The cell pellets were washed once with CGXII

without MOPS and then the cells were incubated in 20 ml CGXII without MOPS and 1% formaldehyde for 20 min at RT to cross-link the regulator protein to the DNA. To stop this reaction, incubation with 125 mM glycine for 5 min followed. Then, cells were washed three times with either TNI20 (20 mM Tris-HCl, 300 mM NaCl, 20 mM Imidazol, pH 8) or buffer A (100 mM Tris-HCl, pH 8; importantly w/o EDTA, to avoid disturbance of DtxR binding) and the pellets were stored overnight at -80°C. For cell disruption and purification, the pellets were resuspended in approximately 20 ml TNI20 or buffer A with cOComplete protease inhibitor (Roche, Basel, Switzerland) and 2 mg RNase A (AppliChem, Darmstadt, Germany) and disrupted at 40,000 psi using the Multi Shot Cell Disrupter (I&L Biosystems, Königswinter, Germany). To shear the chromosomal DNA the samples were sonified 2 x 20 s with the Branson Sonifier 250 (Branson Ultrasonics Corporation, CT, Connecticut, USA) and finally supernatant was collected after ultracentrifugation (150,000 x g, 4°C, 1 h).

The DNA, which was bound by the His-tagged DtxR, was purified using Ni-NTA Agarose column material (Thermo Fisher Scientific, Massachusetts, USA) according to manufacturer's instructions to the gravity flow protocol. Washing of the column was performed using TNI20, while the tagged protein and the bound DNA were eluted with TN buffer with rising imidazole concentrations (20 mM Tris-HCl, 300 mM NaCl, 50/100/200/400 mM Imidazol, pH 8). A Bradford assay was performed to evaluate which eluted fractions will be pooled for further DNA preparation, which were the last three of TNI50 elution and the first three of TNI100.

The DNA bound by the twin-Strep-tagged HrrA was purified using Strep-Tactin XT Superflow column material (IBA Lifesciences, Göttingen, Germany) according to manufacturer's instructions to the gravity flow protocol. Washing of the column was performed using buffer W (100 mM Tris-HCl, 150 mM NaCl, pH 8) and the tagged protein and the bound DNA was eluted with buffer E (100 mM Tris-HCl, 150 mM NaCl, 15 mM D-biotin, pH 8).

After the purification, 1% (w/v) SDS was added to the eluted (and pooled) fractions and incubated overnight at 65°C. Digestion of the protein was accomplished with the addition of 400 µg/ml Proteinase K (AppliChem GmbH, Darmstadt, Germany) at 55°C for 2h. Purification of DNA followed by adding Roti-Phenol/Chloroform/Isoamylalcohol (Carl Roth GmbH, Karlsruhe, Germany) in a 1:1 ratio to the samples and consequent separation of organic phase using Phase Lock Gel (PLG) tubes (VWR International GmbH, Pennsylvania, USA) according to manufacturer's instructions. The aqueous phase was taken off and mixed with 0.1 of the sample volume of 3 M Na-acetate and double the amount of ice-cold EtOH and incubated for 2 h at -20°C. Centrifugation at 16,000 x g, 4°C, 10 min followed. The DNA was precipitated by adding ice-cold 70 % (v/v) EtOH and after another centrifugation, supernatant was

taken off carefully and DNA was dried for 3 h at 50°C and eluted in dH₂O.

ChAP-Seq – Sequencing and Peak Analysis

The isolated DNA fragments (section 3.4) were used for library preparation and indexing with TruSeq DNA PCR-free sample preparation kit (Illumina, Chesterford, UK) according to manufacturer's instructions, leaving out the DNA size selection steps. Libraries were quantified using KAPA library quant kit (Peqlab, Bonn, Germany) and normalized for pooling. These pooled libraries were sequenced using the MiSeq device (Illumina, Chesterford, UK) (paired-end sequencing, read length: 2 x 150 bases). Data analysis as well as base calling was performed with the Illumina instrument software, yielding fastq output files. Further data analysis was based and modified according to Keppel et al. (2020). To remove PCR amplification artifacts, sequencing data was collapsed for each sample. The processed fastq files were mapped to accession NC_003450.3 as *C. glutamicum* reference genome. This was done using Bowtie2 with the following parameters: --ignorequals --local --very-sensitive-local --rfg 9,5 --rdg 9,5 --score-min L,40,1.2 -k 8 --no-unal --no-mixed --threads 8 -l 40 -X 800 (Langmead and Salzberg, 2012; Langmead et al., 2019). The genomic coverage was convoluted with second order Gaussian kernel. The kernel was truncated at 4 sigmas and expanded to the expected peak width. The expected peak width was predicted using the following procedure: (i) All peaks higher than 3 mean coverage were detected. (ii) Points at which coverage dropped below half of the maximal peak height were detected and the distance between those was set as peak width. (iii) The estimated peak width was fixed equal to the median peak width. Convolution profiles were scanned to allow identification of the regions where first derivative changes from positive to negative. Each of these regions was determined as a potential peak with an assigned convolution score (convolution with second order Gaussian kernel centered at the peak position). These filtered peaks were

normalized for inter-sample comparisons and the sum of coverages of all detected peaks was negated from the total genomic coverage. This difference was used as normalization coefficient and was divided by peak intensities.

RESULTS

Genome-wide profiling of DtxR and HrrA DNA-binding

Earlier studies already performed whole-genome expression analyses via DNA microarrays and also RT-qPCR approaches for validating targets of DtxR and HrrA in *Corynebacterium glutamicum* in vitro (Brune et al., 2006; Frunzke et al., 2011; Wennerhold and Bott, 2006). However, in vivo approaches would add even more precise information on a global scale. In order to provide the first genome-wide binding pattern of the transcriptional regulator DtxR, and on top compare it to binding of HrrA, ChAP-Seq experiments using a tagged variant of the protein of interest was performed. While this was already successfully implemented for HrrA (Keppel et al., 2020), previous experiments in our lab demonstrated that both direct C-terminal and N-terminal tagging of DtxR led to a disruption of its function and a growth phenotype resembling a $\Delta dtxR$ strain (Wennerhold and Bott, 2006) (data not shown). Therefore, a flexible linker sequence was added at the C-terminal end of this protein, to avoid any disturbances by the tag in the protein's action (Chen et al., 2013). Growth analysis of the strain expressing the C-terminal His-tagged DtxR variant including the linker showed that there was no growth disturbance neither on standard conditions, nor on iron excess conditions (Figure S1A). Additionally, an N-terminal tagged variant

was tested, which showed a growth defect on iron excess conditions (Figure S1A). Notably, also qPCR analysis confirmed that the C-terminal His-tagged version of *dtxR* is expressed at wild-type levels in the presence of iron ($2^{-\Delta\Delta Ct_{\text{iron excess}}} = 1.11 \pm 0.05$; $2^{-\Delta\Delta Ct_{\text{standard}}} = 1.44 \pm 0.15$, Figure S1B). Analogously to the strain with a His-tagged DtxR, a strain with a twin-Strep-tagged variant of HrrA from previous studies was used (Keppel et al., 2020).

The genome-wide binding of the two regulators DtxR and HrrA was analyzed once under iron excess conditions (100 μM FeSO_4) and once with heme as alternative iron source (4 μM heme). The general procedure is shown schematically in Figure 1A. The genome-wide binding profiles are shown for triplicates of each regulator in Figure 1B and C. In direct comparison, it could be confirmed that HrrA binds to a higher number of genomic targets in comparison to DtxR. Overall, a very similar binding pattern was observed for growth on iron excess and heme, respectively (Figure 1B and 1C). This is not surprising and reflects efficient iron and heme homeostatic processes stabilizing the intracellular pool of chelatable Fe^{2+} and heme, i.e. iron excess conditions support sufficient heme synthesis (Frunzke et al., 2011; Layer, 2021), while iron-starved but heme rich conditions lead to the usage of heme as alternative iron source via heme oxygenase HmuO (Wilks and Schmitt, 1998). Pearson correlations confirmed robust correlation within triplicates of the same samples, while displaying significant differences between the growth conditions that emphasize minor, but substantial variances with respect to the genome-wide binding pattern (Figure 2A and 2C).

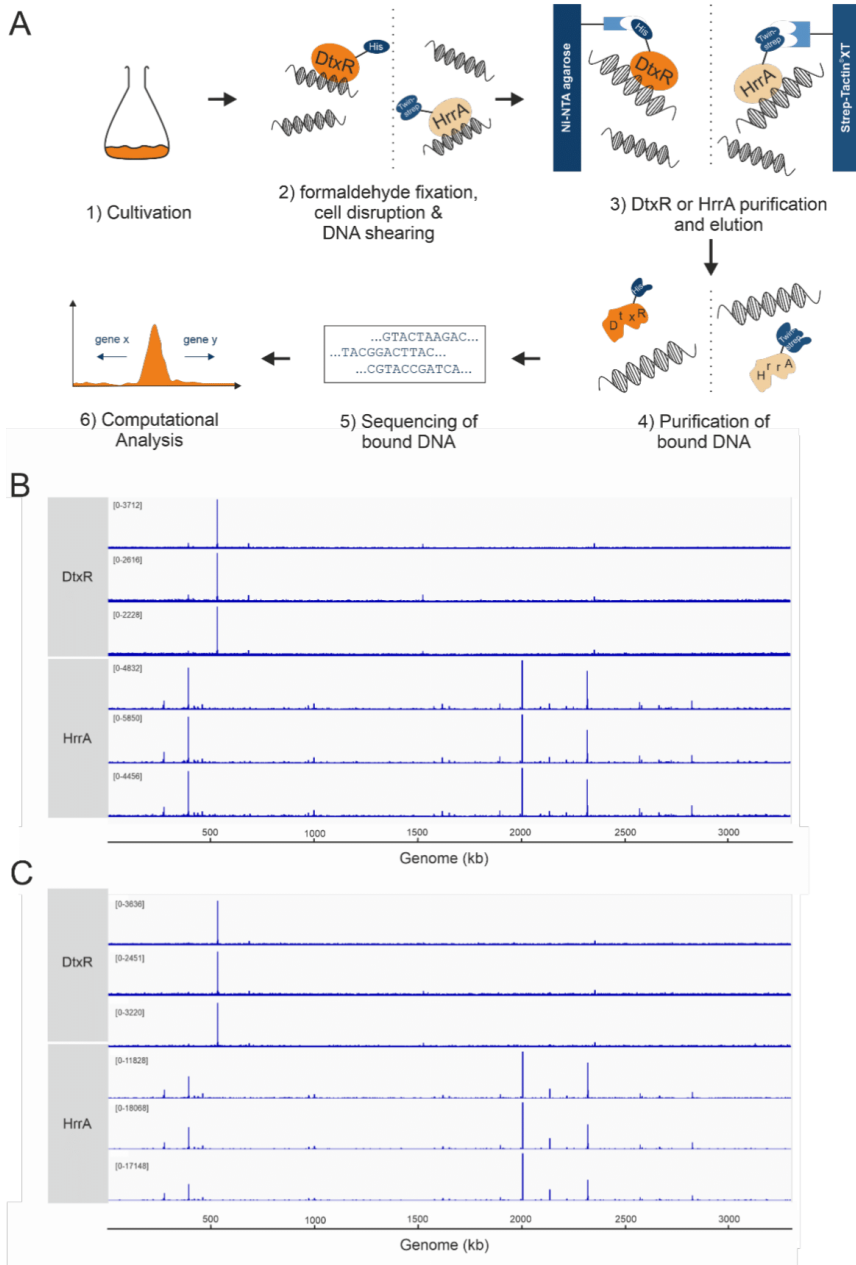


Figure 1: Genome-wide profiling of DtxR and HrrA DNA-binding in *C. glutamicum* (A) Schematic representation of the ChAP-seq experimental setup for both a DtxR His-tagged and a HrrA twin-Strep-tagged variant. (B-C) Mapping of ChAP-seq reads for DtxR and HrrA to the *C. glutamicum* ATCC 13032 genome. DNA was obtained by affinity purification of DtxR and HrrA from cultures grown under iron excess (B; 100 μ M FeSO₄) or heme conditions (C; 4 μ M heme).

For the iron-responsive regulator DtxR, overall 45 genomic targets were found across the tested conditions (Figure 2B, Table S1); almost all located in the upstream region of open reading frames. Among those, we could identify 25 out of 54 targets, which were already described by previous studies using transcriptome analyses and EMSAs (Brune et al., 2006; Wennerhold and Bott, 2006). The most prominent binding peak was found upstream of NCgl0484, encoding a Fe³⁺ siderophore transport system and was already shown to be repressed by DtxR in vitro (Brune et al., 2006). Binding to this target was shown in both iron excess and heme conditions. Interestingly, further 21 yet unknown targets bound by DtxR were found via ChAP-Seq. Among the peaks with the highest coverage, we found the gene NCgl1781 coding for a phage protein, NCgl0193 for a hypothetical protein, *qor3* encoding a putative NADPH:quinone oxidoreductase, the tyrosine recombinase *xerC* and *metH* encoding the homocysteine methyltransferase. Regarding the newly identified targets, ten were detected under iron excess condition and further 14 targets were only present during growth on heme.

By contrast, for the heme-sensitive regulator HrrA, overall 332 targets were identified (Figure 2D, Table S2), with 269 binding in upstream regions and 63 inside open reading frames. 151 out of 231 targets identified by former studies could be confirmed (Keppel et al., 2020). As expected, the most prominent peak for HrrA binding corresponds either to the repression of the myo-inositol-1 or 4-monophosphatase *suhB* or polyphosphate glucokinase *ppgK*, just as found in previous studies (Keppel et al., 2020). Additionally, 183 new targets were identified (41% in the iron excess conditions and 27% found solely during growth on heme), which will be in the focus throughout this study. Among the new targets are for example the central carbon metabolism related targets *aceA*, *pyc* or *tkt*, as well as genes involved in signal transduction, including *cgtR2*, *hrcA*, *hspR*, *pdxR* or *rbsR*. In addition, there are 80 genes, which are bound by HrrA only in the iron

excess condition, which have not been detected in previous studies. This includes the genes *rpoB* encoding the beta subunit of the DNA-directed RNA polymerase, *ohr* encoding a putative organic hydroperoxide resistance and detoxification protein, the universal stress protein encoded by *uspA3* and the gene for the translation initiation factor IF-3 namely *infC*. These results demonstrate the potential for the identification of new targets by sampling under different growth conditions and therefore provide valuable insights into the regulatory role of HrrA.

In relation, the amount of targets between DtxR and HrrA found within this study are in line with the respectively predicted 3% and 21% of the regulatory network in *C. glutamicum* (relation percentage: 3/21 = 0.143; relation targets: 45/334 = 0.135) (Escorcia-Rodríguez et al., 2020).

Peaks of DtxR reveal new binding targets and differences depending on the presence of surplus iron or heme

Representative extracted peaks for all genetic targets of DtxR are shown for the iron excess condition in Figure 3 and for the heme condition in Figure 4. Regarding the peaks with the highest coverages in both conditions, it is striking that the most prominent targets are present in both conditions, including NCgl0484 as already mentioned as the highest peak, but further *irp1*, *sdhDC*, NCgl1781 and NCgl2877. One new target with high binding intensity is the hypothetical protein NCgl1781, which is located in the CGP4 prophage. Interestingly, some targets, which were predicted to be regulated by DtxR based on motif search, but could not yet be shown by in vitro bandshift assays (Brune et al., 2006), but were now identified in the ChAP-Seq experiment. These include genes encoding the putative membrane protein *wzy*, the putative oxidoreductase dehydrogenase *oxiB*, the putative transcriptional regulator NCgl0176 and the tyrosine recombinase *xerC*. The latter one is especially interesting, showing a quite intense peak while also being regulated

by HrrA (Table S2). This target is only regulated by DtxR in the presence of heme (Figure 4). Another quite intense peak found only during growth on heme is visible for the homocysteine methyltransferase *metH*. By contrast, the peak corresponding either to the NADH:quinone oxidoreductase *qor3* or the putative toxin efflux permease *cepA* shows a distinct peak only in iron excess conditions, but not during growth on heme.

In general, for the heme condition (Figure 4), there are significantly more new targets found than in the iron excess condition, again highlighting the importance of binding studies conducted under different conditions.

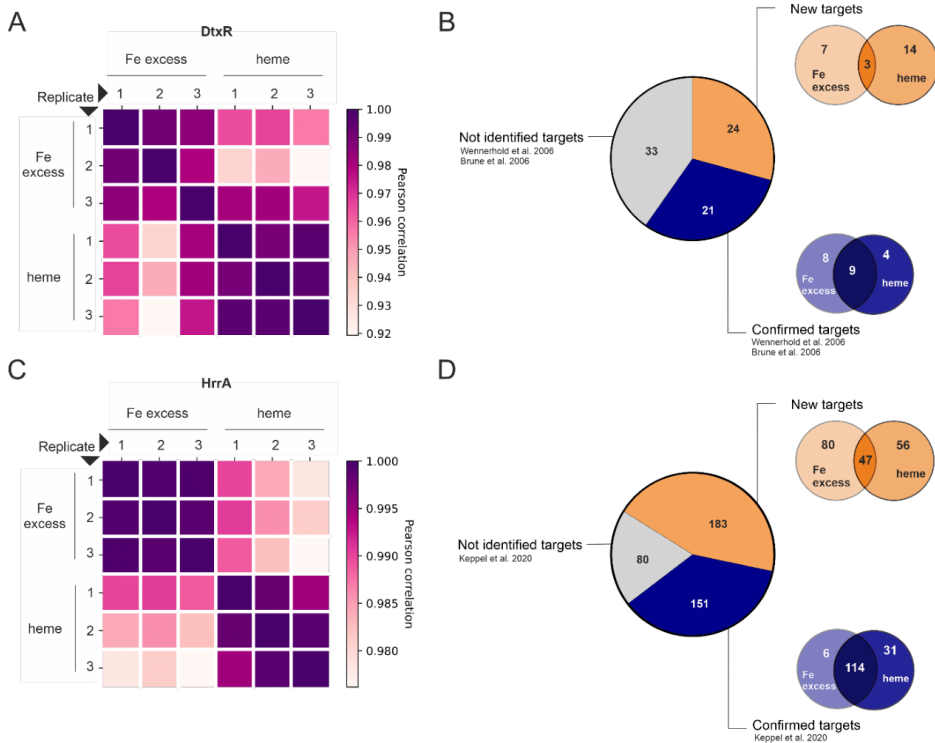


Figure 2: Overview of targets bound by DtxR and HrrA (A) Pearson correlation of identified peaks among all replicates for DtxR binding at the two different conditions of iron excess (100 μ M FeSO_4) and heme (4 μ M). (B) Pie chart comparing targets of DtxR that are new, already confirmed by previous studies and predicted from previous studies (Brune et al., 2006; Wennerhold and Bott, 2006) but not found in this ChAP-Seq splitting up based on conditions. Total = 78. (C) Pearson correlation of identified peaks among all replicates for HrrA binding at the two different conditions of iron excess and heme. (D) Pie chart comparing targets of HrrA that are new, already confirmed by previous studies and predicted from previous studies (Keppel et al., 2020) but not found in this ChAP-Seq splitting up based on conditions. Total = 414.

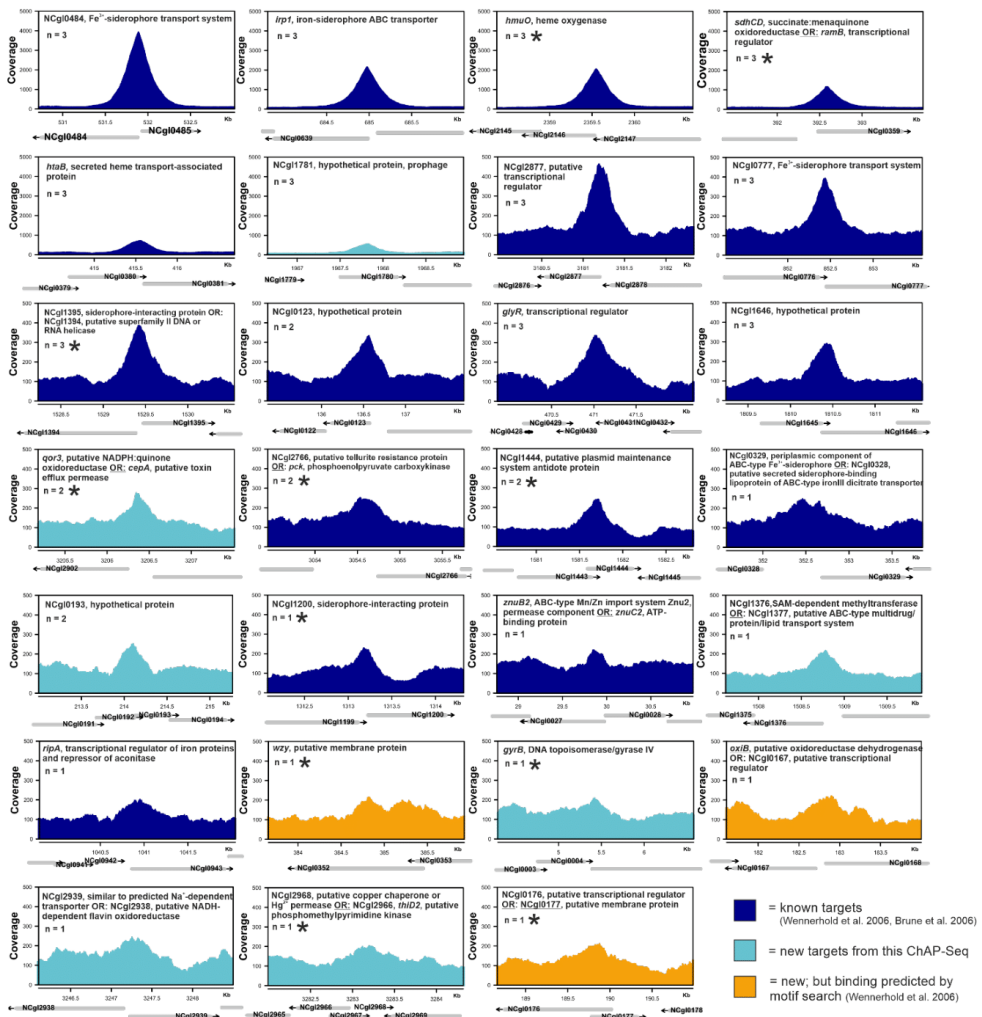


Figure 3: Genomic targets bound by DtxR during growth under iron excess conditions. Coverage of binding peaks (y-axis) plotted against the respective genomic regions of *C. glutamicum* ATCC 13032 (x-axis). Genes are indicated below with grey arrows. Peaks include known targets (dark blue; Wennerhold and Bott (2006) and Brune et al. (2006)), novel targets identified in this study (light blue), and predicted targets of previous studies (orange). The number of replicates where a significant peak could be found is shown in each respective graph as 'n'. '*' marks those targets which are shared with HrrA. 'OR' indicates that regulator binding could affect expression of both divergent genes.

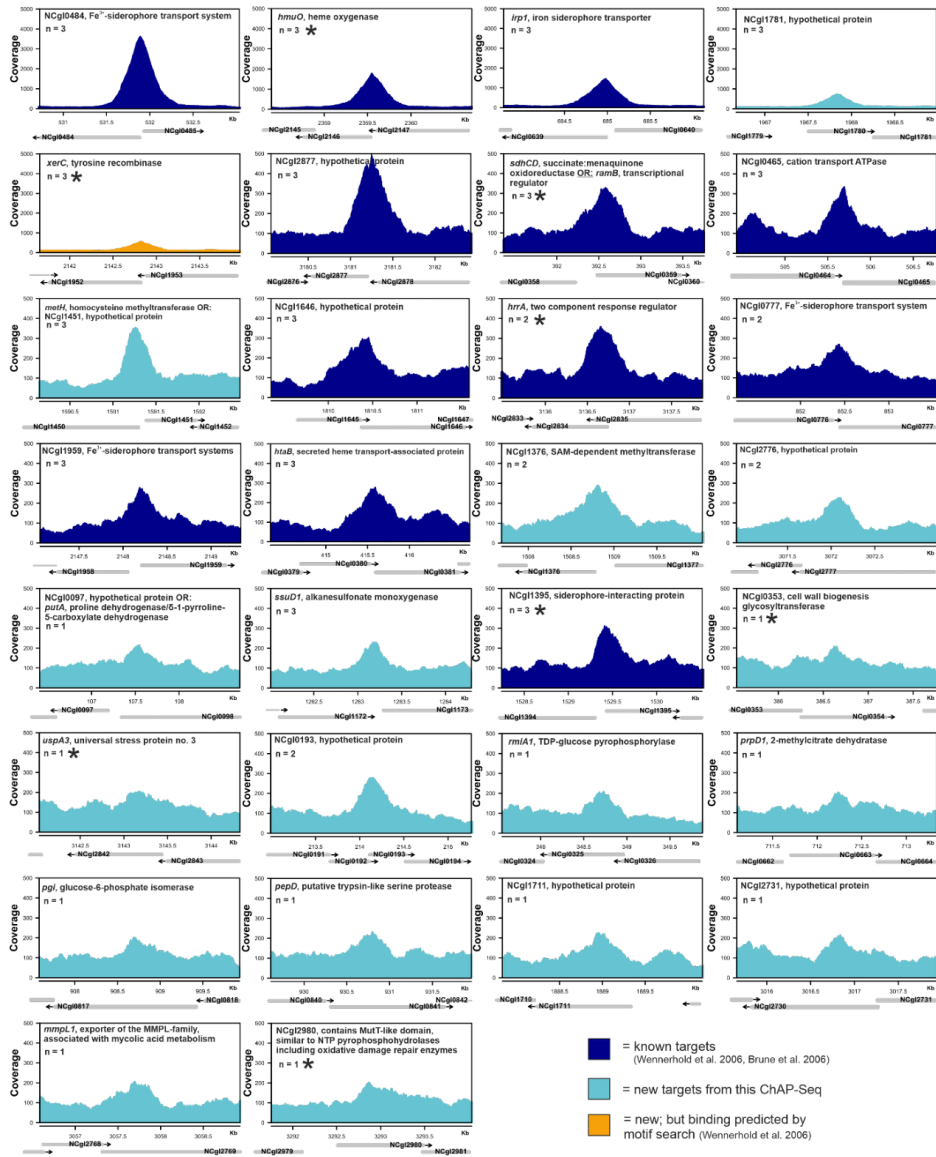


Figure 4: Genomic targets bound by DtxR during growth under heme conditions Coverage of binding peaks (y-axis) plotted against the respective genomic regions of *C. glutamicum* ATCC 13032 (x-axis). Genes are indicated below with grey arrows. Peaks include known targets, identified under iron excess conditions (dark blue; Wennerhold and Bott (2006) and Brune et al. (2006)), novel targets identified in this study (light blue), and predicted targets of previous studies (orange). The number of replicates where a significant peak could be found is shown in each respective graph as 'n'. '*' marks those targets which are shared with HrrA. 'OR' indicates that regulator binding could affect expression of both divergent genes.

Targets with a low peak coverage show higher differential gene expression

ChAP-Seq experiments always result in a high amount of peaks with a weak binding coverage. To address their physiological relevance, we correlated peak intensities of ChAP-Seq experiments with microarray, RT-qPCR and RNA-Seq data obtained previously (Brune et al., 2006; Keppel et al., 2020; Wennerhold and Bott, 2006). Figure 5 represents a comparison of peak intensities for DtxR binding with the differential gene expression levels ($\Delta dtxR/WT$) obtained for microarray analysis by Wennerhold and Bott (2006) and the RT-qPCR results performed by Brune et al. (2006) for the targets identified in all three studies under iron excess conditions. Further comparisons of targets identified in only one of these former studies, are shown in Figure S5A and B. Interestingly, this analysis revealed a consistent anti-proportional correlation of peak intensity and differential gene expression determined by different methods. The highest binding peaks were found in this study for *irp1* and *hmuO*, where differential gene expression levels were shown to be rather low when comparing expression in *C. glutamicum* wild type with a mutant lacking *dtxR*. Analogously, the differential gene expression levels were quite high in NCgl0123 encoding a hypothetical protein and NCgl1646 coding for a putative secreted hydrolase in the prophage CGP3 region, which showed rather low binding peaks.

This is consistent with the pattern observed for HrrA (Keppel et al., 2020), where there is also an anti-proportional relation. This is striking, when comparing the peak for *suhB* and *hmuO*. While the peak for *suhB* is the highest, the $\log_2(\Delta hrrA/WT)$ ratio is one of the lowest. However, for *hmuO*, a low peak intensity correlates with a high differential gene expression for this target in the absence of HrrA.

ChAP-Seq analysis provides a huge amount of binding site sequences. This data also has the potential to improve motif identification. Therefore, analysis on the binding motif was accomplished using the MEME-ChIP tool (Bailey and Elkan, 1994) for both transcriptional regulators and both conditions. For DtxR under iron excess, we found mainly the palindromic consensus sequence GSCTAACCTAANTW (E-value = 9.5×10^{-15}) (Figure 5C). The heme condition led to the similar motif (AGSCTAACCTAAGY, E-value = 6.5×10^{-12}) (Figure S2C). These motifs are shorter but fit well to the motif identified for DtxR by Brune et al. (TAGGTTAG(G/C)CTAACCTAA) and that of *C. diphtheriae* (Kunkle and Schmitt, 2003) and could consequently now be confirmed in vivo within this study.

For HrrA, the found motif from iron excess CMAMCDAAAGTKGA (E-value = 2.4×10^{-40}) and from heme condition CAWHCRAAAGDTKKA (E-value = 9.9×10^{-59}) also corresponds to the motif found by (Keppel et al., 2020), with an even more significant E-value (Figure 5D and S2D).

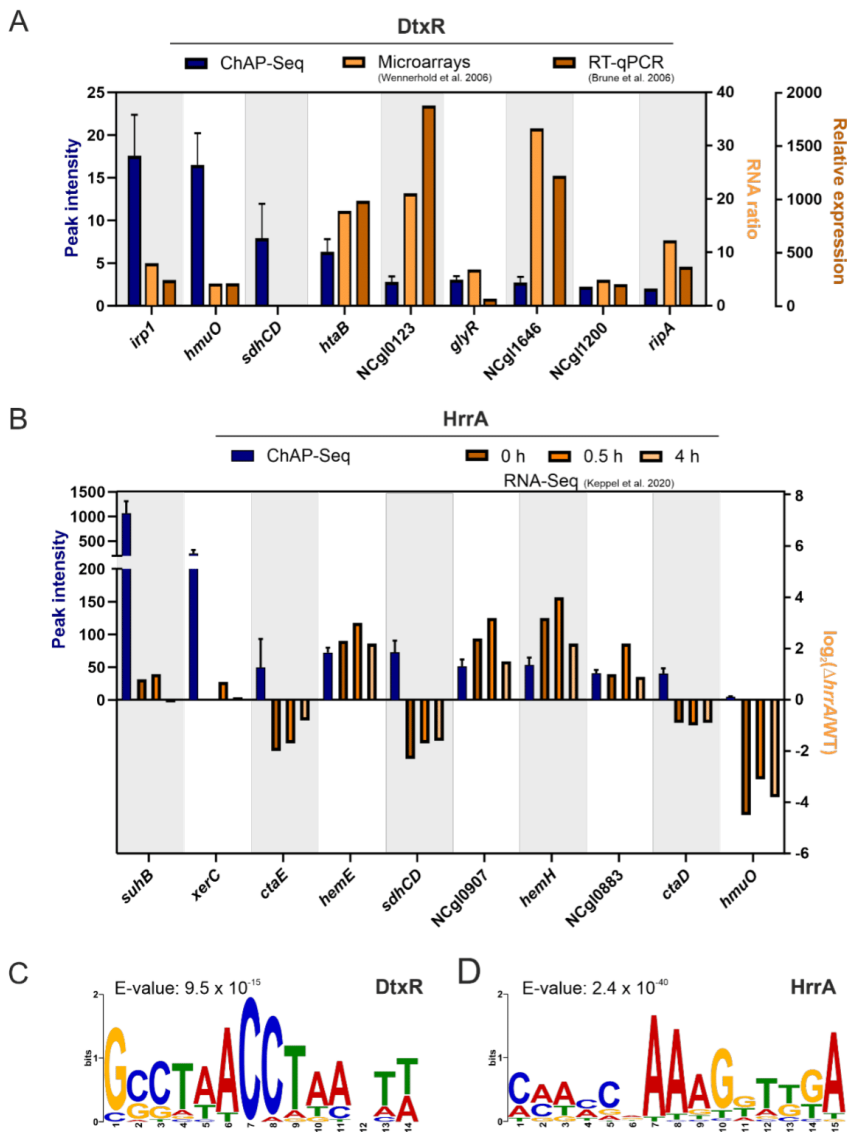


Figure 5: Correlation of ChAP-Seq peak intensity and differential gene expression. (A) Peak intensities of the ChAP-Seq for DtxR under iron excess conditions (dark blue) were compared to the RNA ratios at iron excess (*DtxR*/wild type) from a microarray analysis (Wennerhold and Bott, 2006) (light orange) as well as to the relative expressions under iron excess in the deletion strain *ΔdtxR* compared to wild type analyzed via RT-qPCR (Brune et al., 2006) (dark orange). (B) Peak intensities of the ChAP-Seq of HrrA in the presence of heme (dark blue) was compared to the $\log_2(\Delta hrrA/wild\ type)$ values obtained from the time-resolved RNA-seq in the presence of heme (Keppel et al., 2020) (shades of orange). Further, MEME-ChIP prediction of the DtxR (C) and HrrA (D) binding motif based on ChAP-Seq binding peaks extracted for iron excess conditions is shown (Bailey and Elkan, 1994).

Shared targets of DtxR and HrrA provide insights in interference effects

The analysis of the genome-wide profiling of HrrA and DtxR now, for the first time, enables the comparison of binding patterns for the shared targets of these two regulators, potentially providing insights into regulatory interference. Overall, 16 targets, which were regulated by both DtxR and HrrA could be identified (Figure 6A, Table 3). Examples for binding peaks found are given in Figure 6C-G with their genomic context presented additionally in Figure 6B and Figure S3. An exemplary target showing clear interference of DtxR and HrrA is the promoter of the heme oxygenase *hmuO*. The locations of DtxR and HrrA binding for *hmuO* regulation are in close proximity to each other with significant overlap (Figure 6B-C), hinting for interference of the two regulators in the upstream promoter region. While DtxR acts as a repressor of *hmuO*, HrrA was shown to be crucial for activating *hmuO* expression. For this particular example, we observed a higher coverage of HrrA on heme and a slightly higher coverage of DtxR on iron. A similar trend – with higher coverage for DtxR on iron and HrrA on heme – was also observed for *sdhCD* (Figure 6D). Here, the binding sites are separated by ~100 bp speaking against a direct interference effect.

Regarding peak intensities, a direct comparison between the conditions might be difficult due to different regulator proteins and purification procedures. Nevertheless, a first comparison of the ratios of peak intensities of targets that were bound in both iron and heme conditions gives hints for a trend towards higher peak intensities of DtxR binding in iron conditions than in the presence of heme and

analogously for HrrA a stronger binding at heme conditions (Figure S4). However, an overall trend did not establish when considering all shared targets. For example, DtxR binding to *xerC* was only observed in the presence of heme, while HrrA showed a higher coverage under heme conditions (Figure 6E).

Another shared target is the hypothetical protein NCgl0176 (Figure 6F) encoding a putative transcriptional regulator. For DtxR, the peak intensity is low under iron excess conditions and was not identified at all at heme conditions. The binding region is upstream and at the beginning of the gene. By contrast, HrrA shows a double peak. One is found upstream of NCgl0176 in close proximity to the DtxR region, but not overlapping. The other one is far away inside NCgl0176. Therefore, this second peak might rather account for the regulation of NCgl0177.

Further, we could confirm binding of HrrA to itself, activating the expression of its own gene (Keppel et al., 2020) (Figure 6G). The data suggests that HrrA binding to its own promoter increases with increased heme levels. The DtxR binding site upstream of *hrrA* is slightly upstream, but with no overlap with the HrrA motif as for *hmuO*. Surprisingly, no significant DtxR binding could be detected under iron excess, showing the high sensitivity to slight fluctuations in cultivation conditions or experimental setups.

Overall, there is no conclusive trend that can be summarized for the interference of DtxR and HrrA at the promoter regions of shared targets demonstrating the complexity of regulatory networks – beyond potential interference of two global regulators.

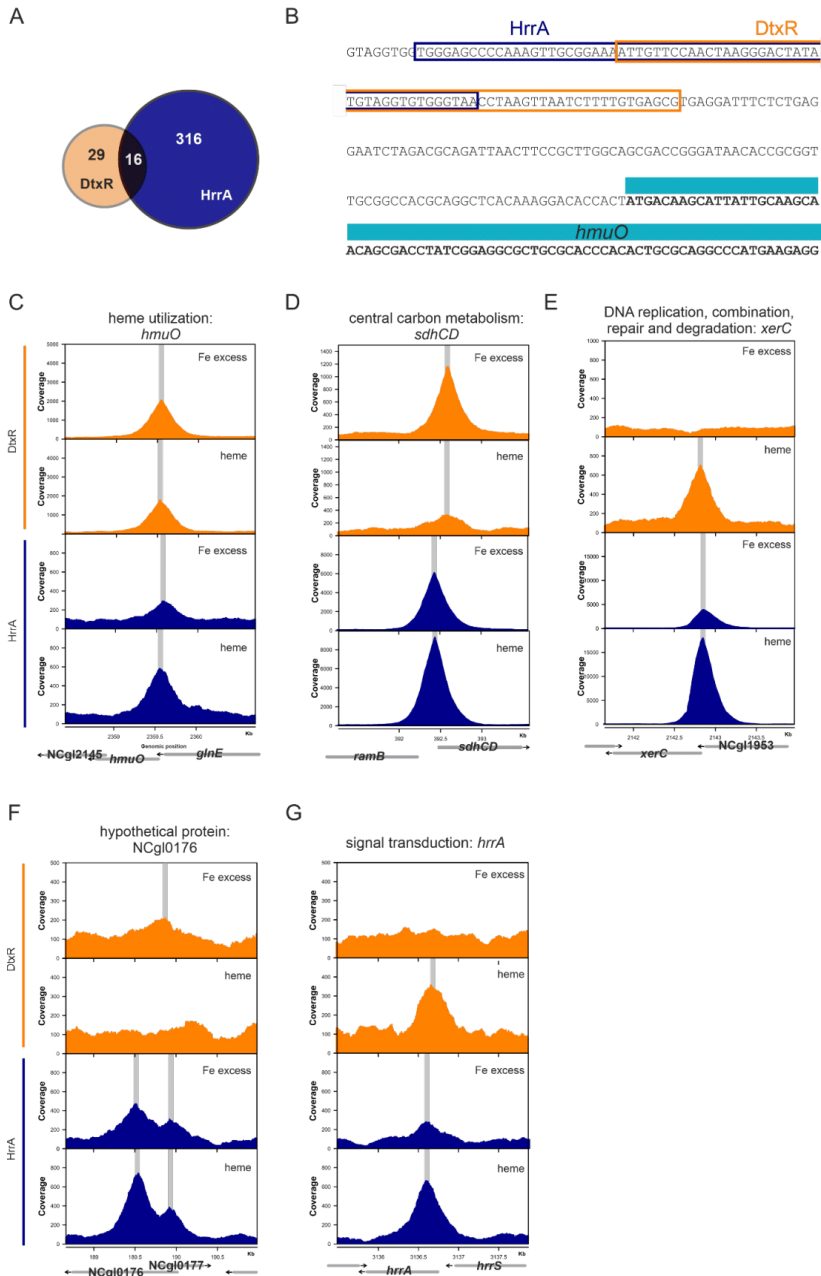


Figure 6: Shared targets of the regulators DtxR and HrrA show interconnection between iron and heme regulatory networks. (A) Quantitative representation of shared targets of the two regulators. (B) Upstream region of *hmuO* (turquoise). Orange boxes represent peak-predicted area of binding by DtxR, blue for binding by HrrA. (C-G) Peak detection in the region of *hmuO*, *sdhCD*, *xerC*, NCgl0176 and *hrrA* respectively as represented by grey arrows below. Orange peaks represent binding of DtxR, blue ones of HrrA. The grey vertical line illustrates the peak maxima.

Table 3: Genes found to be regulated by both DtxR and HrrA

gene number	gene	DtxR Fe excess		DtxR heme		HrrA Fe excess		HrrA heme	
		μ peak intensity	n						
NCgl0005	<i>gyrB</i>	2.01	1	n.d.	0	2.80	2	n.d.	0
NCgl0176		2.03	1	n.d.	0	2.42	3	3.45	1
NCgl0352	<i>wzy</i>	1.94	1	n.d.	0	5.44	3	7.71	3
NCgl0353		n.d.	0	2.02	1	n.d.	0	3.38	1
NCgl0359	<i>sdhC</i> <i>sdhCD</i>	7.93	3	3.16	3	50.47	3	72.92	3
NCgl1200		2.24	1	n.d.	0	n.d.	0	2.50	1
<u>NCgl1395</u>		3.31	3	2.56	3	3.07	3	3.75	3
NCgl1444		2.23	2	n.d.	0	9.48	3	12.28	3
NCgl1952	<i>xerC</i>	n.d.	0	6.54	3	43.06	3	254.09	3
NCgl2146	<i>hmuO</i>	16.51	3	15.80	3	3.01	3	4.96	3
<u>NCgl2766</u>		2.29	3	n.d.	0	3.33	2	n.d.	0
NCgl2834	<i>hrrA</i>	n.d.	0	3.19	2	2.99	3	6.29	3
NCgl2842	<i>uspA3</i>	n.d.	0	2.02	1	3.64	2	n.d.	0
NCgl2902	<i>qor3</i>	2.53	2	n.d.	0	n.d.	0	3.11	3
NCgl2968		1.89	1	n.d.	0	4.71	3	6.75	3
NCgl2980		n.d.	0	2.00	1	2.25	2	n.d.	0

μ = mean value, n = number of replicates with a peak identified, n.d. = no peak detected, underlined = peak was annotated for HrrA for the gene into the other direction, i.e. binding potentially not at same site.

DISCUSSION

In this study, we performed a genome-wide profiling of the global regulators DtxR and HrrA coordinating iron and heme homeostasis in *C. glutamicum*. The obtained results provide valuable insights into the interaction and interference of iron and heme regulatory networks and demonstrate the robust homeostasis conferred by the underlying strategies. Network analysis under different cultivation conditions, further led to the identification of a substantial number of previously unknown targets for both regulators.

Analysis of known targets in iron and heme regulation

Among the genetic regions for which peaks were identified, it is noteworthy that the siderophore transporter NCgl0484 was the main target of DtxR with the highest peak intensity in both iron excess and heme conditions. DtxR represses this siderophore transporter in the presence of iron (Brune et al., 2006). *C. glutamicum* does not produce siderophores on its own, but makes use of those produced by other bacteria. As enough iron or alternative iron sources are present in both conditions, this transporter is strongly

regulated in both conditions avoiding waste of energy. The same applies for further siderophore transporters, e.g. *irp1* and NCgl0777. Interestingly, NCgl0484 is not the best matching motif to the identified one, comparing the three highest peaks, but rather in the following order: *irp1* > *hmuO* > NCgl0484 (MAST: Motif Alignment & Search Tool (Bailey and Gribskov, 1998)). There are further studies, which also were not able to correlate peak height with the matching to the consensus motif (Myers et al., 2013). However, it should be noted, that binding affinities are further influenced by a wide range of factors in vivo like inter- and intramolecular interactions including electrostatic or hydrophobic ones, DNA topology or importantly also interference with other DNA binding proteins (Dorman, 2019; Ponta et al., 1992; Sims et al., 2005).

Moreover, we recognized that the peak intensity of the ChAP-Seq results does negatively correlate with the differential gene expression data, i.e. the highest peaks shown for NCgl0484 and *irp1* do not correspond to highest differential gene expressions ($\Delta dtxR/WT$) analyzed with transcriptomics, but rather opposite. The same applied for the HrrA peak intensity comparison to RNA-Seq results. This negative correlation demonstrates that targets bound with lower peak intensity react more sensible to changes and it further highlights the physiological relevance of weak binding sites in ChAP-Seq experiments. In addition, previous studies also claimed that peak enrichment does not necessarily always correlate with binding strength (Myers et al., 2013).

Although many known DtxR targets from literature were confirmed within this in vivo approach, in total 33 could not be detected, which were already identified to be bound by DtxR in vitro via bandshift assays (Brune et al., 2006; Wennerhold and Bott, 2006). The absence of these targets might be explained either by false-positives or by differently regulation throughout the time, i.e. these targets are regulated rather earlier or in the

later course of cultivation, and have a dependency on cultivation time, stimulus and/or transcription factor concentrations. Recent ChIP-seq analysis of Fur, which is a functional homolog to DtxR in many Gram-negative bacteria, demonstrated a graded response of this transcriptional regulator in *Bacillus subtilis*, caused by different protein-DNA-binding affinities (Pi and Helmann, 2017), i.e. with decreasing iron concentrations Fur derepressed its targets stepwise in 'three waves' and not all at once. Following studies even determined additional targets (Pi and Helmann, 2018). Such a graded response could also be an issue for the two presented transcriptional regulators. Overall, this highlights the importance of binding analyses at different cultivation conditions to fully characterize the highly dynamic binding behavior of global transcriptional regulators. Another reason could be, that nucleoid-associated proteins or other transcription factors mask DtxR binding (Myers et al., 2013; Pfeifer et al., 2016). However, it can further be imagined that the other sites are too weak in binding due to e.g. hardly accessible binding sites and therefore cannot be detected with this experimental setup. An option to overcome this problem might be to overexpress DtxR in order to increase overall cellular copy number, like it was achieved for example in *Mycobacterium tuberculosis* (Galagan et al., 2013b). However, it should be taken into account that this does not mimic the wild type conditions and non-physiologically relevant targets will be bound additionally.

Also in the case of HrrA in total 80 targets, i.e. more than 30%, which were already identified in a ChAP-Seq experiment were not found. Those differences demonstrate the sensitivity of this experimental setup, e.g. in terms of cross-linking or affinity-purification efficiency (Myers et al., 2015; Myers et al., 2013).

Analysis of new targets in iron and heme regulation

Overall, 24 new potential targets of DtxR could be identified. One explanation why

these targets were not found in the former studies could be due to conditional influences as described above, or their impact was below the applied threshold of the microarray analyses. Smaller fold changes in gene expression, which are not statistically set as threshold in these experiments, could be of biological importance (Galagan et al., 2013a). Another reason could be that these experiments were performed in vitro. Transcription factors not always act isolated, but require the combination of several other factors, e.g. any unusual DNA conformation, cooperation with other proteins, etc. (Higo et al., 2012; Wade et al., 2005). To confirm the newly identified targets of DtxR, further studies are necessary. Band shift assays could reveal the binding, but also reporter assays of the respective target genes in wild type compared to a $\Delta dtxR$ strain would be an option giving further hints on their expression dynamics.

Still, interesting new targets of DtxR were found, for example NCg1781. This gene is present in the prophage region CGP4, which is located inside the inducible CGP3 prophage region of *C. glutamicum* NC_003450.3 (Frunzke et al., 2008; Helfrich et al., 2015; Pfeifer et al., 2016). Previous studies already determined targets of DtxR in CGP3 (Wennerhold and Bott, 2006), while it was also shown that the induction of this prophage is triggered by iron-mediated oxidative stress (Boeselager et al., 2018; Frunzke et al., 2008), which could possibly also play a role for CGP4. However, many of those prophage genes regulated by DtxR encode hypothetical proteins and need further investigations for detailed information.

There are several genes, like the newly identified targets *metH* and *xerC*, that are only found bound by DtxR in the heme condition. The gene *metH* encodes for a homocysteine methyltransferase catalyzing the last step of methionine synthesis from homocysteine and was already known to be regulated by the methionine and cysteine

biosynthesis repressor McbR (Rückert et al., 2003). For DtxR of *C. diphtheriae*, binding to methionine related genes *metA* and *mapA* was also predicted (Yellaboina et al., 2004), while Fur, the master regulator of iron in *E. coli*, was likewise shown to regulate methionine biosynthesis via the gene *metH* (Stojiljkovic et al., 1994). In endothelial cells, it has been demonstrated that methionine promotes the catalytic activity of the heme oxygenase and ferritin with the purpose to suppress free radical formation (Erdmann et al., 2005). As DtxR also represses *hmuO* in the presence of iron, repression of *metH* could add on that. This would include a graded response as this regulation only takes place at the heme condition, but however, this requires further investigations.

Focusing on HrrA, we further found 183 new targets. The majority of new targets have been identified under conditions of iron excess, which have not been addressed in previous studies. Most of these targets correspond to hypothetical proteins as well as translation-related and central carbon metabolism targets. Further confirmation of these targets is inevitably necessary to check the influence of this huge amount of targets. The transcriptional regulator AdpA in *Streptomyces griseus* also influences manifold genetic targets, with ChIP-Seq experiments resulting binding peaks for ~1500 sites. However, only ~25% were shown to have function in the regulation of gene expression (Higo et al., 2012). Comparable results were found for AbrB of *Bacillus subtilis* (Chumsakul et al., 2011) or RutR in *Escherichia coli* (Shimada et al., 2008). This effect could speak for e.g. non-functional DNA sites, and should be analyzed for HrrA.

Apart from the prominent targets, we also found a number of weak binding sites, including several potentially new targets. Extensive weak binding was observed for manifold ChIP-Seq analyses (Cao et al., 2010; Galagan et al., 2013a; MacQuarrie et al., 2011; Rhee and Pugh, 2011). Weak interactions can be hypothesized to be a tool allowing to be evolutionary prepared for

fine-tunings (Rhee and Pugh, 2011). It cannot yet be excluded, that these targets are false-positives, but still binding motifs can be found, like e.g. for NCgl0176. Further, the observed anti-correlation of peak binding intensity and differential gene expression highlights that weaker binding can also have a tremendous influence on gene expression and promotes a sensitive reaction to changing conditions. This demonstrates that future research should also pay attention to those small peaks, with a potential lower protein-DNA-binding affinity.

Regarding shared targets of DtxR and HrrA, there are two different interactions. On the one hand, the regulators act in many cases in opposite directions like in the case of *hmuO*. In general, such antagonism was described for other transcriptional regulators like the DtxR homolog IdeR with Lsr2 in *Mycobacterium tuberculosis* (Kurthkoti et al., 2015). On the other hand, for fewer targets these regulators work rather cooperatively in the same direction, like both activating *sdhCD*. Although there is no real pattern observable for DtxR and HrrA interference, several examples like *hmuO* still tend to a small anti-correlation. Therefore, further investigations on the mechanisms of antagonizing as well as synergizing of DtxR and HrrA should be made to evaluate on the intersection of iron and heme regulatory networks.

Conclusion and future perspectives

Overall, our study provides insights into the genome-wide binding profiles of the two global transcriptional regulators DtxR and HrrA. The obtained results emphasize a strong potential for the identification of new targets by performing the profiling via the application of different environmental conditions (iron or heme as iron source). The data also demonstrate the well-balanced homeostasis governed by DtxR and HrrA. The similar binding pattern observed throughout different conditions likely reflects a similar pool of intracellular Fe²⁺ and heme. The fact that targets with a small peak intensity (ChAP-Seq) frequently featured a high

sensitivity towards regulation by the respective transcription factor (high values for differential gene expression) indicated that also targets with a low coverage must not be ignored. In summary, the reported data add to our understanding of the global regulatory network governing iron homeostasis and emphasize that the relation between binding behavior and functional or structural impact of prokaryotic transcription factors exists along a continuum.

CONFLICT OF INTEREST

The authors declare that the research was conducted in the absence of any commercial or financial relationships that could be construed as a potential conflict of interest.

AUTHOR CONTRIBUTIONS

JF and AK conceived and designed the analysis. AK and UV performed the experiments and collected the data. AF contributed data or analysis tools. AK performed the analysis. JF and AK wrote the paper

FUNDING

This work was supported by the Helmholtz Association (grant number W2/W3-096).

ACKNOWLEDGEMENTS

We thank Max Hünnefeld for the support in data analysis.

REFERENCES

- Aft, R.L., and Mueller, G.C. (1984). Hemin-mediated oxidative degradation of proteins. *Journal of Biological Chemistry*, 259(1): 301-305. doi: 10.1016/S0021-9258(17)43657-X.
- Ajioka, R.S., Phillips, J.D., and Kushner, J.P. (2006). Biosynthesis of heme in mammals. *Biochim Biophys Acta*, 1763(7): 723-736. doi: 10.1016/j.bbamcr.2006.05.005.
- Ando, M., Manabe, Y.C., Converse, P.J., Miyazaki, E., Harrison, R., Murphy, J.R., and Bishai, W.R. (2003). Characterization of the role of the divalent metal ion-dependent transcriptional

- repressor MntR in the virulence of *Staphylococcus aureus*. *Infect Immun*, 71(5): 2584-2590. doi: 10.1128/iai.71.5.2584-2590.2003.
- Andrews, S.C., Robinson, A.K., and Rodríguez-Quiriones, F. (2003). Bacterial iron homeostasis. *FEMS Microbiol Rev*, 27(2-3): 215-237. doi: 10.1016/s0168-6445(03)00055-x.
- Bailey, T.L., and Elkan, C. (1994). Fitting a mixture model by expectation maximization to discover motifs in biopolymers. *Proc Int Conf Intell Syst Mol Biol*, 2: 28-36.
- Bailey, T.L., and Gribskov, M. (1998). Combining evidence using p-values: application to sequence homology searches. *Bioinformatics*, 14(1): 48-54. doi: 10.1093/bioinformatics/14.1.48.
- Bibb, L.A., Kunkle, C.A., and Schmitt, M.P. (2007). The ChrA-ChrS and HrrA-HrrS Signal Transduction Systems Are Required for Activation of the *hmuO* Promoter and Repression of the *hemA* Promoter in *Corynebacterium diphtheriae*. *Infect Immun*, 75(5): 2421-2431. doi: 10.1128/iai.01821-06.
- Boeselager, R., Pfeifer, E., and Frunzke, J. (2018). Cytometry meets next-generation sequencing – RNA-Seq of sorted subpopulations reveals regional replication and iron-triggered prophage induction in *Corynebacterium glutamicum*. *Sci Rep*, 8(1): 14856. doi: 10.1038/s41598-018-32997-9.
- Boyd, J., Oza, M.N., and Murphy, J.R. (1990). Molecular cloning and DNA sequence analysis of a diphtheria tox iron-dependent regulatory element (*dtxR*) from *Corynebacterium diphtheriae*. *Proc Natl Acad Sci*, 87(15): 5968-5972. doi: 10.1073/pnas.87.15.5968.
- Brune, I., Werner, H., Hüser, A.T., Kalinowski, J., Pühler, A., and Tauch, A. (2006). The DtxR protein acting as dual transcriptional regulator directs a global regulatory network involved in iron metabolism of *Corynebacterium glutamicum*. *BMC Genom*, 7(1): 21. doi: 10.1186/1471-2164-7-21.
- Cao, Y., Yao, Z., Sarkar, D., Lawrence, M., Sanchez, G.J., Parker, M.H., MacQuarrie, K.L., Davison, J., Morgan, M.T., Ruzzo, W.L., et al. (2010). Genome-wide MyoD binding in skeletal muscle cells: a potential for broad cellular reprogramming. *Dev Cell*, 18(4): 662-674. doi: 10.1016/j.devcel.2010.02.014.
- Capra, E.J., and Laub, M.T. (2012). Evolution of two-component signal transduction systems. *Annu Rev Microbiol*, 66: 325-347. doi: 10.1146/annurev-micro-092611-150039.
- Chen, X., Zaro, J.L., and Shen, W.C. (2013). Fusion protein linkers: property, design and functionality. *Adv Drug Deliv Rev*, 65(10): 1357-1369. doi: 10.1016/j.addr.2012.09.039.
- Chumsakul, O., Takahashi, H., Oshima, T., Hishimoto, T., Kanaya, S., Ogasawara, N., and Ishikawa, S. (2011). Genome-wide binding profiles of the *Bacillus subtilis* transition state regulator AbrB and its homolog Abh reveals their interactive role in transcriptional regulation. *Nucleic Acids Res*, 39(2): 414-428. doi: 10.1093/nar/gkq780.
- Contreras, H., Chim, N., Credali, A., and Goulding, C.W. (2014). Heme uptake in bacterial pathogens. *Curr Opin Chem Biol*, 19: 34-41. doi: 10.1016/j.cbpa.2013.12.014.
- Cornelis, P., Wei, Q., Andrews, S.C., and Vinckx, T. (2011). Iron homeostasis and management of oxidative stress response in bacteria. *Metallomics*, 3(6): 540-549. doi: 10.1039/c1mt00022e.
- Dorman, C.J. (2019). DNA supercoiling and transcription in bacteria: a two-way street. *BMC Mol Biol*, 20(1): 26. doi: 10.1186/s12860-019-0211-6.
- Drazek, E.S., Hammack, C.A., and Schmitt, M.P. (2000). *Corynebacterium diphtheriae* genes required for acquisition of iron from haemin and haemoglobin are homologous to ABC haemin transporters. *Mol Microbiol*, 36(1): 68-84. doi: 10.1046/j.1365-2958.2000.01818.x.
- Eikmanns, B.J., Thum-Schmitz, N., Eggeling, L., Lüdtke, K.-U., and Sahm, H. (1994). Nucleotide sequence, expression and transcriptional analysis of the *Corynebacterium glutamicum gltA* gene encoding citrate synthase. *Microbiology*, 140(8): 1817-1828. doi: 10.1099/13500872-140-8-1817.
- Erdmann, K., Grosser, N., and Schroder, H. (2005). L-methionine reduces oxidant stress in endothelial cells: Role of heme oxygenase-1, ferritin, and nitric oxide. *The AAPS journal*, 7: E195-200. doi: 10.1208/aapsj070118.
- Escorcía-Rodríguez, J., Tauch, A., and Freyre-González, J. (2020). *Corynebacterium glutamicum* Regulation beyond Transcription: Organizing Principles and Reconstruction of an Extended Regulatory Network Incorporating Regulations Mediated by Small RNA and Protein-Protein Interactions. *Microorganisms*, 9(7): 1395. doi: 10.20944/preprints202012.0503.v1.

- Frunzke, J., Bramkamp, M., Schweitzer, J.E., and Bott, M. (2008). Population Heterogeneity in *Corynebacterium glutamicum* ATCC 13032 caused by prophage CGP3. *J Bacteriol*, 190(14): 5111-5119. doi: 10.1128/jb.00310-08.
- Frunzke, J., Gätgens, C., Brocker, M., and Bott, M. (2011). Control of heme homeostasis in *Corynebacterium glutamicum* by the two-component system HrrSA. *J Bacteriol*, 193(5): 1212-1221. doi: 10.1128/jb.01130-10.
- Galagan, J., Lyubetskaya, A., and Gomes, A. (2013a). ChIP-Seq and the complexity of bacterial transcriptional regulation. *Curr Top Microbiol Immunol*, 363: 43-68. doi: 10.1007/82_2012_257.
- Galagan, J.E., Minch, K., Peterson, M., Lyubetskaya, A., Azizi, E., Sweet, L., Gomes, A., Rustad, T., Dolganov, G., Glotova, I., et al. (2013b). The *Mycobacterium tuberculosis* regulatory network and hypoxia. *Nature*, 499(7457): 178-183. doi: 10.1038/nature12337.
- Gibson, D.G., Young, L., Chuang, R.Y., Venter, J.C., Hutchison, C.A., 3rd, and Smith, H.O. (2009). Enzymatic assembly of DNA molecules up to several hundred kilobases. *Nat Methods*, 6(5): 343-345. doi: 10.1038/nmeth.1318.
- Gold, B., Rodriguez, G.M., Marras, S.A., Pentecost, M., and Smith, I. (2001). The *Mycobacterium tuberculosis* IdeR is a dual functional regulator that controls transcription of genes involved in iron acquisition, iron storage and survival in macrophages. *Mol Microbiol*, 42(3): 851-865. doi: 10.1046/j.1365-2958.2001.02684.x.
- Helfrich, S., Pfeifer, E., Krämer, C., Sachs, C.C., Wiechert, W., Kohlheyer, D., Nöh, K., and Frunzke, J. (2015). Live cell imaging of SOS and prophage dynamics in isogenic bacterial populations. *Mol Microbiol*, 98(4): 636-650. doi: 10.1111/mmi.13147.
- Hentschel, E., Mack, C., Gätgens, C., Bott, M., Brocker, M., and Frunzke, J. (2014). Phosphatase activity of the histidine kinases ensures pathway specificity of the ChrSA and HrrSA two-component systems in *Corynebacterium glutamicum*. *Mol Microbiol*, 92(6): 1326-1342. doi: 10.1111/mmi.12633.
- Heyer, A., Gätgens, C., Hentschel, E., Kalinowski, J., Bott, M., and Frunzke, J. (2012). The two-component system ChrSA is crucial for haem tolerance and interferes with HrrSA in haem-dependent gene regulation in *Corynebacterium glutamicum*. *Microbiology*, 158(Pt 12): 3020-3031. doi: 10.1099/mic.0.062638-0.
- Higo, A., Hara, H., Horinouchi, S., and Ohnishi, Y. (2012). Genome-wide distribution of AdpA, a global regulator for secondary metabolism and morphological differentiation in *Streptomyces*, revealed the extent and complexity of the AdpA regulatory network. *DNA Res*, 19(3): 259-273. doi: 10.1093/dnares/dss010.
- Keppel, M., Davoudi, E., Gätgens, C., and Frunzke, J. (2018). Membrane Topology and Heme Binding of the Histidine Kinases HrrS and ChrS in *Corynebacterium glutamicum*. *Front Microbiol*, 9(183): 183. doi: 10.3389/fmicb.2018.00183.
- Keppel, M., Hünnefeld, M., Filipchyk, A., Viets, U., Davoudi, C.F., Krüger, A., Mack, C., Pfeifer, E., Polen, T., Baumgart, M., et al. (2020). HrrSA orchestrates a systemic response to heme and determines prioritization of terminal cytochrome oxidase expression. *Nucleic Acids Res*, 48(12): 6547-6562. doi: 10.1093/nar/gkaa415.
- Kinoshita, S., Udaka, S., and Shimono, M. (2004). Studies on the amino acid fermentation. Part 1. Production of L-glutamic acid by various microorganisms. *J Gen Appl Microbiol*, 50(6): 331-343.
- Krüger, A., Keppel, M., Sharma, V., and Frunzke, J. (2022). The diversity of heme sensor systems - heme-responsive transcriptional regulation mediated by transient heme protein interactions. *FEMS Microbiol Rev*, 46(3): fuac002. doi: 10.1093/femsre/fuac002.
- Kumar, S., and Bandyopadhyay, U. (2005). Free heme toxicity and its detoxification systems in human. *Toxicol Lett*, 157(3): 175-188. doi: 10.1016/j.toxlet.2005.03.004.
- Kunkle, C.A., and Schmitt, M.P. (2003). Analysis of the *Corynebacterium diphtheriae* DtxR regulon: identification of a putative siderophore synthesis and transport system that is similar to the *Yersinia* high-pathogenicity island-encoded yersiniabactin synthesis and uptake system. *J Bacteriol*, 185(23): 6826-6840. doi: 10.1128/jb.185.23.6826-6840.2003.
- Kunkle, C.A., and Schmitt, M.P. (2005). Analysis of a DtxR-regulated iron transport and siderophore biosynthesis gene cluster in *Corynebacterium diphtheriae*. *J Bacteriol*, 187(2): 422-433. doi: 10.1128/jb.187.2.422-433.2005.
- Kurthkoti, K., Tare, P., Paithchowdhury, R., Gowthami, V.N., Garcia, M.J., Colangeli, R., Chatterji, D., Nagaraja, V., and Rodriguez, G.M.

- (2015). The mycobacterial iron-dependent regulator IdeR induces ferritin (*bfrB*) by alleviating Lsr2 repression. *Mol Microbiol*, 98(5): 864-877. doi: 10.1111/mmi.13166.
- Langmead, B., and Salzberg, S.L. (2012). Fast gapped-read alignment with Bowtie 2. *Nat Methods*, 9(4): 357-359. doi: 10.1038/nmeth.1923.
- Langmead, B., Wilks, C., Antonescu, V., and Charles, R. (2019). Scaling read aligners to hundreds of threads on general-purpose processors. *Bioinformatics*, 35(3): 421-432. doi: 10.1093/bioinformatics/bty648.
- Layer, G. (2021). Heme biosynthesis in prokaryotes. *Biochim Biophys Acta Mol Cell Res*, 1868(1): 118861. doi: 10.1016/j.bbamcr.2020.118861.
- MacPhillamy, C., Alinejad-Rokny, H., Pitchford, W.S., and Low, W.Y. (2022). Cross-species enhancer prediction using machine learning. *Genomics*: 110454. doi: 10.1016/j.ygeno.2022.110454.
- MacQuarrie, K.L., Fong, A.P., Morse, R.H., and Tapscott, S.J. (2011). Genome-wide transcription factor binding: beyond direct target regulation. *Trends Genet*, 27(4): 141-148. doi: 10.1016/j.tig.2011.01.001.
- Mascher, T., Helmann, J.D., and Unden, G. (2006). Stimulus Perception in Bacterial Signal-Transducing Histidine Kinases. *Microbiology and molecular biology reviews* : MMBR, 70(4): 910-938. doi: 10.1128/mmb.00020-06.
- Myers, K.S., Park, D.M., Beauchene, N.A., and Kiley, P.J. (2015). Defining bacterial regulons using ChIP-seq. *Methods*, 86: 80-88. doi: 10.1016/j.ymeth.2015.05.022.
- Myers, K.S., Yan, H., Ong, I.M., Chung, D., Liang, K., Tran, F., Keleş, S., Landick, R., and Kiley, P.J. (2013). Genome-scale analysis of *Escherichia coli* FNR reveals complex features of transcription factor binding. *PLoS Genet*, 9(6): e1003565. doi: 10.1371/journal.pgen.1003565.
- Niebisch, A., and Bott, M. (2001). Molecular analysis of the cytochrome bc1-aa3 branch of the *Corynebacterium glutamicum* respiratory chain containing an unusual diheme cytochrome c1. *Arch Microbiol*, 175(4): 282-294. doi: 10.1007/s002030100262.
- Pappenheimer, A.M.J., and Johnson, S.J. (1936). Studies in Diphtheria Toxin Production. I: The Effect of Iron and Copper. *Br J Exp Pathol*, 17(5): 335-341.
- Park, S.T., Peterson, M., Schoolnik, G., Jaini, S., Raman, S., Gomes, A., Galagan, J., and Lyubetskaya, A. (2014). Transcription Factor Binding Site Mapping Using ChIP-Seq. *Microbiol Spectr*, 2. doi: 10.1128/microbiolspec.MGM2-0035-2013.
- Pfeifer, E., Hünnefeld, M., Popa, O., Polen, T., Kohlheyer, D., Baumgart, M., and Frunzke, J. (2016). Silencing of cryptic prophages in *Corynebacterium glutamicum*. *Nucleic Acids Res*, 44(21): 10117-10131. doi: 10.1093/nar/gkw692.
- Pi, H., and Helmann, J.D. (2017). Sequential induction of Fur-regulated genes in response to iron limitation in *Bacillus subtilis*. *Proc Natl Acad Sci USA*, 114(48): 12785-12790. doi: 10.1073/pnas.1713008114.
- Pi, H., and Helmann, J.D. (2018). Genome-Wide Characterization of the Fur Regulatory Network Reveals a Link between Catechol Degradation and Bacillibactin Metabolism in *Bacillus subtilis*. *mBio*, 9(5): e01451-01418. doi: 10.1128/mBio.01451-18.
- Ponka, P. (1999). Cell biology of heme. *Am J Med Sci*, 318(4): 241-256. doi: 10.1097/00000441-199910000-00004.
- Ponta, H., Cato, A.C., and Herrlich, P. (1992). Interference of pathway specific transcription factors. *Biochim Biophys Acta*, 1129(3): 255-261. doi: 10.1016/0167-4781(92)90501-p.
- Qin, S., Yuan, Y., Huang, X., Tan, Z., Hu, X., Liu, H., Pu, Y., Ding, Y.Q., Su, Z., and He, C. (2022). Topoisomerase IIA in adult NSCs regulates SVZ neurogenesis by transcriptional activation of Usp37. *Nucleic Acids Res*, 50(16). doi: 10.1093/nar/gkac731.
- Rhee, H.S., and Pugh, B.F. (2011). Comprehensive genome-wide protein-DNA interactions detected at single-nucleotide resolution. *Cell*, 147(6): 1408-1419. doi: 10.1016/j.cell.2011.11.013.
- Rückert, C., Pühler, A., and Kalinowski, J. (2003). Genome-wide analysis of the l-methionine biosynthetic pathway in *Corynebacterium glutamicum* by targeted gene deletion and homologous complementation. *J Biotechnol*, 104(1): 213-228. doi: 10.1016/s0168-1656(03)00158-5.
- Rustad, T.R., Minch, K.J., Ma, S., Winkler, J.K., Hobbs, S., Hickey, M., Brabant, W., Turkarslan, S., Price, N.D., Baliga, N.S., et al. (2014). Mapping

- and manipulating the *Mycobacterium tuberculosis* transcriptome using a transcription factor overexpression-derived regulatory network. *Genome Biol*, 15(11): 502. doi: 10.1186/s13059-014-0502-3.
- Sambrook, J.F., and Russell, D. (2001). *Molecular Cloning: A Laboratory Manual (3-Volume Set)*, Vol 1 (New York: Cold Spring Harbor Laboratory Press).
- Schäfer, A., Tauch, A., Jäger, W., Kalinowski, J., Thierbach, G., and Pühler, A. (1994). Small mobilizable multi-purpose cloning vectors derived from the *Escherichia coli* plasmids pK18 and pK19: selection of defined deletions in the chromosome of *Corynebacterium glutamicum*. *Gene*, 145(1): 69-73. doi: 10.1016/0378-1119(94)90324-7.
- Schmitt, M.P. (1999). Identification of a two-component signal transduction system from *Corynebacterium diphtheriae* that activates gene expression in response to the presence of heme and hemoglobin. *J Bacteriol*, 181(17): 5330-5340. doi: 10.1128/jb.181.17.5330-5340.1999.
- Shimada, T., Ishihama, A., Busby, S.J., and Grainger, D.C. (2008). The *Escherichia coli* RutR transcription factor binds at targets within genes as well as intergenic regions. *Nucleic Acids Res*, 36(12): 3950-3955. doi: 10.1093/nar/gkn339.
- Sims, P.A., Wong, C.F., Vuga, D., McCammon, J.A., and Sefton, B.M. (2005). Relative contributions of desolvation, inter- and intramolecular interactions to binding affinity in protein kinase systems. *J Comput Chem*, 26(7): 668-681. doi: 10.1002/jcc.20207.
- Stauff, D.L., and Skaar, E.P. (2009). The heme sensor system of *Staphylococcus aureus*. *Contrib Microbiol*, 16: 120-135. doi: 10.1159/000219376.
- Stock, A.M., Robinson, V.L., and Goudreau, P.N. (2000). Two-Component Signal Transduction. *Annu Rev Biochem*, 69(1): 183-215. doi: 10.1146/annurev.biochem.69.1.183.
- Stojiljkovic, I., Bäumlner, A.J., and Hantke, K. (1994). Fur Regulon in Gram-negative Bacteria: Identification and Characterization of New Iron-regulated *Escherichia coli* Genes by a Fur Titration Assay. *Journal of molecular biology*, 236(2): 531-545. doi: 10.1006/jmbi.1994.1163.
- Stojiljkovic, I., Kumar, V., and Srinivasan, N. (1999). Non-iron metalloporphyrins: potent antibacterial compounds that exploit haem/Hb uptake systems of pathogenic bacteria. *Mol Microbiol*, 31(2): 429-442. doi: 10.1046/j.1365-2958.1999.01175.x.
- Thiel, J., Byrne James, M., Kappler, A., Schink, B., and Pester, M. (2019). Pyrite formation from FeS and H₂S is mediated through microbial redox activity. *Proc Natl Acad Sci USA*, 116(14): 6897-6902. doi: 10.1073/pnas.1814412116.
- van der Rest, M.E., Lange, C., and Molenaar, D. (1999). A heat shock following electroporation induces highly efficient transformation of *Corynebacterium glutamicum* with xenogeneic plasmid DNA. *Appl Microbiol Biotechnol*, 52(4): 541-545. doi: 10.1007/s002530051557.
- Wade, J.T., Reppas, N.B., Church, G.M., and Struhl, K. (2005). Genomic analysis of LexA binding reveals the permissive nature of the *Escherichia coli* genome and identifies unconventional target sites. *Genes Dev*, 19(21): 2619-2630. doi: 10.1101/gad.1355605.
- Wennerhold, J., and Bott, M. (2006). The DtxR regulon of *Corynebacterium glutamicum*. *J Bacteriol*, 188(8): 2907-2918. doi: 10.1128/jb.188.8.2907-2918.2006.
- Wennerhold, J., Krug, A., and Bott, M. (2005). The AraC-type Regulator RipA Represses Aconitase and Other Iron Proteins from *Corynebacterium* under Iron Limitation and Is Itself Repressed by DtxR. *The Journal of biological chemistry*, 280(49): 40500-40508. doi: 10.1074/jbc.M508693200.
- White, A., Ding, X., vanderSpek, J.C., Murphy, J.R., and Ringe, D. (1998). Structure of the metal-ion-activated diphtheria toxin repressor/tox operator complex. *Nature*, 394(6692): 502-506. doi: 10.1038/28893.
- Wilks, A. (2002). Heme Oxygenase: Evolution, Structure, and Mechanism. *Antioxid Redox Sign*, 4(4): 603-614. doi: 10.1089/15230860260220102.
- Wilks, A., and Schmitt, M.P. (1998). Expression and Characterization of a Heme Oxygenase (HmuO) from *Corynebacterium diphtheriae*: Iron Acquisition Requires Oxidative Cleavage of the Heme Macrocycle. *J Biol Chem*, 273(2): 837-841. doi: 10.1074/jbc.273.2.837.
- Yellaboina, S., Ranjan, S., Chakhaiyar, P., Hasnain, S.E., and Ranjan, A. (2004). Prediction of DtxR regulon: identification of binding sites and operons controlled by Diphtheria toxin repressor in *Corynebacterium diphtheriae*. *BMC Microbiol*, 4: 38. doi: 10.1186/1471-2180-4-38.

3.3 HrrSA orchestrates a systemic response to heme and determines prioritization of terminal cytochrome oxidase expression

Marc Keppel*, Max Hünnefeld*, Andrei Filipchuk*, Ulrike Viets, Cedric-Farhad Davoudi, **Aileen Krüger**, Christina Mack, Eugen Pfeifer, Tino Polen, Meike Baumgart, Michael Bott, Julia Frunzke

**These authors contributed equally to this work.*

Published in *Nucleic Acids Research*, 2020.

Contributor Role	Contributor
Conceptualization	70% MK, 30% JF
Formal Analysis	30 % MH, 30% AF, 25% MK, 5% CFD, 5% TP, 3% AK, 2% EP
Investigation/Experiments	45% UV, 25% MK, 10% CM, 10% AK, 5% CFD, 5% EP
Methodology	45% MK, 20% AF, 20% MH, 10% CFD, 5% EP
Project Administration	50% MK, 50% JF
Software	50% AF, 40%, MH, 5% EP, 5% TP
Supervision	10% MBA, 20% MBO, 70% JF
Visualization	65% MK, 20% MH, 5% CFD, 5% AF, 5% AK
Writing – Original Draft Preparation	80% MK, 20% JF
Writing – Review & Editing	30% JF, 25% MH, 10% MK, 7% TP, 7% MBA, 7% MBO, 5% AK, 5% AF, 4% UV

Overall contribution AK: 5%

AK performed the TMPD oxidase assay (Figure 3D) and the oxidative stress growth experiments (Figure S8) as well as data analysis and visualization thereof. UV conducted the ChAP-Seq experiments with the support of AK. AK had a minor role on the revision process.

Published online 26 May 2020

Nucleic Acids Research, 2020, Vol. 48, No. 12 6547–6562
doi: 10.1093/nar/gkaa415

HrrSA orchestrates a systemic response to heme and determines prioritization of terminal cytochrome oxidase expression

Marc Keppel^{1,†}, Max Hünnefeld^{1,†}, Andrei Filipchik^{1,†}, Ulrike Viets¹, Cedric-Farhad Davoudi¹, Aileen Krüger¹, Christina Mack¹, Eugen Pfeifer², Tino Polen¹, Meike Baumgart¹, Michael Bott¹ and Julia Frunzke^{1,*}

¹Institute of Bio- und Geosciences, IBG-1: Biotechnology, Forschungszentrum Jülich, 52425 Jülich, Germany and²Microbial Evolutionary Genomics, Institute Pasteur, 75015 Paris, France

Received December 04, 2019; Revised April 26, 2020; Editorial Decision April 29, 2020; Accepted May 05, 2020

ABSTRACT

Heme is a multifaceted molecule. While serving as a prosthetic group for many important proteins, elevated levels are toxic to cells. The complexity of this stimulus has shaped bacterial network evolution. However, only a small number of targets controlled by heme-responsive regulators have been described to date. Here, we performed chromatin affinity purification and sequencing to provide genome-wide insights into *in vivo* promoter occupancy of HrrA, the response regulator of the heme-regulated two-component system HrrSA of *Corynebacterium glutamicum*. Time-resolved profiling revealed dynamic binding of HrrA to more than 200 different genomic targets encoding proteins associated with heme biosynthesis, the respiratory chain, oxidative stress response and cell envelope remodeling. By repression of the extracytoplasmic function sigma factor *sigC*, which activates the *cydABCD* operon, HrrA prioritizes the expression of genes encoding the cytochrome *bc₁-aa₃* supercomplex. This is also reflected by a significantly decreased activity of the cytochrome *aa₃* oxidase in the Δ *hrrA* mutant. Furthermore, our data reveal that HrrA also integrates the response to heme-induced oxidative stress by activating *katA* encoding the catalase. These data provide detailed insights in the systemic strategy that bacteria have evolved to respond to the versatile signaling molecule heme.

INTRODUCTION

Heme (iron bound protoporphyrin IX) is a versatile molecule that is synthesized and used by virtually all aerobic eukaryotic and prokaryotic cells (1). It serves as the prosthetic group of hemoglobins, hydroxylases, catalases, peroxidases and cytochromes (2) and is therefore essential for many cellular processes, such as electron transfer, respiration and oxygen metabolism (3). Furthermore, salvaged heme represents the most important iron source for a variety of pathogenic bacteria (4,5), and also non-pathogenic bacteria can meet their iron demand by degradation of environmental heme. This becomes evident from the diverse set of heme uptake systems and heme oxygenases that catalyze the degradation of the protoporphyrin ring to biliverdin and the concomitant release of carbon monoxide and iron (6).

While heme represents an essential cofactor for a variety of proteins, this molecule also exhibits severe toxicity at high concentrations. Therefore, organisms have evolved sophisticated regulatory networks to tightly control heme uptake, detoxification (including export), synthesis and degradation (4). Several heme-regulated transcription factors have been described, including the heme activator protein (Hap) 1, which is an activator of genes required for aerobic growth of the yeast *Saccharomyces cerevisiae* (7); the transcription factor BACH1 (BTB and CNC homology 1), conserved in mammalian cells (8,9); and the rhizobial Irr protein, which is a heme-regulated member of the Fur family of transcriptional regulators (10–12).

In Gram-positive bacteria, two-component systems (TCSs) appear to play a prevalent role in heme-responsive signaling (13,14), as exemplified by the heme sensor system HssRS of *Staphylococcus aureus* and *Bacillus anthracis*, which controls the expression of the *hrtBA* operon, encoding a heme efflux system in both species (15,16). Remarkably, several members of the *Corynebacteriaceae* family, including the human pathogen *Corynebacterium diph-*

*To whom correspondence should be addressed. Tel: +49 2461 615430; Fax: +49 2461 612710; Email: j.frunzke@fz-juelich.de

†The authors wish it to be known that, in their opinion, the first three authors should be regarded as Joint First Authors.

6548 *Nucleic Acids Research*, 2020, Vol. 48, No. 12

theriae and the biotechnological platform strain *Corynebacterium glutamicum*, have two paralogous TCSs, namely, HrrSA and ChrSA, dedicated to heme-responsive control of gene expression (17–20). The kinases HrrS and ChrS were recently shown to perceive transient changes in heme availability by direct intramembrane interactions with heme (21,22). Heme binding triggers autophosphorylation of the sensor kinase, followed by transfer of the phosphoryl group to the cognate response regulators HrrA and ChrA. In *C. glutamicum*, significant cross-phosphorylation was observed between the closely related systems; however, this crosstalk is proofread by a highly specific phosphatase activity of the kinases toward the cognate response regulators under non-inducing conditions (23). While the ChrSA system appears to be mainly involved in rapid activation of the HrtBA detoxification system (19), previous data suggest that HrrSA coordinates a homeostatic response to heme (18). In recent studies, six direct target operons have been described for HrrA, including genes encoding enzymes involved in heme synthesis (*hemE*, *hemA* and *hemH*), heme utilization (*hmuO*, encoding a heme oxygenase) and the *ctaE-qcrCAB* operon, encoding components of the heme-containing cytochrome *bc₁-aa₃* supercomplex of the respiratory chain (18). Expression of *hrrA* as well as *hmuO* is, furthermore, repressed by the global iron-dependent regulator DtxR in *C. glutamicum* under conditions of sufficient iron supply (24,25) thereby linking iron and heme regulatory networks in this organism.

The branched electron transport chain of *C. glutamicum* consists of the cytochrome *bc₁-aa₃* supercomplex (encoded by *ctaD*, the *ctaCF* operon, and the *ctaE-qcrCAB* operon) and the cytochrome *bd* oxidase, encoded by the first two genes of the *cydABDC* operon (26). Although both the cytochrome *aa₃* oxidase and the *bd* oxidase are involved in the establishment of a proton-motive force, the *aa₃* oxidase is an active proton pump that is responsible for the increased proton translocation number ($6 \text{ H}^+ / 2 \text{ e}^-$) of the cytochrome *bc₁-aa₃* supercomplex compared to that of the *bd* oxidase ($2 \text{ H}^+ / 2 \text{ e}^-$) (26). The presence of the cytochrome *bc₁-aa₃* supercomplex is a characteristic feature of almost all actinobacteria, because members of this phylum lack a soluble cytochrome *c* and instead harbor a diheme cytochrome *c₁* that directly shuttles electrons from the *bc₁* complex to the *aa₃* oxidase (27–32). Furthermore, both terminal oxidases differ in heme content, as the *bc₁-aa₃* supercomplex harbors six heme molecules, while the *bd* oxidase harbors only three. Surprisingly, not much is known about the regulation of terminal oxidases in *C. glutamicum*. In addition to the described activation of the *ctaE-qcr* operon by HrrA, the hydrogen peroxide-sensitive regulator OxyR was described as a repressor of the *cydABDC* operon (33,34). Furthermore, the ECF sigma factor SigC (σ^C) activates expression of the *cydABDC* operon (33,35). For σ^C , a speculated stimulus is a defective electron transfer in the *aa₃* oxidase (35) and such a defect was observed under copper-deprivation or when heme *a* insertion was disturbed, which resulted in activation of the σ^C regulon (36,37).

Interestingly, the regulons of prokaryotic heme regulators described thus far comprise only a low number of direct target genes, which are mostly involved in heme export (e.g. *hrtBA*) or degradation (*hmuO*). This current picture of

prokaryotic heme signaling, however, does not match the complexity of the cellular processes influenced by heme. In this study, we performed a time-resolved and genome-wide binding profiling of HrrA in *C. glutamicum* using chromatin affinity purification and sequencing (ChAP-Seq) of HrrA in *C. glutamicum* showing the transient HrrA promoter occupancy of more than 200 genomic targets in response to heme. The obtained results emphasize that HrrSA is a global regulator of heme homeostasis, which also integrates the response to oxidative stress and cell envelope remodeling. Transcriptome analysis (RNA-Seq) at different time points after heme induction revealed HrrA to be an important regulator of the respiratory chain by coordinating the expression of components of both quinol oxidation branches as well as menaquinol reduction. Remarkably, HrrA was found to prioritize the expression of operons encoding the cytochrome *bc₁-aa₃* supercomplex by repressing *sigC* expression.

MATERIALS AND METHODS

Bacterial strains and growth conditions

Bacterial strains used in this study are listed in Supplementary Table S1. The *C. glutamicum* strain ATCC 13032 was used as wild-type (29) and cultivations were performed in liquid BHI (brain heart infusion, Difco BHI, BD, Heidelberg, Germany), as complex medium or CGXII (38) containing 2% (w/v) glucose as minimal medium. The cells were cultivated at 30°C; if appropriate, 25 µg/ml kanamycin was added. *Escherichia coli* (DH5α and BL21 (DE3)) was cultivated in Lysogeny Broth (Difco LB, BD, Heidelberg, Germany) medium at 37°C in a rotary shaker and for selection, 50 µg/ml kanamycin was added to the medium.

Recombinant DNA work and cloning techniques

Cloning and other molecular methods were performed according to standard protocols (39). As template, chromosomal DNA of *C. glutamicum* ATCC 13032 was used for polymerase chain reaction (PCR) amplification of DNA fragments and was prepared as described previously (40). All sequencing and synthesis of oligonucleotides was performed by Eurofins Genomics (Ebersberg, Germany). For ChAP sequencing, the native *hrrA* was replaced with a twin-strep-tagged version of this gene using a two-step homologous recombination system. This system is based on the suicide vector pK19 *mob-sacB* (41,42), containing 500 bps flanking each site of the targeted sequence inside the *C. glutamicum* genome. The pK19 *mob-sacB hrrA-C-twinstrep* plasmid was constructed using Gibson assembly of PCR products (primers indicated in Supplementary Table S2) and the cut pK19 vector (43).

ChAP-Seq — sample preparation

The preparation of DNA for ChAP sequencing was adapted from (44). The *C. glutamicum* strain ATCC 13032: *hrrA-C-twinstrep* was used for the time series experiment. A preculture was inoculated in liquid BHI medium from a fresh BHI agar plate and incubated for 8–10 h at 30°C in a rotary shaker. Subsequently, cells were transferred into a second

preculture in CGXII medium containing 2% (w/v) glucose and 0 μ M FeSO₄ to starve the cells from iron. Protocatechuic acid (PCA), which was added to the medium, allowed the uptake of trace amounts of iron. From an overnight culture, six main cultures were inoculated to an OD₆₀₀ of 3.0 in 1 l CGXII medium containing 4 μ M hemin as sole iron source. For the time point $t = 0$, the cells were added to 1 l fresh CGXII containing no additional iron source. After 0, 0.5, 2, 4, 9 and 24 h, cells corresponding to an OD₆₀₀ of 3.0 in 1 l were harvested by centrifugation at 4°C, 5000 \times g and washed once in 20 ml CGXII. Subsequently, the cell pellet was resuspended in 20 ml CGXII containing 1% (v/v) formaldehyde to crosslink the regulator protein to the DNA. After incubation for 20 min at RT, the cross linking was stopped by addition of glycine (125 mM), followed by additional incubation of 5 min at RT. After that, the cells were washed three times in buffer A (100 mM Tris-HCl, 1 mM ethylenediaminetetraacetic acid (EDTA), pH = 8.0) and the pellets stored overnight at -80°C. For cell disruption, the pellet was resuspended in buffer A containing 'cOmplete' protease inhibitor cocktail (Roche, Germany) and disrupted using a French press cell (SLM Aisco, Spectronic Instruments, Rochester, NY, USA) five times at 207 MPa. The DNA was fragmented to ~500 bp by sonication (Branson Sonifier 250, Branson Ultrasonics Corporation, CT, USA) and the supernatant was collected after ultra-centrifugation (150 000 \times g, 4°C, 1 h). The DNA bound by the twin-Strep-tagged HrrA protein was purified using Strep-Tactin XT Superflow column material (IBA Lifesciences, Göttingen, Germany) according to the supplier's manual (applying the gravity flow protocol, 1.5 ml column volume). Washing of the column was performed with buffer W (100 mM Tris-HCl, 1 mM EDTA, 150 mM NaCl, pH 8.0) and the tagged protein was eluted with buffer E (100 mM Tris-HCl, 1 mM EDTA, 150 mM NaCl, pH 8.0, added 50 mM D-Biotin). After purification, 1% (w/v) sodium dodecyl sulphate was added to the elution fractions and the samples were incubated overnight at 65°C. For the digestion of protein, 400 μ g/ml Proteinase K (AppliChem GmbH, Darmstadt, Germany) was added and incubated for 3 h at 55°C. Subsequently, the DNA was purified as following: Roti-Phenol/Chloroform/Isoamyl alcohol (Carl Roth GmbH, Karlsruhe, Germany) was added to the samples in a 1:1 ratio and the organic phase was separated using Phase Lock Gel (PLG) tubes (VWR International GmbH, Darmstadt, Germany) according to the supplier's manual. Afterwards, the DNA was precipitated by adding ice-cold ethanol (to a conc. of 70% (v/v) and centrifugation at 16 000 \times g, 4°C for 10 min. The DNA was washed with ice-cold 70% (v/v) ethanol, then dried for 3 h at 50°C and eluted in dH₂O.

ChAP-Seq — sequencing and peak discovery

The obtained DNA fragments of each sample (up to 2 μ g) were used for library preparation and indexing using the TruSeq DNA PCR-free sample preparation kit according to the manufacturer's instruction, yet skipping fragmentation of the DNA and omitting the DNA size selection steps (Illumina, Chesterford, UK). The resulting libraries were quantified using the KAPA library quant kit (Peqlab,

Bonn, Germany) and normalized for pooling. Sequencing of pooled libraries was performed on a MiSeq (Illumina) using paired-end sequencing with a read-length of 2×150 bases. Data analysis and base calling were accomplished with the Illumina instrument software and stored as fastq output files. The sequencing data obtained for each sample were imported into CLC Genomics Workbench (Version 9, Qiagen Aarhus A/S, Aarhus, Denmark) for trimming and base quality filtering. The output was mapped to accession NC.003450.3 as *C. glutamicum* reference genome (29). Genomic coverage was convoluted with second order Gaussian kernel. The kernel was truncated at 4 sigmas (that is all kernel values positioned further then 4 sigmas from the center were set to zero) and expanded to the 'expected peak width'. The expected peak width was estimated via the following procedure: (i) all the peaks higher than 3-fold mean coverage were detected. (ii) Points at which their coverage dropped below $\frac{1}{2}$ of the maximal peak height were found and the distance between them was considered as a peak width. (iii) The 'estimated peak width' was set equal to the median peak width. The convolution profile was scanned in order to find points where first derivative changes its sign from positive to negative (Supplementary Figure S1). Each such point was considered as a potential peak and was assigned with a convolution score (that is convolution with second order Gaussian kernel centred at the peak position). Furthermore, we explored the distribution of the convolution scores. It appeared to resemble normal distribution, but with a heavy right tail. We assumed that this distribution is indeed bimodal of normal distribution (relatively low scores) representing 'noise' and a distribution of 'signal' (relatively high scores). We fit the Gaussian curve to the whole distribution (via `optimize.fit` function from SciPy package; <http://www.scipy.org/>) and set a score thresholds equal mean + 4 sigmas of the fitted distribution. Further filtering with this threshold provided estimated FDR (false discovery rate) of 0.004–0.013 depending on a sample. Filtered peaks were normalized to allow inter-sample comparisons. Sum of coverages of the detected peaks was negated from the total genomic coverage. The resulting difference was used as normalization coefficient; that is peak intensities were divided by this coefficient.

ChAP-Seq — estimation of confidence intervals

To compare peak intensities between the samples, we assessed the significance levels of the detected intensity values by an extensive *in silico* simulation of ChAP-seq experiments along with further peak-detection analyses.

The simulation consisted of the following steps: The reads were artificially generated from *C. glutamicum* genome (NC.003450.3) with the error rate (number of nucleotide mismatches) equal to the average error rate of the real HrrA ChAP-seq reads (estimated from the mapping statistics). The reads were taken from randomly selected spots in the genome (simulation of the non-peak coverage) and from the regions of the detected HrrA binding peaks with the probabilities proportional to the original peak intensities. Thus, we tried to emulate the original binding architecture. We also added a small amount (10% of the total simulated reads) of the sequences heavily affected by mismatches (25%

6550 *Nucleic Acids Research*, 2020, Vol. 48, No. 12

mismatches for the original *C. glutamicum* sequences), as we wanted to account for around 10% of the unmapped reads in the original HrrA ChAP-seq experiments. Finally, the simulated reads were subjected to the computational peak-detection pipeline with the same parameters as in the original analyses. As a result, we obtained the peak intensity values for the detected peaks.

In total, we simulated 200 ChAP-seq samples, each containing 1.14M reads (the average amount of reads in the original samples). For each of the detected peaks we estimated the variation of the reported peak intensity among all the simulations. That is, for each peak intensity we estimated 0.95 confidence interval, as a difference between 97.5 and 2.5 percentiles. We discovered a strong positive correlation (0.94 Pearson) between the width of the confidence intervals and mean intensity (Supplementary Figure S2A). Therefore, we then normalized the width of the confidence intervals to the mean intensity values. The normalized confidence interval width (NCIW) appears to be a convenient metric as it is similar for all peaks, weakly dependent on their intensity. However, for the strongest peaks (peak intensity > 10) the NCIW is limited by 0.2, while for the weaker ones by 0.28 (Supplementary Figure S2B). Then we convert NCIW upper limits to the minimum confident fold changes by the following rule: $\text{min_fold} = (1 + \text{NCIW}/2)/(1 - \text{NCIW}/2)$. Thus, we conclude that for the stronger peaks minimum confident fold change (P -value < 0.05) is ~ 1.23 , while for the weaker peaks it is ~ 1.33 .

RNA-Seq — sample preparation

For RNA sequencing, *C. glutamicum* wild-type and the ΔhrrA mutant strain were cultivated under the same conditions as described for ChAP Sequencing. Both strains did not contain any plasmids and, hence, were cultivated without addition of antibiotics in biological duplicates. After 0 (no heme), 0.5 and 4 h, cells corresponding to an OD_{600} of 3 in 0.1 l were harvested in falcon tubes filled with ice by centrifugation at 4°C and $5000 \times g$ for 10 min and the pellets were stored at -80°C . For the preparation of the RNA, the pellets were resuspended in 800 μl RTL buffer (QIAGEN GmbH, Hilden, Germany) and the cells disrupted by $3 \times 30 \text{ s}$ silica bead beating, 6000 rt/min (Precellys 24, VWR International GmbH, Darmstadt, Germany). After ultracentrifugation ($150\,000 \times g$, 4°C, 1 h), the RNA was purified using the RNeasy Mini Kit (QIAGEN GmbH, Hilden, Germany) according to the supplier's manual. Subsequently, the ribosomal RNA was removed by running twice the workflow of the Ribo-Zero rRNA Removal Kit [Bacterial] (Illumina, CA, USA) in succession. Between steps, the depletion of rRNA as well as the mRNA quality was analysed using the TapeStation 4200 (Agilent Technologies Inc, Santa Clara, USA). After removal of rRNA, the fragmentation of RNA, cDNA strand synthesis and indexing was carried out using the TruSeq Stranded mRNA Library Prep Kit (Illumina, CA, USA) according to the supplier's manual. Afterward, the cDNA was purified using Agencourt AM-Pure XP magnetic beads (Beckman Coulter, IN, USA). The resulting libraries were quantified using the KAPA library quant kit (Peqlab, Bonn, Germany) and normalized for pooling. Pooled libraries were sequenced on a MiSeq (Illu-

mina, CA, USA) generating paired-end reads with a length of 2×75 bases. Data analysis and base calling were performed with the Illumina instrument software and stored as fastq output files.

RNA-Seq — analysis

Sequencing reads quality was explored with the FastQC (<https://www.bioinformatics.babraham.ac.uk/projects/fastqc/>) tool. Since reads appeared to be of a good quality and did not harbor significant fraction of adapters or over-represented sequences, no pre-processing was undertaken. Identical reads were collapsed with a custom script in order to prevent gene levels' misquantification caused by PCR overamplification. Reads were mapped to the *C. glutamicum* genome (NC_003450.3) with Bowtie2 (45). Bowtie2 was run with the following parameters: bowtie2 -1 [path to the reads, 1st mate] -2 [path to the reads, 2nd mate] -S [path to the mappings] -phred33 -sensitive-local -local -score-min C,90 -rdg 9,5 -rfg 9,5 -a --no-unal -l 40 -X 400 --no-mixed --ignorequals.

The reads mapped to multiple locations were split proportionally between parental genes. That is, if 3 reads are mapped to gene A and gene B, expression of gene A is 10 and expression of gene B is 5, then 2 reads will go to gene A and 1 read to gene B. For each *C. glutamicum* gene (46) we assigned an expression value equal to the average read coverage over the gene region. These expression values were then normalized to TPM (transcripts per million) values (47).

Furthermore, we analyzed which genes are significantly differentially expressed between conditions. We set combinatorial thresholds on normalized GEC (gene expression change) $[\text{expr1} - \text{expr2}] / (\text{expr1} + \text{expr2})$ and MGE (mean gene expression) $[\log_2((\text{expr1} + \text{expr2})/2)]$ where 'expr1' is gene expression for the first condition and 'expr2' for the second. Thresholds were set in a way to achieve maximal sensitivity while keeping FDR < 0.05. FDR was estimated as $\text{GECintra} / (\text{GECintra} + \text{GECinter})$; where GECintra is a number of genes passed the thresholds based on intrasample GEC (that is, gene expression change between the replicates for the same condition), GECinter is a number of genes passed the thresholds based on intersample GEC (that is, gene expression change between two different conditions). Threshold function for GEC was defined as: $1 \mid \text{MGE} < C; 2^{**}(-A * \text{MGE}) + B \mid \text{MGE} \geq C$; where A, B, C are parameters to be adjusted. Parameters A, B, C were adjusted with genetic algorithm optimization approach to achieve maximal sensitivity in discovery of differentially expressed genes while keeping FDR below 0.05.

Measurement of cell-associated hemin

C. glutamicum was cultivated in 4 μM hemin as described above (see ChAP-Seq). To measure the cell-associated heme pool, CGXII minimal medium supplemented with 2% (w/v) glucose and 4 μM heme was inoculated to an OD_{600} of 3.5. Samples were taken 0.5, 2, 4, 9 and 24 h after addition of heme. Cells were harvested, resuspended in 100 mM Tris-HCl (pH 8) and adjusted to an OD_{600} of 100. Cells cultivated in 4 μM FeSO_4 supplemented medium were taken

as a control and harvested at the same time points. Absolute spectra of cells reduced with a spatula tip of sodium dithionite were measured at room temperature using the Jasco V560 with a silicon photodiode detector in combination with 5 mm light path cuvettes. Absorption values at 406 nm were normalized by subtracting the measured absorption values of Fe-cultivated cells.

Electrophoretic mobility shift assays (EMSA)

The promoter regions of HrrA target genes (100 bp) were chosen based on the ChAP-Seq analyses and covered the maximal HrrA peak area (for primers see Supplementary Table S2). For quantitative measurements, Cy3-labeled oligonucleotides were used for the generation of the DNA fragments. Before addition of the DNA, HrrA was phosphorylated by incubation for 60 min with MBP-HrrS Δ 1-248 in a ratio of 2:1 and 5 mM adenosine triphosphate. Binding assays were performed in a total volume of 20 μ l using 15 nM DNA and increasing HrrA concentrations (75 and 375 nM) for the qualitative analyses and 10 nM DNA with increasing HrrA concentrations from 5–1000 nM for quantitative analyses, respectively. The binding buffer contained 20 mM Tris-HCl (pH 7.5), 50 mM KCl, 10 mM MgCl₂, 5% (v/v) glycerol, 0.5 mM EDTA and 0.005% (w/v) Triton X-100. After incubation for 20 min at room temperature, the reaction mixtures were loaded onto a 10% native polyacrylamide gel and subsequently separated and documented using a Typhoon TrioTM scanner (GE healthcare). The band intensities of unbound DNA were quantified using Image Studio Lite (Licor, Bad Homburg, Germany). The band intensities were normalized to the lane containing no DNA and plotted against the HrrA concentration in log₁₀ scale. Apparent K_d values were calculated based on at least three gels each using a sigmoidal fit and the software GraphPad Prism 8. For the sigmoidal fit, $Y = 0$ and $Y = 1$ were set as top and bottom constraints. The turning point of the curve was defined as the apparent K_d .

TMPD oxidase assay

C. glutamicum wild-type strain and the Δ hrrA mutant were cultivated to an OD₆₀₀ of 4 in CGXII minimal with or without the addition of 4 μ M hemin. Subsequently, cells were disrupted in a Precellys[®] homogenisator (VWR International GmbH, Darmstadt, Germany) using zirconia/silica-beads (\varnothing 0.1 mm, Roth, Karlsruhe) in 100 mM Tris-HCl (pH 7.5) buffer. Ultracentrifugation at 200 000 $\times g$ for 1 h was used for membrane isolation. The pellet was resuspended in 100 mM Tris-HCl buffer and the protein concentration was determined using a BCA assay. The N,N,N',N'-Tetramethyl-*p*-phenylenediamine (TMPD) oxidase activity in the membrane fraction was measured spectrophotometrically at 562 nm in a TECAN Reader (Thermo Fisher Scientific, Massachusetts, US) by injecting 200 μ M TMPD (37). An extinction coefficient of 10.5 mM⁻¹ cm⁻¹ was used (48). One unit of activity was defined as 1 μ mol of TMPD oxidized per minute. As a control for autooxidation, a sample containing only 100 mM Tris-HCl buffer was recorded after TMPD addition and subtracted from the actual rates.

Significance was evaluated by an unpaired t-test with a 95% confidence interval.

RESULTS

Genome-wide profiling of HrrA promoter occupancy

In previous studies, a number of direct HrrA target operons were described in *C. glutamicum* and *C. diphtheriae*, suggesting an important role of the HrrSA TCS in the control of heme homeostasis (17–20). It has to be noted, that the membrane embedded HrrS sensor kinase is also activated by endogenously synthesized heme (21) and that the addition of external heme leads to a boost of the HrrSA response. In this study, we investigated the genome-wide binding profile of HrrA using chromatin affinity purification of twin-Strep-tagged HrrA combined with DNA sequencing (ChAP-Seq). Importantly, qPCR experiments confirmed wild-type level expression of the twin-Strep-tagged version of HrrA.

To obtain insights into the stimulus-dependent DNA association and dissociation, *C. glutamicum* cells were grown in iron-depleted glucose minimal medium, and samples were obtained before (T₀) and 0.5, 2, 4, 9 and 24 h after the addition of 4 μ M hemin. HrrA was purified, and the bound DNA fragments were sequenced (Figure 1A). We obtained substantial enrichment of known HrrA targets in response to heme (e.g. after 0.5 h: 5-fold *hmuO*, 54-fold *hemE*, 105-fold *ctaE*; Figure 1B–D, respectively) and identified more than 200 previously unknown HrrA-bound regions in the *C. glutamicum* genome (Supplementary Table S3).

As expected, the highest number of peaks was identified at the first time point after the heme pulse (0.5 h), with 199 peaks meeting our applied threshold (distance of <800 bp to the closest downstream or <200 bp to the closest upstream transcription start site (TSS)). In comparison, only 15 peaks showed a more than 2-fold enrichment before hemin addition (T₀, Supplementary Table S3 and Figure S3). It has to be noted, that these 15 peaks detected at T₀ appear to be specific HrrA targets, since none of them was detected in an input control sample. Overall, these data illustrate the fast and transient DNA binding by HrrA in response to heme. In general, the majority of the discovered HrrA binding sites were close to TSSs (Supplementary Figure S4). The binding of HrrA to 11 selected targets was confirmed by electrophoretic mobility shift assays (Supplementary Figure S5), and a palindromic binding motif was deduced (Figure 2B and Supplementary Figure S6).

The HrrA binding patterns depicted in Figure 1B–D are representative of many bound regions. Thirty minutes after the heme pulse, the average peak intensities increased ~2.5-fold in comparison to those at T₀ (Figure 2A). After 2 h of cultivation in hemin, the average peak intensity is declining and is, after 9 h, already below the starting level at T₀ reaching a minimum in stationary phase (24 h). This is likely the result of the pre-cultivation and main cultivation under iron starvation conditions leading to a lowered intracellular heme pool. The dissociation of HrrA from its target promoters is, consequently, caused by rapid depletion of heme and a switch of HrrS from kinase to phosphatase state (23). Heme depletion was confirmed by spectroscopy of *C. glutamicum* cells (Figure 2A, dashed line) and was also obvious upon visual inspection (Supplementary Figure S7).

6552 *Nucleic Acids Research*, 2020, Vol. 48, No. 12

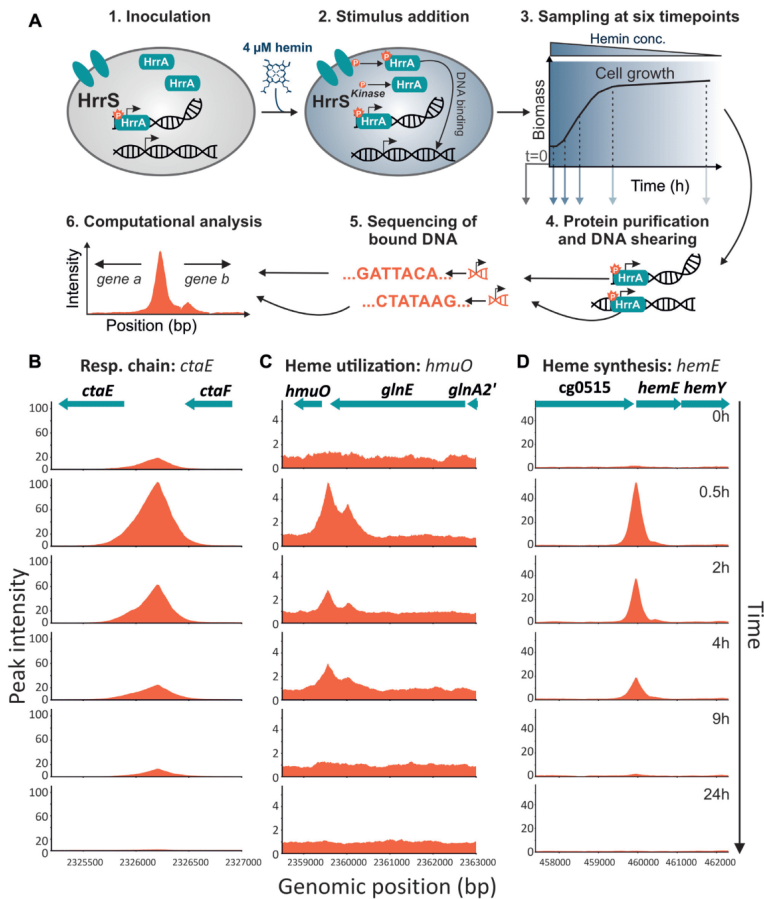


Figure 1. Genome-wide profiling of HrrA binding in response to addition of external heme. (A) ChIP-Seq analysis of the *Corynebacterium glutamicum* strain ATCC 13032::*hrrA-C*-twin-strep grown in iron-depleted glucose minimal medium before and after addition of 4 μ M hemin. The experimental approach is briefly depicted: cells were harvested at the indicated time points, twin-Strep tagged HrrA was purified and co-purified DNA was sequenced to identify HrrA genomic targets. This approach resulted in the identification of more than 200 genomic regions bound by HrrA upon addition of hemin after 30 min. Exemplarily shown is the HrrA binding to regions upstream of operons involved in (B) the respiratory chain (*ctaE*), (C) heme degradation (*hmuO*) and (D) heme biosynthesis (*hemE*).

Of all peaks, that passed our threshold, 128 were upstream of genes encoding hypothetical proteins, while 150 could be assigned to genes with known or predicted function (Figure 2C). Furthermore, we assessed the significance levels of HrrA binding changes between samples from different conditions or/and time-points. It turned out, that for the stronger peaks (peak intensity > 10) the minimum significant fold change (P -value < 0.05) is ~ 1.23 , while for the

weaker peaks (peak intensity < 10) it is ~ 1.33 (see 'Materials and Methods' section).

To analyze the synchronicity in the HrrA regulon, peak intensities were correlated over time. A relatively high correlation between peak intensities for the time points 0.5, 2 and 4 h (Figure 2D) showed that the system reacted proportionally for a majority of the binding sites and the strength of HrrA binding changed in response to heme availability.

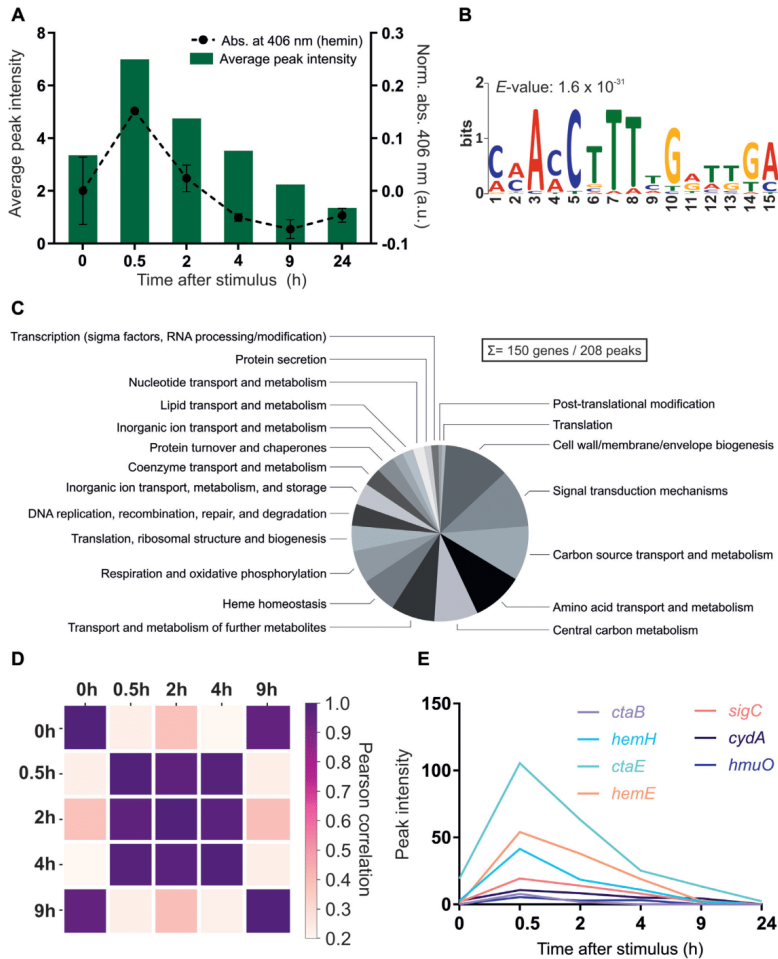


Figure 2. ChAP-Seq analysis revealed HrrA as a global regulator of heme homeostasis in *Corynebacterium glutamicum*. (A) HrrA binding in response to the addition of hemin. The bar plot reflects the average peak intensities among detected peaks in ChAP-Seq experiments (≈ 800 bp to the next TSS). The binding was correlated with the amount of cell-associated hemin (dashed line), measured at corresponding time points by spectroscopy as described in 'Materials and Methods' section. (B) A binding motif was deduced from the sequences of the top 25 peaks ($T_{0.5}$) using MEME v.5 analysis (<http://meme-suite.org>). (C) Pie chart presenting HrrA targets, which can be attributed to known functional categories (total of 272 genes, among which 128 encode proteins of unknown function, e.g. target genes within the CGP3 prophage region were excluded). For a complete overview of HrrA targets, see Supplementary Table S3. (D) Proportional behavior of the HrrA regulon. For each peak that passed the threshold (distance of < 800 bp to the closest downstream or < 200 to the closest upstream TSS) at time point A, the highest peak in the same region (± 50 nt from the center of the peak) was selected for time point B and *vice versa*. Thus, 'paired' peaks for these two time points were obtained, and the Pearson correlation of the intensities of all paired peaks was calculated for all six time points. (E) Peak intensities of selected HrrA targets over time, as identified by ChAP-Seq.

6554 *Nucleic Acids Research*, 2020, Vol. 48, No. 12

Relaxation of the system was observed after 9 h where peak intensities correlated well with T_0 .

The HrrSA TCS coordinates heme homeostasis by integrating the response to oxidative stress and cell envelope remodeling

Our dataset confirmed the binding of HrrA to all previously known targets, including genes encoding components of heme biosynthesis (*hemE*, *hemH* and *hemA*), degradation (*hmuO*) and export (*hrtBA*) pathways and heme-containing complexes of the respiratory chain (*ctaE-qcrCAB* operon and *ctaD*). A comprehensive overview of all identified HrrA targets is presented in Supplementary Table S3; selected target genes are listed in Table 1. Among the more than 180 novel targets identified in this study, we observed HrrA binding upstream of *ctaB*, which encodes a protoheme IX farnesyltransferase that catalyzes the conversion of heme *b* to heme *o* (26) and upstream of *ctaC*, which encodes subunit 2 of the cytochrome *aa3* oxidase. Remarkably, HrrA binding was also observed upstream of the *cydABDC* operon, which encodes the cytochrome *bd* oxidase of the respiratory chain. Altogether, this set of target genes highlights the global role of the HrrSA system in heme-dependent coordination of both branches of the respiratory chain. The HrrA regulon appeared to cover also the aspect of cofactor supply for the respiratory chain, as several HrrA targets encode enzymes involved in menaquinone reduction (*sdhCD*, *lldD* and *lldJ*).

Besides the known heme biosynthesis targets (*hemE*, *hemH* and *hemA*), HrrA binding was also observed upstream of a gene (*hemQ*) encoding a putative dismutase-family protein. However, in actinobacteria, it was proposed that these proteins do not possess chlorite dismutase activity but instead are essential for heme synthesis (49). Furthermore, we observed binding of HrrA upstream of the *chrSA* operon encoding the second TCS involved in heme-dependent regulation in *C. glutamicum*. This finding therefore confirmed the previously postulated cross-regulation of these TCS at the level of transcription (24,50).

Furthermore, HrrA binding was also observed upstream of several genes involved in the oxidative stress response, including *katA*, encoding catalase, *tusG*, encoding a trehalose uptake system (51), and upstream of *gapA* and *gapB* (glyceraldehyde-3-phosphate dehydrogenase, glycolytic and gluconeogenic, respectively) (52,53). In line with these findings, the phenotypic analysis of a *C. glutamicum hrrA* mutant revealed a significantly higher sensitivity to oxidative stress (treatment with H_2O_2) in comparison to the wild-type (Supplementary Figure S8). These findings suggest that the HrrSA system not only controls heme biosynthesis and degradation but also integrates the response to heme-induced oxidative stress.

A further important class of HrrA targets is represented by genes associated with the regulation or maintenance of the *C. glutamicum* cell envelope. The gene products of these previously unknown HrrA targets are, for instance, involved in the synthesis of peptidoglycan (*murA*), the peptidoglycan precursor meso-2,6-diaminopimelate (mDAP), inositol-derived lipids (*ino1*) and arabinogalactan (*aftC*). Furthermore, HrrA binding was revealed upstream of a

number of genes encoding global transcriptional regulators (e.g. *ramA*, *ramB* and *amiR*), adding a further level of complexity to this systemic response to heme.

Temporal dynamics of promoter occupancy reveal hierarchy in the HrrA regulon

With the time-resolved and genome-wide analysis of HrrA binding, we were also able to visualize distinct binding patterns of HrrA in response to addition and depletion of heme. Consequently, we asked whether the binding patterns (ChAP-Seq coverage) could provide information regarding the apparent dissociation constant (K_d) of HrrA to specific genomic targets. We compared the *in vivo* binding patterns of HrrA to *ctaE*, *hmuO* and *cydAB* (Figure 1, 2E and Supplementary Table S3). While a comparably high peak was observed upstream of the *ctaE* promoter—even before the addition of heme (T_0)—the binding of HrrA to the promoter of *hmuO* occurred with apparently high stimulus dependency and appeared to be rather transient, as HrrA was fully dissociated from this promoter 9 h after the addition of hemin (Figure 1B and C).

Subsequently, we determined the *in vitro* affinity of phosphorylated HrrA to the promoter regions of *ctaE*, *cydAB* and *hmuO* (Table 2 and Supplementary Figure S9). Consistent with the ChAP-Seq data, we measured the highest affinity of HrrA to P_{ctaE} with an apparent K_d of 125 nM. We therefore hypothesize that the *ctaE* promoter is a prime target that is constitutively activated by HrrA (Supplementary Table S3) to maintain high gene expression of the operon encoding the *bc1-aa3* supercomplex. In line with this hypothesis, we also found a high HrrA binding peak upstream of the other operons encoding components of the *bc1-aa3* supercomplex (*ctaD* and *ctaCF*, Table 1 and Supplementary Table S3).

In contrast, we measured an almost 3-fold higher apparent K_d (350 nM) for P_{cydAB} , which was consistent with the relatively transient binding pattern observed for this target. With an apparent K_d of 196 nM, the *in vitro* binding affinity of HrrA to the *hmuO* promoter was rather high considering the genomic coverage measured in the ChAP-Seq analysis. However, *in vitro* analysis does not account for the widespread interference among regulatory networks *in vivo*. In the particular example of *hmuO*, the pattern of HrrA binding was likely the result of interference with the global regulator of iron homeostasis, DtxR, which has previously been described to repress *hmuO* expression by binding to adjacent sites (54). Taken together, these results suggest that *in vivo* promoter occupancy is not only influenced by the binding affinity of the regulator to the particular target, but also significantly shaped by network interference. Consequently, high *in vivo* promoter occupancy indicates high binding affinity, but conclusions based on weakly bound regions may be confounded by competition with other binding factors.

HrrA activates the expression of genes encoding components of both branches of the quinol oxidation pathway

To evaluate how HrrA binding affects the expression of individual target genes, we analyzed the transcriptome (RNA-Seq) of the *C. glutamicum* wild-type strain (ATCC 13032) as

Table 1. Selected target genes of HrrA

Locus tag	Gene name	Annotation	Dist. TSS ^a	Peak intensity ^b	log ₂ (Δ hrrA/wt) ^c T 0.5 h	log ₂ (Δ hrrA/wt) ^c T 4 h
Heme homeostasis/metabolism						
cg2445	<i>hmuO</i>	Heme oxygenase	43	5.4	-3.1	-3.8
cg0516	<i>hemE</i>	Uroporphyrinogen decarboxylase	17	54	3.1	2.2
cg0497	<i>hemA</i>	Glutamyl-tRNA reductase	-162	13	0.7	1.0
cg0517	<i>hemY</i>	Protoporphyrinogen oxidase	429	3.0	2.8	1.6
cg2079	<i>hemQ</i>	Putative chlorite dismutase-family protein, conserved		19	2.8	1.8
cg3156	<i>htaD</i>	Secreted heme transport-associated protein	-108	15	-0.3	-1.1
cg1734	<i>hemH</i>	Ferrochelatase	21	41	4.0	2.2
cg3247	<i>hrrA</i>	Heme-dependent response regulator	108	3.7	n.d.	n.d.
cg2201	<i>chrS</i>	Heme-dependent histidine kinase (<i>chrSA</i> operon)	32	2.5	-0.4	1.3
cg2202	<i>hrrB</i>	Heme exporter (<i>hrrBA</i> operon)	78	2.5	-1.0	4.3
Respiratory chain						
cg2406	<i>ctaE</i>	Cytochrome <i>aa3</i> oxidase, subunit 3	307	105	-1.7	-0.8
cg2780	<i>ctaD</i>	Cytochrome <i>aa3</i> oxidase, subunit 1	197	36	-1.1	-0.9
cg1301	<i>cydA</i>	Cytochrome <i>bd</i> oxidase	192	11	-0.7	-2.6
cg2409	<i>ctaC</i>	Cytochrome <i>aa3</i> oxidase, subunit 2	47	22	-1.4	-1.0
cg1773	<i>ctaB</i>	Protoheme IX farnesyltransferase	667	7.9	0.4	-1.4
cg0445	<i>sdhC</i>	Succinate:menaquinone oxidoreductase, cytochrome b subunit	83	38	-1.7	-1.6
cg3226		L-lactate permease, operon with <i>lldD</i>	533	5.5	-1.7	0.9
Glucose uptake						
cg2121	<i>ptsH</i>	Phosphocarrier protein HPr, general component of PTS	-70	2.1	-1.2	-0.3
cg1537	<i>ptsG</i>	Glucose-specific EIIBC component EIIGlc of PTS	70	1.6	-1.1	-0.1
cg2091	<i>ppgG</i>	Polyphosphate glucokinase	199	266	0.2	-0.8
cg0223	<i>iolTI</i>	Myo-Inositol transporter 1, alternative glucose uptake system	73	2.0	-1.0	-0.7
Signal transduction						
cg0986	<i>amtR</i>	Master regulator of nitrogen control, repressor, TetR-family	366	1.8	0.3	0.1
cg2461	<i>benR</i>	Transcriptional regulator, LuxR-family	229	5.6	-0.1	-1.2
cg2761	<i>cpdA</i>	cAMP phosphodiesterase	309	4.2	0.4	-0.5
cg0309	<i>sigC</i>	Extracytoplasmic-function σ factor, control of branched quinol oxidation pathway	29	19	2.1	0.6
cg0444	<i>ramB</i>	Transcriptional regulator, involved in acetate metabolism	83	38	-0.7	-0.6
cg2831	<i>ramA</i>	Transcriptional regulator, acetate metabolism, LuxR-family	-10	2.1	-0.5	0.6
Oxidative stress						
cg0310	<i>katA</i>	Catalase	132	19	-0.7	-1.2
cg0831	<i>tusG</i>	Trehalose uptake system, ABC-type, permease protein	-30	1.8	0.0	-0.2
cg1791	<i>gapA</i>	Glyceraldehyde-3-phos. dehydrogenase, glycolysis	86	3.9	-0.3	-0.4
cg1069	<i>gapB</i>	Glyceraldehyde-3-phos. dehydrogenase, gluconeogenesis	175	2.4	1.6	-0.1
Cell envelope						
cg2077	<i>aftC</i>	arabinofuranosyltransferase	271	3.0	-0.3	-0.2
cg3323	<i>inoI</i>	D-myo-inositol-1-phosphate synthase	-46	4.2	1.7	0.6
cg0337	<i>whcA</i>	WhiB homolog, role in SigH-mediated oxidative stress response	-21	2.1	-0.5	-0.7
cg0306	<i>lysC</i>	Aspartate kinase	32	13	0.7	0.1
cg0422	<i>murA</i>	UDP-N-acetylenolpyruvoylglucosamine reductase	591	3.5	-0.3	-0.1

^aDistance of the HrrA binding peak, identified via ChAP-Seq, to the start codon (TSS).^bThe corresponding peak intensity.^cRelative ratio of the transcript levels of the Δ hrrA deletion mutant compared to the wild-type (log₂ fold change). The values are derived from a comparison between the two strains 0.5 and 4 h after hemin addition. The log₂(Δ hrrA/wt) value for was not determined for the deleted *hrrA* gene (n.d.).This table summarizes results from the HrrA ChAP-Seq analysis of the *C. glutamicum* strain ATCC 13032::hrrA-C-twinstep and the transcriptome analysis of *C. glutamicum* wild-type and strain Δ hrrA (complete datasets are provided in Supplementary Tables S3 and 4, respectively). For both experiments, cells were grown on glucose minimal medium and 4 M heme (see 'Materials and Methods' section).

6556 *Nucleic Acids Research*, 2020, Vol. 48, No. 12

Table 2. Apparent K_d values of HrrA to the promoters of *hmuO*, *ctaE*, *sigC* and *cydA*

Promoter	Function	Apparent K_d value (nM)	95% confidence interval (nM)	R^2	Peak intensity after hemin addition (ChAP-Seq)
P_{hmuO}	Heme oxygenase	196	182–212	0.95	10
P_{ctaE}	Cytochrome <i>aa3</i> oxidase	125	117–132	0.97	53
P_{sigC}	ECF sigma factor σ^C	271	247–299	0.96	25
P_{cydA}	Cytochrome <i>bd</i> oxidase	350	318–386	0.96	18

The affinity of phosphorylated HrrA to the indicated regions was measured using purified protein in increasing concentrations and its ability to shift 10 nM DNA fragments of ~100 bp size covering the maximal ChAP-Seq peak (for detailed information, see Supplementary Figure S9).

well as a $\Delta hrrA$ mutant (Supplementary Table S4). Analogous to the ChAP-Seq experiments, RNA-Seq analysis was performed prior to the addition of heme (T_0) as well as 0.5 and 4 h after the heme pulse (in medium containing no other iron source). The RNA-Seq analysis was performed in two independent biological replicates (for inter-replicate variation, see Supplementary Table S5).

At T_0 , before the addition of heme, already 212 genes showed a more than 2-fold altered expression level in $\Delta hrrA$ cells compared to wild-type cells ($\Delta hrrA/wt$). Directly after the addition of heme (0.5 h), the expression of 309 genes changed more than 2-fold. (Supplementary Table S4 and Figure 3A, orange dots). Of these genes, 174 were upregulated and 135 were downregulated in the *hrrA* deletion strain. Four hours after addition of heme, only 167 genes exhibited a >2-fold increase or decrease (scatter plots for additional time points are presented in Supplementary Figure S10).

The *hrrA* expression decreased after 0.5 h upon the addition of heme, which was likely caused by DtxR repression in response to increased intracellular iron levels (Figure 3B) (24). In contrast, after 4 h of cultivation, *hrrA* levels significantly increased, reflecting the depletion of heme as an alternative iron source and dissociation of DtxR. Furthermore, differential gene expression analysis revealed HrrA to be an activator of all genes encoding components of the respiratory chain (*ctaE*, *ctaD*, *ctaF* and *cydAB*) and as a repressor of heme biosynthesis (*hemA*, *hemE* and *hemH*) (Figure 3C). The impact on the cytochrome *bc₁-aa₃* supercomplex was also confirmed by measuring the activity of the *aa₃* oxidase, which was about 2-fold reduced in a *hrrA* mutant in comparison to the wild-type when grown on heme (Figure 3D). Additionally, expression of *lldD* (L-lactate dehydrogenase) as well as *sdhCD* (succinate dehydrogenase) contributing to the reduced menaquinone pool was downregulated more than 3-fold upon deletion of *hrrA*. In addition to these considerable differences between the wild-type and the $\Delta hrrA$ mutant, we also observed decreased mRNA levels of genes involved in the oxidative stress response (e.g. *kata*) or cell envelope remodeling (e.g. *murA*) in the $\Delta hrrA$ mutant, suggesting HrrA to be an activator of these targets.

In some cases, promoter occupancy by HrrA did not result in altered expression levels of the particular target gene in a $\Delta hrrA$ mutant under the tested conditions (Table 1 and Supplementary Table S3). This finding is, however, not surprising considering the multiplicity of signals and regulators affecting gene expression. Under changing environmental conditions, transcription factor binding will not necessarily always be translated in an altered gene expression of the

respective target. When we compare the results obtained from RNA-Seq and ChAP-Seq analysis, 269 genes out of 309 genes featuring an >2-fold change in gene expression did not show HrrA binding in their upstream promoter region. Looking at all HrrA targets (ChAP-Seq analysis) on a global scale, there is, nevertheless, a significantly higher impact on gene expression in a strain lacking *hrrA* for all targets bound by HrrA in comparison to non-targets (unbound, Supplementary Figure S11). Overall, 109 out of 228 HrrA targets featured a significantly altered gene expression in the *hrrA* mutant (64 increased and 55 decreased).

HrrA determines the prioritization of terminal cytochrome oxidases by repression of *sigC*

The results from ChAP-Seq and RNA-Seq experiments highlight the important role of HrrA in the control of the respiratory chain, including cofactor supply. Our data revealed that HrrA activates the expression of genes encoding the cytochrome *bc₁-aa₃* supercomplex (*ctaE-qcrCAB*, *ctaD*, *ctaCF*) and of *cydAB*, encoding the cytochrome *bd* branch of the respiratory chain (Figure 4 and Supplementary Table S3). Remarkably, the mRNA profiles of the corresponding operons exhibited significantly delayed activation of *cydAB* in response to heme, which was abolished in the $\Delta hrrA$ mutant (Figure 4). In contrast, *ctaE* expression was significantly higher in wild-type cells, even before hemin addition (T_0), but showed a further induction after stimulus addition (T 0.5 h, Supplementary Table S4). Notably, we also observed binding of HrrA upstream of *sigC*, encoding an ECF sigma factor that was shown to be involved in the activation of the *cydABDC* operon (35). The mRNA level of *sigC* increased more than 2-fold in the $\Delta hrrA$ mutant, indicating HrrA to be a repressor of this gene (Figure 4). Consistent with this hypothesis, *sigC* expression was slightly decreased in response to the addition of heme, which correlated with increased HrrA peak intensity (Figure 4F). Additionally, the higher *cydAB* expression, observed in the $\Delta hrrA$ strain before addition of stimulus (Figure 4B) is likely the effect of increased *sigC* expression (Figure 4C). Dissociation of HrrA from P_{sigC} at a later time point (4 h after heme pulse) led to derepression of *sigC* coinciding with an increased expression of *cydAB* in the wild-type. Because *cydAB* levels were constitutively low in the $\Delta hrrA$ mutant in response to heme, we hypothesized that activation by HrrA together with an additional boost by SigC (Figure 5) leads to delayed activation of *cydAB* after the heme pulse. This regulation enables cells to channel most of the available heme pool into the more efficient cytochrome *bc₁-aa₃* supercomplex.

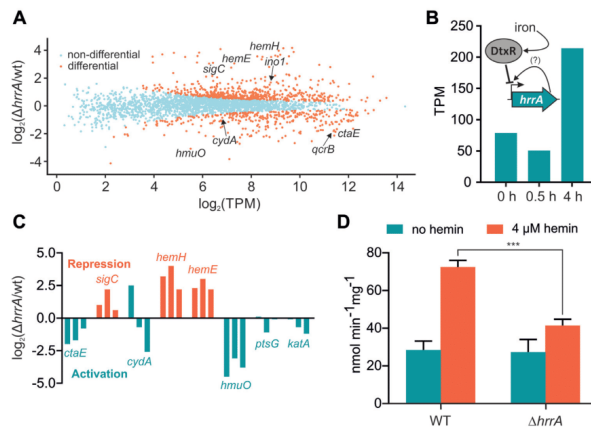


Figure 3. Differential gene expression analysis of wild-type *Corynebacterium glutamicum* and a $\Delta hrrA$ mutant. (A) Differential gene expression analysis (RNA-Seq) revealed 120 upregulated and 154 downregulated genes in the *hrrA* deletion strain compared to the wild-type (in transcripts per million, TPM) after 30 min of cultivation in iron-depleted glucose minimal medium containing 4 μ M heme. (B) Expression levels of *hrrA* (TPM) 0, 0.5 and 4 h after the addition of hemin. A scheme depicts HrrA autoregulation and iron-dependent DtxR repression (24). (C) Impact of *hrrA* deletion on the transcript levels of six selected target genes at three different time points (0, 0.5, 4 h; orange: HrrA acts as a repressor, turquoise: HrrA acts as an activator). (D) Measurement of cytochrome *aa3* oxidase activity using the TMPD oxidase assay in *C. glutamicum* wild-type and $\Delta hrrA$ grown with or without 4 μ M heme.

The lower apparent K_d of HrrA for the *ctaE* promoter (125 nM) compared to P_{cydAB} (350 nM) or P_{sigC} (270 μ M) also reflects this prioritization of HrrA targets (Table 2). Consequently, this almost 3-fold decrease in affinity (apparent K_d) increases the threshold for HrrSA activity to control these targets.

HrrA activates PTS-dependent and -independent glucose uptake

Besides the activation of all components constituting the respiratory chain, ChAP-Seq experiments and transcriptome analysis revealed HrrA as a direct activator of genes encoding components of the phosphotransferase (PTS) system (*ptsH* and *ptsG*) and of *iolT1* encoding inositol permease with a reported function as a PTS-independent glucose uptake system (55). Remarkably, the gene *ppgK*, encoding the polyphosphate glucokinase was among the targets with the highest HrrA peak and showed reduced expression in the 4 h sample (Table 1 and Supplementary Table S4). These results emphasize that cellular respiration and glucose uptake is coordinated via the HrrSA system in response to cellular heme levels.

DISCUSSION

In this work, we applied a genome-wide approach to study the ‘heme-responsive regulator’ HrrA in *C. glutamicum* and identified more than 200 genomic target regions of this response regulator. This intriguingly diverse set of target genes, encoding enzymes involved in heme biosynthesis, heme-containing proteins and components of the respiratory chain as well as proteins involved in oxidative stress response, glucose uptake and cell envelope remodeling, pro-

vided unprecedented insight into the systemic response to heme coordinated by the TCS HrrSA.

In Gram-positive bacteria, TCSs appear to play a central role in transient heme sensing, and heme-responsive systems have been described in several prominent pathogens, including *C. diphtheriae*, *S. aureus* and *B. anthracis* (15–18). However, for all prokaryotic heme regulatory systems, only a small number of target genes have been described to date, focusing on targets involved in degradation (*hmuO* (18,56)), heme export (*hrtBA* (19,57)) or heme biosynthesis (*hemA* (18,20)). Systems orthologous to HrrSA are present in almost all corynebacterial species and the high amino acid sequence identity shared by the response regulators (87%, between *C. glutamicum* and *C. diphtheriae* HrrA) suggests that the important role of HrrSA in the control of heme homeostasis is conserved. In many corynebacteria, including *C. diphtheriae*, control of heme homeostasis is shaped by the tight interplay of HrrSA with a second heme-dependent system, ChrSA. While the present study emphasized that HrrSA governs a large and complex homeostatic response, the only known target of the response regulator ChrA in *C. glutamicum* is the divergently located operon *hrtBA* encoding a heme export system. There is, however, also evidence for a cross-regulation between the TCSs, not only by cross-phosphorylation but also on the transcriptional level (23,24). In *C. diphtheriae*, evidence for more overlap between the regulons of the TCSs has been provided, since both response regulators were shown to control a common set of target genes including *hrtBA*, *hemA* and *hmuO* (20,58). Genome-wide analysis of these systems have, however, not been performed so far and *in vitro* protein–DNA interaction studies may not necessarily reflect the *in vivo* promoter preferences of these highly similar systems.

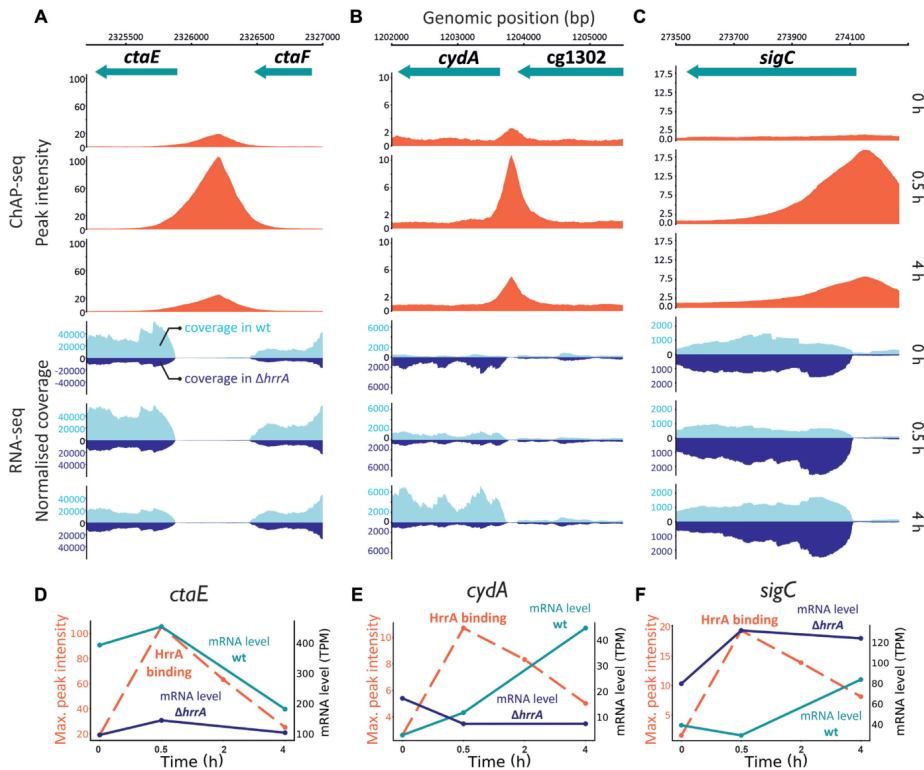
6558 *Nucleic Acids Research*, 2020, Vol. 48, No. 12

Figure 4. HrrA prioritizes the expression of genes encoding components of the *bc1-aa3* supercomplex. Depicted are HrrA binding peaks as identified by ChAP-Seq analysis (Figures 1 and 2) in comparison to the normalized coverage of RNA-Seq results (wild-type and the $\Delta hrrA$ mutant) for the genomic loci of *ctaE* (A and D), *sigC* (B and E) and *cydA* (C and F). D–F: HrrA binding (max. peak intensities measured by ChAP-Seq experiments) and the mRNA levels (in transcripts per million, TPM) of the respective genes in the $\Delta hrrA$ strain as well as in wild-type *Corynebacterium glutamicum* cells 0, 0.5 and 4 h after the addition of heme.

Coping with heme stress

While being an essential cofactor for many proteins, heme causes severe toxicity to cells at high levels (4). In mammalian cells, the BACH1 regulator is inactivated by heme binding and plays a key role in maintaining the balance of the cellular heme pool (8,59). Heme oxygenases are targets of various heme-dependent regulators (18,60–61), and consistent with this principle, the mammalian *HMOX1* gene, encoding an NADPH-dependent oxygenase, is regulated by BACH1 (59). Other identified BACH1 targets are involved in redox regulation, the cell cycle, and apoptosis as well as subcellular transport processes (9,62–63).

Although neither the regulator nor the constitution of the regulon is conserved, the responses of BACH1 and HrrSA share a similar logic. Analogous to eukaryotic BACH1, we

observed HrrA-mediated activation of genes involved in the oxidative stress response, including *katA*, which appears to be required to counteract oxidative stress caused by elevated heme levels (Supplementary Figure S8).

Remarkably, HrrA binding was also observed upstream of both *gapA* and *gapB*, which encode glyceraldehyde-3-phosphate dehydrogenases (GapDHs) involved in glycolysis and gluconeogenesis, respectively. Previous studies in baker's yeast and mammalian cells have revealed that oxidative stress may block glycolysis by inhibiting GapDH (53,64). Furthermore, GapDH of *C. diphtheriae* was recently shown to be redox-controlled by S-mycothiolation (65). Slight activation of *gapA* by HrrA may thus counteract an impaired glycolytic flux under conditions of heme stress.

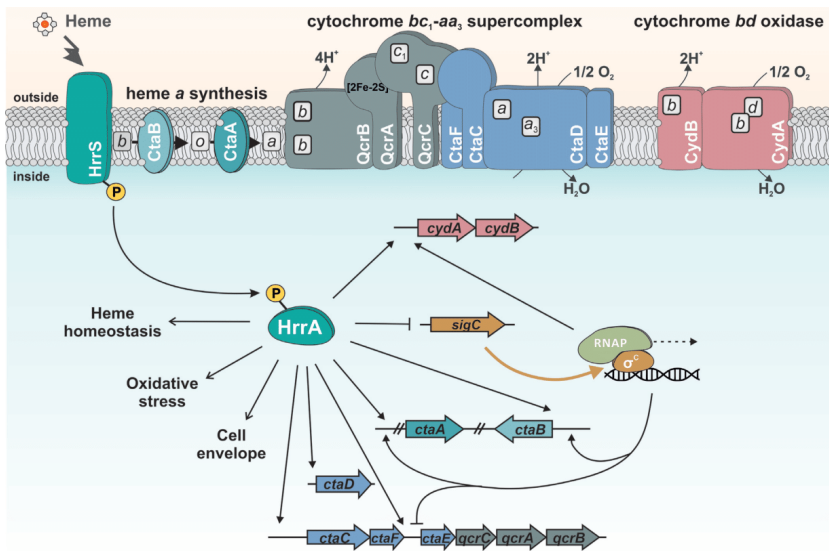


Figure 5. Model of heme-responsive control of components of the respiratory chain by HrrSA. The results of this study reveal HrrSA as a global regulator of heme homeostasis coordinating the expression of genes involved in heme biosynthesis, oxidative stress responses, glucose uptake and cell envelope remodeling. Genes encoding the components of the branched respiratory chain of *Corynebacterium glutamicum* comprise an important part of the HrrA regulon. While HrrA acts as an activator of almost all components (*ctaE-qcrCAB*, *ctaB*, *cydAB*), it represses transcription of the *sigC* gene encoding an important sigma factor required for *cydAB* expression. This regulatory network architecture consequently confers prioritization to the synthesis of the more efficient proton pump, the cytochrome *bc*₁-*aa*₃ supercomplex. Bordered boxes, b, c, a, d: heme b, heme c, heme a, heme d.

Furthermore, several HrrA targets play a role in the biosynthesis and remodeling of the corynebacterial cell envelope, including *inol*, which is required for the synthesis of inositol-derived lipids (66), *lysC*, providing the peptidoglycan precursor meso-2,6-diaminopimelate (mDAP) and *murA* (Table 1). Taken together, these insights emphasize the important role of the HrrSA system in the control of heme stress responses.

From networks to function

Genome-wide analysis of regulatory networks may provide important hints toward the physiological function of genes. An example is provided by the HrrA-dependent regulation of *cg2079* (*hemQ*), described in this study (Table 1). In actinobacteria, it was recently proposed that these proteins inherit an essential role in heme biosynthesis (49,67). The finding that HrrA binds to the promoter of this gene and represses its expression supports a role of HemQ in heme biosynthesis in *C. glutamicum*. Among the direct targets of HrrA are many further targets encoding proteins of unknown function, including several ABC transport systems with a potential role in heme uptake or export. Therefore, this dataset provides guidance for further functional analysis of these HrrA targets to decipher their role in heme homeostasis.

Coordinated control of the respiratory chain

Among the most significantly affected targets in the Δ *hrrA* mutant were many genes encoding components of the respiratory chain (26). These genes comprise all the genes constituting the cytochrome *bc*₁-*aa*₃ branch of the respiratory chain (*ctaE-qcrCAB*, *ctaCF* and *ctaD*) (68); genes encoding the cytochrome *bd* branch (*cydAB* (26)); *ctaA* (69) and *ctaB* (70), encoding enzymes responsible for heme a synthesis; and *lldD* and *dld*, encoding lactate dehydrogenases that contribute to the reduced menaquinone pool (26) (Figure 4; Supplementary Figure S12 and Table S3).

In a recent study, Toyoda and Inui described the ECF sigma factor σ^C to be an important regulator of both branches of the *C. glutamicum* respiratory chain. The *ctaE-qcrCAB* operon was shown to be significantly downregulated after σ^C overexpression due to binding of the sigma factor to the antisense strand of the promoter (35). Here, we demonstrated that this repression is counteracted by HrrA, which not only represses *sigC* but also activates *ctaE-qcrCAB* expression. While the two proteins have antagonistic effects on the expression of the supercomplex, both σ^C and HrrA positively regulate the *cyd* operon, encoding the cytochrome *bd* branch of the respiratory chain (Figure 5).

Interestingly, a hierarchy in the regulon was reflected by the differences in the apparent K_d values of HrrA with P_{cydA} and P_{sigC} , which were 2-fold lower than those with the pro-

6560 *Nucleic Acids Research*, 2020, Vol. 48, No. 12

motor of *ctaE*. These findings were also consistent with the ChAP-Seq experiments, where the peaks upstream of *ctaE* and *ctaD* were among the highest peaks at T_0 and after 0.5 h (Figure 4A). These data suggest that under conditions of sufficient heme supply, production of the cytochrome *bc*₁–*aa*₃ supercomplex is preferred, which is highly effective but requires the incorporation of six heme molecules (in contrast to only three molecules for the synthesis of the *bd* oxidase). Repression of *sigC* by HrrA and the relatively low affinity to the *cydAB* promoter results in delayed production of the *bd* branch. Under the applied aerobic conditions, available heme is thus first channeled to the cytochrome *bc*₁–*aa*₃ supercomplex before the cytochrome *bd* oxidase is used, which is less efficient but has a higher oxygen affinity. Remarkably, HrrA was also found to activate expression of genes involved in PTS-dependent (*ptsH* and *ptsG*) and -independent (*iolTT*) glucose uptake thereby ensuring a high glucose uptake rate under conditions of active cellular respiration.

Interference with other regulatory networks

Deletion of the *hrrA* gene led to more than 2-fold upregulation of 174 genes, while 135 genes were downregulated after the addition of heme. Several other genes were significantly affected but to a lesser extent. Remarkably, among the direct target genes controlled by HrrA, we identified several prominent global regulators, including the regulators of acetate metabolism *ramA* and *ramB* (71, 72), and *amtR* encoding the master regulator of nitrogen control (73). Furthermore, *cpdA* encoding a cAMP phosphodiesterase playing a key role in the control of cellular cAMP levels in *C. glutamicum* (74) was found to be under direct control of HrrA. These examples illustrate the profound influence of HrrA on cellular networks and the systemic response cells have programmed to respond to heme availability.

CONCLUSION

Genome-wide analyses of targets controlled by prokaryotic transcription factors will change our view on many systems we believe to know. In this study, we provide an unprecedented insight into the systemic response to heme coordinated by the TCS HrrSA. Given the many properties of this molecule, the complexity of this response is actually not surprising but paves the way for further functional analysis of HrrA targets with so far unknown functions in heme homeostasis.

DATA AVAILABILITY

The custom-developed software used in this study is publicly available at GitHub repository under the link <https://github.com/afilipch/afp>.

All sequencing data were deposited in the GEO database under the accession numbers GSE121962 (ChAP-Seq) and GSE120924 (RNA-Seq).

SUPPLEMENTARY DATA

Supplementary Data are available at NAR Online.

ACKNOWLEDGEMENTS

We thank Eva Davoudi for fruitful discussions and critical reading of the manuscript. We thank Helga Etterich for her practical help with the sequencing experiments.

FUNDING

German Research Foundation [FR 2759/4-1]; European Research Council [ERC-StG-2017, 757563]; Helmholtz Association [W2/W3-096]. Funding for open access charge: Forschungszentrum Jülich, European Research Council [757563].

Conflict of interest statement. None declared.

REFERENCES

1. Ponka, P. (1999) Cell biology of heme. *Am. J. Med. Sci.*, **318**, 241–256.
2. Layer, G., Reichelt, J., Jahn, D. and Heinz, D.W. (2010) Structure and function of enzymes in heme biosynthesis. *Protein Sci.*, **19**, 1137–1161.
3. Ajioka, R.S., Phillips, J.D. and Kushner, J.P. (2006) Biosynthesis of heme in mammals. *Biochim. Biophys. Acta*, **1763**, 723–736.
4. Anzaldi, L.L. and Skaar, E.P. (2010) Overcoming the heme paradox: heme toxicity and tolerance in bacterial pathogens. *Infect. Immun.*, **78**, 4977–4989.
5. Huang, W. and Wilks, A. (2017) Extracellular heme uptake and the challenge of bacterial cell membranes. *Annu. Rev. Biochem.*, **86**, 799–823.
6. Wilks, A. (2002) Heme oxygenase: evolution, structure, and mechanism. *Antioxid. Redox. Signal.*, **4**, 603–614.
7. Hickman, M.J. and Winston, F. (2007) Heme levels switch the function of Hap1 of *Saccharomyces cerevisiae* between transcriptional activator and transcriptional repressor. *Mol. Cell. Biol.*, **27**, 7414–7424.
8. Ogawa, K., Sun, J., Taketani, S., Nakajima, O., Nishitani, C., Sassa, S., Hayashi, N., Yamamoto, M., Shibahara, S., Fujita, H. et al. (2001) Heme mediates depression of Maf recognition element through direct binding to transcription repressor Bach1. *EMBO J.*, **20**, 2835–2843.
9. Warnatz, H.J., Schmidt, D., Manke, T., Piccini, I., Sultan, M., Borodina, T., Balzereit, D., Wruck, W., Soldatov, A., Vingron, M. et al. (2011) The BTB and CNC homology 1 (BACH1) target genes are involved in the oxidative stress response and in control of the cell cycle. *J. Biol. Chem.*, **286**, 23521–23532.
10. Qi, Z., Hamza, I. and O'Brian, M.R. (1999) Heme is an effector molecule for iron-dependent degradation of the bacterial iron response regulator (Irr) protein. *Proc. Natl. Acad. Sci. U.S.A.*, **96**, 13056–13061.
11. Qi, Z. and O'Brian, M.R. (2002) Interaction between the bacterial iron response regulator and ferrochelatase mediates genetic control of heme biosynthesis. *Mol. Cell*, **9**, 155–162.
12. O'Brian, M.R. (2015) Perception and homeostatic control of iron in the rhizobia and related bacteria. *Annu. Rev. Microbiol.*, **69**, 229–245.
13. Torres, V.J., Stauff, D.L., Pishchany, G., Bezbradica, J.S., Gordy, L.E., Iturregui, J., Anderson, K.L., Dunman, P.M., Joyce, S. and Skaar, E.P. (2007) A *Staphylococcus aureus* regulatory system that responds to host heme and modulates virulence. *Cell Host Microbe*, **1**, 109–119.
14. Mike, L.A., Choby, J.E., Brinkman, P.R., Olive, L.Q., Dutter, B.F., Ivan, S.J., Gibbs, C.M., Sulikowski, G.A., Stauff, D.L. and Skaar, E.P. (2014) Two-component system cross-regulation integrates *Bacillus anthracis* response to heme and cell envelope stress. *PLoS Pathog.*, **10**, e1004044.
15. Stauff, D.L. and Skaar, E.P. (2009) The heme sensor system of *Staphylococcus aureus*. *Contrib. Microbiol.*, **16**, 120–135.
16. Stauff, D.L. and Skaar, E.P. (2009) *Bacillus anthracis* HsRS signalling to HrtAB regulates haem resistance during infection. *Mol. Microbiol.*, **72**, 763–778.
17. Bibb, L.A., Kunkle, C.A. and Schmitt, M.P. (2007) The ChrA-ChrS and HrrA-HrrS signal transduction systems are required for activation of the *imuO* promoter and repression of the *hemA* promoter in *Corynebacterium diphtheriae*. *Infect. Immun.*, **75**, 2421–2431.

18. Frunzke, J., Gätgens, C., Brocker, M. and Bott, M. (2011) Control of heme homeostasis in *Corynebacterium glutamicum* by the two-component system HrrSA. *J. Bacteriol.*, **193**, 1212–1221.
19. Heyer, A., Gätgens, C., Hentschel, E., Kalinowski, J., Bott, M. and Frunzke, J. (2012) The two-component system ChrSA is crucial for haem tolerance and interferes with HrrSA in haem-dependent gene regulation in *Corynebacterium glutamicum*. *Microbiology*, **158**, 3020–3031.
20. Burgos, J.M. and Schmitt, M.P. (2016) The ChrSA and HrrSA two-component systems are required for transcriptional regulation of the hema promoter in *Corynebacterium diphtheriae*. *J. Bacteriol.*, **198**, 2419–2430.
21. Keppel, M., Davoudi, E., Gätgens, C. and Frunzke, J. (2018) Membrane topology and heme binding of the histidine kinases HrrS and ChrS in *Corynebacterium glutamicum*. *Front. Microbiol.*, **9**, 183.
22. Ito, Y., Nakagawa, S., Komagata, A., Ikeda-Saito, M., Shiro, Y. and Nakamura, H. (2009) Heme-dependent autophosphorylation of a heme sensor kinase, ChrS, from *Corynebacterium diphtheriae* reconstituted in proteoliposomes. *FEBS Lett.*, **583**, 2244–2248.
23. Hentschel, E., Mack, C., Gätgens, C., Bott, M., Brocker, M. and Frunzke, J. (2014) Phosphatase activity of the histidine kinases ensures pathway specificity of the ChrSA and HrrSA two-component systems in *Corynebacterium glutamicum*. *Mol. Microbiol.*, **92**, 1326–1342.
24. Keppel, M., Piepenbreier, H., Gätgens, C., Fritz, G. and Frunzke, J. (2019) Toxic but tasty—temporal dynamics and network architecture of heme-responsive two-component signaling in *Corynebacterium glutamicum*. *Mol. Microbiol.*, **111**, 1367–1381.
25. Wennerhold, J. and Bott, M. (2006) The DtxR regulon of *Corynebacterium glutamicum*. *J. Bacteriol.*, **188**, 2907–2918.
26. Bott, M. and Niebisch, A. (2003) The respiratory chain of *Corynebacterium glutamicum*. *J. Biotechnol.*, **104**, 129–153.
27. Kao, W.C., Kleinschroth, T., Nitschke, W., Baymann, F., Neehaul, Y., Hellwig, P., Richers, S., Vonck, J., Bott, M. and Hunte, C. (2016) The obligate respiratory supercomplex from Actinobacteria. *Biochim. Biophys. Acta*, **1857**, 1705–1714.
28. Niebisch, A. and Bott, M. (2001) Molecular analysis of the cytochrome *bc₁-aa₃* branch of the *Corynebacterium glutamicum* respiratory chain containing an unusual diheme cytochrome *c₁*. *Arch. Microbiol.*, **175**, 282–294.
29. Kalinowski, J., Bathe, B., Bartels, D., Bischoff, N., Bott, M., Burkowski, A., Dusch, N., Eggeling, L., Eikmanns, B.J., Gaigalat, L. et al. (2003) The complete *Corynebacterium glutamicum* ATCC 13032 genome sequence and its impact on the production of L-aspartate-derived amino acids and vitamins. *J. Biotechnol.*, **104**, 5–25.
30. Ikeda, M. and Nakagawa, S. (2003) The *Corynebacterium glutamicum* genome: features and impacts on biotechnological processes. *Appl. Microbiol. Biotechnol.*, **62**, 99–109.
31. Sone, N., Nagata, K., Kojima, H., Tajima, J., Koder, Y., Kanamaru, T., Noguchi, S. and Sakamoto, J. (2001) A novel hydrophobic diheme c-type cytochrome. Purification from *Corynebacterium glutamicum* and analysis of the QcrCBA operon encoding three subunit proteins of a putative cytochrome reductase complex. *Biochim. Biophys. Acta*, **1503**, 279–290.
32. Niebisch, A. and Bott, M. (2003) Purification of a cytochrome *bc-aa₃* supercomplex with quinol oxidase activity from *Corynebacterium glutamicum*. Identification of a fourth subunit of cytochrome *aa₃* oxidase and mutational analysis of diheme cytochrome *c₁*. *J. Biol. Chem.*, **278**, 4339–4346.
33. Teramoto, H., Inui, M. and Yukawa, H. (2013) OxyR acts as a transcriptional repressor of hydrogen peroxide-inducible antioxidant genes in *Corynebacterium glutamicum* R. *FEBS J.*, **280**, 3298–3312.
34. Milse, J., Petri, K., Ruckert, C. and Kalinowski, J. (2014) Transcriptional response of *Corynebacterium glutamicum* ATCC 13032 to hydrogen peroxide stress and characterization of the OxyR regulon. *J. Biotechnol.*, **190**, 40–54.
35. Toyoda, K. and Inui, M. (2016) The extracytoplasmic function sigma factor sigma(C) regulates expression of a branched quinol oxidation pathway in *Corynebacterium glutamicum*. *Mol. Microbiol.*, **100**, 486–509.
36. Morosov, X., Davoudi, C.F., Baumgart, M., Brocker, M. and Bott, M. (2018) The copper-deprivation stimulant of *Corynebacterium glutamicum* comprises proteins for biogenesis of the actinobacterial cytochrome *bc₁-aa₃* supercomplex. *J. Biol. Chem.*, **293**, 15628–15640.
37. Davoudi, C.F., Ramp, P., Baumgart, M. and Bott, M. (2019) Identification of Surf1 as an assembly factor of the cytochrome *bc₁-aa₃* supercomplex of Actinobacteria. *Biochim. Biophys. Acta Bioenerget.*, **1860**, 148033.
38. Keilhauer, C., Eggeling, L. and Sahn, H. (1993) Isoleucine synthesis in *Corynebacterium glutamicum*: molecular analysis of the *ilvB-ilvN-ilvC* operon. *J. Bacteriol.*, **175**, 5595–5603.
39. Sambrook, J.F. and Russell, D.W. (2001) In: *Molecular Cloning: A Laboratory Manual*. 3rd edn. Cold Spring Harbor Laboratory Press, NY.
40. Eikmanns, B.J., Thum-Schmitz, N., Eggeling, L., Ludtke, K.U. and Sahn, H. (1994) Nucleotide sequence, expression and transcriptional analysis of the *Corynebacterium glutamicum* gltA gene encoding citrate synthase. *Microbiology*, **140**, 1817–1828.
41. Niebisch, A. and Bott, M. (2001) Molecular analysis of the cytochrome *bc₁-aa₃* branch of the *Corynebacterium glutamicum* respiratory chain containing an unusual diheme cytochrome *c₁*. *Arch. Microbiol.*, **175**, 282–294.
42. Schäfer, A., Tauch, A., Jäger, W., Kalinowski, J., Thierbach, G. and Pühler, A. (1994) Small mobilizable multi-purpose cloning vectors derived from the *Escherichia coli* plasmids pK18 and pK19: selection of defined deletions in the chromosome of *Corynebacterium glutamicum*. *Gene*, **145**, 69–73.
43. Gibson, D.G., Young, L., Chuang, R.Y., Venter, J.C., Hutchison, C.A. 3rd and Smith, H.O. (2009) Enzymatic assembly of DNA molecules up to several hundred kilobases. *Nat. Methods*, **6**, 343–345.
44. Pfeifer, E., Hünnefeld, M., Popa, O., Polen, T., Kohlheyer, D., Baumgart, M. and Frunzke, J. (2016) Silencing of cryptic prophages in *Corynebacterium glutamicum*. *Nucleic Acids Res.*, **44**, 10117–10131.
45. Langmead, B. and Salzberg, S.L. (2012) Fast gapped-read alignment with Bowtie 2. *Nat. Methods*, **9**, 357–359.
46. Baumgart, M., Unthan, S., Kloss, R., Radek, A., Polen, T., Tenhaef, N., Müller, M.F., Kubler, A., Siebert, D., Bruhl, N. et al. (2018) *Corynebacterium glutamicum* Chassis C1*: Building and testing a novel platform host for synthetic biology and industrial biotechnology. *ACS Synth. Biol.*, **7**, 132–144.
47. Pachter, L. (2011) Models for transcript quantification from RNA-Seq. *Conference Proceedings*. arXiv: <https://arxiv.org/abs/1104.3889>, 13 May 2011, preprint: not peer reviewed.
48. Sakamoto, J., Shibata, T., Mine, T., Miyahara, R., Torigoe, T., Noguchi, S., Matsushita, K. and Sone, N. (2001) Cytochrome c oxidase contains an extra charged amino acid cluster in a new type of respiratory chain in the amino-acid-producing Gram-positive bacterium *Corynebacterium glutamicum*. *Microbiology*, **147**, 2865–2871.
49. Dailey, H.A. and Gerdes, S. (2015) HemQ: an iron-coproporphyrin oxidative decarboxylase for protoheme synthesis in Firmicutes and Actinobacteria. *Arch. Biochem. Biophys.*, **574**, 27–35.
50. Frunzke, J., Gätgens, C., Brocker, M. and Bott, M. (2011) Control of heme homeostasis in *Corynebacterium glutamicum* by the two-component system HrrSA. *J. Bacteriol.*, **193**, 1212–1221.
51. Alvarez-Peral, F.J., Zaragoza, O., Pedreno, Y. and Arguelles, J.C. (2002) Protective role of trehalose during severe oxidative stress caused by hydrogen peroxide and the adaptive oxidative stress response in *Candida albicans*. *Microbiology*, **148**, 2599–2606.
52. Kuehne, A., Emmert, H., Soehle, J., Winnefeld, M., Fischer, F., Wenck, H., Gallinat, S., Terstegen, L., Lucius, R., Hildebrand, J. et al. (2015) Acute activation of oxidative pentose phosphate pathway as First-Line response to oxidative stress in human skin cells. *Mol. Cell*, **59**, 359–371.
53. Ralsler, M., Wamelink, M.M., Latkolik, S., Jansen, E.E., Lehrach, H. and Jakobs, C. (2009) Metabolic reconfiguration precedes transcriptional regulation in the antioxidant response. *Nat. Biotechnol.*, **27**, 604–605.
54. Wennerhold, J. and Bott, M. (2006) The DtxR regulon of *Corynebacterium glutamicum*. *J. Bacteriol.*, **188**, 2907–2918.
55. Lindner, S.N., Seibold, G.M., Henrich, A., Kramer, R. and Wendisch, V.F. (2011) Phosphotransferase system-independent glucose utilization in *Corynebacterium glutamicum* by inositol permeases and glucokinases. *Appl. Environ. Microbiol.*, **77**, 3571–3581.
56. Bibb, L.A., King, N.D., Kunkle, C.A. and Schmitt, M.P. (2005) Analysis of a heme-dependent signal transduction system in

6562 *Nucleic Acids Research*, 2020, Vol. 48, No. 12

- Corynebacterium diphtheriae*: deletion of the *chrAS* genes results in heme sensitivity and diminished heme-dependent activation of the *hmuO* promoter. *Infect. Immun.*, **73**, 7406–7412.
57. Bibb, L.A. and Schmitt, M.P. (2010) The ABC transporter HrtAB confers resistance to hemin toxicity and is regulated in a hemin-dependent manner by the ChrAS two-component system in *Corynebacterium diphtheriae*. *J. Bacteriol.*, **192**, 4606–4617.
 58. Bibb, L.A. and Schmitt, M.P. (2010) The ABC transporter, HrtAB, confers resistance to hemin toxicity and is regulated in a hemin-dependent manner by the ChrAS two-component system in *Corynebacterium diphtheriae*. *J. Bacteriol.*, **192**, 4606–4617.
 59. Sun, J., Hoshino, H., Takaku, K., Nakajima, O., Muto, A., Suzuki, H., Tashiro, S., Takahashi, S., Shibahara, S., Alam, J. *et al.* (2002) Hemoprotein Bach1 regulates enhancer availability of heme oxygenase-1 gene. *EMBO J.*, **21**, 5216–5224.
 60. Ratliff, M., Zhu, W., Deshmukh, R., Wilks, A. and Stojilkovic, I. (2001) Homologues of neisserial heme oxygenase in gram-negative bacteria: degradation of heme by the product of the *pigA* gene of *Pseudomonas aeruginosa*. *J. Bacteriol.*, **183**, 6394–6403.
 61. Schmitt, M.P. (1997) Transcription of the *Corynebacterium diphtheriae* *hmuO* gene is regulated by iron and heme. *Infect. Immun.*, **65**, 4634–4641.
 62. Hintze, K.J., Katoh, Y., Igarashi, K. and Theil, E.C. (2007) Bach1 repression of ferritin and thioredoxin reductase1 is heme-sensitive in cells and in vitro and coordinates expression with heme oxygenase1, beta-globin, and NAD(P)H quinone (oxido) reductase1. *J. Biol. Chem.*, **282**, 34365–34371.
 63. Dhakshinamoorthy, S., Jain, A.K., Bloom, D.A. and Jaiswal, A.K. (2005) Bach1 competes with Nrf2 leading to negative regulation of the antioxidant response element (ARE)-mediated NAD(P)H:quinone oxidoreductase 1 gene expression and induction in response to antioxidants. *J. Biol. Chem.*, **280**, 16891–16900.
 64. Kuehne, A., Emmert, H., Soehle, J., Winnefeld, M., Fischer, F., Wene, H., Gallinat, S., Terstegen, L., Lucius, R., Hildebrand, J. *et al.* (2015) Acute activation of oxidative pentose phosphate pathway as First-Line response to oxidative stress in human skin cells. *Mol. Cell*, **59**, 359–371.
 65. Hillion, M., Imber, M., Pedre, B., Bernhardt, J., Saleh, M., Loi, V.V., Maaß, S., Becher, D., Astolfi Rosado, L., Adrian, L. *et al.* (2017) The glyceraldehyde-3-phosphate dehydrogenase GapDH of *Corynebacterium diphtheriae* is redox-controlled by protein S-mycothiolation under oxidative stress. *Sci. Rep.*, **7**, 5020.
 66. Baumgart, M., Luder, K., Grover, S., Gatgens, C., Besra, G.S. and Frunzke, J. (2013) IpsA, a novel LacI-type regulator, is required for isonitrol-derived lipid formation in *Corynebacteria* and *Mycobacteria*. *BMC Biol.*, **11**, 122.
 67. Dailey, H.A., Dailey, T.A., Gerdes, S., Jahn, D., Jahn, M., O'Brian, M.R. and Warren, M.J. (2017) Prokaryotic heme Biosynthesis: Multiple pathways to a common essential product. *Microbiol. Mol. Biol. Rev.*, **81**, e00048-16.
 68. Niebisch, A. and Bott, M. (2003) Purification of a cytochrome *bc-aa3* supercomplex with quinol oxidase activity from *Corynebacterium glutamicum*. Identification of a fourth subunit of cytochrome *aa3* oxidase and mutational analysis of diheme cytochrome *c1*. *J. Biol. Chem.*, **278**, 4339–4346.
 69. Mueller, J.P. and Taber, H.W. (1989) Isolation and sequence of *ctaA*, a gene required for cytochrome *aa3* biosynthesis and sporulation in *Bacillus subtilis*. *J. Bacteriol.*, **171**, 4967–4978.
 70. Svensson, B., Lubben, M. and Hederstedt, L. (1993) *Bacillus subtilis* CtaA and CtaB function in haem A biosynthesis. *Mol. Microbiol.*, **10**, 193–201.
 71. Auchter, M., Cramer, A., Huser, A., Ruckert, C., Emer, D., Schwarz, P., Arndt, A., Lange, C., Kalinowski, J., Wendisch, V.F. *et al.* (2011) RamA and RamB are global transcriptional regulators in *Corynebacterium glutamicum* and control genes for enzymes of the central metabolism. *J. Biotechnol.*, **154**, 126–139.
 72. Shah, A., Blombach, B., Gauttam, R. and Eikmanns, B.J. (2018) The RamA regulon: complex regulatory interactions in relation to central metabolism in *Corynebacterium glutamicum*. *Appl. Microbiol. Biotechnol.*, **102**, 5901–5910.
 73. Burkovski, A. (2007) Nitrogen control in *Corynebacterium glutamicum*: proteins, mechanisms, signals. *J. Microbiol. Biotechnol.*, **17**, 187–194.
 74. Schulte, J., Baumgart, M. and Bott, M. (2017) Identification of the cAMP phosphodiesterase CpdA as novel key player in cAMP-dependent regulation in *Corynebacterium glutamicum*. *Mol. Microbiol.*, **103**, 534–552.

3.4 A pseudokinase version of the histidine kinase ChrS promotes high heme tolerance of *Corynebacterium glutamicum*

Krüger A., Frunzke J.

Published in *Frontiers in Microbiology*, 2022.

Contributor Role	Contributor
Conceptualization	60% AK, 40% JF
Formal Analysis	100% AK
Investigation/Experiments	100% AK
Methodology	100% AK
Project Administration	50% AK, 50% JF
Software	100% AK
Supervision	50% AK, 50% JF
Visualization	100% AK
Writing – Original Draft Preparation	70% AK, 30% JF
Writing – Review & Editing	50% AK, 50% JF

Overall contribution AK: 80%

All of the presented experimental work was performed by AK, except for whole genome sequencing (Table 1) conducted by Ulrike Viets and qPCR on *hrtB* expression (Figure S4) which was done by the student Elvira Mukinovic, supervised by AK. Data analysis and visualization was performed by AK. The manuscript was mainly written by AK, and revised by JF and AK.



OPEN ACCESS

EDITED BY
Ulrike Kappler,
The University of Queensland, Australia

REVIEWED BY
Miaomiao Shi,
The University of Chicago,
United States
Haibi Wang,
Cornell University, United States

*CORRESPONDENCE
Julia Frunzke
j.frunzke@fz-juelich.de

SPECIALTY SECTION
This article was submitted to
Microbial Physiology and Metabolism,
a section of the journal
Frontiers in Microbiology

RECEIVED 18 July 2022
ACCEPTED 18 August 2022
PUBLISHED 07 September 2022

CITATION
Krüger A and Frunzke J (2022) A
pseudokinase version of the histidine
kinase ChrS promotes high heme
tolerance of *Corynebacterium
glutamicum*.
Front. Microbiol. 13:997448.
doi: 10.3389/fmicb.2022.997448

COPYRIGHT
© 2022 Krüger and Frunzke. This is an
open-access article distributed under
the terms of the [Creative Commons
Attribution License \(CC BY\)](https://creativecommons.org/licenses/by/4.0/). The use,
distribution or reproduction in other
forums is permitted, provided the
original author(s) and the copyright
owner(s) are credited and that the
original publication in this journal is
cited, in accordance with accepted
academic practice. No use, distribution
or reproduction is permitted which
does not comply with these terms.

A pseudokinase version of the histidine kinase ChrS promotes high heme tolerance of *Corynebacterium glutamicum*

Aileen Krüger and Julia Frunzke*

Forschungszentrum Jülich GmbH, Institute for Bio- and Geosciences 1, Jülich, Germany

Heme is an essential cofactor for almost all living cells by acting as prosthetic group for various proteins or serving as alternative iron source. However, elevated levels are highly toxic for cells. Several corynebacterial species employ two paralogous, heme-responsive two-component systems (TCS), ChrSA and HrrSA, to cope with heme stress and to maintain intracellular heme homeostasis. Significant cross-talk at the level of phosphorylation between these systems was previously demonstrated. In this study, we have performed a laboratory evolution experiment to adapt *Corynebacterium glutamicum* to increasing heme levels. Isolated strains showed a highly increased tolerance to heme growing at concentrations of up to 100 μM . The strain featuring the highest heme tolerance harbored a frameshift mutation in the catalytic and ATPase-domain (CA-domain) of the *chrS* gene, converting it into a catalytically-inactive pseudokinase (ChrS_CA-fs). Reintroduction of the respective mutation in the parental *C. glutamicum* strain confirmed high heme tolerance and showed a drastic upregulation of *hrtBA* encoding a heme export system, conserved in Firmicutes and Actinobacteria. The strain encoding the ChrS pseudokinase variant showed significantly higher heme tolerance than a strain lacking *chrS*. Mutational analysis revealed that induction of *hrtBA* in the evolved strain is solely mediated via the cross-phosphorylation of the response regulator (RR) ChrA by the kinase HrrS and BACTH assays revealed the formation of heterodimers between HrrS and ChrS. Overall, our results emphasize an important role of the ChrS pseudokinase in high heme tolerance of the evolved *C. glutamicum* and demonstrate the promiscuity in heme-dependent signaling of the paralogous two-component systems facilitating fast adaptation to changing environmental conditions.

KEYWORDS

adaptive laboratory evolution (ALE), heme, pseudokinase, two-component system (TCS), histidine kinase, CA-domain

Introduction

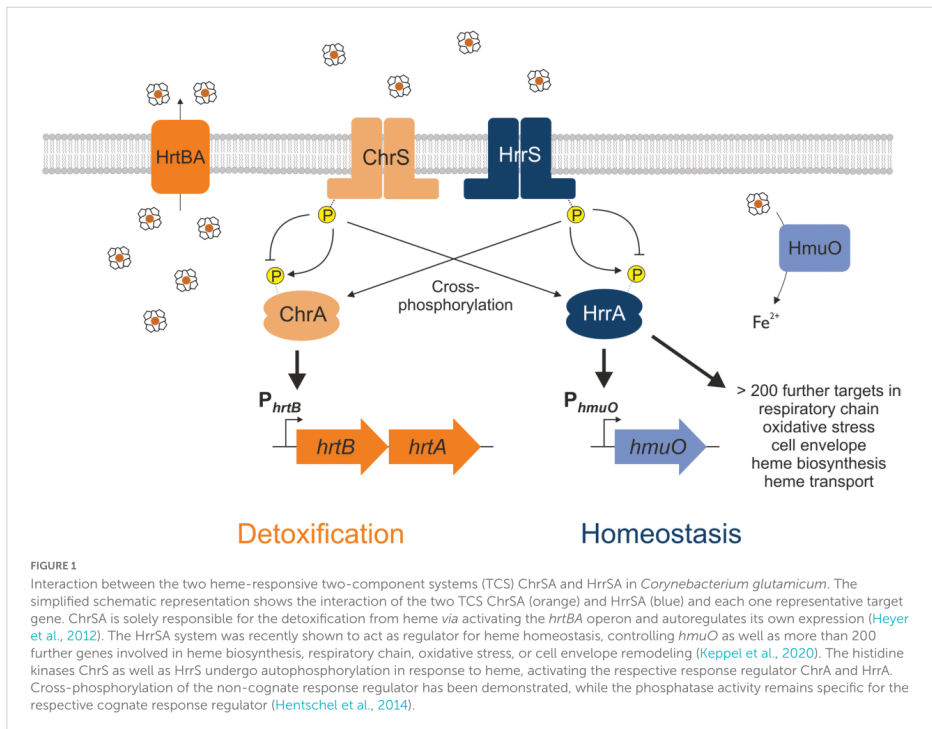
Heme constitutes 95% of functional iron in the human body and is a key molecule for almost all living cells (Ponka, 1999; Andrews et al., 2003) acting as cofactor for many important proteins, including cytochromes, hydroxylases, catalases, peroxidases (Ajioka et al., 2006; Layer et al., 2010), and serving as alternative iron source (Anzaldi and Skaar, 2010). Nevertheless, elevated levels of this iron-bound protoporphyrin are highly cytotoxic. While this toxicity partially originates from the redox-active iron, causing the formation of reactive oxygen species (Kumar and Bandyopadhyay, 2005), a not yet unraveled porphyrin-related toxicity is furthermore suggested (Stojiljkovic et al., 1999). Consequently, organisms have evolved sophisticated mechanisms ensuring heme homeostasis (Padmanaban et al., 1989; Anzaldi and Skaar, 2010). Among those, systems enhancing heme tolerance play an important role in both pathogenic and non-pathogenic prokaryotes. Known strategies include mechanisms of (i) heme sequestration (e.g., HemS of *Yersinia enterocolitica* Stojiljkovic and Hantke, 1994), (ii) heme degradation (e.g., IsdG of *Bacillus anthracis* Skaar et al., 2006), and (iii) heme export by the HrtBA system (Stauff and Skaar, 2009b; Heyer et al., 2012; Nakamura et al., 2022). The heme-dedicated ATP-binding cassette efflux pump HrtBA is a highly conserved system and predominantly found in Firmicutes and Actinobacteria (Krüger et al., 2022). Recent structural studies shed light on the mechanism HrtBA employs to sequester and extrude heme from the cytoplasmic membrane (Nakamura et al., 2022).

In Gram-positive bacteria, two-component systems (TCS) play a predominant role in the regulation of heme homeostasis (Bibb et al., 2007; Stauff and Skaar, 2009a; Hentschel et al., 2014; Keppel et al., 2019; Krüger et al., 2022). The prototypical TCS consists of a membrane-bound histidine kinase (HK), which undergoes autophosphorylation at a conserved histidine residue upon stimulus perception. Subsequently, the phosphoryl group is transferred to a conserved aspartate residue of a cytoplasmic response regulator (RR) resulting in an appropriate output, e.g., altering gene expression (Stock et al., 2000; Mascher et al., 2006; Laub and Goulian, 2007). HKs may be composed of multiple domains with a significant architectural diversity, but typically consist of an N-terminal transmembrane domain and a C-terminal transmitter domain. The transmitter domain can be split up in the dimerization and histidine phosphotransfer (DHp) domain and the catalytic and ATPase (CA) domain (Dutta et al., 1999; Gao and Stock, 2009). The CA-domain comprises four sequence motifs, including N, G1, F, and G2 boxes, which bind ATP in a pocket using an ATP lid and are consequently necessary for the autophosphorylation reaction (Kim and Forst, 2001; Wolanin et al., 2002). The DHp-domain possesses the H box motif harboring the conserved histidine residue which is phosphorylated upon stimulus

perception (Dutta et al., 1999), as well as the X box, which is required for dimerization. The DHp- and CA-domain are connected *via* a flexible linker, which probably also supports keeping the RR in place during the phosphotransfer reaction (Casino et al., 2009). Many HKs are bifunctional possessing also a phosphatase motif and subsequently acting both as kinase and phosphatase for the RR (Perego and Hoch, 1996; Laub and Goulian, 2007; Hentschel et al., 2014). Furthermore, also catalytically inactive variants of kinases have been identified, referred to as pseudokinases, that can act as important signaling modulators by various mechanisms (Raju and Shaw, 2015; Kung and Jura, 2019; Kwon et al., 2019; Mace and Murphy, 2021).

Gene duplication events facilitate the evolution of TCS signaling enabling the integration of new input signals and diversification of the gene regulatory network. Members of the *Corynebacteriaceae* family, including the Gram-positive soil bacterium *Corynebacterium glutamicum*, represent an interesting example of a recent gene duplication event, encoding two paralogous two-component systems that both respond to the multifaceted molecule heme (Figure 1). After sensing heme availability *via* intramembrane interaction (Ito et al., 2009; Keppel et al., 2018), the TCS ChrSA acts as an activator of the *hrtBA* operon encoding the heme export system (Heyer et al., 2012). In contrast, the paralogous TCS HrrSA is a global regulator of heme homeostasis controlling more than 200 genomic targets including inter alia genes involved in heme biosynthesis, respiration as well as *hmuO*, encoding heme oxygenase (Keppel et al., 2020). Strikingly, a high level of cross-phosphorylation between the systems was observed (Keppel et al., 2019), while phosphatase activity of these HKs remains specific to their cognate RR (Hentschel et al., 2014).

In this study, we addressed the question how this underlying signaling cascade consisting of two paralogous TCSs facilitates fast adaptation to high heme levels, such as encountered by pathogenic species in the mammalian host, using the non-pathogenic *C. glutamicum* as a model. Understanding the mechanisms underlying microbial heme tolerance are not only important for the control of bacterial infections but also of biotechnological relevance for the engineering of a microbial production host demanding high product tolerance (Ko et al., 2021). Adaptive laboratory evolution (ALE) of *C. glutamicum* to increased heme levels resulted in the isolation of highly heme-tolerant clones bearing mutations in the CA-domain of ChrS. The catalytically inactive ChrS pseudokinase was shown to be required for the efficient activation of ChrA *via* the paralogous HK HrrS. Overall, this study demonstrated the potential of this ALE approach to provide new mechanistic insights in heme-dependent signaling and highlights the flexibility of paralogous TCS signaling facilitating the fast adaptation to enhanced heme levels.



Materials and methods

Bacterial strains and growth conditions

Bacterial strains used in this study are listed in [Supplementary Table 1](#). For standard cultivation, *C. glutamicum* cells ATCC 13032 (wild type) and derivatives were streaked on agar plates (17 g/l) containing brain heart infusion (BHI) (Difco, BD, Heidelberg, Germany) (37 g/l) and inoculated at 30°C overnight. One single colony was picked and incubated for approximately 8 h at 30°C in 5 ml BHI in reaction tubes (for cultivation in shake flasks) or in 1 ml BHI in deep-well plates (VWR International, PA, United States) (for microtiter cultivation). This first pre-culture was used to inoculate the second pre-culture 1:10 in CGXII minimal medium (Keilhauer et al., 1993) supplemented with 2% (w/v) glucose but without any iron source to starve the cells from iron allowing the usage of heme as alternative iron source in the main culture. CGXII medium without FeSO₄ is in the following referred to as “iron-free CGXII.” If appropriate, 25 µg/ml kanamycin was added to the medium.

Incubation followed shaking at 120 rpm over night at 30°C. For the main experiment, cultures were inoculated to an OD₆₀₀ of 1 in iron-free CGXII with 2% (w/v) glucose, and the respective amount of hemin (Sigma-Aldrich, St. Louis, United States). For simplicity, hemin is further referred to as heme throughout this study.

For the ALE experiment, the main culture was grown in deep-well plates for 1–3 days and then freshly transferred at an OD₆₀₀ of 1 for the next batch. After the 13th inoculation, glycerol stocks of each population were frozen at –80°C. This allowed a restreaking of each potentially heterogeneous population on BHI-agar plates and picking of single evolved clones. Online monitoring of bacterial growth was performed using the BioLector® microtiter cultivation system of Beckman Coulter GmbH (Baesweiler) (Kensy et al., 2009). Backscatter (a.u.) was measured in 30 min intervals as scattered light with a wavelength of 620 nm (gain: 20); YFP-fluorescence was measured at an excitation wavelength of 508 nm and an emission wavelength of 532 nm (gain: 80). Specific fluorescence (a.u.) was calculated by dividing the YFP-signal by the backscatter signal for each measurement.

Escherichia coli strains including DH5 α and BTH101 were cultivated in Lysogeny Broth (10 g/l tryptone, 5 g/l yeast extract, 10 g/l NaCl) medium at 37°C in a rotary shaker and if needed for selection, 50 μ g/ml kanamycin or 100 μ g/ml ampicillin was added to the medium.

Recombinant DNA work

Standard molecular methods were performed according to Sambrook and Russell (2001). For polymerase chain reactions (PCR) amplification of DNA fragments, chromosomal DNA of *C. glutamicum* ATCC 13032 was used as template and prepared as described previously (Eikmanns et al., 1994). Synthesis of oligonucleotides as well as sequencing was performed by Eurofins Genomics (Ebersberg, Germany).

Plasmids were constructed by amplifying DNA fragments using the respective oligonucleotides (Supplementary Tables 2, 3) and enzymatically ligated into a pre-cut vector backbone using Gibson assembly (Gibson et al., 2009).

For the deletion of genes in the genome of *C. glutamicum*, the suicide vector pK19-*mobsacB* was used (Schäfer et al., 1994). Electrocompetent *C. glutamicum* cells were transformed with the respective isolated plasmids by electroporation (van der Rest et al., 1999). Subsequently, the first and second recombination events were performed and verified as described in previous studies (Niebisch and Bott, 2001). The respective deletion was confirmed by amplification and sequencing.

Whole genome sequencing

Whole genome resequencing of *C. glutamicum* strains isolated during the ALE experiment was performed using next generation sequencing (NGS). Genomic DNA was prepared using the NucleoSpin microbial DNA kit (Macherey-Nagel, Düren, Germany) according to manufacturer's instructions. Concentrations of the purified genomic DNA were measured using Qubit 2.0 fluorometer (Invitrogen, Carlsbad, CA, United States) according to manufacturer's instructions. The purified genomic DNA was used for the preparation for genome sequencing using NEBNext Ultra II DNA Library Kit for Illumina (New England BioLabs, Frankfurt am Main) and MiSeq Reagent Kit v2 (300-cycles) (Illumina, San Diego, CA, United States), according to manufacturer's instructions. A MiSeq system (Illumina, San Diego, CA, United States) was used for sequencing. Data analysis and base calling were accomplished with the Illumina instrument software. FASTQ output files were analyzed for single nucleotide polymorphisms using

PathoSystems Resource Integration Center (PATRIC) 3.6.12 (Davis et al., 2020).

Gradient plates

For heme gradient plates, the different mutant strains were cultivated in triplicates as described above using deep-well plates for the first and second pre-culture. Subsequently, cultures were harvested and resuspended to an OD₆₀₀ of 1 in 0.9% NaCl. For each spot, 2 μ l of the respective samples were spotted on the gradient plates. The gradient plates were always prepared freshly. Therefore, 30 ml of iron-free CGXII with 2% (w/v) glucose, and 17 g/l Bacto Agar (Difco, BD, Heidelberg, Germany) was poured into a squared agar plate, which was in inclined position. Then, after drying of the first layer, the incline was removed and further 30 ml of iron-free CGXII containing 2% glucose, and 15 μ M heme were poured in the plates so that a heme gradient results.

Bacterial two-hybrid assays

Bacterial two-hybrid plate assays for the qualitative assessment of protein-protein interactions

Bacterial two-hybrid assays were performed based on the BACTH kit according to manufacturer's instructions (Euromedex, Souffelweyersheim, France). This method is based on the two fragments T25 and T18 of the catalytic domain of the adenylate cyclase from *Bordetella pertussis*, which is only active when these two fragments are physically in close contact. Therefore, T25 and T18 were each fused once to ChrS, ChrS-Ala245fs, and HrrS. If the HKs interact with each other, this allows a functional complementation of T25 and T18, leading to cAMP synthesis, which binds to the catabolic activator protein (CAP). cAMP/CAP complexes are pleiotropic regulators of gene transcription in *E. coli* and therefore turn on the expression of e.g., the *lac* operon.

Therefore, *E. coli* BTH101, which lack adenylate cyclase activity, were transformed with two plasmids of heterologous proteins fused once to T25 and once to T18. This approach was directly diluted and spotted as 10⁰, 10⁻¹, and 10⁻² dilutions on LB plates containing 40 μ g/ml X-Gal, 50 μ g/ml kanamycin, 100 μ g/ml ampicillin, and 0.5 mM IPTG and incubated approximately 24 h at 30°C. Bacteria producing interacting proteins will form blue colonies. Otherwise, the colonies remain white. This allowed to check also for heterogeneity in expression. Additionally, the approach was also plated on LB plates only with antibiotics, to

allow picking for further biological replicates for the β -galactosidase assay.

Bacterial two-hybrid β -galactosidase measurements

Transformed *E. coli* strains (compare 1.5.1) were re-cultivated in deep-well plates as triplicates in LB media with 50 μ g/ml kanamycin, 100 μ g/ml ampicillin and 0.5 mM IPTG. OD₆₀₀ of the overnight cultures was measured in a Tecan Reader (Thermo Fisher Scientific, Massachusetts, United States). The β -galactosidase assay was adapted according to a previous study for 96-well plates (Griffith and Wolf, 2002). Per sample, 1 ml Z-buffer (60 mM Na₂HPO₄ \times 12H₂O, 40 mM NaH₂PO₄ \times H₂O, 10 mM KCl, 1 mM MgSO₄ \times 7H₂O, 50 mM β -mercaptoethanol) was mixed with 20 μ l 0.1% SDS, 40 μ l chloroform and 200 μ l of cell culture. The solution was resuspended 15 times for permeabilization. 100 μ l of the permeabilized cells were put into a microtiter plate, where each 20 μ l of 4 mg/ml o-nitrophenol- β -galactosidase (ONPG) was added. When a yellowish color was observable (10 min), 50 μ l of 1 M Na₂CO₃ was added for reaction termination. Using the Tecan Reader (Thermo Fisher Scientific, Massachusetts, United States), A₄₂₀ and A₅₅₀ was measured. The Miller Unit, representing the standardized amount of β -Gal activity, was calculated using the following formula:

$$1 \text{ MU} = 1000 * \frac{(A_{420} - (A_{550} * 1.75))}{(t * v * A_{600})} \quad (1)$$

With A₄₂₀ being the absorbance of the yellow o-nitrophenol, A₅₅₀ the scatter from the cell debris, 1.75 is the factor which needs to be multiplied with A₅₅₀ to approximate scatter observed at 420 nm, t is time in minutes, v is the volume of the culture employed in the plate and A₆₀₀ for the cell density. The value of A₆₀₀ was calibrated to proper OD₆₀₀.

DNA microarrays

For the analysis of the transcriptome, *C. glutamicum* wild type and *C. glutamicum* ChrS-Ala245fs were cultivated in triplicates as described above in 50 ml CGXII medium containing 2% glucose, no FeSO₄ and 4 μ M heme in shake flasks. Cells were harvested after 6 h, when the wild type reached an OD₆₀₀ around 2.5 and the mutated strain around 5. The cell suspension was centrifuged at 4,250 \times g, 10 min, 4°C in falcons filled with ice. The resulting pellets were frozen in liquid nitrogen and stored at -80°C. The following RNA preparation, cDNA synthesis, microchip hybridization, scanning, and overall evaluation was performed as described in previous studies (Baumgart et al., 2013). The microarray

data described in this study are available at NCBI's Gene Expression Omnibus under the GEO accession number GSE206796.

Results

Adaptive laboratory evolution of *Corynebacterium glutamicum* toward tolerance of high heme levels depends on the heme exporter HrtBA

Previous studies reported a crucial role of the two-component system ChrSA for heme tolerance of *C. glutamicum* (Heyer et al., 2012). Figures 2A,B show characteristic growth curves of the *C. glutamicum* wild type (Figure 2A) and the deletion mutant Δ hrtBA (Figure 2B) on increasing concentrations of heme. Growing on standard conditions with 36 μ M FeSO₄ as iron source, the wild type displayed a growth rate of $0.42 \pm 0.01 \text{ h}^{-1}$. Lower heme concentrations between 2.5 and 5 μ M showed strongly reduced growth rates of 0.16 ± 0.003 and $0.20 \pm 0.003 \text{ h}^{-1}$, respectively, and reduced backscatter levels compared to the cultivation under non-limiting conditions. Higher concentrations between 10 and 15 μ M heme exhibited restored backscatter levels and growth rates of 0.22 ± 0.005 and $0.27 \pm 0.012 \text{ h}^{-1}$, but were accompanied by an elongated lag phase as a result of heme toxicity. This effect of toxicity was even more evident for the growth of a strain lacking the operon *hrtBA*. While growth on standard conditions and low concentrations of heme were comparable to the WT, higher concentrations led to a significantly elongated lag phase of ~35 and 50 h, respectively.

To elucidate mechanisms promoting high heme tolerance, we performed an ALE experiment applying increasing concentrations of heme to *C. glutamicum* wild type and the Δ hrtBA strain (Figure 2C). The ALE was accomplished in CGXII minimal medium, with 13 repetitive batch cultivations and started from each four independent single colonies, yielding four evolving populations. Batch cultures were started on 10 μ M heme and were stepwise increased to finally reach 60 μ M heme in the case of *C. glutamicum* wild type. From *C. glutamicum* wild type populations, four single clones were isolated from agar plates after the 13th batch cultivation and then further characterized in liquid culture (Figure 2D). Further analysis on earlier inoculation steps was also performed (Supplementary Figure 1). Remarkably, all isolates from the 13th inoculation were able to grow in the re-cultivation on medium containing up to 100 μ M heme where growth of the parental strain was completely inhibited. By contrast, heme levels above 15 μ M heme remained toxic to the Δ hrtBA strain and could not be increased throughout

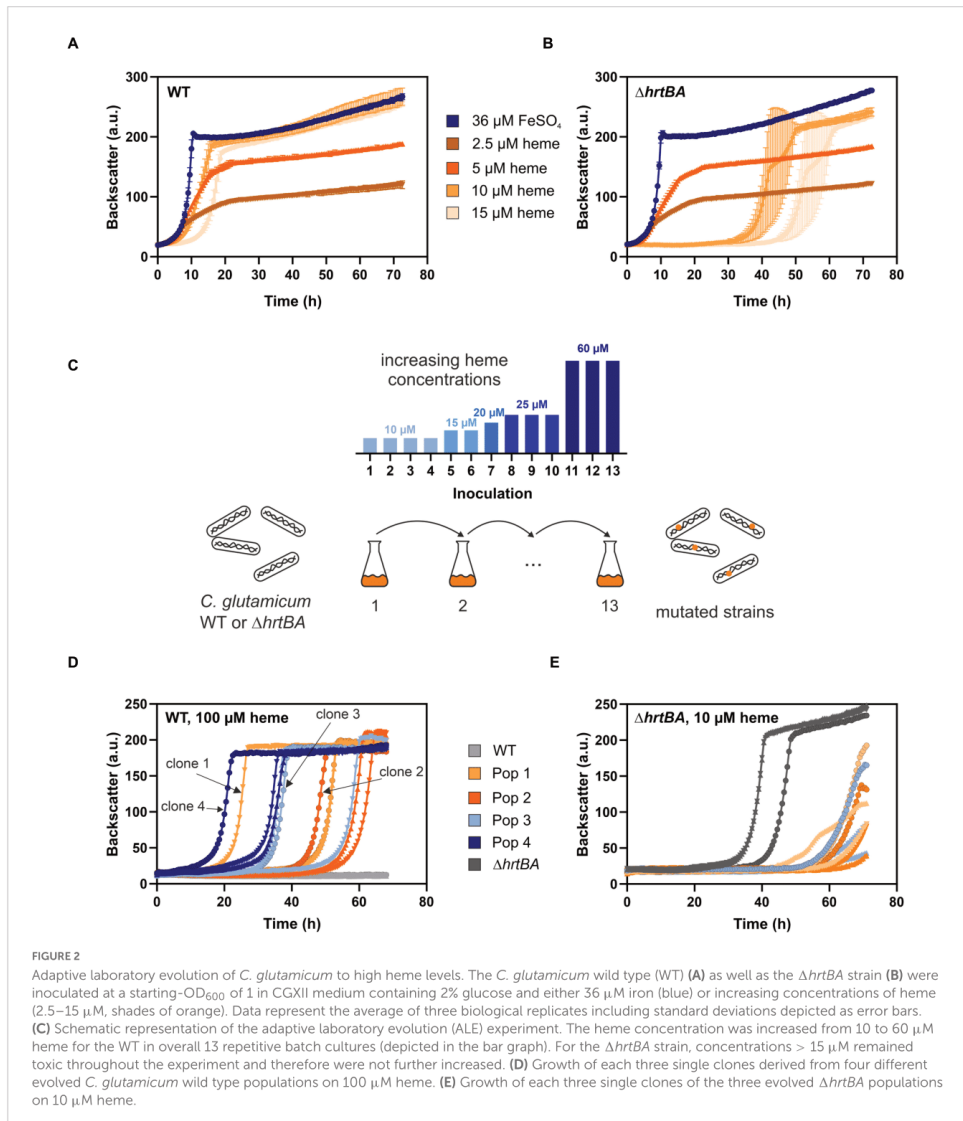


FIGURE 2

Adaptive laboratory evolution of *C. glutamicum* to high heme levels. The *C. glutamicum* wild type (WT) (A) as well as the $\Delta hrtBA$ strain (B) were inoculated at a starting- OD_{600} of 1 in CGXII medium containing 2% glucose and either 36 μM iron (blue) or increasing concentrations of heme (2.5–15 μM , shades of orange). Data represent the average of three biological replicates including standard deviations depicted as error bars. (C) Schematic representation of the adaptive laboratory evolution (ALE) experiment. The heme concentration was increased from 10 to 60 μM heme for the WT in overall 13 repetitive batch cultures (depicted in the bar graph). For the $\Delta hrtBA$ strain, concentrations > 15 μM remained toxic throughout the experiment and therefore were not further increased. (D) Growth of each three single clones derived from four different evolved *C. glutamicum* wild type populations on 100 μM heme. (E) Growth of each three single clones of the three evolved $\Delta hrtBA$ populations on 10 μM heme.

the ALE experiment without killing the cells. Only three of the four starting populations survived 13 inoculations and for these, no significant adaptation was observed throughout the ALE experiment (Figure 2E). These results already underlined that HrtBA represents a key factor for the adaptation of *C. glutamicum* to high heme levels.

Mutations in the catalytic- and ATPase domain of ChrS lead to significantly improved growth on heme

Whole genome sequencing of the four isolated clones from the ALE experiment revealed that all of them possess a mutation

in the gene encoding the HK ChrS (Table 1). Remarkably, in all four cases, the catalytic- and ATPase (CA) domain was affected. For clone 2, a stop codon was inserted directly at the beginning of the CA-domain, while clone 3 possesses an amino acid exchange inside and close to the start of this domain. Strikingly, clone 1 and 4 (evolved in two independent cell lines) showed the exact same frameshift mutation for alanine at position 245, immediately after the dimerization and histidine phosphotransfer (DHP) domain of ChrS. This mutation also affects the linker between the CA- and DHP-domain. Since the strains carrying this mutation showed the highest heme tolerance, evolved clone number 1, in the following referred to as 1.fs, was further analyzed within this study.

Reintegration of this mutation into the wild type parental strain confirmed that this frameshift mutation in *chrS* led to highly improved growth on heme (Figure 3A and Supplementary Figure 2). Protein structure prediction via AlphaFold2 shows the truncated CA-domain of ChrS-Ala245fs with additional 60 amino acids caused by the frameshift resulting in a presumably catalytically-inactive pseudokinase variant (Figure 3B; Jumper et al., 2021; Varadi et al., 2021).

The 1.fs strain showed normal growth under standard conditions. However, it outcompeted the wild type in the presence of heme at all concentrations tested, but not under iron starved conditions (Figures 3C,D and Supplementary Figure 2). A heme gradient plate experiment further confirmed the improved heme tolerance of the evolved clone 1.fs, and showed that this is also the case for the reintegrated pseudokinase variant ChrS-Ala245fs (Figure 3E).

The ChrS pseudokinase promotes increased *hrtBA* expression and is crucial for the improved growth on heme

The main known target of ChrA is the *hrtBA* operon encoding a heme export system. To unravel the impact of the frame-shift mutation in *chrS* on its activation kinetics, *hrtBA* reporter assays were performed, using the reporter plasmid pJC1-P_{*hrtBA*}-*eyfp* (Heyer et al., 2012). In fact, reporter assays (Figure 4A) showed a > 10-fold elevated expression of *hrtBA* in the evolved clone 1.fs compared to the WT. This also applies for strain carrying the reintegrated gene variant (Supplementary Figure 3A) and was further confirmed by qPCR (Supplementary Figure 4). Strikingly, *hrtBA* expression was constitutively high also during cultivation under standard conditions, i.e., without external addition of heme (Supplementary Figure 3).

In the following, we further analyzed the growth and *hrtBA* expression of the evolved clone in comparison to different mutant strains, including the deletion mutants Δ *chrS* and Δ *chrS* Δ *hrrS* as well as the phosphatase mutant *chrS*-Q191A

(Figures 3E, 4A; Hentschel et al., 2014). Heme gradient plates showed that the complete deletion of the *chrS* gene also led to an improved growth compared to the WT. This is caused by the abolished dephosphorylation of ChrA by its cognate kinase/phosphatase ChrS, allowing constant *hrtBA* expression due to cross talk with HrrS. The delay in *hrtBA* expression is explained by the less sensitive response of HrrS to heme (Keppel et al., 2019). Interestingly, the Δ *chrS* deletion strain grew worse than the evolved strain 1.fs. This is in line with the lower *hrtBA* expression level in comparison to 1.fs. These results indicated that the remaining part of ChrS, which is present in the evolved clone, must play a crucial role for this high activation. Strikingly, 1.fs also significantly outperformed the phosphatase mutant *chrS*-Q191A in terms of growth and *hrtBA* expression.

Considering that the frame-shift mutation in *chrS* likely abolished the catalytic activity of the ChrS kinase, we wondered whether activation of ChrA is solely dependent on HrrS. Cross-talk between the kinases was previously described (Hentschel et al., 2014) and might explain the activation of the *hrtBA* operon in the evolved clone. To test this hypothesis, the *hrrS* gene was deleted in evolved strain 1.fs and compared to a Δ *hrrS* mutant in the parental background. Figure 4B shows that upon deletion of *hrrS*, 1.fs grew with an elongated lag phase of ~50 h, which is even longer than for the WT. This result was in agreement with reporter assays showing that *hrrS* deletion also led to an abolishment of the *hrtBA* expression in 1.fs (Figure 4C). These results confirmed our hypothesis that HrrS is essential for activating *hrtBA* expression in the evolved clone encoding the catalytically-inactive pseudokinase of ChrS. Deletion of *hrrA* in the evolved variant did not influence its improved heme tolerance, therefore indicating that this is mainly an effect of HrrS activating ChrA (Supplementary Figure 5A,B). Overexpression of *chrA* also improved the heme tolerance to some extent (Supplementary Figure 5C). Interestingly, a plasmid-based overexpression of *hrtBA* in the WT background led to growth defects, probably caused by severe iron/heme starvation due to the excessive heme export (Supplementary Figure 6). This is further supported by comparative transcriptome analyses showing a higher upregulation in the strain overexpressing *hrtBA* compared to the evolved clone. This demonstrates the necessity of a tight balance between export and intracellular iron availability to maintain homeostasis while achieving optimal heme tolerance.

To investigate if the truncated version of ChrS still plays a role in the phosphotransfer to ChrA, we exchanged the conserved histidine residue at position 186 to an alanine (Figure 4D). This amino acid exchange did, however, not significantly influence the heme tolerance of strain 1.fs. Therefore, it can be assumed that the truncated version of ChrS does not participate in the phosphotransfer via autophosphorylation at the histidine 186.

Based on these results, we postulated that a lack of the catalytic activity of ChrS is beneficial for *C. glutamicum* heme

TABLE 1 Key mutations identified in *C. glutamicum* strains featuring increased heme tolerance.

Clone	Type	Variance nucleotides	Variance amino acids	Locus
1.fs, 4.fs	Frameshift	733delG	Ala245fs	cg2201 Sensor histidine kinase ChrS
2.*	Non-sense	862C > T	Gln288*	
3. <	Missense	916A > C	Thr306Pro	

The * is the symbol for the insertion of a stop-codon. Similar, the > indicates an amino acid exchange.

tolerance. In line with this hypothesis, an in-frame deletion of the CA-domain of *chrS* led to improved growth on heme compared to the wild type. However, this strain did not reach comparably high heme tolerance like the 1.fs strain (Figure 4E). Upon additional deletion of the DHP-domain, this growth advantage was abolished suggesting the necessity of homo- or heterodimerization and/or interaction with ChrA.

ChrS and HrrS form heterodimers *in vivo*

In general, HKs act as homodimers. However, based on the fact that the autophosphorylation histidine residue of ChrS in the evolved mutant 1.fs was not relevant for its growth benefit on heme (Figure 4D), we aimed to investigate the homo- and heterodimerization properties of the *C. glutamicum* HKs ChrS and HrrS and the pseudokinase ChrS (ChrS_CA-fs).

To assess these protein-protein interactions between the respective monomers ChrS, HrrS and the truncated HK variant ChrS_CA-fs, we performed bacterial two-hybrid (BACTH) assays (Euromedex, Souffelweyersheim, France). The plate assays in Figure 5A as well as the quantitative β -galactosidase assay in Figure 5B show that homodimerization for both the native and the evolved HKs was observed when these fusion proteins were produced as C-terminal fusions in *E. coli*. The assays also revealed heterodimerization of the native HKs, while there was no significant evidence for heterodimerization of the truncated ChrS_CA-fs version. Similar results were observed when the proteins were produced as N-terminal fusions (Supplementary Figure 7).

In a next set of experiments, we investigated the interaction between the sensor kinases and the RRs. Here, BACTH assays confirmed the interaction of ChrS with ChrA and HrrS with HrrA, as well as the cross-talk between ChrS and HrrA. Interaction was not observed for ChrS_CA-fs and neither ChrA nor HrrA within the β -galactosidase assay, although a slight signal appeared to be visible on plates (Figure 5). However, the assays did also not reveal the already reported cross-talk between HrrS and ChrA (Hentschel et al., 2014) demonstrating also the limitations of the *in vivo* approach based on the *E. coli* system. Therefore, a direct interaction between ChrA and the evolved ChrS_CA-fs in the *C. glutamicum in vivo* background should not be excluded.

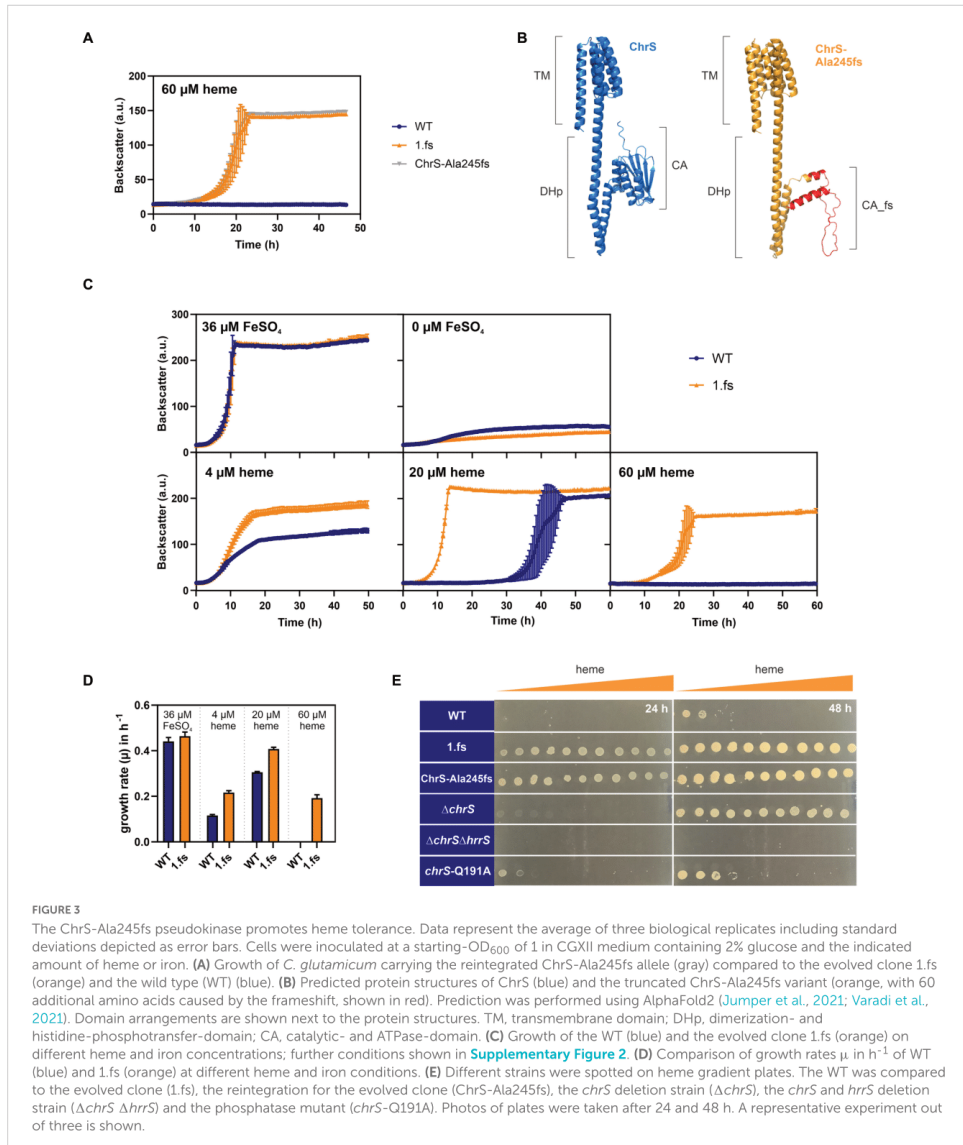
Heme-binding proteins contribute to heme tolerance

Within this study, we showed the crucial role of the HrtBA export system for *C. glutamicum* heme tolerance. To identify further potentially relevant factors, we performed a comparative transcriptome analysis of the ChrS-Ala245fs strain and *C. glutamicum* wild type (Table 2). As expected, the *hrtBA* operon showed significantly increased mRNA levels in the evolved clone (~150-fold increase). Besides *hrtBA*, several other heme-related targets also showed increased expression levels, including the TCS *chrSA* itself, *hmuO* encoding heme oxygenase and the heme transport system *hmuU*. Quantitative PCR confirmed unaltered expression levels of *hrrS* (Supplementary Figure 4). Strikingly, all genes encoding known heme-binding proteins were significantly upregulated. Furthermore, many targets of the DtxR regulon were upregulated (Wennerhold and Bott, 2006), while targets of the RipA regulon were downregulated (Wennerhold et al., 2005). This indicates that the evolved clone encounters a strong iron depletion, most likely caused by the extreme heme export. This is in line with a growth defect of this strain under iron starvation conditions (Figure 3C).

To test whether the upregulation of heme-binding proteins could also contribute to heme tolerance mediated by heme sequestration, we further analyzed the impact of heme binding proteins by the construction of serial deletions (Figure 6). A strain lacking the heme binding proteins *hmuT*, *htaA*, *htaB*, *htaC*, and *htaD* showed wild typical growth at low (4 μ M) and high (20 μ M) heme levels. However, at moderate (10 μ M) heme concentrations, the mutant showed a significant growth defect. These results suggested that heme sequestration *via* heme-binding proteins could promote heme tolerance at moderate levels.

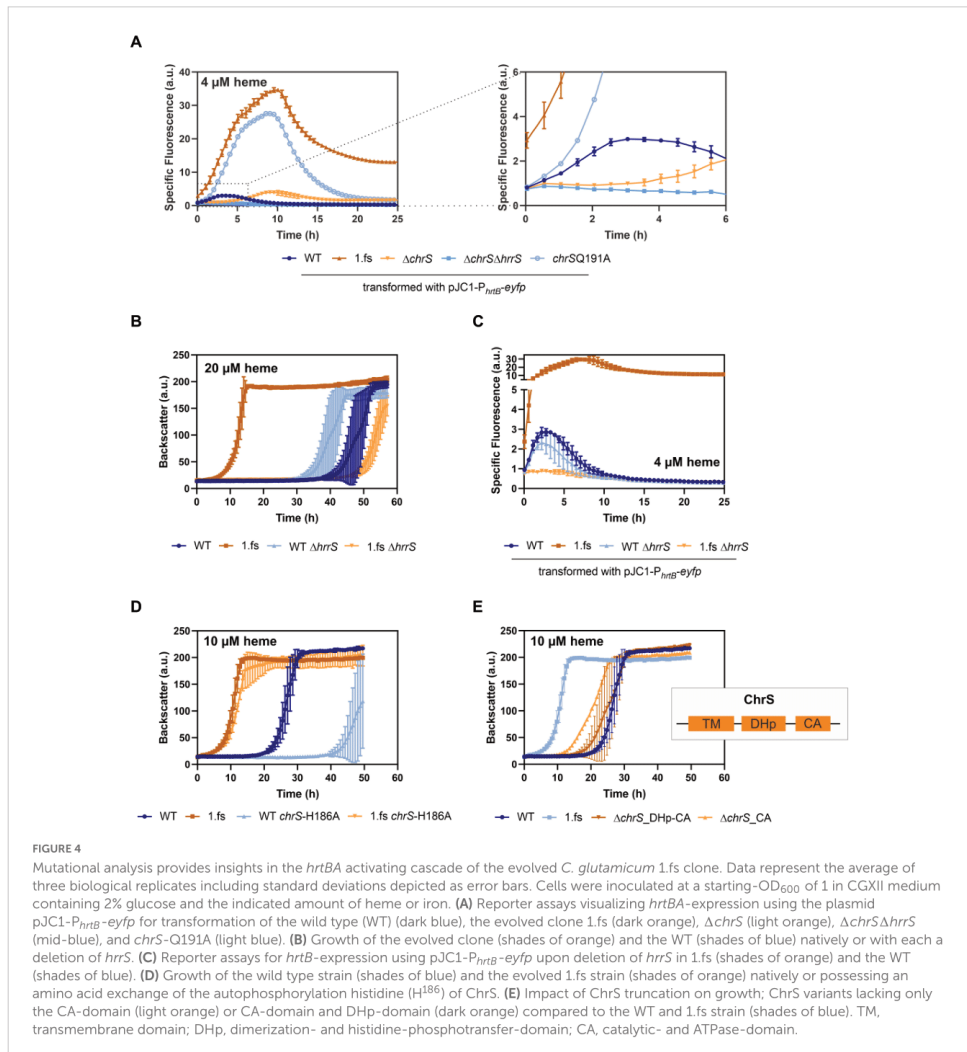
Discussion

In this study, we pursued a laboratory evolution approach to adapt *C. glutamicum* ATCC 13032 to high heme levels. This ALE approach resulted in the isolation of strains harboring a frameshift mutation in the *chrS* HK gene yielding a catalytically inactive pseudokinase, which was shown to promote high heme tolerance of up to 100 μ M. This effect could mainly be attributed



to the strong upregulation of the heme exporter HrtBA and was strictly dependent on phosphotransfer *via* the non-cognate HK HrrS to the RR ChrA. Further mutational analysis confirmed that the conserved histidine residue of the ChrS pseudokinase (ChrS_CA-fs) was not involved in this phosphotransfer reaction.

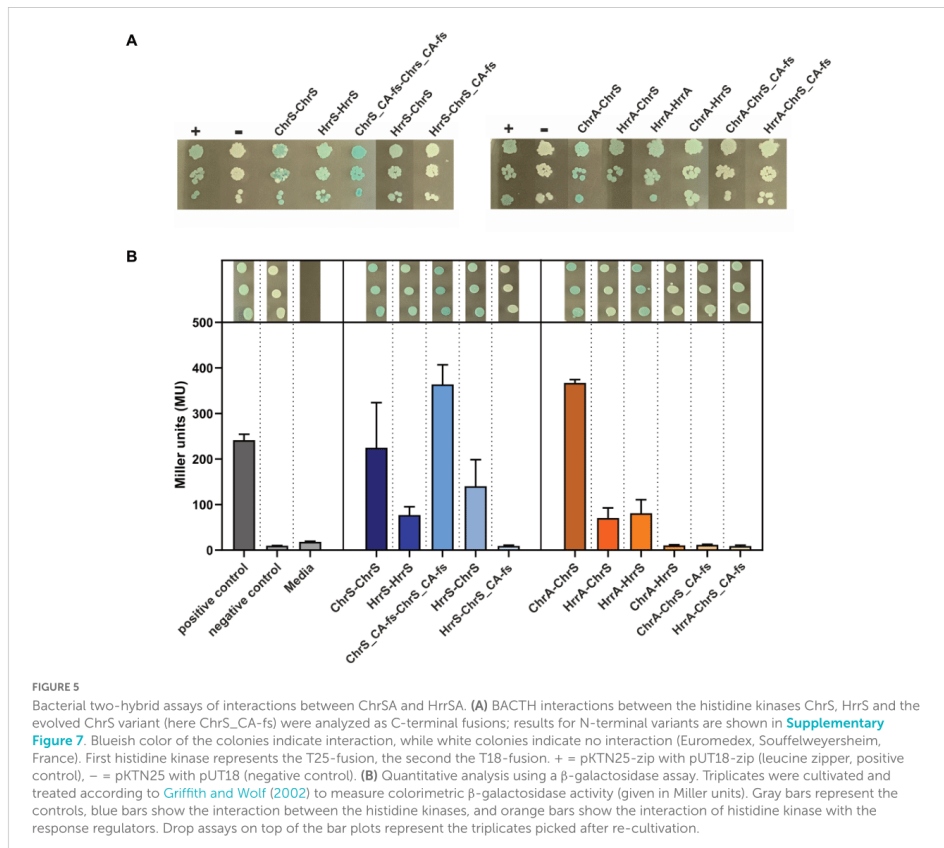
Continuously high *hrrS* expression levels observed in our evolved 1.fs strain are in agreement with a defect in ChrS phosphatase function of this strain. Remarkably, the evolved strains encoding the truncated pseudokinase variant ChrS showed significantly higher heme tolerance



and higher *hrtBA* expression levels compared to a phosphatase deficient strain *chrS*-Q191A or a strain lacking *chrS* completely (Δ *chrS*) (Hentschel et al., 2014). Consequently, dephosphorylation of ChrA seems to be abolished in the mutant clones, but the presence of the ChrS pseudokinase is apparently further beneficial for enhancing heme tolerance.

Our results indicate that the catalytically inactive version of ChrS promotes—directly or indirectly—the efficient

phosphotransfer reaction from the paralogous HrrS to ChrA leading to the constitutive activation of *hrtBA* (due to the absence of ChrS phosphatase activity). Gene duplication is a powerful evolutionary driving force and the presence of paralogs has previously been shown to be beneficial for adaptations to new environmental conditions (Gevers et al., 2004; Bratlie et al., 2010). In our study, the interaction between the two paralogous TCs HrrSA and ChrSA enabled fast adaptation and the evolution of novel



functionality of the signaling cascade based on the pseudokinase version of ChrS.

Pseudokinases are described as kinases lacking catalytic functions, but can contribute to signaling *via* functioning as allosteric modulators, dynamic scaffolds, or competitors of protein-protein interactions ([Reiterer et al., 2014](#); [Kwon et al., 2019](#); [Tomoni et al., 2019](#)). An example for a bacterial pseudokinase is DivL from *Caulobacter crescentus*. DivL controls the autophosphorylation of another HK CckA mediated by the phosphorylation status of the RR DivK. The direct interaction with DivL is required for maximal kinase activity of CckA, but this is achieved by a yet unknown mechanism ([Iniesta et al., 2010](#); [Tsokos et al., 2011](#); [Francis and Porter, 2019](#)). It was shown that neither the ATPase domain nor the autophosphorylation residue of DivL is necessary for its function ([Reisinger et al., 2007](#))—which is similar

to the scenario observed for ChrS in this study. It can therefore be hypothesized that the catalytically inactive ChrS pseudokinase has a stimulating effect on HrrS activity, e.g., by influencing its “on” or “off” states. An alternative or additional reason for enhanced phosphotransfer could also be the recruitment of ChrA *via* the ChrS pseudokinase fostering phosphotransfer from HrrS by the formation of heterodimers. In fact, heterodimerization between the native versions of ChrS and HrrS could be demonstrated using BACTH assays speaking for a direct signaling between ChrS and HrrS *in vivo*. However, interaction could not be observed with the truncated version of ChrS, but it has to be kept in mind that the *E. coli* based BACTH does not perfectly reflect the *C. glutamicum* *in vivo* situation. Here, we also observed high upregulation of the *chrSA* operon itself offering also enhanced levels of RR acceptor protein.

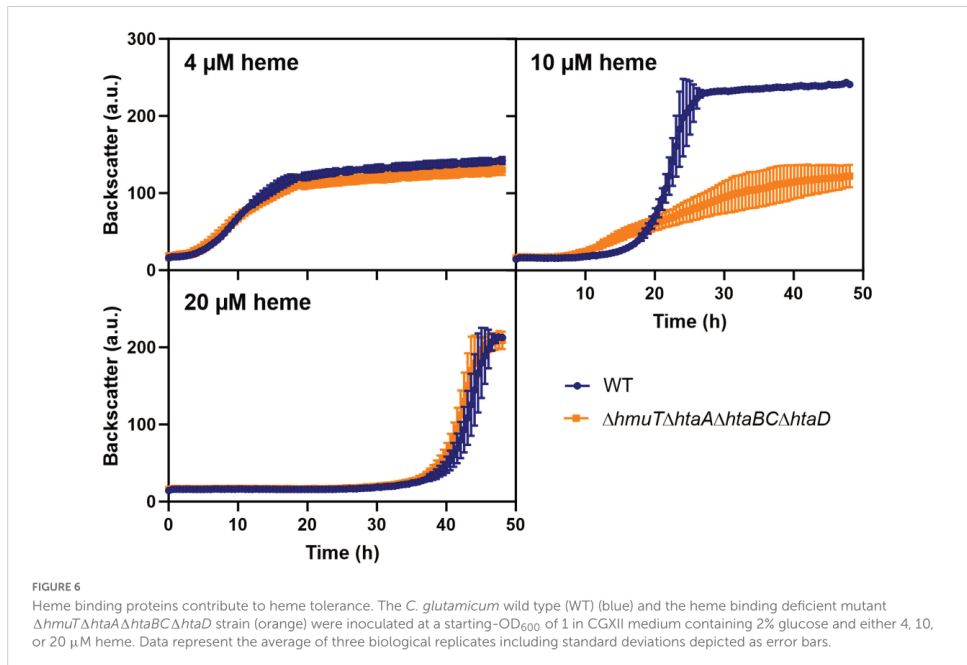
TABLE 2 Comparative transcriptome analysis of *C. glutamicum* wild type and *C. glutamicum* *chrS*-Ala245fs growing on 4 μ M heme.

Category and cg gene number	Gene designation and description of product	mRNA ratio ^a	P-value
Heme-related genes			
cg0468	<i>hmuU</i> , hemin transport system, permease protein	16.90	0.05
cg2200	<i>chrA</i> , two-component system, response regulator	8.85	0.01
cg2201	<i>chrS</i> , two-component system, signal transduction histidine kinase	43.60	0.04
cg2202	<i>hrtB</i> , ABC-type transport system, permease component	170.13	0.00
cg2204	<i>hrtA</i> , ABC-type transport system, ATPase component	151.54	0.00
cg2445	<i>hmuO</i> , heme oxygenase	8.30	0.01
Heme-binding proteins			
cg0466	<i>htaA</i> , secreted heme-transport associated protein	5.80	0.01
cg0467	<i>hmuT</i> , hemin-binding periplasmic protein precursor	21.23	0.06
cg0470	<i>htaB</i> , secreted heme transport-associated protein	66.64	0.02
cg0471	<i>htaC</i> , secreted heme transport-associated protein	16.87	0.04
cg3156	<i>htaD</i> , secreted heme transport-associated protein	18.64	0.05
DtxR regulon			
cg0160	Hypothetical protein cg0160	2.98	0.00
cg1120	<i>ripA</i> , transcriptional regulator of iron proteins, AraC family	5.76	0.10
cg1419	Putative Na ⁺ -dependent transporter	4.85	0.01
cg1476	<i>thiC</i> , thiamine biosynthesis protein ThiC	2.48	0.04
cg1695	Putative plasmid maintenance system antidote protein	0.34	0.05
cg1930	Putative secreted hydrolase	5.68	0.01
cg1930	Putative secreted hydrolase	5.68	0.01
cg1931	Putative secreted protein	9.98	0.05
cg1931	Putative secreted protein	9.98	0.05
cg2311	SAM-dependent methyltransferase	3.47	0.00
cg2444	Hypothetical protein cg2444	4.67	0.01
cg2782	<i>ftn</i> , ferritin-like protein	0.32	0.06
cg2796	MMGE/PRPD family protein	11.01	0.00
cg2962	Uncharacterized enzyme involved in biosynthesis of extracellular polysaccharides	6.69	0.02
RipA regulon			
cg0310	<i>kata</i> , catalase	0.14	0.00
cg0445	<i>sdhC</i> , succinate dehydrogenase	0.36	0.02
cg0446	<i>sdhA</i> , succinate dehydrogenase	0.40	0.00
cg0447	<i>sdhB</i> , succinate dehydrogenase	0.45	0.00
cg1343	<i>narH</i> , probable respiratory nitrate reductase oxidoreduct	0.49	0.03
cg1344	<i>narG</i> , nitrate reductase 2, alpha subunit	0.30	0.00
cg1487	<i>leuC</i> , isopropylmalate isomerase large subunit	0.29	0.01
cg1737	<i>acn</i> , aconitate hydratase	0.29	0.01
cg2636	<i>catA1</i> , catechol 1,2-dioxygenase	0.03	0.00
cg3048	<i>pta</i> , phosphate acetyltransferase	0.24	0.00

^aExpression of selected genes given as the mRNA ratio of the evolved strain compared to the WT (>2-fold or < 0.5-fold, p-value < 0.05). Data represent the average of three biological replicates (for a complete list of up- and downregulated genes, see [Supplementary Table 4](#)).

Although only a few reports on heterodimerization of HKs exist up to date (Capra and Laub, 2012; Willett and Crosson, 2017), studies in e.g., *Pseudomonas aeruginosa* showed that the HK RetS directly controls the HK GacS on three different levels by heterooligomerization (Goodman et al., 2009; Jing et al., 2010; Francis et al., 2018). Such pivotal (multiple) regulatory roles of heterodimers or -oligomers could also play a role in

the native *C. glutamicum* system. In previous studies, HrrS was shown to act as “kickstarter” of the ChrSA-mediated response and the absence of HrrS led to a delayed promoter activation of *hrtBA* (Keppel et al., 2019). Consistently, heterooligomerization of HrrS with ChrS could support the fast activation of ChrA when heme becomes available, e.g., by cross-phosphorylation on the HK-level. An alternative option could be an indirect



communication between ChrS and HrrS *via* another—yet unknown—component involved in cross-signaling (Buelow and Raivio, 2010; Salvado et al., 2012).

Apart from the conserved heme export system HrtBA, transcriptome analysis gave further hints for additional players contributing to heme tolerance in *C. glutamicum*. Here, we observed a high upregulation of all genes encoding heme-binding proteins and a deletion mutant showed reduced tolerance to intermediate heme levels. In fact, heme-binding proteins could serve a detoxifying role *via* heme sequestration, as described throughout the literature for other organisms, including HbpC of *Bartonella henselae* (Rodén et al., 2012), HemS of *Yersinia enterocolitica* (Stojiljkovic and Hantke, 1994) or HupZ of Group A *Streptococcus*, which has been recently hypothesized to function as heme chaperone (Lyles et al., 2022).

Moreover, several transport systems are differently expressed in the evolved strains. Export of further toxic heme-related products, or even import of neutralizing compounds coping with H_2O_2 , like e.g., described for the ribulose-5-phosphate 3-epimerase in *Escherichia coli* or the Mn(II) uptake system of *Neisseria gonorrhoeae* importing manganese (Horsburgh et al., 2002; Seib et al., 2004; Sobota and Imlay, 2011), could also aid at tolerating heme. Of special interest is e.g., the operon cg2675-cg2678, which encodes an ABC-type

transport system and was found also to be regulated by the heme-responsive RR HrrA (Keppel et al., 2020). Future studies on these systems, are however, required to elucidate their role in heme tolerance or homeostatic processes.

The appearance of a ChrS pseudokinase was not yet described to occur naturally in corynebacterial strains (Bott and Brocker, 2012). However, our experimental approach demonstrated their ability to quickly adapt to high heme levels, which is for example relevant for virulence conditions in the mammalian host (Stauff and Skaar, 2009a). In the soil environment, a constant expression of the *hrtBA* operon is likely too costly as reflected by the strong upregulation of the iron starvation response in the evolved clones, including the regulon of DtxR (Wennerhold and Bott, 2006) and the downregulation of RipA targets (Wennerhold et al., 2005). The native cascade consequently rather facilitates a fast but transient activation of *hrtBA* in response to heme levels (Keppel et al., 2019).

Strains featuring an elevated heme tolerance are also highly interesting for the biotechnological production of heme, which is commercially produced for medical uses or the food sector for artificial meat products. Recent metabolic engineering efforts resulted in *E. coli* (Kwon et al., 2003; Zhao et al., 2018) and *C. glutamicum* heme-producing strains (Ko et al., 2021)

achieving heme yields of about 0.14–0.61 mmol mol⁻¹. In this context, the pseudokinase variant of ChrS described in this study might aid future metabolic engineering approaches to promote efficient heme export and high product tolerance.

Data availability statement

The datasets presented in this study can be found in online repositories. The names of the repository/repositories and accession number(s) can be found in the article/[Supplementary material](#).

Author contributions

JF and AK conceived and designed the analysis and wrote the manuscript. AK performed the experiments and collected the data, contributed to data and analysis tools, and performed the analysis. Both authors contributed to the article and approved the submitted version.

Funding

This work was supported by the Helmholtz Association (grant no. W2/W3-096).

References

- Ajioka, R. S., Phillips, J. D., and Kushner, J. P. (2006). Biosynthesis of heme in mammals. *Biochim. Biophys. Acta* 1763, 723–736. doi: 10.1016/j.bbamcr.2006.05.005
- Andrews, S. C., Robinson, A. K., and Rodriguez-Quiriones, F. (2003). Bacterial iron homeostasis. *FEMS Microbiol. Rev.* 27, 215–237. doi: 10.1016/S0168-6445(03)00055-X
- Anzaldi, L. L., and Skaar, E. P. (2010). Overcoming the heme paradox: Heme toxicity and tolerance in bacterial pathogens. *Infect. Immun.* 78, 4977–4989. doi: 10.1128/IAI.00613-10
- Baumgart, M., Luder, K., Grover, S., Gätgens, C., Besra, G. S., and Frunzke, J. (2013). IpsA, a novel LacI-type regulator, is required for inositol-derived lipid formation in *Corynebacteria* and *Mycobacteria*. *BMC Biol.* 11:122. doi: 10.1186/1741-7007-11-122
- Bibb, L. A., Kunkle, C. A., and Schmitt, M. P. (2007). The ChrA-ChrS and HrrA-HrrS signal transduction systems are required for activation of the *hmuO* promoter and repression of the *hemaA* promoter in *Corynebacterium diphtheriae*. *Infect. Immun.* 75, 2421–2431. doi: 10.1128/IAI.01821-06
- Bott, M., and Brocker, M. (2012). Two-component signal transduction in *Corynebacterium glutamicum* and other corynebacteria: On the way towards stimuli and targets. *Appl. Microbiol. Biotechnol.* 94, 1131–1150. doi: 10.1007/s00253-012-4060-x
- Bratlie, M. S., Johansen, J., Sherman, B. T., Huang, D. W., Lempicki, R. A., and Drablos, F. (2010). Gene duplications in prokaryotes can be associated with environmental adaptation. *BMC Genomics* 11:588. doi: 10.1186/1471-2164-11-588
- Buelow, D. R., and Raivio, T. L. (2010). Three (and more) component regulatory systems – auxiliary regulators of bacterial histidine kinases. *Mol. Microbiol.* 75, 547–566. doi: 10.1111/j.1365-2958.2009.06982.x
- Capra, E. J., and Laub, M. T. (2012). Evolution of two-component signal transduction systems. *Annu. Rev. Microbiol.* 66, 325–347. doi: 10.1146/annurev-micro-092611-150039
- Casino, P., Rubio, V., and Marina, A. (2009). Structural insight into partner specificity and phosphoryl transfer in two-component signal transduction. *Cell* 139, 325–336. doi: 10.1016/j.cell.2009.08.032
- Davis, J. J., Wattam, A. R., Aziz, R. K., Brettin, T., Butler, R., Butler, R. M., et al. (2020). The PATRIC bioinformatics resource center: Expanding data and analysis capabilities. *Nucleic Acids Res.* 48, D606–D612. doi: 10.1093/nar/gkz943
- Dutta, R., Qin, L., and Inouye, M. (1999). Histidine kinases: Diversity of domain organization. *Mol. Microbiol.* 34, 633–640. doi: 10.1046/j.1365-2958.1999.01646.x
- Eikmanns, B. J., Thum-Schmitz, N., Eggeling, L., Lüttke, K.-U., and Sahl, H. (1994). Nucleotide sequence, expression and transcriptional analysis of the *Corynebacterium glutamicum* *gltA* gene encoding citrate synthase. *Microbiology* 140, 1817–1828. doi: 10.1099/13500872-140-8-1817
- Francis, V. I., and Porter, S. L. (2019). Multikinase networks: Two-component signaling networks integrating multiple stimuli. *Annu. Rev. Microbiol.* 73, 199–223. doi: 10.1146/annurev-micro-020518-115846
- Francis, V. I., Waters, E. M., Finton-James, S. E., Gori, A., Kadioglu, A., Brown, A. R., et al. (2018). Multiple communication mechanisms between sensor kinases are crucial for virulence in *Pseudomonas aeruginosa*. *Nat. Commun.* 9:2219. doi: 10.1038/s41467-018-04640-8

Acknowledgments

We thank Ulrike Viets for whole genome sequencing, Tino Polen for help with the microarrays and upload to databases and Elvira Mukinovic for assisting with the qPCR experiments.

Conflict of interest

AK and JF were employed by the Forschungszentrum Jülich GmbH.

Publisher's note

All claims expressed in this article are solely those of the authors and do not necessarily represent those of their affiliated organizations, or those of the publisher, the editors and the reviewers. Any product that may be evaluated in this article, or claim that may be made by its manufacturer, is not guaranteed or endorsed by the publisher.

Supplementary material

The Supplementary Material for this article can be found online at: <https://www.frontiersin.org/articles/10.3389/fmicb.2022.997448/full#supplementary-material>

- Gao, R., and Stock, A. M. (2009). Biological insights from structures of two-component proteins. *Annu. Rev. Microbiol.* 63, 133–154. doi: 10.1146/annurev.micro.091208.073214
- Gevers, D., Vandepoel, K., Smillion, C., and Van de Peer, Y. (2004). Gene duplication and biased functional retention of paralogs in bacterial genomes. *Trends Microbiol.* 12, 148–154. doi: 10.1016/j.tim.2004.02.007
- Gibson, D. G., Young, L., Chuang, R. Y., Venter, J. C., Hutchison, C. A. III, and Smith, H. O. (2009). Enzymatic assembly of DNA molecules up to several hundred kilobases. *Nat. Methods* 6, 343–345. doi: 10.1038/nmeth.1318
- Goodman, A. L., Merighi, M., Hyodo, M., Ventre, I., Filloux, A., and Lory, S. (2009). Direct interaction between sensor kinase proteins mediates acute and chronic disease phenotypes in a bacterial pathogen. *Genes Dev.* 23, 249–259. doi: 10.1101/gad.1739009
- Griffith, K. L., and Wolf, R. E. Jr. (2002). Measuring beta-galactosidase activity in bacteria: Cell growth, permeabilization, and enzyme assays in 96-well arrays. *Biochem. Biophys. Res. Commun.* 290, 397–402. doi: 10.1006/bbrc.2001.6152
- Hentschel, E., Mack, C., Gatgens, C., Bott, M., Brocker, M., and Frunzke, J. (2014). Phosphatase activity of the histidine kinases ensures pathway specificity of the ChrSA and HrrSA two-component systems in *Corynebacterium glutamicum*. *Mol. Microbiol.* 92, 1326–1342. doi: 10.1111/mmi.12633
- Heyer, A., Gatgens, C., Hentschel, E., Kalinowski, J., Bott, M., and Frunzke, J. (2012). The two-component system ChrSA is crucial for haem tolerance and interferes with HrrSA in haem-dependent gene regulation in *Corynebacterium glutamicum*. *Microbiology* 158, 3020–3031. doi: 10.1099/mic.0.062638-0
- Horsburgh, M. J., Wharton, S. J., Karavolos, M., and Foster, S. J. (2002). Manganese: Elemental defence for a life with oxygen. *Trends Microbiol.* 10, 496–501. doi: 10.1016/S0966-842X(02)02462-9
- Iniesta, A. A., Hillson, N. J., and Shapiro, L. (2010). Cell pole-specific activation of a critical bacterial cell cycle kinase. *Proc. Natl. Acad. Sci. U.S.A.* 107, 7012–7017. doi: 10.1073/pnas.1001767107
- Ito, Y., Nakagawa, S., Komagata, A., Ikeda-Saito, M., Shiro, Y., and Nakamura, H. (2009). Heme-dependent autophosphorylation of a heme sensor kinase, ChrS, from *Corynebacterium diphtheriae* reconstituted in proteoliposomes. *FEBS Lett.* 583, 2244–2248. doi: 10.1016/j.febslet.2009.06.001
- Jing, X., Jaw, J., Robinson, H. H., and Schubot, F. D. (2010). Crystal structure and oligomeric state of the RetS signaling kinase sensory domain. *Proteins* 78, 1631–1640. doi: 10.1002/prot.22679
- Jumper, J., Evans, R., Pritzel, A., Green, T., Figurnov, M., Ronneberger, O., et al. (2021). Highly accurate protein structure prediction with AlphaFold. *Nature* 596, 583–589. doi: 10.1038/s41586-021-03819-2
- Keilhauer, C., Eggeling, L., and Sahn, H. (1993). Isoleucine synthesis in *Corynebacterium glutamicum*: Molecular analysis of the *ilvB-ilvN-ilvC* operon. *J. Bacteriol.* 175, 5595–5603. doi: 10.1128/jb.175.17.5595-5603.1993
- Kensy, F., Zang, E., Faulhammer, C., Tan, R.-K., and Büchs, J. (2009). Validation of a high-throughput fermentation system based on online monitoring of biomass and fluorescence in continuously shaken microtiter plates. *Microb. Cell Fact.* 8:31. doi: 10.1186/1475-2859-8-31
- Keppel, M., Davoudi, E., Gätgens, C., and Frunzke, J. (2018). Membrane topology and heme binding of the histidine kinases HrrS and ChrS in *Corynebacterium glutamicum*. *Front. Microbiol.* 9:183. doi: 10.3389/fmicb.2018.002183
- Keppel, M., Hünnefeld, M., Filipchik, A., Viets, U., Davoudi, C. F., Krüger, A., et al. (2020). HrrSA orchestrates a systemic response to heme and determines prioritization of terminal cytochrome oxidase expression. *Nucleic Acids Res.* 48, 6547–6562. doi: 10.1093/nar/gkaa415
- Keppel, M., Piepenbreier, H., Gatgens, C., Fritz, G., and Frunzke, J. (2019). Toxic but tasty - temporal dynamics and network architecture of heme-responsive two-component signaling in *Corynebacterium glutamicum*. *Mol. Microbiol.* 111, 1367–1381. doi: 10.1111/mmi.14226
- Kim, D. J., and Forst, S. (2001). Genomic analysis of the histidine kinase family in bacteria and archaea. *Microbiology (Reading)* 147, 1197–1212. doi: 10.1099/00221287-147-5-1197
- Ko, Y. J., Kim, M., You, S. K., Shin, S. K., Chang, J., Choi, H. J., et al. (2021). Animal-free heme production for artificial meat in *Corynebacterium glutamicum* via systems metabolic and membrane engineering. *Metabolic Eng.* 66, 217–228. doi: 10.1016/j.ymben.2021.04.013
- Krüger, A., Keppel, M., Sharma, V., and Frunzke, J. (2022). The diversity of heme sensor systems - heme-responsive transcriptional regulation mediated by transient heme protein interactions. *FEMS Microbiol. Rev.* 46:fua002. doi: 10.1093/femsre/fua002
- Kumar, S., and Bandyopadhyay, U. (2005). Free heme toxicity and its detoxification systems in human. *Toxicol. Lett.* 157, 175–188. doi: 10.1016/j.toxlet.2005.03.004
- Kung, J. E., and Jura, N. (2019). Prospects for pharmacological targeting of pseudokinases. *Nat. Rev. Drug Discov.* 18, 501–526. doi: 10.1038/s41573-019-0018-3
- Kwon, A., Scott, S., Tajuale, R., Yeung, W., Kochut, K. J., Eyers, P. A., et al. (2019). Tracing the origin and evolution of pseudokinases across the tree of life. *Sci. Signal.* 12:eaav3810. doi: 10.1126/scisignal.aav3810
- Kwon, S. J., Boer, A. L. D., Petri, R., and Schmidt-Dannert, C. (2003). High-Level production of porphyrins in metabolically engineered *Escherichia coli*: Systematic extension of a pathway assembled from overexpressed genes involved in heme biosynthesis. *Appl. Environ. Microbiol.* 69, 4875–4883. doi: 10.1128/AEM.69.8.4875-4883.2003
- Laub, M. T., and Goulian, M. (2007). Specificity in two-component signal transduction pathways. *Annu. Rev. Genet.* 41, 121–145. doi: 10.1146/annurev.genet.41.042007.170548
- Layer, G., Reichelt, J., Jahn, D., and Heinz, D. W. (2010). Structure and function of enzymes in heme biosynthesis. *Protein Sci.* 19, 1137–1161. doi: 10.1002/pro.405
- Lyles, K. V., Thomas, L. S., Ouellette, C., Cook, L. C. C., and Eichenbaum, Z. (2022). HupZ, a unique heme-binding protein, enhances group A *Streptococcus* fitness during mucosal colonization. *Front. Cell. Infect. Microbiol.* 12:867963. doi: 10.3389/fcimb.2022.867963
- Mace, P. D., and Murphy, J. M. (2021). There's more to death than life: Noncatalytic functions in kinase and pseudokinase signaling. *J. Biol. Chem.* 296:100705. doi: 10.1016/j.jbc.2021.100705
- Mascher, T., Helmann, J. D., and Uuden, G. (2006). Stimulus perception in bacterial signal-transducing histidine kinases. *Microbiol. Mol. Biol. Rev.* 70, 910–938. doi: 10.1128/MMBR.00020-06
- Nakamura, H., Hisano, T., Rahman, M. M., Toshi, T., Shirouzu, M., and Shiro, Y. (2022). Structural basis for heme detoxification by an ATP-binding cassette-type efflux pump in gram-positive pathogenic bacteria. *Proc. Natl. Acad. Sci. U.S.A.* 119:e2123385119. doi: 10.1073/pnas.2123385119
- Niebisch, A., and Bott, M. (2001). Molecular analysis of the cytochrome bc1-a3 branch of the *Corynebacterium glutamicum* respiratory chain containing an unusual dihemetic cytochrome c1. *Arch. Microbiol.* 175, 282–294. doi: 10.1007/s002010100262
- Padmanaban, G., Venkateswar, V., and Rangarajan, P. N. (1989). Haem as a multifunctional regulator. *Trends Biochem. Sci.* 14, 492–496. doi: 10.1016/0968-0004(89)90182-5
- Perego, M., and Hoch, J. A. (1996). Protein aspartate phosphatases control the output of two-component signal transduction systems. *Trends Genet.* 12, 97–101. doi: 10.1016/0168-9525(96)81420-X
- Ponka, P. (1999). Cell biology of heme. *Am. J. Med. Sci.* 318, 241–256. doi: 10.1016/S0002-9629(15)40628-7
- Raju, S., and Shaw, A. S. (2015). What is the point of pseudokinases? *Elife* 4:e07771. doi: 10.7554/eLife.07771
- Reisinger, S. J., Huntwork, S., Viollier, P. H., and Ryan, K. R. (2007). DivI performs critical cell cycle functions in *Caulobacter crescentus* independent of kinase activity. *J. Bacteriol.* 189, 8308–8320. doi: 10.1128/JB.00868-07
- Reiterer, V., Eyers, P. A., and Farhan, H. (2014). Day of the dead: Pseudokinases and pseudophosphatases in physiology and disease. *Trends Cell Biol.* 24, 489–505. doi: 10.1016/j.tcb.2014.03.008
- Roden, J. A., Wells, D. H., Chomel, B. B., Kasten, R. W., and Koehler, J. E. (2012). Hemin binding protein C is found in outer membrane vesicles and protects *Bartonella henselae* against toxic concentrations of hemin. *Infect. Immun.* 80, 929–942. doi: 10.1128/IAI.05769-11
- Salvado, B., Vilaprinco, E., Karathia, H., Sorribas, A., and Alves, R. (2012). Two component systems: Physiological effect of a third component. *PLoS One* 7:e31095. doi: 10.1371/journal.pone.0031095
- Sambrook, J. F., and Russell, D. (2001). *Molecular cloning: A laboratory manual (3-Volume Set)*, Vol. 1. New York, NY: Cold Spring Harbor Laboratory Press.
- Schäfer, A., Tauch, A., Jäger, W., Kalinowski, J., Thierbach, G., and Pühler, A. (1994). Small mobilizable multi-purpose cloning vectors derived from the *Escherichia coli* plasmids pK18 and pK19: Selection of defined deletions in the chromosome of *Corynebacterium glutamicum*. *Gene* 145, 69–73. doi: 10.1016/0378-1119(94)90324-7
- Seib, K. L., Tseng, H. J., McEwan, A. G., Apicella, M. A., and Jennings, M. P. (2004). Defenses against oxidative stress in *Neisseria gonorrhoeae* and *Neisseria meningitidis*: Distinctive systems for different lifestyles. *J. Infect. Dis.* 190, 136–147. doi: 10.1086/421299

- Skaar, E. P., Gaspar, A. H., and Schneewind, O. (2006). *Bacillus anthracis* IsdG, a heme-degrading monooxygenase. *J. Bacteriol.* 188, 1071–1080. doi: 10.1128/JB.188.3.1071-1080.2006
- Sobota, J. M., and Imlay, J. A. (2011). Iron enzyme ribulose-5-phosphate 3-epimerase in *Escherichia coli* is rapidly damaged by hydrogen peroxide but can be protected by manganese. *Proc. Natl. Acad. Sci. U.S.A.* 108, 5402–5407. doi: 10.1073/pnas.1100410108
- Stauff, D. L., and Skaar, E. P. (2009b). The heme sensor system of *Staphylococcus aureus*. *Contrib. Microbiol.* 16, 120–135. doi: 10.1159/000219376
- Stauff, D. L., and Skaar, E. P. (2009a). *Bacillus anthracis* HssRS signaling to HrtAB regulates heme resistance during infection. *Mol. Microbiol.* 72, 763–778. doi: 10.1111/j.1365-2958.2009.06684.x
- Stock, A. M., Robinson, V. L., and Goudreau, P. N. (2000). Two-component signal transduction. *Annu. Rev. Biochem.* 69, 183–215. doi: 10.1146/annurev.biochem.69.1.183
- Stojiljkovic, I., and Hantke, K. (1994). Transport of haemin across the cytoplasmic membrane through a haemin-specific periplasmic binding-protein-dependent transport system in *Yersinia enterocolitica*. *Mol. Microbiol.* 13, 719–732. doi: 10.1111/j.1365-2958.1994.tb00465.x
- Stojiljkovic, I., Kumar, V., and Srinivasan, N. (1999). Non-iron metalloporphyrins: Potent antibacterial compounds that exploit haem/Hb uptake systems of pathogenic bacteria. *Mol. Microbiol.* 31, 429–442. doi: 10.1046/j.1365-2958.1999.01175.x
- Tomoni, A., Lees, J., Santana, A. G., Bolanos-Garcia, V. M., and Bastida, A. (2019). Pseudokinases: From allosteric regulation of catalytic domains and the formation of macromolecular assemblies to emerging drug targets. *Catalysts* 9:778. doi: 10.3390/catal9090778
- Tskos, C. G., Perchuk, B. S., and Laub, M. T. (2011). A dynamic complex of signaling proteins uses polar localization to regulate cell-fate asymmetry in *Caulobacter crescentus*. *Dev. Cell* 20, 329–341. doi: 10.1016/j.devcel.2011.01.007
- van der Rest, M. E., Lange, C., and Molenaar, D. (1999). A heat shock following electroporation induces highly efficient transformation of *Corynebacterium glutamicum* with xenogenic plasmid DNA. *Appl. Microbiol. Biotechnol.* 52, 541–545. doi: 10.1007/s002530051557
- Varadi, M., Anyango, S., Deshpande, M., Nair, S., Natassia, C., Yordanova, G., et al. (2021). AlphaFold Protein Structure Database: Massively expanding the structural coverage of protein-sequence space with high-accuracy models. *Nucleic Acids Res.* 50, D439–D444. doi: 10.1093/nar/gkab1061
- Wennerhold, J., and Bott, M. (2006). The DtxR regulon of *Corynebacterium glutamicum*. *J. Bacteriol.* 188, 2907–2918. doi: 10.1128/JB.188.8.2907-2918.2006
- Wennerhold, J., Krug, A., and Bott, M. (2005). The AraC-type regulator RipA represses aconitase and other iron proteins from *Corynebacterium* under iron limitation and is itself repressed by DtxR^{*}. *J. Biol. Chem.* 280, 40500–40508. doi: 10.1074/jbc.M508693200
- Willett, J. W., and Crosson, S. (2017). Atypical modes of bacterial histidine kinase signaling. *Mol. Microbiol.* 103, 197–202. doi: 10.1111/mmi.13525
- Wolanin, P. M., Thomason, P. A., and Stock, J. B. (2002). Histidine protein kinases: Key signal transducers outside the animal kingdom. *Genome Biol.* 3:REVIEWS3013. doi: 10.1186/gb-2002-3-10-reviews3013
- Zhao, X. R., Choi, K. R., and Lee, S. Y. (2018). Metabolic engineering of *Escherichia coli* for secretory production of free haem. *Nat. Catalysis* 1, 720–728. doi: 10.1038/s41929-018-0126-1

4. Appendix

4.1 Supplemental material to “A genome-wide analysis of the interconnection of iron- and heme-dependent regulatory networks governed by DtxR and HrrA in *Corynebacterium glutamicum*”

Supplemental material to: A genome-wide analysis of the interconnection of iron- and heme-dependent regulatory networks governed by DtxR and HrrA in *Corynebacterium glutamicum*

Aileen Krüger¹, Ulrike Viets¹, Andrei Filipchuk¹, Julia Frunzke^{1*}

¹ Forschungszentrum Jülich GmbH, Institute for Bio- and Geosciences 1, IBG1, 52425 Jülich, Germany

***Correspondence:**

Corresponding Author
j.frunzke@fz-juelich.de

Figures

Figure S1: Analysis of a *C. glutamicum* strain with a tagged DtxR variant.

Figure S2: Further comparison of ChAP-Seq peak intensities to expression levels and binding motifs.

Figure S3: Peak location along selected shared target genes of DtxR and HrrA.

Figure S4: Ratios of iron and heme peak intensities.

Tables

Table S1: Complete dataset of genome wide DtxR binding (ChAP-Seq) at iron excess (100 μM FeSO_4) and heme (4 μM heme) conditions in triplicates.

Table S2: Complete dataset of genome wide HrrA binding (ChAP-Seq) at iron excess (100 μM FeSO_4) and heme (4 μM heme) conditions in triplicates.

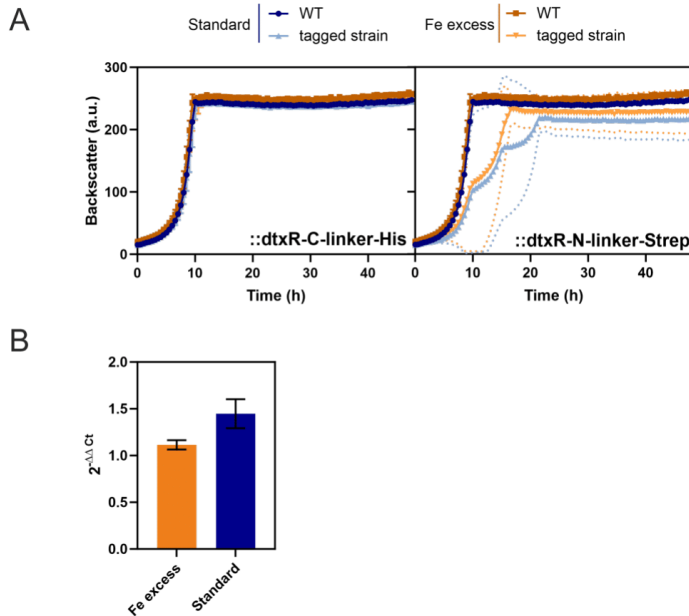


Figure S1: Analysis of a *C. glutamicum* strain with a tagged DtxR variant. (A) The wild type as well as the strain WT::*dtxR*-C-linker-His with a C-terminally His-tagged DtxR variant (left) and the strain WT::*dtxR*-N-linker-Strep with an N-terminally Strep-tagged DtxR variant (right) were inoculated from a fresh agar plate in 1 ml BHI in deep-well plates (VWR International, PA, USA) and incubated for 8 h at 30°C, 900 rpm. As a second pre-culture, cells were transferred 1:10 in 1 ml CGXII with 2% glucose and incubated for approximately 16 h at 30°C, 900 rpm. As main culture, cells were inoculated at a starting- OD_{600} of 1 in CGXII medium containing 2% glucose and either the standard amount of iron (36 μ M $FeSO_4$) or iron excess (100 μ M $FeSO_4$) in the BioLector® microtiter cultivation system of Beckman Coulter GmbH (Baesweiler) (Kensy et al., 2009). Data represents the average of three biological replicates including standard deviations depicted as error bars. (B) The WT::*dtxR*-C-linker-His strain was further analyzed in a qPCR experiment. Same cultivation as described above was performed, harvesting cells in ice-falcons at an OD_{600} of 5. Using the Luna One-Step RT-qPCR Kit (New England Biolabs, Frankfurt am Main) according to manufacturer's instructions, qPCR was performed in the qTower (Analytik Jena, Jena) and analyzed using qPCRsoft 3.1 (Analytik Jena, Jena). As a reference gene for normalization, the housekeeping gene *ddh* (A156-*ddh*-qPCR-fw CCGGAAAGCAAACCCACAAG; A157-*ddh*-qPCR-rv CTCGAGTCTGAAGGTTGCTT) was used (Frunzke et al., 2008), besides the target gene *dtxR* (A312-*dtxR*-qPCR-fw TTGAGCAGTCCAGGCACTC; A313-*dtxR*-qPCR-rv TTTCTACGGGACTGCATGT). Data represents two biological and three technical replicates. Fold-change was calculated according to the $2^{-\Delta\Delta Ct}$ (Livak and Schmittgen, 2001).

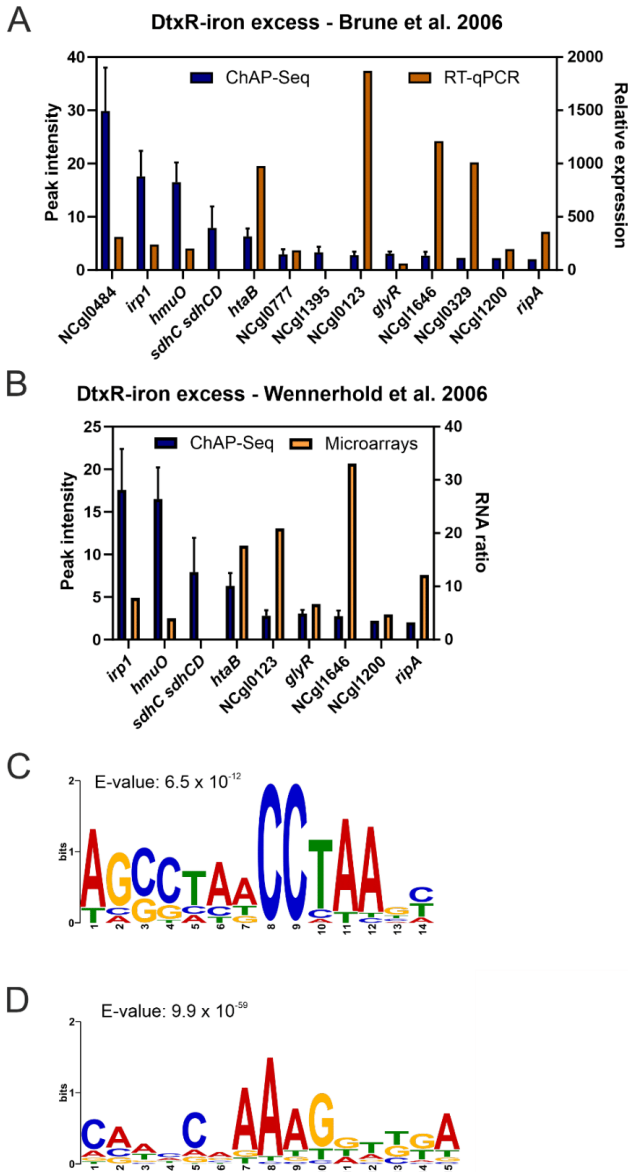


Figure S2: Further comparison of ChAP-Seq peak intensities to expression levels and binding motifs. Peak intensities of the ChAP-Seq for DtxR under iron excess conditions (dark blue) were compared to (A) to the relative expression in iron excess in the deletion strain $\Delta dtxR$ compared to wild type obtained from RT-qPCR (Brune et al., 2006) (dark orange) or (B) the RNA ratio at iron excess between the wild type and the deletion strain $\Delta dtxR$ from a microarray analysis (Wennerhold and Bott, 2006) (light orange). (C) Predicted binding motif of DtxR by MEME-ChIP (Bailey and Elkan, 1994) from ChAP-Seq data of heme conditions. (D) Predicted binding motif of HrrA by MEME-ChIP (Bailey and Elkan, 1994) from ChAP-Seq data of heme conditions.

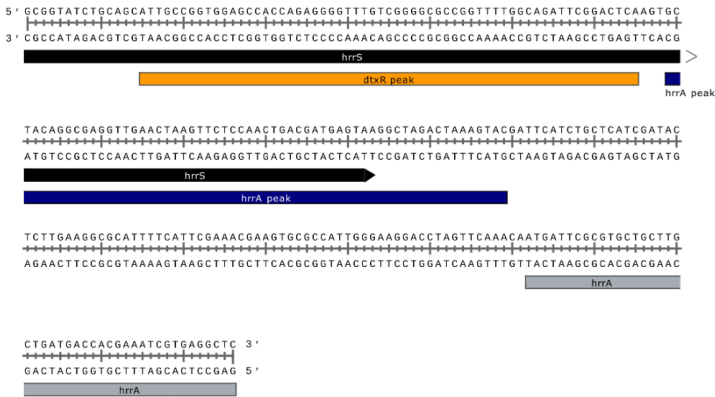
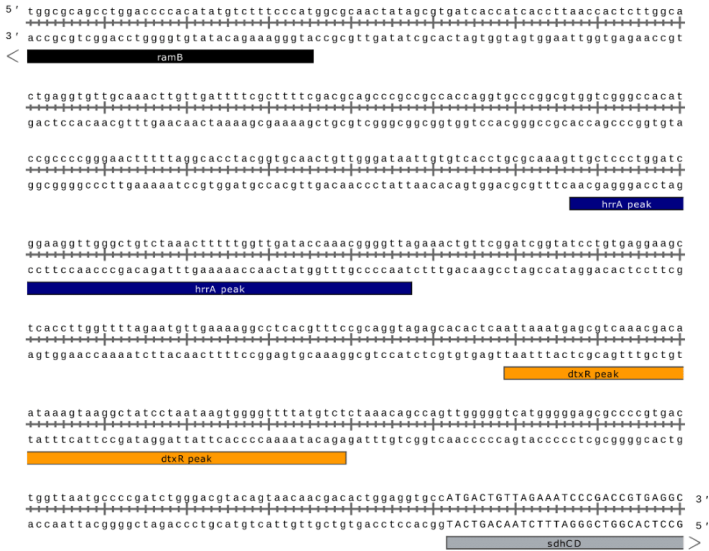
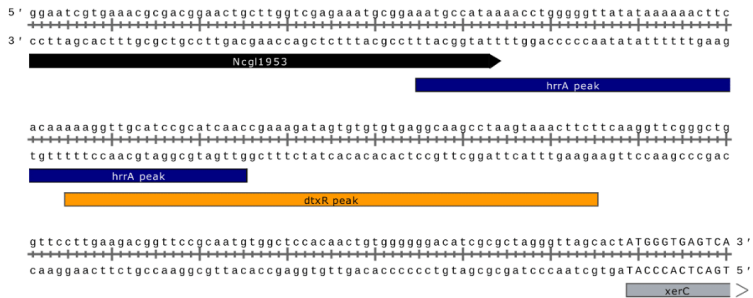
A *hrrA*B *sdhCD*

Figure S3: Peak location along selected shared target genes of DtxR and HrrA. The sequences around the identified peaks corresponding to shared target genes of DtxR and HrrA including (A) *hmuO*, (B) *sdhCD*, (C) *xerC* and (D) *NCgl0176* were extracted using SnapGene software (www.snapgene.com). The gene of interest, which was identified to be regulated by these transcriptional regulators, is shown in grey. Further genes in that region are shown in black. The region of the DtxR peak is shown in orange and for HrrA in blue.

C *xerC*

D NCgl0176

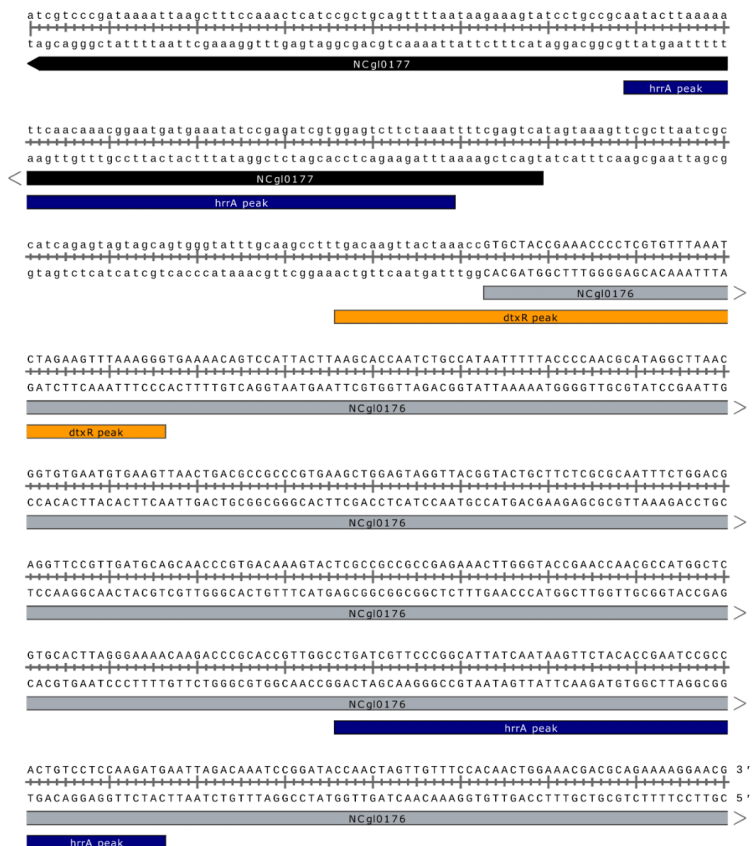


Figure S3 (continued).

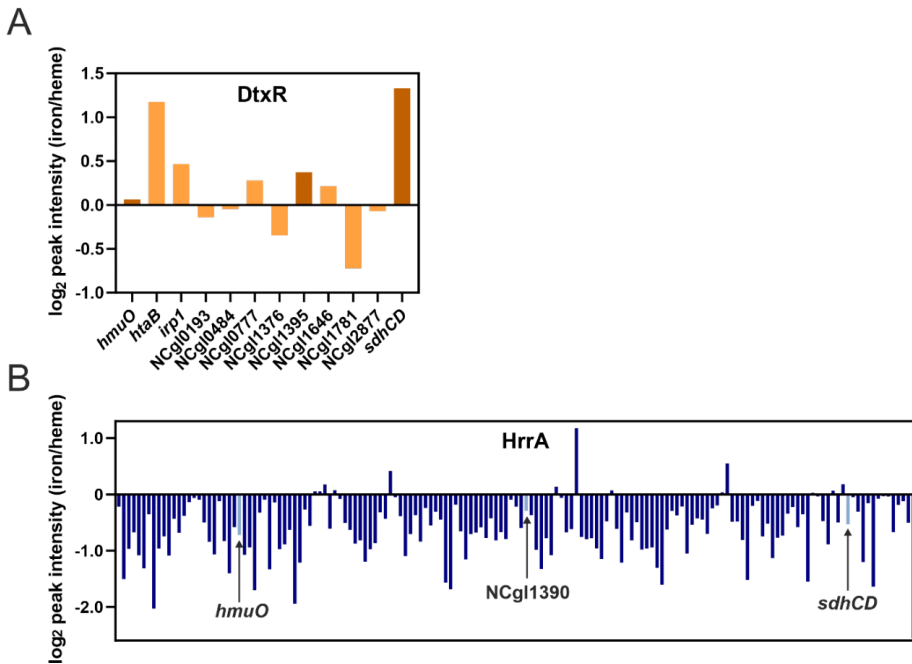


Figure S4: Ratios of iron and heme peak intensities. The ratio between the peak intensities at the two different conditions was calculated for those targets where a signal in both conditions could be identified. Therefore, the mean of peak intensity at the iron condition was divided by the mean of that in the presence of heme. Taking the logarithm to the basis of 2 allows evaluation with all targets representing values above 0 to be potentially more regulated in iron conditions, while below 0 more in heme condition by the respective regulator. (A) Ratios for target binding by DtxR. Shared targets with HrrA are shown in dark orange. A tendency for stronger iron binding can be suggested. (B) Ratios for target binding by HrrA. Shared targets with DtxR are shown in light blue. A clear trend for stronger binding at heme conditions can be drawn.

Table S1: Complete dataset of genome wide DtxR binding (ChAP-Seq) at iron excess (100 μ M FeSO₄) and heme (4 μ M heme) conditions in triplicates.

NCgI number	gene name	annotation	distance to tss	distance to atg	iron excess			heme		
					1	2	3	1	2	3
NCgI0005	<i>gyrB</i>	DNA topoisomerase/gyrase IV, subunit B (EC:5.99.1.3)	-35	3	n.d.	n.d.	2.007	n.d.	n.d.	n.d.
NCgI0027	<i>znuB2</i>	ABC-type Mn/Zn import system Znu2, permease component	-94	-94	2.133	n.d.	n.d.	n.d.	n.d.	n.d.
NCgI0097		None	350	350	n.d.	n.d.	n.d.	2.124	n.d.	n.d.
NCgI0123		None	-2	-2	3.267	2.353	n.d.	n.d.	n.d.	n.d.
NCgI0168	<i>oxiB</i>	putative oxidoreductase dehydrogenase	-53	-53	n.d.	2.076	n.d.	n.d.	n.d.	n.d.
NCgI0176		None	-71	98	n.d.	2.030	n.d.	n.d.	n.d.	n.d.
NCgI0193		None	-17	-17	2.241	n.d.	n.d.	n.d.	2.797	n.d.
NCgI0193		None	8	8	n.d.	2.399	n.d.	n.d.	2.319	n.d.
NCgI0325	<i>rmIA1</i>	TDP-glucose pyrophosphorylase, Glucose-1-phosphate thymidyltransferase (EC:2.7.7.24)	-240	-240	n.d.	n.d.	n.d.	n.d.	2.000	n.d.
NCgI0329		None	-9	-9	2.268	n.d.	n.d.	n.d.	n.d.	n.d.
NCgI0352	<i>wzy</i>	putative membrane protein, involved in polysaccharide polymerization, horizontally transferred	-644	-392	n.d.	1.938	n.d.	n.d.	n.d.	n.d.
NCgI0353		None	398	448	n.d.	n.d.	n.d.	2.018	n.d.	n.d.
NCgI0359	<i>sdhC</i> <i>sdhCD</i>	succinate:menaquinone oxidoreductase, cytochrome b subunit	-99	116	11.501	8.720	3.572	3.222	2.999	3.250
NCgI0381	<i>htaB</i>	secreted heme transport-associated protein	79	112	7.128	7.244	4.575	n.d.	2.679	n.d.
NCgI0381	<i>htaB</i>	secreted heme transport-associated protein	31	64	n.d.	n.d.	n.d.	2.655	n.d.	3.061
NCgI0430	<i>glyR</i>	transcriptional regulator of glyA cg1133, ArsR-family	15	15	3.240	3.368	2.598	n.d.	n.d.	n.d.
NCgI0465		None	38	38	n.d.	n.d.	n.d.	3.116	2.759	2.079
NCgI0484		FecCD transport family%3B similar to ABC-type cobalamin/Fe3+-siderophore transport system	15	97	38.986	27.361	23.260	36.114	24.434	31.900
NCgI0639	<i>irp1</i>	putative iron-siderophore ABC transporter, secreted siderophore-binding lipoprotein	-2	50	21.599	18.871	12.250	14.481	11.157	12.473
NCgI0664	<i>prpD1</i>	2-methylcitrate dehydratase	466	502	n.d.	n.d.	n.d.	n.d.	2.040	n.d.
NCgI0777		None	27	185	3.888	3.045	1.948	2.691	n.d.	2.192
NCgI0817	<i>pgi</i>	glucose-6-phosphate isomerase (EC:5.3.1.9)	-707	-679	n.d.	n.d.	n.d.	n.d.	2.000	n.d.
NCgI0841	<i>pepD</i>	putative trypsin-like serine protease PepD, EC:3.4.21	-474	-474	n.d.	n.d.	n.d.	n.d.	n.d.	2.268
NCgI0943	<i>ripA</i>	transcriptional regulator of iron proteins and repressor of aconitase, AraC-family	-43	13	2.025	n.d.	n.d.	n.d.	n.d.	n.d.
NCgI1173		alkanesulfonate monooxygenase, FMN/H2-dependent aliphatic sulfonate monooxygenase EC:1.14.14.5	174	174	n.d.	n.d.	n.d.	2.089	2.599	2.306
NCgI1200	<i>ssuD1</i>	None	37	70	2.241	n.d.	n.d.	n.d.	n.d.	n.d.
NCgI1376		None	28	32	2.106	n.d.	n.d.	n.d.	n.d.	n.d.
NCgI1376		None	128	132	n.d.	n.d.	n.d.	2.478	n.d.	n.d.

NCgl1376		None		87	91	n.d.	n.d.	n.d.	n.d.	n.d.	2.872
NCgl1395		None		71	71	3.834	n.d.	2.096	n.d.	2.054	2.986
NCgl1395		None		48	48	n.d.	4.014	n.d.	n.d.	2.639	n.d.
NCgl1444		None		64	149	2.376	2.076	n.d.	n.d.	n.d.	n.d.
NCgl1450	<i>metH</i>	homocysteine methyltransferase, methionine synthase EC:2.1.1.13		54	54	n.d.	n.d.	n.d.	n.d.	3.045	n.d.
NCgl1450	<i>metH</i>	homocysteine methyltransferase, methionine synthase EC:2.1.1.13		16	16	n.d.	n.d.	n.d.	n.d.	3.519	3.402
NCgl1646		None		-36	215	2.889	3.322	1.978	n.d.	2.903	1.920
NCgl1646		None		34	179	n.d.	n.d.	n.d.	n.d.	n.d.	2.230
NCgl1711		None		-346	-123	n.d.	n.d.	n.d.	n.d.	2.119	n.d.
NCgl1781		None		433	433	5.562	4.153	2.627	7.223	5.479	7.673
NCgl1952	<i>xerC</i>	tyrosine recombinase		11	114	n.d.	n.d.	n.d.	n.d.	5.594	7.038
NCgl1959		similar to ABC-type cobalamin/Fe3+-siderophores transport systems		13	19	n.d.	n.d.	n.d.	2.691	2.359	2.608
NCgl2146	<i>hmuO</i>	heme oxygenase		31	137	20.573	15.641	13.312	17.243	13.477	16.668
NCgl2731		None		463	674	n.d.	n.d.	n.d.	n.d.	n.d.	2.041
NCgl2766		similar to tellurite resistance protein and related permeases		196	196	2.457	n.d.	1.978	n.d.	n.d.	n.d.
NCgl2766		similar to tellurite resistance protein and related permeases		153	153	n.d.	2.445	n.d.	n.d.	n.d.	n.d.
NCgl2769	<i>mmpL1</i>	exporter of the MMPL-family, associated with mycolic acid metabolism		-440	-440	n.d.	n.d.	n.d.	n.d.	1.880	n.d.
NCgl2776		None		426	426	n.d.	n.d.	n.d.	2.266	n.d.	2.419
NCgl2834	<i>hrrA</i>	two component response regulator, control of heme homeostasis		-62	177	n.d.	n.d.	n.d.	2.903	n.d.	3.477
NCgl2842	<i>uspA3</i>	universal stress protein no. 3 / protein E		-265	-197	n.d.	n.d.	n.d.	2.018	n.d.	n.d.
NCgl2877		similar to predicted transcriptional regulators		15	80	4.482	4.291	2.893	n.d.	n.d.	4.422
NCgl2902		similar to predicted transcriptional regulators		50	115	n.d.	n.d.	n.d.	4.603	3.199	n.d.
NCgl2902	<i>gor3</i>	putative NADPH:quinone oxidoreductase (EC:1.6.5.5)		137	137	2.700	2.353	n.d.	n.d.	n.d.	n.d.
NCgl2939		similar to predicted Na+-dependent transporter		-90	-90	n.d.	2.215	n.d.	n.d.	n.d.	n.d.
NCgl2968		contains heavy-metal-associated domain		-16	16	n.d.	n.d.	1.889	n.d.	n.d.	n.d.
NCgl2980		contains MutT-like domain, similar to NTP pyrophosphohydrolases including oxidative damage repair enzymes		-328	-328	n.d.	n.d.	n.d.	n.d.	n.d.	2.003

Table S2: Complete dataset of genome wide DtxR binding (ChAP-Seq) at iron excess (100 μ M FeSO₄) and heme (4 μ M heme) conditions in triplicates.

NCgl number	gene	annotation	distance to tss	distance atg	iron excess			heme			
					1	2	3	1	2	3	
NCgl0003	<i>recF</i>	recombination protein RecF	23	82	n.d.	n.d.	n.d.	n.d.	n.d.	n.d.	2,449
NCgl0005	<i>gyrB</i>	DNA topoisomerase/gyrase IV, subunit B (EC:5.99.1.3)	-9	29	n.d.	3,069	2,539	n.d.	n.d.	n.d.	n.d.
NCgl0007		None	-442	-376	n.d.	2,518	n.d.	n.d.	n.d.	n.d.	n.d.
NCgl0007		None	-386	-320	n.d.	n.d.	n.d.	n.d.	n.d.	2,432	n.d.
NCgl0023	<i>ohr</i>	putative organic hydroperoxide resistance/detoxification protein	668	796							
NCgl0023	<i>ohr</i>	putative organic hydroperoxide resistance/detoxification protein	702	830							
NCgl0031		similar to type II (general) secretory pathway (IISP) family proteins and heme exporter protein CcmA	-481	-481							
NCgl0046	<i>fhaA</i>	cytoplasmic protein with FHA and DUF domain	37	264	2,563	2,636	n.d.	n.d.	n.d.	2,662	n.d.
NCgl0055		None	-106	-77	4,373	4,643	5,441	3,501	5,028	n.d.	n.d.
NCgl0056		None	248	248	2,981	n.d.	n.d.	3,562	4,535	5,550	n.d.
NCgl0069		similar to D-isomer specific 2-hydroxyacid dehydrogenase, NAD binding domain	2443	2493							
NCgl0069		similar to D-isomer specific 2-hydroxyacid dehydrogenase, NAD binding domain	4812	4862							
NCgl0069		similar to D-isomer specific 2-hydroxyacid dehydrogenase, NAD binding domain	2462	2512							
NCgl0069		similar to D-isomer specific 2-hydroxyacid dehydrogenase, NAD binding domain	4771	4821							
NCgl0078		None	4582	4582							
NCgl0078		None	4549	4549							
NCgl0083	<i>ureA</i>	urease V subunit (EC:3.5.1.5)	535	559							
NCgl0098	<i>putA</i>	proline dehydrogenase/δ-1-pyrroline-5-carboxylate dehydrogenase (EC:1.5.99.8)	19	101							
NCgl0098	<i>putA</i>	proline dehydrogenase/δ-1-pyrroline-5-carboxylate dehydrogenase (EC:1.5.99.8)	-18	64							
NCgl0106		None	3480	3736							
NCgl0117	<i>hde</i>	putative esterase/lipase protein (EC:3.1.1.3)	306	306	2,619	3,305	2,176	5,343	5,126	3,918	n.d.
NCgl0126		Probably involved in cell wall biogenesis	327	433							
NCgl0154	<i>iolR</i>	repressor of myo-inositol utilization genes, GntR-family, essential on gluconeogenic substrates	-860	-723	2,229	n.d.	n.d.	2,395	2,530	n.d.	n.d.
NCgl0155	<i>iolC</i>	carbohydrate kinase, myo-inositol catabolism	1156	1214	n.d.	2,243	n.d.	n.d.	n.d.	2,394	n.d.
NCgl0161	<i>iolG</i>	putative oxidoreductase, myo-inositol 2-dehydrogenase (EC:1.1.1.18)	249	249	3,036	4,053	3,537	8,168	9,004	9,577	n.d.
NCgl0171	<i>cspA</i>	cold-shock protein A, contains signal peptide for secretion	-47	133							
NCgl0176		None	-43	224							
NCgl0177		None	262	397							

NCgI0184	<i>embB (embC)</i>	arabinosyltransferase	-824	-824	n.d.	n.d.	n.d.	2,702	n.d.	n.d.	n.d.
NCgI0184	<i>embB (embC)</i>	arabinosyltransferase	-749	-749	n.d.	n.d.	n.d.	n.d.	n.d.	2,550	2,177
NCgI0187		None	-8	-5	2,256	n.d.	n.d.	n.d.	n.d.	n.d.	n.d.
NCgI0187		None	-676	-673	2,173	2,243	n.d.	n.d.	n.d.	n.d.	n.d.
NCgI0189		None	598	598	n.d.	n.d.	2,584	n.d.	n.d.	n.d.	n.d.
NCgI0196		None	174	174	n.d.	n.d.	n.d.	2,518	2,760	2,449	n.d.
NCgI0199		None	-1331	-1048	4,011	4,446	4,262	8,291	8,643	6,421	n.d.
NCgI0207	<i>moaB</i>	molybdopterin cofactor biosynthesis protein, Mog-family	18	288	n.d.	n.d.	2,358	n.d.	n.d.	n.d.	n.d.
NCgI0219		None	275	275	n.d.	2,597	n.d.	n.d.	n.d.	n.d.	n.d.
NCgI0236		None	6521	6580	n.d.	n.d.	n.d.	n.d.	n.d.	n.d.	2,557
NCgI0237	<i>aspT (ospB)</i>	aspartate aminotransferase, AT class I (EC:2.6.1.1)	46	230	2,173	n.d.	n.d.	n.d.	n.d.	n.d.	n.d.
NCgI0237	<i>aspT (ospB)</i>	aspartate aminotransferase, AT class I (EC:2.6.1.1)	-52	132	n.d.	2,282	n.d.	n.d.	n.d.	n.d.	n.d.
NCgI0245	<i>leuA</i>	2-isopropylmalate synthase (EC:2.3.3.13)	-1393	-1154	2,591	n.d.	2,584	4,913	5,389	4,081	n.d.
NCgI0246		similar to permeases of the drug/metabolite transporter (DMT) superfamily	23	202	8,134	7,909	8,433	13,143	16,858	13,114	n.d.
NCgI0250	<i>sigC</i>	RNA polymerase σ factor, ECF-family, control of branched quinol oxidation pathway	53	53	9,499	13,771	9,794	22,724	26,980	26,336	n.d.
NCgI0268	<i>cgrR1</i>	two component response regulator	-9	-9	n.d.	n.d.	n.d.	3,378	n.d.	n.d.	n.d.
NCgI0275	<i>whcA (whiB4)</i>	negative role in SigH-mediated oxidative stress response, WhiB homolog	-51	103	n.d.	2,400	n.d.	n.d.	2,958	2,503	n.d.
NCgI0279	<i>phdA (fadD1)</i>	acyl:CoA ligase transmembrane protein	163	163	4,819	5,902	4,353	6,019	7,723	8,815	n.d.
NCgI0302		distinct helicase with a unique C-terminal domain including a metal-binding cysteine cluster	-42	50	n.d.	3,620	3,763	n.d.	n.d.	n.d.	n.d.
NCgI0302		distinct helicase with a unique C-terminal domain including a metal-binding cysteine cluster	235	336	n.d.	3,305	n.d.	n.d.	n.d.	n.d.	n.d.
NCgI0303		cold-shock protein A2	-60	108	2,396	n.d.	n.d.	n.d.	n.d.	n.d.	n.d.
NCgI0316		None	366	366	3,315	3,541	3,582	5,650	9,694	8,597	n.d.
NCgI0333		member of the peptidase S9A	-151	-151	2,340	n.d.	n.d.	n.d.	n.d.	n.d.	n.d.
NCgI0333		member of the peptidase S9A	-194	-194	n.d.	2,558	n.d.	3,562	6,145	4,734	n.d.
NCgI0342		None	-699	-455	4,903	5,351	5,033	9,827	9,957	8,108	n.d.
NCgI0344	<i>wzx</i>	putative translocase involved in export of a cell surface polysaccharide, horizontally transferred	-1150	-871	3,900	4,485	n.d.	5,589	5,718	5,768	n.d.
NCgI0344	<i>wzx</i>	putative translocase involved in export of a cell surface polysaccharide, horizontally transferred	583	862	2,702	4,053	2,947	3,194	4,206	3,156	n.d.
NCgI0344	<i>wzx</i>	putative translocase involved in export of a cell surface polysaccharide, horizontally transferred	-670	-391	n.d.	n.d.	n.d.	3,439	3,746	4,897	n.d.
NCgI0345	<i>murA</i>	UDP-N-acetylglucosamine 1-carboxyvinyltransferase (EC:2.5.1.7), horizontally transferred	-1387	-1303	2,229	2,636	n.d.	n.d.	2,629	n.d.	n.d.

NCg 0345	<i>murA</i>	UDP-N-acetylglucosamine 1-carboxyvinyltransferase (EC:2.5.1.7), horizontally transferred	580	664	n.d.	n.d.	3.310	n.d.	n.d.	n.d.	n.d.
NCg 0347		None	-90	-82	2.424	3.187	1.950	n.d.	n.d.	3.122	3.047
NCg 0347		None	485	759	n.d.	n.d.	n.d.	n.d.	3.255	n.d.	n.d.
NCg 0347		None	-118	-110	n.d.	n.d.	n.d.	n.d.	2.702	n.d.	n.d.
NCg 0347		None	399	673	n.d.	n.d.	n.d.	n.d.	n.d.	2.892	n.d.
NCg 0349		None	-264	-264	n.d.	n.d.	n.d.	n.d.	2.641	3.056	n.d.
NCg 0349		None	-231	-231	n.d.	n.d.	n.d.	n.d.	n.d.	n.d.	3.863
NCg 0349		None	472	472	n.d.	n.d.	2.358	n.d.	n.d.	n.d.	n.d.
NCg 0350		None	1	66	2.646	3.581	n.d.	2.334	n.d.	n.d.	n.d.
NCg 0350		None	-441	-376	n.d.	2.518	n.d.	n.d.	n.d.	n.d.	n.d.
NCg 0351	<i>uagA1</i>	UDP-glucose 6-dehydrogenase (EC:1.1.1.22), horizontally transferred	-478	-255	n.d.	n.d.	n.d.	2.457	n.d.	n.d.	n.d.
NCg 0352	<i>wzy</i>	putative membrane protein, involved in polysaccharide polymerization, horizontally transferred	55	307	4.875	6.925	4.534	7.063	8.938	7.128	n.d.
NCg 0353		None	-17	15	n.d.	n.d.	n.d.	3.378	n.d.	n.d.	n.d.
NCg 0354		member of the isoleucine patch superfamily	-3	288	2.646	3.266	n.d.	n.d.	3.713	2.394	n.d.
NCg 0359	<i>sdhC sdhD</i>	succinate:menaquinone oxidoreductase, cytochrome b subunit	61	276	44.877	60.790	45.748	60.925	92.934	64.915	n.d.
NCg 0367		similar to permeases of the major facilitator superfamily	-88	-46	2.284	2.479	n.d.	2.395	n.d.	n.d.	n.d.
NCg 0367		similar to permeases of the major facilitator superfamily	-37	5	n.d.	n.d.	2.403	n.d.	3.615	3.374	n.d.
NCg 0375	<i>copA (ctpA, ctpV)</i>	copper-transporting P-type ATPase (EC:3.6.3.4)	-12	17	n.d.	n.d.	2.358	n.d.	n.d.	n.d.	n.d.
NCg 0377	<i>htaA</i>	secreted heme transport-associated protein	31	173	2.813	n.d.	2.448	4.606	4.765	5.278	n.d.
NCg 0377	<i>htaA</i>	secreted heme transport-associated protein	-9	133	n.d.	2.361	n.d.	n.d.	n.d.	n.d.	n.d.
NCg 0385		None	388	388	16.714	17.863	18.907	33.840	46.105	34.498	n.d.
NCg 0390	<i>gpmA</i>	phosphoglyceromutase (EC:5.4.2.1), also important role for cell division and morphology	19	26	1.978	n.d.	n.d.	n.d.	n.d.	n.d.	n.d.
NCg 0390	<i>gpmA</i>	phosphoglyceromutase (EC:5.4.2.1), also important role for cell division and morphology	-44	-37	n.d.	2.361	n.d.	n.d.	n.d.	n.d.	n.d.
NCg 0391	<i>senX3 (cgt54)</i>	two component sensor kinase	38	38	n.d.	n.d.	2.176	n.d.	n.d.	n.d.	n.d.
NCg 0400		None	360	433	13.455	16.958	15.960	23.338	29.444	22.908	n.d.
NCg 0405	<i>gsuR</i>	transcriptional activator of <i>gsuABCD</i> genes, LysR-family	-45	11	4.680	4.761	3.582	7.554	9.070	7.509	n.d.
NCg 0410		None	16	16	n.d.	n.d.	n.d.	2.457	2.728	2.884	n.d.

NCgI0420	<i>hemE</i>	uroporphyrinogen decarboxylase (EC:4.1.1.37), involved in heme biosynthesis	17	17	26.937	30.493	24.620	68.356	80.972	67.690
NCgI0422	<i>hemL</i>	glutamate-1-semialdehyde 2,1-aminomutase, AT class II EC:5.4.3.8 involved in heme biosynthesis	-228	-228	2.006	n.d.	n.d.	n.d.	n.d.	n.d.
NCgI0425	<i>ccsA</i>	cytochrome c biogenesis protein, membrane protein, DsbD-family	198	198	n.d.	n.d.	2.312	n.d.	n.d.	n.d.
NCgI0427	<i>ccsB</i>	cytochrome c assembly membrane protein, CcsA-family	-29	-29	n.d.	n.d.	n.d.	2.334	n.d.	n.d.
NCgI0435	<i>menE</i>	O-succinylbenzoic acid-CoA ligase (EC:6.2.1.26), involved in menaquinone biosynthesis	-561	-559	4.596	n.d.	4.489	5.712	7.361	7.672
NCgI0435	<i>menE</i>	O-succinylbenzoic acid-CoA ligase (EC:6.2.1.26), involved in menaquinone biosynthesis	-529	-527	n.d.	4.997	n.d.	n.d.	n.d.	n.d.
NCgI0445	<i>pitA</i>	low-affinity phosphate transport protein, Pit-family	395	550	n.d.	2.479	n.d.	n.d.	n.d.	n.d.
NCgI0455		None	1257	1257	5.794	6.610	5.940	7.738	13.441	13.331
NCgI0455		None	-13	-13	2.674	3.856	3.264	3.439	5.652	3.591
NCgI0459	<i>rplK</i>	50S ribosomal protein L11	9	161	n.d.	n.d.	2.267	n.d.	n.d.	n.d.
NCgI0461	<i>pwkR/gabR</i>	putative transcriptional regulator, similar to <i>purR</i> of <i>Bacillus subtilis</i> that regulates purine catabolism	-667	-667	n.d.	n.d.	n.d.	2.825	n.d.	3.428
NCgI0461	<i>pwkR/gabR</i>	putative transcriptional regulator, similar to <i>purR</i> of <i>Bacillus subtilis</i> that regulates purine catabolism	-593	-593	n.d.	n.d.	2.222	n.d.	3.319	n.d.
NCgI0461	<i>pwkR/gabR</i>	putative transcriptional regulator, similar to <i>purR</i> of <i>Bacillus subtilis</i> that regulates purine catabolism	-119	-119	n.d.	n.d.	n.d.	n.d.	2.596	n.d.
NCgI0461	<i>pwkR/gabR</i>	putative transcriptional regulator, similar to <i>purR</i> of <i>Bacillus subtilis</i> that regulates purine catabolism	-26	-26	n.d.	2.361	n.d.	n.d.	n.d.	n.d.
NCgI0468	<i>rplJ</i>	50S ribosomal protein L10	-1	250	n.d.	2.715	2.312	n.d.	n.d.	n.d.
NCgI0471	<i>rpoB</i>	DNA-directed RNA polymerase β subunit (EC:2.7.6), essential	-9	218	3.064	2.794	2.494	n.d.	n.d.	n.d.
NCgI0475		None	213	213	n.d.	2.676	n.d.	n.d.	n.d.	n.d.
NCgI0476	<i>rpsL</i>	30S ribosomal protein S12	-94	168	2.396	n.d.	n.d.	n.d.	n.d.	n.d.
NCgI0476	<i>rpsL</i>	30S ribosomal protein S12	-43	219	n.d.	n.d.	2.856	n.d.	n.d.	n.d.
NCgI0478	<i>fusA</i>	elongation factor EF-2/G EC:3.6.5.3	-118	-14	n.d.	2.439	n.d.	n.d.	n.d.	n.d.
NCgI0505	<i>fahD</i>	formate dehydrogenase accessory protein	-283	-283	n.d.	n.d.	n.d.	2.764	3.089	2.775
NCgI0515	<i>rpsH</i>	30S ribosomal protein S8	-5	227	n.d.	n.d.	2.222	n.d.	n.d.	n.d.
NCgI0522	<i>creB</i>	putative membrane protein	203	252	3.482	n.d.	n.d.	n.d.	n.d.	n.d.
NCgI0522	<i>creB</i>	putative membrane protein	-10	39	3.426	4.053	3.537	6.817	8.051	6.638
NCgI0522	<i>creB</i>	putative membrane protein	363	412	n.d.	n.d.	n.d.	5.650	6.474	6.421
NCgI0532	<i>secY</i>	preprotein translocase subunit	34	147	2.451	n.d.	n.d.	n.d.	n.d.	n.d.
NCgI0532	<i>secY</i>	preprotein translocase subunit	588	701	n.d.	n.d.	n.d.	2.395	2.465	n.d.
NCgI0532	<i>secY</i>	preprotein translocase subunit	-30	83	n.d.	2.203	2.403	n.d.	n.d.	n.d.

NCgI0536	<i>infA</i>	translational initiation factor IF-1	59	147	n.d.	2,400	n.d.	n.d.	n.d.	n.d.	n.d.
NCgI0541	<i>rplQ</i>	50S ribosomal protein L17	4	4	n.d.	n.d.	n.d.	n.d.	n.d.	3,746	3,210
NCgI0553		None	-449	-357	2,507	n.d.	3,174	4,975	4,929	4,407	
NCgI0553		None	-471	-379	n.d.	2,321	n.d.	n.d.	n.d.	n.d.	n.d.
NCgI0556	<i>rplM</i>	50S ribosomal protein L13	-66	75	2,674	n.d.	n.d.	n.d.	n.d.	n.d.	n.d.
NCgI0556	<i>rplM</i>	50S ribosomal protein L13	-134	7	n.d.	n.d.	2,403	2,395	n.d.	n.d.	n.d.
NCgI0556	<i>rplM</i>	50S ribosomal protein L13	15	156	n.d.	3,069	n.d.	n.d.	n.d.	n.d.	n.d.
NCgI0557	<i>rpsI</i>	30S ribosomal protein S9	409	409	n.d.	n.d.	n.d.	n.d.	2,530	n.d.	n.d.
NCgI0570		similar to sugar kinases	24	24	8,329	8,381	7,028	8,107	12,290	7,672	
NCgI0604	<i>phr</i>	deoxyribodipyrimidine photolyase (EC:4.1.99.3)	-1087	-940	n.d.	n.d.	n.d.	n.d.	2,530	n.d.	n.d.
NCgI0611	<i>dnaE2</i>	DNA polymerase III subunit α (EC:2.7.7)	-1335	-1335	n.d.	2,282	2,539	2,641	4,502	4,462	
NCgI0623		None	255	255	8,385	10,623	9,657	12,836	16,891	12,352	
NCgI0646		similar to ABC-type cobalamin/Fe3+-siderophores transport systems	36	72	10,920	13,378	11,788	14,064	17,055	13,603	
NCgI0648		similar to tRNA-processing ribonuclease BN	-144	-144	2,368	2,321	2,403	3,009	3,845	2,829	
NCgI0659	<i>pyc</i>	pyruvate carboxylase (EC:6.4.1.1)	-749	-693	n.d.	n.d.	n.d.	n.d.	3,122	n.d.	n.d.
NCgI0670	<i>accBC</i>	biotin carboxylase and biotin carboxyl carrier protein EC:6.3.4.14,6.4.1.2,6.4	12	194	n.d.	2,558	n.d.	n.d.	n.d.	n.d.	n.d.
NCgI0675	<i>maf</i>	putative septum formation protein Maf-like protein	-290	-290	n.d.	n.d.	n.d.	n.d.	2,662	n.d.	n.d.
NCgI0694	<i>tusG</i>	trehalose uptake system, ABC-type, permease protein	-25	-25	n.d.	n.d.	2,176	3,071	3,549	3,754	
NCgI0710	<i>manC (rmlA2)</i>	GDP-mannose pyrophosphorylase, mannose-1-phosphate guanylyltransferase GDP EC:2.7.2.2	-486	-302	n.d.	n.d.	n.d.	3,316	4,042	3,700	
NCgI0725	<i>psrp-1</i>	putative ribosome-associated protein Y	-147	-67	2,841	n.d.	n.d.	n.d.	n.d.	n.d.	n.d.
NCgI0725	<i>psrp-1</i>	putative ribosome-associated protein Y	-80	0	n.d.	2,636	n.d.	n.d.	n.d.	n.d.	n.d.
NCgI0726	<i>secA1</i>	preprotein translocase, essential	309	391	n.d.	n.d.	3,264	n.d.	n.d.	n.d.	n.d.
NCgI0732		None	0	62	4,067	5,154	3,854	9,458	14,394	14,909	
NCgI0736		None	53	53	4,262	4,722	4,625	12,283	14,591	16,977	
NCgI0753	<i>pdxR</i>	pyridoxal phosphate biosynthesis transcriptional regulator, aminotransferase, GntR-family	-120	-120	n.d.	n.d.	n.d.	n.d.	n.d.	2,340	
NCgI0756		None	129	151	n.d.	n.d.	n.d.	n.d.	n.d.	3,265	
NCgI0757		None	66	105	n.d.	n.d.	n.d.	3,255	n.d.	n.d.	n.d.
NCgI0757		None	149	188	n.d.	3,069	n.d.	n.d.	3,713	n.d.	n.d.

NCg0773	None	-538	-538	n.d.	n.d.	n.d.	2.596	2.503
NCg0775	None	4556	4690	2.396	n.d.	2.131	n.d.	n.d.
NCg0775	None	4469	4603	n.d.	2.479	n.d.	n.d.	n.d.
NCg0776	None	2991	3071	n.d.	2.361	n.d.	n.d.	n.d.
NCg0780	None	384	384	2.284	2.715	n.d.	3.685	4.173
NCg0780	None	3516	3516	n.d.	n.d.	n.d.	2.887	n.d.
NCg0780	None	62	62	n.d.	2.125	2.403	2.764	4.141
NCg0780	None	3567	3567	n.d.	n.d.	n.d.	n.d.	3.265
NCg0786	<i>cspB</i>	-7	59	n.d.	2.282	n.d.	n.d.	n.d.
NCg0794	phosphoserine aminotransferase, AT class IV EC:2.6.1.52, loss causes serine-auxotrophic	160	220	2.479	n.d.	2.040	2.579	3.352
NCg0794	phosphoserine aminotransferase, AT class IV EC:2.6.1.52, loss causes serine-auxotrophic	203	263	n.d.	2.794	n.d.	n.d.	n.d.
NCg0795	citrate synthase [EC:2.3.3.1]	-936	-742	5.627	6.453	6.756	12.652	15.478
NCg0797	acetyl-coenzyme A carboxylase carboxyl transferase (EC:6.4.1.2)	-84	81	n.d.	n.d.	n.d.	2.764	2.925
NCg0829	master regulator of nitrogen control, repressor, TetR- family	382	423	n.d.	n.d.	n.d.	2.211	2.760
NCg0834	50S ribosomal protein L28	12	126	n.d.	2.794	2.403	n.d.	n.d.
NCg0839	two component response regulator	87	199	n.d.	n.d.	n.d.	n.d.	2.563
NCg0840	two component sensor kinase	-555	-555	3.566	2.794	3.718	7.431	7.723
NCg0867	transposase fragment	59	357	2.424	n.d.	2.312	n.d.	2.432
NCg0883	None	57	57	16.463	20.067	18.227	39.552	46.368
NCg0884	None	-131	-131	3.148	2.597	2.494	4.913	4.831
NCg0900	glyceraldehyde-3-phosphate dehydrogenase gluconogenesis	194	274	n.d.	n.d.	n.d.	2.579	3.746
NCg0907	similar to permeases of the major facilitator superfamily	21	21	30.113	34.467	32.010	53.370	60.663
NCg0914	similar to ABC-type multidrug/protein/lipid transport system	386	454	5.711	6.374	4.081	6.264	11.272
NCg0917	None	59	59	n.d.	2.361	n.d.	n.d.	n.d.
NCg0927	None	-1115	-948	n.d.	n.d.	2.312	4.422	3.878
NCg0927	None	-1090	-923	n.d.	2.243	n.d.	n.d.	n.d.
NCg0929	<i>lysI</i>	549	549	3.231	n.d.	3.673	n.d.	4.788

NCgi0929	<i>lysI</i>	L-lysine permease	524	524	n.d.	4,171	n.d.	3,255	n.d.	n.d.
NCgi0935	<i>eno</i>	enolase EC:4.2.1.11 phosphopyruvate hydratase	290	360	n.d.	n.d.	n.d.	n.d.	2,728	n.d.
NCgi0935	<i>eno</i>	enolase EC:4.2.1.11 phosphopyruvate hydratase	-5	53	n.d.	2,479	n.d.	n.d.	n.d.	n.d.
NCgi0947		None	28	74	n.d.	2,164	n.d.	n.d.	n.d.	n.d.
NCgi0968	<i>ssuI</i>	NADPH-dependent FMN reductase (EC:1.5.1.29) required for sulfonate and sulfonate ester utilization	-28	192	n.d.	2,439	n.d.	2,395	2,793	n.d.
NCgi0968	<i>ssuI</i>	NADPH-dependent FMN reductase (EC:1.5.1.29) required for sulfonate and sulfonate ester utilization	-86	134	n.d.	n.d.	2,222	n.d.	n.d.	n.d.
NCgi0978		None	-1928	-1776	n.d.	2,563	2,676	n.d.	3,194	4,239
NCgi0978		None	-1877	-1725	n.d.	n.d.	n.d.	n.d.	n.d.	3,102
NCgi0993	<i>tnp9a</i>	transposase	-466	-387	n.d.	n.d.	n.d.	n.d.	2,596	2,340
NCgi1038		similar to LimB	-296	-296	n.d.	2,518	n.d.	n.d.	n.d.	n.d.
NCgi1053		None	1	79	n.d.	n.d.	2,131	n.d.	n.d.	n.d.
NCgi1069		None	-26	22	n.d.	2,243	n.d.	n.d.	n.d.	n.d.
NCgi1093		None	538	538	n.d.	n.d.	n.d.	n.d.	2,629	2,394
NCgi1096		None	108	108	n.d.	2,813	3,148	3,718	4,176	n.d.
NCgi1096		None	94	94	n.d.	n.d.	n.d.	n.d.	n.d.	7,197
NCgi1098		None	-831	-831	n.d.	n.d.	n.d.	n.d.	3,378	4,075
NCgi1104	<i>cydA</i>	cytochrome bd oxidase, subunit I	190	190	n.d.	8,441	10,387	7,663	11,055	13,506
NCgi1133	<i>lysA</i>	diaminopimelate decarboxylase (EC:4.1.1.20)	-47	121	n.d.	4,986	5,390	5,259	12,652	13,375
NCgi1144	<i>mog</i>	putative molybdopterin biosynthesis MOG protein	335	512	n.d.	2,203	n.d.	n.d.	n.d.	n.d.
NCgi1147		similar to hemolysins and related proteins containing CBS domains	-510	-390	n.d.	n.d.	n.d.	n.d.	2,395	2,629
NCgi1153	<i>prfA</i>	peptide chain release factor 1 RF-1	504	636	n.d.	n.d.	n.d.	n.d.	2,457	2,563
NCgi1158	<i>atpI</i>	putative protein, conserved, maybe related to Mg2+ uptake	143	143	n.d.	n.d.	n.d.	n.d.	n.d.	2,465
NCgi1159	<i>atpB</i>	F1FO-ATP synthase, a-subunit of FO part	316	316	n.d.	2,145	n.d.	n.d.	n.d.	n.d.
NCgi1200		None	292	325	n.d.	n.d.	n.d.	n.d.	n.d.	2,498
NCgi1202	<i>pfkA (pfk)</i>	6-phosphofructokinase EC:2.7.1.11	-6	-6	n.d.	n.d.	2,176	n.d.	n.d.	n.d.
NCgi1203	<i>rbsR</i>	transcriptional repressor of the ribose importer RbsACBD, LacI-family	-304	-230	n.d.	n.d.	n.d.	n.d.	n.d.	3,812
NCgi1241	<i>odx</i>	oxaloacetate decarboxylase	-158	-158	n.d.	2,321	n.d.	2,825	4,929	4,135
NCgi1250		None	1080	1080	n.d.	3,176	n.d.	n.d.	n.d.	n.d.

NCg11736	None	13	170	3,426	4,604	3,673	4,668	7,854	7,563
NCg11742	None	-35	2	2,396	3,344	2,584	3,992	6,441	5,768
NCg11742	None	-709	-672	n.d.	2,243	n.d.	n.d.	n.d.	n.d.
NCg11755	None	53	53	n.d.	2,203	n.d.	4,176	5,159	5,332
NCg11769	similar DNA topoisomerase III	981	1005	n.d.	2,558	n.d.	n.d.	n.d.	n.d.
NCg11787	None	-35	-27	n.d.	2,361	n.d.	3,009	3,713	3,156
NCg11793	None	265	265	n.d.	n.d.	n.d.	2,395	2,530	2,449
NCg11806	None	652	652	3,315	4,013	2,992	2,641	4,239	2,938
NCg11806	None	-621	-621	n.d.	n.d.	n.d.	2,334	n.d.	2,612
NCg11806	None	-546	-546	n.d.	n.d.	n.d.	n.d.	2,859	n.d.
NCg11815	None	458	628	n.d.	n.d.	n.d.	n.d.	2,859	2,394
NCg11822	arabinofuranosyltransferase	320	416	n.d.	n.d.	n.d.	2,702	n.d.	n.d.
NCg11822	arabinofuranosyltransferase	262	358	n.d.	n.d.	n.d.	n.d.	3,418	3,428
NCg11824	None	3	123	12,925	16,604	13,013	20,329	24,646	20,133
NCg11829	None	124	192	n.d.	n.d.	n.d.	2,457	n.d.	n.d.
NCg11834	myc-inositol-1-or 4-monophosphatase (EC:3.1.3.25)	-133	-133	309,597	411,601	308,450	799,329	1,256,148	1,155,077
NCg11873	None	-696	-656	n.d.	n.d.	n.d.	n.d.	3,188	n.d.
NCg11875	glutamate uptake system, ABC-type, ATP-binding protein	2675	2675	n.d.	n.d.	n.d.	2,579	n.d.	n.d.
NCg11890	None	326	326	2,535	3,344	2,992	6,203	6,474	7,890
NCg11903	putative kinase / FMN adenylyltransferase (EC:2.7.1.26), maybe involved in riboflavin metabolism, riboflavin	941	941	n.d.	n.d.	n.d.	2,395	n.d.	n.d.
NCg11911	implicated in transcription termination	-33	47	n.d.	2,203	n.d.	n.d.	n.d.	n.d.
NCg11915	ABC-type peptide transport system, secreted component	211	268	13,315	15,345	13,013	17,135	29,017	23,180
NCg11919	prolyl-tRNA synthetase (EC:6.1.1.15)	-803	-803	n.d.	n.d.	n.d.	n.d.	2,728	n.d.
NCg11921	None	228	228	n.d.	n.d.	n.d.	n.d.	2,596	2,721
NCg11922	None	-459	-402	n.d.	n.d.	n.d.	n.d.	2,563	n.d.
NCg11929	None	48	282	3,398	3,541	2,630	3,194	5,126	3,646
NCg11930	None	83	225	n.d.	n.d.	2,403	n.d.	n.d.	n.d.
NCg11940	1-deoxy-D-xylulose 5-phosphate reductoisomerase (EC:1.1.1.267)	51	51	2,284	2,558	n.d.	2,887	3,516	3,047

NGgl1941		None		64	143	n.d.	n.d.	2,494	n.d.	n.d.	n.d.
NGgl1946	<i>cdsA</i>	phosphatidate cytidyltransferase (EC:2.7.7.41)		-536	-536	n.d.	n.d.	n.d.	2,272	n.d.	n.d.
NGgl1952	<i>xerC</i>	tyrosine recombinase		31	134	39,027	52,055	38,086	177,676	306,438	278,159
NGgl2026	<i>glgX</i>	glycogen debranching enzyme (EC:3.2.1.68)		-298	-298	17,522	25,024	21,491	35,806	43,181	35,858
NGgl2027		None		127	127	2,312	2,203	2,448	3,624	4,568	n.d.
NGgl2027		None		89	89	n.d.	n.d.	n.d.	n.d.	n.d.	4,081
NGgl2048		cobalamin-independent		289	330	n.d.	n.d.	n.d.	3,132	n.d.	n.d.
NGgl2048		cobalamin-independent		80	121	n.d.	n.d.	n.d.	n.d.	n.d.	2,557
NGgl2048		cobalamin-independent		135	176	n.d.	n.d.	n.d.	n.d.	n.d.	3,451
NGgl2054		None		219	449	2,786	n.d.	n.d.	n.d.	n.d.	n.d.
NGgl2054		None		194	424	n.d.	3,620	2,176	3,808	5,028	3,265
NGgl2055		None		-900	-900	n.d.	2,203	2,222	3,869	4,568	4,680
NGgl2104	<i>plsC</i>	1-acyl-sn-glycerol-3-phosphate acetyltransferase		14	92	n.d.	n.d.	n.d.	2,518	n.d.	n.d.
NGgl2104	<i>plsC</i>	1-acyl-sn-glycerol-3-phosphate acetyltransferase		75	153	n.d.	n.d.	n.d.	n.d.	3,286	2,938
NGgl2112	<i>ctaE</i>	cytochrome aa3 oxidase, subunit 3		71	71	n.d.	n.d.	n.d.	80,393	n.d.	68,996
NGgl2113		None		-71	-71	63,708	76,883	64,927	137,510	158,132	105,887
NGgl2115	<i>ctaC</i>	cytochrome aa3 oxidase, subunit 2		57	243	10,446	10,584	10,564	16,705	20,177	16,215
NGgl2128	<i>lipA</i>	lipoyl synthase/synthetase (EC:2.8.1.-)		-27	67	2,730	2,479	2,902	3,808	4,666	4,081
NGgl2146	<i>hmuO</i>	heme oxygenase		54	160	2,813	3,226	2,992	4,790	5,751	n.d.
NGgl2146	<i>hmuO</i>	heme oxygenase		80	186	n.d.	n.d.	n.d.	n.d.	n.d.	4,353
NGgl2167	<i>aceE</i>	pyruvate dehydrogenase, E1 subunit of PDHC		0	70	n.d.	n.d.	2,312	n.d.	n.d.	n.d.
NGgl2174	<i>acpM</i>	acyl carrier protein ACP		589	589	3,426	3,856	4,353	9,704	12,126	11,209
NGgl2195		None		-59	-4	3,621	4,525	3,355	7,554	8,413	6,149
NGgl2198	<i>glyS</i>	βlycyl-tRNA synthetase (EC:6.1.1.14)		-53	122	n.d.	2,676	n.d.	n.d.	n.d.	n.d.
NGgl2207		None		440	440	n.d.	n.d.	n.d.	n.d.	2,366	n.d.
NGgl2211	<i>hrcA</i>	heat-inducible transcription repressor, HrcA-family		-243	-240	n.d.	n.d.	n.d.	n.d.	n.d.	2,449
NGgl2216	<i>fabD15</i>	long-chain fatty acid CoA ligase (EC:6.2.1.3)		11	210	2,061	3,462	n.d.	2,887	n.d.	n.d.
NGgl2217	<i>malQ</i>	4-α-glucanotransferase (EC:2.4.1.25)		-3	7	n.d.	n.d.	2,403	n.d.	n.d.	n.d.
NGgl2228	<i>brnQ</i>	branched-chain amino acid uptake carrier, Na+-coupled?		236	346	2,869	2,479	2,630	4,176	4,798	3,754

NCgI2236	None	160	181	6.853	8.932	6.529	14.617	19.651	20.840
NCgI2247	malate synthase (EC:2.3.3.9), part of glyoxylate shunt	66	249	2.368	2.164	n.d.	n.d.	n.d.	n.d.
NCgI2247	malate synthase (EC:2.3.3.9), part of glyoxylate shunt	142	325	n.d.	n.d.	n.d.	2.641	n.d.	n.d.
NCgI2248	isocitrate lyase (EC:4.1.3.1), part of glyoxylate shunt	32	143	n.d.	n.d.	n.d.	n.d.	n.d.	2.449
NCgI2252	None	-38	27	n.d.	3.856	2.584	n.d.	n.d.	n.d.
NCgI2253	None	506	538	2.841	n.d.	n.d.	n.d.	n.d.	n.d.
NCgI2254	None	-717	-717	2.396	n.d.	n.d.	n.d.	n.d.	n.d.
NCgI2254	None	-701	-701	n.d.	2.164	n.d.	5.650	7.657	7.509
NCgI2261	30S ribosomal protein S20	166	321	n.d.	n.d.	n.d.	n.d.	n.d.	2.340
NCgI2280	50S ribosomal protein L21	29	205	n.d.	2.518	n.d.	n.d.	n.d.	n.d.
NCgI2296	None	-448	-448	n.d.	n.d.	2.222	n.d.	n.d.	n.d.
NCgI2304	ATP-dependent protease ATP-binding subunit	8	83	2.201	n.d.	2.675	n.d.	n.d.	n.d.
NCgI2309	β -ketoacyl-CoA thiolase (EC:2.3.1.174)	241	241	n.d.	n.d.	2.176	2.211	n.d.	n.d.
NCgI2309	β -ketoacyl-CoA thiolase (EC:2.3.1.174)	200	200	n.d.	n.d.	n.d.	n.d.	3.319	n.d.
NCgI2316	similar to restriction endonucleases	-554	-516	n.d.	n.d.	n.d.	n.d.	2.662	n.d.
NCgI2324	transcriptional regulator, LuxR-family	225	291	3.928	4.604	3.582	8.045	9.070	6.584
NCgI2326	benzoate membrane transport protein, , benzoate:H+ symporter BenE-family	-261	-261	n.d.	n.d.	n.d.	n.d.	2.498	n.d.
NCgI2326	benzoate membrane transport protein, , benzoate:H+ symporter BenE-family	-315	-315	n.d.	n.d.	n.d.	n.d.	n.d.	3.102
NCgI2350	similar to ATPases of various ABC-type transport systems, contains duplicated ATPase	5	5	11.115	13.850	11.063	16.091	25.139	14.365
NCgI2355	putative aminotransferase class-III, pyridoxal-phosphate dependent	185	226	n.d.	n.d.	n.d.	3.562	3.451	4.081
NCgI2358	similar to short-chain alcohol dehydrogenases	-18	11	20.642	22.506	21.174	29.234	31.285	18.174
NCgI2384	hydroxypyruvate isomerase (EC:5.3.1.22)	1288	1312	n.d.	n.d.	n.d.	n.d.	3.319	2.503
NCgI2410	None	-816	-816	n.d.	n.d.	n.d.	2.518	n.d.	n.d.
NCgI2422	cAMP phosphodiesterase	301	301	2.229	n.d.	2.222	7.984	9.037	10.284
NCgI2434	None	-444	-411	n.d.	n.d.	n.d.	2.395	n.d.	n.d.
NCgI2434	None	-497	-464	n.d.	n.d.	n.d.	n.d.	3.220	3.591
NCgI2437	cytochrome aa3 oxidase, subunit 1	211	323	18.190	20.185	18.363	38.016	49.227	33.410
NCgI2443	ribonucleotide-diphosphate reductase α subunit (EC:1.17.4.1), essential for aerobic growth	-68	-68	3.315	3.974	3.582	6.387	9.366	8.108

NCgi2446a	None	-42	49	n.d.	2.400	n.d.	n.d.	n.d.	n.d.
NCgi2447	COG3001:hypothetical protein	-275	-275	n.d.	n.d.	2.312	n.d.	n.d.	n.d.
NCgi2465	involved in lipoprotein release, ATPases	-115	-45	2.229	n.d.	n.d.	2.887	2.892	n.d.
NCgi2466	similar to sugar phosphate isomerases/epimerases	540	540	2.340	3.108	n.d.	n.d.	n.d.	n.d.
NCgi2466	similar to sugar phosphate isomerases/epimerases	2887	2887	n.d.	n.d.	n.d.	2.887	n.d.	n.d.
NCgi2466	similar to sugar phosphate isomerases/epimerases	2836	2836	n.d.	n.d.	n.d.	n.d.	n.d.	3.265
NCgi2466	similar to sugar phosphate isomerases/epimerases	501	501	n.d.	n.d.	2.494	n.d.	n.d.	n.d.
NCgi2471	<i>pdvO</i>	1338	1512	2.702	n.d.	n.d.	n.d.	n.d.	n.d.
NCgi2471	adenosylcobalamin-dependent diol dehydratase y (EC:4.2.1.28)	3719	3893	n.d.	n.d.	n.d.	2.887	n.d.	n.d.
NCgi2471	adenosylcobalamin-dependent diol dehydratase y (EC:4.2.1.28)	3667	3841	n.d.	n.d.	n.d.	n.d.	n.d.	3.265
NCgi2471	adenosylcobalamin-dependent diol dehydratase y (EC:4.2.1.28)	1383	1557	n.d.	2.912	2.267	n.d.	n.d.	n.d.
NCgi2472	transcriptional regulator, acetate metabolism, LuxR-family	-9	65	3.009	2.990	3.038	2.825	3.418	2.394
NCgi2472	transcriptional regulator, acetate metabolism, LuxR-family	242	316	n.d.	n.d.	n.d.	n.d.	n.d.	2.285
NCgi2473	<i>cysK</i>	-242	-164	n.d.	n.d.	2.720	n.d.	n.d.	n.d.
NCgi2473	O-acetylserine thiol-lyase, cysteine synthase (EC:2.5.1.47), loss causes cysteine auxotrophy	-383	-305	n.d.	2.794	n.d.	n.d.	n.d.	n.d.
NCgi2482	O-acetylserine thiol-lyase, cysteine synthase (EC:2.5.1.47), loss causes cysteine auxotrophy	-66	-66	3.482	3.895	3.401	3.316	6.178	4.299
NCgi2491	phosphate uptake regulator	1562	1713	n.d.	2.321	n.d.	n.d.	n.d.	n.d.
NCgi2492	catalyzes the formation of 4-aminobenzoate and pyruvate from 4-amino-4-deoxychorismate								
NCgi2492	None	-72	-72	n.d.	n.d.	2.131	n.d.	n.d.	n.d.
NCgi2569	2-C-methyl-D-erythritol 2,4-cyclodiphosphate synthase (EC:4.6.1.12)	499	546	n.d.	3.148	n.d.	7.677	5.685	5.169
NCgi2574	None	65	111	10.808	13.181	13.103	19.407	32.961	24.540
NCgi2577	None	292	292	2.368	2.400	n.d.	n.d.	3.779	3.156
NCgi2581	None	-269	-269	n.d.	n.d.	1.950	n.d.	n.d.	n.d.
NCgi2589	None	-237	-237	2.674	n.d.	2.494	3.071	4.141	3.210
NCgi2591	None	-1280	-1280	n.d.	2.597	n.d.	n.d.	n.d.	n.d.
NCgi2592	lincomycin resistance protein	-717	-635	3.482	3.738	n.d.	9.151	14.426	16.814
NCgi2592	lincomycin resistance protein	-676	-594	n.d.	n.d.	3.264	n.d.	n.d.	n.d.
NCgi2602	GTP cyclohydrolase I (EC:3.5.4.16)	-34	150	n.d.	n.d.	n.d.	n.d.	2.465	2.340

NCgl2648		None		1430	1630	n.d.	2.676	n.d.	n.d.	n.d.
NCgl2655	<i>plnG</i>	serine/threonine protein kinase		-207	-86	n.d.	n.d.	n.d.	2.202	n.d.
NCgl2659		None		535	535	n.d.	n.d.	n.d.	2.563	n.d.
NCgl2663	<i>purT</i>	5-phosphoribosylglycinamide transformylase		-59	227	n.d.	n.d.	n.d.	2.457	3.188
NCgl2664		None		-661	-565	n.d.	2.558	2.494	n.d.	3.319
NCgl2666	<i>tnp8a</i>	transposase fragment		210	445	n.d.	2.833	n.d.	n.d.	n.d.
NCgl2673	<i>fdx</i>	fructose-bisphosphate aldolase (EC:4.1.2.13)		-45	-1	3.816	n.d.	3.219	4.238	4.436
NCgl2673	<i>fdx</i>	fructose-bisphosphate aldolase (EC:4.1.2.13)		-5	39	n.d.	4.407	n.d.	n.d.	n.d.
NCgl2674		similar to alpha-1%2C6-mannanase		-8	141	3.593	3.974	3.355	5.466	6.967
NCgl2699	<i>hspR</i>	transcriptional regulator involved in heat shock response, MerR-family		350	435	n.d.	n.d.	n.d.	n.d.	2.394
NCgl2702	<i>dnaK</i>	chaperone DnaK, heat shock protein		-328	-310	n.d.	n.d.	2.539	n.d.	n.d.
NCgl2703		None		-31	-31	3.677	n.d.	3.038	n.d.	4.929
NCgl2703		None		579	579	2.535	n.d.	n.d.	n.d.	4.075
NCgl2703		None		5	5	n.d.	3.659	n.d.	3.808	n.d.
NCgl2703		None		553	553	n.d.	n.d.	n.d.	3.685	n.d.
NCgl2716	<i>cysD</i>	sulfate adenylyltransferase subunit 2 (EC:2.7.4), loss causes sulfide/cysteine auxotrophy		99	99	n.d.	n.d.	n.d.	n.d.	2.285
NCgl2719	<i>cysJ (fpr2)</i>	sulfite reductase flavoprotein, Ferredoxin-NADP+ reductase (EC:1.18.1.2)		-432	-326	3.064	n.d.	2.675	n.d.	n.d.
NCgl2720		None		445	445	n.d.	n.d.	n.d.	2.272	n.d.
NCgl2726	<i>tatC</i>	citrate uptake transporter, substrate binding protein		-165	-67	2.646	2.558	2.947	n.d.	3.286
NCgl2748		contains integrase core domain		613	613	n.d.	2.282	n.d.	2.702	2.530
NCgl2752	<i>htrAD</i>	secreted heme transport-associated protein		-125	148	4.791	4.918	5.305	15.907	17.745
NCgl2762		None		1476	1479	2.451	n.d.	2.448	n.d.	2.465
NCgl2765	<i>pck</i>	phosphoenolpyruvate carboxykinase GTP (EC:4.1.1.32)		-30	7	2.758	n.d.	n.d.	n.d.	n.d.
NCgl2765	<i>pck</i>	phosphoenolpyruvate carboxykinase GTP (EC:4.1.1.32)		-3	65	n.d.	3.895	n.d.	n.d.	n.d.
NCgl2768		None		15	15	4.429	7.791	4.851	n.d.	3.428
NCgl2768		None		-13	-13	n.d.	n.d.	n.d.	3.869	4.371
NCgl2770		None		212	212	n.d.	2.243	2.403	2.948	3.265
NCgl2777	<i>cop1</i>	trehalose corynomycolyl transferase (EC:2.3.1.122), <i>cop1</i> , <i>cmt1</i> , and <i>cmt2</i> can replace each other in the synthesis		-18	193	n.d.	2.164	n.d.	2.764	n.d.

NCgI2787		None	-133	-108	4.541	4.840	4.897	5.773	7.953	6.257
NCgI2789	<i>psp5</i>	putative secreted protein	-1704	-1704	2.897	3.462	2.856	3.194	3.549	2.285
NCgI2791		similar to predicted hydrolases of the HAD superfamily	183	183	2.953	2.676	3.038	3.746	6.211	5.278
NCgI2794	<i>farR</i>	transcriptional regulator involved in amino acid biosynthesis, GntR-family	43	43	2.173	n.d.	n.d.	n.d.	n.d.	n.d.
NCgI2809		catalyzes the formation of phosphoenolpyruvate from pyruvate	92	133	2.312	3.777	n.d.	n.d.	n.d.	n.d.
NCgI2810	<i>ldhA (ldh)</i>	NAD-dependent L-lactate dehydrogenase	-36	55	2.563	n.d.	n.d.	n.d.	n.d.	n.d.
NCgI2816		similar to permeases of the major facilitator superfamily	530	603	3.120	3.817	3.627	8.721	10.779	10.883
NCgI2826	<i>sodA (sod)</i>	manganese superoxide dismutase (EC:1.15.1.1)	9	101	n.d.	3.148	2.312	n.d.	n.d.	n.d.
NCgI2834	<i>hrrA (cgtR11)</i>	two component response regulator, control of heme homeostasis	29	111	2.619	3.541	2.811	6.019	6.277	6.584
NCgI2842	<i>uspA3</i>	universal stress protein no. 3 / protein E	-446	-378	n.d.	n.d.	3.582	n.d.	n.d.	n.d.
NCgI2842	<i>uspA3</i>	universal stress protein no. 3 / protein E	-46	22	n.d.	3.699	n.d.	n.d.	n.d.	n.d.
NCgI2842	<i>uspA3</i>	universal stress protein no. 3 / protein E	12	80	n.d.	n.d.	3.128	n.d.	n.d.	n.d.
NCgI2843		putative alkanal monooxygenase α chain	-82	68	n.d.	n.d.	2.494	n.d.	n.d.	n.d.
NCgI2843		putative alkanal monooxygenase α chain	3	153	n.d.	2.321	n.d.	n.d.	n.d.	n.d.
NCgI2843		putative alkanal monooxygenase α chain	1443	1593	n.d.	2.203	2.131	n.d.	n.d.	n.d.
NCgI2843		putative alkanal monooxygenase α chain	1477	1627	n.d.	n.d.	n.d.	n.d.	2.498	n.d.
NCgI2845		None	-9	40	2.256	3.187	2.448	n.d.	n.d.	n.d.
NCgI2847		similar to pneumococcal surface protein A	3091	3168	n.d.	n.d.	n.d.	2.887	n.d.	n.d.
NCgI2847		similar to pneumococcal surface protein A	3041	3118	n.d.	n.d.	n.d.	n.d.	n.d.	3.265
NCgI2861		None	0	0	2.479	2.794	2.675	n.d.	n.d.	n.d.
NCgI2861		None	34	34	n.d.	n.d.	n.d.	n.d.	2.859	2.884
NCgI2874	<i>trxB1</i>	thioredoxin no. 1 (EC:5.3.4.1)	5	29	n.d.	2.243	n.d.	n.d.	n.d.	n.d.
NCgI2881	<i>rpsF</i>	30S ribosomal protein S6	-6	79	2.368	2.990	n.d.	n.d.	n.d.	n.d.
NCgI2885		None	107	257	2.117	n.d.	n.d.	n.d.	n.d.	n.d.
NCgI2888		None	-5	-5	2.758	3.620	3.854	4.483	6.309	6.366
NCgI2894	<i>ino1</i>	D-myo-inositol-1-phosphate synthase	-48	165	9.220	12.551	9.113	9.274	14.755	14.691
NCgI2897	<i>dps</i>	starvation-induced DNA protection protein	-2	-2	n.d.	2.321	2.584	n.d.	n.d.	n.d.
NCgI2902	<i>qor3</i>	putative NADPH:quinone oxidoreductase (EC:1.6.5.5)	-24	-24	n.d.	n.d.	n.d.	2.579	2.990	3.754
NCgI2905	<i>gntK</i>	putative gluconate kinase (EC:2.7.1.12)	-97	-61	n.d.	n.d.	2.403	n.d.	n.d.	2.612
NCgI2911		None	228	332	n.d.	n.d.	2.131	n.d.	n.d.	n.d.

NCgI2916	None	18	18	n.d.	n.d.	2,312	n.d.	n.d.	n.d.	n.d.	n.d.
NCgI2924	similar to Na ⁺ /H ⁺ -dicarboxylate symporters	-1	188	2,368	n.d.	n.d.	n.d.	n.d.	n.d.	n.d.	n.d.
NCgI2925	tryptophan-specific permease, 5-methyltryptophan resistance	-28	34	n.d.	2,597	2,267	n.d.	n.d.	n.d.	n.d.	n.d.
NCgI2938	member of the Old Yellow Enzyme family	-953	-755	n.d.	n.d.	n.d.	n.d.	2,702	2,629	n.d.	n.d.
NCgI2952	methylacetate reductase (EC:1.3.1.32)	465	465	n.d.	n.d.	n.d.	n.d.	n.d.	n.d.	2,666	2,666
NCgI2968	contains heavy-metal-associated domain	-37	-5	4,596	4,643	4,897	n.d.	5,466	8,051	6,747	6,747
NCgI2980	contains MutT-like domain, similar to NTP pyrophosphohydrolases including oxidative damage repair enzymes	-34	-34	2,368	n.d.	n.d.	n.d.	n.d.	n.d.	n.d.	n.d.
NCgI2980	contains MutT-like domain, similar to NTP pyrophosphohydrolases including oxidative damage repair enzymes	31	31	n.d.	n.d.	2,131	n.d.	n.d.	n.d.	n.d.	n.d.
NCgI2991	functions to insert inner membrane proteins into the IM in <i>Escherichia coli</i> , interacts with transmembrane segments, functions in both Sec-dependent and -independent membrane insertion, similar to Oxa1p in mitochondria	-669	-437	n.d.	n.d.	n.d.	n.d.	n.d.	n.d.	2,775	2,775
NCgI2993	50S ribosomal protein L34	-8	254	n.d.	2,676	n.d.	n.d.	n.d.	n.d.	n.d.	n.d.
NCgI2993	50S ribosomal protein L34	33	295	n.d.	n.d.	2,494	n.d.	n.d.	n.d.	n.d.	n.d.

References

- Bailey, T.L., and Elkan, C. (1994). Fitting a mixture model by expectation maximization to discover motifs in biopolymers. *Proc Int Conf Intell Syst Mol Biol*, 2: 28-36.
- Brune, I., Werner, H., Hüser, A.T., Kalinowski, J., Pühler, A., and Tauch, A. (2006). The DtxR protein acting as dual transcriptional regulator directs a global regulatory network involved in iron metabolism of *Corynebacterium glutamicum*. *BMC Genom*, 7(1): 21. doi: 10.1186/1471-2164-7-21.
- Frunzke, J., Bramkamp, M., Schweitzer, J.E., and Bott, M. (2008). Population Heterogeneity in *Corynebacterium glutamicum* ATCC 13032 caused by prophage CGP3. *J Bacteriol*, 190(14): 5111-5119. doi: 10.1128/jb.00310-08.
- Kensy, F., Zang, E., Faulhammer, C., Tan, R.-K., and Büchs, J. (2009). Validation of a high-throughput fermentation system based on online monitoring of biomass and fluorescence in continuously shaken microtiter plates. *Microb Cell Factories*, 8(1): 31. doi: 10.1186/1475-2859-8-31.
- Livak, K.J., and Schmittgen, T.D. (2001). Analysis of relative gene expression data using real-time quantitative PCR and the $2^{-\Delta\Delta Ct}$ Method. *Methods*, 25(4): 402-408. doi: 10.1006/meth.2001.1262.
- Wennerhold, J., and Bott, M. (2006). The DtxR regulon of *Corynebacterium glutamicum*. *J Bacteriol*, 188(8): 2907-2918. doi: 10.1128/jb.188.8.2907-2918.2006.

4.2 Supplemental material to “HrrSA orchestrates a systemic response to heme and determines prioritization of terminal cytochrome oxidase expression”

1 Supplementary Information for

2

3 **HrrSA orchestrates a systemic response to heme and determines prioritisation of terminal**
 4 **cytochrome oxidase expression**

5

6 Marc Keppel^{1#}, Max Hünnefeld^{1#}, Andrei Filipchik^{1#}, Ulrike Viets¹, Cedric-Farhad Davoudi¹, Aileen
 7 Krüger¹, Eugen Pfeifer², Christina Mack¹, Tino Polen¹, Meike Baumgart¹, Michael Bott¹, and Julia
 8 Frunzke^{1*}

9

10 ¹Institute of Bio- und Geosciences, IBG-1: Biotechnology, Forschungszentrum Jülich, 52425 Jülich,
 11 Germany

12 ²Microbial Evolutionary Genomics, Institute Pasteur, 75015 Paris, France

13

14

15 *Corresponding author:

16 Julia Frunzke; Email: j.frunzke@fz-juelich.de; Phone: +49 2461 615430

17

18 #These authors contributed equally to this work.

19

20 **This PDF file includes:**

21

22 Figure S1: Schematic overview of the convolution profiling.

23 Figure S2: Assessment of significance for the reported peak intensity values.

24 Figure S3: Global binding pattern of HrrA in the *C. glutamicum* genome in response to
 25 hemin addition.

26 Figure S4: Distribution of distances from HrrA binding peaks centers to the closest gene
 27 start site (transcription start site, TSS).

28 Figure S5: HrrA binding to selected target promotor regions.

29 Figure S6: Derivation of a HrrA binding motif revealed a weakly conserved palindromic
 30 sequence.

31 Figure S7: Visual inspection of *C. glutamicum* cells before and after addition of heme.

32 Figure S8: Growth assays revealed an increased sensitivity of $\Delta hrrA$ cells against oxidative
 33 stress.

34 Figure S9: Binding affinity of HrrA to selected target promoters.

35 Figure S10: Time-resolved differential gene expression analysis.

36 Figure S11: Correlation of HrrA binding and expression change.

37 Figure S12: HrrA coordinates expression of *ctaA* and *ctaB* in response to heme.

38

39 Table S1: Bacterial strains and plasmids used in this study.

40 Table S2: Oligonucleotides used in this study.

41 Table S5: Pearson correlation for the gene expression values (TPM) between the two
 42 biological replicates.

43

44 SI References

45

46

47 **Other supplementary materials for this manuscript include the following separate files:**

48 Table S3: Full Dataset, binding peaks HrrA and transcriptome analysis of *C. glutamicum*
 49 wild type and $\Delta hrrA$.

50 Table S4: Filtered dataset of time resolved transcriptome analysis of *C. glutamicum* wild
 51 type and $\Delta hrrA$ with genes showing at least two-fold alteration.

52

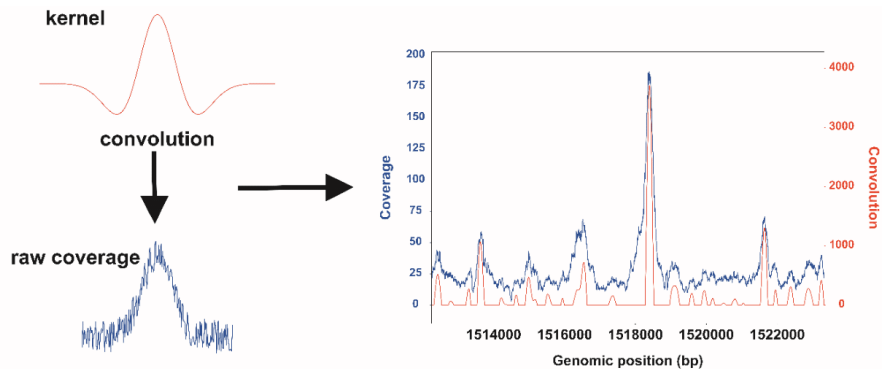
53

54

55 **Supplementary Figures**

56

57

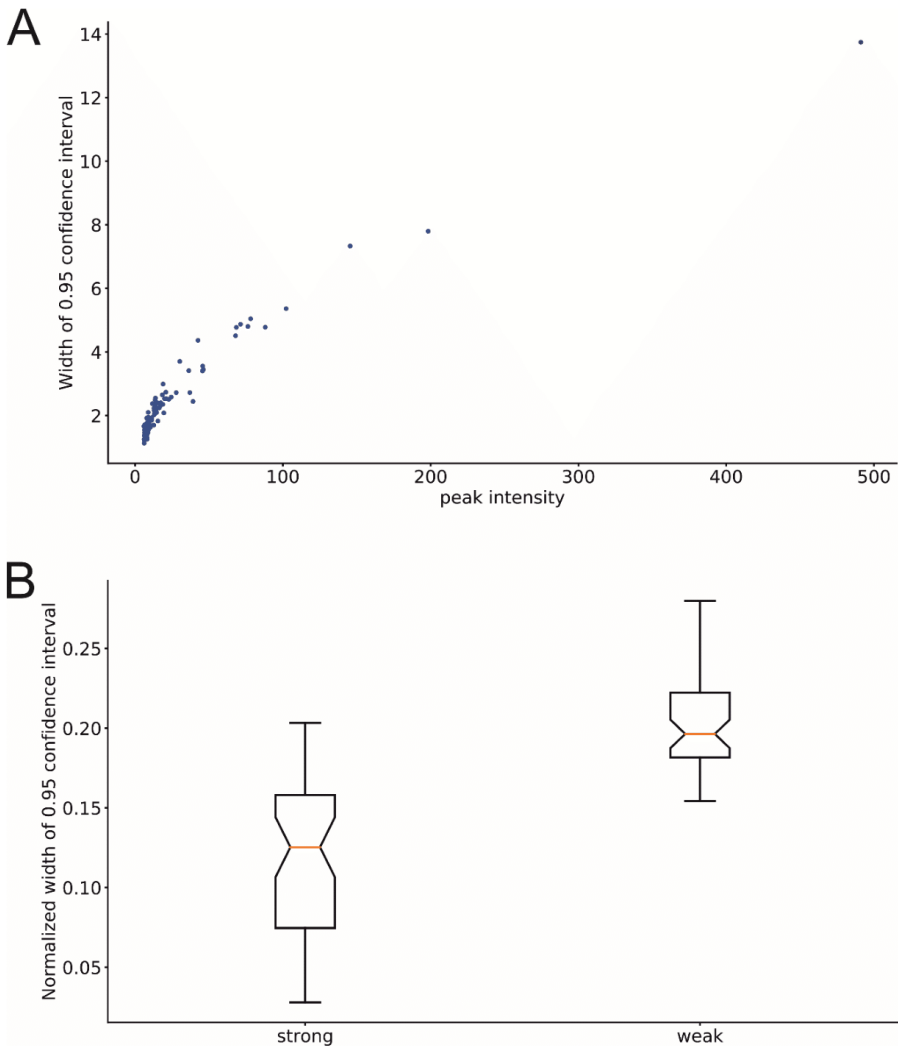


58

59

60 **Figure S1: Schematic overview of the convolution profiling.** Read coverage was convolved
61 with negative second order Gaussian kernel. The convolved read coverage was then scanned
62 to discover the local maxima (peaks).

63



64

65

66

67

68

69

70

71

72

73

74

75

Figure S2: Assessment of significance for the reported peak intensity values. (A) The error of peak intensity value (0.95 confidence intervals width) linearly depends on its absolute value. The stronger the peak the less the confidence in its absolute value. In contrast, the relative error normalized to peak intensity is similar for peaks of various strength, hence can be used as universal measure for significance assessment. (B) Distribution of the normalized confidence intervals width (NCIW) among the detected peaks. The distribution is represented as box plots with box edges at 1st and 3rd quantiles and box whiskers at minimum and maximum values. For the weak peaks (peak intensity <10) average NCIW is around 0.2 and limited by 0.28, while for the strong ones the average NCIW is around 0.13 and limited by 0.2. The upper limits were taken for the final estimation, as the most conservative confidence evaluation was pursued.

76

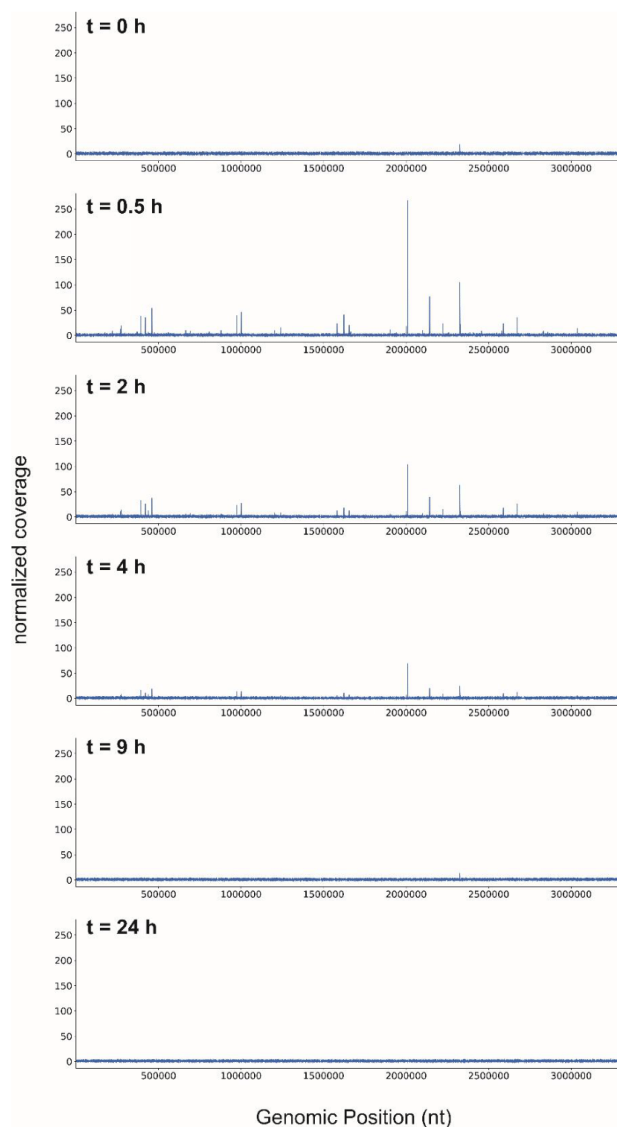
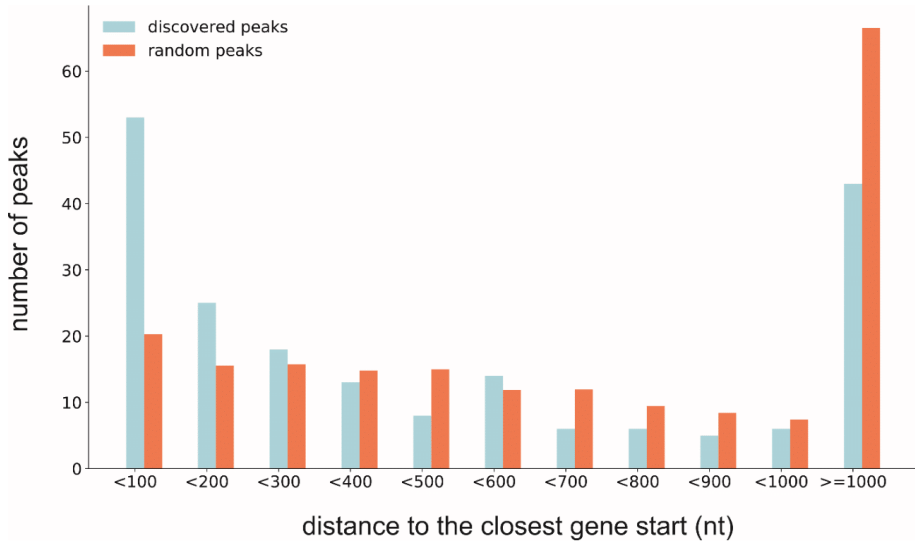
77
78
79
80
81
82
83
84
85

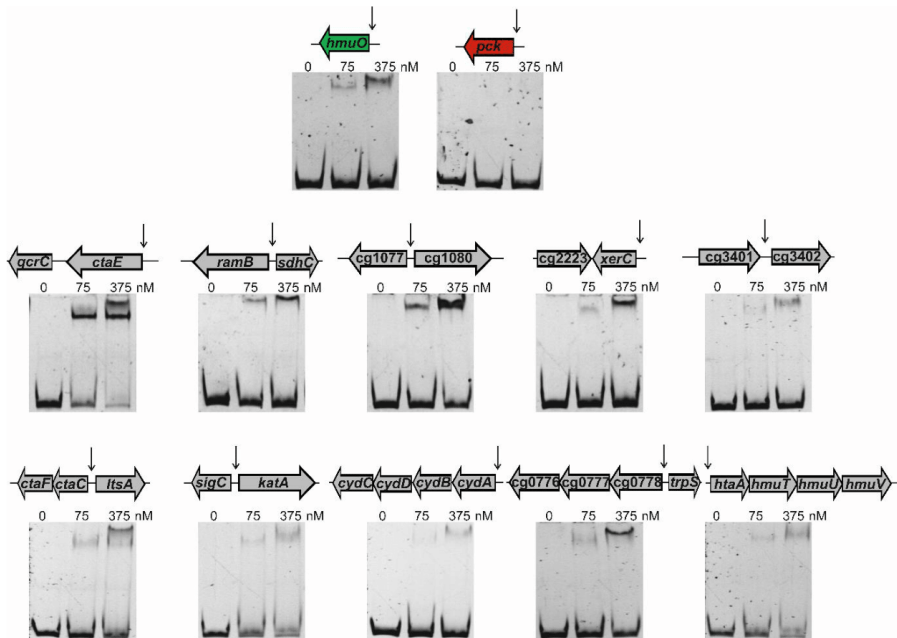
Figure S3: Global binding pattern of HrrA in the *C. glutamicum* genome in response to hemin addition. Genomic coverage (number of reads covering a particular genomic position) was normalized to the average coverage of the regions not harbouring binding peaks. Thus, depicted peak intensities are comparable between different time points. The strain *C. glutamicum::hrrA-C-twinstrep* was cultivated in CGXII minimal medium (lacking FeSO₄) supplemented with 2% (w/v) glucose and 4 μM hemin was added at 0 h. Cells were harvested at different time points as described in Figure 1.

4



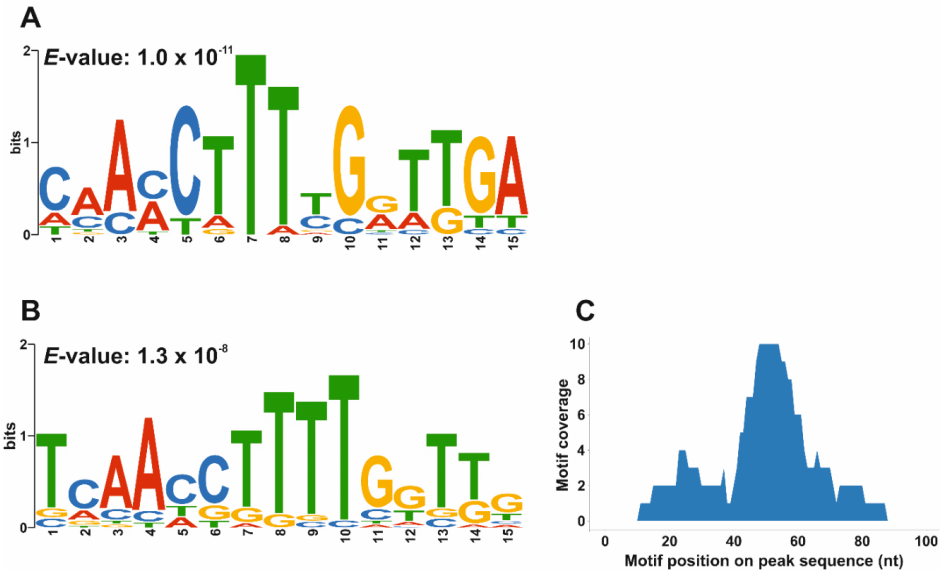
86
87
88
89
90
91
92
93

Figure S4: Distribution of distances from HrrA binding peaks centres to the closest downstream gene start site (transcription start site, TSS). As a background (red color), random peaks of the same width as real ones were generated. Random peak generation was performed 100 times and resulting distance distributions were then averaged into a single background distribution. Peaks with a distance of <100 nt can also be found up to 60 nt downstream of the TSS.



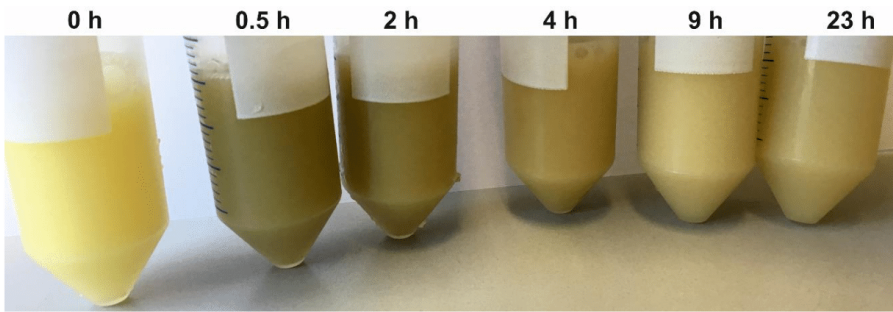
94
95
96
97
98
99
100
101

Figure S5: HrrA binding to selected target promoter regions. Protein-DNA interactions were validated by electrophoretic mobility shift assays (EMSA) using 15 nM DNA fragments covering 50 bp up- and downstream of the maximal ChAP-Seq peak height and an increasing protein monomer concentration of 0, 75 and 375 nM. The genomic location of the maximal peak height found in the ChAP-Seq experiments is indicated by an arrow. As control, the promoter regions of *hmuO* (positive control) and *pck* (negative control) were used.



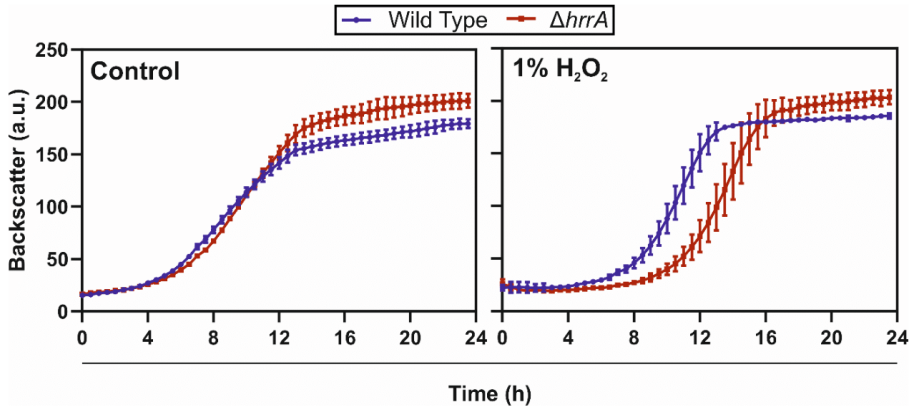
102
103
104
105
106
107
108
109
110

Figure S6: Derivation of a HrrA binding motif revealed a weakly conserved palindromic sequence. Sequences of all peaks with at least two-fold increased coverage (T_0) (A) or 100 bp of the tested EMSA DNA fragments (Figure S5) (B) were used for a MEME v.5 analysis (<http://meme-suite.org>). (C) Shown is the position of identified motif sequences within the analysed peak sequences used in (B). The majority of HrrA motifs centre at the position of the peak maximum (at 50 nt).



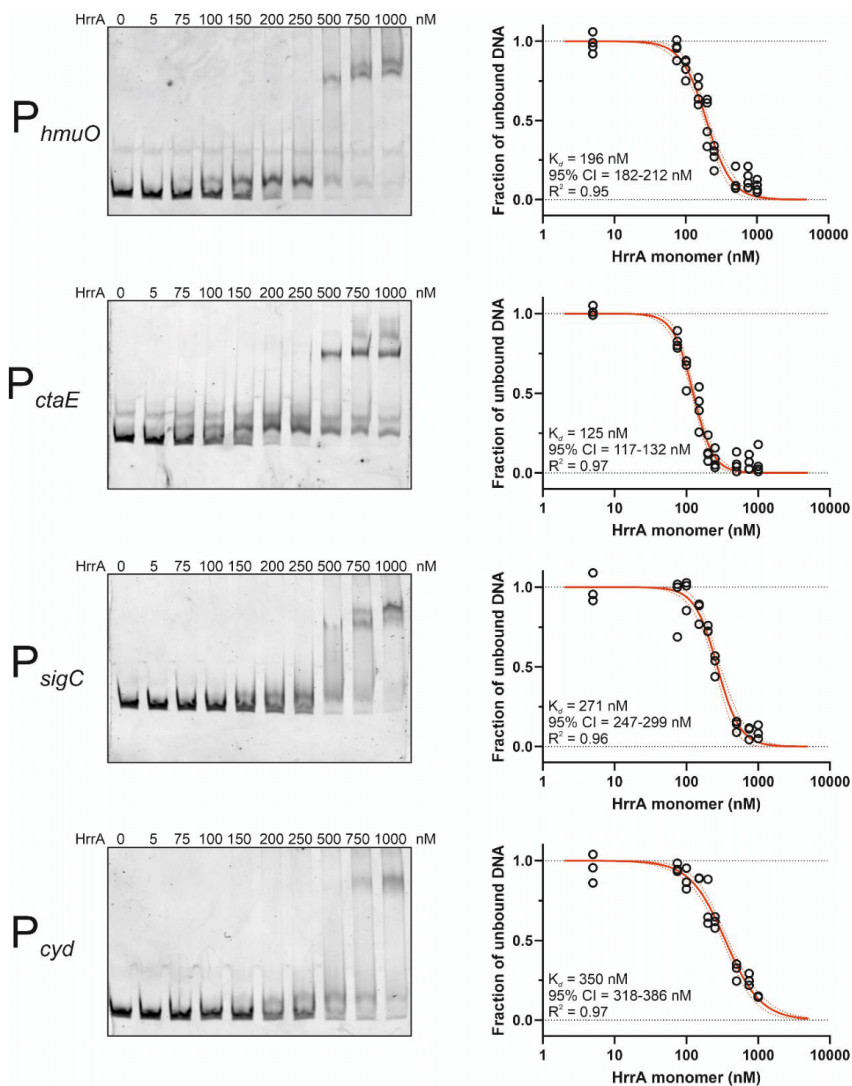
111
112
113
114
115
116
117
118
119

Figure S7: Visual inspection of *C. glutamicum* cells before and after addition of heme. Iron-starved *C. glutamicum* wild type cells were cultivated in CGXII medium (2 % (w/v) glucose, without FeSO_4) and cells were harvested at different time points before and after the addition of $4 \mu\text{M}$ heme. Cell pellets were subsequently resuspended in Tris buffer (100 mM Tris-HCl, 1 mM EDTA, pH 8.0) and adjusted to an OD_{600} of 3.5.



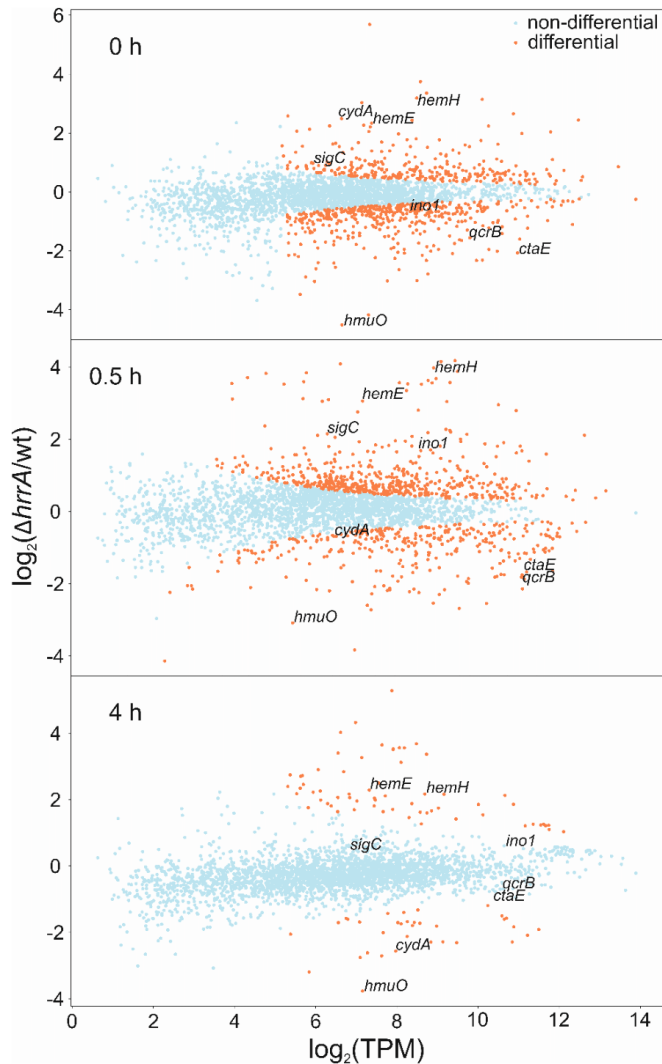
120
121
122
123
124
125
126
127
128
129
130

Figure S8: Growth assays revealed an increased sensitivity of *C. glutamicum* $\Delta hrrA$ against oxidative stress. Iron-starved *C. glutamicum* wild type as well as the mutant strain $\Delta hrrA$ were inoculated to an OD₆₀₀ of 1 in CGXII medium (2% (w/v) glucose, 4 μ M hemin, without FeSO₄) and subsequently incubated for 15 min at RT either with 1% (v/v) H₂O₂ or without. This incubation time of 15 min served as avoidance of misleading backscatter measurements due to foam generation. After the incubation, cells were transferred to microtiter plates and cultivated in a microbioreactor cultivation system. Growth curves shown are based on backscatter measurements (expressed in arbitrary units (a.u.)) of three biological replicates. The error bars represent the standard deviation of these replicates.



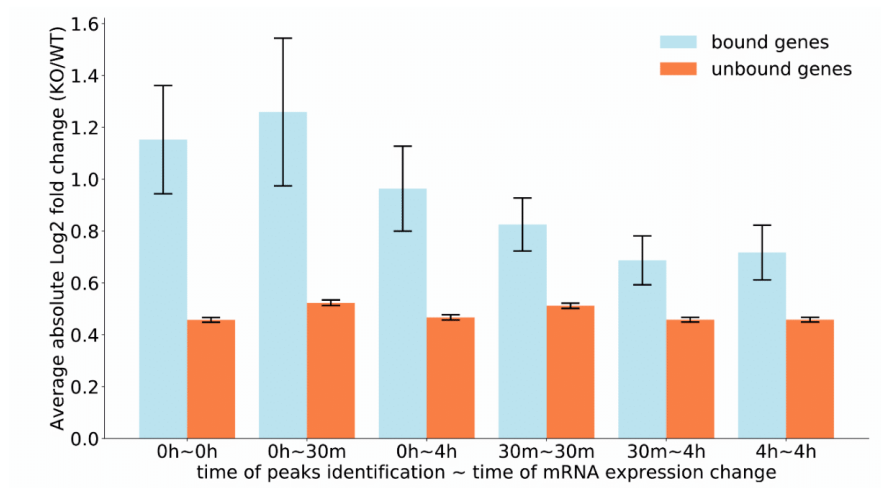
131
 132
 133
 134
 135
 136
 137
 138
 139
 140
 141
 142

Figure S9: Binding affinity of HrrA to selected target promoters. Depicted are representative images of quantitative EMSAs used for analysis of protein-DNA interaction and the calculation of HrrA affinities to the different promoters. For the analysis, 10 nM Cy3-labelled 98-105 bp DNA fragments containing the maximal ChAP-Seq peak height were used with increasing amounts of HrrA (given as monomers). Determination of unbound DNA in EMSA studies allowed the calculation of HrrA binding affinities to different target promoters. Quantification of unbound DNA band intensities was performed using Image Studio Lite (Licor, Bad Homburg, Germany) and apparent K_d values were calculated using GraphPad Prism 7. The calculation of apparent K_d values is based on 3-4 gels each. Black dotted lines represent top and bottom constraints for the fit. Red dotted lines represent the 95% confidence level. CI, confidence interval.



143
 144
 145
 146
 147
 148
 149
 150
 151
 152

Figure S10: Time-resolved differential gene expression analysis. Shown is the log₂ fold change in gene expression (Δ*hrrA* versus wild type) along with a log₂ mean expression (expression averaged for Δ*hrrA* and WT samples) in transcripts per million (TPM). Orange dots represent significantly differentially expressed genes with an empirical FDR < 0.05 (see material and methods). Wild type and Δ*hrrA* *C. glutamicum* strains were grown in CGXII medium (without FeSO₄) supplemented with 2% (w/v) glucose and 4 μM hemin (T₀ is prior addition of hemin; for details on cultivation and sample preparation see material and methods).



153

154

Figure S11: Correlation of HrrA binding and expression change. For the time-points 0h, 0.5h, 4h all the *C. glutamicum* protein-coding genes with decent expression (>10 TPM in $\Delta hrrA$ and WT samples) were split into groups: bound by HrrA (the ones which have an HrrA binding peak within 800 nt region upstream or 200 nt downstream to the transcription start site) and unbound. For these groups mean absolute log2 fold change ($\Delta hrrA/WT$) was calculated for the time-points 0h, 0.5h, 4 h along with standard error of the mean.

156

157

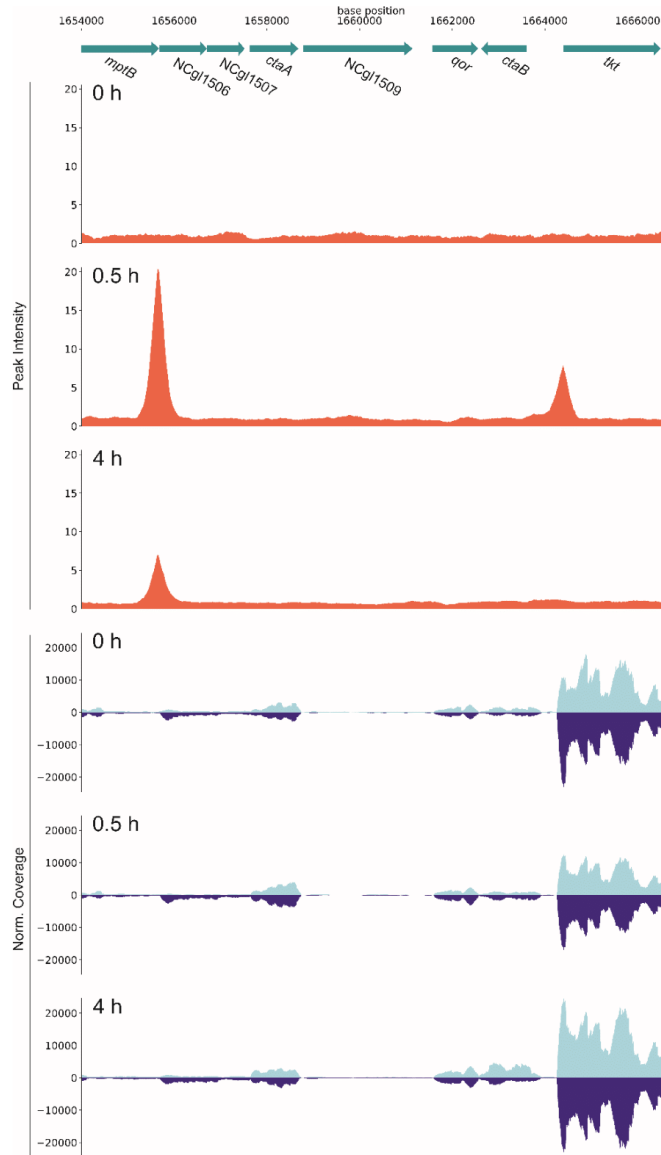
158

159

160

161

162



163
164
165
166
167
168
169
170

Figure S12: HrrA coordinates expression of *ctaA* and *ctaB* in response to heme. Shown are the ChAP-Seq (orange) and RNA-Seq (blue) results focusing on the *ctaA* and *ctaB* locus in the genome of *C. glutamicum*. Depicted is the genomic region between *mptB* (cg1766) and *tkt* (cg1774). For the cultivation, CGXII medium supplemented with 2% (w/v) glucose and 4 μ M hemin was inoculated with iron starved cells from a stationary culture and adjusted to an OD₆₀₀ of 3.5. Samples were analysed at the indicated time points as described in material and methods.

171

172 **Supplementary Tables**

173

174 **Table S1: Bacterial strains and plasmids used in this study.** Oligonucleotides used for the
175 construction of the plasmids are listed in Table S2.

176

177

Strain	Relevant characteristics	Reference
<i>Escherichia coli</i>		
DH5 α	<i>fhuA2 lac(del)U169 phoA glnV44 Φ80' lacZ(del)M15 gyrA96 recA1 relA1 endA1 thi-1 hsdR17</i> ; for general cloning purposes	Invitrogen
BL21(DE3)	B F ⁻ <i>ompT gal dcm lon hsdS_B(r_B⁻m_B⁻) λ(DE3 [<i>lacI lacUV5-T7p07 ind1 sam7 nin5</i>] [<i>malB</i>]_{K-12}(λ^S); overexpression of proteins.</i>	(1)
<i>Corynebacterium glutamicum</i>		
<i>C. glutamicum</i> ATCC 13032	Biotin-auxotrophic wild type strain	(2)
<i>C. glutamicum</i> Δ<i>hrrA</i>	Derivative of ATCC 13032 with in-frame deletion of the <i>hrrA</i> gene (cg3247).	(3)
<i>C. glutamicum</i>::<i>hrrA</i>-C-<i>twinstrep</i>	Derivative of ATCC 13032 encoding a C-terminally <i>twinstrep</i> -tagged version of <i>hrrA</i> (cg3247).	This study
Plasmids		
Name	Resistance	Source
pK19 <i>mob sacB</i>	Kanamycin	(4)
pK19 <i>mob sacB_hrrA</i> -C- <i>twinstrep</i>	Kanamycin	This study

178

179

180 **Table S2: Oligonucleotides used in this study.**181
182

#	Name	Sequence
Construction of pK19 <i>mob sacB_hrrA-C-twinstrep</i>		
1	<i>hrrA</i> -LF-twin-strep_fw	CAAGCTTGCATGCCTGCAGGTGCAGCGCGGAATCGACGTCATCTTG
2	<i>hrrA</i> -LF-twin-strep_rv	ACCTAAAGCCTTGCAGCAACCCCGCTATTTTTCGAACTGCGGGTGG
3	<i>hrrA</i> -RF_fw	GAGCCACCCGAGTTTCGAAAAATAGCGGGGTTGCTGCAAGGC
4	<i>hrrA</i> -RF_rv	ATTCGAGCTCGGTACCCGGGATCCCCGGAATCAATACACCCGGC
Amplification of DNA probes for EMSAs		
5	<i>P_{hmuO}</i> (EMSA) fw	GAGAAATCCTCACGCTCAC
6	<i>P_{hmuO}</i> (EMSA) fw-Cy3	Cy3-GAGAAATCCTCACGCTCAC
7	<i>P_{hmuO}</i> (EMSA) rv	GGTGGGAGCCCCAAGTTG
8	<i>P_{ctaE}</i> (EMSA) fw	CCCAAAGTGGTTCCGCAGG
9	<i>P_{ctaE}</i> (EMSA) fw-Cy3	Cy3-CCCAAAGTGGTTCCGCAGG
10	<i>P_{ctaE}</i> (EMSA) rv	ACGCCTTTTATTCGGGTTT
11	<i>P_{pck}</i> (EMSA) fw	CTTTCTATGGAGATGATCG
12	<i>P_{pck}</i> (EMSA) rv	CGATTTAAATGGACCCTAAAC
13	<i>P_{ramB}</i> (EMSA) fw	CCTGCGCAAAGTTGCTCCCTG
14	<i>P_{ramB}</i> (EMSA) rv	CTCACAGGATACCGATCCGAAC
15	<i>P_{cg1080}</i> (EMSA) fw	CGCTCCTCTGTGGGATTTGTC
16	<i>P_{cg1080}</i> (EMSA) rv	GCCTTCACTCCCTCAAAC
17	<i>P_{xerC}</i> (EMSA) fw	CTTAGGCTTGCCTCACACAC
18	<i>P_{xerC}</i> (EMSA) rv	AATGCGGAAATGCCATAAAACC
19	<i>P_{cg3402}</i> (EMSA) fw	CATAGGGGTATAGCCTTGAG
20	<i>P_{cg3402}</i> (EMSA) rv	CAGTGTGCGCAGGTCATGCC
21	<i>P_{ctaC}</i> (EMSA) fw	GGAATACCTAAAGTCTAGGC
22	<i>P_{ctaC}</i> (EMSA) rv	GTAGGAACGTAGGGGTAAG
23	<i>P_{sigC/katA}</i> (EMSA) fw	GGTCACCATAAAGGTGTGTAG
24	<i>P_{sigC/katA}</i> (EMSA) fw-Cy3	Cy3-GGTCACCATAAAGGTGTGTAG
25	<i>P_{sigC/katA}</i> (EMSA) rv	GCCACCAATAATCAGCCC
26	<i>P_{cyd}</i> (EMSA) fw	GTTCCCGCTCACAGCTTAAC
27	<i>P_{cyd}</i> (EMSA) fw-Cy3	Cy3-GTTCCCGCTCACAGCTTAAC
28	<i>P_{cyd}</i> (EMSA) rv	GGTGACTTGTAACAAGGGG
29	<i>P_{trpS}</i> (EMSA) fw	GACTTGTTTACCCAAGCAATAC
30	<i>P_{trpS}</i> (EMSA) rv	CCGGTGAGGCAACATTTACC
31	<i>P_{htaA}</i> (EMSA) fw	GTCATGATGGCGTCTCGGGC
32	<i>P_{htaA}</i> (EMSA) rv	GTAATCAACGCACAAATG

183
184
185
186

Table S3: Complete Dataset of genome wide HrrA binding (ChAP-seq) and time resolved transcriptome analysis of *C. glutamicum* wild type and Δ hrrA (RNA-seq). For ChAP-seq analysis, the strain *C. glutamicum*::hrrA-C-twinstrep was cultivated in CGXII minimal medium supplemented with 2% (w/v) glucose and 4 μ M hemin, was harvested at different time points as described in Figure 1. For RNA-Seq, wild type cells and a Δ hrrA strain were cultivated accordingly and harvested 0 h, 0.5 h and 4 h after hemin addition. Column 1 and 2 show the the gene locus (ID) and gene name. Column 3 indicates the distance of the peak maximum to the translational start site of the gene and column 4 indicates the distance to the transcription start site. In light grey (510), ChAP-seq peak intensities are indicated at 0 h, 0.5 h, 2 h, 4 h, 9 h and 24 h after hemin addition. In green (11-13) and red (14-16), the measured mRNA levels of the corresponding genes in the wild type strain (green) and a Δ hrrA strain (red) are shown (in transcripts per million, mean of two biological replicates). All further information can be found in the full table in Keppel et al. (2018).

Gene ID	Gene name	Dist ance ATG	Dist ance to TSS	ChAP-Seq						mRNA wt			mRNA Δ hrrA		
				t=0	t=0.5	t=2	t=4	t=9	t=24	t=0	t=0.5	t=4	t=0	t=0.5	t=4
				cg0074		205	205	0.0	2.1	2.2	2.1	0.0	0.0	7.0	1.5
cg0075		79	-108	0.0	2.1	2.2	2.1	0.0	0.0	136.5	65.7	68.4	93.7	40.4	64.3
cg0076		280	280	0.0	2.3	2.3	2.0	0.0	0.0	22.6	6.0	15.8	12.0	3.8	12.0
cg0113	<i>ureA</i>	557	533	0.0	1.8	1.6	0.0	0.0	0.0	408.2	163.9	118.3	165.2	216.3	93.4
cg0128		166	166	0.0	1.7	1.9	1.6	0.0	0.0	10.6	6.9	17.4	5.8	12.5	13.0
cg0129	<i>putA</i>	90	8	0.0	1.7	1.9	1.6	0.0	0.0	179.4	90.1	179.3	132.3	113.6	95.6
cg0153	<i>hde</i>	302	302	0.0	3.8	3.7	2.5	0.0	0.0	20.5	18.0	30.6	21.5	21.4	15.9
cg0163		428	322	0.0	2.0	1.9	1.6	0.0	0.0	165.9	302.2	181.6	56.6	50.7	87.6
cg0204	<i>iolG</i>	253	253	0.0	6.4	4.3	3.1	0.0	0.0	21.3	39.7	59.0	25.7	26.6	37.4
cg0222		410	275	0.0	3.2	3.1	2.4	0.0	0.0	43.0	28.1	37.7	22.1	25.2	22.0
cg0223	<i>iolT1</i>	158	73	0.0	2.0	1.9	1.7	0.0	0.0	18.4	11.8	37.5	14.9	6.0	23.0
cg0247		180	180	0.0	2.2	1.7	1.5	0.0	0.0	40.4	21.2	28.5	37.2	34.6	23.3
cg0251		71	-71	1.3	1.6	2.3	1.4	0.0	0.0	108.3	67.8	107.3	95.5	80.8	85.0
cg0284		122	-159	0.0	1.8	2.0	0.0	0.0	0.0	95.7	76.4	103.8	109.7	85.9	88.3
NCg10236		169	110	1.3	1.3	1.3	1.3	1.2	1.0	0.0	0.1	0.0	0.0	0.1	0.3
cg0296	<i>dnaZX</i>	73	73	0.0	1.6	1.7	0.0	0.0	0.0	191.0	145.7	237.7	139.6	145.4	188.8
cg0304		214	35	0.0	13	11	5.9	0.0	0.0	96.2	39.6	71.9	90.0	67.5	53.8
cg0306	<i>lysC</i>	32	32	0.0	13	11	5.9	0.0	0.0	601.5	598.3	692.6	722.9	970.1	764.5
cg0309	<i>sigC</i>	29	29	1.5	19	14	8.1	1.7	0.0	39.1	29.2	83.7	79.7	131.6	124.0
cg0310	<i>katA</i>	175	132	1.5	19	14	8.1	1.7	0.0	1980.0	5988.3	1699.9	1847.3	3600.9	734.7
cg0330	<i>cgfR1</i>	24	24	0.0	3.0	2.7	1.9	0.0	0.0	25.8	15.3	19.7	13.8	19.7	16.5
cg0336	<i>pbp1a</i>	533	243	0.0	2.1	2.0	1.6	0.0	0.0	413.5	221.9	224.6	224.0	153.7	194.9
cg0337	<i>whcA (whiB4)</i>	133	-21	0.0	2.1	2.0	1.6	0.0	0.0	1195.5	1024.2	1111.8	755.4	742.4	677.5
cg0341	<i>phdA (fadD1)</i>	175	175	0.0	2.6	2.7	2.0	1.5	0.0	5.0	3.3	9.8	4.5	2.2	3.7
cg0390		350	350	0.0	3.4	3.6	2.0	0.0	0.0	95.4	96.1	55.0	59.1	90.1	43.3
cg0420		641	641	0.0	7.3	4.9	4.4	0.0	0.0	192.3	99.2	161.1	50.3	62.0	41.3
cg0420		164	-164	0.0	3.0	2.4	2.3	0.0	0.0	192.3	99.2	161.1	50.3	62.0	41.3
cg0422	<i>murA</i>	675	591	0.0	3.5	2.4	2.5	0.0	0.0	230.1	157.2	218.4	237.6	144.1	205.0
cg0424		89	-97	0.0	2.2	1.5	0.0	0.0	0.0	194.0	149.5	254.4	183.3	135.3	216.8
cg0437	<i>wzy</i>	312	60	0.0	4.0	3.4	2.7	0.0	0.0	154.8	119.9	212.2	88.7	124.0	160.7
cg0438		35	3	0.0	2.3	1.7	0.0	0.0	0.0	416.0	360.2	458.3	385.8	399.8	263.8
cg0438		79	29	0.0	2.3	1.7	1.8	0.0	0.0	416.0	360.2	458.3	385.8	399.8	263.8
cg0439		326	35	0.0	2.3	1.7	0.0	0.0	0.0	194.3	209.8	254.1	169.3	227.8	203.2
cg0439		281	-10	0.0	2.3	1.7	1.8	0.0	0.0	194.3	209.8	254.1	169.3	227.8	203.2
cg0444	<i>ramB</i>	213	198	3.1	38	33	16	3.1	0.0	673.0	725.4	470.9	353.7	439.9	319.0

cg0445	<i>sdhC</i> <i>sdhCD</i>	298	83	3.1	38	33	16	3.1	0.0	1917.1	2911.0	2339.4	392.3	884.6	760.6
cg0453		4	-38	0.0	2.4	2.0	0.0	0.0	0.0	220.6	312.2	502.2	438.4	562.0	417.4
cg0465		45	45	0.0	2.8	2.3	2.2	0.0	0.0	5.6	1.1	8.6	3.9	1.1	11.3
cg0466	<i>htaA</i>	185	43	0.0	2.8	2.3	2.2	0.0	0.0	19.4	8.6	77.7	3.0	3.0	72.5
cg0475		370	370	0.0	36	26	11	2.2	0.0	612.1	709.0	1603.6	1108.3	1378.3	1607.6
cg0495		434	44	0.0	7.1	13	8.1	0.0	0.0	39.2	24.8	46.5	30.9	33.6	33.7
cg0497	<i>hemA</i>	34	-162	0.0	7.1	13	8.1	0.0	0.0	115.4	487.8	136.3	636.4	765.8	274.8
cg0500	<i>qsuR</i>	16	-40	0.0	4.8	4.1	2.9	0.0	0.0	38.8	25.7	20.4	22.2	20.1	14.0
cg0501	<i>qsuA</i>	260	80	0.0	4.8	4.1	2.9	0.0	0.0	59.3	85.9	25.4	44.9	50.4	24.8
cg0505		7	7	0.0	1.9	1.6	1.4	0.0	0.0	79.4	59.2	81.2	126.7	93.2	41.2
cg0516	<i>hemE</i>	17	17	0.0	54	38	19	2.6	0.0	56.8	34.8	52.6	281.2	277.5	249.6
cg0517	<i>hemY</i>	624	429	0.0	0.0	3.0	0.0	0.0	0.0	65.7	37.6	96.6	215.2	258.1	297.0
cg0524	<i>ccsB</i>	38	-38	0.0	2.2	2.2	1.5	0.0	0.0	95.5	234.0	292.9	112.7	300.6	375.5
cg0545	<i>pitA</i>	3	-158	0.0	1.6	1.4	0.0	1.4	0.0	105.9	51.6	206.8	138.9	81.9	289.6
cg0557		9	-9	0.0	3.0	3.2	2.3	0.0	0.0	24.4	25.0	28.3	33.8	55.8	42.7
cg0559	<i>ispB</i>	154	80	0.0	3.0	3.2	2.3	0.0	0.0	271.6	230.9	253.5	213.1	263.4	273.8
cg0566	<i>gabT</i>	748	748	0.0	3.9	2.6	1.7	0.0	0.0	3.2	4.1	3.2	3.0	3.4	3.0
cg0614		654	654	0.0	2.1	1.5	1.6	0.0	0.0	78.5	197.6	53.7	73.5	143.1	33.6
cg0630	<i>rplR</i>	141	-141	0.0	1.8	0.0	0.0	0.0	0.0	1311.6	798.0	3689.9	2113.0	2820.0	4967.9
cg0636	<i>creB</i>	54	5	0.0	6.6	4.2	4.2	0.0	0.0	50.9	50.2	18.7	42.2	31.1	13.1
cg0636	<i>creB</i>	451	402	0.0	3.5	2.5	0.0	0.0	0.0	50.9	50.2	18.7	42.2	31.1	13.1
cg0647	<i>secY</i>	708	595	0.0	1.8	1.4	0.0	0.0	0.0	652.3	537.6	587.1	651.5	477.7	563.0
cg0656	<i>rplQ</i>	14	-14	0.0	2.9	2.1	1.8	0.0	0.0	1374.9	750.8	3061.1	1423.5	1461.1	4076.1
cg0671		710	710	0.0	3.2	2.6	2.5	0.0	0.0	7.9	1.9	8.9	3.5	4.1	3.2
cg0673	<i>rplM</i>	36	-177	0.0	2.0	1.7	1.4	0.0	0.0	1752.3	1550.6	4184.6	2711.2	2511.7	5649.7
cg0688		17	17	0.0	3.9	3.8	2.7	1.4	0.0	49.4	41.5	114.3	65.5	75.2	90.1
cg0752		504	381	0.0	1.9	1.5	1.5	0.0	0.0	111.5	135.6	286.1	158.2	186.8	387.3
cg0753		250	250	0.0	10	6.3	4.6	0.0	0.0	238.0	301.2	328.1	442.7	531.1	190.0
cg0778		65	29	0.0	8.8	7.3	4.2	0.0	0.0	130.6	80.6	111.9	149.8	121.9	154.5
cg0779	<i>trpS</i>	95	95	0.0	8.8	7.3	4.2	0.0	0.0	333.0	247.9	506.6	247.4	304.5	315.6
cg0780		140	-140	0.0	2.0	0.0	0.0	0.0	0.0	459.5	359.3	184.0	211.0	218.1	149.2
cg0823	<i>ntaA</i>	32	-32	1.2	1.5	1.2	1.2	1.1	1.2	5.3	1.8	5.6	4.2	2.1	3.0
cg0831	<i>tusG</i>	30	-30	0.0	1.8	1.4	0.0	0.0	0.0	146.7	129.7	452.5	130.2	128.9	403.2
cg0842		58	58	0.0	1.7	1.4	0.0	0.0	0.0	21.8	22.1	121.0	35.8	42.5	90.8
cg0875		54	-8	0.0	4.5	3.4	2.1	0.0	0.0	3.8	4.0	3.5	2.2	3.2	1.7
cg0876	<i>sigH</i>	114	-17	0.0	4.5	3.4	2.1	0.0	0.0	208.6	342.9	347.9	249.1	313.8	260.4
cg0880		54	54	0.0	7.7	5.0	3.4	0.0	0.0	67.0	45.0	63.2	76.9	70.9	51.2
cg0931		69	69	0.0	2.3	1.6	1.5	1.2	1.0	26.8	17.1	7.7	16.8	12.5	5.3
cg0948	<i>serC</i>	207	147	0.0	2.8	2.3	1.7	0.0	0.0	800.8	553.5	595.8	662.8	839.1	927.2
cg0949	<i>gltA</i>	519	140	0.0	2.8	2.3	1.7	0.0	0.0	4125.6	2270.2	2535.7	2959.2	1630.9	3228.6
cg0950	<i>fkpA</i>	692	630	0.0	10	6.5	4.0	0.0	0.0	689.3	547.7	1184.1	718.0	952.9	1436.1
cg0951	<i>accD3</i>	69	-96	0.0	4.3	1.8	2.2	0.0	0.0	508.0	728.0	395.4	134.3	156.3	119.4
cg0986	<i>amtR</i>	407	366	0.0	1.8	1.4	1.4	0.0	0.0	274.1	242.2	233.6	208.3	295.3	241.8
cg0986	<i>amtR</i>	460	419	0.0	0.0	0.0	0.0	0.0	0.0	274.1	242.2	233.6	208.3	295.3	241.8
cg1044		431	431	0.0	2.0	1.4	0.0	0.0	0.0	272.8	189.1	678.3	468.8	436.8	465.6
cg1050		57	57	0.0	40	24	14	1.6	0.0	49.5	26.5	90.1	102.2	119.1	170.4

cg1051		149	-149	0.0	2.8	2.1	1.7	0.0	0.0	25.8	28.8	68.1	49.4	69.8	63.0
cg1051		102	-102	0.0	2.8	2.1	0.0	1.2	0.0	25.8	28.8	68.1	49.4	69.8	63.0
cg1052	<i>cmt3</i>	277	233	0.0	2.8	2.1	1.7	0.0	0.0	220.6	155.6	176.1	172.6	220.6	96.2
cg1052	<i>cmt3</i>	230	186	0.0	2.8	2.1	0.0	1.2	0.0	220.6	155.6	176.1	172.6	220.6	96.2
cg1069	<i>gapB (gapX)</i>	295	215	0.0	2.4	2.1	1.4	0.0	0.0	75.8	96.1	538.2	89.4	304.8	503.9
cg1069	<i>gapB (gapX)</i>	255	175	0.0	2.4	2.1	1.4	0.0	0.0	75.8	96.1	538.2	89.4	304.8	503.9
cg1077		33	33	4.1	47	28	15	2.4	0.0	4.4	2.8	7.2	23.0	25.6	21.1
cg1080		50	17	4.1	47	28	15	2.4	0.0	26.9	12.1	52.1	130.4	206.2	200.5
NCgl0914		450	382	0.0	3.4	2.3	1.9	0.0	0.0	33.5	24.2	100.2	51.3	44.2	71.0
cg1105	<i>lysI</i>	553	553	0.0	3.8	2.5	2.1	0.0	0.0	23.3	14.4	13.7	20.3	17.9	11.2
cg1111	<i>eno</i>	389	319	0.0	2.2	1.7	0.0	0.0	0.0	2231.6	1416.8	3740.6	2553.3	1758.9	3184.7
cg1145	<i>fumC (fum)</i>	115	78	0.0	2.2	1.3	1.3	0.0	0.0	664.9	719.6	1499.4	674.7	1209.2	1530.5
cg1147	<i>ssul</i>	203	-17	0.0	2.2	1.3	1.3	0.0	0.0	416.4	258.7	159.8	255.5	180.0	170.9
cg1157	<i>fbp</i>	869	767	0.0	2.0	1.3	0.0	0.0	0.0	825.0	876.1	861.3	518.3	842.0	903.0
cg1179		782	740	0.0	2.2	1.7	1.3	0.0	0.0	85.5	114.7	85.8	101.9	105.8	60.6
cg1288		775	666	0.0	1.9	0.0	1.3	0.0	0.0	25.6	62.2	19.7	16.6	43.4	19.0
cg1289		534	534	0.0	2.0	1.3	1.4	0.0	0.0	13.2	31.6	13.4	8.2	24.3	13.7
cg1292		113	113	0.0	3.0	2.0	1.6	0.0	0.0	83.4	29.6	351.0	77.3	41.0	325.7
cg1301	<i>cydA</i>	192	192	2.6	11	8.3	5.0	4.5	0.0	30.3	117.6	446.8	173.5	74.3	74.5
cg1316		443	383	0.0	1.8	1.3	0.0	0.0	0.0	94.7	62.3	100.3	85.5	68.2	91.2
cg1334	<i>lysA</i>	114	-54	2.2	16	9.0	6.4	1.8	0.0	328.0	330.5	530.0	273.3	337.0	588.8
cg1355	<i>prfA</i>	627	495	0.0	1.7	1.4	1.2	0.0	0.0	503.3	222.0	398.3	442.1	256.2	472.0
cg1359		176	176	0.0	1.6	0.0	0.0	0.0	0.0	158.8	83.5	159.7	131.3	112.9	139.3
cg1454		274	248	0.0	1.5	0.0	0.0	0.0	0.0	84.5	130.3	101.3	124.8	145.9	67.8
cg1456		154	-166	0.0	1.5	0.0	0.0	0.0	0.0	110.4	132.3	151.7	97.3	104.4	109.8
cg1458	<i>odx</i>	144	-144	0.0	2.1	1.4	0.0	0.0	0.0	238.6	153.4	371.2	212.6	253.8	418.5
cg1467		250	116	0.0	1.9	1.2	1.1	0.0	0.0	16.7	12.1	4.5	9.8	10.9	5.3
cg1474		138	-138	0.0	2.8	1.3	1.5	0.0	0.0	48.2	54.8	70.8	43.8	40.3	47.6
cg1484		-64	-97	0.0	3.1	0.0	1.4	0.0	0.0	100.1	191.4	101.6	141.4	187.3	107.5
cg1484		-20	-53	0.0	3.1	1.9	1.4	0.0	0.0	100.1	191.4	101.6	141.4	187.3	107.5
cg1485		254	187	0.0	2.4	1.6	0.0	0.0	0.0	50.5	40.6	26.7	34.3	35.1	22.3
cg1485		124	57	0.0	3.1	0.0	1.4	0.0	0.0	50.5	40.6	26.7	34.3	35.1	22.3
cg1485		80	13	0.0	3.1	1.9	1.4	0.0	0.0	50.5	40.6	26.7	34.3	35.1	22.3
cg1526		46	-46	0.0	2.1	1.7	1.4	0.0	0.0	3.1	1.3	2.1	3.3	2.1	1.5
cg1527		83	83	0.0	2.1	1.7	1.4	0.0	0.0	29.9	28.7	21.3	23.8	27.6	15.2
cg1531	<i>rpsA</i>	409	261	0.0	2.3	1.7	1.3	0.0	0.0	1779.3	1823.5	4049.0	1999.6	2520.4	5095.3
cg1537	<i>ptsG</i>	325	70	0.0	1.6	1.4	0.0	0.0	0.0	2393.3	1757.4	1855.8	2649.0	825.0	1779.5
cg1538	<i>coaE</i>	144	144	0.0	3.7	2.4	1.8	0.0	0.0	829.0	534.1	501.4	693.8	494.2	355.0
cg1568	<i>ugpA</i>	228	228	0.0	0.0	0.0	1.6	1.5	1.4	27.9	17.6	16.8	23.2	14.7	8.7
cg1583	<i>argD</i>	191	191	0.0	1.5	1.4	0.0	0.0	0.0	129.9	110.1	178.2	401.3	1329.5	356.0
cg1603		35	35	0.0	3.6	1.9	1.4	0.0	0.0	274.0	374.8	334.0	213.7	355.6	309.2
cg1628		13	-62	0.0	4.9	2.9	2.0	0.0	0.0	60.3	198.4	19.6	41.0	362.6	31.7
cg1629	<i>secA2</i>	225	193	0.0	4.9	2.9	2.0	0.0	0.0	119.5	101.9	164.4	94.7	127.1	143.8
cg1636		14	-110	0.0	4.1	1.7	1.3	0.0	0.0	86.6	130.8	152.6	88.4	167.2	132.1
cg1639		56	-56	0.0	1.6	1.0	1.2	0.0	0.0	89.2	106.8	125.5	73.0	116.4	110.1
cg1668		155	155	0.0	2.0	1.4	1.2	0.0	0.0	155.9	123.3	164.7	200.6	213.3	238.0
cg1691	<i>arc (mpa)</i>	74	74	0.0	1.9	1.3	0.0	0.0	0.0	452.4	360.3	200.9	361.6	307.9	161.6

cg1695		210	-37	0.0	24	13	5.8	3.0	0.0	302.1	434.4	172.6	171.1	211.4	62.1
cg1695		165	80	3.2	24	13	0.0	3.0	0.0	302.1	434.4	172.6	171.1	211.4	62.1
cg1701	<i>metH</i>	718	718	0.0	2.2	1.3	1.4	0.0	0.0	1376.3	1208.0	102.7	1037.7	859.8	175.3
cg1731		126	126	0.0	4.5	2.6	2.0	1.4	0.0	470.8	324.9	753.6	401.6	493.1	521.4
cg1734	<i>hemH</i>	21	21	2.7	41	18	11	2.0	0.0	78.6	68.1	156.0	731.7	1086.0	692.5
cg1736		87	-60	0.0	8.3	4.7	3.1	0.0	0.0	48.2	30.3	37.3	38.3	35.7	26.1
cg1737	<i>acn</i>	267	-59	0.0	8.3	4.7	3.1	0.0	0.0	2242.6	3962.9	1878.7	1175.0	3469.1	1605.0
cg1767		27	27	0.0	21	13	7.0	0.0	0.0	41.4	16.3	48.6	130.8	139.3	129.6
cg1773	<i>ctaB</i>	789	667	0.0	7.9	1.8	0.0	0.0	0.0	96.0	73.4	313.9	73.8	101.1	115.2
cg1791	<i>gapA (gap)</i>	269	86	2.9	3.9	3.0	2.3	2.2	0.0	6401.7	3734.5	6577.6	9354.4	3023.7	5159.7
cg1801	<i>rpe</i>	67	67	0.0	2.6	1.6	1.2	0.0	0.0	350.8	379.0	445.3	356.6	384.5	414.8
cg1841	<i>aspS</i>	189	79	0.0	1.7	0.0	0.0	0.0	0.0	355.0	264.9	550.4	258.2	268.4	550.7
cg1842		43	43	0.0	1.7	0.0	0.0	0.0	0.0	542.0	357.4	234.1	400.4	324.9	223.1
cg1893	<i>act4</i>	462	267	0.0	2.2	1.4	1.3	0.0	0.0	139.7	88.8	103.4	122.9	101.9	75.5
cg1894		124	-124	0.0	2.2	1.4	1.3	0.0	0.0	276.3	246.1	250.9	213.1	251.2	186.7
cg1898		743	590	0.0	2.9	1.9	1.7	0.0	0.0	2.2	0.3	1.0	1.7	0.0	0.8
cg1905		286	139	0.0	2.1	2.0	1.4	0.0	0.0	573.4	901.6	1744.0	487.4	967.2	1131.7
NCgl1628		961	776	0.0	1.6	1.1	0.0	0.0	0.0	26.4	15.5	46.2	25.4	30.5	32.9
cg1918		682	682	0.0	1.8	1.5	0.0	0.0	0.0	140.4	93.9	103.1	75.1	55.2	70.8
cg1923		156	-156	0.0	1.9	1.3	0.0	0.0	0.0	3.1	2.9	2.8	3.1	3.2	2.8
cg1925		348	348	0.0	2.4	1.2	1.3	0.0	0.0	118.4	79.7	49.7	95.8	118.5	48.2
cg1926		170	170	0.0	2.0	1.4	0.0	0.0	0.0	47.7	33.5	29.6	25.1	52.5	23.4
cg1926		130	130	0.0	2.0	1.4	0.0	0.0	0.0	47.7	33.5	29.6	25.1	52.5	23.4
cg1959	<i>priP</i>	16	-180	0.0	3.3	1.9	1.8	0.0	0.0	4.8	2.6	2.7	3.6	2.6	2.0
cg1981		556	556	0.0	2.4	0.0	0.0	0.0	0.0	12.9	7.0	6.1	9.4	5.7	4.4
cg1981		476	476	0.0	0.0	1.5	1.6	0.0	0.0	12.9	7.0	6.1	9.4	5.7	4.4
cg1981		438	438	0.0	0.0	1.5	1.6	0.0	0.0	12.9	7.0	6.1	9.4	5.7	4.4
cg1981		47	-47	0.0	1.8	1.5	0.0	0.0	0.0	12.9	7.0	6.1	9.4	5.7	4.4
cg2005		340	139	0.0	2.7	1.8	2.0	0.0	0.0	15.8	14.8	11.9	15.8	14.2	9.1
cg2014		78	-78	0.0	12	6.6	4.9	0.0	0.0	109.7	122.2	54.1	50.9	57.2	33.9
cg2021		298	298	0.0	3.3	1.5	1.4	0.0	0.0	14.9	12.8	9.0	12.0	10.9	6.5
NCgl1731		523	245	0.0	1.8	1.2	1.5	0.0	0.0	1651.6	952.3	737.2	1404.5	786.8	620.6
cg2031		164	7	0.0	3.0	1.7	1.5	0.0	0.0	91.8	112.3	78.4	96.8	72.4	62.2
cg2037		7	-44	0.0	3.3	1.8	1.5	0.0	0.0	89.9	92.4	82.1	81.6	98.5	68.9
NCgl1755		43	43	0.0	5.8	2.2	2.0	0.0	0.0	187.9	298.7	148.3	210.3	217.9	122.8
NCgl1787		14	-22	0.0	2.8	2.1	1.3	0.0	0.0	8.3	9.7	17.1	9.7	12.6	9.5
NCgl1793		260	260	0.0	2.3	1.6	1.5	0.0	0.0	1.5	0.0	0.5	0.8	0.3	0.0
NCgl1815		677	507	0.0	1.6	1.2	1.1	1.0	1.1	9.2	5.4	4.1	6.8	4.6	3.4
cg2077	<i>aftC</i>	367	271	0.0	3.0	1.9	1.3	0.0	0.0	271.9	331.4	130.5	162.6	263.7	113.2
cg2079	<i>hemQ</i>	133	13	2.0	19	11	6.9	1.7	0.0	177.1	109.0	460.8	630.7	773.5	1641.3
cg2080		140	67	2.0	19	11	6.9	1.7	0.0	692.7	882.1	402.4	448.6	636.8	338.1
cg2085		164	96	0.0	0.0	1.5	1.4	0.0	0.0	281.8	252.3	351.3	259.5	252.7	257.4
cg2085		202	134	0.0	1.9	1.5	1.4	0.0	0.0	281.8	252.3	351.3	259.5	252.7	257.4
cg2090	<i>suhB</i>	129	-129	2.3	266	104	70	1.6	0.0	166.2	117.0	181.7	287.2	242.2	164.6
cg2091	<i>ppgK</i>	199	199	2.3	266	104	70	1.6	0.0	472.0	443.9	878.6	494.4	502.2	499.5
cg2121	<i>ptsH</i>	25	-70	0.0	2.1	1.2	0.0	0.0	0.0	2765.7	3056.9	2443.1	3448.2	1299.4	1981.3

cg2155		326	326	0.0	5.0	2.6	1.9	0.0	0.0	464.3	371.5	396.7	644.6	640.5	329.9
cg2181	<i>oppA</i>	274	217	2.2	10	7.2	3.9	1.7	0.0	1304.7	133.3	1967.7	433.8	136.2	1525.0
cg2187		279	279	0.0	2.1	0.0	0.0	0.0	0.0	88.0	55.0	41.6	36.9	39.0	40.4
cg2195		284	50	0.0	2.5	1.5	1.5	0.0	0.0	6624.2	8846.7	1167.9	8905.6	1165.1	11955.3
cg2201	<i>chrS (cgt58)</i>	4	4	0.0	2.5	1.4	1.0	0.0	0.0	36.8	490.1	23.7	11.6	363.7	57.5
cg2202	<i>hrtB</i>	107	107	0.0	2.5	1.4	1.0	0.0	0.0	42.7	5528.5	12.0	4.7	2771.7	240.2
cg2208	<i>dxr</i>	44	44	0.0	3.2	2.4	1.8	0.0	0.0	48.8	32.4	96.3	51.3	58.8	72.1
cg2211		200	121	0.0	3.2	2.4	1.8	0.0	0.0	1747.7	2114.1	2363.5	808.6	1629.5	1453.7
cg2224	<i>xerC</i>	129	26	2.4	78	40	20	1.8	0.0	42.7	26.5	31.3	43.0	42.1	33.3
cg2311		113	113	0.0	4.2	2.8	2.1	0.0	0.0	99.7	50.0	135.3	47.2	48.7	163.2
cg2343		422	192	0.0	6.3	3.8	3.2	0.0	0.0	84.4	124.2	79.7	103.6	115.6	54.7
cg2398	<i>plsC</i>	153	75	0.0	2.3	1.8	1.4	0.0	0.0	441.4	656.1	325.5	243.1	242.3	147.8
cg2406	<i>ctaE</i>	307	307	19	105	63	25	13	2.3	3935.0	4547.1	1818.0	965.4	1446.9	1039.4
cg2409	<i>ctaC</i>	233	47	1.9	22	12	6.3	2.1	0.0	2698.8	3552.2	2684.1	1037.3	1403.6	1371.5
cg2409	<i>ctaC</i>	270	84	1.9	22	12	6.3	2.1	0.0	2698.8	3552.2	2684.1	1037.3	1403.6	1371.5
cg2410	<i>ltsA</i>	286	199	1.9	22	12	6.3	2.1	0.0	153.0	136.3	203.1	135.0	142.7	168.0
cg2410	<i>ltsA</i>	249	162	1.9	22	12	6.3	2.1	0.0	153.0	136.3	203.1	135.0	142.7	168.0
cg2423	<i>lipA</i>	127	33	0.0	3.3	2.3	1.9	0.0	0.0	677.5	1675.7	452.8	678.3	1702.6	462.5
cg2445	<i>hmuO</i>	149	43	0.0	5.4	2.8	3.1	0.0	0.0	185.3	80.4	263.1	8.3	9.6	19.1
cg2445	<i>hmuO</i>	625	519	0.0	3.6	1.7	2.0	0.0	0.0	185.3	80.4	263.1	8.3	9.6	19.1
cg2473	<i>acpM</i>	586	586	0.0	6.6	3.7	2.6	0.0	0.0	188.3	140.2	247.5	253.0	278.1	175.4
cg2495		43	43	0.0	6.7	4.3	3.4	0.0	0.0	90.2	69.8	104.0	91.0	70.3	67.5
cg2496		-1	-56	0.0	6.7	4.3	3.4	0.0	0.0	128.3	109.5	140.6	122.9	145.0	113.5
cg2521	<i>fadD15</i>	184	-15	0.0	1.3	1.6	1.5	0.0	0.0	284.8	254.5	209.6	250.1	244.5	204.5
cg2523	<i>malQ</i>	84	74	0.0	1.3	1.6	1.5	0.0	0.0	1629.8	1167.4	1339.1	1106.0	998.8	1039.7
cg2537	<i>brnQ</i>	345	235	0.0	3.9	2.9	2.0	1.5	0.0	178.7	133.9	150.6	158.3	187.0	169.8
cg2546		183	162	0.0	8.6	5.3	3.5	1.3	0.0	5.3	4.0	12.1	3.2	3.7	16.2
cg2557		114	37	0.0	1.8	1.3	0.0	0.0	0.0	25.4	20.2	114.8	15.5	21.9	125.7
cg2625	<i>pcaF</i>	219	219	0.0	2.0	1.8	1.6	0.0	0.0	817.0	323.1	19.9	207.6	77.2	17.5
cg2641	<i>benR</i>	295	229	0.0	5.6	4.0	3.1	0.0	0.0	24.0	26.5	45.7	22.3	24.3	20.4
cg2675		9	-9	0.0	9.6	4.7	3.3	0.0	0.0	571.8	1357.7	18.0	859.1	399.3	61.0
cg2680	<i>argD2</i>	227	186	0.0	3.5	2.4	1.9	0.0	0.0	163.7	187.2	213.7	111.0	133.2	175.3
cg2683		99	72	0.0	0.0	0.0	1.2	1.2	1.1	3.4	3.0	2.6	2.1	1.9	1.8
cg2685		13	-16	2.8	24	18	10	2.8	0.0	148.4	71.3	80.6	115.3	121.8	129.2
cg2686		120	120	2.8	24	18	10	2.8	0.0	369.7	437.3	188.7	427.0	395.4	128.0
cg2734	<i>pncA</i>	31	-5	1.1	0.0	0.0	1.0	1.2	1.2	212.4	222.3	240.2	196.2	212.1	166.2
cg2761	<i>cpdA</i>	309	309	0.0	4.2	3.4	2.1	0.0	0.0	102.3	170.8	175.7	92.7	221.3	122.7
cg2780	<i>ctaD</i>	309	197	3.5	36	27	13	5.0	1.6	3107.7	5452.0	3251.3	1682.3	2653.4	1786.1
cg2786	<i>nrdE</i>	31	-31	0.0	4.4	2.6	2.3	0.0	0.0	259.3	313.0	413.0	239.1	225.8	407.4
cg2812		47	-117	0.0	2.4	2.0	1.8	0.0	0.0	123.2	500.3	206.7	149.8	417.3	131.5
cg2822		278	278	1.2	1.2	0.0	1.2	1.3	0.0	6.9	4.1	4.7	5.2	2.4	1.8
cg2831	<i>ramA</i>	64	-10	0.0	2.1	1.6	1.5	1.9	0.0	231.9	249.2	136.6	157.4	183.8	203.5
cg2842	<i>phoU</i>	65	-65	0.0	2.5	1.9	1.7	0.0	0.0	337.4	364.5	216.2	232.8	358.1	183.3

cg2944	<i>ispF</i>	529	482	0.0	7.4	4.8	2.7	0.0	1.5	198.3	136.8	209.3	164.9	178.5	173.2
cg2949		113	67	1.6	9.6	7.2	4.2	0.0	0.0	726.8	1005.1	1597.1	507.1	868.1	963.8
cg2952		302	302	0.0	2.2	1.8	1.6	0.0	0.0	648.1	603.4	542.0	410.3	544.5	462.4
cg2953	<i>vdh</i>	19	-47	0.0	2.1	0.0	0.0	0.0	0.0	59.9	30.3	155.4	45.7	50.6	108.5
cg3050		523	523	0.0	2.0	1.8	0.0	0.0	0.0	301.9	288.8	463.0	387.4	501.7	393.5
cg3054	<i>purT</i>	254	-32	0.0	2.3	1.8	1.8	0.0	0.0	194.4	198.6	224.2	144.8	140.4	153.8
cg3068	<i>fda</i>	6	-38	0.0	4.2	2.8	2.8	0.0	0.0	1017.3	656.7	1791.0	1350.1	1107.9	1835.1
cg3069		148	-1	0.0	4.8	3.1	2.6	0.0	0.0	241.0	221.7	317.2	362.8	317.4	218.3
cg3100	<i>dnaK</i>	335	215	0.0	2.8	2.3	1.9	0.0	0.0	153.7	1668.7	949.8	109.1	965.5	1171.5
cg3101		596	596	0.0	2.0	2.3	1.7	0.0	0.0	393.2	430.1	327.3	106.2	126.7	178.9
cg3101		4	4	0.0	2.8	2.3	1.9	0.0	0.0	393.2	430.1	327.3	106.2	126.7	178.9
cg3114	<i>cysN</i>	558	558	0.0	2.2	2.2	0.0	0.0	0.0	5360.9	5660.6	40.7	3871.6	3522.6	477.9
cg3118	<i>cysI</i>	138	86	0.0	2.0	1.9	0.0	0.0	0.0	6141.7	6683.3	58.0	5086.3	4183.2	498.1
cg3119	<i>cysJ (fpr2)</i>	245	139	0.0	2.0	1.9	0.0	0.0	0.0	6749.5	6238.2	39.4	5613.2	4179.1	453.8
cg3127	<i>tctC</i>	64	-162	0.0	1.9	2.1	1.8	0.0	1.1	7.6	9.5	27.8	8.6	8.8	14.7
NCgI2748		601	601	0.0	2.4	2.3	2.0	1.5	0.0	15.1	15.0	15.9	24.2	20.6	12.2
cg3156	<i>htaD</i>	165	-108	2.3	14	11	6.0	1.9	0.0	6.6	1.0	50.9	2.8	0.8	24.1
cg3173		24	24	0.0	0.0	2.1	1.6	0.0	0.0	335.5	210.7	320.6	253.5	217.7	279.7
cg3175		231	231	0.0	3.2	2.6	2.4	0.0	0.0	63.4	46.9	74.8	59.1	68.7	63.0
cg3194		273	273	0.0	4.4	4.1	2.7	0.0	0.0	22.4	7.9	43.1	16.4	11.0	28.6
cg3195		108	-133	0.0	4.4	4.1	2.7	0.0	0.0	54.8	24.0	3057.3	93.5	15.3	617.3
cg3199		181	181	0.0	3.4	3.7	2.4	0.0	0.0	51.3	29.5	81.5	33.6	43.5	69.9
cg3226		606	533	0.0	3.4	3.6	2.2	0.0	0.0	2579.1	569.4	83.9	1161.8	178.5	151.9
cg3247	<i>hrrA (cgtR11)</i>	107	25	0.0	3.7	3.4	2.1	0.0	0.0	82.1	52.6	226.1	0.0	0.0	0.0
NCgI2861		44	44	0.0	2.7	2.4	1.8	0.0	0.0	779.6	978.2	23.3	474.2	440.8	20.7
cg3317		3	-3	0.0	4.1	3.4	2.7	0.0	0.0	136.9	212.9	224.2	221.8	340.1	368.3
cg3322		199	79	0.0	4.2	4.5	3.2	1.7	0.0	19.4	85.8	57.8	18.4	167.2	72.3
cg3323	<i>ino1</i>	167	-46	0.0	4.2	4.5	3.2	1.7	0.0	449.9	218.3	1284.7	302.3	712.6	1928.5
cg3332	<i>qor3</i>	9	-9	0.0	1.9	1.7	0.0	0.0	0.0	76.4	107.1	188.0	107.2	182.5	108.7
cg3336	<i>gntK</i>	67	-103	0.0	2.0	1.6	1.6	0.0	0.0	69.1	78.2	47.7	58.7	64.5	40.7
cg3400	<i>thiD2</i>	242	242	0.0	3.3	2.7	2.6	0.0	0.0	6.3	2.9	3.9	4.9	2.0	2.1
cg3402		9	-41	0.0	3.3	2.7	2.6	0.0	0.0	1464.6	2591.0	28.3	1863.5	1236.0	24.2

Table S4: Filtered dataset of time resolved transcriptome analysis of *C. glutamicum* wild type and $\Delta hrrA$ with genes showing at least two-fold alteration in gene expression. Wild type cells and a $\Delta hrrA$ strain were cultivated in CGII minimal medium supplemented with 2% (w/v) glucose and 4 μ M hemin and harvested 0 h, 0.5 h and 4 h after hemin addition. Column 1 and 2 show the gene locus (ID) and gene name. In green (3-5) and red (6-8), the measured mRNA levels of the corresponding genes in the wild type strain (green) and a $\Delta hrrA$ strain (red) are shown (in transcripts per million, mean of two biological replicates). Column 9-11 show the \log_2 -fold change of $\Delta hrrA$ in comparison to the wild type after 0 h, 0.5 h, or 4 h of incubation in hemin containing medium. The presented genes were filtered for at least two-fold altered fold-change in one of the measured time points and for a p-value <0.05. All further information can be found in the full table in Keppel et al. (2018).

Gene ID	Gene name	mRNA wt			mRNA $\Delta hrrA$			$\log_2(\Delta hrrA/wt)$		
		t=0	t=0.5	t=4	t=0	t=0.5	t=4	t=0	t=0.5	t=4
cg0012	<i>ssuR</i>	783.2	319.1	5.9	160.5	103.2	20.4	-2.3	-1.6	1.8
cg0061	<i>rodA</i>	146.9	344.0	222.8	169.4	166.3	155.6	0.2	-1.0	-0.5
cg0160		7.8	2.0	3.6	2.4	0.6	18.7	-1.7	-1.7	2.4
cg0161		494.5	397.9	287.3	80.6	88.9	133.9	-2.6	-2.2	-1.1
cg0162		306.1	327.4	201.3	66.6	50.4	99.2	-2.2	-2.7	-1.0
cg0163		165.9	302.2	181.6	56.6	50.7	87.6	-1.6	-2.6	-1.1
cg0165		31.6	114.3	88.2	26.0	26.2	43.6	-0.3	-2.1	-1.0
cg0230	<i>gltD</i>	57.0	427.7	8.4	147.6	96.4	6.4	1.4	-2.1	-0.4
cg0256		42.1	5.4	39.3	9.4	0.3	20.8	-2.2	-4.1	-0.9
cg0314	<i>brnF</i>	37.5	47.5	14.2	29.1	19.8	6.9	-0.4	-1.3	-1.0
cg0315	<i>brnE</i>	50.5	39.6	16.2	34.2	19.4	11.0	-0.6	-1.0	-0.6
cg0318	<i>arsC1 (arsB2)</i>	39.6	90.2	19.4	29.6	32.9	15.2	-0.4	-1.5	-0.4
cg0319	<i>arsC2 (arsX)</i>	86.2	116.4	34.9	77.2	50.3	25.5	-0.2	-1.2	-0.5
cg0421	<i>wzx</i>	69.7	36.7	60.2	20.7	14.8	14.4	-1.8	-1.3	-2.1
cg0445	<i>sdhC sdhCD</i>	1917.1	2911.0	2339.4	392.3	884.6	760.6	-2.3	-1.7	-1.6
cg0446	<i>sdhA</i>	1156.2	2662.4	2224.9	278.2	768.3	774.9	-2.1	-1.8	-1.5
cg0447	<i>sdhB</i>	458.1	2731.7	2527.3	229.8	798.8	839.3	-1.0	-1.8	-1.6
cg0455		634.7	578.7	24.9	364.1	261.3	24.2	-0.8	-1.1	0.0
cg0456		276.6	580.5	17.8	320.0	253.6	19.4	0.2	-1.2	0.1
cg0463	<i>csaR</i>	537.5	3066.3	45.3	705.1	926.5	39.9	0.4	-1.7	-0.2
cg0464	<i>copA (ctpA, ctpV)</i>	1863.7	4490.5	27.0	1442.6	1033.9	30.1	-0.4	-2.1	0.2
cg0466	<i>htaA</i>	19.4	8.6	77.7	3.0	3.0	72.5	-2.7	-1.5	-0.1
cg0635	<i>creA</i>	48.5	32.8	6.7	18.9	12.7	5.4	-1.4	-1.4	-0.3
cg0676		29.7	17.3	19.7	12.8	7.9	17.5	-1.2	-1.1	-0.2
cg0683		873.3	449.8	145.3	850.1	218.0	148.4	0.0	-1.0	0.0
cg0755	<i>metY</i>	3615.4	2977.0	54.7	2088.5	1365.4	304.6	-0.8	-1.1	2.5
cg0793		321.7	183.1	246.2	141.7	83.5	153.9	-1.2	-1.1	-0.7
cg0898	<i>pdxS</i>	701.1	228.4	772.2	517.3	111.3	907.8	-0.4	-1.0	0.2
cg0922		35.6	16.4	43.8	13.6	5.2	106.2	-1.4	-1.7	1.3
cg0923		440.6	466.9	147.2	134.2	124.0	92.2	-1.7	-1.9	-0.7
cg0926		140.1	27.1	228.7	27.0	12.8	718.5	-2.4	-1.1	1.7
cg0927		415.1	29.5	215.7	52.6	13.6	644.6	-3.0	-1.1	1.6
cg0951	<i>accD3</i>	508.0	728.0	395.4	134.3	156.3	119.4	-1.9	-2.2	-1.7
cg1120	<i>ripA</i>	77.0	55.3	105.7	33.8	26.1	339.2	-1.2	-1.1	1.7
cg1225	<i>benK3 (pcaK)</i>	1672.9	600.3	42.2	1190.0	207.5	27.4	-0.5	-1.5	-0.6
cg1226	<i>pobB (pobA)</i>	2600.5	682.1	60.3	1874.0	314.8	37.4	-0.5	-1.1	-0.7
cg1313		393.1	139.4	77.5	149.2	65.4	33.4	-1.4	-1.1	-1.2
cg1405		518.3	297.8	119.3	202.5	97.0	135.6	-1.4	-1.6	0.2
cg1411	<i>rbsA</i>	29.9	22.5	51.6	16.1	10.5	61.5	-0.9	-1.1	0.3
cg1412	<i>rbsC</i>	27.8	24.0	50.7	17.9	11.8	69.2	-0.6	-1.0	0.4
cg1424	<i>lysE</i>	613.8	368.3	8.3	300.9	89.8	9.1	-1.0	-2.0	0.1
cg1425	<i>lysG</i>	57.5	49.0	17.5	38.9	21.6	14.7	-0.6	-1.2	-0.3
cg1537	<i>ptsG</i>	2393.3	1757.4	1855.8	2649.0	825.0	1779.5	0.1	-1.1	-0.1

cg1555		127.2	736.5	83.3	120.1	297.6	71.6	-0.1	-1.3	-0.2
cg1695		302.1	434.4	172.6	171.1	211.4	62.1	-0.8	-1.0	-1.5
cg1705	<i>arsB1 (arsC2)</i>	53.1	112.9	48.8	42.1	54.9	45.0	-0.3	-1.0	-0.1
cg1738	<i>acnR</i>	173.0	368.6	74.8	78.8	171.9	60.3	-1.1	-1.1	-0.3
cg1759		2544.1	4176.3	834.1	3478.9	1899.3	830.8	0.5	-1.1	0.0
cg1760	<i>sufU</i>	3043.1	4005.4	883.6	3669.2	1828.7	869.8	0.3	-1.1	0.0
cg1761	<i>sufS</i>	3417.4	3789.5	758.6	3412.6	1567.9	766.3	0.0	-1.3	0.0
cg1762	<i>sufC</i>	4638.9	4619.6	946.1	4230.5	1871.9	954.6	-0.1	-1.3	0.0
cg1763	<i>sufD</i>	5218.2	4722.5	1051.6	4286.1	2202.4	1067.8	-0.3	-1.1	0.0
cg1778	<i>zwf</i>	411.2	728.0	294.8	316.8	321.9	243.7	-0.4	-1.2	-0.3
cg1779	<i>opcA</i>	382.6	823.1	302.5	338.8	342.5	267.3	-0.2	-1.3	-0.2
cg1780	<i>pgi (devB)</i>	184.5	399.9	181.9	208.7	198.5	157.0	0.2	-1.0	-0.2
cg1787	<i>ppc</i>	1217.0	447.6	467.2	735.7	177.9	332.6	-0.7	-1.3	-0.5
cg1861	<i>rel</i>	494.7	736.1	327.6	305.5	338.3	227.1	-0.7	-1.1	-0.5
cg1962		135.4	183.8	90.8	98.1	86.3	63.5	-0.5	-1.1	-0.5
cg2012		20.8	26.5	10.8	14.0	12.7	6.3	-0.6	-1.1	-0.8
cg2014		109.7	122.2	54.1	50.9	57.2	33.9	-1.1	-1.1	-0.7
NCgl1729		22.6	15.1	11.8	13.0	6.6	10.4	-0.8	-1.2	-0.2
cg2106		1096.6	3586.5	265.7	851.3	1615.4	206.4	-0.4	-1.2	-0.4
cg2117	<i>ptsl</i>	1629.4	565.0	1067.6	1799.1	204.8	910.0	0.1	-1.5	-0.2
cg2118	<i>fruR</i>	3069.0	1111.2	852.6	3750.8	251.3	510.3	0.3	-2.1	-0.7
cg2119	<i>pfkB (fruK)</i>	2340.6	1037.4	848.4	2908.1	213.2	510.7	0.3	-2.3	-0.7
cg2120	<i>ptsF</i>	2834.9	2472.9	931.9	3460.9	431.2	548.2	0.3	-2.5	-0.8
cg2121	<i>ptsH</i>	2765.7	3056.9	2443.1	3448.2	1299.4	1981.3	0.3	-1.2	-0.3
cg2204	<i>hrtA</i>	34.7	4329.7	11.2	2.8	2134.6	185.5	-3.7	-1.0	4.0
cg2329		55.3	113.0	27.6	40.7	48.0	14.6	-0.4	-1.2	-0.9
cg2381		108.4	196.0	87.6	90.9	97.9	87.7	-0.3	-1.0	0.0
cg2397		204.1	146.9	135.7	79.5	72.3	106.6	-1.4	-1.0	-0.3
cg2398	<i>plsC</i>	441.4	656.1	325.5	243.1	242.3	147.8	-0.9	-1.4	-1.1
cg2403	<i>qcrB</i>	1531.9	4192.8	2001.6	533.1	1209.8	1227.5	-1.5	-1.8	-0.7
cg2404	<i>qcrA (qcrA1)</i>	2308.3	4502.3	1893.6	612.3	1254.2	1153.9	-1.9	-1.8	-0.7
cg2405	<i>qcrC</i>	2729.9	4308.4	1782.9	692.9	1294.4	1034.6	-2.0	-1.7	-0.8
cg2406	<i>ctaE</i>	3935.0	4547.1	1818.0	965.4	1446.9	1039.4	-2.0	-1.7	-0.8
cg2408	<i>ctaF</i>	1375.0	2402.0	1615.9	575.2	824.0	934.6	-1.3	-1.5	-0.8
cg2409	<i>ctaC</i>	2698.8	3552.2	2684.1	1037.3	1403.6	1371.5	-1.4	-1.3	-1.0
cg2438		371.3	475.9	337.4	341.6	138.6	169.3	-0.1	-1.8	-1.0
cg2445	<i>hmuO</i>	185.3	80.4	263.1	8.3	9.6	19.1	-4.5	-3.1	-3.8
cg2559	<i>aceB</i>	295.1	156.7	228.5	145.9	54.2	159.1	-1.0	-1.5	-0.5
cg2560	<i>aceA</i>	61.0	16.9	212.8	13.9	8.4	260.7	-2.1	-1.0	0.3
cg2624	<i>pcaR</i>	616.9	252.4	25.5	190.1	106.2	15.4	-1.7	-1.2	-0.7
cg2625	<i>pcaF</i>	817.0	323.1	19.9	207.6	77.2	17.5	-2.0	-2.1	-0.2
cg2626	<i>pcaD</i>	1150.5	606.2	36.7	349.9	132.0	34.0	-1.7	-2.2	-0.1
cg2629	<i>pcaB</i>	2832.7	1115.4	156.2	2377.9	555.3	60.4	-0.3	-1.0	-1.4
cg2630	<i>pcaG</i>	5111.6	2096.4	232.9	5046.4	999.5	93.3	0.0	-1.1	-1.3
cg2636	<i>catA1 (catA)</i>	143.3	298.3	821.6	49.7	62.5	230.6	-1.5	-2.3	-1.8
cg2638	<i>benB</i>	4.4	6.6	7.3	3.9	1.6	1.1	-0.2	-2.0	-2.7
cg2639	<i>benC</i>	5.2	6.7	5.9	1.8	1.5	2.1	-1.6	-2.2	-1.5
cg2674		349.7	1095.0	285.3	877.5	491.2	225.6	1.3	-1.2	-0.3
cg2675		571.8	1357.7	18.0	859.1	399.3	61.0	0.6	-1.8	1.8
cg2676		891.9	1635.4	12.3	855.5	432.6	63.4	-0.1	-1.9	2.4
cg2677		1213.2	1710.5	11.0	845.1	438.1	72.0	-0.5	-2.0	2.7
cg2678		1362.4	1661.0	15.7	756.1	465.6	79.0	-0.8	-1.8	2.3
cg2697		26.5	20.5	12.0	14.0	9.9	8.1	-0.9	-1.1	-0.6

cg2732	<i>gntV (gntK)</i>	61.2	33.8	6.5	36.9	8.0	10.6	-0.7	-2.1	0.7
cg2739		32.7	59.3	9.0	21.7	29.2	9.0	-0.6	-1.0	0.0
cg2780	<i>ctaD</i>	3107.7	5452.0	3251.3	1682.3	2653.4	1786.1	-0.9	-1.0	-0.9
cg2810	<i>cynT</i>	212.1	944.4	26.1	94.1	164.4	35.7	-1.2	-2.5	0.5
cg2833	<i>cysK</i>	8886.8	7276.4	611.9	4250.2	2372.2	2635.8	-1.1	-1.6	2.1
cg2836	<i>sucD</i>	45.7	35.7	576.0	87.0	16.6	171.2	0.9	-1.1	-1.8
cg2838		283.1	1219.4	86.3	197.3	579.0	93.3	-0.5	-1.1	0.1
cg2867	<i>mpx</i>	284.8	487.7	311.2	195.9	172.1	208.8	-0.5	-1.5	-0.6
cg2925	<i>ptsS</i>	3076.8	629.6	1200.2	4006.3	144.1	674.8	0.4	-2.1	-0.8
cg2939	<i>siaG</i>	35.4	22.2	36.7	41.0	9.9	26.8	0.2	-1.2	-0.5
cg2940	<i>sial</i>	19.8	23.7	33.5	31.4	9.4	25.5	0.7	-1.3	-0.4
cg3101		393.2	430.1	327.3	106.2	126.7	178.9	-1.9	-1.8	-0.9
cg3109		12.4	12.0	4.8	8.2	5.2	2.6	-0.6	-1.2	-0.9
cg3112	<i>cysZ</i>	4747.4	5718.7	15.8	4079.5	2666.5	166.0	-0.2	-1.1	3.4
cg3141	<i>hmp</i>	825.6	454.8	8.7	238.8	170.1	12.5	-1.8	-1.4	0.5
cg3145		7.5	9.4	5.8	5.7	2.2	2.2	-0.4	-2.1	-1.4
cg3176		430.2	422.9	189.2	92.0	98.6	137.5	-2.2	-2.1	-0.5
cg3213		74.6	260.6	15.5	104.4	122.7	9.7	0.5	-1.1	-0.7
cg3216	<i>gntP</i>	383.5	166.1	178.6	212.9	60.1	89.0	-0.8	-1.5	-1.0
cg3226		2579.1	569.4	83.9	1161.8	178.5	151.9	-1.2	-1.7	0.9
cg3227	<i>lldD</i>	4147.0	905.9	134.2	1808.7	311.1	408.9	-1.2	-1.5	1.6
cg3234		129.2	557.6	59.9	89.6	262.7	56.7	-0.5	-1.1	-0.1
NCgl2845		1.5	7.1	10.4	1.5	2.4	14.2	-0.1	-1.6	0.4
cg3277		181.8	804.8	57.2	198.6	265.1	43.7	0.1	-1.6	-0.4
cg3280		1436.3	6136.9	43.1	1447.1	2940.8	26.3	0.0	-1.1	-0.7
NCgl2858a		459.2	4055.7	22.0	685.8	1736.3	13.0	0.6	-1.2	-0.8
cg3281	<i>copB</i>	1250.1	2882.3	27.1	647.3	1133.8	16.0	-0.9	-1.3	-0.8
cg3282		1870.4	2441.3	31.0	957.1	923.6	23.4	-1.0	-1.4	-0.4
NCgl2861		779.6	978.2	23.3	474.2	440.8	20.7	-0.7	-1.2	-0.2
cg3284	<i>copS (cgtS9)</i>	15.5	22.6	22.4	6.2	8.7	10.7	-1.3	-1.4	-1.1
cg3285	<i>copR (cgtR9)</i>	25.0	31.0	19.7	7.3	14.2	5.6	-1.8	-1.1	-1.8
cg3286		107.6	212.5	77.3	17.8	56.2	59.4	-2.6	-1.9	-0.4
cg3287	<i>copO</i>	45.5	91.0	37.4	6.6	24.3	32.9	-2.8	-1.9	-0.2
cg3334	<i>cepA</i>	310.8	263.7	22.4	17.4	18.8	6.8	-4.2	-3.8	-1.7
cg3374	<i>cye1</i>	993.8	1177.7	27.2	610.7	554.7	26.2	-0.7	-1.1	-0.1
cg3385	<i>catA3 (rhcD2)</i>	94.1	35.1	49.3	86.0	16.5	30.8	-0.1	-1.1	-0.7
cg3387	<i>iolT2</i>	127.1	33.4	56.0	62.0	13.6	37.2	-1.0	-1.3	-0.6
cg3399		1182.9	1521.5	10.6	602.5	241.8	47.0	-1.0	-2.7	2.1
cg3402		1464.6	2591.0	28.3	1863.5	1236.0	24.2	0.3	-1.1	-0.2

187 **Table S5: Pearson correlation for the gene expression values (TPM) between the two**
 188 **biological replicates.** Transcriptome expression estimates for all the three time-points and both
 189 KO and WT conditions show high reproducibility. The genes with low expression (combined
 190 expression in replicates < 5 TPM) were not included in this analysis.
 191

Time Point	WT	KO
0 h	0.9987	0.9994
0.5 h	0.9990	0.9984
4 h	0.9974	0.9964

192

193 References

194

- 195 1. Studier, F.W. and Moffatt, B.A. (1986) Use of bacteriophage T7 RNA polymerase to direct
 196 selective high-level expression of cloned genes. *J. Mol. Biol.*, **189**, 113-130.
- 197 2. Kalinowski, J., Bathe, B., Bartels, D., Bischoff, N., Bott, M., Burkovski, A., Dusch, N.,
 198 Eggeling, L., Eikmanns, B.J., Gaigalat, L. *et al.* (2003) The complete *Corynebacterium*
 199 *glutamicum* ATCC 13032 genome sequence and its impact on the production of L-
 200 aspartate-derived amino acids and vitamins. *J Biotechnol*, **104**, 5-25.
- 201 3. Frunzke, J., Gätgens, C., Brocker, M. and Bott, M. (2011) Control of heme homeostasis in
 202 *Corynebacterium glutamicum* by the two-component system HrrSA. *J Bacteriol*, **193**, 1212-
 203 1221.
- 204 4. Schäfer, A., Tauch, A., Jager, W., Kalinowski, J., Thierbach, G. and Pühler, A. (1994) Small
 205 mobilizable multi-purpose cloning vectors derived from the *Escherichia coli* plasmids pK18
 206 and pK19: selection of defined deletions in the chromosome of *Corynebacterium*
 207 *glutamicum*. *Gene*, **145**, 69-73.
 208

4.3 Supplemental material to “A pseudokinase version of the histidine kinase ChrS promotes high heme tolerance of *Corynebacterium glutamicum*”

Supplemental material to: A pseudokinase version of the histidine kinase ChrS promotes high heme tolerance of *Corynebacterium glutamicum*

This file includes:

Figure S1: Adaptive laboratory evolution of *C. glutamicum* to high heme levels.

Figure S2: The ChrS-Ala245fs pseudokinase promotes heme tolerance.

Figure S3: HrtB-reporter assay.

Figure S4: qPCR analysis comparing expression levels of *hrtB* and *hrrS* in the *C. glutamicum* WT in comparison to the evolved strain.

Figure S5: ChrA is crucial for the activation of *hrtBA*, while *hrrA* does not affect the growth advantage of the evolved clone.

Figure S6: Plasmid-based overexpression of *hrtBA* does not lead to the same heme tolerance as in the evolved clone 1.fs due to too excessive heme export

Figure S7: BACTH with N-terminal tagged variants of the HKs ChrS and HrrS.

Table S1: Bacterial strains used within this study.

Table S2: Oligonucleotides used in this study.

Table S3: Plasmids used within this study

Table S4: Comparative transcriptome analysis of *C. glutamicum* WT and *C. glutamicum* ChrS-Ala245fs during growth on 4 μ M heme.

Figures

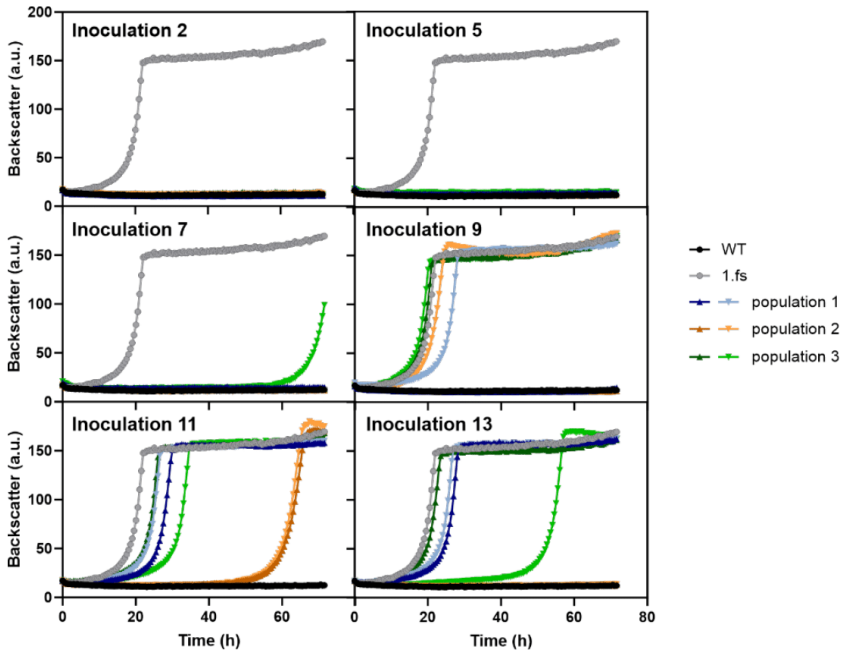


Figure S1: Adaptive laboratory evolution of *C. glutamicum* to high heme levels. *C. glutamicum* ATCC 13032 (WT, black) as well as the evolved strain (1.fs, grey) and each two single clones of the different populations 1 to 3 (blue, orange, green) from the respective inoculation steps in the ALE experiment were inoculated at a starting- OD_{600} of 1 in CGXII medium containing 2% glucose and 100 μ M heme.

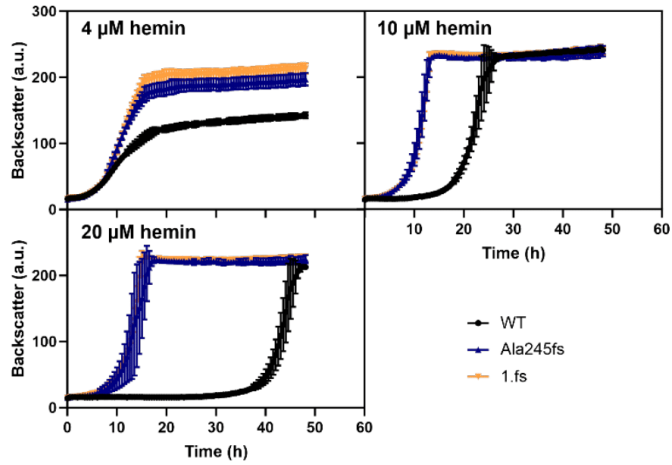


Figure S2: The ChrS-Ala245fs pseudokinase promotes heme tolerance. Data represent the averages of three biological replicates including standard deviations. Reintegration of the point mutation Ala245fs in the parental *chrS* (blue) gene shows that this single mutation leads to enhanced heme tolerance of the evolved clone 1.fs (orange) compared to the WT (black) under all tested conditions.

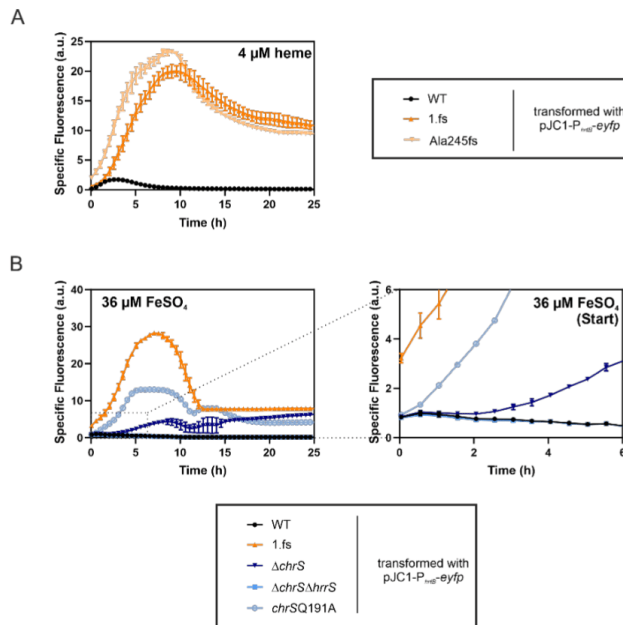


Figure S3: HrtB-reporter assay. Data represent the averages for three biological replicates including standard deviations as error bars. Cells were inoculated at a starting-OD₆₀₀ of 1 in CGXII medium containing 2% glucose and the indicated amount of heme or iron. (A) Reporter assays for *hrtB*-expression using the plasmid pJC1-P_{*hrtB*}-*eyfp* for transformation of the WT (black), evolved clone 1.fs (orange) and the reintegration strain with Ala245fs in ChrS (light orange). The *hrtB* expression for the evolved strain 1.fs and the reintegration strain ChrS-Ala245fs is comparable in the presence of 4 μM heme. (B) Reporter assays for *hrtB*-expression using the plasmid pJC1-P_{*hrtB*}-*eyfp* for transformation of the WT (black), evolved clone 1.fs (orange), ΔchrS (dark blue), $\Delta\text{chrS}\Delta\text{hrrS}$ (mid-blue) and chrS-Q191A (light blue). 1.fs shows an extreme high upregulation of the heme exporter even at standard conditions (36 μM FeSO₄, no presence of added heme).

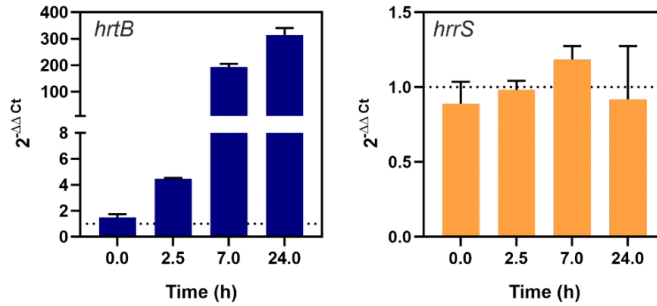


Figure S4: qPCR analysis comparing expression levels of *hrtB* and *hrrS* in the *C. glutamicum* WT in comparison to the evolved strain. The *C. glutamicum* WT and the imitated strain ChrS-Ala245fs were cultivated in 50 ml CGXII medium with 2% glucose and 4 μ M heme in 500 ml shaking flasks. After 0, 2.5, 7 and 24 h, a sample was taken in ice-falcons for RNA isolation via the Monarch Total RNA Miniprep Kit (New England BioLabs, Frankfurt am Main). Using the Luna One-Step RT-qPCR Kit (New England BioLabs, Frankfurt am Main) according to manufacturer's instructions, qPCR was performed in the qTower (Analytik Jena, Jena) and analyzed using qPCRsoft 3.1 (Analytik Jena, Jena). As a reference gene for normalization, the housekeeping gene *ddh* (A156-*ddh*-qPCR-fw CCGGAAAGCAAACCCACAAG; A157-*ddh*-qPCR-rv CTCGGAGTCGAAGTTGCTT) was used (Frunzke et al., 2008), besides the target genes *hrtB* (A269-*hrtB*-qPCR-fw TCCGATTTAGCCTCACTCGC; A270-*hrtB*-qPCR-rv AGTGACATCTGTTCGCCCTG) or *hrrS* (A463-*hrrS*-qPCR-fw AGTTCAACCTCGCCTGTAGC; A464-*hrrS*-qPCR-rv GATGGAATTGCACGGCGAAG). Data represent two biological and three technical replicates. Fold-change was calculated according to the $2^{-\Delta\Delta C_t}$ (Livak and Schmittgen, 2001).

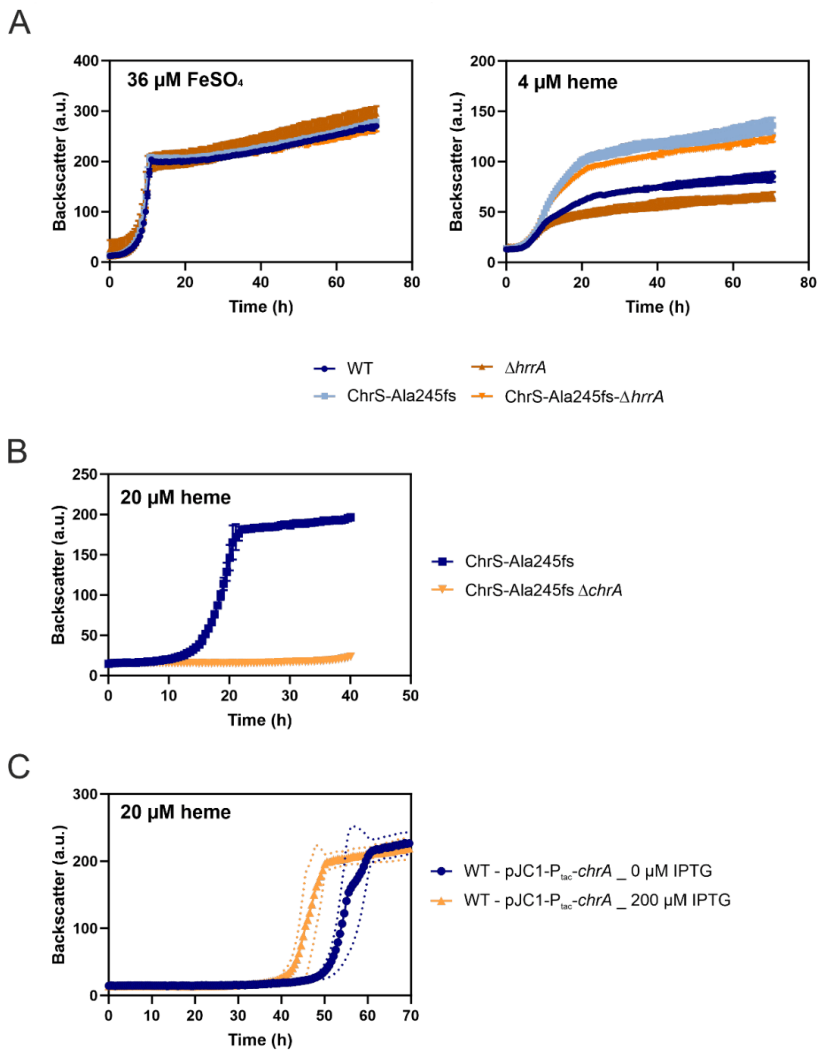


Figure S5: ChrA is crucial for the activation of *hrtBA*, while HrrA does not affect the growth advantage of the evolved clone. Cells were inoculated at a starting- OD_{600} of 1 in CGII medium containing 2% glucose and the indicated amount of heme or iron. (A) *C. glutamicum* WT (dark blue), the strain encoding the pseudokinase ChrS-Ala245fs (light blue) and strains carrying an additional deletion of *hrrA* (shades of orange) were cultivated under standard conditions (36 μM FeSO_4) and with 4 μM heme. The deletion of *hrrA* does not significantly affect the growth advantage of the strain encoding the ChrS pseudokinase. (B) Deletion of *chrA* abolished the growth of the evolved clone on heme. (C) The WT strain was transformed with the overexpression plasmid pJC1- P_{tac} -*chrA* and cultivated with 20 μM heme and either without (blue) or with 200 μM IPTG (orange) for induction. Upon *chrA* overexpression, the strain shows slightly increased heme tolerance. Data represent the averages of three biological replicates including standard deviations.

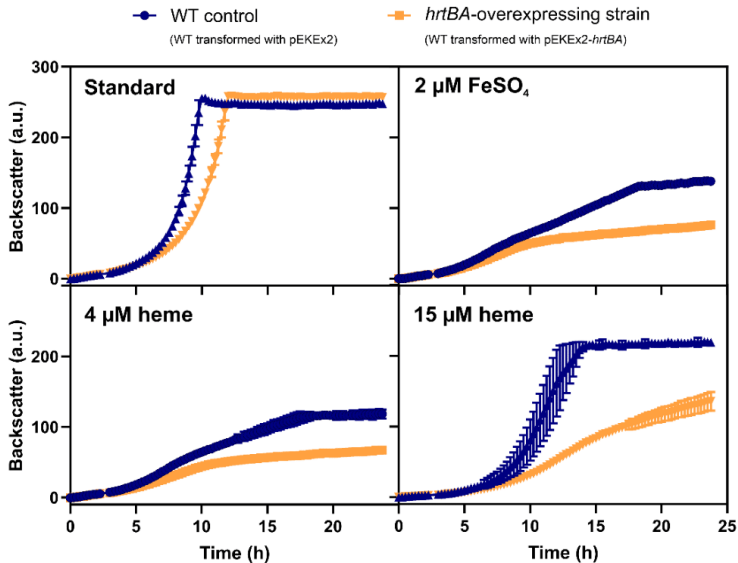


Figure S6: Plasmid-based overexpression of *hrtBA* does not lead to the same heme tolerance as in the evolved clone 1.fs due to too excessive heme export. *C. glutamicum* WT was transformed with an empty plasmid pEKEx2 (Eikmanns et al., 1994) (blue) and a *hrtBA* overexpressing plasmid pEKEx2-*lacI*-*P_{tac}*-*hrtBA* (Heyer et al., 2012) (orange). Cells were inoculated at a starting- OD_{600} of 1 in CGXII medium containing 2% glucose, 25 $\mu\text{g}/\text{ml}$ kanamycin, 100 μM IPTG for induction and the indicated amount of heme or iron. Standard refers to 36 μM FeSO_4 . The overexpression of *hrtBA* did lead to a growth defect in every condition tested, probably caused by too excessive heme export leading to a severe iron starvation phenotype. As comparison, microarrays of WT compared to the evolved clone presented in this study showed a ~ 150 -fold upregulation of *hrtBA* (p-value: 0.002), while this overexpressing strain shows a ~ 400 -fold upregulation (p-value: 0.002) (data not shown).

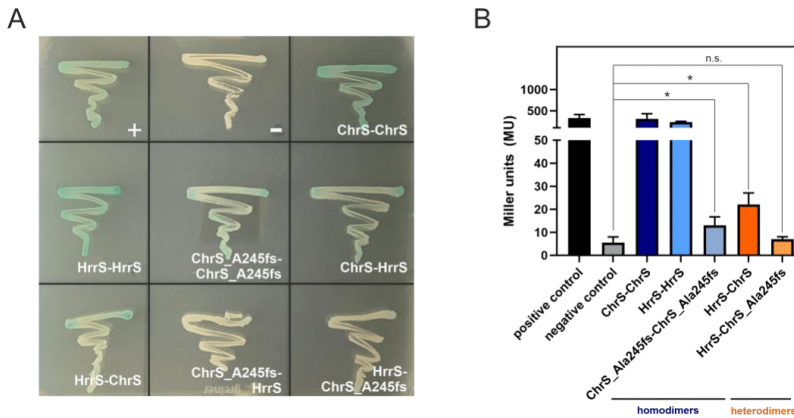


Figure S6: BACTH with N-terminal tagged variants of the HKs ChrS and HrrS. (A) Interactions between the histidine kinases ChrS, HrrS and the ChrS pseudokinase variant (here ChrS_Ala245fs). Blueish color of the colonies indicates a direct interaction, while white represents no interaction. The first HK represents a T25-fusion, the second a T18-fusion. + = pKTN25-zip with pUT18-zip (leucine zipper, positive control), - = pKTN25 with pUT18 (negative control). (B) After transformation, cells were plated, and for each combination, three single colonies were picked for further quantitative analysis using a β -galactosidase assay. Triplicates were re-cultivated overnight and treated according to Griffith and Wolf (2002) to measure colorimetric β -galactosidase activity. Miller units were calculated and are represented in this bar graph. Black and grey bars represent the controls, blue bars show homodimer interactions, and orange bars show heterodimer interactions. Significance was evaluated by an unpaired t-test with a 95% confidence interval.

Tables

Table S1: Bacterial strains used in this study.

Strain	Characteristics	Reference
<i>C. glutamicum</i> ATCC 13032	Wild type (WT), biotin auxotroph	Kinoshita et al. (2004)
$\Delta hrtBA$	ATCC 13032 derivative with deletion of <i>hrtBA</i>	Heyer et al. (2012)
1.fs	ATCC 13032 evolved on heme, frameshift mutant, <i>chrS</i> -730delG	This work
<i>chrS</i> -Ala245fs	ATCC 13032 derivative with 730delG leading to frameshift at Ala245, limitation of 1.fs	This work
$\Delta chrS$	ATCC 13032 derivative with deletion of <i>chrS</i>	Hentschel et al. (2014)
$\Delta chrS\Delta hrrS$	ATCC 13032 derivative with deletion of <i>chrS</i> and <i>hrrS</i>	Hentschel et al. (2014)
<i>chrS</i> -Q191A	ATCC 13032 derivative with amino acid exchange Q191A in <i>chrS</i> , phosphatase mutant	Hentschel et al. (2014)
$\Delta hrrS$	ATCC 13032 derivative with deletion of <i>hrrS</i>	Hentschel et al. (2014)
1.fs $\Delta hrrS$	Evolution clone 1.fs derivative with deletion of <i>hrrS</i>	This work
<i>chrS</i> -H186A	ATCC 13032 derivative with amino acid exchange H186A in <i>chrS</i> , affects autophosphorylation histidine	This work
1.fs <i>chrS</i> -H186A	Evolution clone 1.fs derivative with amino acid exchange H186A in <i>chrS</i> , affects autophosphorylation histidine	This work
$\Delta chrS_DHP-CA$	ATCC 13032 derivative with deletion of the whole DHP and CA domain of <i>chrS</i>	This work
$\Delta chrS_CA$	ATCC 13032 derivative with deletion of the whole DHP and CA domain of <i>chrS</i>	This work
$\Delta hmuT\Delta htaA\Delta htaBC\Delta htaD$	ATCC 13032 derivative with deletion of <i>hmuT</i> , <i>htaA</i> , <i>htaBC</i> and <i>htaD</i>	This work
<i>E. coli</i> DH5 α	F ⁻ ϕ 80lacZ Δ M15 Δ (lacZYA-argF)U169 recA1 endA1 hsdR17(rK ⁻ mK [*]) phoA supE44 thi-1 gyrA96 relA1 λ^{-} ; for general cloning purposes	Invitrogen
<i>E. coli</i> BTH101	F ⁻ , <i>cya</i> -99, <i>ara</i> D139, <i>gal</i> E15, <i>gal</i> K16, <i>rps</i> L1 (Str ^r), <i>hsd</i> R2, <i>mcr</i> A1, <i>mcr</i> B1; reporter strain for BACTH assay	Euromedex

Table S2: Oligonucleotides used in this study.

Oligonucleotide	Sequence 5' → 3'	Use
Construction of deletion plasmid pK19-mobsacB-<i>chrS</i>-Ala245fs		
A250- <i>chrS</i> -730delG-lf_fw	CAGGTCGACTCTAGAGGATCGACCGGAGCCTGCGTATTGG	Left flank
A251- <i>chrS</i> -730delG-lf_rv	CGGCAGATCCGCCCAATGAG	
A252- <i>chrS</i> -730delG-rf_fw	CTCATTGGGCGGATCTGCCG	Right flank
A253- <i>chrS</i> -730delG-rf_rv	GTA AACGACGGCCAGTGAATTGCATCATCTGGGGTGCCACC	
A260- <i>chrS</i> -seq	GGATGATCCGAGGCGTTAAGC	Sequencing <i>chrS</i> region
Construction of deletion plasmid pK19-mobsacB-Δ<i>hrrS</i>		
A303-DhrrS-leftflank_fw	CAGGTCGACTCTAGAGGATCGATTGGTGAACACGATGACCGCG	Left flank
A304-DhrrS-leftflank-rv	GTCTGTAACCGAGCATCTCTCCTA CTAGGCTTGACTGCATGCGTGC	
A305-DhrrS-rightflank_fw	GAGAGATGCTCGGTTACAGAC GGCGAGGTTGAAC TAAGTTCTCC	Right flank
A306-DhrrS-rightflank-rv	GTA AACGACGGCCAGTGAATTGGGGTGACAGTGTGGAGTCACC	
A307-DhrrS-seq3-fw	CCATGGGTGCCACTGATG	Sequencing of <i>hrrS</i> region
A308-DhrrS-seq4-rv	GTTACGTGGGGTGAGTGAGG	
Construction of plasmid pK19-mobsacB-<i>chrS</i>-H186A for amino acid exchange		
A322- <i>chrS</i> -H186A-lf_fw	CAGGTCGACTCTAGAGGATCGACCATCGCCCGAATTGAGAGAG	Left flank
A323- <i>chrS</i> -H186A-lf_rv	CTGCGCCACAGTGTCCGGCTATTTGCGCCGCTATGCCG	
A324- <i>chrS</i> -H186A-rf_fw	CGCATAGCGGGCGAAATAGCCGACACTGTGGCGCAG	Right flank
A325- <i>chrS</i> -H186A-rf_rv	GTA AACGACGGCCAGTGAATTGCGAAATCCAGTTCCCGATCCG	
A326- <i>chrS</i> -HIS-seq_fw	GTACGACCAAAGTCGGATTCGCG	Sequencing of <i>chrS</i> region
A327- <i>chrS</i> -HIS-seq_rv	GCGCAACAACGGGATGATCATC	
A328- <i>chrS</i> -HISclose-seq_rv	CTCCGCCAAATTATCAGTGTCG	
Construction of deletion plasmids for the deletion of <i>ChrS</i> regions		
A298-DchrS-CAdomain-leftflank_fw	CAGGTCGACTCTAGAGGATCCACCGCTGAAATCCGCGATCATC	Left flank for deletion of CA-domain
A299-DchrS-CAdomain-leftflank-rv	GTCTGTAACCGAGCATCTCTCCTA TCTGCCTCCATCGCATCAGGTAA	
A300-DchrS-CAdomain-rightflank_fw	GAGAGATGCTCGGTTACAGAC CCGCCGTTTTCCCTATCCAC	Right flank for deletion of CA-domain
A301-DchrS-CAdomain-rightflank-rv	GTA AACGACGGCCAGTGAATTGCGCCACCAAGGACAGCACTTC	
A314-DchrS-DHp-leftflank_fw	CAGGTCGACTCTAGAGGATCCTAGCCAAGCGACCATGCGC	Left flank for deletion of DHp- and CA-domain
A315-DchrS-DHp-leftflank-rv	GTCTGTAACCGAGCATCTCTCCTA TGCCTGCTCGCCAGCGCTTT	
A300-DchrS-CAdomain-rightflank_fw	GAGAGATGCTCGGTTACAGAC CCGCCGTTTTCCCTATCCAC	Right flank for deletion of DHp- and CA-domain
A301-DchrS-CAdomain-rightflank-rv	GTA AACGACGGCCAGTGAATTGCGCCACCAAGGACAGCACTTC	
A265- <i>ChrS</i> -CA-fw	CAGTGTGATCACGACCCG	Sequencing of <i>chrS</i>
A266- <i>ChrS</i> -CA-rv	GACTTTTACCCTGGCCTCAG	
Construction of plasmids for deletion of heme binding proteins		
A160- <i>htaA</i> -leftflank_fw	CAGGTCGACTCTAGAGGATCCCATGTGGCGTCGACGAACC	Left flank for deletion of
A161- <i>htaA</i> -leftflank-rv	GTCTGTAACCGAGCATCTCTCCTA GCTCCTCATCCGATACGAGG	

		<i>htaA</i> and <i>hmuT</i>
A185-hmuT-rightflank-fw	GAGAGATGCTCGGTTACAGAC GTCGCCGACGCTTCCATTGC	Right flank for deletion of <i>htaA</i> and <i>hmuT</i>
A186-hmuT-rightflank-rv	GTAAACGACGGCCAGTGAATTG CACAACCATCTACTCGCCGCC	
A051-seq-hmuhtaA-2-fw	GTGTCTGAGCCATGGGATCGC	Sequencing of <i>htaA</i> and <i>hmuT</i>
A188-hmuT-seq-rv	CGGTCCGACGCTTAGCTATAGC	
A165-htaB-leftflank_fw	CAGGTCGACTCTAGAGGATCG TCCCGTGTCTTGCTCAGC	Left flank for deletion of <i>htaB</i> and <i>htaC</i>
A166-htaB-leftflank-rv	GTCTGTAACCGAGCATCTCTCCTA GTGAGAGCAACGAGCGCACG	
A173-htaC-rightflank-fw	GAGAGATGCTCGGTTACAGAC GCTGAGTGGTTCTACAGGTCGG	Right flank for deletion of <i>htaB</i> and <i>htaC</i>
A174-htaC-rightflank-rv	GTAAACGACGGCCAGTGAATTG GAAGCCGCACAGTAAAGAGCGC	
A169-htaB-seq-fw	CCGCCACCTCGGTATCGCAC	Sequencing of <i>htaB</i> and <i>htaC</i>
A176-htaC-seq-rv	GCATCAACGTCACCTGACCG	
A177-htaD-leftflank_fw	CAGGTCGACTCTAGAGGATCG TTCGATCCCGTACCAGCGC	Left flank for deletion of <i>htaD</i>
A178-htaD-leftflank-rv	GTCTGTAACCGAGCATCTCTCCTA CAGCGGTCAGTACTGCGAAAGC	
A179-htaD-rightflank-fw	GAGAGATGCTCGGTTACAGAC GGGCCAGCTGAACTACGAAGG	Right flank for deletion of <i>htaD</i>
A180-htaD-rightflank-rv	GTAAACGACGGCCAGTGAATTG CCCTTACCAAACGTTGGTCTGC	
A181-htaD-seq-fw	GCGCCACCTTTTACTACTGCCG	Sequencing of <i>htaD</i>
A182-htaD-seq-rv	CCAGAGAAACCGTACCACGG	
Sequencing primers for pK19-constructs		
M13_fw	CGCCAGGGTTTTCCAGTCAC	Sequencing of plasmid
M13_rv	AGCGGATAACAATTTACACAGGA	
Construction of plasmid for overexpression of chrA		
J545-lacI-Ptac_fw	AGCGACGCCGAGGGGGATCCT CAAGCCTTCGTCAGTGGTCCC	<i>Ptac</i> and <i>lacI</i> as inducible promoter
J546-lacI-Ptac_rv	ATGATATCTCCTTCTTAAAGTTCA GGATCCTCTAGAGTCGACCTGC	<i>chrA</i> insert
A523-ChrA_oex_fw	TGAACCTTTAAGAAGGAGATATCAT GTGATCCGTATTCTGTTGGCTG	
A524-ChrA-oex_rv	AAAACGACGGCCAGTACTAGCT AGATAAATCCGCGCTGTCTG	
Sequencing primers for pJ1-constructs		
pJ1-MCS-fw	CAGGGACAAGCCACCCGCACA	Sequencing of plasmid
pJ1-MCS-rv	GGAAGCTAGAGTAAGTAGTTCGC	
Bacterial two-hybrid assays		
Note: for pKTN25 and pUT18 constructs, the same primers were used only backbone varied		
A380-BACTH-NT25-ChrS-lf_fw	GCATGCCTGCAGGTCGACT GTGAAAAGTACCCAAGCGACCA	Insert ChrS and ChrS_CAs -> Differing Template
A381-BACTH-NT25-ChrS-rf_rv	GCTCGGTACCCGGGGATCCT TATCTTGGTCTTTTGTGGATAG	Insert HrrS
A382-BACTH-NT25-HrrS-lf_fw	GCATGCCTGCAGGTCGACT ATGCAGTCAAGCCTAGATCG	
A383-BACTH-NT25-HrrS-rf_rv	GCTCGGTACCCGGGGATCCT CATCGTCAGTTGGAGAACTTAG	Insert ChrA
A455-BACTH-NT25-ChrA-lf_fw	GCATGCCTGCAGGTCGACT GTGATCCGTATTCTGTTGGCTG	
A456-BACTH-NT25-ChrA-rf_rv	GCTCGGTACCCGGGGATCGATA ATCCGCGCTGTCTGGCT	
A457-BACTH-NT25-HrrA-lf_fw	GCATGCCTGCAGGTCGACT ATGATTCCGCGTGTCTGCTGC	Insert HrrA
A458-BACTH-NT25-HrrA-rf_rv	GCTCGGTACCCGGGGATCCAG CAGCCCTGCTCACGTG	

A357-pUT18seq_fw	GGTGTCTGGGGCTGGCTTAAC	Sequencing
M13_rv	AGCGATAACAATTCACACAGGA	pKTN25 constructs
M13_fw	CGCCAGGGTTTTCCAGTCAC	Sequencing
M13_rv	AGCGATAACAATTCACACAGGA	pUT18 constructs

Bold = overlap to backbone; **orange** = overlap of inserts

Table S3: Plasmids used in this study.

Plasmid	Characteristics	Reference
pK19- <i>mobsacB</i>	Contains negative (<i>sacB</i>) and positive (Kan ^r) selection markers for genomic integration and deletion, MCS cut with EcoRI/BamHI	Schäfer et al. (1994)
pK19- <i>mobsacB-chrS-Ala245fs</i>	Derivative of pK19 <i>mobsacB</i> deletion of a single guanine at position 730 in <i>chrS</i> , leading to a frameshift after Ala245; Kan ^r	This work
pK19- <i>mobsacB-ΔhrrS</i>	Derivative of pK19 <i>mobsacB</i> for partial <i>hrrS</i> gene deletion; Kan ^r	Hentschel et al. (2014)
pK19- <i>mobsacB-chrS-H186A</i>	Derivative of pK19 <i>mobsacB</i> for amino acid exchange at the autophosphorylation histidine (H186A) in <i>chrS</i> ; Kan ^r	This work
pK19- <i>mobsacB-ΔchrS_DHp-CA</i>	Derivative of pK19 <i>mobsacB</i> for partial deletion of <i>chrS</i> , deletion of DHP and CA-domain; Kan ^r	This work
pK19- <i>mobsacB-ΔchrS_CA</i>	Derivative of pK19 <i>mobsacB</i> for partial deletion of <i>chrS</i> , deletion of CA-domain Kan ^r	This work
pK19- <i>mobsacB-ΔchrA</i>	Derivative of pK19 <i>mobsacB</i> for partial <i>chrA</i> gene deletion; Stop Codon included; Kan ^r	This work
pK19- <i>mobsacB-ΔhrrA</i>	Derivative of pK19 <i>mobsacB</i> for partial <i>hrrA</i> gene deletion; Stop Codon included; Kan ^r	(Frunzke et al., 2011)
pJC1- <i>venus-term-BS</i>	<i>E. coli</i> - <i>C. glutamicum</i> shuttle vector; derivative of pJC1 (Cremer et al., 1990), containing the terminator sequence of <i>Bacillus subtilis</i> behind <i>venus</i> ; <i>oriV_{Ec}</i> ; Kan ^r	Baumgart et al. (2013)
pJC1- <i>P_{hrtB}-eyfp</i>	Derivative of pJC1- <i>venus-term-BS</i> , containing <i>eyfp</i> under the control of the promoter <i>P_{hrtB}</i>	Heyer et al. (2012)
pJC1- <i>P_{tac}-chrA</i>	Derivative of pJC1- <i>venus-term-BS</i> , containing <i>chrA</i> under the control of the promoter <i>P_{tac}</i> and <i>lacI</i>	This work
pKTN25	C-terminal T25 protein fusion plasmid, pSU40 derivative, MCS cut with XbaI/BamHI; Kan ^r	Euromedex
pUT18	C-terminal T18 protein fusion plasmid, pUC19 derivative, MCS cut with XbaI/BamHI; Amp ^r	Euromedex
pKT25- <i>zip</i>	Derivative of pKT25, leucine zipper of GCN4 fused to T25, serves as positive control; Kan ^r	Euromedex
pUT18C- <i>zip</i>	Derivative of pUT18C, leucine zipper of GCN4 fused to T18, serves as positive control; Amp ^r	Euromedex
pKTN25- <i>chrS</i>	Derivative of pKT25 for <i>ChrS</i> with T25 N-terminally fused; Kan ^r	This work
pKTN25- <i>chrS_CA-fs</i>	Derivative of pKT25 for <i>ChrS-Ala245fs</i> (evolution variant) with T25 N-terminally fused; Kan ^r	This work
pKTN25- <i>hrrS</i>	Derivative of pKT25 for <i>HrrS</i> with T25 N-terminally fused; Kan ^r	This work
pUT18- <i>chrS</i>	Derivative of pUT18C for <i>ChrS</i> with T18 N-terminally fused; Amp ^r	This work
pUT18- <i>chrS_CA-fs</i>	Derivative of pUT18C for <i>ChrS-Ala245fs</i> (evolution variant) with T18 N-terminally fused; Amp ^r	This work
pUT18- <i>hrrS</i>	Derivative of pUT18C for <i>HrrS</i> with T18 N-terminally fused; Amp ^r	This work
pKTN25- <i>chrA</i>	Derivative of pKT25 for <i>ChrA</i> with T25 N-terminally fused; Kan ^r	This work

pUT18- <i>chrA</i>	Derivative of pUT18 for ChrA with T18 N-terminally fused; Amp ^r	This work
--------------------	--	-----------

Table S4: Comparative transcriptome analysis of *C. glutamicum* WT and *C. glutamicum* *chr5*-Ala245fs during growth on 4 μ M heme.

Gene	Average	p-value	Annotation
cg2202	170.13	0.00	<i>hrtB</i> , ABC-type transport system, permease component
cg2204	151.54	0.00	<i>hrtA</i> , ABC-type transport system, ATPase component
cg0470	66.64	0.02	<i>htaB</i> , secreted heme transport-associated protein
cg2201	43.60	0.04	<i>cgtS8</i> , two-component system, signal transduction histidine kinase
cg0467	21.23	0.06	<i>hmuT</i> , hemin-binding periplasmic protein precursor
cg3369	21.13	0.00	Rieske-type iron-sulfur protein
cg3156	18.64	0.05	<i>htaD</i> , secreted heme transport-associated protein
cg0468	16.90	0.05	<i>hmuU</i> , hemin transport system, permease protein
cg0471	16.87	0.04	<i>htaC</i> , secreted heme transport-associated protein
cg0771	15.90	0.05	secreted siderophore-binding lipoprotein
cg1418	12.64	0.06	secreted siderophore-binding lipoprotein
cg2796	11.01	0.00	MMGE/PRPD family protein
cg1931	9.98	0.05	putative secreted protein
cg2200	8.85	0.01	<i>cgtR8</i> , two-component system, response regulator
cg2445	8.30	0.01	<i>hmuO</i> , heme oxygenase <i>hmuO</i> , heme oxygenase uncharacterized enzyme involved in biosynthesis of extracellular polysaccharides
cg2962	6.69	0.02	
cg0466	5.80	0.01	<i>htaA</i> , secreted heme-transport associated protein
cg1120	5.76	0.10	<i>ripA</i> , transcriptional regulator of iron proteins, AraC family
cg0927	5.76	0.02	siderophore ABC transporter, permease protein
cg0924	5.75	0.01	secreted siderophore-binding lipoprotein
cg1930	5.68	0.01	putative secreted hydrolase
cg3404	5.24	0.00	secreted siderophore-binding lipoprotein
cg0926	5.05	0.02	siderophore ABC transporter, permease protein putative Na ⁺ -dependent transporter putative Na ⁺ -dependent transporter
cg1419	4.85	0.01	
cg2444	4.67	0.01	hypothetical protein cg2444 hypothetical protein cg2444
cg0360	4.43	0.02	putative phosphatase
cg0590	4.24	0.00	siderophore ABC transporter, permease protein secreted siderophore-binding lipoprotein secreted siderophore-binding lipoprotein
cg0922	4.19	0.12	
cg0768	4.08	0.00	siderophore ABC transporter, ATP-binding protein
cg2311	3.47	0.00	SAM-dependent methyltransferase
cg0589	3.42	0.03	siderophore ABC transporter, ATP-binding protein
cg2283	3.40	0.02	hypothetical protein cg2283 ABC-type dipeptide/oligopeptide/nickel transport systems, secreted component
cg2678	3.33	0.13	
cg2061	3.16	0.00	<i>psp3</i> , putative secreted protein
cg0769	3.07	0.00	siderophore ABC transporter, permease protein
cg1327	3.06	0.03	bacterial regulatory proteins, Crp family <i>bbp</i> , penicillin-binding protein, putative D-alanyl-D-alanine carboxypeptidase
cg2199	3.05	0.08	
cg3219	3.03	0.01	<i>ldhA</i> , NAD-dependent L-lactate dehydrogenase
cgr05	3.02	0.05	23S ribosomal RNA geneID:3345511 putative secreted or membrane protein putative secreted or membrane protein
cg0752	2.98	0.02	
cg0160	2.98	0.00	hypothetical protein cg0160 hypothetical protein cg0160
cg1966	2.97	0.03	hypothetical protein cg1966

cg0282	2.97	0.03	hypothetical protein cg0282
cg1514	2.91	0.02	secreted protein
cg3254	2.88	0.03	hypothetical protein cg3254 hypothetical protein cg3254
cg3218	2.87	0.00	pyruvate kinase
cg2052	2.76	0.00	putative secreted protein
cg0528	2.76	0.06	putative secreted protein
cg4005	2.71	0.01	putative secreted protein
cgtrNA_3542	2.68	0.09	
cg1291	2.65	0.01	hypothetical protein cg1291 hypothetical protein cg1291
cg0780	2.65	0.05	membrane protein ribonuclease BN-like family <i>tnp23a</i> (ISCg23a), transposase-fragment <i>tnp23a</i> (ISCg23a), transposase-fragment
cg1513	2.48	0.17	
cg1476	2.48	0.04	<i>thiC</i> , thiamine biosynthesis protein ThiC ABC-type dipeptide/oligopeptide/nickel transport system, permease component
cg2677	2.47	0.06	
cg2833	2.40	0.02	<i>cysK</i> , O-acetylserine (thiol)-lyase
cg2777	2.39	0.00	hypothetical protein cg2777
cg3192	2.31	0.00	putative secreted or membrane protein
cg1744	2.31	0.01	<i>pacL</i> , cation-transporting ATPase
cg3169	2.30	0.01	<i>pck</i> , phosphoenolpyruvate carboxykinase (GTP)
cg3100	2.30	0.04	<i>dnaK</i> , molecular chaperone Dnak
cg0704	2.29	0.07	hypothetical protein cg0704
cg2793	2.29	0.00	hypothetical protein cg2793
cg1884	2.25	0.01	hypothetical protein cg1884 hypothetical protein cg1884
cg2431	2.22	0.02	putative transcriptional regulator
cg2613	2.21	0.00	<i>mdh</i> , malate dehydrogenase <i>mdh</i> , malate dehydrogenase
cg3099	2.20	0.05	<i>grpE</i> , molecular chaperone GrpE (heat shock protein)
cg0683	2.16	0.05	permease <i>ykoC</i> , transmembrane component YkoC of energizing module of thiamin-regulated ECF transporter for hydroxymethylpyri
cg1229	2.15	0.01	
cg2794	2.11	0.03	hypothetical protein cg2794
cg1883	2.11	0.00	putative secreted protein
cg3008	2.11	0.01	<i>porA</i> , main cell wall channel protein
cg1917	2.10	0.06	hypothetical protein cg1917
cg1881	2.06	0.01	predicted iron-dependent peroxidase, secreted protein
cg3073	2.05	0.02	<i>sseA1</i> , probable thiosulfate sulfurtransferase protein
cg1942	2.05	0.09	putative secreted protein putative secreted protein
cg1328	2.04	0.01	putative copper chaperone
cg2845	2.03	0.17	<i>pstC</i> , ABC-type phosphate transport system, permease component
cg3103	2.01	0.16	hypothetical protein cg3103
cg0759	0.50	0.06	<i>prpD2</i> , 2-methylcitrate dehydratase
cg3047	0.50	0.02	<i>ackA</i> , acetate/propionate kinase
cg0706	0.49	0.02	conserved hypothetical membrane protein
cg3327	0.49	0.06	<i>dps</i> , starvation-induced DNA protecting protein <i>tusF</i> , ABC transporter, membrane spanning protein, trehalose uptake system
cg0832	0.49	0.01	<i>tusE</i> , bacterial extracellular solute-binding protein, trehalose uptake system
cg0834	0.49	0.05	
cg1314	0.49	0.02	<i>putP</i> , proline transport system
cg1343	0.49	0.03	<i>narH</i> , probable respiratory nitrate reductase oxidoreduct

cg3282	0.48	0.01	cation transport ATPase hypothetical protein cg0472 hypothetical protein cg0472 hypothetical protein cg0472
cg0472	0.48	0.01	hypothetical protein cg0472
cg3212	0.48	0.00	putative carboxymuconolactone decarboxylase subunit
cg1052	0.47	0.00	<i>cmt3</i> , corynomycylol transferase
cg2887	0.46	0.13	<i>phoS</i> , two component sensor kinase
cg0447	0.45	0.00	<i>sdhB</i> , succinate dehydrogenase <i>sdhB</i> , succinate dehydrogenase
cg3283	0.44	0.01	hypothetical protein predicted by Glimmer
cg0046	0.44	0.09	probable ABC transport protein, ATP-binding compon
cg1603	0.43	0.01	hypothetical protein cg1603
cg3386	0.42	0.06	<i>tcbF</i> , maleylacetate reductase
cg0404	0.42	0.01	nitroreductase family
cg0798	0.41	0.25	<i>prpC1</i> , 2-methylcitrate synthase
cg1090	0.41	0.07	<i>ggtB</i> , probable gamma-glutamyltranspeptidase precursor PR
cg0446	0.40	0.00	<i>sdhA</i> , succinate dehydrogenase
cg0899	0.39	0.00	<i>pdxT</i> , pyridoxine biosynthesis enzyme
cg0898	0.39	0.00	<i>pdxS</i> , pyridoxine biosynthesis enzyme <i>yggB</i> , small-conductance mechanosensitive channel <i>yggB</i> , small-conductance mechanosensitive channel <i>yggB</i> , small-conductance mechanosensitive channel
cg1434	0.39	0.12	mechanosensitive channel
cg1108	0.38	0.01	<i>porC</i> , putative secreted protein <i>porC</i> , putative secreted protein
cg0936	0.38	0.02	<i>rpf1</i> , resuscitation promoting factor
cg0518	0.37	0.02	<i>hemL</i> , glutamate-1-semialdehyde 2,1-aminomutase
cg1066	0.36	0.01	<i>urtE</i> , ABC-type urea uptake system, ATP binding protein
cg2953	0.36	0.02	<i>xylC</i> , benzaldehyde dehydrogenase <i>xy/C</i> , benzaldehyde dehydrogenase
cg0915	0.36	0.01	<i>ftsX</i> , putative cell division protein
cg0445	0.36	0.02	<i>sdhC</i> , succinate dehydrogenase
cg0444	0.35	0.06	<i>ramB</i> , transcriptional regulator, involved in acetate metabolism
cg3096	0.35	0.00	<i>ald</i> , alcohol dehydrogenase
cg1341	0.35	0.01	<i>narI</i> , respiratory nitrate reductase 2 gamma chain
cg1377	0.35	0.04	<i>ssuC</i> , aliphatic sulfonates transmembrane ABC transporterprotein
cg2631	0.34	0.00	<i>pcaH</i> , protocatechuate dioxygenase beta subunit
cg1695	0.34	0.05	putative plasmid maintenance system antidote protein
cg1132	0.34	0.12	<i>coaA</i> , pantothenate kinase
cg1452	0.34	0.27	hypothetical protein cg1452
cg1376	0.34	0.01	<i>ssuD1</i> , alkanesulfonate monooxygenase
cg1380	0.33	0.01	<i>ssuA</i> , aliphatic sulfonate binding protein
cg2782	0.32	0.06	<i>ftn</i> , ferritin-like protein
cg1612	0.31	0.04	acetyltransferase acetyltransferase
cg3107	0.31	0.01	<i>adhA</i> , Zn-dependent alcohol dehydrogenase
cg2778	0.31	0.01	hypothetical protein cg2778
cg1342	0.31	0.01	<i>narJ</i> , nitrate reductase delta chain
cg1379	0.31	0.02	<i>ssuB</i> , aliphatic sulfonates ATP-binding ABC transporterprotein
cg1344	0.30	0.00	<i>narG</i> , nitrate reductase 2, alpha subunit
cg2307	0.30	0.05	hypothetical protein cg2307
cg1737	0.29	0.01	<i>acn</i> , aconitate hydratase
cg1487	0.29	0.01	<i>leuC</i> , isopropylmalate isomerase large subunit

cg2610	0.27	0.00	ABC-type dipeptide/oligopeptide/nickel transport system, secreted component ABC-type dipeptide/oligopeptide/nickel transport system, secreted component
cg2629	0.26	0.00	<i>pcaB</i> , ?-carboxy-cis,cis-muconate cycloisomerase <i>pcaB</i> , ?-carboxy-cis,cis-muconate cycloisomerase
cg2937	0.26	0.14	ABC-type dipeptide/oligopeptide/nickel transport system, secreted component ABC-type dipeptide/oligopeptide/nickel transport system, secreted component ABC-type dipeptide/oligopeptide/nickel transport system, secreted component
cg1109	0.24	0.03	<i>porB</i> , anion-specific porin precursor
cg1153	0.24	0.02	<i>seuC</i> , monooxygenase for sulfonate ester utilization
cg3048	0.24	0.00	<i>pta</i> , phosphate acetyltransferase
cg0961	0.23	0.00	homoserine O-acetyltransferase
cg1156	0.22	0.02	<i>ssuD2</i> , monooxygenase for sulfonate utilization
cg1152	0.21	0.02	<i>seuB</i> , monooxygenase for sulfonate ester utilization <i>ssuI</i> , FMN-binding protein required for sulfonate and sulfonate ester utilization <i>ssuI</i> , FMN-binding protein required for sulfonate and sulfonate ester utilization
cg1147	0.20	0.01	ABC-type peptide transport system, permease component
cg2182	0.19	0.01	ABC-type peptide transport system, permease component
cg0228	0.19	0.07	sensor histidine kinase of two-component system, fragment
cg3195	0.18	0.00	flavin-containing monooxygenase (FMO)
cg0310	0.14	0.00	<i>katA</i> , catalase <i>katA</i> , catalase
cg3303	0.08	0.03	transcriptional regulator PadR-like family <i>benK1</i> , putative benzoate transport protein <i>benK1</i> , putative benzoate transport protein
cg2642	0.06	0.00	transport protein
cg2636	0.03	0.00	<i>catA1</i> , catechol 1,2-dioxygenase <i>catA1</i> , catechol 1,2-dioxygenase

References

- Baumgart, M., Luder, K., Grover, S., Gätgens, C., Besra, G.S., and Frunzke, J. (2013). IpsA, a novel LacI-type regulator, is required for inositol-derived lipid formation in *Corynebacteria* and *Mycobacteria*. *BMC Biology* *11*, 122.
- Cremer, J., Eggeling, L., and Sahm, H. (1990). Cloning the *dapA dapB* cluster of the lysine-secreting bacterium *Corynebacterium glutamicum*. *Molecular and General Genetics MGG* *220*, 478-480.
- Eikmanns, B.J., Thum-Schmitz, N., Eggeling, L., Lüdtke, K.-U., and Sahm, H. (1994). Nucleotide sequence, expression and transcriptional analysis of the *Corynebacterium glutamicum gltA* gene encoding citrate synthase. *Microbiology* *140*, 1817-1828.
- Frunzke, J., Bramkamp, M., Schweitzer, J.E., and Bott, M. (2008). Population Heterogeneity in *Corynebacterium glutamicum* ATCC 13032 caused by prophage CGP3. *J Bacteriol* *190*, 5111-5119.
- Frunzke, J., Gätgens, C., Brocker, M., and Bott, M. (2011). Control of heme homeostasis in *Corynebacterium glutamicum* by the two-component system HrrSA. *Journal of Bacteriology* *193*, 1212-1221.
- Griffith, K.L., and Wolf, R.E., Jr. (2002). Measuring beta-galactosidase activity in bacteria: cell growth, permeabilization, and enzyme assays in 96-well arrays. *Biochem Biophys Res Commun* *290*, 397-402.
- Hentschel, E., Mack, C., Gatgens, C., Bott, M., Brocker, M., and Frunzke, J. (2014). Phosphatase activity of the histidine kinases ensures pathway specificity of the ChrSA and HrrSA two-component systems in *Corynebacterium glutamicum*. *Molecular Microbiology* *92*, 1326-1342.
- Heyer, A., Gatgens, C., Hentschel, E., Kalinowski, J., Bott, M., and Frunzke, J. (2012). The two-component system ChrSA is crucial for haem tolerance and interferes with HrrSA in haem-dependent gene regulation in *Corynebacterium glutamicum*. *Microbiology* *158*, 3020-3031.
- Kinoshita, S., Udaka, S., and Shimono, M. (2004). Studies on the amino acid fermentation. Part 1. Production of L-glutamic acid by various microorganisms. *The Journal of General and Applied Microbiology* *50*, 331-343.
- Livak, K.J., and Schmittgen, T.D. (2001). Analysis of relative gene expression data using real-time quantitative PCR and the 2(-Delta Delta C(T)) Method. *Methods* *25*, 402-408.
- Schäfer, A., Tauch, A., Jäger, W., Kalinowski, J., Thierbach, G., and Pühler, A. (1994). Small mobilizable multi-purpose cloning vectors derived from the *Escherichia coli* plasmids pK18 and pK19: selection of defined deletions in the chromosome of *Corynebacterium glutamicum*. *Gene* *145*, 69-73.

4.4 Supplemental material to section “2.7 Evolution towards the production of heme”

Experimental work on this topic was conceptualized by Julia Frunzke and Aileen Krüger and conducted by Janik Göddecke in the context of his master thesis supervised and mainly planned by Aileen Krüger. HPLC measurements were performed with the help of Astrid Wirtz from the research group of Dr. Tino Polen at the Forschungszentrum Jülich.

Table S1: Bacterial strains used in this study

Table S2: Plasmids used in this study

Table S3: Oligonucleotides used in this study

Method 1: Acetonitrile extraction for HPLC sample preparation

Method 2: High performance liquid chromatography (HPLC) for heme measurements

Table S1: Bacterial strains used in this study

Strain	Characteristics	Reference
<i>C. glutamicum</i> ATCC 13032	Wild type (WT), biotin auxotroph	Kinoshita et al. (2004)
WT:: <i>P_{hrtB}_pfkA</i>	Integrated HrtB-biosensor construct (terminator, <i>chrS-hrtB</i> intergenic region and first 30 bp of <i>hrtB</i> followed by a stopcodon, RBS and linker) upstream of <i>pfkA</i> in <i>C. glutamicum</i>	This work
<i>E. coli</i> DH5 α	<i>F</i> ⁻ ϕ 80 <i>lacZ</i> Δ M15 Δ (<i>lacZYA-argF</i>)U169 <i>recA1 endA1 hsdR17(rK⁻ mK[*]) phoA supE44 thi-1 gyrA96 relA1</i> λ ⁻ ; for general cloning purposes	Invitrogen

Table S2: Plasmids used in this study

Plasmid	Characteristics	Reference
pJC1- <i>venus-term-BS</i>	<i>E. coli-C. glutamicum</i> shuttle vector; derivative of pJC1 (Cremer et al., 1990), containing the terminator sequence of <i>Bacillus subtilis</i> behind <i>venus</i> ; <i>oriV_{Ec}</i> <i>oriV_{Cg}</i> ; Kan ^r	Baumgart et al. (2013)
pJC1- <i>P_{hrtB}-eyfp</i>	Derivative of pJC1- <i>venus-term-BS</i> , containing <i>eyfp</i> under the control of the promoter <i>P_{hrtB}</i>	Heyer et al. (2012)
pK19- <i>mobsacB</i>	Contains negative (<i>sacB</i>) and positive (Kan ^r) selection markers for genomic integration and deletion, MCS cut with EcoRI/BamHI	Schäfer et al. (1994)
pK19- <i>mobsacB-P_{hrtB}_pfkA</i>	Derivative of pK19 <i>mobsacB</i> for integration of the HrtB-biosensor construct upstream of <i>pfkA</i>	This study

Table S3: Oligonucleotides used in this study

Oligonucleotide	Sequence (5' → 3')	Use	Template
Plasmid construction of integration plasmid pK19- <i>mobsacB</i> -P _{<i>hrtB</i>} - <i>pfkA</i>			
A414_ <i>pfkA</i> _leftflank_fw	CCTGCAGGTCGACTCTAGAGAGAGATCG CCCCGATAAGTTT	Left flank for integration in front of <i>pfkA</i>	Genomic DNA <i>C. glutamicum</i>
A415_ <i>pfkA</i> _leftflank_rv	<u>TCTTCTCTCATCCGCCAAAA</u> TCTGACC ATCTTATTTAATCGCCA		
A416_ <i>term</i> _fw	TTTGGCGGATGAGAGAAGA	Terminator sequence	pJC1_ <i>venus</i> _Term-BS
A417_ <i>term</i> _rv	CAAAAGAGTTTGTAGAAACGCA		
A418_ <i>IR_hrtB</i> _fw	GTTTCTACAAACTCTTTTGCCACCACG ATAGATCAACT	Intergenic region (IR) between <i>chrS</i> and <i>hrtB</i> , first 30 bp of <i>hrtB</i> , Stop, RBS and linker	Genomic DNA <i>C. glutamicum</i>
A419_ <i>IR_hrtB</i> _rv	<u>ATGATATCTCCTTCTTAAAGTTCATGCG</u> GTGAGTTCTTTTAGTC		
A420_ <i>pfkA</i> _rightflank_fw	<u>TGAACTTTAAGAAGGAGATATCATATGC</u> GAATTGCTACTCTCACG	Right flank for integration in front of <i>pfkA</i>	Genomic DNA <i>C. glutamicum</i>
A421_ <i>pfkA</i> _rightflank_rv	TTGTAAAACGACGGCCAGT GATACCTGC GTGCAGAGCAAT		
Sequencing primers			
JG1_ <i>pfkA</i> _fw	CGCGCTCAGCAAGGCATAAG	Sequencing of <i>pfkA</i> region	
JG2_ <i>pfkA</i> _rv	GCGCACGTGGATCTCATCAG		
M13_fw	CGCCAGGGTTTTCCAGTCAC	Sequencing of pK19 plasmids	
M13_rv	AGCGGATAACAATTTCCACACAGGA		

bold = overlap backbone, **blue** = overlap terminator (start), **orange** = overlap terminator (end), underlined = Stop, ribosomal binding site (RBS), linker

Method 1: Acetonitrile extraction for HPLC sample preparation

This method was used to prepare extracts from cell pellets, which can be further analyzed in regards to total heme content using high performance liquid chromatography (HPLC). For this purpose, cells were cultivated for ~24 h in CGXII supplemented with 2% glucose and 100 μM FeSO₄. After centrifugation at 12000 x g for 5 minutes of cell suspension corresponding to an OD₆₀₀ of 100, the supernatant was discarded and the cell pellet was resuspended in 100 μL acidic acetonitrile preparations (acetonitrile : 1.6M HCl), as modified from Espinas et al. (2012) and Fyrestam and Östman, (2017). For the extraction, samples were shaken in a vortex (IKA, Königswinter, Germany) for 20 minutes. After another centrifugation, the resulting supernatant was sterile filtered using a 0.2 μm filter (AcroPrep™ Advance, 96-well plate with 0.2 μm PTFE membrane, VWR, USA) and could finally be used for further HPLC analysis.

Method 2: High performance liquid chromatography (HPLC) for heme measurements

In this method, heme was separated from its cell sample in a reversed phase chromatography. Simultaneously, standards were used to properly identify and quantify heme contents. HPLC samples were prepared as described in Method 1, while hemin standards (0 μM – 20 μM) were diluted in acetonitrile, to fit the extraction method. Overall, the HPLC method was developed based on several previous studies (Fyrestam and Östman, 2017; Wakamatsu et al. 2009). The substance specific adsorption was measured at 400 nm in a diode array detection unit (DAD). For separation, an Agilent 1260 Infinity II Prime LC System (Agilent Technologies, Inc., Santa Clara, US) with the Ascentis Express Peptide ES-C18 reversed phase column (Sigma Aldrich, St. Louis, US) was employed. A sample volume of 10 μl was injected. The filtered sample was separated at 50°C using a linear gradient of two solvents (A: 200 mM ammonium acetate buffer; B: methanol) with a volume flow of 0.5 ml/min and a total analysis time of 20 minutes. The measurement started with a stationary ratio of 80% solvent A in solvent B for 2 minutes and changed to 10% solvent A in solvent B in a linear gradient over 10 minutes. After a total analysis time of 16.5 min, the initial situation of 20% solvent A in solvent B was restored. A heme peak could be identified after about 12.5 minutes. Consequently, the data obtained was analyzed using OpenLab CDR software (Beckman Coulter GmbH, Baesweiler, Germany), Excel (Microsoft, US) and Graph Pad Prism 9 (Graphpad Software, Inc., California), quantifying heme content from a standard curve based on peak areas.

References

- Baumgart, M., Luder, K., Grover, S., Gätgens, C., Besra, G.S., and Frunzke, J. (2013). IpsA, a novel LacI-type regulator, is required for inositol-derived lipid formation in *Corynebacteria* and *Mycobacteria*. *BMC Biology*, 11(1): 122. doi: 10.1186/1741-7007-11-122.
- Espinas, N.A., Kobayashi, K., Takahashi, S., Mochizuki, N., and Masuda, T. (2012). Evaluation of Unbound Free Heme in Plant Cells by Differential Acetone Extraction. *Plant and Cell Physiology*, 53(7): 1344-1354. doi: 10.1093/pcp/pcs067.
- Fyrestam, J., and Östman, C. (2017). Determination of heme in microorganisms using HPLC-MS/MS and cobalt(III) protoporphyrin IX inhibition of heme acquisition in *Escherichia coli*. *Anal Bioanal Chem*, 409(30): 6999-7010. doi: 10.1007/s00216-017-0610-5.
- Heyer, A., Gätgens, C., Hentschel, E., Kalinowski, J., Bott, M., and Frunzke, J. (2012). The two-component system ChrSA is crucial for haem tolerance and interferes with HrrSA in haem-dependent gene regulation in *Corynebacterium glutamicum*. *Microbiology*, 158(Pt 12): 3020-3031. doi: 10.1099/mic.0.062638-0.
- Kinoshita, S., Udaka, S., and Shimono, M. (2004). Studies on the amino acid fermentation. Part 1. Production of L-glutamic acid by various microorganisms. *J Gen Appl Microbiol*, 50(6): 331-343.
- Schäfer, A., Tauch, A., Jäger, W., Kalinowski, J., Thierbach, G., and Pühler, A. (1994). Small mobilizable multi-purpose cloning vectors derived from the *Escherichia coli* plasmids pK18 and pK19: selection of defined deletions in the chromosome of *Corynebacterium glutamicum*. *Gene*, 145(1): 69-73. doi: 10.1016/0378-1119(94)90324-7.
- Wakamatsu, J., Odagiri, H., Nishimura, T., and Hattori, A. (2009). Quantitative determination of Zn protoporphyrin IX, heme and protoporphyrin IX in Parma ham by HPLC. *Meat Sci*, 82(1): 139-142. doi: 10.1016/j.meatsci.2008.12.011.

4.5 Impact of CO₂/HCO₃⁻ Availability on Anaplerotic Flux in Pyruvate Dehydrogenase Complex-Deficient *Corynebacterium glutamicum* Strains

Krüger A.*, Wiechert J.*, Gätgens C., Polen T., Mahr R. and Frunzke J.

*These authors contributed equally to this work.

Published in *Journal of Bacteriology*, 2019.

Contributor Role	Contributor
Conceptualization	30% JW, 30% JF, 20% AK, 20% RM
Formal Analysis	75% AK, 20% RM, 5% TP
Investigation/Experiments	80% AK, 10% CG, 10% RM
Methodology	25% AK, 25% JW, 25% JF, 15% RM, 10% CG
Project Administration	70% JW, 30% JF
Software	100% TP
Supervision	70% JW, 30% JF
Visualization	100% AK
Writing – Original Draft Preparation	80% JF, 10% AK, 10% JW
Writing – Review & Editing	70% JF, 20% AK, 10% JW

Overall contribution AK: 30%

The main contribution of AK to this article was on the experimental and editing site in the context of her master thesis supervised by JW. JW planned most of the experimental work, which was mainly conducted by AK. Exceptions are the uHPLC measurements (Figure 5) and the PKH67 cell staining coupled to flow cytometry (Figure 7B), which were performed by RM, the GC-ToF analysis that was done by Jochem Gätgens (Table S1) and the overexpression experiment of glyoxylate shunt, which was accomplished by CG (Figure 6B). TP performed the bioinformatic analysis of whole genome sequencing (Table 5). All visualizations and further data analyses were done by AK. The original draft was mainly prepared by JF, as well as the revision process.



Impact of CO₂/HCO₃⁻ Availability on Anaplerotic Flux in Pyruvate Dehydrogenase Complex-Deficient *Corynebacterium glutamicum* Strains

Aileen Krüger,^a Johanna Wiechert,^a Cornelia Gätgens,^a Tino Polen,^a Regina Mahr,^b  Julia Frunzke^a

^aInstitut für Bio- und Geowissenschaften, IBG-1: Biotechnology, Forschungszentrum Jülich, Jülich, Germany

^bSenseUp GmbH, Forschungszentrum Jülich, Jülich, Germany

ABSTRACT The pyruvate dehydrogenase complex (PDHC) catalyzes the oxidative decarboxylation of pyruvate, yielding acetyl coenzyme A (acetyl-CoA) and CO₂. The PDHC-deficient *Corynebacterium glutamicum* $\Delta aceE$ strain therefore lacks an important decarboxylation step in its central metabolism. Additional inactivation of *pyc*, encoding pyruvate carboxylase, resulted in a >15-h lag phase in the presence of glucose, while no growth defect was observed on gluconeogenic substrates, such as acetate. Growth was successfully restored by deletion of *ptsG*, encoding the glucose-specific permease of the phosphotransferase system (PTS), thereby linking the observed phenotype to the increased sensitivity of the $\Delta aceE \Delta pyc$ strain to glucose catabolism. In this work, the $\Delta aceE \Delta pyc$ strain was used to systematically study the impact of perturbations of the intracellular CO₂/HCO₃⁻ pool on growth and anaplerotic flux. Remarkably, all measures leading to enhanced CO₂/HCO₃⁻ levels, such as external addition of HCO₃⁻, increasing the pH, or rerouting metabolic flux via the pentose phosphate pathway, at least partially eliminated the lag phase of the $\Delta aceE \Delta pyc$ strain on glucose medium. In accordance with these results, inactivation of the urease enzyme, lowering the intracellular CO₂/HCO₃⁻ pool, led to an even longer lag phase, accompanied by the excretion of L-valine and L-alanine. Transcriptome analysis, as well as an adaptive laboratory evolution experiment with the $\Delta aceE \Delta pyc$ strain, revealed the reduction of glucose uptake as a key adaptive measure to enhance growth on glucose-acetate mixtures. Taken together, our results highlight the significant impact of the intracellular CO₂/HCO₃⁻ pool on metabolic flux distribution, which becomes especially evident in engineered strains exhibiting low endogenous CO₂ production rates, as exemplified by PDHC-deficient strains.

IMPORTANCE CO₂ is a ubiquitous product of cellular metabolism and an essential substrate for carboxylation reactions. The pyruvate dehydrogenase complex (PDHC) catalyzes a central metabolic reaction contributing to the intracellular CO₂/HCO₃⁻ pool in many organisms. In this study, we used a PDHC-deficient strain of *Corynebacterium glutamicum*, which additionally lacked pyruvate carboxylase ($\Delta aceE \Delta pyc$). This strain featured a >15-h lag phase during growth on glucose-acetate mixtures. We used this strain to systematically assess the impact of alterations in the intracellular CO₂/HCO₃⁻ pool on growth in glucose-acetate medium. Remarkably, all measures enhancing CO₂/HCO₃⁻ levels successfully restored growth. These results emphasize the strong impact of the intracellular CO₂/HCO₃⁻ pool on metabolic flux, especially in strains exhibiting low endogenous CO₂ production rates.

KEYWORDS *Corynebacterium glutamicum*, L-valine, anaplerosis, carbon dioxide, pyruvate carboxylase, pyruvate dehydrogenase complex

Citation Krüger A, Wiechert J, Gätgens C, Polen T, Mahr R, Frunzke J. 2019. Impact of CO₂/HCO₃⁻ availability on anaplerotic flux in pyruvate dehydrogenase complex-deficient *Corynebacterium glutamicum* strains. *J Bacteriol* 201:e00387-19. <https://doi.org/10.1128/JB.00387-19>.

Editor Anke Becker, Philipps-Universität Marburg

Copyright © 2019 American Society for Microbiology. All Rights Reserved.

Address correspondence to Regina Mahr, r.mahr@senseup.de, or Julia Frunzke, j.frunzke@fz-juelich.de.

A.K. and J.W. contributed equally to this work.

Received 6 June 2019

Accepted 19 July 2019

Accepted manuscript posted online 29 July 2019

Published 20 September 2019

CO_2 is an inevitable product and, at the same time, an essential substrate of microbial metabolism. In water, CO_2 is in equilibrium with bicarbonate (HCO_3^-) and CO_3^{2-} , and this equilibrium is influenced by the pH of the medium (1). As products of decarboxylating reactions and substrates for carboxylation, CO_2 and HCO_3^- are involved in various metabolic processes. Consequently, the intracellular $\text{CO}_2/\text{HCO}_3^-$ pool has a significant impact on metabolic fluxes, such as anaplerosis, especially in the early phase of cultivation, when the cell density is low (2).

During aerobic growth, the pyruvate dehydrogenase complex (PDHC), which is conserved in various microbial species, catalyzes an important reaction contributing to the intracellular $\text{CO}_2/\text{HCO}_3^-$ pool (3, 4). The PDHC is a multienzyme complex belonging to the family of 2-oxo acid dehydrogenase complexes, which also include the α -ketoglutarate dehydrogenase complex and the branched-chain 2-keto acid dehydrogenase (3, 5). In particular, the PDHC catalyzes the oxidative decarboxylation of pyruvate to acetyl coenzyme A (acetyl-CoA) and CO_2 .

The Gram-positive actinobacterium *Corynebacterium glutamicum* represents an important platform strain used in industrial biotechnology for the production of amino acids, proteins, and various other value-added products (6–10). In this organism, the PDHC represents a central target for engineering the metabolic pathways of pyruvate-derived products, including L-valine, isobutanol, ketoisovalerate, and L-lysine. To this end, various studies have focused on the reduction or complete abolishment of PDHC activity in order to improve precursor availability (4, 11–13). Due to the deficiency of PDHC activity, however, cells are not able to grow on glucose as a single carbon source, a difficulty that can be circumvented by the addition of acetyl-CoA refueling substrates, such as acetate. In the presence of both carbon sources—glucose and acetate—PDHC-deficient strains initially form biomass from acetate and subsequently convert glucose into products (e.g., L-valine or L-alanine) in the stationary phase (12). In contrast to *Escherichia coli* or *Bacillus subtilis*, *C. glutamicum* does not normally show the typical diauxic growth behavior but prefers cometabolism of many carbon sources (10, 14). Co-utilization of glucose and acetate has been studied in detail, showing that while the consumption rates of both carbon sources decrease, total carbon consumption is comparable to that with growth on either carbon source alone, which is regulated by SugR activity (15). Further examples of sugars or organic acids with which glucose is cometabolized include fructose (16), lactate (17), pyruvate (14), and gluconate (18). It has been shown that upon growth on a mixture of glucose and acetate, the glyoxylate shunt is active and is required to fuel the oxaloacetate pool in wild-type (WT) *C. glutamicum* (15). Here it should be noted that the glyoxylate shunt is active in the presence of acetate but is repressed by glucose (19).

For growth on glycolytic carbon sources, organisms depend on tricarboxylic acid (TCA) cycle-replenishing reactions constituting the anaplerotic node (or phosphoenolpyruvate [PEP]-pyruvate-oxaloacetate node), comprising different carboxylating and decarboxylating reactions (20). Consequently, flux via these reactions is influenced by the intracellular $\text{CO}_2/\text{HCO}_3^-$ pool. In contrast to most other organisms, *C. glutamicum* possesses both anaplerotic carboxylases, namely, the PEP carboxylase (PEPCx) (EC 4.1.1.31) encoded by the *ppc* gene (21, 22) and the pyruvate carboxylase (PCx) (EC 6.4.1.1) encoded by *pyc* (20, 23). These two C_3 -carboxylating enzymes catalyze bicarbonate-dependent reactions yielding oxaloacetate from PEP or pyruvate, respectively. It has been shown that in *C. glutamicum*, these two enzymes can replace each other to a certain extent, depending on the intracellular concentrations of the respective effectors for each enzyme. However, under standard conditions during growth on glucose, the biotin-containing PCx contributes 90% of the main anaplerotic activity, in contrast to PEPCx (23). Remarkably, the Michaelis-Menten constants of both carboxylases are about 30-fold higher than those in *Escherichia coli* PEPCx (24). Apparently, a low $\text{CO}_2/\text{HCO}_3^-$ pool may thus limit anaplerotic flux, which is of special relevance in early phases, when the biomass concentration is low but high aeration may strip dissolved CO_2 from the medium.

Several studies have revealed the inhibitory effect of low partial CO_2 pressure ($p\text{CO}_2$)

on microbial growth (2, 25, 26). In the case of *C. glutamicum*, low pCO_2 led to a significant drop in the growth rate in turbidostatic continuous cultures (27) as well as in batch cultures (28). It was further demonstrated that the reduced flux through anaplerotic reactions under low $\text{CO}_2/\text{HCO}_3^-$ levels led to increased production of the pyruvate-derived amino acids L-alanine and L-valine (28).

While several previous studies have focused on the impact of CO_2 by altering the partial CO_2 pressure in the process, we applied targeted genetic perturbations to systematically assess the impact of the intracellular $\text{CO}_2/\text{HCO}_3^-$ pool on the anaplerotic flux and growth of *C. glutamicum*. In this study, we focused on PDHC-deficient strains exhibiting a reduced intracellular $\text{CO}_2/\text{HCO}_3^-$ pool during growth on glucose-acetate mixtures. The effect of low $\text{CO}_2/\text{HCO}_3^-$ levels became even more evident upon the additional deletion of the *pyc* gene, encoding the dominant anaplerotic enzyme, leading to a drastically elongated lag phase for a *C. glutamicum* $\Delta aceE \Delta pyc$ strain during growth on glucose-acetate mixtures. This effect could be attributed to reduced tolerance of glucose by these strains and was successfully complemented by the deletion of *ptsG*, encoding the glucose-specific permease of the phosphotransferase system (PTS). Remarkably, growth was successfully restored by increasing the intracellular $\text{CO}_2/\text{HCO}_3^-$ pool by the addition of bicarbonate, by increasing the pH, by rerouting metabolic flux over the pentose phosphate pathway (PPP), or by refueling the oxaloacetate pool by the addition of TCA cycle intermediates to the growth medium. Finally, adaptive laboratory evolution (ALE) of the *C. glutamicum* $\Delta aceE \Delta pyc$ strain on minimal medium containing glucose and acetate revealed the abolishment of glucose uptake as a key adaptive strategy to allow for growth on acetate.

RESULTS

A lowered intracellular $\text{CO}_2/\text{HCO}_3^-$ pool impacts the growth of PDHC-deficient strains. The pyruvate dehydrogenase complex (PDHC) contributes to a key metabolic reaction in the central metabolism by catalyzing the oxidative decarboxylation of pyruvate to acetyl-CoA (Fig. 1), thereby producing 1 molecule of CO_2 and 1 molecule of NADH per molecule of pyruvate. Previous studies have already revealed that PDHC-deficient strains feature ~2-fold-decreased excretion of CO_2 during exponential growth (29). It is therefore reasonable to assume that a reduction in the intracellular $\text{CO}_2/\text{HCO}_3^-$ pool has an impact on metabolic flux distribution in PDHC-deficient strains. A simple growth comparison of wild-type *C. glutamicum* and a strain lacking the *aceE* gene (and thus PDHC deficient) revealed a slightly increased lag phase for the $\Delta aceE$ strain, which became especially evident when cells were grown in microtiter plates, while the maximal growth rate appeared to be unaffected ($0.40 \pm 0.01 \text{ h}^{-1}$ for the $\Delta aceE$ strain and $0.41 \pm 0.01 \text{ h}^{-1}$ for the WT) (Fig. 2A). Remarkably, this lag phase was completely eliminated by the addition of 100 mM HCO_3^- , suggesting that the effect is attributable to the lowered intracellular $\text{CO}_2/\text{HCO}_3^-$ pool of this mutant (Fig. 2B).

In *C. glutamicum*, the pyruvate carboxylase (PCx) encoded by *pyc* is the dominating HCO_3^- -dependent anaplerotic enzyme required for refueling the TCA cycle via oxaloacetate during growth on glycolytic carbon sources (23). In the next experiment, we deleted *pyc* in the $\Delta aceE$ background in order to examine the influence of different $\text{CO}_2/\text{HCO}_3^-$ levels on bicarbonate-dependent anaplerosis. Remarkably, the additional deletion of the *pyc* gene resulted in an elongated lag phase of about 20 h and a reduced growth rate for the $\Delta aceE \Delta pyc$ strain (maximum growth rate $[\mu_{\text{max}}]$, $0.27 \pm 0.02 \text{ h}^{-1}$, in contrast to $0.40 \pm 0.01 \text{ h}^{-1}$ for the $\Delta aceE$ strain) during cultivation in CGXII minimal medium containing glucose and acetate (Fig. 2A). An extended lag phase was also observed for the Δpyc single mutant, but the lag phase was significantly less prominent than that for the PDHC-deficient $\Delta aceE \Delta pyc$ variant (Fig. 2C). The growth defects of both strains were successfully complemented by reintroducing the *pyc* gene on plasmid pJ1 under the control of its own promoter (Fig. 2C). Remarkably, this extended lag phase was observed only in the presence of glucose, not during cultivation on minimal medium containing acetate as the sole carbon source (Fig. 2A).

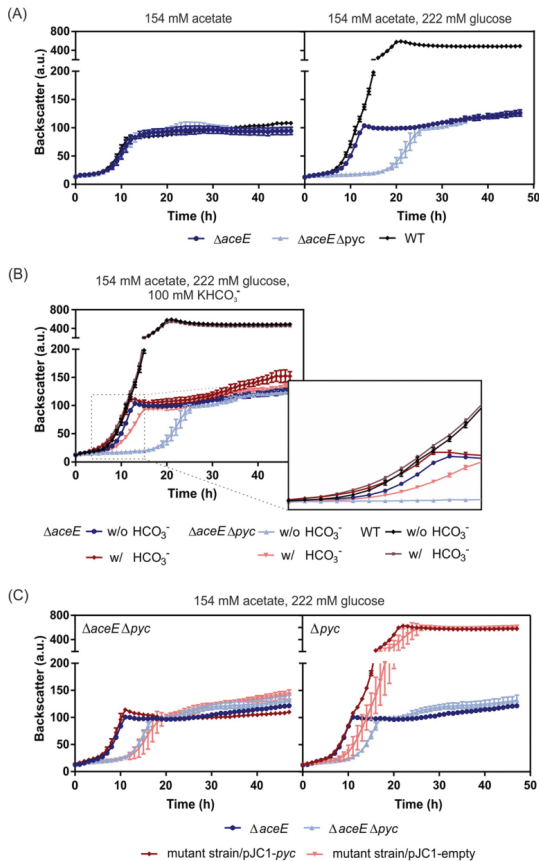


FIG 2 Impact of glucose on *aceE* and *pyc* mutant strains. The growth curves shown are based on the backscatter measurements (expressed in arbitrary units [a.u.]) in a microtiter cultivation system inoculated at an OD_{600} of 1. Data represent the averages for three biological replicates; error bars, standard deviations. (A) The *C. glutamicum* $\Delta aceE$ and $\Delta aceE \Delta pyc$ strains, as well as the wild type, were inoculated in CGXII medium containing 154 mM acetate (left) or 154 mM acetate plus 222 mM glucose (right). (B) The $\Delta aceE$ and $\Delta aceE \Delta pyc$ strains, as well as WT cells, were cultivated in CGXII medium containing 154 mM acetate and 222 mM glucose, either with (w/) or without (w/o) 100 mM KHCO_3^- . The box zooms in on the time interval between 4 h and 15 h. (C) The $\Delta aceE \Delta pyc$ (left) and Δpyc (right) strains were transformed with the $pJC1-pyc$ plasmid for complementation of the *pyc* deletion or with the $pJC1$ -empty vector as a control. Cultures were inoculated in CGXII medium containing 154 mM acetate, 222 mM glucose, and 25 $\mu\text{g}/\text{ml}$ kanamycin.

h^{-1} for the $\Delta aceE \Delta pyc$ parental strain and $0.39 \pm 0.02 \text{ h}^{-1}$ for the $\Delta aceE \Delta pyc \Delta ptsG$ strain) but resulted in reduced final backscatter values, comparable to those with growth on acetate alone (Fig. 3B). Strains lacking the *ptsG* gene consumed only minor amounts of glucose, while the $\Delta aceE$ and $\Delta aceE \Delta pyc$ strains consumed glucose after entering the stationary phase (see Fig. S2 in the supplemental material). The glucose uptake rate of the $\Delta aceE \Delta pyc$ strain, $10.87 \pm 4.95 \text{ nmol min}^{-1} \text{ g}^{-1}$, was significantly lower than that of the $\Delta aceE$ strain, $16.81 \pm 3.01 \text{ nmol min}^{-1} \text{ g}^{-1}$ (Table 1). In contrast, deletion of *ptsG* did not restore growth on either the PTS substrate fructose (see Fig.

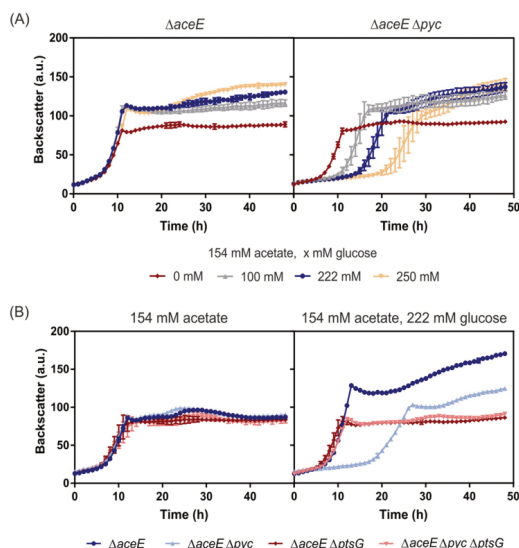


FIG 3 Influence of glucose consumption on the growth of *C. glutamicum* $\Delta aceE$ and *C. glutamicum* $\Delta aceE \Delta pyc$. The growth curves shown are based on the backscatter measurements in a microtiter cultivation system, inoculated at an OD_{600} of 1. (A) The $\Delta aceE$ (left) and $\Delta aceE \Delta pyc$ (right) strains were inoculated to an OD_{600} of 1 in CGXII medium containing 154 mM acetate and either no glucose or 100 mM, 222 mM, or 250 mM glucose. (B) Deletion of the *ptsG* gene in the $\Delta aceE$ and $\Delta aceE \Delta pyc$ strains restored growth on glucose-acetate mixtures relative to that for the $\Delta aceE$ and $\Delta aceE \Delta pyc$ parental strains. Data represent the averages for three biological replicates; error bars, standard deviations.

S3), which is imported mainly by the permease encoded by *ptsF* (30, 31), or the non-PTS sugar ribose (see Fig. S4). Taken together, these findings clearly link the observed growth defect of the $\Delta aceE \Delta pyc$ strain on glucose-acetate mixtures to the uptake of residual amounts of glucose.

Increased HCO_3^- availability improves anaplerotic flux in *pyc* mutants. Next, we used different strategies to alter the intracellular CO_2/HCO_3^- pool. This was achieved by (i) supplementing the medium with HCO_3^- , (ii) mutating the endogenous urease gene producing CO_2 from urea in the early growth phase, (iii) increasing the pH of the growth medium, or (iv) rerouting metabolic flux via the pentose phosphate pathway (Fig. 4).

As with the $\Delta aceE$ parental strain, the addition of 100 mM HCO_3^- eliminated the lag phase for PDHC-deficient strains lacking the *pyc* gene (Fig. 2B) during microtiter plate cultivation on glucose-acetate mixtures. Restoration of growth was not possible in a

TABLE 1 Glucose consumption rates of PDHC-deficient *C. glutamicum* strains in the exponential-growth phase^a

Mutation(s)	Glucose consumption rate (nmol min ⁻¹ g ⁻¹) ^b
$\Delta aceE$	16.81 ± 3.01
$\Delta aceE \Delta pyc$	10.87 ± 4.95
$\Delta aceE \Delta ptsG$	7.24 ± 3.97
$\Delta aceE \Delta pyc \Delta ptsG$	7.32 ± 1.88

^aFor an overview of glucose consumption over the entire time course of the experiment, including the stationary phase, see Fig. S2 in the supplemental material.

^bValues are means ± standard deviations for three independent biological replicates.

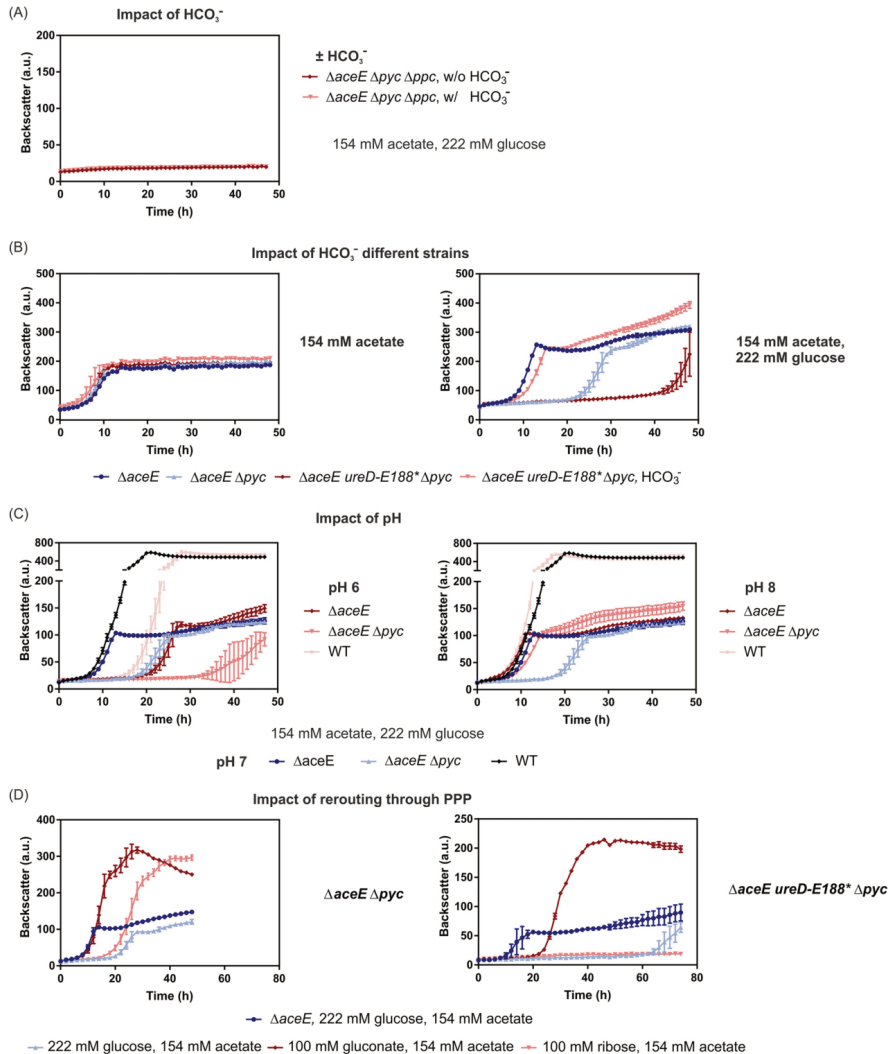


FIG 4 Increased availability of HCO_3^- improved anaplerotic flux via PEPcX in *pyc*-deficient *C. glutamicum* strains. The growth curves shown are based on the backscatter measurements in a microtiter cultivation system, inoculated at an OD_{600} of 1. Symbols represent the backscatter means for biological triplicates ($n = 3$). (A) The $\Delta aceE \Delta pyc \Delta ppc$ strain was inoculated in CGXII medium containing 154 mM acetate and 222 mM glucose (w/o HCO_3^-), and if indicated, 100 mM KHCO_3^- was added (w/ HCO_3^-). (B) The $\Delta aceE$, $\Delta aceE \Delta pyc$, and $\Delta aceE ureD-E188^* \Delta pyc$ strains were cultivated in CGXII medium containing 154 mM acetate (left) or 154 mM acetate and 222 mM glucose (right) with or without the addition of KHCO_3^- . (C) The $\Delta aceE$ and $\Delta aceE \Delta pyc$ strains, as well as the WT, were cultivated in CGXII medium containing 154 mM acetate and 222 mM glucose adjusted to a pH of 6 (left) or 8 (right), and growth was compared to that with cultivation at pH 7. (D) The $\Delta aceE$ strain and the $\Delta aceE \Delta pyc$ (left) or $\Delta aceE ureD-E188^* \Delta pyc$ (right) strain were inoculated in different growth media containing 154 mM acetate and either 222 mM glucose, 100 mM gluconate, or 100 mM ribose.

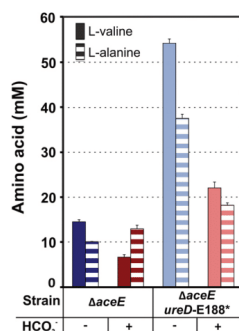


FIG 5 The intracellular $\text{CO}_2\text{-HCO}_3^-$ pool significantly affects L-valine production. The influence of carbonate on the L-alanine and L-valine production of *C. glutamicum* $\Delta aceE$ and *C. glutamicum* $\Delta aceE ureD-E188^*$ was investigated. Shown are L-valine and L-alanine titers in the supernatant after 28 h of cultivation in the microtiter cultivation system. Data represent average values from three independent biological replicates using uHPLC.

strain lacking both anaplerotic enzymes PCx and PEPCx, indicating that the positive effect of HCO_3^- on the $\Delta aceE \Delta pyc$ strain depends on the increased flux over PEPCx (Fig. 4A; see also Fig. S5 in the supplemental material). In contrast to the finding for PCx-deficient strains, no negative impact of glucose on the growth of the $\Delta aceE \Delta ppc$ strain was observed (see Fig. S6), confirming again the superior role of PCx in *C. glutamicum* (23, 32). Interestingly, we also observed a significant impact of the culture volume on the growth of the $\Delta aceE \Delta pyc$ strain. Since efficient liquid-air mixing continuously removes CO_2 from the culture medium, the lag phase of the $\Delta aceE \Delta pyc$ strain was much more prominent during microtiter plate cultivation (~17 h) than in cultures in shake flasks (a ~7-h lag phase in 100-ml cultures and a ~13-h lag phase in 50 ml) (see Fig. S7).

The urease enzyme, catalyzing the degradation of urea to ammonium and carbon dioxide, represents a further important contributor to the intracellular $\text{CO}_2/\text{HCO}_3^-$ pool, especially in the early exponential phase, when cell densities and decarboxylation reaction rates are low. In a previous study, the *ureD-E188** mutation was found to abolish urease activity in *C. glutamicum* and to enhance L-valine production by PDHC-deficient strains (33). In this study, we introduced the *ureD-E188** mutation into the $\Delta aceE \Delta pyc$ background so as to examine the influence of an even lower $\text{CO}_2/\text{HCO}_3^-$ level on anaplerosis in this strain background. The additional inactivation of the urease enzyme resulted in a significantly elongated lag phase of about 46 h, which could also be complemented by the addition of HCO_3^- (Fig. 4B), demonstrating the importance of the $\text{CO}_2/\text{HCO}_3^-$ pool during the initial growth phase. Furthermore, we assessed the impact of urease mutation on the production of L-valine and L-alanine by the $\Delta aceE$ and $\Delta aceE ureD-E188^*$ strains and the effect of complementation via HCO_3^- addition. Within 28 h of cultivation, the $\Delta aceE$ strain produced 15 mM L-valine and 10 mM L-alanine as by-products, while the $\Delta aceE ureD-E188^*$ strain accumulated 54 mM L-valine and 38 mM L-alanine (Fig. 5). The addition of HCO_3^- , however, significantly reduced L-valine production, by 54% for the $\Delta aceE$ strain and 59% for the $\Delta aceE ureD-E188^*$ strain. The concentration of the by-product L-alanine increased by 22% for the $\Delta aceE$ strain and decreased by 51% for the $\Delta aceE ureD-E188^*$ strain (Fig. 5). The examples of L-valine and L-alanine production illustrate the important role of the intracellular $\text{CO}_2/\text{HCO}_3^-$ levels on metabolic flux in PDHC-deficient strains.

Another approach to influencing the extracellular HCO_3^- availability was to change the pH conditions (2). According to the Bjerrum plot, CO_2 is predominant under acidic conditions, while CO_3^{2-} is the dominant form under alkaline conditions. At a pH of

about 8, HCO_3^- is the prevalent form. Since HCO_3^- is the substrate of the anaplerotic enzymes PCx and PEPCx, the pH in the cultivation medium was adjusted to 8 using KOH, leading to an equilibrium shift toward higher HCO_3^- availability. As a negative control, the pH was adjusted to 6 using HCl. While the growth of both strains tested was retarded at pH 6, it was significantly enhanced at pH 8 (Fig. 4C). Thus, elevation of the culture pH improved the growth of PDHC-deficient strains, likely by increasing anaplerotic flux.

The PPP includes another decarboxylation reaction in the central carbon metabolism, the reaction catalyzed by 6-phosphogluconate dehydrogenase (6PGDH), that contributes to the intracellular $\text{CO}_2/\text{HCO}_3^-$ pool. Remarkably, the lag phases of the $\Delta aceE \Delta pyc$ and $\Delta aceE ureD-E188^+ \Delta pyc$ strains were mostly complemented during growth on acetate and gluconate—the latter entering the PPP via gluconate-6-phosphate (Fig. 4D). Growth on ribose, which enters the PPP via ribulose-5-phosphate and thereby bypasses the decarboxylation catalyzed by 6PGDH, showed a significantly elongated lag phase in *pyc*-deficient strains (Fig. 4D). In a further experiment, metabolic/glycolytic flux was rerouted through the PPP by deleting *pgi*, encoding glucose-6-phosphate isomerase. However, deletion of *pgi* resulted in a severe growth defect in the $\Delta aceE$ background. In this context, the growth of the $\Delta aceE \Delta pyc$ strain featured only minor, nonsignificant improvement (see Fig. S8 in the supplemental material).

Taken together, our findings highlight the important impact of the intracellular $\text{CO}_2/\text{HCO}_3^-$ pool on metabolic flux in the central carbon metabolism. This is especially evident in the $\Delta aceE \Delta pyc$ strain, which lacks a central decarboxylation reaction and the key carboxylase PCx in *C. glutamicum*.

Refueling the TCA cycle improves the growth of *pyc* mutants. Glucose catabolism requires sufficient anaplerotic flux to replenish TCA cycle intermediates, providing precursors for various anabolic pathways. Therefore, we tested whether the addition of TCA cycle intermediates would complement the negative impact of glucose on the growth of the $\Delta aceE \Delta pyc$ strain. Remarkably, all TCA cycle intermediates tested (succinate, malate, citrate, and the glutamate-containing dipeptide Glu-Ala) reduced the extended lag phase of the $\Delta aceE \Delta pyc$ strain during growth on glucose-acetate mixtures (Fig. 6A). The value of Δt was defined to give the percentage change of lag phase time compared to the first doubling time of the $\Delta aceE$ and $\Delta aceE \Delta pyc$ strains on glucose-acetate mixtures (100%). The dipeptide Glu-Ala and succinate reduced the elongated lag phase to high extents, by 90% ($\Delta t = 10\%$) and 85% ($\Delta t = 15\%$), respectively, while the effects of citrate and malate were weaker (Δt , 40% and 38%, respectively) (Table 2).

Based on previous studies, it was known that the glyoxylate shunt might be switched off during growth on glucose-acetate mixtures, due to the inhibitory effect of glucose (34). In this study, overexpression of the *aceA* and *aceB* genes, encoding the glyoxylate shunt enzymes isocitrate lyase and malate synthase, resulted in a significantly shorter lag phase for the $\Delta aceE \Delta pyc$ strain (Fig. 6B). These genes were overexpressed by use of the pJC1 vector harboring an inducible P_{tac} promoter in front of either of two synthetic operon variants (pJC1- P_{tac} -*aceA*-*aceB* and pJC1- P_{tac} -*aceB*-*aceA*). However, it must be noted that for the $\Delta aceE$ strain, overexpression of *aceA* and *aceB* led to lag phases slightly longer than those with the empty-vector control (Fig. 6B). Expression from the leaky P_{tac} promoter yielded the best result, while induction with isopropyl- β -D-thiogalactopyranoside (IPTG) resulted in severe growth defects (data not shown).

Unusual intermediate accumulation or depletion can provide valuable information regarding intracellular flux imbalances causing the observed growth defects. Gas chromatography–time of flight (GC-ToF) experiments were performed for analysis of the metabolic states by comparing samples of the $\Delta aceE$ strain during the early-exponential phase, the $\Delta aceE \Delta pyc$ strain at the same time point during the lag phase, and the $\Delta aceE \Delta pyc$ strain during the early exponential phase (Fig. S9 in the supplemental material shows the sampling scheme). Additionally, samples of both PDHC-

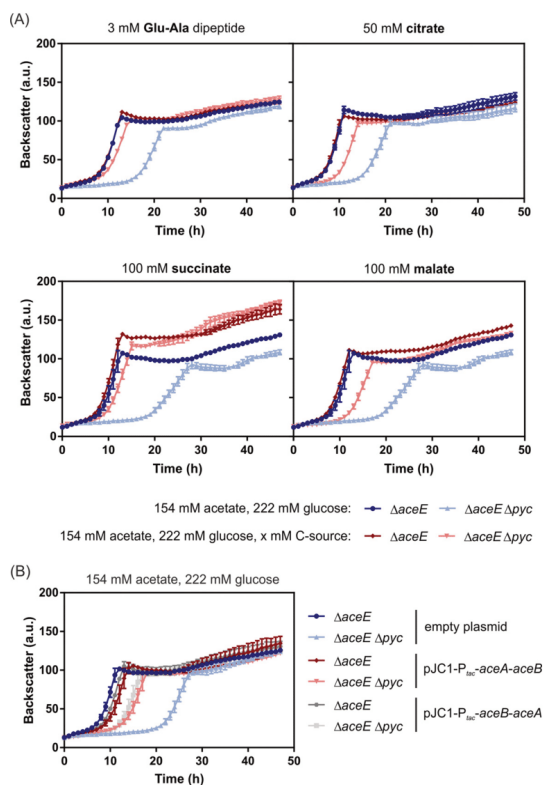


FIG 6 Refueling the TCA cycle to complement the glucose intolerance of the $\Delta aceE$ Δprc strain. The growth curves shown are based on the backscatter measurements in a microtiter cultivation system, while symbols represent the backscatter means for biological triplicates ($n = 3$). The $\Delta aceE$ and $\Delta aceE \Delta prc$ strains were inoculated to an OD_{600} of 1 into CGXII medium with 154 mM acetate and 222 mM glucose. (A) The TCA cycle-fueling carbon source glutamate (3 mM Glu-Ala dipeptide), citrate (50 mM), succinate (100 mM), or malate (100 mM) was added to the medium in order to analyze the effect on lag phase complementation (shades of red). As a control, growth on 154 mM acetate and 222 mM glucose is shown for the $\Delta aceE$ (dark blue) and $\Delta aceE \Delta prc$ (light blue) strains in each experiment. (B) The $\Delta aceE$ and $\Delta aceE \Delta prc$ strains were transformed with the pJC1-P_{lac}-aceA-aceB or pJC1-P_{lac}-aceB-aceA plasmid for simultaneous overexpression of the glyoxylate shunt enzymes isocitrate lyase (encoded by *aceA*) and malate synthase (encoded by *aceB*), while the $\Delta aceE \Delta prc$ and Δprc strains transformed with the empty pJC1 vector served as controls. Cultures were inoculated to an OD_{600} of 1 in CGXII medium containing 154 mM acetate, 222 mM glucose, and 25 $\mu\text{g/ml}$ kanamycin.

deficient strains cultivated with 100 mM HCO_3^- were measured, and WT cells in exponential phase were used as a reference (see Table S1). No significant intermediate accumulation and no occurrence of unusual compounds was observed in the lag-phase sample of the $\Delta aceE \Delta prc$ strain relative to all other samples. Although oxaloacetate cannot be measured by this method, complete depletion of oxaloacetate-derived aspartate was detected in $\Delta aceE \Delta prc$ cells during the lag phase but not during the exponential phase or in HCO_3^- -complemented samples. This result supports the hypothesis that oxaloacetate depletion is the key reason for the elongated lag phase.

In order to identify oxaloacetate depletion as a key growth-limiting factor and to decouple this effect from anaplerosis-dependent replenishment, the Δprc , $\Delta prc \Delta prp$,

TABLE 2 Overview of the lag phases and growth rates of the *C. glutamicum* $\Delta aceE$ and $\Delta aceE \Delta pyc$ strains cultivated with different TCA cycle carbon sources^a

Added carbon source (concn [mM])	<i>C. glutamicum</i> $\Delta aceE$			<i>C. glutamicum</i> $\Delta aceE \Delta pyc$		
	Lag phase ^b	Δt (%) ^c	Growth rate (h ⁻¹)	Lag phase ^b	Δt (%) ^c	Growth rate (h ⁻¹)
None	–	0	0.41 ± 0.01	+	100	0.27 ± 0.02
Glu-Ala (3)	–	0	0.35 ± 0.01	+	10	0.33 ± 0.01
Citrate (50)	–	0	0.39 ± 0.01	+	40	0.35 ± 0.01
Succinate (100)	–	–8	0.36 ± 0.01	+	15	0.34 ± 0.02
Malate (100)	–	–8	0.35 ± 0.01	+	38	0.35 ± 0.02

^aThe strains were cultivated in CGXII medium containing 154 mM acetate and 222 mM glucose with or without a TCA cycle carbon source.

^b+, lag phase greater than or equal to the lag phase observed for the strain on 154 mM acetate with 222 mM glucose; +, shorter lag phase; –, no lag phase.

^cThe difference between the first doubling time of the $\Delta aceE$ strain and that of the $\Delta aceE \Delta pyc$ strain was defined as 100%.

and $\Delta aceE \Delta pyc \Delta ppc$ strains were tested in the presence of different TCA cycle intermediates. Here, mutants lacking both anaplerotic reactions (PCx and PEPc)—the $\Delta pyc \Delta ppc$ and $\Delta aceE \Delta pyc \Delta ppc$ strains—were not able to grow on glucose-acetate mixtures at all (Fig. 4A; also Fig. S5 in the supplemental material). Again, all TCA cycle intermediates were able to complement the glucose sensitivity of these *pyc*-deficient strains, and the growth of the $\Delta pyc \Delta ppc$ and $\Delta aceE \Delta pyc \Delta ppc$ strains was effectively restored (Table 3). Nevertheless, slight differences were observed, which might also be caused by differences in the uptake of these carbon sources.

Adaptation of *C. glutamicum* $\Delta aceE \Delta pyc$ to growth on glucose and acetate. In a previous study, Kotte et al. reported on an elongated lag phase of *E. coli* as a result of glucose-gluconeogenic substrate shifts (35). This phenomenon was ascribed to the formation of a small subpopulation that is able to start growing after carbon source switches (35). Usually, the growth of a small subpopulation is obscured by typical bulk measurements but can be visualized by single-cell approaches, such as flow cytometry (FC). To this end, the membranes of $\Delta aceE$ and $\Delta aceE \Delta pyc$ cells were stained using the nontoxic green fluorescent dye PKH67 prior to inoculation. During cellular growth, the amount of fluorescent dye is diluted by membrane synthesis, leading to a decrease in the level of single-cell PKH67 fluorescence (35). Stained $\Delta aceE$ and $\Delta aceE \Delta pyc$ cells were cultivated in minimal medium containing glucose and acetate (Fig. 7A). As a nonproliferating control, $\Delta aceE \Delta pyc$ cells were incubated in glucose as the sole carbon source. Using flow cytometry, membrane staining was analyzed during cultivation at the single-cell level (Fig. 7B). While the mean of the fluorescence of the whole $\Delta aceE$ population decreased from 2.7×10^4 arbitrary units (AU) to 7.5×10^2 AU, the mean of the fluorescence of the $\Delta aceE \Delta pyc$ population incubated in glucose medium alone shifted from 3.1×10^4 AU to 1.3×10^3 AU, resulting from a minor dilution/bleaching of fluorescence intensity during incubation. Remarkably, both the $\Delta aceE$ and $\Delta aceE \Delta pyc$ strains featured rather heterogeneous adaptation behavior on glucose-acetate mixtures, which was apparently delayed in the $\Delta aceE \Delta pyc$ strain, reflecting the elongated

TABLE 3 Overview of the lag phases and growth rates of the *C. glutamicum* Δpyc , $\Delta pyc \Delta ppc$, and $\Delta aceE \Delta pyc \Delta ppc$ strains cultivated with different TCA cycle carbon sources^a

Added carbon source (concn [mM])	Result for the <i>C. glutamicum</i> strain with the following mutation(s):					
	Δpyc		$\Delta pyc \Delta ppc$		$\Delta aceE \Delta pyc \Delta ppc$	
	Δt_{lag} (h) ^b	Growth rate (h ⁻¹) ^c	Δt_{lag} (h)	Growth rate (h ⁻¹)	Δt_{lag} (h)	Growth rate (h ⁻¹)
None	6 h	0.17 ± 0.02	No growth		No growth	
Glu-Ala (3)	ND	ND	8	0.21 ± 0.01	30	0.14 ± 0.01
Citrate (50)	3	0.19 ± 0.01	5	0.26 ± 0.01	8	0.20 ± 0.03
Succinate (100)	2	0.2 ± 0.02	3	0.16 ± 0.03	5	0.12 ± 0.03
Malate (100)	3	0.21 ± 0.01	17	0.18 ± 0.01	18	0.24 ± 0.01

^aStrains were cultivated in CGXII medium containing 154 mM acetate and 222 mM glucose with or without a TCA cycle carbon source.

^bDifference in lag phase duration between the $\Delta aceE$ strain growing on a glucose-acetate mixture and the strain of interest growing on the respective carbon source(s). ND, not determined.

^cFor comparison, the growth rate in a glucose-acetate mixture was 0.41 h⁻¹ for the $\Delta aceE$ strain and 0.28 h⁻¹ for the $\Delta aceE \Delta pyc$ strain in this experiment.

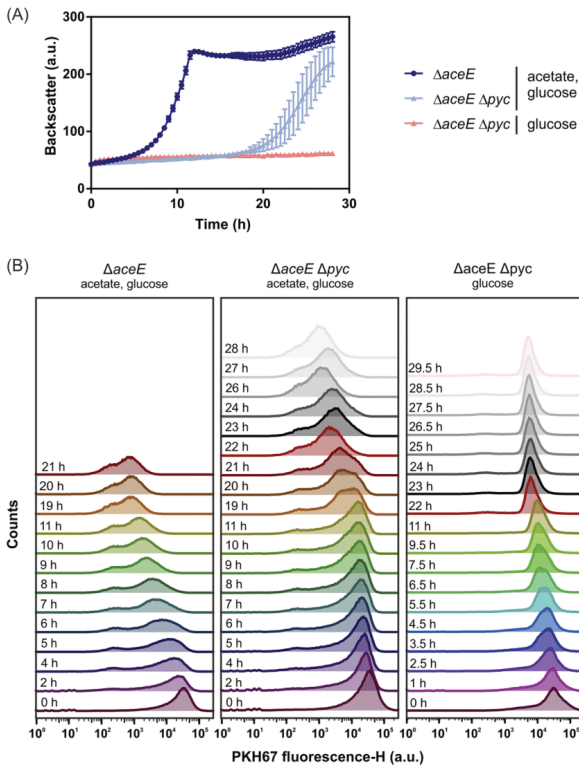


FIG 7 Heterogeneous adaptation of *C. glutamicum* $\Delta aceE$ and *C. glutamicum* $\Delta aceE \Delta pyc$ during growth on glucose and acetate. To identify a potential growing subpopulation, the fluorescent dye PKH67 was used to stain the membranes of $\Delta aceE$ and $\Delta aceE \Delta pyc$ cells prior to cultivation. The cells were cultivated in a microtiter cultivation system in the presence of 154 mM acetate and 222 mM glucose. As a nongrowing control, the $\Delta aceE \Delta pyc$ strain was additionally incubated in CGXII medium containing solely 222 mM glucose. (A) Cell growth was monitored online using a microtiter cultivation system. (B) Staining intensities were measured on the single-cell level during cultivation using flow cytometry (with three biological replicates). Shown are the frequencies of PKH67 staining intensities of one representative culture of each sample over the time course of cultivation. H, height; Counts, cell count.

lag phase. Already in the early phase of cultivation, the populations split into two subpopulations of low and high PKH67 fluorescence, indicating that only a few cells started to proliferate, while a fraction of the population was not able to grow under the same conditions (36–38).

To study the adaptation of the $\Delta aceE \Delta pyc$ strain, comparative transcriptome analyses were performed using DNA microarrays. To this end, $\Delta aceE$ and $\Delta aceE \Delta pyc$ cells were harvested at comparable optical densities (ODs) during early exponential phase (see Fig. S9 in the supplemental material). Both strains were cultivated in CGXII medium with 154 mM acetate and 222 mM glucose. Under the conditions chosen, a total of 354 genes showed significantly altered mRNA levels. While 121 genes were at least 1.7-fold upregulated ($P < 0.05$), 233 genes were 0.7-fold downregulated ($P < 0.05$) in the $\Delta aceE \Delta pyc$ strain (see Table S2). An overview of expression changes of selected genes is shown in Table 4. Among the various changes in the levels of gene expression,

TABLE 4 Comparative transcriptome analysis of *C. glutamicum* $\Delta aceE \Delta pyc$ and *C. glutamicum* $\Delta aceE$ during growth on glucose and acetate^a

Function and gene locus	Gene name	Annotation	mRNA ratio	P
PTS component				
cg1537	<i>ptsG</i>	Glucose-specific enzyme IIBC component of PTS	<u>0.59</u>	0.02
cg2117	<i>ptsI</i>	PEP:sugar phosphotransferase system enzyme I	<u>0.67</u>	0.01
cg2121	<i>ptsH</i>	Phosphocarrier protein HPr of PTS	1.16	<i>0.11</i>
myo-Inositol transport				
cg0223	<i>iolT1</i>	myo-Inositol transporter	1.97	0.04
cg3387	<i>iolT2</i>	myo-Inositol transporter	1.41	<i>0.19</i>
Transcriptional regulation of <i>ptsG</i>				
cg2783	<i>gntR1</i>	Transcriptional regulator, GntR family	0.76	0.05
cg1935	<i>gntR2</i>	Transcriptional regulator, GntR family	0.97	<i>0.46</i>
cg2115	<i>sugR</i>	DeoR-type transcriptional regulator of <i>ptsG</i> , <i>ptsS</i> , and <i>ptsF</i>	0.79	0.03
Acetate metabolism				
cg3047	<i>ackA</i>	Acetate/propionate kinase	1.99	0.01
cg3048	<i>pta</i>	Phosphate acetyltransferase	1.34	0.04
cg2560	<i>aceA</i>	Isocitrate lyase	1.70	<i>0.12</i>
cg2559	<i>aceB</i>	Malate synthase	1.88	0.02
Anaplerosis				
cg1787	<i>ppc</i>	Phosphoenolpyruvate carboxylase	0.91	<i>0.32</i>
cg3169	<i>pck</i>	Phosphoenolpyruvate carboxykinase (GTP)	0.72	0.03
cg1458	<i>odx</i>	Oxaloacetate decarboxylase	1.07	<i>0.32</i>
cg3335	<i>malE</i>	Malic enzyme	<u>0.48</u>	<i>0.26</i>
Other functions in the central carbon metabolism				
cg0973	<i>pgi</i>	Glucose-6-phosphate isomerase	0.44	0.03
cg2291	<i>pyk</i>	Pyruvate kinase	<u>0.59</u>	0.01
cg2891	<i>pqo</i>	Pyruvate:quinone oxidoreductase	<u>0.47</u>	0.02

^aThe expression of selected genes encoding central metabolic enzymes or regulators is given as the ratio of the mRNA level in the $\Delta aceE \Delta pyc$ strain to that in the $\Delta aceE$ strain. mRNA ratios of ≤ 0.70 are underlined, and mRNA ratios of ≥ 1.70 are shown in boldface. P values of >0.05 (from three biological replicates) are italicized. For the complete data set, see Table S4 in the supplemental material.

we observed 0.59-fold and 0.67-fold downregulation of the PTS components *ptsG* and *ptsI*, respectively, in the $\Delta aceE \Delta pyc$ strain, in line with the decreased glucose uptake rates of this strain (Table 1). In contrast, *iolT1*, encoding the myo-inositol transporter, which is responsible, *inter alia*, for PTS-independent glucose uptake, was upregulated (39, 40). This is in line with the fact that the *ptsG*-deficient strains still consumed minor amounts of glucose. Interestingly, genes involved in acetate metabolism, including *aceA* and *aceB*, constituting the glyoxylate shunt, displayed increased mRNA levels in the $\Delta aceE \Delta pyc$ strain. This may also represent an important adaptive mechanism, since the glyoxylate shunt needs to be active in the $\Delta aceE \Delta pyc$ strain to compensate for the loss of TCA cycle intermediates during coconsumption of acetate and glucose, as demonstrated by the effect of *aceA-aceB* overexpression in this study (Fig. 6B). While the mRNA levels of genes encoding anaplerotic enzymes did not show significant changes, the glycolytic genes *pgi* and *pyk* featured ~ 2 -fold-reduced levels in the $\Delta aceE \Delta pyc$ mutant. This might well reflect an adaptive mechanism, since downregulation of *pyk* would reduce flux from PEP to pyruvate, and reduced expression of *pgi* would probably lead to increased flux through the PPP, contributing an additional decarboxylation step.

Less is more: ALE of the $\Delta aceE \Delta pyc$ strain reveals rapid inactivation of glucose uptake. In order to identify key mutations abolishing the lag phase of the $\Delta aceE \Delta pyc$ strain, an adaptive laboratory evolution (ALE) experiment was performed. In this ALE experiment, *C. glutamicum* $\Delta aceE \Delta pyc$ was grown in CGXII minimal medium containing 154 mM acetate and 222 mM glucose in 16 repetitive-batch cultures overall. Remarkably, after 8 inoculations, a significantly shortened lag phase was already observed; after 10 inoculations, the $\Delta aceE \Delta pyc$ strain featured a lag phase similar to that of the

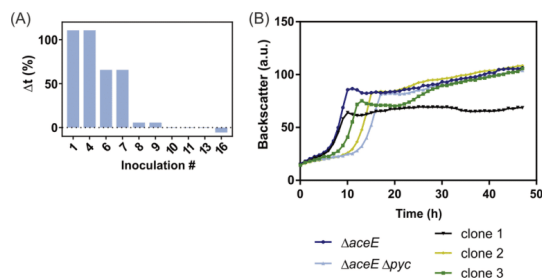


FIG 8 Adaptive laboratory evolution of *C. glutamicum* $\Delta aceE$ Δpyc . Growth was analyzed for single inoculation steps obtained from the adaptive laboratory evolution (ALE) approach, which was performed with the $\Delta aceE$ Δpyc strain in the presence of glucose and acetate. Growth curves are shown based on the backscatter measurements in a microtiter cultivation system. Symbols represent the backscatter means. (A) For growth analysis on the population level, glycerol stocks prepared during the ALE experiment were used for the inoculation of a first preculture in BHI medium supplemented with 51 mM acetate. The second preculture, in CGXII medium containing 154 mM acetate, was then used for inoculation of the main culture in CGXII medium containing 154 mM acetate and 222 mM glucose (starting OD_{600} 1). Shown is the development of the relative lag phase duration after repetitive inoculations of the $\Delta aceE$ Δpyc strain in media containing glucose and acetate. The difference in the first doubling time between the $\Delta aceE$ and $\Delta aceE$ Δpyc strains was set to 100%. For each inoculation, the difference in the lag phase from that for the $\Delta aceE$ strain was calculated and is given as a percentage. (B) Single clones were isolated from batches 7 (clone 1), 8 (clone 2), and 10 (green) and were cultivated as described above. The $\Delta aceE$ and $\Delta aceE$ Δpyc strains served as controls. These single clones were further analyzed by genome sequencing (Table 5).

$\Delta aceE$ strain (Fig. 8A). In contrast, serial cultivation transfers in CGXII medium containing solely acetate did not lead to improved growth in a glucose-acetate medium, indicating that glucose exerted evolutionary selection pressure (see Fig. S10 in the supplemental material). Genome resequencing of the three selected glucose-acetate clones for which data are presented in Fig. 8B revealed mutations in the *ptsI* gene, encoding the EI enzyme of the PTS, in two independently evolved clones (Table 5). This is in agreement with the reduced biomass formation of both clones, in which glucose uptake was apparently abolished to optimize growth on acetate. The third clone showed only slightly accelerated growth, but biomass formation was not impaired. Here, sequencing revealed a mutation in the *rpsC* gene, encoding the ribosomal S3 protein.

In summary, it was indeed possible to eliminate the observed lag phase of the $\Delta aceE$ Δpyc strain ascribed to glucose sensitivity by an adaptive laboratory evolution approach. Especially, the mutations identified in the *ptsI* gene are in agreement with other experiments emphasizing the high selective pressure exerted by glucose on PCx-deficient strains when the intracellular HCO_3^- levels are limiting.

DISCUSSION

During growth on glucose, the pyruvate dehydrogenase complex catalyzes a central metabolic reaction contributing to the intracellular CO_2/HCO_3^- pool. In this study, we systematically perturbed the intracellular CO_2/HCO_3^- pool of PDHC-deficient *C. glutamicum* strains in order to monitor the impact on growth and anaplerotic flux. Even the PDHC-deficient strain *C. glutamicum* $\Delta aceE$ features a slightly elongated lag phase on glucose-acetate mixtures relative to that of the wild type, while no difference in growth is observed when strains are growing on gluconeogenetic substrates, such as acetate.

TABLE 5 Key mutations identified in an adaptive laboratory evolution experiment with *C. glutamicum* $\Delta aceE$ Δpyc

Clone no.	Batch no.	Gene locus	Gene name	Annotation	Mutation
1	7	cg2117	<i>ptsI</i>	EI enzyme, general component of PTS (EC 2.7.3.9)	Exchange, R132H
2	8	cg0601	<i>rpsC</i>	30S ribosomal protein S3	Exchange, R225H
3	10	cg2117	<i>ptsI</i>	EI enzyme, general component of PTS (EC 2.7.3.9)	Exchange, G155

This is remarkable, since this strain catabolizes only a minor fraction of the glucose provided in the exponential-growth phase but turns to the production of L-valine and L-alanine from glucose in the stationary phase (11, 12). The growth defect of *C. glutamicum* $\Delta aceE$ was, however, successfully complemented by the addition of HCO_3^- , which had no significant effect on the growth of wild-type cells, thus hinting at problems caused by impaired anaplerotic flux in this strain background. By comparing the CO_2 production rates of the *C. glutamicum* $\Delta aceE$ strain and the wild type, Bartek et al. were able to show in a previous study that the $\Delta aceE$ strain excretes only around $0.83 \text{ mmol of CO}_2 \text{ g}^{-1} \text{ h}^{-1}$, while the wild type excretes ca. $1.65 \text{ mmol of CO}_2 \text{ g}^{-1} \text{ h}^{-1}$ (29). The lower CO_2 production rates of the PDHC-deficient strain already indicate a significant impact on the intracellular $\text{CO}_2/\text{HCO}_3^-$ pool affecting metabolic flux distribution, especially at low cell densities, when $\text{CO}_2/\text{HCO}_3^-$ is limiting.

The anaplerotic node comprises the essential link between glycolysis/gluconeogenesis and the TCA cycle (20). In contrast to most other organisms, *C. glutamicum* possesses both anaplerotic carboxylases, PEPCx (encoded by *ppc*) and PCx (encoded by *pyc*), catalyzing the anaplerotic bicarbonate-dependent reactions to yield oxaloacetate from PEP or pyruvate, respectively. It was shown that in *C. glutamicum*, these two enzymes can replace each other to a certain extent, depending on the intracellular concentrations of the respective effectors for each enzyme. However, during growth on glucose, the biotin-containing PCx contributes 90% to the main anaplerotic activity, in contrast to PEPCx (23, 32). In our study, deletion of the *pyc* gene resulted in a severely elongated lag phase ($>15 \text{ h}$) of the $\Delta aceE \Delta pyc$ strain when glucose was present in the medium. Retarded growth of Δpyc strains has been observed previously, and in line with our data, other studies also reported a severe growth defect of a Δpyc strain under low $\text{CO}_2/\text{HCO}_3^-$ levels (23, 28). This effect appeared to be even more severe when the cells were grown in microtiter plates under CO_2 -stripping conditions (low culture volume, high air mixing) than when they were grown in higher culture volumes (see Fig. S7 in the supplemental material). The PDHC-deficient mutant strain *C. glutamicum* $\Delta aceE \Delta pyc$ was found to react very sensitively to small changes in intracellular bicarbonate availability and was therefore used as a test platform with which to assess systematically the impact of perturbations affecting the intracellular $\text{CO}_2/\text{HCO}_3^-$ pool. While addition of HCO_3^- , an increase in the pH, and higher culture volumes rescued the strain, mutation of the urease accessory protein (*ureD*-E188*), which lowers the intracellular $\text{CO}_2/\text{HCO}_3^-$ pool, resulted in an even more severe phenotype. It was not possible to restore growth if the second anaplerotic gene, *ppc*, was deleted as well, confirming that the measures mentioned above fostered the flux over the remaining anaplerotic reaction catalyzed by PEPCx.

The mutation in *ureD* was revealed by a previous biosensor-driven evolution approach selecting for mutations enhancing L-valine production in *C. glutamicum* (33). In that study, inactivation of the urease enzyme by the *ureD*-E188* mutation reduced the anaplerotic flux via PCx, resulting in increased precursor availability of pyruvate-derived products, such as L-valine and L-alanine (33). In the present study, we confirmed this finding by complementation with HCO_3^- , counteracting the effect of the *ureD*-E188* mutation. In another study, by Blombach et al., lower $\text{CO}_2/\text{HCO}_3^-$ levels also triggered enhanced production of L-valine and L-alanine by *C. glutamicum* during shake flask cultivation (28). However, a positive impact of anaplerotic reactions has been confirmed for other products, for example, oxaloacetate-derived products, such as L-lysine. In those studies, attempts to overexpress *pyc* or the introduction of deregulated variants significantly improved L-lysine production (41, 42). However, in spite of great efforts and success in the development of L-lysine production strains, the impact of altered $\text{CO}_2/\text{HCO}_3^-$ levels has not been systematically assessed so far.

Residual glucose consumption by PDHC-deficient *C. glutamicum* strains has already been reported in previous studies (11, 12, 29). The results of this work, however, emphasize that mutants lacking the major anaplerotic route via PCx (Δpyc mutants) are under strong evolutionary pressure in the presence of glucose. Although the strains would be able to grow on the acetate supplied in the growth medium, increasing levels

of glucose resulted in a severely elongated lag phase (as long as >40 h with 250 mM) for *C. glutamicum* $\Delta aceE \Delta pyc$. Besides the above-mentioned efforts to increase the CO_2/HCO_3^- pool, the deletion of the *ptsG* gene itself effectively restored growth on glucose but not on other PTS substrates and not on ribose. These results indicate that growth retardation is not the result of PtsG-dependent regulation as known for *E. coli* (43, 44).

Furthermore, among the three key mutations identified in the ALE experiment, two single nucleotide polymorphisms (SNPs) obtained from independent cell lines were located within the *ptsI* gene, encoding the EI component of the PTS. These findings clearly highlight the problems of residual glucose consumption in strains featuring impaired anaplerotic flux. One reason for the observed growth phenotype might be stress resulting from the intracellular accumulation of sugar phosphates. In *Escherichia coli*, sugar phosphate stress can be caused by the accumulation of any sugar phosphates due to a block in glycolysis (45), e.g., by mutations in *pgi* or *pfkA* (46), or due to excessive glucose uptake caused, e.g., by overexpression of *uhpT*, encoding a sugar phosphate permease (47). The resulting metabolic imbalance causes growth inhibition. For example, in *C. glutamicum*, accumulation of several sugar phosphates, such as fructose-1,6-bisphosphate or PEP, inhibits the key enzyme of the glyoxylate shunt, isocitrate lyase, already at low concentrations (34). To counteract this stress, *E. coli* triggers SgrR, which, in turn, activates SgrS by an unknown signal. The transcription factor SgrS then prevents further uptake of glucose by downregulation of *ptsG* (45, 48, 49). This is in line with the finding of our study showing a slight downregulation of *ptsG* upon resumed growth of the $\Delta aceE \Delta pyc$ strain (Table 4). This reduction of glucose uptake via the PTS, which converts PEP to pyruvate during glucose transport, also contributes to increased PEP availability for the remaining anaplerotic reaction catalyzed by PEPCK. Further, this is in line with an upregulation of *iolT1*, which ensures minor usage of glucose without PEP depletion (39, 40). In this context, the downregulation of the *pyk* gene in the $\Delta aceE \Delta pyc$ strain can also be interpreted as a potential adaptation to increase the PEP pool, fostering anaplerotic flux. All these strategies counteracting PEP depletion underline the fact that under these conditions, the anaplerotic enzyme PEPCK is not able to deliver appropriate amounts of oxaloacetate in the $\Delta aceE \Delta pyc$ strain.

During growth on gluconeogenic carbon sources—such as acetate—the transcriptional repressor SugR represses the expression of the PTS genes in *C. glutamicum*, including the glucose-specific *ptsG* gene but also *ptsF*, *ptsS*, and general components, such as *ptsI* and *ptsH* (50–52). Derepression appears to be triggered by the accumulation of fructose-6-phosphate (F6P), which is generated from glucose-6-phosphate entering glycolysis. Consequently, F6P accumulation leads to an increase in glucose consumption rates, resulting in parallel catabolization of glucose and acetate (15). The fact that the PDHC-deficient strains are also subject to regulation by SugR has been demonstrated by studies showing that the $\Delta aceE \Delta sugR$ strain leads to glucose consumption rates as much as 4-fold higher (53).

In aerobic glucose-based bioprocesses, the endogenous production of CO_2 is typically sufficiently high to promote microbial growth even at low cell densities. However, it is well known that the anaerobic growth of some bacteria, such as *E. coli*, requires an external supply of CO_2/HCO_3^- to avoid long lag phases (25, 54, 55). The critical impact of CO_2/HCO_3^- levels may become especially evident under conditions where the endogenous CO_2 production rate becomes limiting. This was nicely demonstrated by a recent study of Bracher et al., who showed that long lag phases of engineered, but nonevolved, *Saccharomyces cerevisiae* strains during xylose fermentation could be avoided by sparging the bioreactor cultures with CO_2-N_2 mixtures (56). Alternatively, the addition of L-aspartate, whose transamination provides oxaloacetate, which refuels the TCA cycle, completely abolished the long adaptation phase of the respective yeast strains. In line with these findings, a recent ^{13}C flux analysis with *E. coli* revealed that considerable turnover of lipids via β -oxidation appears to be required for growth on xylose to enhance the intracellular CO_2/HCO_3^- pool to a growth-promoting level that

enables anaplerotic flux (57). These findings are in good agreement with our demonstration in this study that the elongated lag phase of the *C. glutamicum* $\Delta aceE \Delta pyc$ strain can be eliminated by various measures, either by increasing the intracellular $\text{CO}_2/\text{HCO}_3^-$ level or by refueling the TCA cycle with various intermediates, such as citrate, malate, or succinate.

Overall, oxaloacetate depletion appeared to represent a key issue causing the delayed growth of the $\Delta aceE \Delta pyc$ strain. Our data revealed that this is caused by impaired anaplerotic flux on glucose due to low intracellular $\text{CO}_2/\text{HCO}_3^-$ levels as well as reduced activities of glyoxylate cycle enzymes. As known from several organisms, the activity of glyoxylate shunt enzymes is tightly repressed during growth on glucose. In *C. glutamicum*, the transcription of *aceA* (encoding isocitrate lyase) and *aceB* (encoding malate synthase) is repressed by RamB in the presence of glucose (58) and is activated by RamA in the presence of acetate (59). The PDHC-deficient strains in this study were grown on glucose-acetate mixtures. In an earlier study by Wendisch et al., it was emphasized that the anaplerotic function is entirely achieved by the glyoxylate cycle enzymes when wild-type *C. glutamicum* is grown on glucose plus acetate (15). They further revealed that this function can be partly complemented by PEPcX or PCx (15). However, the possibility remains that the glyoxylate cycle enzymes, especially isocitrate lyase, are repressed in the PDHC-deficient mutants due to accumulation of, e.g., sugar phosphates caused by the PDHC and/or *pyc* inactivation. Reinscheid et al. (1994) claimed that the sugar phosphates 3-phosphoglycerate, 6-phosphogluconate, and fructose 1,6-bisphosphate cause inhibition of the isocitrate lyase in *C. glutamicum* (34). Although transcriptional regulation of the glyoxylate shunt is different, isocitrate lyases of *E. coli* are also repressed by glucose catabolites (60–62). Consequently, a repressed glyoxylate shunt due to glucose catabolite accumulation probably also accounts for oxaloacetate depletion in PDHC-deficient strains; this is especially problematic for the $\Delta aceE \Delta pyc$ strain, which cannot complement this depletion by anaplerotic pathways due to lower intracellular $\text{CO}_2/\text{HCO}_3^-$ levels.

Taken together, these results emphasize the important impact of the intracellular $\text{CO}_2/\text{HCO}_3^-$ pool on metabolic flux distribution, which is especially relevant in engineered strains exhibiting lower endogenous CO_2 production rates, as exemplified by PDHC-deficient strains in this study, but also by the performance of pentose-fermenting yeast and *E. coli* strains (56, 57). Consequently, the lack of an important by-product, such as CO_2 released by the PDHC, may have a significant impact on cellular metabolism and growth, especially on glycolytic substrates demanding high flux via anaplerotic reactions.

MATERIALS AND METHODS

Bacterial strains and growth conditions. All bacterial strains and plasmids used in this study are listed in Tables 6 and 7, respectively. Mutant strains are based on the wild-type *Corynebacterium glutamicum* strain ATCC 13032 (63).

Standard cultivation of *C. glutamicum* $\Delta aceE$ cells and derivatives was performed on brain heart infusion (BHI; Difco; BD, Heidelberg, Germany) agar plates containing 51 mM potassium acetate (referred to here as acetate) (ChemSolute; Th. Geyer, Stuttgart, Germany) at 30°C for 2 days. One single colony was picked and was incubated for 8 to 10 h at 30°C in either 4.5 ml or 1 ml BHI containing 154 mM acetate in reaction tubes or deep-well plates (VWR International, PA, USA), respectively. First precultures were used to inoculate second precultures in CGXII minimal medium (64) supplemented with 154 mM acetate either as 10-ml cultures in shake flasks or in 1-ml volumes in deep-well plates. After overnight growth, a main culture was inoculated at an optical density at 600 nm (OD_{600}) of 1 in CGXII medium containing 154 mM acetate and either 222 mM D-(+)-glucose monohydrate (Riedel-de Haën, Seelze, Germany) (referred to here as glucose) or any other carbon source as stated, e.g., D-(–)-fructose (Sigma-Aldrich, Taufkirchen, Germany) (referred to as fructose), D-(+)-sucrose (Roth, Karlsruhe, Germany) (referred to as sucrose), D-gluconic acid sodium salt (Sigma-Aldrich, Taufkirchen, Germany) (referred to as gluconate), D-(–)-ribose (Sigma-Aldrich, Taufkirchen, Germany) (referred to as ribose), citric acid monohydrate (Merck Millipore, Darmstadt, Germany) (referred to as citrate), H-Glu-Ala-OH (Bachem AG, Bubendorf, Switzerland) (referred to as Glu-Ala), succinic acid (Sigma-Aldrich, Taufkirchen, Germany) (referred to as succinate), or L-malic acid (Merck Millipore, Darmstadt, Germany) (referred to as malate). To increase the extracellular availability of bicarbonate, 100 mM potassium HCO_3^- (Merck Millipore, Darmstadt, Germany) was added to the basic CGXII solution. The pH was adjusted to 7, and subsequently, the medium was passed through a sterile filter before inoculation. In order to analyze the effects of different pH levels, either HCl (to lower the pH) or KOH (to increase the pH) was added to the CGXII basis, which was sterile

TABLE 6 Bacterial strains used in this study

Strain	Characteristics	Source or reference
<i>C. glutamicum</i>		
ATCC 13032	Wild type, biotin auxotroph	S. Kinoshita et al. (77)
$\Delta aceE$ strain	ATCC 13032 derivative with deletion of <i>aceE</i>	M. E. Schreiner et al. (5)
$\Delta aceE \Delta pyc$ strain	ATCC 13032 derivative with deletions of <i>aceE</i> and <i>pyc</i>	This work
$\Delta aceE \Delta ptsG$ strain	ATCC 13032 derivative with deletions of <i>aceE</i> and <i>ptsG</i>	This work
$\Delta aceE \Delta pyc \Delta ptsG$ strain	ATCC 13032 derivative with deletions of <i>aceE</i> , <i>pyc</i> , and <i>ptsG</i>	This work
$\Delta aceE \Delta pgi$ strain	ATCC 13032 derivative with deletions of <i>aceE</i> and <i>pgi</i>	This work
$\Delta aceE \Delta pyc \Delta pgi$ strain	ATCC 13032 derivative with deletions of <i>aceE</i> , <i>pyc</i> , and <i>pgi</i>	This work
$\Delta aceE \Delta ppc$ strain	ATCC 13032 derivative with deletions of <i>aceE</i> and <i>ppc</i>	This work
$\Delta aceE \Delta pyc \Delta ppc$ strain	ATCC 13032 derivative with deletions of <i>aceE</i> , <i>pyc</i> , and <i>ppc</i>	This work
$\Delta aceE ureD-E188^*$ strain	ATCC 13032 derivative with deletion of <i>aceE</i> and with <i>ureD-E188^*</i> (Glu188 replaced by the stop codon)	R. Mahr et al. (33)
$\Delta aceE ureD-E188^* \Delta pyc$ strain	ATCC 13032 derivative with deletions of <i>aceE</i> and <i>pyc</i> and with <i>ureD-E188^*</i> (Glu188 replaced by the stop codon)	This work
Δpyc strain	ATCC 13032 derivative with deletion of <i>pyc</i>	P. G. Peters-Wendisch et al. (23)
$\Delta pyc \Delta ppc$ strain	ATCC 13032 derivative with deletions of <i>aceE</i> and <i>ppc</i>	A. Schwentner et al. (78)
<i>E. coli</i> DH5 α	F ⁻ $\phi 80lac\Delta M15 \Delta(lacZYA-argF)U169 recA1 endA1 hsdR17(r_k^- m_k^+) phoA supE44 thi-1 gyrA96 relA1 \lambda^-$; for general cloning purposes	Invitrogen

filtered afterwards. For cultivations in the presence of TCA cycle-filling/refueling substrates, 50 mM citric acid monohydrate (citrate), 3 mM H-Glu-Ala-OH dipeptide (Glu-Ala), 100 mM succinic acid (succinate), or 100 mM L-malic acid (malate) was used. In experiments where gluconate or ribose was used as the carbon source, 100 mM D-gluconic acid sodium salt or 100 mM D-ribose was added, respectively. Biomass formation was monitored during cultivation in shake flasks by measuring the OD₆₀₀ or by measuring backscatter values during microtiter plate cultivation. Where necessary, the medium was also supplemented with 25 μ g/ml kanamycin.

Escherichia coli DH5 α was used for cloning and plasmid isolation. Cells were directly inoculated from a glycerol stock or from a lysogeny broth (LB) agar plate and were grown in shake flasks in LB medium at 37°C. If necessary for selection, the medium was also supplemented with 50 μ g/ml kanamycin.

TABLE 7 Plasmids used in this study

Plasmid	Characteristics	Source or reference
pK19 <i>mobsacB</i>	Contains negative (<i>sacB</i>) and positive (Kan ^r) selection markers for genomic integration and deletion	A. Schäfer et al. (70)
pK19 <i>mobsacB</i> - Δpyc	Kan ^r ; derivative of pK19 <i>mobsacB</i> for partial <i>pyc</i> gene deletion, containing only the first 499 bp and last 493 bp of <i>pyc</i> , with the deletion of 2,429 bp in the middle	P. G. Peters-Wendisch et al. (23)
pK19 <i>mobsacB</i> - $\Delta ptsG$	Kan ^r ; derivative of pK19 <i>mobsacB</i> for partial <i>ptsG</i> gene deletion, containing only the last 491 bp of <i>ptsG</i> , with the deletion of the first 1,561 bp	This work
pK19 <i>mobsacB</i> - Δpgi	Kan ^r ; derivative of pK19 <i>mobsacB</i> for <i>pgi</i> gene deletion, containing only the last 537 bp of <i>pgi</i> , with the deletion of the first 1,086 bp	This work
pK19 <i>mobsacB</i> - Δppc	Kan ^r ; derivative of pK19 <i>mobsacB</i> for partial <i>ppc</i> gene deletion, containing only the first 391 bp and last 447 bp of <i>ppc</i> , with the deletion of 1,922 bp in the middle	J. Buchholz et al. (13)
pK19 <i>mobsacB</i> - <i>ureD-E188^*</i>	Kan ^r ; derivative of pK19 <i>mobsacB</i> for <i>ureD</i> gene truncation by replacing Glu188 in <i>ureD</i> with the stop codon	R. Mahr et al. (33)
pJC1	Kan ^r <i>oriV_{Ec}</i> <i>oriV_{Cg}</i> ; <i>E. coli</i> - <i>C. glutamicum</i> shuttle vector	J. Cremer et al. (79)
pJC1- <i>venus-term-BS</i>	Kan ^r ; derivative of pJC1, containing the terminator sequence of <i>Bacillus subtilis</i> behind <i>venus</i>	M. Baumgart et al. (74)
pJC1- <i>pyc</i>	Kan ^r ; derivative of pJC1- <i>venus-term-BS</i> , containing <i>pyc</i> under the control of its native promoter P _{<i>pyc</i>}	This work
pJC1-P _{<i>tac</i>} - <i>aceA-aceB</i>	Kan ^r ; derivative of pJC1- <i>venus-term-BS</i> , containing <i>lacI</i> and <i>aceA</i> followed by a linking sequence (5'-ACTAGAAATAATTTTGTTTAACTTTAAGAAGGAGATATACAT-3') and <i>aceB</i> under the control of the inducible promoter P _{<i>tac</i>}	This work
pJC1-P _{<i>tac</i>} - <i>aceB-aceA</i>	Kan ^r ; derivative of pJC1- <i>venus-term-BS</i> , containing <i>lacI</i> and <i>aceB</i> followed by a linking sequence (5'-ACTAGAAATAATTTTGTTTAACTTTAAGAAGGAGATATACAT-3') and <i>aceA</i> under the control of the inducible promoter P _{<i>tac</i>}	This work

Microtiter plate cultivation. Online monitoring of growth and/or pH was performed in 48-well microtiter FlowerPlates (m2p-labs GmbH, Baesweiler, Germany) sealed with sterile breathable rayon film (VWR International, PA) in a BioLector microtiter cultivation system (m2p-labs GmbH, Baesweiler, Germany) (65). The cultivation conditions were adjusted as described previously (66), and biomass formation was recorded every 15 min as the backscattered light intensity (light wavelength, 620 nm; signal gain factor of 20) for 24 to 72 h at 30°C and 1,200 rpm. pH measurements were performed with 48-well microtiter FlowerPlates equipped with pH optodes. The data obtained were evaluated using BioLector (m2p-labs, Baesweiler, Germany) and GraphPad Prism 7 (GraphPad Software, Inc., San Diego, CA) software.

ALE. Adaptive laboratory evolution (ALE) of *C. glutamicum* $\Delta aceE$ and *C. glutamicum* $\Delta aceE \Delta pyc$ was performed in deep-well plates (VWR International, PA) in a main culture of 1 ml CGXII medium containing either 154 mM acetate and 222 mM glucose or solely 154 mM acetate (as a control without selection pressure) adjusted to an OD₆₀₀ of 1. Cells were cultivated for 2 to 3 days before the next generation was inoculated, starting at an OD₆₀₀ of 1, and cultivated again for 2 to 3 days. After each generation step, glycerol stocks of cultures were prepared (20% glycerol) and were stored at -80°C, allowing growth analysis and DNA sequencing of cultures from individual inoculations. In total, 16 serial transfers were analyzed.

Cloning techniques and recombinant DNA work. Standard molecular biology methods were performed according to J. Sambrook and D. W. Russell (67). *C. glutamicum* ATCC 13032 chromosomal DNA was used as the template for PCR amplification of DNA fragments and was prepared as described previously (68). DNA fragment and plasmid sequencing, as well as synthesis of oligonucleotides, was performed by Eurofins Genomics (Ebersberg, Germany).

For the construction of plasmids (see Table S3 in the supplemental material), DNA fragments were amplified using the respective oligonucleotides (see Table S4) and were enzymatically assembled into a vector backbone according to reference 69.

To achieve genomic deletion of *pyc*, *ptsG*, *ppc*, and *pgi*, two-step homologous recombination using the pK19mobsacB system (70) was implemented. The suicide plasmids (compare Table 7 with Table S2 in the supplemental material) were isolated from *E. coli* cells using the QIAprep spin miniprep kit (Qiagen, Hilden, Germany). Electrocompetent *C. glutamicum* $\Delta aceE$ and *C. glutamicum* $\Delta aceE \Delta pyc$ cells were transformed with these plasmids by electroporation (71). The first and second recombination events were performed and verified as described in previous studies (72). The deletion of *pyc*, *ptsG*, *ppc*, and *pgi* was reviewed by amplification and sequencing using primers shown in Table S1.

Measurement of glucose concentrations. To measure the glucose concentration of the culture medium at different time points, cultivation was performed in 50 ml in shaking flasks. During cultivation, 0.5-ml samples were taken every 3 h and were centrifuged (16,000 × g). The supernatant was collected and was stored at -20°C until use.

The actual glucose concentration was measured using a D-glucose UV test kit (R-Biopharm, Darmstadt, Germany), and calculations were done, according to the manufacturer's instructions. Absorption was measured at 340 nm.

Further calculations of the glucose uptake rates could be done based on the glucose concentrations and OD₆₀₀ values obtained. According to reference 18, the following equation was used to determine the glucose concentration in nanomoles per gram (dry weight) per hour:

$$\left(\frac{S}{M}\right) \cdot \mu \left[\left(\frac{\text{nmol} \cdot \text{liter}^{-1} \cdot \text{OD}_{600}^{-1}}{\text{gDW} \cdot \text{liter}^{-1} \cdot \text{OD}_{600}^{-1}} \right) \cdot \text{h}^{-1} \right] = \left[\frac{\text{nmol}}{\text{gDW} \cdot \text{h}} \right]$$

where *S* represents the slope of the glucose concentration versus the OD₆₀₀ (expressed as nanomoles per liter per OD₆₀₀ unit), *M* is the correlation between the dry weight and the OD₆₀₀ (expressed in grams [dry weight] per liter per OD₆₀₀ unit), and μ is the growth rate per hour. According to A. Kabus et al. (73), an OD₆₀₀ of 1 corresponds to 0.25 g (dry weight) liter⁻¹, so this value was used as *M* throughout these calculations.

Quantification of amino acid production. Using ultrahigh-performance liquid chromatography (uHPLC), amino acids were quantified as *ortho*-phthalaldehyde derivatives by automatic precolumn derivatization. Derivatives were separated by reverse-phase chromatography on an Agilent (Santa Clara, CA) 1290 Infinity LC ChemStation equipped with a fluorescence detector. As the eluent for the Zorbax Eclipse amino acid analysis (AAA) column (particle size, 3.5 μ m; inside diameter, 4.6 mm; length, 75 mm; Agilent, Santa Clara, CA), a gradient of Na-borate buffer (10 mM Na₂HPO₄, 10 mM Na₂B₄O₇, [pH 8.2]; adapted to operator's guide) and methanol was applied. Prior to analysis, samples were centrifuged for 10 min at 16,000 × g and 4°C and were diluted 1:100.

Monitoring of cellular proliferation by cell staining. For the staining of proliferating cells, the PKH67 green fluorescent cell linker kit for general cell membrane labeling (Sigma-Aldrich, Munich, Germany) was used, and the protocol was adapted according to the work of O. Kotte et al. (35). From an exponentially growing preculture in CGXII minimal medium containing 222 mM glucose and 154 mM acetate, 1.5 × 10⁹ cells were harvested by centrifugation for 4 min at 4,000 × g and 4°C. Then the cells were washed again in 5 ml ice-cold CGXII basic solution, without MgSO₄, CaCl₂, biotin, trace elements, or protocatechuic acid. For staining, the cell pellet was resuspended in 500 μ l dilution buffer C (Sigma-Aldrich, Munich, Germany) at room temperature, and a freshly prepared mixture of 10 μ l PKH67 dye (Sigma-Aldrich, Munich, Germany) and 500 μ l dilution buffer C was added. Subsequently, cells were incubated for 3 min at room temperature, and afterwards, 4 ml ice-cold filtered CGXII basic solution containing 1% (wt/vol) bovine serum albumin, 1 mM MgSO₄, and 0.1 mM CaCl₂ was added. Then the cells were centrifuged for 4 min at 4,000 × g and 4°C, and the cell pellet was washed twice. Finally, the cells

were resuspended in CGXII minimal medium containing 222 mM glucose and 154 mM acetate and were cultivated in a microtiter cultivation system.

Flow cytometry. Flow cytometric (FC) analyses were conducted on a FACSAria II flow cytometer (Becton, Dickinson, San Jose, CA) equipped with a blue solid-state laser (excitation, 488 nm). Forward-scatter characteristics (FSC) and side-scatter characteristics (SSC) were recorded as small-angle and orthogonal scatters of the 488-nm laser, respectively. PKH67 fluorescence was detected using a 502-nm long-pass and 530/30-nm band-pass filter set. FACSDiva software, version 6.0, was used to monitor the measurements. During analyses, thresholding on FSC was applied to remove background noise. For FC analyses, PKH67-stained culture samples were diluted to an OD_{600} of 0.05 in FACSFlow sheath fluid buffer (BD, Heidelberg, Germany). FlowJo (version 10.0.8) analysis software was used to visualize and evaluate the data (Tree Star, Ashland, OR).

DNA microarrays. For analysis of the transcriptome, *C. glutamicum* $\Delta aceE$ and *C. glutamicum* $\Delta aceE \Delta pyc$ were cultivated in triplicate as described above in 50 ml CGXII medium containing 154 mM acetate and 222 mM glucose in shake flasks. After reaching exponential phase at an OD_{600} of ca. 12 to 15, the cell suspension was harvested by centrifugation ($4,256 \times g$, 10 min, 4°C). The resulting pellet was directly frozen in liquid nitrogen and was stored at -80°C . RNA preparation and cDNA synthesis, as well as microchip hybridization, scanning, and evaluation, were performed as described in previous studies (74).

GC-ToF MS analysis. For analysis of the metabolome, samples of *C. glutamicum* $\Delta aceE$ in the exponential phase, as well as samples of *C. glutamicum* $\Delta aceE \Delta pyc$ in the stationary and exponential phases, were taken, and cells were disrupted using hot methanol. Further sample preparation, derivatization, mass spectrometry (MS) operation, and peak identification were accomplished according to the method of N. Paczia et al. (75) in an Agilent (Santa Clara, CA) 6890N gas chromatograph coupled to a Waters (Milford, MA) Micromass GCT Premier high-resolution ToF MS. Known metabolites were identified using the in-house database JuPoD, the commercial database NIST17 (National Institute of Standards and Technology, USA), and the GMD database (Max Planck Institute of Molecular Plant Physiology, Golm, Germany) (76).

Whole-genome sequencing. In order to sequence the whole genome of *C. glutamicum* $\Delta aceE \Delta pyc$ mutants from the ALE experiment using next-generation sequencing (NGS), genomic DNA was prepared using the NucleoSpin microbial DNA kit (Macherey-Nagel, Düren, Germany) according to the manufacturer's instructions. Subsequently, the concentrations of the purified genomic DNA were measured using a Qubit 2.0 fluorometer (Invitrogen, Carlsbad, CA) according to the manufacturer's instructions. Overall, 4 μg purified genomic DNA was employed for the preparation for genome sequencing using a TruSeq DNA library prep kit and a MiSeq reagent kit, version 1 (Illumina, San Diego, CA, USA), according to the manufacturer's instructions. The sequencing run was performed in a MiSeq system (Illumina, San Diego, CA). Data analysis and base calling were performed with the Illumina instrument software. The resulting FASTQ output files were examined using CLC Genomics Workbench 9 (Qiagen, Aarhus, Denmark).

Accession number(s). The microarray data determined in this study are available at NCBI's Gene Expression Omnibus under accession number GSE134218.

SUPPLEMENTAL MATERIAL

Supplemental material for this article may be found at <https://doi.org/10.1128/JB.00387-19>.

SUPPLEMENTAL FILE 1, PDF file, 1.4 MB.

ACKNOWLEDGMENTS

We thank Jochem Gätgens for performing GC-ToF analyses, and we thank Bastian Blombach and Stephan Noack for fruitful discussions.

We acknowledge financial support by the Helmholtz Association (grant W2/W3-096).

REFERENCES

- Bailey JE, Ollis DF. 1986. Biochemical engineering fundamentals. McGraw-Hill, New York, NY.
- Blombach B, Takors R. 2015. CO₂—intrinsic product, essential substrate, and regulatory trigger of microbial and mammalian production processes. *Front Bioeng Biotechnol* 3:108. <https://doi.org/10.3389/fbioe.2015.00108>.
- de Kok A, Hengeveld AF, Martin A, Westphal AH. 1998. The pyruvate dehydrogenase multi-enzyme complex from Gram-negative bacteria. *Biochim Biophys* 1385:353–366. [https://doi.org/10.1016/S0167-4838\(98\)00079-X](https://doi.org/10.1016/S0167-4838(98)00079-X).
- Eikmanns BJ, Blombach B. 2014. The pyruvate dehydrogenase complex of *Corynebacterium glutamicum*: an attractive target for metabolic engineering. *J Biotechnol* 192(Pt B):339–345. <https://doi.org/10.1016/j.jbiotec.2013.12.019>.
- Schreiner ME, Fiuir D, Holátko J, Pátek M, Eikmanns BJ. 2005. E1 enzyme of the pyruvate dehydrogenase complex in *Corynebacterium glutamicum*: molecular analysis of the gene and phylogenetic aspects. *J Bacteriol* 187:6005–6018. <https://doi.org/10.1128/JB.187.17.6005-6018.2005>.
- Becker J, Rohles CM, Wittmann C. 2018. Metabolically engineered *Corynebacterium glutamicum* for bio-based production of chemicals, fuels, materials, and healthcare products. *Metab Eng* 50:122–141. <https://doi.org/10.1016/j.ymben.2018.07.008>.
- Kogure T, Inui M. 2018. Recent advances in metabolic engineering of *Corynebacterium glutamicum* for bio-production of value-added aromatic chemicals and natural products. *Appl Microbiol Biotechnol* 102:8685–8705. <https://doi.org/10.1007/s00253-018-9289-6>.
- Wang X, Zhang H, Quinn PJ. 2018. Production of L-valine from metabolically engineered *Corynebacterium glutamicum*. *Appl Microbiol Biotechnol* 102:4319–4330. <https://doi.org/10.1007/s00253-018-8952-2>.
- Wendisch VF, Mindt M, Pérez-García F. 2018. Biotechnological production of mono- and diamines using bacteria: recent progress, applications, and perspectives. *Appl Microbiol Biotechnol* 102:3583–3594. <https://doi.org/10.1007/s00253-018-8890-z>.

10. Eggeling L, Bott M. 2005. Handbook of *Corynebacterium glutamicum*. Academic Press, Boca Raton, FL.
11. Blombach B, Schreiner ME, Bartek T, Oldiges M, Eikmanns BJ. 2008. *Corynebacterium glutamicum* tailored for high-yield L-valine production. Appl Microbiol Biotechnol 79:471–479. <https://doi.org/10.1007/s00253-008-1444-z>.
12. Blombach B, Schreiner ME, Holatko J, Bartek T, Oldiges M, Eikmanns BJ. 2007. L-Valine production with pyruvate dehydrogenase complex-deficient *Corynebacterium glutamicum*. Appl Environ Microbiol 73:2079–2084. <https://doi.org/10.1128/AEM.02826-06>.
13. Buchholz J, Schwentner A, Brunnenkan B, Gabris C, Grimm S, Gerstmeier R, Takors R, Eikmanns BJ, Blombach B. 2013. Platform engineering of *Corynebacterium glutamicum* with reduced pyruvate dehydrogenase complex activity for improved production of L-lysine, L-valine, and 2-ketoisovalerate. Appl Environ Microbiol 79:5566–5575. <https://doi.org/10.1128/AEM.01741-13>.
14. Cocaign M, Monnet C, Lindley ND. 1993. Batch kinetics of *Corynebacterium glutamicum* during growth on various carbon substrates: use of substrate mixtures to localise metabolic bottlenecks. Appl Microbiol Biotechnol 40:526–530. <https://doi.org/10.1007/BF00175743>.
15. Wendisch VF, de Graaf AA, Sahn H, Eikmanns BJ. 2000. Quantitative determination of metabolic fluxes during coutilization of two carbon sources: comparative analyses with *Corynebacterium glutamicum* during growth on acetate and/or glucose. J Bacteriol 182:3088–3096. <https://doi.org/10.1128/JB.182.11.3088-3096.2000>.
16. Dominguez H, Cocaign-Bousquet M, Lindley ND. 1997. Simultaneous consumption of glucose and fructose from sugar mixtures during batch growth of *Corynebacterium glutamicum*. Appl Microbiol Biotechnol 47:600–603. <https://doi.org/10.1007/s002530050980>.
17. Stansen C, Uy D, Delaunay S, Eggeling L, Goergen J-L, Wendisch VF. 2005. Characterization of a *Corynebacterium glutamicum* lactate utilization operon induced during temperature-triggered glutamate production. Appl Environ Microbiol 71:5920–5928. <https://doi.org/10.1128/AEM.71.10.5920-5928.2005>.
18. Frunzke J, Engels V, Hasenbein S, Gätgens C, Bott M. 2008. Co-ordinated regulation of gluconate catabolism and glucose uptake in *Corynebacterium glutamicum* by two functionally equivalent transcriptional regulators, GntR1 and GntR2. Mol Microbiol 67:305–322. <https://doi.org/10.1111/j.1365-2958.2007.06020.x>.
19. Wendisch VF, Spies M, Reinscheid DJ, Schnicke S, Sahn H, Eikmanns BJ. 1997. Regulation of acetate metabolism in *Corynebacterium glutamicum*: transcriptional control of the isocitrate lyase and malate synthase genes. Arch Microbiol 168:262–269. <https://doi.org/10.1007/s002030050497>.
20. Sauer U, Eikmanns BJ. 2005. The PEP-pyruvate-oxaloacetate node as the switch point for carbon flux distribution in bacteria. FEMS Microbiol Rev 29:765–794. <https://doi.org/10.1016/j.femsre.2004.11.002>.
21. Eikmanns BJ, Follett MT, Griot MU, Sinskey AJ. 1989. The phosphoenolpyruvate carboxylase gene of *Corynebacterium glutamicum*: molecular cloning, nucleotide sequence, and expression. Mol Gen Genet 218:330–339. <https://doi.org/10.1007/BF00331286>.
22. O'Regan M, Thierbach G, Bachmann B, Villeval D, Lepage P, Viret JF, Lemoine Y. 1989. Cloning and nucleotide sequence of the phosphoenolpyruvate carboxylase-coding gene of *Corynebacterium glutamicum* ATCC13032. Gene 77:237–251. [https://doi.org/10.1016/0378-1119\(89\)90072-3](https://doi.org/10.1016/0378-1119(89)90072-3).
23. Peters-Wendisch PG, Kreutzer C, Kalinowski J, Patek M, Sahn H, Eikmanns BJ. 1998. Pyruvate carboxylase from *Corynebacterium glutamicum*: characterization, expression and inactivation of the *pyc* gene. Microbiology 144:915–927. <https://doi.org/10.1099/00221287-144-4-915>.
24. Kai Y, Matsumura H, Inoue T, Terada K, Nagara Y, Yoshinaga T, Kihara A, Tsumura K, Izui K. 1999. Three-dimensional structure of phosphoenolpyruvate carboxylase: a proposed mechanism for allosteric inhibition. Proc Natl Acad Sci U S A 96:823–828. <https://doi.org/10.1073/pnas.96.3.823>.
25. Repaske R, Repaske AC, Mayer RD. 1974. Carbon dioxide control of lag period and growth of *Streptococcus sanguis*. J Bacteriol 117:652–659.
26. Talley RS, Baugh CL. 1975. Effects of bicarbonate on growth of *Neisseria gonorrhoeae*: replacement of gaseous CO₂ atmosphere. Appl Microbiol 29:469–471.
27. Bäumchen C, Knoll A, Husemann B, Seletzky J, Maier B, Dietrich C, Amoabediny G, Buchs J. 2007. Effect of elevated dissolved carbon dioxide concentrations on growth of *Corynebacterium glutamicum* on D-glucose and L-lactate. J Biotechnol 128:868–874. <https://doi.org/10.1016/j.biotech.2007.01.001>.
28. Blombach B, Buchholz J, Busche T, Kalinowski J, Takors R. 2013. Impact of different CO₂/HCO₃⁻ levels on metabolism and regulation in *Corynebacterium glutamicum*. J Biotechnol 168:331–340. <https://doi.org/10.1016/j.biotech.2013.10.005>.
29. Bartek T, Blombach B, Lang S, Eikmanns BJ, Wiechert W, Oldiges M, Noh K, Noack S. 2011. Comparative ¹³C metabolic flux analysis of pyruvate dehydrogenase complex-deficient, L-valine-producing *Corynebacterium glutamicum*. Appl Environ Microbiol 77:6644–6652. <https://doi.org/10.1128/AEM.00575-11>.
30. Dominguez H, Lindley ND. 1996. Complete sucrose metabolism requires fructose phosphotransferase activity in *Corynebacterium glutamicum* to ensure phosphorylation of liberated fructose. Appl Environ Microbiol 62:3878–3880.
31. Moon MW, Kim HJ, Oh TK, Shin CS, Lee JS, Kim SJ, Lee JK. 2005. Analyses of enzyme II gene mutants for sugar transport and heterologous expression of fructokinase gene in *Corynebacterium glutamicum* ATCC 13032. FEMS Microbiol Lett 244:259–266. <https://doi.org/10.1016/j.femsle.2005.01.053>.
32. Peters-Wendisch PG, Eikmanns BJ, Thierbach G, Bachmann B, Sahn H. 1993. Phosphoenolpyruvate carboxylase in *Corynebacterium glutamicum* is dispensable for growth and lysine production. FEMS Microbiol Lett 112:269–274. <https://doi.org/10.1111/j.1574-6968.1993.tb06461.x>.
33. Mahr R, Gätgens C, Gätgens J, Polen T, Kalinowski J, Frunzke J. 2015. Biosensor-driven adaptive laboratory evolution of L-valine production in *Corynebacterium glutamicum*. Metab Eng 32:184–194. <https://doi.org/10.1016/jymben.2015.09.017>.
34. Reinscheid DJ, Eikmanns BJ, Sahn H. 1994. Characterization of the isocitrate lyase gene from *Corynebacterium glutamicum* and biochemical analysis of the enzyme. J Bacteriol 176:3474–3483. <https://doi.org/10.1128/jb.176.12.3474-3483.1994>.
35. Kotte O, Volkmer B, Radzikowski JL, Heinemann M. 2014. Phenotypic bistability in *Escherichia coli*'s central carbon metabolism. Mol Syst Biol 10:736. <https://doi.org/10.1525/msb.20135022>.
36. Takhaveev V, Heinemann M. 2018. Metabolic heterogeneity in clonal microbial populations. Curr Opin Microbiol 45:30–38. <https://doi.org/10.1016/j.cmb.2018.02.004>.
37. Heinemann M, Zenobi R. 2011. Single cell metabolomics. Curr Opin Biotechnol 22:26–31. <https://doi.org/10.1016/j.copbio.2010.09.008>.
38. Davis KM, Isberg RR. 2016. Defining heterogeneity within bacterial populations via single cell approaches. Bioessays 38:782–790. <https://doi.org/10.1002/bies.201500121>.
39. Ikeda M, Mizuno Y, Awane SI, Hayashi M, Mitsuhashi S, Takeno S. 2011. Identification and application of a different glucose uptake system that functions as an alternative to the phosphotransferase system in *Corynebacterium glutamicum*. Appl Microbiol Biotechnol 90:1443–1451. <https://doi.org/10.1007/s00253-011-3210-x>.
40. Lindner SN, Seibold GM, Henrich A, Krämer R, Wendisch VF. 2011. Phosphotransferase system-independent glucose utilization in *Corynebacterium glutamicum* by inositol permeases and glucokinases. Appl Environ Microbiol 77:3571–3581. <https://doi.org/10.1128/AEM.02713-10>.
41. Peters-Wendisch PG, Schiel B, Wendisch VF, Katsoulidis E, Mockel B, Sahn H, Eikmanns BJ. 2001. Pyruvate carboxylase is a major bottleneck for glutamate and lysine production by *Corynebacterium glutamicum*. J Mol Microbiol Biotechnol 3:295–300.
42. Kortmann M, Mack C, Baumgart M, Bott M. 2019. Pyruvate carboxylase variants enabling improved lysine production from glucose identified by biosensor-based high-throughput fluorescence-activated cell sorting screening. ACS Synth Biol 8:274–281. <https://doi.org/10.1021/acssynbio.8b00510>.
43. Chatterjee R, Millard CS, Champion K, Clark DP, Donnelly MI. 2001. Mutation of the *ptsG* gene results in increased production of succinate in fermentation of glucose by *Escherichia coli*. Appl Environ Microbiol 67:148–154. <https://doi.org/10.1128/AEM.67.1.148-154.2001>.
44. Wang Q, Wu C, Chen T, Chen X, Zhao X. 2006. Expression of galactose permease and pyruvate carboxylase in *Escherichia coli ptsG* mutant increases the growth rate and succinate yield under anaerobic conditions. Biotechnol Lett 28:89–93. <https://doi.org/10.1007/s10529-005-4952-2>.
45. Vanderpool CK, Gottesman S. 2007. The novel transcription factor SgrR coordinates the response to glucose-phosphate stress. J Bacteriol 189:2238–2248. <https://doi.org/10.1128/JB.01689-06>.
46. Morita T, El-Kazzaz W, Tanaka Y, Inada T, Aiba H. 2003. Accumulation of glucose 6-phosphate or fructose 6-phosphate is responsible for destabilization of glucose transporter mRNA in *Escherichia coli*. J Biol Chem 278:15608–15614. <https://doi.org/10.1074/jbc.M300177200>.

47. Kadner RJ, Murphy GP, Stephens CM. 1992. Two mechanisms for growth inhibition by elevated transport of sugar phosphates in *Escherichia coli*. *J Gen Microbiol* 138:2007–2014. <https://doi.org/10.1099/0021287-138-10-2007>.
48. Kessler JR, Cobe BL, Richards GR. 2017. Stringent response regulators contribute to recovery from glucose phosphate stress in *Escherichia coli*. *Appl Environ Microbiol* 83:e01636-17. <https://doi.org/10.1128/aem.01636-17>.
49. Vanderpool CK, Gottesman S. 2004. Involvement of a novel transcriptional activator and small RNA in post-transcriptional regulation of the glucose phosphoenolpyruvate phosphotransferase system. *Mol Microbiol* 54:1076–1089. <https://doi.org/10.1111/j.1365-2958.2004.04348.x>.
50. Engels V, Wendisch VF. 2007. The DeoR-type regulator SugR represses expression of *ptsG* in *Corynebacterium glutamicum*. *J Bacteriol* 189:2955–2966. <https://doi.org/10.1128/JB.01596-06>.
51. Gaigalat L, Schlüter JP, Hartmann M, Mormann S, Tauch A, Pühler A, Kalinowski J. 2007. The DeoR-type transcriptional regulator SugR acts as a repressor for genes encoding the phosphoenolpyruvate:sugar phosphotransferase system (PTS) in *Corynebacterium glutamicum*. *BMC Mol Biol* 8:104. <https://doi.org/10.1186/1471-2199-8-104>.
52. Tanaka Y, Teramoto H, Inui M, Yukawa H. 2008. Regulation of expression of general components of the phosphoenolpyruvate:carbohydrate phosphotransferase system (PTS) by the global regulator SugR in *Corynebacterium glutamicum*. *Appl Microbiol Biotechnol* 78:309–318. <https://doi.org/10.1007/s00253-007-1313-1>.
53. Blombach B, Arndt A, Aucher M, Eikmanns BJ. 2009. L-Valine production during growth of pyruvate dehydrogenase complex-deficient *Corynebacterium glutamicum* in the presence of ethanol or by inactivation of the transcriptional regulator SugR. *Appl Environ Microbiol* 75:1197–1200. <https://doi.org/10.1128/AEM.02351-08>.
54. Repaske R, Clayton MA. 1978. Control of *Escherichia coli* growth by CO₂. *J Bacteriol* 135:1162–1164.
55. Valley G, Rettger LF. 1927. The influence of carbon dioxide on bacteria. *J Bacteriol* 14:101–137.
56. Bracher JM, Martínez-Rodríguez OA, Dekker WJC, Verhoeven MD, van Maris AJA, Pronk JT. 2019. Reassessment of requirements for anaerobic xylose fermentation by engineered, non-evolved *Saccharomyces cerevisiae* strains. *FEMS Yeast Res* 19. <https://doi.org/10.1093/femsyr/foy104>.
57. Gonzalez JE, Long CP, Antoniewicz MR. 2017. Comprehensive analysis of glucose and xylose metabolism in *Escherichia coli* under aerobic and anaerobic conditions by ¹³C metabolic flux analysis. *Metab Eng* 39:9–18. <https://doi.org/10.1016/j.jymben.2016.11.003>.
58. Gerstmeir R, Cramer A, Dangel P, Schaffer S, Eikmanns BJ. 2004. RamB, a novel transcriptional regulator of genes involved in acetate metabolism of *Corynebacterium glutamicum*. *J Bacteriol* 186:2798–2809. <https://doi.org/10.1128/JB.186.9.2798-2809.2004>.
59. Cramer A, Gerstmeir R, Schaffer S, Bott M, Eikmanns BJ. 2006. Identification of RamA, a novel LuxR-type transcriptional regulator of genes involved in acetate metabolism of *Corynebacterium glutamicum*. *J Bacteriol* 188:2554–2567. <https://doi.org/10.1128/JB.188.7.2554-2567.2006>.
60. Kornberg HL. 1966. The role and control of the glyoxylate cycle in *Escherichia coli*. *Biochem J* 99:1–11. <https://doi.org/10.1042/bj0990001>.
61. MacKintosh C, Nimmo HG. 1988. Purification and regulatory properties of isocitrate lyase from *Escherichia coli* ML308. *Biochem J* 250:25–31. <https://doi.org/10.1042/bj2500025>.
62. Robertson EF, Reeves HC. 1986. Purification and characterization of isocitrate lyase from *Escherichia coli*. *Curr Microbiol* 14:347–350. <https://doi.org/10.1007/BF01568702>.
63. Kalinowski J, Bathe B, Bartels D, Bischoff N, Bott M, Burkovski A, Dusch N, Eggeling L, Eikmanns BJ, Gaigalat L, Goesmann A, Hartmann M, Huthmacher K, Krämer R, Linke B, McHardy AC, Meyer F, Möckel B, Pfefferle W, Pühler A, Rey DA, Rückert C, Rupp O, Sahn H, Wendisch VF, Wiegäbe I, Tauch A. 2003. The complete *Corynebacterium glutamicum* ATCC 13032 genome sequence and its impact on the production of L-aspartate-derived amino acids and vitamins. *J Biotechnol* 104:5–25. [https://doi.org/10.1016/S0168-1656\(03\)00154-8](https://doi.org/10.1016/S0168-1656(03)00154-8).
64. Keilhauer C, Eggeling L, Sahn H. 1993. Isoleucine synthesis in *Corynebacterium glutamicum*: molecular analysis of the *ilvB-ilvN-ilvC* operon. *J Bacteriol* 175:5595–5603. <https://doi.org/10.1128/jb.175.17.5595-5603.1993>.
65. Kensy F, Zang E, Faulhammer C, Tan RK, Büchs J. 2009. Validation of a high-throughput fermentation system based on online monitoring of biomass and fluorescence in continuously shaken microtiter plates. *Microb Cell Fact* 8:31. <https://doi.org/10.1186/1475-2859-8-31>.
66. Mustafi N, Grünberger A, Kohlheyer D, Bott M, Frunzke J. 2012. The development and application of a single-cell biosensor for the detection of L-methionine and branched-chain amino acids. *Metab Eng* 14:449–457. <https://doi.org/10.1016/j.jymben.2012.02.002>.
67. Sambrook J, Russell DW. 2001. Molecular cloning: a laboratory manual, 3rd ed. Cold Spring Harbor Laboratory Press, Cold Spring Harbor, NY.
68. Eikmanns BJ, Thum-Schmitz N, Eggeling L, Ludtke K-U, Sahn H. 1994. Nucleotide sequence, expression and transcriptional analysis of the *Corynebacterium glutamicum gltA* gene encoding citrate synthase. *Microbiology* 140:1817–1828. <https://doi.org/10.1099/13500872-140-8-1817>.
69. Gibson DG, Young L, Chuang RY, Venter JC, Hutchison CA, Smith HO. 2009. Enzymatic assembly of DNA molecules up to several hundred kilobases. *Nat Methods* 6:343–345. <https://doi.org/10.1038/nmeth.1318>.
70. Schäfer A, Tauch A, Jäger W, Kalinowski J, Thierbach G, Pühler A. 1994. Small mobilizable multi-purpose cloning vectors derived from the *Escherichia coli* plasmids pK18 and pK19: selection of defined deletions in the chromosome of *Corynebacterium glutamicum*. *Gene* 145:69–73. [https://doi.org/10.1016/0378-1119\(94\)90324-7](https://doi.org/10.1016/0378-1119(94)90324-7).
71. van der Rest ME, Lange C, Molenaar D. 1999. A heat shock following electroporation induces highly efficient transformation of *Corynebacterium glutamicum* with xenogeneic plasmid DNA. *Appl Microbiol Biotechnol* 52:541–545. <https://doi.org/10.1007/s002530051557>.
72. Niebisch A, Bott M. 2001. Molecular analysis of the cytochrome *bc₁-aa₃* branch of the *Corynebacterium glutamicum* respiratory chain containing an unusual diHEME cytochrome *c₁*. *Arch Microbiol* 175:282–294. <https://doi.org/10.1007/s002030100262>.
73. Kabus A, Georgi T, Wendisch VF, Bott M. 2007. Expression of the *Escherichia coli pntAB* genes encoding a membrane-bound transhydrogenase in *Corynebacterium glutamicum* improves L-lysine formation. *Appl Microbiol Biotechnol* 75:47–53. <https://doi.org/10.1007/s00253-006-0804-9>.
74. Baumgart M, Luder K, Grover S, Gätgens C, Besra GS, Frunzke J. 2013. IpsA, a novel LacI-type regulator, is required for inositol-derived lipid formation in *Corynebacteria* and *Mycobacteria*. *BMC Biol* 11:122. <https://doi.org/10.1186/1741-7007-11-122>.
75. Paczia N, Nilgen A, Lehmann T, Gätgens J, Wiechert W, Noack S. 2012. Extensive exometabolome analysis reveals extended overflow metabolism in various microorganisms. *Microb Cell Fact* 11:122. <https://doi.org/10.1186/1475-2859-11-122>.
76. Hummel J, Strehmel N, Selbig J, Walther D, Kopka J. 2010. Decision tree supported substructure prediction of metabolites from GC-MS profiles. *Metabolomics* 6:322–333. <https://doi.org/10.1007/s11306-010-0198-7>.
77. Kinoshita S, Udaka S, Shimono M. 2004. Studies on the amino acid fermentation. Part 1. Production of L-glutamic acid by various microorganisms. *J Gen Appl Microbiol* 50:331–343.
78. Schwentner A, Feith A, Münch E, Busche T, Rückert C, Kalinowski J, Takors R, Blombach B. 2018. Metabolic engineering to guide evolution: creating a novel mode for L-valine production with *Corynebacterium glutamicum*. *Metab Eng* 47:31–41. <https://doi.org/10.1016/j.jymben.2018.02.015>.
79. Cremer J, Eggeling L, Sahn H. 1990. Cloning the *dapA dapB* cluster of the lysine-secreting bacterium *Corynebacterium glutamicum*. *Mol Gen Genet* 220:478–480. <https://doi.org/10.1007/BF00391757>.

4.6 Supplemental material to “Impact of CO₂/HCO₃⁻ Availability on Anaplerotic Flux in Pyruvate Dehydrogenase Complex-Deficient *Corynebacterium glutamicum* Strains”

1 **Supplemental Material to:**

2 The impact of CO₂/HCO₃⁻ availability on anaplerotic flux in PDHC-deficient
3 *Corynebacterium glutamicum* strains

4

5 Aileen Krüger^a, Johanna Wiechert^a, Cornelia Gätgens^a, Tino Polen^a, Regina Mahr^{b#} and
6 Julia Frunzke^{a#}

7

8 ^a Institut für Bio- und Geowissenschaften, IBG-1: Biotechnology, Forschungszentrum
9 Jülich, 52425 Jülich, Germany

10

11 ^b SenseUp GmbH, c/o Campus Forschungszentrum Jülich, 52425 Jülich, Germany

12

13

14 **Content:**

15

16 **Table S1:** Peak areas for compounds determined via GC-ToF analysis for PDHC-deficient
17 strains.

18 **Table S2:** Analysis of differential gene expression (0.7- and 1.7-fold change) of *C.*
19 *glutamicum* $\Delta aceE \Delta pyc$ and $\Delta aceE$ growing on CGXII containing 154 mM acetate and
20 222 mM glucose.

21 **Table S3:** Overview on plasmids constructed in this study.

22 **Table S4:** Oligonucleotides used in this work.

23

24 **Figure S1:** Effect of different PTS-sugars on growth of *C. glutamicum* $\Delta aceE$ and $\Delta aceE$
25 Δpyc .

26 **Figure S2:** Growth and glucose consumption of different *C. glutamicum* PDHC-deficient
27 strains.

28 **Figure S3:** Effect of PTS-sugar fructose on growth of *ptsG*-deficient *C. glutamicum* $\Delta aceE$
29 and $\Delta aceE \Delta pyc$.

30 **Figure S4:** Effect of gluconate and ribose on growth of *ptsG*-deficient *C. glutamicum*
31 $\Delta aceE \Delta pyc$.

32 **Figure S5:** Addition of HCO₃⁻ restored growth defects of *pyc*-deficient *C. glutamicum*
33 strains

34 **Figure S6:** Growth of the PEPCx-deficient strain $\Delta aceE \Delta ppc$.

35 **Figure S7:** Effect of culture volume on the growth of *C. glutamicum* $\Delta aceE$ and $\Delta aceE$
36 Δpyc .

37 **Figure S8:** Deletion of *pgi* in PDHC-deficient strains to reroute flux through the pentose
38 phosphate pathway.

39 **Figure S9:** Growth phase dependent sampling of *C. glutamicum* $\Delta aceE$ and $\Delta aceE \Delta pyc$
40 for DNA microarrays and GC-ToF analysis.

41 **Figure S10:** Adaptive laboratory evolution of *C. glutamicum* $\Delta aceE \Delta pyc$ on acetate.

42

43 **Table S1: Peak areas for compounds determined via GC-ToF analysis for PDHC-**
 44 **deficient strains.**

	Area					
	WT	$\Delta aceE$ E1*	$\Delta aceE$ Δprc E1*	$\Delta aceE$ Δprc E2*	$\Delta aceE$ HCO ₃ **	$\Delta aceE$ Δprc HCO ₃ **
<u>Amino acids</u>						
Alanine	2503	1303	845	8321	3277	5299
Aspartate	998	402	<1	383	296	460
Glutamine	6603	2554	1393	4430	3060	4166
Glutamate	30122	9836	3249	21157	17374	21093
N-acetyl-Glutamate	305	178	116	140	144	216
Glycine	197	110	-	168	164	192
Lysine	217	124	112	216	174	257
Proline	9611	4918	432	8127	8609	4835
Proline+CO ₂	917	625	73	620	737	407
Serine	90	52	<1	-	68	80
Valine	177	436	753	1125	410	285
<u>Glycolysis</u>						
Glucose	3819	10761	7152	5901	3702	3270
Glycerol + Phosphate	1591	804	801	929	1248	1262
Glycerol-3-phosphate	1229	751	299	666	928	961
3-phospho-Glycerate	49	78	35	51	117	111
Pyruvate	51	85	-	278	156	492
<u>TCA cycle</u>						
Malate	218	259	-	90	-	214
Succinate	1689	2135	597	2848	2093	5719
<u>Further</u>						
Lactate	2436	934	784	915	1686	401
Trehalose	31837	11813	29109	7409	32045	8603
Urea	233	193	168	144	247	69

45 Strains were cultivated in 50 ml CGXII containing 154 mM acetate and 222 mM glucose. Compounds were identified
 46 based on retention time using in-house database JuPoD.* = E1 corresponds to the first sample extraction where $\Delta aceE$
 47 reached in the exponential phase, while $\Delta aceE \Delta prc$ was still in lag phase. E2 corresponds to the second sample
 48 extraction where $\Delta aceE \Delta prc$ reached the exponential phase. ** = Medium was supplemented with 100 mM HCO₃.

49

50 **Table S2: Analysis of differential gene expression (0.7- and 1.7-fold change) of *C.***
 51 ***glutamicum* $\Delta aceE \Delta pyc$ and $\Delta aceE$ growing on CGXII containing 154 mM acetate**
 52 **and 222 mM glucose. mRNA ratio ≤ 0.70 = downregulation in $\Delta aceE \Delta pyc$ (shaded in**
 53 **red), mRNA ratio ≥ 1.7 = upregulation in $\Delta aceE \Delta pyc$ (shaded in green), p-values < 0.05 .**

Gene	Annotation	mRNA ratio	p-value
cg0791	<i>pyc</i> , pyruvate carboxylase	0.01	0.01
cg1377	<i>ssuC</i> , aliphatic sulfonates transmembrane ABC transporterprotein	0.04	0.02
cg1376	<i>ssuD1</i> , alkanesulfonate monooxygenase	0.06	0.01
cg1379	<i>ssuB</i> , aliphatic sulfonates ATP-binding ABC transporterprotein	0.08	0.00
cg0120	esterase/lipase/thioesterase family protein	0.12	0.00
cg0111	hypothetical protein cg0111	0.17	0.00
cg3219	<i>ldhA</i> , NAD-dependent L-lactate dehydrogenase	0.18	0.02
cg1147	<i>ssuI</i> , FMN-binding protein required for sulfonate and sulfonate ester utilization	0.19	0.00
cg1156	<i>ssuD2</i> , monooxygenase for sulfonate utilization	0.20	0.00
cg2962	uncharacterized enzyme involved in biosynthesis of extracellular polysaccharides	0.23	0.00
cg1905	hypothetical protein cg1905	0.25	0.00
cg2320	predicted transcriptional regulator	0.26	0.00
cg3226	putative L-lactate permease	0.27	0.01
cg1484	putative secreted protein	0.28	0.01
cg3315	bacterial regulatory protein, MarR family	0.28	0.00
cg0957	<i>fas-IB</i> , fatty acid synthase	0.29	0.02
cg3118	<i>cysI</i> , sulfite reductase (hemoprotein)	0.31	0.02
cg1907	putative phosphopantothenoylecysteine synthetase/decarboxylase	0.31	0.01
cg0812	<i>dtsR1</i> , acetyl/propionyl-CoA carboxylase beta chain	0.31	0.01
cg1906	hypothetical protein cg1906	0.32	0.00
cg1454	putative aliphatic sulfonates uptake ABC transporter secreted solute-binding protein	0.32	0.01
cg2958	<i>butA</i> , L-2,3-butanediol dehydrogenase/acetoin reductase	0.33	0.02
cg3179	<i>fadD2</i> , acyl-CoA synthase	0.35	0.00

cg3117	hypothetical protein cg3117	0.36	0.01
cg0683	permease	0.36	0.00
cg3316	universal stress protein UspA or related nucleotide-binding protein	0.37	0.00
cg2685	short chain dehydrogenase	0.37	0.03
cg1380	<i>ssuA</i> , aliphatic sulfonate binding protein	0.38	0.02
cg0277	<i>dccT</i> , dicarboxylate uptake system (succinate, fumarate or L-malate)	0.40	0.04
cg3119	<i>cysJ</i> , probable sulfite reductase (flavoprotein)	0.41	0.00
cg0175	secreted protein, signal peptide	0.41	0.02
cg3116	<i>cysH</i> , phosphoadenosine-phosphosulfate reductase	0.42	0.01
cg1003	5-formyltetrahydrofolate cyclo-ligase	0.42	0.03
cg1268	<i>glgA</i> , glycogen synthase	0.42	0.02
cg3227	<i>lldD</i> , quinone-dependent L-lactate dehydrogenase LldD	0.43	0.01
cg1066	<i>urtE</i> , ABC-type urea uptake system, ATP binding protein	0.43	0.01
cg0241	hypothetical protein cg0241	0.44	0.00
cg1399	permease of the major facilitator superfamily	0.44	0.01
cg0973	<i>pgi</i> , glucose-6-phosphate isomerase	0.44	0.03
cg0240	membrane protein	0.45	0.00
cg2645	<i>clpP1</i> , ATP-dependent Clp protease proteolytic subunit	0.45	0.01
cg2699	hypothetical protein cg2699	0.45	0.03
cg0284	drug exporter of the RND superfamily	0.45	0.04
cg2891	<i>pgo</i> , pyruvate chinon oxidoreductase	0.47	0.02
cg1744	<i>pacL</i> , cation-transporting ATPase	0.47	0.03
cg2707	hypothetical protein cg2707	0.47	0.01
cg2953	<i>xyIC</i> , benzaldehyde dehydrogenase	0.48	0.01
cg2456	Zn-ribbon protein, possibly nucleic acid-binding	0.48	0.02
cg2715	hypothetical protein cg2715	0.48	0.01
cg1740	putative nucleoside-diphosphate-sugar epimerase	0.48	0.00
cg0697	hypothetical protein cg0697	0.49	0.02
cg2342	dehydrogenase	0.49	0.02
cg0514	hypothetical membrane protein	0.49	0.00
cg3112	predicted permease	0.49	0.03

cg3092	hypothetical protein cg3092	0.50	0.03
cg0316	secreted protein	0.50	0.00
cg3223	NADPH-dependent FMN reductase	0.50	0.01
cg1741	hypothetical protein cg1741	0.50	0.01
cg0359	hypothetical protein cg0359	0.51	0.03
cg1345	<i>narK</i> , putative nitrate/nitrite transporter	0.51	0.04
cg3218	pyruvate kinase	0.52	0.01
cg0129	<i>putA</i> , proline dehydrogenase/delta-1-pyrroline-5-carboxylate dehydrogenase	0.52	0.00
cg2910	transcriptional regulator, LacI family	0.52	0.00
cg2800	<i>pgm</i> , phosphoglucomutase	0.52	0.02
cg1080	putative multicopper oxidase	0.52	0.00
cg3224	<i>LldR</i> , Repressor of the cg3226- <i>lldD</i> lactate operon	0.52	0.01
cg1081	ABC-type multidrug transport system, ATPase component	0.52	0.00
cg1742	hypothetical protein cg1742	0.52	0.01
cg1619	putative DNA gyrase inhibitor	0.53	0.01
cg2890	putative amino acid processing enzyme	0.53	0.01
cg3279	putative dehydrogenase-fragment	0.53	0.02
cg1045	hypothetical protein cg1045	0.53	0.04
cg1246	hypothetical protein cg1246	0.53	0.01
cg0892	hypothetical protein cg0892	0.53	0.04
cg0387	<i>adhE</i> , putative zinc-type alcohol dehydrogenase transmembrane	0.53	0.03
cg2500	bacterial regulatory proteins, ArsR family	0.53	0.03
cg2118	transcriptional regulator of sugar metabolism, DeoR family	0.53	0.01
cg2810	Na ⁺ /H ⁺ -dicarboxylate symporter family	0.54	0.02
cg1647	ABC-type multidrug transport system, permease component	0.54	0.00
cg1002	putative secreted protein	0.54	0.01
cg1452	hypothetical protein cg1452	0.55	0.00
cg3402	copper chaperone	0.55	0.01
cg3004	<i>gabD2</i> , succinic semialdehyde dehydrogenase	0.55	0.00
cg2305	<i>hisD</i> , histidinol dehydrogenase	0.55	0.05
cg3304	<i>dnaB</i> , replicative DNA helicase	0.55	0.00

cg1068	probable oxidoreductase	0.55	0.01
cg1374	hypothetical protein cg1374	0.56	0.01
cg3280	putative secreted protein	0.56	0.02
cg1238	hypothetical protein cg1238	0.56	0.02
cg0039	putative transcriptional regulator	0.56	0.01
cg1111	<i>eno</i> , phosphopyruvate hydratase	0.57	0.03
cg1618	hypothetical protein cg1618	0.57	0.01
cg3340	<i>dadA</i> , putative D-amino acid dehydrogenase (deaminating)	0.57	0.02
cg2318	putative secreted vitamin B12-binding lipoprotein	0.57	0.00
cg0807	hypothetical protein cg0807	0.57	0.03
cg2598	hypothetical protein cg2598	0.57	0.00
cg3225	putative serine/threonine-specific protein phosphatase	0.57	0.03
cg2340	ABC-type amino acid transport system, secreted component	0.57	0.00
cg0513	hypothetical membrane protein	0.58	0.00
cg0777	siderophore ABC transporter, ATP-binding protein	0.58	0.02
cg1545	permease of the major facilitator superfamily	0.58	0.04
cg0755	<i>metY</i> , O-acetylhomoserine sulfhydrylase	0.58	0.01
cg2537	<i>brnQ</i> , branched-chain amino acid uptake carrier	0.58	0.03
cg1525	<i>polA</i> , DNA polymerase I	0.58	0.01
cg0685	homolog of metal-dependent protease, putative molecular chaperone	0.58	0.01
cg2291	<i>pyk</i> , pyruvate kinase	0.58	0.01
cg2770	hypothetical protein cg2770	0.58	0.03
cg3128	ABC-type transport system, ATPase component	0.59	0.01
cg0780	membrane protein ribonuclease BN-like family	0.59	0.01
cg0611	secreted protein	0.59	0.00
cg0176	permease	0.59	0.02
cg0358	hydrolase or acyltransferase	0.59	0.01
cg0122	putative glycerol 3-phosphate dehydrogenase	0.59	0.05
cg2304	<i>hisC</i> , histidinol-phosphate aminotransferase	0.59	0.01
cg1537	<i>ptsG</i> , glucose-specific enzyme II BC component of PTS	0.59	0.02
cg1791	<i>gap</i> , glyceraldehyde-3-phosphate dehydrogenase	0.59	0.02

cg0976	<i>pcrA</i> , ATP-dependent helicase PCRA	0.59	0.01
cg0260	<i>moaC</i> , molybdenum cofactor biosynthesis protein C	0.60	0.03
cg0464	<i>ctpA</i> , copper-transporting ATPase	0.60	0.02
cg0662	FAD/FMN-containing dehydrogenase	0.60	0.03
cg2247	hypothetical protein cg2247	0.60	0.02
cg1017	<i>metS</i> , methionyl-tRNA synthetase	0.60	0.02
cg1330	similar to GTP pyrophosphokinase	0.60	0.00
cg2459	<i>ptpA</i> , protein-tyrosine-phosphatase	0.60	0.01
cg0766	<i>icd</i> , isocitrate dehydrogenase	0.60	0.01
cg2877	<i>avtA</i> , aminotransferase, uses alanine, keto-isovalerate and ketobutyrate	0.61	0.01
cg2743	<i>fas-IA</i> , fatty acid synthase	0.61	0.04
cg2457	hypothetical protein cg2457	0.61	0.02
cg1195	sulfate permease or related transporter (MFS superfamily)	0.61	0.01
cg2556	uncharacterized iron-regulated membrane protein	0.61	0.00
cg1027	<i>dld</i> , D-lactate dehydrogenase	0.61	0.02
cg0404	nitroreductase family	0.61	0.00
cg2835	predicted acetyltransferase	0.61	0.01
cg3399	permease of the major facilitator superfamily	0.62	0.05
cg2162	<i>thyX</i> , alternative thymidylate synthase	0.62	0.02
cg0896	hypothetical protein cg0896	0.62	0.02
cg2104	<i>galE</i> , UDP-glucose 4-epimerase	0.62	0.02
cg0131	putative oxidoreductase	0.62	0.00
cg3057	putative secreted protein	0.62	0.00
cg1790	<i>pgk</i> , phosphoglycerate kinase	0.62	0.02
cg2558	related to aldose 1-epimerase	0.62	0.00
cg2554	<i>rbsK2</i> , probable ribokinase protein	0.62	0.02
cg2536	<i>metC</i> , cystathionine beta-lyase	0.62	0.00
cg0239	hypothetical protein cg0239	0.63	0.02
cg2178	<i>nusA</i> , transcription elongation factor NusA	0.63	0.04
cg1908	hypothetical protein cg1908	0.63	0.05
cg1603	hypothetical protein cg1603	0.63	0.02

cg1247	putative secreted protein	0.63	0.00
cg3228	hypothetical protein cg3228	0.63	0.04
cg1106	hypothetical protein cg1106	0.63	0.03
cg3158	<i>nagA2</i> , beta-N-acetylglucosaminidase precursor	0.63	0.02
cg1691	<i>arc</i> , AAA+ ATPase ARC, pupylation machinery	0.63	0.00
cg0781	membrane protein	0.63	0.04
cg0934	hypothetical protein cg0934	0.63	0.02
cg2867	<i>gpx</i> , glutathione peroxidase	0.64	0.02
cg1683	superfamily II DNA and RNA helicase	0.64	0.01
cg2605	predicted acetyltransferase	0.64	0.02
cg1883	putative secreted protein	0.64	0.05
cg3331	<i>ogt</i> , methylated-DNA--protein-cysteine methyltransferase	0.64	0.00
cg1375	putative thioredoxin	0.64	0.01
cg2529	<i>treS</i> , trehalose synthase (maltose alpha-D-glucosyltransferase)	0.64	0.00
cg1400	DNA polymerase III subunit epsilon	0.64	0.00
cg2778	hypothetical protein cg2778	0.64	0.01
cg2248	hypothetical protein cg2248	0.64	0.01
cg0684	<i>papA</i> , prolyl aminopeptidase A	0.64	0.02
cg2577	predicted multitransmembrane, metal-binding protein	0.64	0.04
cg2431	putative transcriptional regulator	0.64	0.01
cg1831	bacterial regulatory protein, ArsR family	0.65	0.05
cg3332	putative quinone oxidoreductase	0.65	0.01
cg0712	secreted protein	0.65	0.00
cg1599	hypothetical protein cg1599	0.65	0.00
cg0297	hypothetical protein cg0297	0.65	0.03
cg2455	hypothetical protein cg2455	0.65	0.01
cg2572	hypothetical protein cg2572	0.65	0.01
cg0512	<i>hemB</i> , delta-aminolevulinic acid dehydratase	0.65	0.00
cg0171	secreted protein	0.65	0.00
cg2521	<i>fadD15</i> , long-chain fatty acid CoA ligase	0.65	0.01
cg0174	putative transport protein	0.65	0.04
cg1680	hypothetical protein cg1680	0.65	0.01

cg0376	<i>dnaX</i> , putative DNA polymerase III, delta subunit	0.65	0.03
cg2033	putative secreted protein	0.66	0.02
cg0680	hypothetical protein cg0680	0.66	0.04
cg2924	<i>cysS</i> , cysteinyl-tRNA synthetase	0.66	0.01
cg1206	PEP phosphonmutase or related enzyme	0.66	0.01
cg3236	<i>msrA</i> , peptide methionine sulfoxide reductase	0.66	0.00
cg0481	<i>mshA</i> , glycosyltransferase	0.66	0.01
cg0686	acetyltransferase, GNAT family	0.66	0.02
cg1035	TatD related DNase	0.66	0.03
cg3067	hypothetical protein cg3067	0.66	0.01
cg0388	Zn-dependent hydrolase	0.66	0.04
cg2193	putative lysophospholipase	0.66	0.01
cg1018	probable ATP-dependent DNA helicase protein	0.66	0.03
cg1423	putative oxidoreductase (related to aryl-alcohol dehydrogenase)	0.66	0.01
cg1284	<i>lipT</i> , type B carboxylesterase	0.67	0.03
cg2597	<i>rne</i> , probable ribonuclease E (RNase E) protein	0.67	0.05
cg0796	<i>prpD1</i> , 2-methylcitrate dehydratase	0.67	0.01
cg2117	<i>ptsI</i> , phosphoenolpyruvate:sugar phosphotransferase system enzyme	0.67	0.01
cg0081	putative tautomerase	0.67	0.01
cg1630	<i>odhI</i> , essential for glutamine utilization, regulates ODH activity	0.67	0.03
cg2795	NADPH quinone reductase or related Zn-dependent oxidoreductase	0.67	0.02
cg3253	<i>mcbR</i> , TetR-type transcriptional regulator of sulfur metabolism	0.67	0.03
cg1600	predicted rRNA methylase	0.68	0.01
cg3069	hypothetical protein cg3069	0.68	0.02
cg3068	<i>fda</i> , fructose-bisphosphate aldolase	0.68	0.01
cg0067	<i>gabD3</i> , succinate-semialdehyde dehydrogenase (NADP+)	0.68	0.00
cg0450	hypothetical protein cg0450	0.68	0.04
cg2687	<i>metB</i> , cystathionine gamma-synthase	0.68	0.00
cg2323	<i>treY</i> , maltooligosyl trehalose synthase	0.68	0.01
cg3185	hypothetical protein cg3185	0.68	0.01
cg1384	putative NUDIX hydrolase	0.68	0.00

cg3350	<i>nagK</i> , fumarylpyruvate hydrolase	0.68	0.04
cg0232	hypothetical secreted protein	0.69	0.00
cg2432	MUTT/NUDIX family protein	0.69	0.03
cg3034	<i>def</i> , peptide deformylase	0.69	0.02
cg2421	<i>sucB</i> , dihydrolipoamide acetyltransferase	0.69	0.00
cg1401	<i>ligA</i> , DNA ligase	0.69	0.03
cg3423	<i>trxC</i> , thioredoxin	0.69	0.01
cg0128	secreted protein, signal peptide	0.69	0.03
cg0496	thiol-disulfide isomerase or thioredoxin	0.69	0.05
cg1048	haloacid dehalogenase/epoxide hydrolase family	0.69	0.03
cg0015	<i>gyrA</i> , DNA gyrase subunit A	0.69	0.03
cg0854	<i>pmmA</i> , phosphomannomutase	0.69	0.01
cg1318	DNA repair exonuclease	0.69	0.03
cg0873	<i>aroA</i> , 3-phosphoshikimate 1-carboxyvinyltransferase	0.69	0.01
cg0154	haloacid dehalogenase-like hydrolase	0.70	0.04
cg2444	hypothetical protein cg2444	0.70	0.03
cg0745	NAD-dependent deacetylase	0.70	0.01
cg2716	<i>hyi</i> , hydroxypyruvate isomerase	0.70	0.02
cg3154	<i>udgA2</i> , UDP-glucose 6-dehydrogenase	0.70	0.01
cg0910	inositol monophosphatase	0.70	0.03
cg0489	hypothetical membrane protein	0.70	0.00
cg3168	SAM-dependent methyltransferase	0.70	0.01
cg3015	hypothetical protein cg3015	1.70	0.01
cg1414	uncharacterized component of ribose/xylose transport systems	1.70	0.00
cg1355	<i>prfA</i> , peptide chain release factor 1	1.71	0.02
cg2138	<i>gluC</i> , glutamate permease	1.71	0.03
cg1366	<i>atpA</i> , ATP synthase subunit A	1.71	0.05
cg3008	<i>porA</i> , main cell wall channel protein	1.72	0.03
cg2374	<i>murE</i> , UDP-N-acetylmuramoylalanyl-D-glutamate--2,6-diaminopimelate ligase	1.72	0.03
cg1367	<i>atpG</i> , ATP synthase subunit C	1.72	0.02
cg2272	mutM1, formamidopyrimidine-DNA glycosylase	1.73	0.00

cg1498	RecG-like helicase	1.73	0.01
cg0719	<i>crtYe</i> , C50 carotenoid epsilon cyclase	1.74	0.01
cg3266	<i>tnp5c</i> (ISCg5c), transposase	1.74	0.00
cg1706	<i>arsC1</i> , arsenate reductase	1.74	0.02
cg2263	hypothetical protein cg2263	1.75	0.00
cg1314	<i>putP</i> , proline transport system	1.75	0.00
cg1349	membrane protein containing CBS domain	1.75	0.03
cg1122	putative secreted protein	1.75	0.05
cg1412	ribose/xylose/arabinose/galactoside ABC-type transport system, permease component	1.75	0.02
cg1123	<i>greA</i> , transcription elongation factor GreA	1.76	0.03
cg0577	<i>rpoC</i> , DNA-directed RNA polymerase beta subunit	1.78	0.03
cg1617	GTP-binding protein EngA	1.78	0.01
cg2990	<i>speE</i> , spermidine synthase	1.78	0.00
cg2624	<i>pcaR</i> , transcriptional regulator of 4-hydroxybenzoate, protocatechuate, p-cresol pathway	1.78	0.02
cg0690	<i>groES</i> , chaperonin 10 Kd subunit	1.78	0.01
cg2807	<i>tnp11a</i> (ISCg11a), transposase-fragment	1.79	0.00
cg1041	<i>pdxK</i> , pyridoxal/pyridoxine/pyridoxamine kinase	1.79	0.00
cg2184	ATPase component of peptide ABC-type transport system, contains duplicated ATPase domains	1.79	0.00
cg3027	<i>mrpE</i> , hypothetical protein cg3027	1.80	0.02
cg2600	<i>tnp1d</i> (ISCg1d), transposase	1.80	0.00
cg0203	<i>iolE</i> , 2-Keto-myo-inositol dehydratase	1.80	0.00
cg0621	substrate-specific component SCO2325 of predicted cobalamin ECF transporter	1.81	0.00
cg1218	<i>ndnR</i> , transcriptional repressor of NAD de novo biosynthesis genes	1.81	0.00
cg1586	<i>argG</i> , argininosuccinate synthase	1.82	0.01
cg2269	predicted permease	1.82	0.00
cg1413	secreted sugar-binding protein	1.82	0.01
cg0717	<i>crtEb</i> , hypothetical protein cg0717	1.82	0.00
cg0057	<i>pknB</i> , eukaryotic-type serine/threonine kinase	1.83	0.00
cg1602	<i>recN</i> , DNA repair protein RecN	1.86	0.00
cg2467	ABC transporter ATP-binding protein	1.86	0.00

cg2196	putative secreted or membrane protein	1.86	0.05
cg3385	<i>catA3</i> , catechol 1,2-dioxygenase	1.86	0.00
cg1149	hypothetical protein cg1149	1.87	0.04
cg1364	<i>atpF</i> , ATP synthase subunit B	1.88	0.02
cg2559	<i>aceB</i> , malate synthase	1.88	0.02
cg0693	<i>groEL</i> , 60 KDA chaperonin (protein CPN60) (groel protein) C-terminal fragment	1.88	0.04
cg1363	<i>atpE</i> , ATP synthase subunit C	1.88	0.02
cg0691	<i>groEL</i> , 60 KDA chaperonin (protein CPN60) (HSP60)-N-terminal fragment	1.89	0.02
cg1040	ATPase component of ABC transporters with duplicated ATPase domains	1.90	0.00
cg1902	putative secreted protein	1.91	0.02
cg0692	<i>tnp1c</i> (ISCg1c), transposase	1.92	0.00
cg1418	secreted siderophore-binding lipoprotein	1.92	0.00
cg1213	<i>tnp1a</i> (ISCg1a), transposase	1.93	0.04
cg2052	putative secreted protein	1.94	0.02
cg2676	ABC-type dipeptide/oligopeptide/nickel transport systems, permease component	1.94	0.01
cg1780	<i>devB</i> , 6-phosphogluconolactonase	1.94	0.01
cg1362	<i>atpB</i> , ATP synthase subunit A	1.95	0.03
cg2265	<i>smc</i> , chromosome segregation ATPase	1.96	0.00
cg0204	<i>iolG</i> , putative oxidoreductase myo-inositol 2-dehydrogenase	1.96	0.04
cg3386	<i>tcbF</i> , maleylacetate reductase	1.96	0.01
cg0223	<i>iolT1</i> , myo-Inositol transporter	1.97	0.04
cg1488	<i>leuD</i> , isopropylmalate isomerase small subunit	1.97	0.00
cg1354	<i>rho</i> , transcription termination factor Rho	1.98	0.01
cg1792	putative transcriptional regulator-WhiA homolog	1.98	0.01
cg2470	secreted ABC transporter substrate-binding protein	1.98	0.00
cg3047	<i>ackA</i> , acetate/propionate kinase	1.99	0.01
cg1417	acetyltransferase	2.00	0.00
cg1348	membrane protein containing CBS domain	2.01	0.03
cg1725	<i>mutA</i> , methylmalonyl-CoA mutase, subunit	2.01	0.01
cg0062	<i>ppp</i> , protein phosphatase	2.02	0.02

cg1779	<i>opcA</i> , putative subunit of glucose-6-P dehydrogenase	2.04	0.01
cg0323	conserved hypothetical secreted protein	2.05	0.01
cg3195	flavin-containing monooxygenase (FMO)	2.06	0.04
cg1812	<i>pyrF</i> , orotidine 5-phosphate decarboxylase	2.07	0.02
cg1344	<i>narG</i> , nitrate reductase 2, alpha subunit	2.07	0.01
cg0417	<i>capD</i> , probable dTDP-glucose 4,6-dehydratase transmembrane protein	2.08	0.00
cg1813	<i>carB</i> , carbamoyl-phosphate synthase large subunit	2.12	0.01
cg3363	<i>trpB</i> , tryptophan synthase subunit beta	2.14	0.00
cg0720	<i>crtI2</i> , phytoene dehydrogenase (desaturase)	2.15	0.01
cg0321	Na ⁺ /H ⁺ antiporter subunit	2.16	0.01
cg0419	glycosyltransferase	2.16	0.01
cg1365	<i>atpH</i> , ATP synthase subunit D	2.16	0.01
cg0418	putative aminotransferase	2.17	0.01
cg0325	hypothetical protein cg0325	2.22	0.02
cg1215	<i>nadC</i> , quinolinate phosphoribosyltransferase	2.23	0.01
cg3016	hypothetical protein cg3016	2.24	0.01
cg3096	<i>ald</i> , alcohol dehydrogenase	2.24	0.04
cg2939	ABC-type dipeptide/oligopeptide/nickel transport system, fused permease and ATPase components	2.29	0.02
cg3028	<i>mrpF</i> , hypothetical protein cg3028	2.32	0.00
cg3029	<i>mrpG</i> , multisubunit Na ⁺ /H ⁺ antiporter, g subunit	2.34	0.01
cg3025	<i>mrpC</i> , hypothetical protein cg3025	2.34	0.01
cg2675	ATPase component of ABC-type transport system, contains duplicated ATPase domains ATPase component of ABC-type transport system, contains duplicated ATPase domains	2.36	0.01
cg1582	<i>argB</i> , acetylglutamate kinase	2.37	0.04
cg2240	<i>thiF</i> , molybdopterin biosynthesis protein MoeB	2.38	0.04
cg3391	<i>oxiD</i> , myo-Inositol dehydrogenase	2.40	0.00
cg0324	<i>mnhD</i> , NADH dehydrogenase subunit N	2.41	0.01
cg2610	ABC-type dipeptide/oligopeptide/nickel transport system, secreted component	2.46	0.00
cg3017	hypothetical protein cg3017	2.54	0.00
cg0837	hypothetical protein cg0837	2.66	0.03

cg0322	predicted conserved membrane protein	2.69	0.00
cg3026	<i>mrpD</i> , NADH-ubiquinone oxidoreductase/multisubunit Na ⁺ /H ⁺ antiporter, D subunit	2.86	0.01
cg3390	<i>myo</i> -Inositol catabolism, sugar phosphate isomerase/epimerase	2.89	0.01
cg3360	<i>trpG</i> , anthranilate synthase component II	2.97	0.01
cg0059	<i>pknA</i> , serine/threonine protein kinase	3.01	0.00
cg0838	helicase	3.06	0.01
cg3359	<i>trpE</i> , anthranilate synthase component I	3.08	0.00
cg0165	ABC-2 type transporter	3.12	0.01
cg0061	<i>rodA</i> , putative FTSW/RODA/SPOVE family cell cycle protein	3.13	0.00
cg1724	<i>meaB</i> , accessory protein of methylmalonylCoA mutase	3.18	0.01
cg0018	hypothetical membrane protein	3.19	0.00
cg0163	N-acetylglucosaminyltransferase	3.21	0.00
cg1583	<i>argD</i> , acetylornithine aminotransferase	3.26	0.01
cg0060	<i>pbpA</i> , D-alanyl-D-alanine carboxypeptidase	3.31	0.00
cg3362	<i>trpCF</i> , bifunctional indole-3-glycerol phosphate synthase/phosphoribosylanthranilate isomerase	3.31	0.01
cg0162	membrane spanning protein	3.33	0.00
cg1214	<i>nadS</i> , cysteine desulfurase-like protein involved in Fe-S cluster assembly	3.44	0.00
cg2636	<i>catA1</i> , catechol 1,2-dioxygenase	3.50	0.01
cg1584	<i>argF</i> , ornithine carbamoyltransferase	3.81	0.01
cg3361	<i>trpD</i> , anthranilate phosphoribosyltransferase	3.83	0.01
cg1585	<i>argR</i> , arginine repressor	3.96	0.00
cg0844	type II restriction enzyme, methylase subunit	6.36	0.00
cg2430	hypothetical protein cg2430	13.96	0.00

55 **Table S3: Overview on plasmids constructed in this study.** In Table 2 in the main text
 56 provides a list of all plasmids used in this study.

Plasmid	Backbone	Restriction-enzymes	Oligonucleotides for insert	Template	Method
pK19 <i>mobsacB</i> - Δ <i>ptsG</i> -P3	pK19 <i>mobsacB</i> (1)	EcoRI, BamHI	A7-ptsG-leftflank-fw A8-ptsG-leftflank-rv A9-ptsG-rightflank-fw A10-ptsG-rightflank-rv	Genomic DNA (<i>C. glutamicum</i>)	Gibson assembly
pK19 <i>mobsacB</i> - Δ <i>pgi</i>	pK19 <i>mobsacB</i> (1)	EcoRI, BamHI	A21-pgi-leftflank-fw A22-pgi-leftflank-rv A23-pgi-rightflank-fw A24-pgi-rightflank-rv	Genomic DNA (<i>C. glutamicum</i>)	Gibson assembly
pJC1- <i>pyc</i>	pJC1- <i>venus</i> - term-BS (2)	BamHI, BcuI	A31- <i>pyc</i> -pJC1-fw A32- <i>pyc</i> -pJC1-rv	Genomic DNA (<i>C. glutamicum</i>)	Gibson assembly

57

58

59 **Table S4: Oligonucleotides used in this work.**

Oligonucleotide	Sequence 5'→3'	Use
Primer for sequencing and strain verification		
A1-seq- <i>pyc</i> -fw	CTGCGCCACGGTTTTGTGAAG	Sequencing <i>pyc</i>
A2-seq- <i>pyc</i> -rv	CAACCACATCTGCACTGCGATC	Sequencing <i>pyc</i>
A14-seq- <i>ptsG</i> -flanks-fw	GGCTCACTGACGTTGACAGTG	Sequencing <i>ptsG</i>
A15-seq- <i>ptsG</i> -flanks-rv	GATATCGCGGGCAACTTGGTC	Sequencing <i>ptsG</i>
A17-seq- <i>pgi</i> -fw	GTGATGGCACCTGCCGATTC	Sequencing <i>pgi</i>
A18-seq- <i>pgi</i> -rv	CGGAATCCACGAAATCGCCG	Sequencing <i>pgi</i>
104- <i>aceE</i> int-seq-fw	CCAGGGCTCCTTCTTTACCAATG	Sequencing <i>aceE</i>
105- <i>aceE</i> int-seq-rv	CGTTCCTCCCGGCACTGTG	Sequencing <i>aceE</i>
<i>ppc</i> del_fw	GGAATAGACTCGCTCGGC	Sequencing <i>ppc</i>
<i>ppc</i> del_rv	GTGAACAGGCTCTCGATGC	Sequencing <i>ppc</i>
<i>ureD</i> _E188*_fw	CGGACTCCCATAGGGAAGTTTTG	Sequencing <i>ureD</i>
<i>ureD</i> _E188*_rv	CAAAACCTCCCTATCGGGAGTCCG	Sequencing <i>ureD</i>
596- <i>aceA</i> -Seq-rv	CGAGTTCCTTCTGGAACCTAGCG	Sequencing <i>aceA</i>
599- <i>aceA</i> -Seq-rv2	CTTCGGTGCGTGCGATTTTCATC	Sequencing <i>aceA</i>
597- <i>aceB</i> -Seq-fw	CTTCGAAGACTCCGTTGCAGC	Sequencing <i>aceB</i>
598- <i>aceB</i> -Seq-rv	TTGTTGAGCTCACGGGTGAAG	Sequencing <i>aceB</i>
600- <i>aceB</i> -Seq-rv2	GAGCAAGCAGCTCGCGGTG	Sequencing <i>aceB</i>
M19-M13-fw	CACTGACCCTTTTGGGACCGC	Sequencing of pK19 <i>mobsacB</i>
M20-M13-rv	AGCGGATAACAATTCACACAGGA	Sequencing of pK19 <i>mobsacB</i>
R12-pJC1-MCS-fw	CAGGGACAAGCCACCCGCACA	Sequencing of inserts in pJC1
R13-pJC1-MCS-rv	GGAAGCTAGAGTAAGTAGTTCGC	Sequencing of inserts in pJC1
Construction of plasmid pK19<i>mobsacB</i>-Δ<i>ptsG</i>-P3 used for deletion of <i>ptsG</i>		
A7- <i>ptsG</i> -leftflank-fw	<u>CAGGTCGACTCTAGAGGATCGCTTTTGGCGGGCGC</u> TTCGG	Left flank fw Δ <i>ptsG</i>
A8- <i>ptsG</i> -leftflank-rv	<u>GTCTGTAACCGAGCATCTCTCGTCAAACCTTTCTA</u> AACGTAGGGTCTG	Left flank rv Δ <i>ptsG</i>
A9- <i>ptsG</i> -rightflank-fw	<u>GAGAGATGCTCGGTTACAGACCAGCTAAGCCGAAG</u> CTGGCCG	Right flank fw Δ <i>ptsG</i>
A10- <i>ptsG</i> -rightflank-rv	<u>GTAATAACGACGGCCAGTGAATTGTTACTCGTTCTT</u> GCCGTTGACCTTG	Right flank rv Δ <i>ptsG</i>

Construction of plasmid pK19*mobsacB*- Δ *pgi* used for deletion of *pgi*

A21- <i>pgi</i> -leftflank-fw	<u>CAGGTCGACTCTAGAGGATCCAGCACCCGACAAACA</u> CGATC	Left flank fw Δ <i>pgi</i>
A22- <i>pgi</i> -leftflank-rv	<u>GTCTGTAACCGAGCATCTCTC</u> GAAAACTCCTTTAT TGTCGTTAAATAAC	Left flank rv Δ <i>pgi</i>
A23- <i>pgi</i> -rightflank-fw	<u>GAGAGATGCTCGGTTACAGACC</u> CTGTTTCCACTGG CACTG	Right flank fw Δ <i>pgi</i>
A24- <i>pgi</i> -rightflank-rv	<u>GTA AACGACGCGCCAGTGAATTGCTAC</u> TATTGTC GCGGTACC	Right flank rv Δ <i>pgi</i>

Construction of plasmid pJC1-*pyc* used for overexpression of *pyc*

A31- <i>pyc</i> -pJC1-fw	<u>AGCGACGCCGACGGGGATCCGGATTGCTTTGTGC</u> ACTCCTGG	<i>pyc</i> fw, including promoter region
A32- <i>pyc</i> -pJC1-rv	<u>AAAACGACGCCAGTACTAGCAGAAAGTTTAGGA</u> AACGACGAC	<i>pyc</i> rv

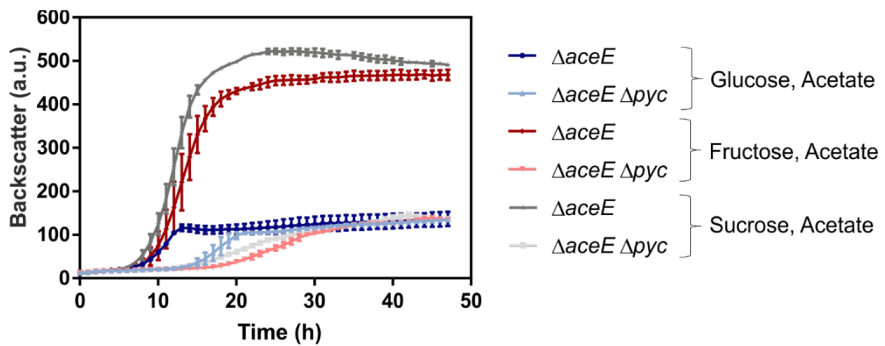
Construction of plasmid pJC1-*pyc* used for overexpression of *aceA* and *aceB*

588- <i>aceA</i> -fw	<u>CTGAACTTTAAGAAGGAGATATCATATGTCAAACG</u> TTGAAAGCCACG	Insert 1 <i>aceA</i> fw
589- <i>aceA</i> -linker-rv	<u>CATATGTATATCTCCTTCTTAAAGTTAAACAAAAT</u> <u>TATTCTAGTCTAGTTGTGGA</u> ACTGGCCTTCTTC	Insert 1 <i>aceA</i> rv, including linker
590- <i>aceB</i> -linker-fw	<u>GTTTAACTTTAAGAAGGAGATATACATATGACTGA</u> ACAGGAACTGTTGTCTG	Insert 2 <i>aceB</i> fw, including linker
591- <i>aceB</i> -rv	<u>CTGTAAAACGACGCCAGTACTAGTTAGTTTTTTG</u> CTTTGAACTCGCGGC	Insert 2 <i>aceB</i> rv

Construction of plasmid pJC1-*pyc* used for overexpression of *aceB* and *aceA*

584- <i>aceB</i> -fw	<u>CTGAACTTTAAGAAGGAGATATCATATGACTGAAC</u> AGGAACTGTTGTCTG	Insert 1 <i>aceB</i> fw
585- <i>aceB</i> -linker-rv	<u>ATGTATATCTCCTTCTTAAAGTTAAACAAAATTAT</u> <u>TTCTAGTTAGTTTTTTGCTTGA</u> ACTCGCGG	Insert 1 <i>aceB</i> rv, including linker
586- <i>aceA</i> -linker-fw	<u>GTTTAACTTTAAGAAGGAGATATACATATGTCAA</u> CGTTGAAAGCCACG	Insert 2 <i>aceA</i> fw, including linker
587- <i>aceA</i> -rv	<u>CTGTAAAACGACGCCAGTACTAGCTAGTTGTGGA</u> ACTGGCCTTCTTC	Insert 2 <i>aceA</i> rv

60 Underlined = complementary to backbone, **red** = linker sequence; fw = forward, rv = reverse



63

64 **Figure S1: Effect of different PTS-sugars on growth of *C. glutamicum* $\Delta aceE$ and**65 **$\Delta aceE \Delta pyc$.** The strains $\Delta aceE$ and $\Delta aceE \Delta pyc$ were inoculated to an OD_{600} of 1 in

66 CGXII containing 154 Mm acetate and 222 mM of varying PTS sugars: glucose (shades

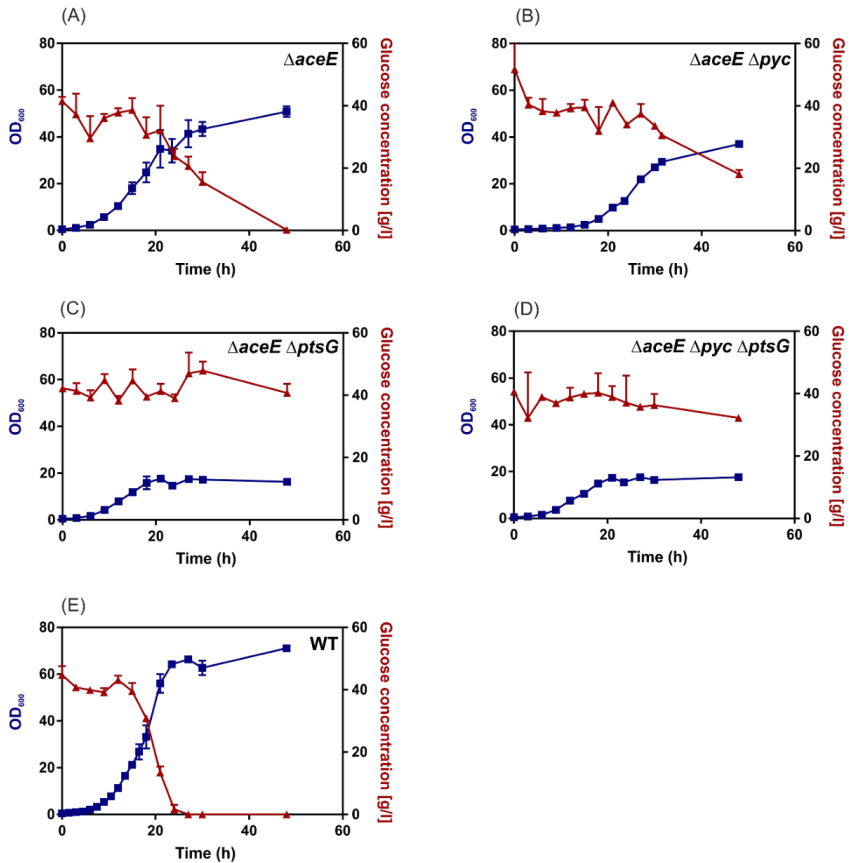
67 of blue), fructose (shades of red), or sucrose (shades of grey). Growth curves shown are

68 based on the backscatter measurements in a microtiter cultivation system. Symbols

69 represent the backscatter means and error bars their standard deviations of biological

70 triplicates.

71



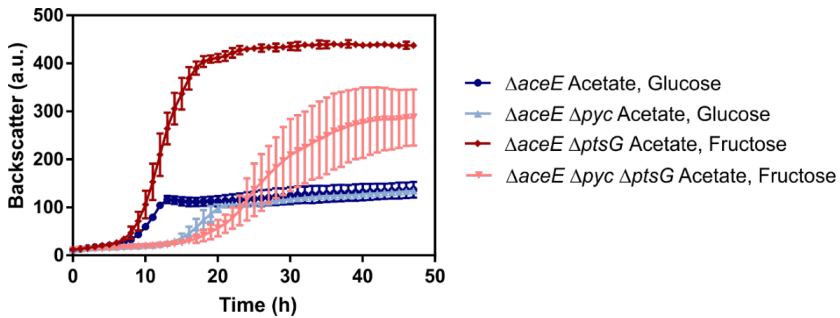
72

73 **Figure S2: Growth and glucose consumption of different *C. glutamicum* PDHC-**
 74 **deficient strains.** The PDHC-deficient strains $\Delta aceE$, $\Delta aceE \Delta pyc$, $\Delta aceE \Delta ptsG$, $\Delta aceE$
 75 $\Delta pyc \Delta ptsG$ as well as the wild type (WT) as control were inoculated to an OD₆₀₀ of 1 each
 76 in 50 ml CGXII containing 154 mM acetate and 222 mM glucose. OD₆₀₀ measurements
 77 (blue graphs) and sampling for glucose measurements were performed every 3 h until 33
 78 h and once additionally at 48 h. (A-E) Measurement of glucose concentration was
 79 performed with the D-Glucose UV-Test Kit (r-biopharm, Darmstadt, Germany) (red

80 graphs). Symbols represent the OD₆₀₀ means and error bars their standard deviations of
81 biological triplicates.

82

83



84

85 **Figure S3: Effect of PTS-sugar fructose on growth of *ptsG*-deficient *C. glutamicum***86 ***ΔaceE* and *ΔaceE Δpyc*.** Growth curves shown are based on the backscatter87 measurements in a microtiter cultivation system, inoculated at an OD₆₀₀ of 1. Symbols

88 represent the backscatter means and error bars their standard deviations of biological

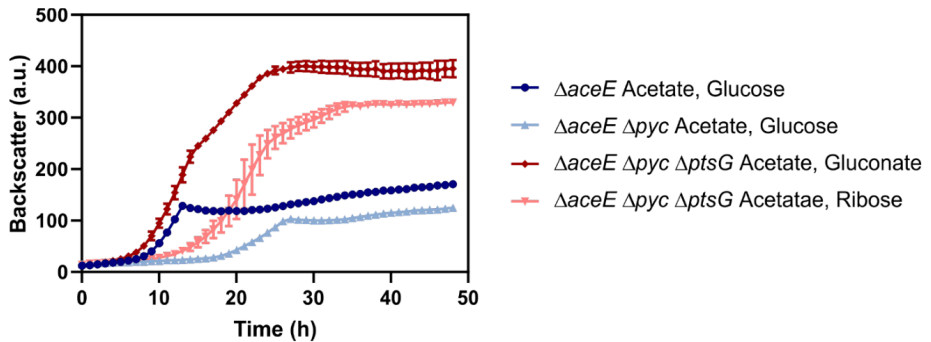
89 triplicates. Deletion of the *ptsG* gene was accomplished using the pK19*mobsacB*-system90 for both strains *ΔaceE* and *ΔaceE Δpyc*. These *ΔptsG* strains (shades of red) were

91 cultivated in a microtiter cultivation system in CGXII containing 154 mM acetate and 222

92 mM fructose. Strains *ΔaceE* and *ΔaceE Δpyc* cultivated in 154 mM acetate and 222 mM

93 glucose served as control, and are shown in shades of blue.

94



95

96 **Figure S4: Effect of gluconate and ribose on growth of *ptsG*-deficient *C. glutamicum***97 **$\Delta aceE \Delta pyc$.** Growth curves shown are based on the backscatter measurements in a98 microtiter cultivation system, inoculated at an OD₆₀₀ of 1. Symbols represent the

99 backscatter means and error bars their standard deviations of biological

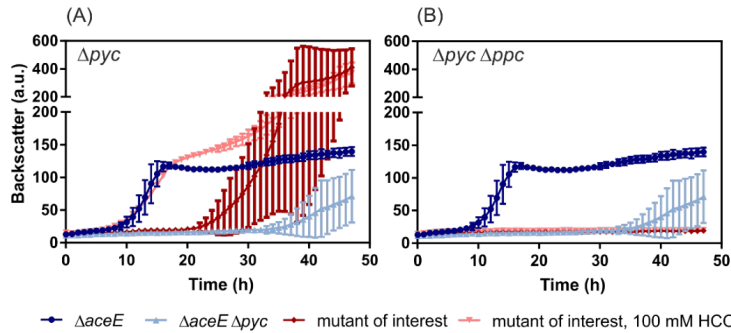
100 triplicates. Deletion of the *ptsG* gene was accomplished using the pK19*mobsacB*-system101 for both strains $\Delta aceE$ and $\Delta aceE \Delta pyc$. These $\Delta ptsG$ strains (shades of red) were

102 cultivated in a microtiter cultivation system in CGXII containing 154 mM acetate and 222

103 mM gluconate (dark red) or 154 mM acetate and 222 mM ribose (light red). Strains $\Delta aceE$ 104 and $\Delta aceE \Delta pyc$ cultivated in 154 mM acetate and 222 mM glucose served as control,

105 and are shown in shades of blue.

106



107

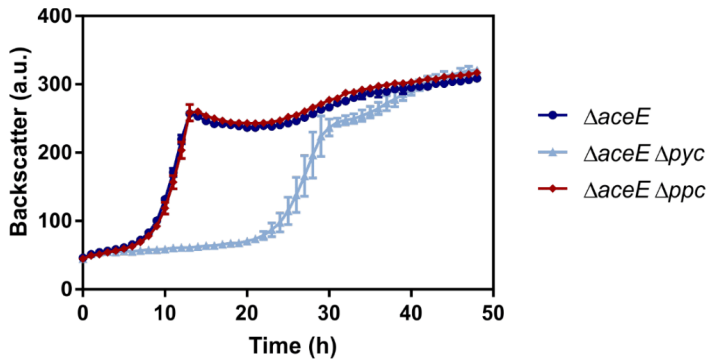
108 **Figure S5: Addition of HCO_3^- restored growth defects of *pyc*-deficient**109 ***C. glutamicum* strains.** The strains (A) Δpyc and (B) $\Delta pyc \Delta ppc$ were inoculated to an110 OD_{600} of 1 in CGXII media containing 154 mM acetate and 222 mM glucose (shown in111 dark red) or additionally 100 mM $KHCO_3^-$ (shown in light red). Further, $\Delta aceE$ and $\Delta aceE$ 112 Δpyc in CGXII media containing 154 mM acetate and 222 mM glucose were cultivated as

113 controls (shown in shades of blue). Growth curves shown are based on the backscatter

114 measurements in a microtiter cultivation system. Symbols represent the backscatter

115 means and error bars their standard deviations of biological triplicates.

116



117

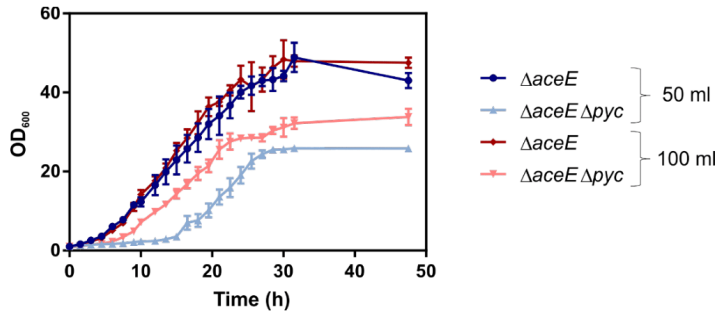
118 **Figure S6: Growth of the PEPCx-deficient strain $\Delta aceE \Delta ppc$.** The strain $\Delta aceE \Delta ppc$ 119 was inoculated to an OD_{600} of 1 in CGXII media containing 154 mM acetate and 222 mM120 glucose (red). Further, $\Delta aceE$ and $\Delta aceE \Delta pyc$ in CGXII media containing 154 mM

121 acetate and 222 mM glucose were cultivated as controls (shown in shades of blue).

122 Growth curves shown are based on the backscatter measurements in a microtiter

123 cultivation system. Symbols represent the backscatter means and error bars the standard

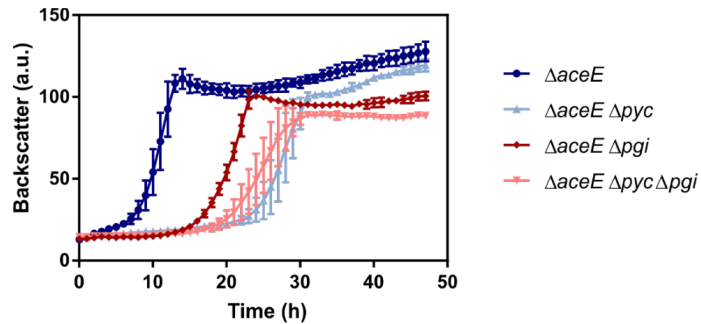
124 deviations of biological triplicates.



125

126 **Figure S7: Effect of culture volume on the growth of *C. glutamicum* $\Delta aceE$ and**
 127 **$\Delta aceE \Delta pyc$.** Main cultures of $\Delta aceE$ and $\Delta aceE \Delta pyc$ were inoculated to an OD_{600} of 1
 128 in CGXII containing 154 mM acetate and 222 mM glucose once in 50 ml in a 500 ml
 129 shaking flask (shades of blue) and once in 100 ml in a 1 l shaking flask (shades of red).
 130 Cultivation was performed in an orbital shaker. Growth curves shown are based on OD_{600}
 131 measurements which were performed every 90 minutes until 33 h, and an additional
 132 measurement after 48 h. Symbols represent the OD_{600} means and error bars their
 133 standard deviations of biological triplicates.

134

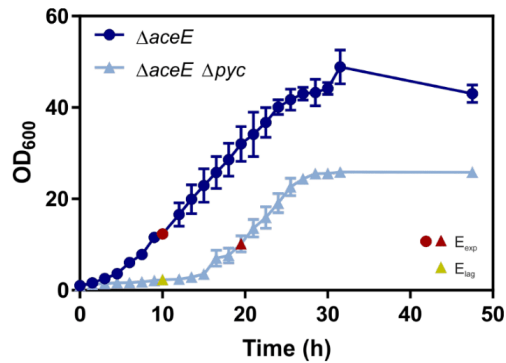


135

136 **Figure S8: Deletion of *pgi* in PDHC-deficient strains to reroute flux through the**
137 **pentose phosphate pathway.** Deletion of the *pgi* gene was accomplished using the
138 *pK19mobsacB* system for both strains $\Delta aceE$ and $\Delta aceE \Delta pyc$. Generated strains were
139 inoculated in a microtiter cultivation system to an OD_{600} of 1 in CGXII containing 154 mM
140 acetate and 222 mM glucose. Additionally, the parental strains $\Delta aceE$ and $\Delta aceE \Delta pyc$
141 served as control, and are shown in shades of blue, while $\Delta aceE \Delta pgi$ and $\Delta aceE \Delta pyc$
142 Δpgi are shown in shades of red. Growth curves shown are based on the backscatter
143 measurements in a microtiter cultivation system. Symbols represent the backscatter
144 means and error bars their standard deviations of biological triplicates.

145

146



147

148 **Figure S9: Growth phase dependent sampling of *C. glutamicum* $\Delta aceE$ and $\Delta aceE$** 149 **Δpyc for DNA microarrays and GC-ToF analysis.** The strains $\Delta aceE$ and $\Delta aceE \Delta pyc$ 150 were cultivated. The main culture was inoculated to an OD₆₀₀ of 1 in 50 ml CGXII

151 containing 154 mM acetate and 222 mM glucose. Cultivation was performed in 500 ml

152 shaking flasks. Growth curves shown are based on OD₆₀₀ measurements which were

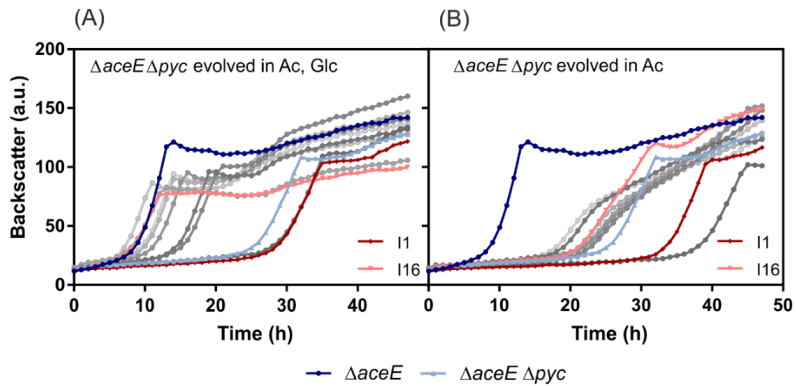
153 performed every 90 minutes until 33 h, and an additional measurement after 48 h. Colored

154 data points indicate the time where samples were taken: red = sampling time point during

155 exponential phase (E_{exp}) used for DNA microarrays and GC-ToF analysis, yellow =156 sampling time point during lag phase of $\Delta aceE \Delta pyc$ (E_{lag}) additionally used for GC-ToF

157 experiments.

158



159

160 **Figure S10: Adaptive laboratory evolution of *C. glutamicum* $\Delta aceE \Delta pyc$ on acetate.**

161 Growth analysis of single inoculation steps obtained from the adaptive laboratory evolution
 162 (ALE) approach which was performed with the strain $\Delta aceE \Delta pyc$ (A) with selection
 163 pressure in CGXII containing 154 mM acetate and 222 mM glucose and (B) without
 164 selection pressure in CGXII containing solely 154 mM acetate. Growth curves are shown
 165 based on the backscatter measurements in a microtiter cultivation system. For growth
 166 analysis on population level, glycerol stocks which were prepared after batch number 1,
 167 4, 6, 7, 8, 9, 10, 11, 13 and 16 during ALE were directly used for the inoculation of a first
 168 pre-culture in BHI supplemented with 51 mM acetate. The second pre-culture in CGXII
 169 containing 154 mM acetate was then used for inoculation of the main culture in CGXII
 170 containing 154 mM acetate and 222 mM glucose (start OD_{600} of 1). The first and last
 171 inoculations are shown in shades of red. The parental strains $\Delta aceE$ and $\Delta aceE \Delta pyc$
 172 (shades of blue) served as controls. Symbols represent the backscatter means. I =
 173 Inoculation.

174

175 **References**

- 176 1. Schäfer A, Tauch A, Jäger W, Kalinowski J, Thierbach G, Pühler A. 1994. Small
177 mobilizable multi-purpose cloning vectors derived from the *Escherichia coli*
178 plasmids pK18 and pK19: selection of defined deletions in the chromosome of
179 *Corynebacterium glutamicum*. *Gene* 145:69-73 doi:10.1016/0378-1119(94)90324-
180 7.
- 181 2. Baumgart M, Luder K, Grover S, Gätgens C, Besra GS, Frunzke J. 2013. IpsA, a
182 novel LacI-type regulator, is required for inositol-derived lipid formation in
183 *Corynebacteria* and *Mycobacteria*. *BMC Biol* 11 doi:10.1186/1741-7007-11-122.

184

Acknowledgements

At first, I want to express my special thanks to Prof. Dr. Julia Frunzke for giving me the opportunity to work on this exciting and diverse topic, for inspiring discussions and for her support in both my personal and academic development.

Furthermore, I would like to thank Prof. Dr. Lutz Schmitt for agreeing to be my co-supervisor.

Thanks to all the colleagues of the IBG-1 institute for the nice working atmosphere and the constant helpfulness. Special thanks goes to all former and current group members of AG Bacterial Networks and Interactions, especially Johanna Wiechert, Eva Davoudi, Roberto Stella, Max Hünnefeld, Larissa Kever, Tom Luthe, Vikas Sharma, Ulrike Viets, Cornelia Gätgens, Aël Hardy, Sebastian Erdrichs, Janik Göttsche, Bente Rackow, Isabelle Mohnen, Biel Badia Roigé, Marc Keppel. Thank you for this exceptionally nice working atmosphere, for fruitful discussions and valuable input, funny lunch breaks, wonderful group evenings and the great time!

Especially, I want to thank Johanna for her motivating support and help in every situation whenever needed, as well as for the nice atmosphere in the office and our inspiring weekly 'Eisengang'. Special thanks to Larissa for encouraging talks as colleague and friend, fruitful discussions and mutual motivation and support during daily tea breaks.

I would particularly like to thank Ulli for her reliable, motivating and excellent technical support in the lab with various ChAP-Seq trials. I also want to thank Conni helping with several cloning issues whenever needed.

Moreover, I would like to thank Janik for his motivated and great work during his master thesis, which I had the chance to supervise.

Thanks to the proofreading gang - Tom, Johanna, Bente - for their time and valuable input.

Ich möchte ich mich ganz besonders bei meinen Eltern, meiner Familie und meinen Freunden bedanken, die immer hinter mir stehen, immer an mich glauben und auf deren Hilfe ich wirklich immer bauen kann!

Ein besonderer Dank gilt Madleen, die mich nicht nur stetig mit Nervennahrung versorgt hat, sondern auch immer voller lieber motivierender Worte hinter mir steht!

Zum Schluss möchte ich mich noch von Herzen bei Ben bedanken für die liebevolle Rundumversorgung, für die kontinuierliche Unterstützung und Motivation, für die stetige Aufmunterung. Für alles!

Eidesstattliche Erklärung

Hiermit versichere ich an Eides Statt, dass die Dissertation von mir selbständig und ohne unzulässige fremde Hilfe unter Beachtung der „Grundsätze zur Sicherung guter wissenschaftlicher Praxis an der Heinrich-Heine-Universität Düsseldorf“ erstellt worden ist. Die Dissertation wurde in der vorgelegten oder in ähnlicher Form noch bei keiner anderen Institution eingereicht. Ich habe bisher keine erfolglosen Promotionsversuche unternommen.

Aileen Krüger

Band / Volume 253

Topological magnonic properties of two-dimensional magnetic materials

L. Zhang (2022), xx, 154 pp

ISBN: 978-3-95806-621-2

Band / Volume 254

Role of secondary metabolites in antiphage defense in *Streptomyces*

Aël Hardy (2022), IV, 193 pp

ISBN: 978-3-95806-633-5

Band / Volume 255

Neutron Scattering

Lectures of the JCNS Laboratory Course held at Forschungszentrum Jülich and at the Heinz-Maier-Leibnitz Zentrum Garching

edited by T. Brückel, S. Förster, M. Kruteva, M. Zobel, and R. Zorn (2022), ca. 300 pp

ISBN: 978-3-95806-634-2

Band / Volume 256

Magnetoelectric Interactions in Multiferroic Thin-film Heterosystems and Nanostructures

H. Gökdemir (2022), x, 140 pp

ISBN: 978-3-95806-635-9

Band / Volume 257

High-Performance Computing Approach to Hybrid Functionals in the All-Electron DFT Code FLEUR

M. Redies (2022), xi, 109 pp

ISBN: 978-3-95806-639-7

Band / Volume 258

Establishing regulatable expression systems in the acetic acid bacterium

***Gluconobacter oxydans* 621H**

P. M. Fricke (2022), VIII, 187 pp

ISBN: 978-3-95806-642-7

Band / Volume 259

Density-Functional Perturbation Theory within the All-Electron Full-Potential Linearized Augmented Plane-Wave Method: Application to Phonons

C.-R. Gerhorst (2022), xvi, 317 pp

ISBN: 978-3-95806-649-6

Band / Volume 260

Crystal and Magnetic Structure of CrAs under Extreme Conditions

A. Eich (2022), viii, 235 pp

ISBN: 978-3-95806-655-7

Band / Volume 261

Applications of transcription factor-based biosensors for strain development and evolutionary engineering

R. G. Stella (2022), x, 128 pp

ISBN: 978-3-95806-657-1

Band / Volume 262

Strömungsmechanische Simulation und experimentelle Validierung des kryogenen Wasserstoff-Moderators für die Europäische Spallationsneutronenquelle ESS

Y. Beßler (2022), XXIV, 154, xxxiii pp

ISBN: 978-3-95806-660-1

Band / Volume 263

**9th Georgian-German School and Workshop in Basic Science
September 12 – 16, 2022 | Kutaisi, Tbilisi | Georgia**

A. Kacharava, E. Portius, N. J. Shah, H. Ströher (2022)

ISBN: 978-3-95806-664-9

Band / Volume 264

Self-assembly of Au-Fe₃O₄ dumbbell nanoparticles

N. Nandakumaran (2022), xiv, 234 pp

ISBN: 978-3-95806-666-3

Band / Volume 265

Time-resolved and three-dimensional characterisation of magnetic states in nanoscale materials in the transmission electron microscope

T. Weßels (2023), xx, 211 pp

ISBN: 978-3-95806-685-4

Band / Volume 266

Dissecting iron and heme regulatory networks and adaptation to heme stress in *Corynebacterium glutamicum*

A. Krüger (2023), IV, 274 pp

ISBN: 978-3-95806-686-1

Weitere **Schriften des Verlags im Forschungszentrum Jülich** unter
<http://www.zb1.fz-juelich.de/verlagextern1/index.asp>

Schlüsseltechnologien / Key Technologies

Band / Volume 266

ISBN 978-3-95806-686-1